

USE OF QUASI-STATIC FRICITION CONE PENETROMETER DATA  
TO PREDICT LOAD CAPACITY OF DISPLACEMENT PILES

By

LARRY C. NOTTINGHAM

A DISSERTATION PRESENTED TO THE GRADUATE COUNCIL OF  
THE UNIVERSITY OF FLORIDA  
IN PARTIAL FULFILLMENT OF THE REQUIREMENTS FOR THE  
DEGREE OF DOCTOR OF PHILOSOPHY

UNIVERSITY OF FLORIDA

1975

DEDICATION

To Carol, John and Amy for patiently enduring.

#### ACKNOWLEDGEMENTS

The author thanks Dr. J. H. Schmertmann for serving as Chairman of his Supervisory Committee and for the expert guidance he provided during the course of this study. He is also grateful to David L. Freed for his assistance in performing some of the tests and for independently evaluating a portion of the data.

The effort of Professors J. H. Schaub, B. Ruth, and W. Zimpfer, who served as members of the Supervisory Committee, is gratefully acknowledged. A round of applause is also accorded to Bill Whitehead for his moral support and to Howard Brown for his expert workmanship in fabricating the many strange gadgets required for performing the field tests.

Finally, appreciation is expressed to the Florida Department of Transportation for financing this research project and for providing the author with employment during his stay at the University of Florida.

## TABLE OF CONTENTS

ACKNOWLEDGEMENTS	iii
LIST OF SYMBOLS AND ABBREVIATIONS	vii
ABSTRACT	xii
1 INTRODUCTION	
1.1 Research Justification	1
1.2 Purpose and Scope	6
2 SUMMARY OF PREVIOUS WORK	
2.1 Penetrometer History	9
2.2 CPT Methods for Predicting Pile Point Capacity	13
2.3 CPT Methods for Predicting Pile Side Friction	34
2.4 Summary	39
3 MODEL PILE TEST SITES	
3.1 Fairbanks Site	40
3.2 Beville Site	42
3.3 Paines Prairie Site	54
3.4 Pile-Soil Friction Tests	72
4 EQUIPMENT FOR MODEL PILE RESEARCH	
4.1 Penetrometer Equipment	78
4.2 Model Piles	81
4.3 Pile Driving and Load Testing Equipment	85
5 MODEL PILE TESTING TECHNIQUES	
5.1 Penetration Testing	99
5.2 Pile Load Testing in Sand	105
5.3 Pile Load Testing in Clay	112
5.4 Pile Tip Load Cell Operation	121
6 MODEL PILE TEST DATA	
6.1 Cone Penetrometer Soundings	124
6.2 Model Pile Driving Data	125
6.3 Fairbanks Site Pile Load Tests	125
6.4 Beville Site Pile Load Tests	125
6.5 Paines Prairie Pile Tests	130
6.6 Definition of Failure Load	131
6.7 Side Friction and Tip Resistance Corrections	134

7	MODEL PILE CAPACITY PREDICTIONS IN SAND	147
7.1	Data Summary	147
7.2	Pile Tip Resistance	147
7.3	Pile Side Friction	185
7.4	Shaft Resistance of Step-Taper Piles	209
7.5	Total Pile Capacity Predictions	213
7.6	Design Safety Factors for Piles in Sand	221
8	MODEL PILE CAPACITY PREDICTIONS IN CLAY	232
8.1	Currently Available Prediction Methods	232
8.2	Possible Methods of Using CPT Data	241
8.3	Model Pile Point Capacity Predictions	243
8.4	Model Pile Side Friction Predictions	247
8.5	Step-Taper Pile Shaft Resistance	260
8.6	Total Capacity Predictions	264
8.7	Time Effects on Pile Capacity	267
8.8	Conclusions	270
9	FULL-SCALE PILE TEST RESULTS	272
9.1	West Palm Beach Tests	272
9.2	Jefferson County Tests	276
9.3	Tarver, Georgia, Load Test	277
9.4	Blount Island Tests	278
10	FULL-SCALE PILE CAPACITY PREDICTIONS	283
10.1	Description of Prediction Methods Used	283
10.2	Comparison of Predicted and Measured Capacities	288
10.3	Evaluation of Prediction Accuracy Safety Factors	293
11	RECOMMENDED CPT FILE CAPACITY DESIGN PROCEDURES	296
11.1	Introduction	296
11.2	Tip Bearing Capacity	296
11.3	Side Friction on Constant Section Piles	298
11.4	Tapered Pile Shaft Resistance	307
11.5	Safety Factors	311
11.6	Limitations and Precautions	315
12	CONCLUSIONS AND RECOMMENDATIONS	317
12.1	Conclusions	317
12.2	Significant Contributions of the Research	326
12.3	Recommendations for Additional Research	328
	LIST OF REFERENCES	330
	APPENDIX A - FAIRBANKS SITE TEST RESULTS	335
	APPENDIX B - BEVILLE SITE TEST RESULTS	355

APPENDIX C - PAINES PRAIRIE SITE TEST RESULTS	462
APPENDIX D - FULL-SCALE PILE TEST RESULTS	494
BIOGRAPHY	553

## LIST OF SYMBOLS AND ABBREVIATIONS

$A_s$	= Pile shaft surface area
$A'_s$	= Pile surface area between cone sounding intervals
$A''_s$	= Pile surface area over a specified depth interval
$A_{step}$	= Step bearing area of a step-taper pile
$A_{s/si}$	= Equivalent pile step area per cone sounding interval
$\bar{A}_{s/si}$	= Average pile step area per cone sounding interval for a specified soil layer
$A_t$	= Pile tip area
$a_r$	= Coefficient of compressibility
$B$	= Pile width or diameter
$C$	= A constant used in penetrometer field data reduction
$C_c$	= Compression index
$C_{me}$	= Mechanical penetrometer tip capacity correction factor
CPT	= Cone penetration test
CRP	= Constant rate of penetration
$c$	= Cohesion
$c$	= Penetrometer calibration constant
$c'$	= Effective cohesion
$D_c$	= Critical embedment depth
$D_r$	= Relative density
$d$	= Depth below ground surface
$d$	= Pile tip depth
$E$	= Prediction error
$E$	= Pressuremeter modulus
$E_r$	= Remolded modulus of elasticity

$E_u$	= Undisturbed modulus of elasticity
e	= Natural logarithm base
e	= Void ratio
FDOT	= Florida Department of Transportation
FR	= Penetrometer friction ratio
FS	= Factor of safety
$F_s$	= Pile side friction
$F_1$	= Safety factor component
$F_2$	= Safety factor component
$f_p$	= Unit pile side friction
$f_s$	= Penetrometer sleeve friction
$\bar{f}_s$	= Average penetrometer sleeve friction
$f_{se}$	= Electrical penetrometer sleeve friction
$f_{sm}$	= Mechanical penetrometer sleeve friction
G	= Penetrometer gauge or chart recorder reading
K	= Coefficient of lateral earth pressure
K	= Ratio of unit pile friction to penetrometer sleeve friction
$K_f^t$	= Ratio of final drained radial stress acting on a pile to the initial vertical effective stress
$K_0$	= Coefficient of at-rest earth pressure
k	= Ratio of maximum pile friction to penetrometer sleeve friction
$k_v$	= Coefficient of permeability in the vertical direction
L	= Embedded length of pile
LETCO	= Law Engineering Testing Company
LR	= Load relaxation
l	= Depth below ground surface to a specified point
ML	= Maintained load

$N_c$	= Bearing capacity factor
$N_q$	= Bearing capacity factor
$N_Y$	= Bearing capacity factor
$n$	= A symbol or subscript used as a counter
$n$	= Dimensionless parameter used in pile friction reduction study
$n$	= Soil layer number
OCR	= Overconsolidation ratio
OD	= Outside diameter
P	= Total pile capacity
$p_L$	= Pressuremeter limit pressure
$Q_s$	= Tapered pile shaft resistance
$Q_{step}$	= Step bearing component of tapered pile shaft resistance
$q_c$	= Unit cone bearing capacity
$q_c^*$	= Average $q_c$ in the vicinity of a pile diameter step
$q_{ce}$	= Electrical penetrometer unit bearing capacity
$\bar{q}_{ce}$	= Average electrical penetrometer bearing capacity
$q_{cm}$	= Mechanical penetrometer unit bearing capacity
$\bar{q}_{cm}$	= Average mechanical penetrometer bearing capacity
$q_{c1}$	= Average $q_c$ value below pile tip
$q_{c2}$	= Average $q_c$ above pile tip
$q_p$	= Unit pile tip bearing capacity
$q_s$	= Unit bearing capacity at pile diameter step
$q_{step}$	= Unit bearing capacity at pile diameter step
$q_{ult}$	= Ultimate unit tip bearing capacity
$R_f$	= Pile friction reduction factor
r	= Subscript denoting remolded
S	= Ratio of cone bearing capacity to unit bearing resistance at pile diameter step

$s_t$	= Ratio of remolded to undisturbed shear strength
$s$	= Distance between test pile and reaction piles
$s_u$	= Undrained shear strength
$\bar{s}_u$	= Average undrained shear strength
$s_{uu}$	= Undisturbed undrained shear strength
$t_{\alpha/2}$	= Students t-distribution value
$u$	= Pore pressure
$u$	= Subscript denoting undrained
$u$	= Subscript denoting undisturbed
$ult$	= Subscript denoting ultimate capacity
$w$	= Water content
$y$	= Subscript denoting yield capacity
$\alpha$	= Ratio of pile adhesion to undrained shear strength
$\alpha'$	= Ratio of pile adhesion to penetrometer sleeve friction
$\beta$	= Ratio of pile friction to vertical effective stress
$\gamma$	= Total unit weight
$\gamma_{nat}$	= Natural or in-place unit weight
$\delta$	= Pile-soil friction angle
$\delta'$	= Effective or drained pile-soil friction angle
$\delta_u$	= Pile settlement at ultimate capacity
$\delta_y$	= Pile settlement at yield capacity
$\Delta F_s$	= Pile side friction correction
$\Delta Q_t$	= Pile tip resistance correction
$\epsilon$	= Strain
$\lambda$	= Vijayvergiya and Focht's pile friction coefficient
$\lambda'$	= Modified pile friction coefficient

- $\mu$  = Average or mean value  
 $\mu$  = Bjerrum's field vane shear strength correction factor  
 $\sigma'_c$  = Maximum past preconsolidation pressure  
 $\sigma'_D$  = Standard deviation  
 $\sigma'_{rf}$  = Final drained radial stress acting on a pile  
 $\sigma'_{vi}$  = Effective vertical stress before pile driving  
 $\sigma'_v$  = Effective vertical stress  
 $\bar{\sigma}'_v$  = Average effective vertical stress over total pile length  
 $\phi$  = Angle of internal friction  
 $\phi'$  = Effective angle of internal friction  
 $\phi_d$  = Drained angle of internal friction  
 $\omega$  = Pile settlement excluding reaction pile effects  
 $\omega_0$  = Pile settlement including reaction pile effects

Abstract of Dissertation Presented to the Graduate Council  
of the University of Florida in Partial Fulfillment of the Requirements  
for the Degree of Doctor of Philosophy

USE OF QUASI-STATIC FRICTION CONE PENETROMETER DATA  
TO PREDICT LOAD CAPACITY OF DISPLACEMENT PILES

By

Larry C. Nottingham

June, 1975

Chairman: John H. Schmertmann

Major Department: Civil Engineering

A study to determine the applicability of quasi-static friction cone penetrometer data for predicting the load capacity of displacement piles is presented. The study included performing and evaluating 108 load tests on large-scale model piles, from which load capacity prediction equations were developed. Data from load tests on 15 full-scale piles were used to verify the equations developed from the model pile tests.

Three types of model piles were used in the study: a 4.0 in square precast concrete pile; a 4.0 in diameter pipe pile; and a step-taper pile with section diameters ranging from 2.9 to 4.5 in. All piles were driven and tested under field conditions to simulate an actual pile situation, and each pile was instrumented to permit separation of total load capacity into end bearing and side friction components. Each test site was investigated with a Begemann mechanical friction sleeve penetrometer and a Fugro electrical friction sleeve penetrometer, and tests were conducted in both cohesive and granular soils. The different combinations of soil types, penetrometer types,

and pile types investigated permitted development of design equations applicable to a wide variety of situations.

The results of this study show that the Begemann procedure for estimating pile end bearing capacity in granular soils provided good agreement with the load test results and is a valid design tool. It is also demonstrated that the Begemann procedure is valid for cohesive soils and electrical penetrometer data. When using mechanical penetrometer data for cohesive soils, it is necessary to correct the penetrometer data for tip mantle friction effects before the data can be used to predict pile end bearing capacity.

Equations and design curves are developed and presented to permit estimating pile side friction from penetrometer sleeve friction ( $f_s$ ) data. The equations provide answers which agree well with measured side friction resistance on the model piles and the total predicted capacity for full-scale piles, obtained by adding predicted end resistance and side friction, agree well with measured total capacity. It is shown that  $f_s$  values in granular soils differ significantly for the mechanical and electrical penetrometers, primarily because of end bearing on the lower beveled portion of the mechanical penetrometer friction sleeve. Separate design curves which account for this difference are presented for each penetrometer type. A conventional undrained shear strength approach is recommended for predicting pile side friction in cohesive soils. For the soils investigated, it is shown that measured  $f_s$  values are approximately equal for the two penetrometers used and that  $f_s$  is approximately equal to the undrained shear strength of the soil, as determined from conventional laboratory tests.

Drained friction methods of estimating side friction in cohesive soils are also evaluated, and it is concluded that the drained friction approach will ultimately provide a more accurate and fundamentally more correct solution to the pile friction problem.

A method of estimating the shaft resistance of step-taper piles is presented in which the shaft resistance is divided into side friction and step-bearing components. Side friction is estimated using equations for a constant section pile and step bearing is estimated from cone-bearing resistance at the diameter step levels. Predictions obtained in this manner agreed well with measured shaft resistance. The prediction method for step-taper piles is extended for use with continuously tapered piles and used to estimate the capacity of full-scale timber piles. The agreement between measured and predicted capacity is good.

It is concluded that the quasi-static cone penetrometer is a valuable tool for estimating the load capacity of displacement piles.

## CHAPTER 1

### INTRODUCTION

#### 1.1 Research Justification

The problem of predicting the load carrying capacity of driven piles has plagued engineers for many years and has received much attention from both research and practical engineers. The vast amount of literature available on this subject attests to the magnitude of the problem.

At present, most engineers use one or both of the following methods for estimating the capacity of a driven pile:

1. Static analysis based on an evaluation of properties of the soil into which the pile will be driven.
2. Dynamic analysis based on behavior of the pile during driving.

Each method has its own advantages and disadvantages and, in many instances, neither method has given very satisfactory results.

Dynamic methods are based on work-energy principles for the hammer-pile-soil system. The inability of most dynamic methods to consistently provide accurate answers is generally thought to be caused by:

1. The difficulty in accurately determining hammer energy and the energy losses which occur in the hammer-pile-soil system.
2. Changes in soil strength or resistance that occurs between the time the pile is driven and the time it is loaded.

Recently developed dynamic methods based on wave propagation theory have eliminated some of the inaccuracies associated with previous dynamic methods, but are still subject to the second limitation listed above. Regardless of accuracy, all dynamic methods are subject to the severe limitation that the pile must be driven before a load capacity prediction can be made.

Static predictions are usually made by treating side friction and end bearing as independent components of total pile resistance. Side friction in granular soils is generally estimated using an equation of the following form:

$$F_S = K \sigma'_V A_S \tan \delta \quad (1.1)$$

where

$F_S$  = Pile side friction

$K$  = Coefficient of lateral earth pressure

$\sigma'_V$  = Average effective overburden stress

$A_S$  = Pile surface area

$\delta$  = Pile-soil friction angle

In principle, this equation seems to provide a reasonable approximation of the behavior one would expect, but correlations of estimated and measured side friction resistance have not been good. One difficulty in using this type of analysis is selecting an appropriate value for  $K$ . Lambe and Whitman (1969), in a summary of work of several investigators, report  $K$  values ranging from 0.3 to 3.0.

Another shortcoming of Eq 1.1 was pointed out by Vesic (1964), who presented experimental results indicating that unit pile friction in sands does not increase linearly with depth as implied by Eq 1.1, but approaches a constant value at a depth which depends on the pile size

and relative density of the sand. However, these results are somewhat questionable because of possible arching and boundary effects in the laboratory test bins in which Vesic's tests were conducted. Also, friction distribution was not actually measured, but was inferred from total friction data. More recently, Vesic (1970) summarized the results of load tests performed on instrumented piles by several investigators and concluded that the distribution of friction on piles in sands is probably parabolic with a maximum value occurring near the mid-length of the pile.

Pile side friction in cohesive soils is usually estimated by using an approach similar to that proposed by Tomlinson (1957). In this method, unit side friction is assumed equal to the undrained shear strength of the soil times a reduction factor which is dependent on the magnitude of the undrained shear strength. This method sometimes gives satisfactory results but it is difficult to justify using undrained strength properties to evaluate the capacity of a pile which will ultimately attain load support through drained friction.

Static analysis methods for computing pile end bearing capacity generally use an equation of the following form:

$$Q_t = A_t q_{ult} = A_t (cN_c + \frac{\gamma B}{2} N_y + \gamma d N_q) \quad (1.2)$$

where

$Q_t$  = Ultimate tip load capacity

$A_t$  = Pile tip area

$q_{ult}$  = Ultimate unit tip bearing capacity

$c$  = Soil cohesion

$\gamma$  = Unit weight of soil

$N_c, \gamma, q$  = Bearing capacity factors

B = Pile width or diameter

d = Pile tip depth

In granular soils, Eq 1.2 reduces to:

$$Q_t = A_t \gamma d N_q \quad (1.3)$$

since c is zero and the  $N_y$  term is negligible in most instances. The problem then becomes one of choosing an appropriate value for  $N_q$ . Engineers agree that  $N_q$  is a function of the angle of internal friction ( $\phi$ ); but as shown in Fig 1.1, there is a wide variation of opinion concerning the actual form of the relationship. The questions concerning the  $\phi - N_q$  relationship, coupled with the difficulty of determining the in situ value of  $\phi$  for a granular soil, create serious doubts about the reliability of the theory.

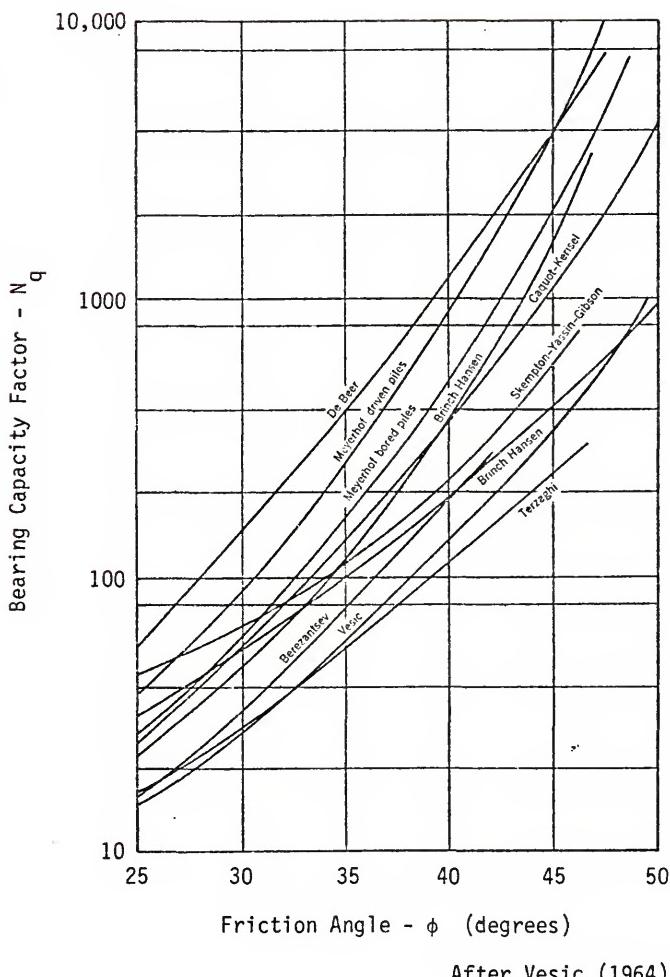
Eq 1.2 is usually reduced to the following form for piles in cohesive soils:

$$Q_t = A_t (N_c + \gamma d) \quad (1.4)$$

While there is less disagreement about the correct value of  $N_c$  than there is concerning  $N_q$ , the importance of the tip bearing contribution in relation to total pile capacity is much less in clays than in sands. Thus, accurately predicting tip bearing capacity in clays does little to improve the accuracy of the total capacity determined from a static analysis.

While it is difficult to place much faith in pile capacities computed in accordance with the previously outlined static methods, engineers continue to use these methods for the following reasons:

1. Dynamic prediction methods often do not provide any better results and the predictions are not available until the pile is driven.



BEARING CAPACITY FACTOR FOR DEEP CIRCULAR FOUNDATIONS

FIGURE 1.1

2. It is often difficult to justify the cost of a pile load testing program on small projects.
3. Even when pile load testing can be justified, it is desirable to evaluate the probable performance of different pile types, sizes, and lengths during the design stage of a project in order to intelligently plan the field testing program.

The quasi-static cone penetrometer offers an alternate approach to the pile capacity prediction problem. The cone penetrometer, which can be thought of as a model displacement pile, provides a means of measuring unit tip resistance and unit side friction. By making these measurements at frequent depth intervals, it is possible to develop almost continuous resistance profiles. These measurements are made in situ; thus, the problems of obtaining representative undisturbed samples and determining correct values of the appropriate soil properties in the laboratory are eliminated. Also, the need for estimating values for intermediate parameters ( $K$ ,  $N_q$ , etc.) is eliminated because direct measures of unit tip resistance and side friction are provided.

The cone penetrometer has been used as a tool for estimating pile capacity for a number of years. This use has been restricted mainly to a few European countries and to piles which derive their load capacity primarily through tip resistance in sands or other hard soils; however, outside of the Netherlands there is no generally accepted method of using cone data for this purpose.

### 1.2 Purpose and Scope

This research project was undertaken to systematically evaluate the cone penetrometer as a tool for estimating the load capacity of driven displacement piles. The initial objectives of the research

program were to evaluate several pile types in both cohesive and granular soils. The program was divided into two phases to accomplish this objective with a reasonable investment of time and money. The first phase consisted of performing a large number of model pile tests in both granular and cohesive soils to provide data from which a general prediction method could be developed. The second phase consisted of performing and evaluating full-scale pile load tests in order to check the prediction method against true field conditions and make any necessary revisions. All model pile test sites were investigated with both the Begemam type mechanical friction sleeve penetrometer and the Fugro type electrical friction sleeve penetrometer. Full-scale pile load test sites were investigated with the Begemam mechanical penetrometer.

The model pile testing program was conducted using large-scale models at field sites in order to minimize scale effects and the problems associated with testing in artificial soil deposits in the laboratory. Three types of model piles were tested: a 4 in diameter pipe pile; a 4 in square concrete pile; and a step-taper pile varying from 2-5/8 to 4-1/2 in in diameter. A total of 108 load tests were conducted on piles driven at 37 different locations.

Data from static load tests conducted on 15 full-scale piles were included in the research program. This included data on square concrete, steel pipe, Raymond step-taper and timber piles. The full-scale test sites were scattered throughout Florida and encompassed a variety of soil conditions.

Prediction methods utilizing cone penetration test (CPT) data were formulated on the basis of the model pile test results. Methods

were developed for independently estimating both tip resistance and side friction (or shaft resistance) for each of the three model pile types. These prediction methods were used to estimate the capacity of each of the full-scale piles tested and the resulting prediction was compared with the actual pile capacity. Based on both model and full-scale pile capacity prediction correlations, simple conservative CPT capacity prediction methods are recommended for design use. These recommended design methods represent the end product of this dissertation.

## CHAPTER 2

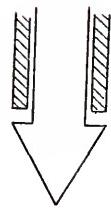
### SUMMARY OF PREVIOUS WORK

#### 2.1 Penetrometer History

Penetrometers were one of the first tools used as an indirect means of soil exploration. Early penetrometer testing consisted of driving or forcing a metal rod into the ground to locate hard or soft layers of soil. Significant improvements to this technique were made around 1930 with the development of the dynamic standard penetration test in the United States and the static deep sounding test method in Holland. Since that time, numerous types of penetrometers, both static and dynamic, have been developed and used for soil exploration. These range in size from miniature hand-operated pocket penetrometers to probes almost one foot in diameter.

This research project deals only with Dutch-type, quasi-static penetrometers. The term quasi-static is used because this type of penetrometer is forced into the ground at a constant speed rather than being subjected to a truly static loading condition. Dynamic penetrometers were not considered because of the problem of relating dynamic penetration resistance to the static behavior of a loaded pile. It seems obvious that pile behavior should correlate better with the results of penetration tests that are directly related to static soil behavior.

The stages of evolution of the Dutch-type mechanical penetrometer are shown in Fig 2.1. The original equipment (Fig 2.1a) was developed



(a)

Original Dutch  
Penetrometer



(b)

Dutch Mantle  
Penetrometer



(c)

Begemann Friction  
Sleeve Penetrometer

#### DIFFERENT TYPES OF MECHANICAL CONE PENETROMETERS

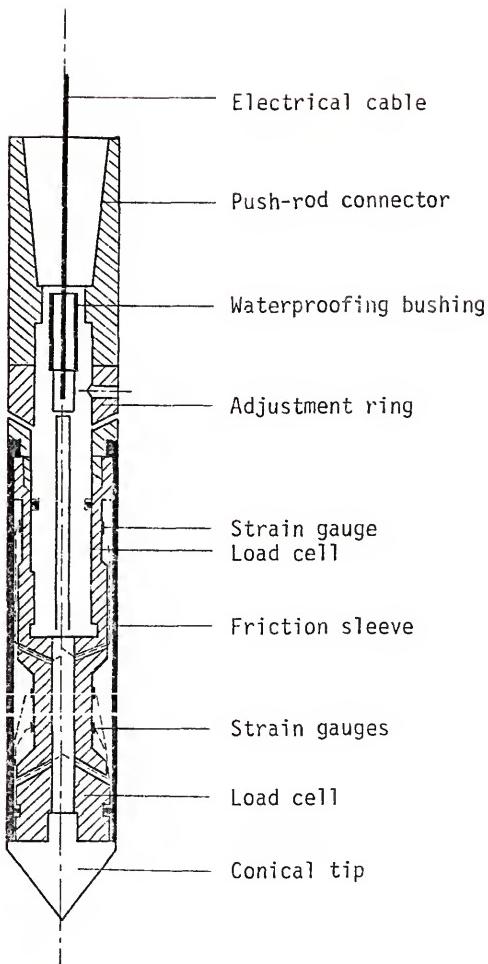
FIGURE 2.1

in the early 1930's at the Delft Soil Mechanics Laboratory. This penetrometer consisted of a conical point connected to a steel push-rod. The push-rod was isolated from the surrounding soil by a sleeve or system of outer rods. Using this system, penetration tests could be conducted at different depths by alternately pushing on the inner and outer rods. The design and operation of this equipment has been described by Vermeiden (1948).

Experience showed that soil particles sometimes entered the mechanism of the original penetrometer tip, resulting in erroneous readings because of friction between the moving parts. To eliminate this problem, the mantle cone shown in Fig 2.1b was developed at the Delft Laboratory. The tapered mantle located just above the cone tip was designed to prevent soil particles from entering and fouling the mechanism. This design proved to be very efficient and continues to be used throughout the world today.

The Dutch mantle cone has been used extensively in Holland for estimating pile capacities with varying degrees of success: Begemann (1953) became dissatisfied with using total outer rod friction for estimating pile side friction and developed the adhesion jacket cone shown in Fig 2.1c. This penetrometer is similar to the mantle cone, but provides a movable friction sleeve just above the tip for measurement of local friction between the soil and sounding rods.

Recent developments in this field have led to electrical penetrometer tips. The Fugro electrical friction sleeve penetrometer is shown in Fig 2.2. The most significant differences between the mechanical and electrical tips are as follows:



FUGRO ELECTRICAL FRICTION SLEEVE PENETROMETER

FIGURE 2.2

1. With the electrical tip, penetration resistance is measured by strain gauge load cells in the tip rather than at the ground surface as with the mechanical tip. This eliminates possible errors resulting from friction between the inner and outer rods.
2. There is no relative movement between the parts of the electrical cone as there is with the mechanical cone.
3. The electrical penetrometer is pushed into the ground continuously as opposed to the alternate pushing on the inner and outer rods of the mechanical penetrometer.
4. The Fugro penetrometer does not have a recessed section immediately behind the cone point.
5. The friction sleeve of the Fugro penetrometer does not have a beveled surface at its lower end as does the Begemann penetrometer. This eliminates the possibility of end bearing on the friction sleeve.
6. The friction sleeve of the Fugro penetrometer is located closer to the cone tip than that of the Begemann penetrometer.

Electrical penetrometers have also been developed which incorporate inclinometers and piezometers. The general features of electrical penetrometers and the Fugro design have been described by de Ruiter (1971).

Both the Begemann mechanical friction sleeve penetrometer and the Fugro electrical friction sleeve penetrometer were used in this study. As will be pointed out in a later chapter, the penetrometer shape and method of operation can have a significant effect on CPT results. For this reason, caution should be exercised in using the findings of this study with data gathered using different types of penetrometers.

## 2.2 CPT Methods for Predicting Pile Point Capacity

### 2.2.1 General

Since its inception, the quasi-static cone penetrometer has been used as a tool for designing pile foundations. Based on published

literature, it appears that pile design and general soil exploration have been the main areas of use for CPT data.

According to Begemann (1969b) early efforts to use CPT data for pile design were directed toward estimating the maximum depth to which a pile could be driven. He reports that the maximum driving depth for a normal concrete pile was generally taken as the depth where the total cone resistance (point resistance plus total rod friction) reached 4500 to 5000 kg. This approach was soon abandoned in favor of using CPT data for making independent estimates of pile point resistance and side friction.

### 2.2.2 Early Point Capacity Prediction Methods

Engineers quickly realized that the cone penetrometer could be considered as a small-scale model pile and that there should be some relationship between the cone point resistance ( $q_c$ ) and pile point resistance. However, discussions in the literature indicate that there was considerable disagreement concerning the form of the relationship.

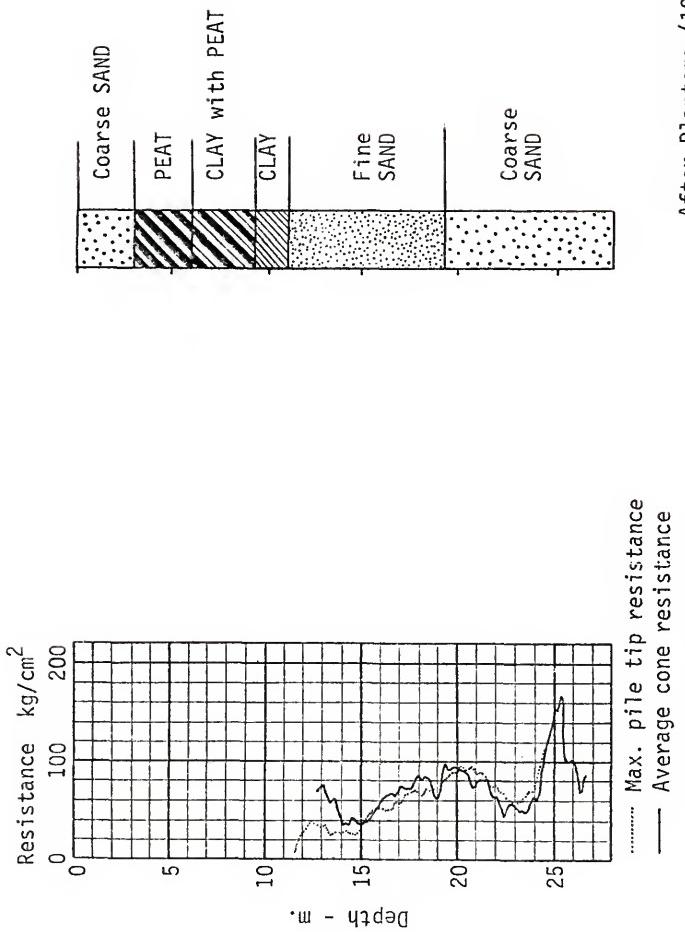
Huizinga (1951) reports on early efforts in Holland to estimate pile point resistance from CPT data. He states that pile point resistance was computed using  $q_c$  as unit point bearing capacity and indicates that some type of averaging procedure was used to account for varying  $q_c$  values in the zone of soil that would be influenced by the pile point; however, he did not describe the details of the averaging procedure. The agreement between measured and predicted point resistance values contained in this report was generally good.

An interesting and informative experiment concerning the relationship between penetrometer and pile point resistance was conducted by Plantema (1948). To evaluate this relationship, he placed a steel

sleeve around a 42.6 cm square concrete pile to eliminate side friction and installed the pile by jacking, continuously measuring the point resistance. The soil profile at the site consisted of about 12 m of soft clay and peat followed by a thick layer of medium dense sand. A comparison between the pile point resistance and the average  $q_c$  profile from six soundings is shown in Fig 2.3. The agreement is very good except through the top 3 m of the sand layer, where the pile resistance was much less than the cone resistance. Based on these data, Plantema concluded that pile point resistance could be computed directly from  $q_c$  data.

Meyerhof (1951) developed a theoretical method for bearing capacity analysis and applied the method to load test results on both shallow and deep foundations. Based on the results of this study, he concluded that for deep foundations bearing in sand, it is better to estimate bearing capacity directly from CPT logs than to use theoretical bearing capacity equations. However, he points out that there is a danger in extrapolating CPT data to a pile which only penetrates a short distance into a dense layer because the much smaller diameter cone will give unit resistance much larger than that which will act on a larger pile.

Van der Veen and Boersma (1957) reported the results of load tests on 15 concrete piles in Amsterdam in which CPT data was used to evaluate pile point resistance. They recognized the importance of accounting for scale effects when transposing resistance values from the small diameter cone to a much larger pile and attempted to account for these effects by averaging cone resistance values over a depth interval from  $aB$  above the pile base to  $bB$  below the base where  $B$  is the equivalent



After Plantema (1948)

PLANTEMA'S EXPERIMENTAL PILE POINT RESISTANCE DATA

FIGURE 2.3

pile diameter. A trial-and-error analysis of data from the 15 pile load tests indicated that  $a$  varied from about 1.5 to 12 while  $b$  varied from 1 to 2. They arrived at these ranges by using various combinations of  $a$  and  $b$  values to determine which combinations gave average  $q_c$  values corresponding most closely to measured pile point resistances. Furthermore, they reported that the most probable values of  $a$  and  $b$  appeared to be 3.75 and 1.0, respectively. Pile point resistances computed using these values varied from about 50 to 150% of the values determined from the pile load tests.

Menzenbach (1961) used Van der Veen's computation method to evaluate the results of 88 pile load tests and performed a statistical analysis of the resulting prediction ratios (prediction ratio = predicted pile point resistance/measured resistance). In general, he found a large range of scatter (from approximately 40 to 220%); however, by eliminating very large piles and test sites with  $q_c$  resistances over  $100 \text{ kg/cm}^2$ , the prediction ratio scatter was reduced considerably. Based on this, he concluded that more attention should be given to the scale effect (ratio of cone diameter to pile diameter) and the type and strength of soil. He also pointed out the importance of the procedure used in determining the pile failure load and concluded that use of different failure criteria is probably responsible for a considerable portion of the prediction ratio scatter.

Mohan et al. (1963) also applied Van der Veen's prediction method to a number of load tests on cast-in-place concrete piles in fine to medium sands. These data showed that the predicted pile point resistance varied from 100 to 150% of the actual resistance. CPT logs were not presented for the individual pile test sites, so the nature of the

soil profile could not be determined for locations where  $q_c$  data led to a significant over-prediction.

CPT data were used by Bogdanovic (1961) to analyze the results of load tests performed on driven concrete piles in Yugoslavia. In addition, one test was performed in which a 30 x 30 cm pile was continuously jacked in to a depth of 13 m with the penetration resistance being continuously recorded. The pile penetrated about 10 m of soft clayey soil and approximately 3 m into a dense gravelly sand layer. Pile resistance was estimated from CPT data in the following manner:

1. Pile shaft resistance was assumed equal to the total penetrometer shaft resistance at a corresponding depth times the ratio of the circumference of the penetrometer to that of the pile.
2. The pile point resistance was taken as the average of the  $q_c$  values from 4B above the pile base to 2B below the base, or as the average of the minimum  $q_c$  values over the same interval.

The measured resistance of the jacked-in pile corresponded closely with the predicted resistance except when the pile was penetrating the upper portion of the dense sand layer. In this case, the pile resistance was considerably less than the predicted resistance. Capacity predictions using the same procedure were compared to load test results from the driven piles, and the correlation was generally good. Based on these results, Bogdanovic concluded that pile capacities could be reasonably estimated from CPT data and that better point resistance estimates are obtained by averaging cone resistance values obtained from an envelope drawn through the minimum  $q_c$  values rather than by averaging the actual values.

Most of the previously cited investigators evaluated the accuracy with which they were able to predict pile point resistances and recommended safety factors which should be applied to the  $q_c$  based predictions.

The size of these safety factors provide a means of evaluating the accuracy of the method and comparing it with the accuracy of other methods. Most authors recommended that composite safety factors varying from 2.5 to 3.0 be applied to the predicted ultimate resistance to determine allowable working loads.

It should be noted that the composite safety factor consists of two components:  $F_1$ , which accounts for the inaccuracy of the prediction method, and  $F_2$ , which is the desired ratio between the maximum allowable working load and the actual ultimate pile resistance. All of the authors agreed that the maximum working load should not exceed 60% of the ultimate pile capacity; thus, the value of  $F_2$  is approximately 1.7. This results in an  $F_1$  value of 1.4 to 1.8.

The recommended composite safety factors are comparable to those normally used with other currently available static analysis methods which indicates that the early CPT methods were as accurate, if not more so, than other available methods of evaluating point resistance of piles driven in sands.

References pertaining to the use of CPT data for predicting pile point resistance in clays apparently do not exist. This is mainly due to the CPT method being developed in countries where the geology is such that piles are driven through soft clays and organic soils into underlying sands.

### 2.2.3 Research Concerning Scale Effects

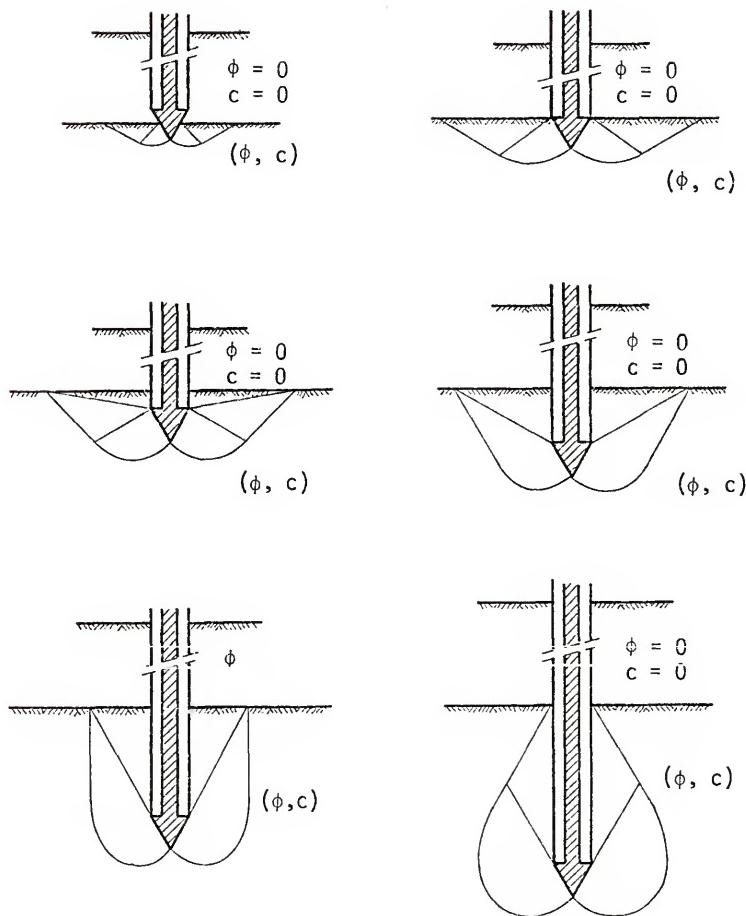
The preceding section shows that early attempts to predict pile point capacity from CPT data were generally successful whether the unit point bearing capacity was taken directly as the  $q_c$  value at the pile point level or taken as the average of  $q_c$  values for some distance

above and below the pile point. However, according to Sanglerat (1972), there was still some skepticism regarding use of this method because of cases in which measured pile point capacity was only a fraction of the  $q_c$  value at the same level. Much of this controversy centered around data obtained by Kerisel (1961) from tests on piles and penetrometers in artificial sand deposits. Kerisel's data showed that the bearing capacity of large piles was considerably less than that of the penetrometers in dense sand; however, the tests were conducted at shallow depths and the discrepancy was thought to be the result of the difference in size between the penetrometer and piles.

Considerable insight into this problem was provided by de Beer (1963) in a thorough study of the effect of pile or penetrometer size on the ultimate point bearing capacity. By considering penetrometers of different size, de Beer showed that all penetrometers should ultimately attain the same point resistance and that the depth at which this constant value occurs should be proportional to the penetrometer size.

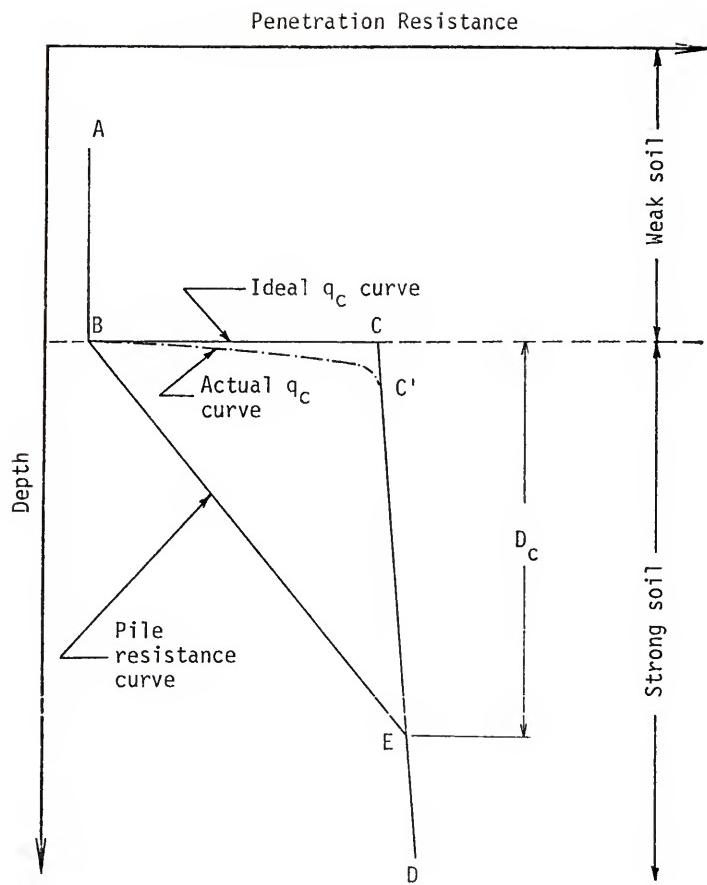
The explanation offered by de Beer for this phenomenon was that the bearing capacity failure which occurs beneath the cone tip gradually changes from that for a shallow foundation to that of a deep one, as shown in Fig 2.4. During the transition between the shallow and deep type base failure, the point resistance increases linearly with depth, but after the deep foundation condition is reached, point resistance only increases slightly with increased penetration.

The effect of this phenomenon on the point resistance of a pile driven into a dense layer underlying a weaker layer can be seen by referring to Fig 2.5. If the layers were penetrated by a probe of



TRANSITION FROM SHALLOW TO DEEP BEARING CAPACITY FAILURE

FIGURE 2.4



DE BEER SCALE EFFECT DIAGRAM

FIGURE 2.5

zero diameter, the depth of embedment effect would be eliminated and the penetration resistance would follow the idealized curve ABCD. However, if a large diameter pile were pushed into the second layer, the point resistance would not equal that of the zero diameter probe until the pile reached a depth corresponding to the deep foundation condition (point E). The depth at which this condition is met is termed the critical depth ( $D_c$ ). De Beer showed that it is reasonable to assume that the pile resistance curve between points A and E varies linearly; thus, the pile resistance at any intermediate depth could be determined if the idealized penetration resistance curve and  $D_c$  were known.

Although it is not possible to use a probe of zero diameter to determine the idealized curve, the small diameter cone penetrometer (3.57 cm) comes close to meeting this condition (curve ABC'D) and the cone penetration resistance curve is a reasonable approximation of the idealized curve. The correct value of  $D_c$  is more difficult to determine. Meyerhoff (1951), de Beer (1963), and others have shown that  $D_c$  is a function of the foundation size; thus, it is more convenient to express this depth in terms of the ratio of the foundation size to the critical depth, i.e.,  $(D/B)_c$ . Both experimental and theoretical studies have shown that  $(D/B)_c$  for sands is a function of the sand density and varies from about 5 for loose sands to about 15 to 20 for dense sands.

Results of research performed by Vesic (1964) and Kerisel (1964) tend to confirm de Beer's theory concerning the depth of embedment effect. Vesic's tests were performed on penetrometers and model piles in sands placed at different densities in a laboratory test chamber. The results of his tests on 4.0 in diameter piles are shown in Fig 2.6.

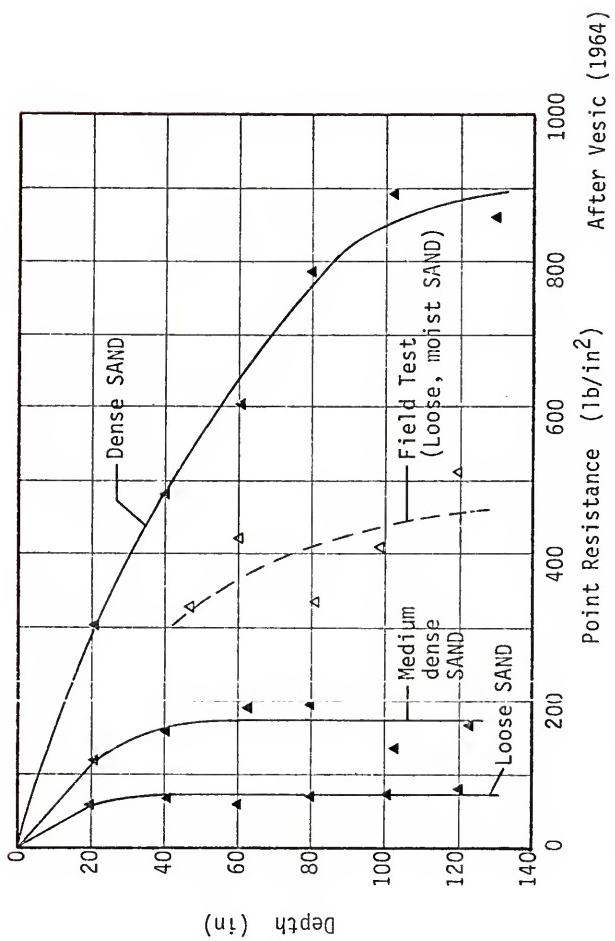


FIGURE 2.6

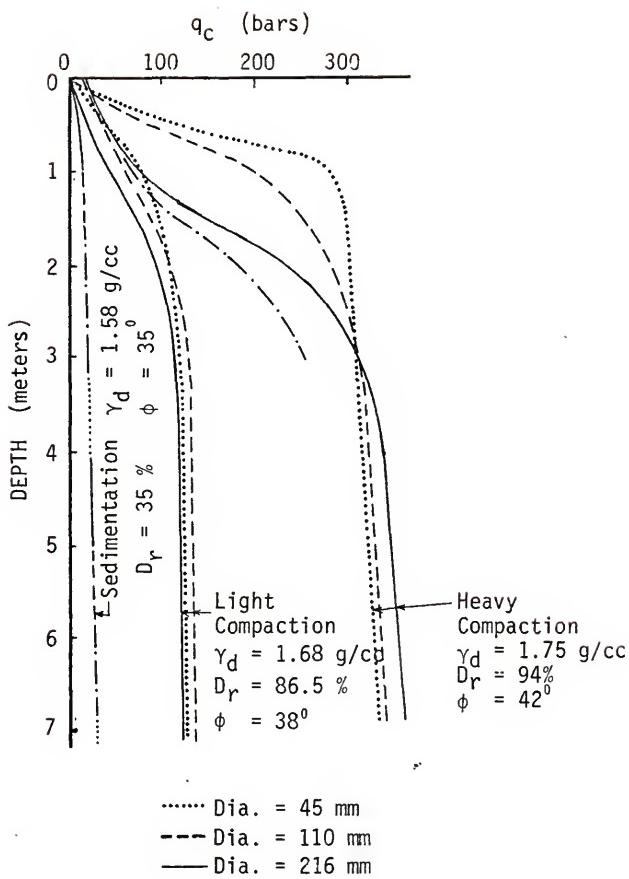
The experimental curves in this figure show that the pile point resistance increased almost linearly with depth to a certain point after which the value remained almost constant. Values for  $(D/B)_c$  varied from about 6 for loose sand ( $D_r \approx 10\%$ ) to about 25 for dense sands ( $D_r \approx 80\%$ ). Kerasel obtained similar results using 4.5 to 32.0 cm diameter penetrometers and piles in a sand compacted to three different densities. His results, shown in Fig 2.7, indicate  $(D/B)_c$  values of about 20 for dense sand and approximately 5 for loose sand.

Both Vesic's and Kerasel's experiments were performed in rigid wall test chambers and the test results may have been affected by arching between the piles and chamber walls and other boundary effects. However, the general trends shown by their work are believed to be correct because of the similar data obtained by both researchers and the general agreement between their findings and the results of Plantema and Bogdanovic's full-scale pile tests described in Section 2.2.2.

In summary, it appears that accounting for the scale factors in a manner similar to that proposed by de Beer is the key to making accurate pile point capacity predictions from CPT data when the actual pile embedment is less than the critical embedment as determined by  $(D/B)_c$ . The scale factor has no effect when the actual embedment is greater than  $D_c$  as long as the soil resistance remains unchanged.

#### 2.2.4 Recent Dutch Prediction Methods

The literature indicates that Dutch engineers were refining their prediction methods at the same time that de Beer, Kerasel, and Vesic's research was being conducted. The bases for these refinements have been described by Begemann (1963) as follows:



KERISEL'S EXPERIMENTAL PENETRATION RESISTANCE CURVES

FIGURE 2.7

1. It was noted that the point resistance of a pile with its point at the interface between two soil layers was approximately equal to the average cone penetration resistance of the two layers. From this, they concluded that the soil above and below a pile tip contribute almost equally to the pile point resistance.
2. The failure at the pile base was assumed to follow the classic logarithmic spiral shape as shown in Fig 2.8.

From this observation and assumption, it was concluded that the pile capacity prediction equation should take the following form:

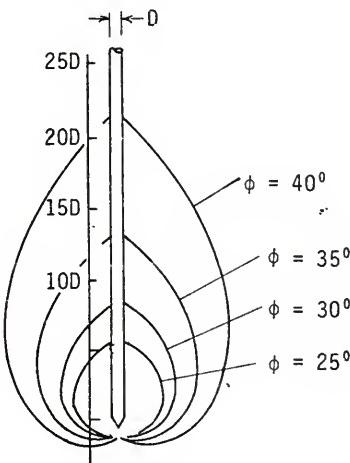
$$q_p = \frac{q_{c1} + q_{c2}}{2} \quad (2.1)$$

where

$q_p$  = unit pile point bearing capacity

$q_{c1}$  = average  $q_c$  value below the pile tip

$q_{c2}$  = average  $q_c$  value above the pile point



LOG SPIRAL FAILURE SURFACES

FIGURE 2.8

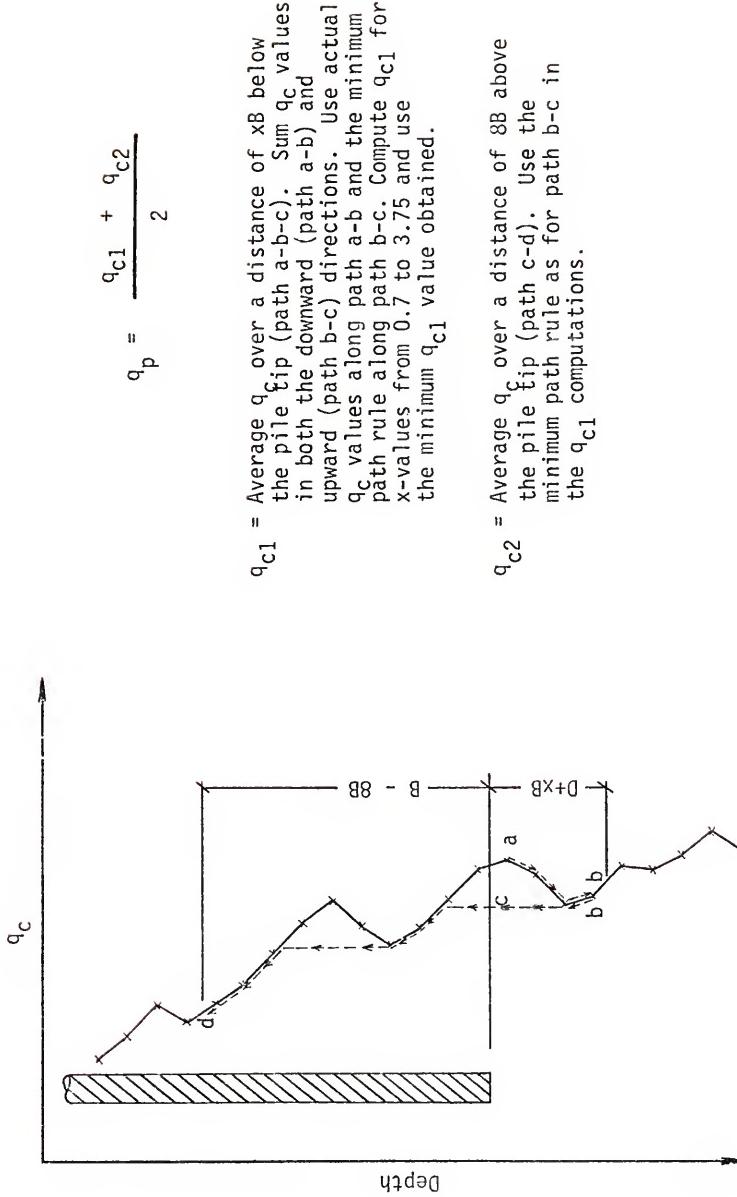
The rupture surfaces in Fig 2.8 indicate that the distances over which  $q_{c1}$  and  $q_{c2}$  should be determined are dependent on the strength of the soil. In his 1963 paper, Begemann suggested that it was usually adequate to average  $q_{c2}$  to a distance of  $8B$  above the pile point and  $q_{c1}$  over  $3.5B$  below the point, using the following equation for  $q_{c1}$ :

$$q_{c1} = \frac{(q_1 + q_2 + \dots + q_n) + nq_n}{2n} \quad (2.2)$$

where  $q_1, q_2 \dots q_n$  are the cone sounding values to a distance of  $3.5B$  below the pile base. Additional weight was given to the sounding value at a depth of  $3.5B$  to account for the fact that a significant portion of the failure surface runs horizontally through the soil at this level. Begemann recommends that this method be used only in cases where  $q_c$  remains approximately constant or decreases below the pile tip. A method for the case when  $q_c$  increases with depth below the pile point was not presented. He also notes that the method represented by Eqs 2.1 and 2.2 generally gives more reliable answers than does the method proposed earlier by Van der Veen and Boersma (1957).

More recently, this method has been further refined to account for the presence of thin layers or zones of weak soil which could affect the shape and position of the rupture surface at the pile base. Eq 2.1 is still used to compute the unit pile tip resistance; however,  $q_{c1}$  and  $q_{c2}$  are determined in the following manner (refer to Fig 2.9):

1. Starting with the first  $q_c$  value below the pile base,  $q_c$  values are summed to a distance of  $xB$  below the base (path a-b). The summation process is then continued in an upward direction until the pile base level is reached (path b-c). During the upward summation, the stipulation is made that no  $q_c$  value can be greater than the value at the next lower level. If this condition is encountered, the  $q_c$  value at the higher level is reduced to equal that at the lower level. The effect of this requirement can



be seen by examining path b-c in Fig 2.9. This averaging process is carried out using values of  $x$  (from the  $xB$  term) varying from 0.70 to 3.75, and  $q_{c1}$  is taken as the minimum average value obtained.

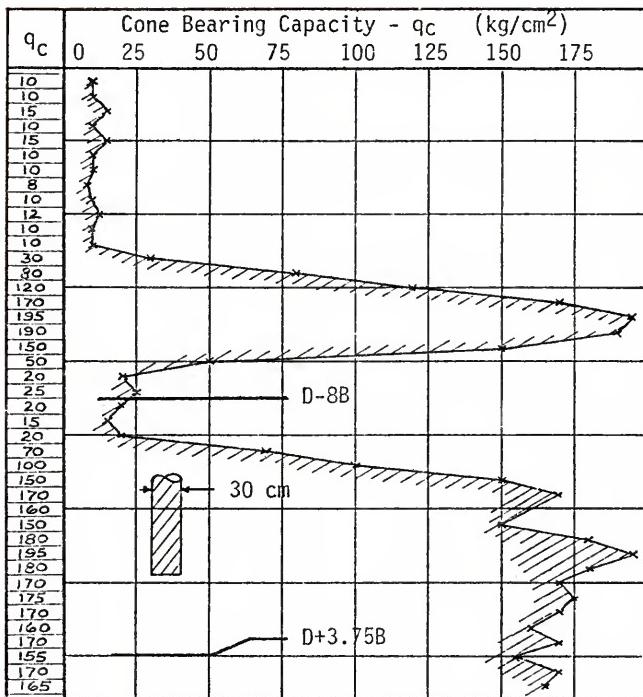
2. The averaging interval for  $q_{c2}$  is the same as before (from the pile base to a distance  $8B$  above it); however, the same minimum path rule is used as was used along path b-c in computing  $q_{c1}$ . Furthermore, the first  $q_c$  value above the base cannot be greater than the last value used in the  $q_{c2}$  summation.

An example computation made using this method is shown in Fig 2.10.

Fig 2.11 shows the application of this method to the type of two-layer system studied by de Beer (weak layer with constant  $q_c$  overlying a strong layer of constant  $q_c$ ). This shows that the two methods give considerably different results even when a  $(D/B)_c$  value of 8 is used with de Beer's method. The difference results primarily because de Beer's method does not recognize that the pile point will sense the presence of the stronger layer before reaching the layer interface. From a practical point of view, Begemann's method is more useful because the  $q_c$  averaging procedure automatically accounts for the scale effect, thus eliminating the need for estimating the exact position of soil layer boundaries. This method can also be easily applied to cases where  $q_c$  varies considerably over short distances as is often the case in practical situations.

The application of Begemann's method to a 'typical' CPT log and a range of pile sizes is shown in Fig 2.12. The point resistance curves become smoother as the pile diameter increases and approaches an envelope drawn through the minimum  $q_c$  values for large piles. This is in agreement with the experimental findings of Bogdanovic (1961), Plantema (1948), and others.

During a recent conference on penetration testing, Heijnen (1974)



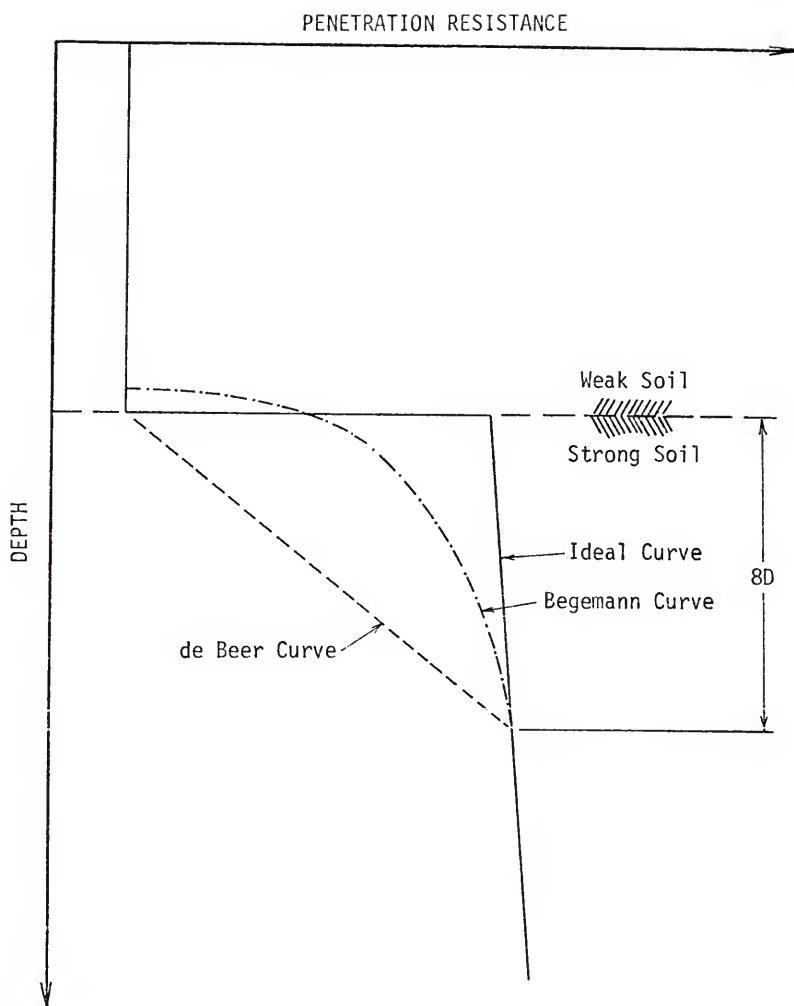
#### EXAMPLE COMPUTATION

x	xB (cm)	Trial computation for $q_{c1}$	$q_{c1}$
0.7	21	$q_{c1} = 1/2(170 + 170)$	170.0
1.0	30	$= 1/4(170 + 175 + 175 + 170)$	172.5
1.5	45	Same as for $x = 1.0$	172.5
2.0	60	$= 1/6(170 + 175 + 4(170))$	170.8
2.5	75	$= 1/8(170 + 175 + 170 + 5(160))$	164.4
3.0	90	$= 1/10(170+175+170+160+2(170)+4(160))$	165.5
3.5	105	Same as for $x = 3.0$	165.5
3.75	112.5	$= 1/12(170+175+170+160+170+7(155))$	160.8
			Min.

$$q_{c2} = 1/12(3(155) + 4(150) + 100 + 70 + 20 + 2(15)) = 107.1$$

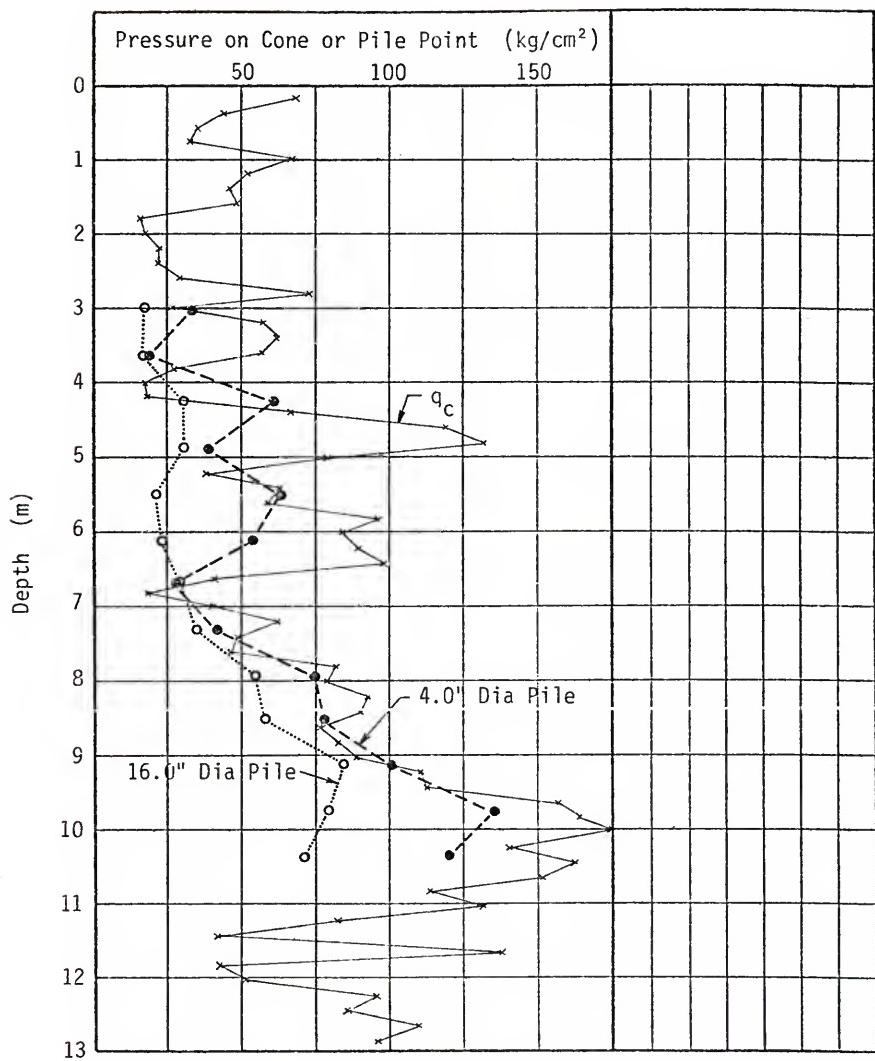
$$q_p = 1/2(160.8 + 107.1) = \underline{133.9 \text{ kg/cm}^2}$$

EXAMPLE COMPUTATION USING THE BEGEMANN PROCEDURE  
FIGURE 2.10



COMPARISON OF BEGEMANN AND DE BEER'S PREDICTED PILE POINT CAPACITY CURVES

FIGURE 2.11



TIP RESISTANCE CURVES FOR DIFFERENT SIZE PILES

FIGURE 2.12

indicated the prediction method herein described as the Begemann method is now commonly used in The Netherlands. Fugro, Inc., an international consulting organization, also uses a very similar procedure. It is also interesting to note that representatives from 16 of the 26 countries attending the European Symposium on Penetration Testing reported that CPT data are used in their countries to estimate pile capacity.

Although the Begemann procedure for estimating pile tip capacity has been used successfully by a number of individuals and organizations, there are some questions concerning the assumptions on which the method is based. The main area of controversy is the assumed rupture surface. To the author's knowledge, there is no available evidence to show such a rupture surface develops at the base of a deep foundation. The current thinking seems to be that deep foundation base failures occur as compression-type failures in which the soil beneath the pile tip is compressed and displaced in a downward and outward direction. The fact that the Begemann procedure gives good answers is probably a result of the method being empirically developed from a large number of correlations between CPT and pile tip capacity data rather than to the correctness of the assumed rupture surface. The  $q_c$  averaging procedure reasonably accounts for the effects of the soil above and below the pile tip and the log-spiral rupture surface is a convenient, although probably incorrect, way of explaining these effects.

### 2.3 CPT Methods for Predicting Pile Side Friction

#### 2.3.1 General

As noted in the previous section, most of the early efforts to

relate pile capacity to penetrometer resistance were directed toward predicting the pile point resistance, and relatively little attention was given to the side friction problem. However, the early literature cites some instances where attempts were made to predict side friction from CPT data, and more attention has been given to this matter since the development of the adhesion jacket cone. The highlights of this work are summarized in the following sections.

### 2.3.2 Early Methods for Predicting Side Friction

Prior to 1953, only the Dutch mantle cone was available for use, and the only measure of side friction which could be obtained with this equipment was total friction on the entire string of push-rods. Because of this limitation, the early efforts to predict pile side friction were directed toward relating measured values of pile friction to the total penetrometer rod resistance over the same depth of soil. Several engineers, for example Bogdanovic (1961) and Huizinga (1951), assumed that unit friction acting on the pile surface was equal to the unit friction acting on the cone rods and estimated the pile friction by multiplying the total rod friction by the ratio of the perimeters of the rods and pile. They recognized that this would probably give a conservative estimate for pile friction because the actual unit pile friction should be greater than the unit friction on the smooth cone rods.

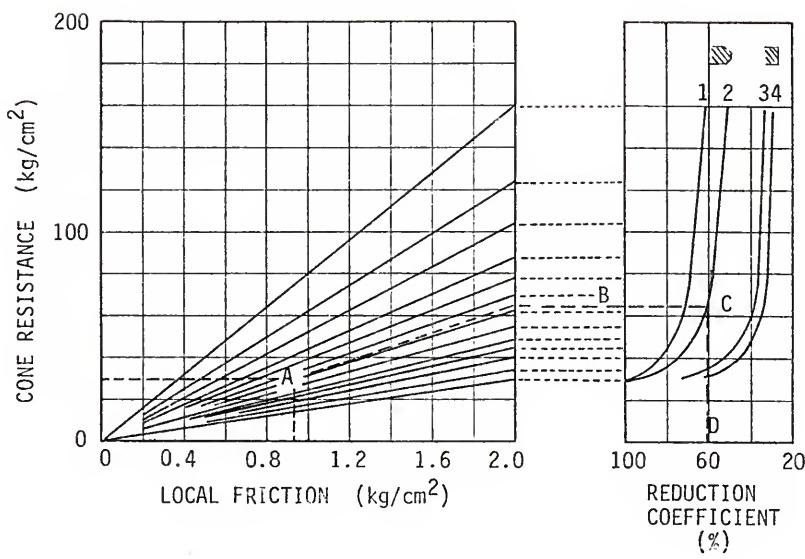
Huizinga noted from his data that, on the average, measured values of pile friction were about twice the value computed by assuming equal unit friction on the rods and pile. Meyerhoff (1956) reported finding a similar relationship for piles driven in sand. Although there was reasonable agreement between average measured pile friction and the

average predicted value computed by assuming that unit pile friction was twice that acting on the cone rods, there was a great amount of scatter between the values for individual tests. Thus, confidence in friction capacities computed according to this method was not very great.

### 2.3.3 Begemann's Method for Predicting Side Friction

Begemann (1953 and 1969a) presented some typical curves showing the variation of total rod friction with penetration depth and explained why it would be unreasonable to expect accurate pile friction predictions from these data. He cited several examples where total rod friction decreased with additional penetration, indicating a soil layer had been encountered which was applying negative friction to the rods, a situation which could not possibly exist. Begemann thought this was primarily due to loss in soil strength due to remolding as more and more rods passed a certain soil layer and showed experimentally that this remolding could cause the apparent negative friction effect in some soils. Lateral movement of the slender cone rods would also tend to enlarge the hole surrounding the rods and reduce friction at the soil-rod contact.

To provide a more reliable means of estimating pile side friction, Begemann developed the adhesion jacket cone in 1953. Since that time, he has analyzed the results of a large number of load tests to develop a side friction prediction method. The results of this work are summarized in Fig 2.13 and are presented in more detail by Begemann (1965 and 1969b). It should be noted that these design curves were developed on the basis of pile uplift tests and are intended to provide an estimate of uplift friction capacity rather than friction capacity under

LEGEND

- 1 - Wooden pile
- 2 - Prefab pile with 45 degree point
- 3 - Open-end steep pipe and I-beam pile
- 4 - Pointless prefab pile

After Begemann (1965)

BEGEMANN'S GRAPH FOR ESTIMATING PILE SIDE FRICTION

FIGURE 2.13

compression loading. However, Begemann (1969b) reports that some test results indicate that the differences between friction in uplift and compression are small enough to neglect. Furthermore, Begemann (1973) used these curves to predict the frictional capacity of a steel H-pile loaded in compression and obtained good correlation between the predicted and measured friction.

The manner in which these design curves are used is as follows:

1. The average  $q_c$  and  $f_s$  values for the soil layer in question are computed and a point corresponding to these values is located on the  $q_c-f_s$  graph, i.e., point A in Fig 2.13.
2. A straight line is extended through the origin and point A to intersect the right margin of the  $q_c-f_s$  graph (point B).
3. A horizontal line is drawn through point B to intersect the appropriate pile type curve on the reduction coefficient graph (point C).
4. The reduction coefficient is determined by projecting a vertical line through point C to intersect the reduction coefficient scale.
5. The predicted unit pile friction is determined by multiplying the average local sleeve friction by the reduction coefficient; thus, a reduction coefficient of 100% amounts to no reduction at all, and a small reduction coefficient amounts to a large reduction in local friction.

Begemann also presented similar curves for cast-in-place concrete piles and pressure-injected piles.

According to Begemann's design curves, the friction which will act on a driven pile is a function of the type and strength of soil ( $q_c$  and  $f_s$ ), the type of pile, and the point angle of the pile. The curves also indirectly indicate that the shape of the pile is important since the reduction factors for wooden piles (which are normally tapered) are greater than the factors for straight-sided steel or concrete piles.

#### 2.4 Summary

Based on this literature review, it appears that the current CPT methods for predicting the point resistance of piles are the result of a great deal of research work and numerous correlation studies using results of load tests on full-size piles. The prediction method currently in use in The Netherlands provides results which agree well with actual measurements of pile behavior even though the rupture surface assumed in the development of this method may be incorrect. Most of the test results used in the development of the current prediction method were obtained from piles driven in sands. Very little work has been done with respect to predicting pile point resistance in clays from CPT data.

CPT methods for predicting pile side friction are almost solely the result of Begemann's work with tension piles. Begemann has obtained good correlation with his method and measured pile tension capacities; however, the literature contains very few examples of application of this method to piles loaded in compression.

## CHAPTER 3

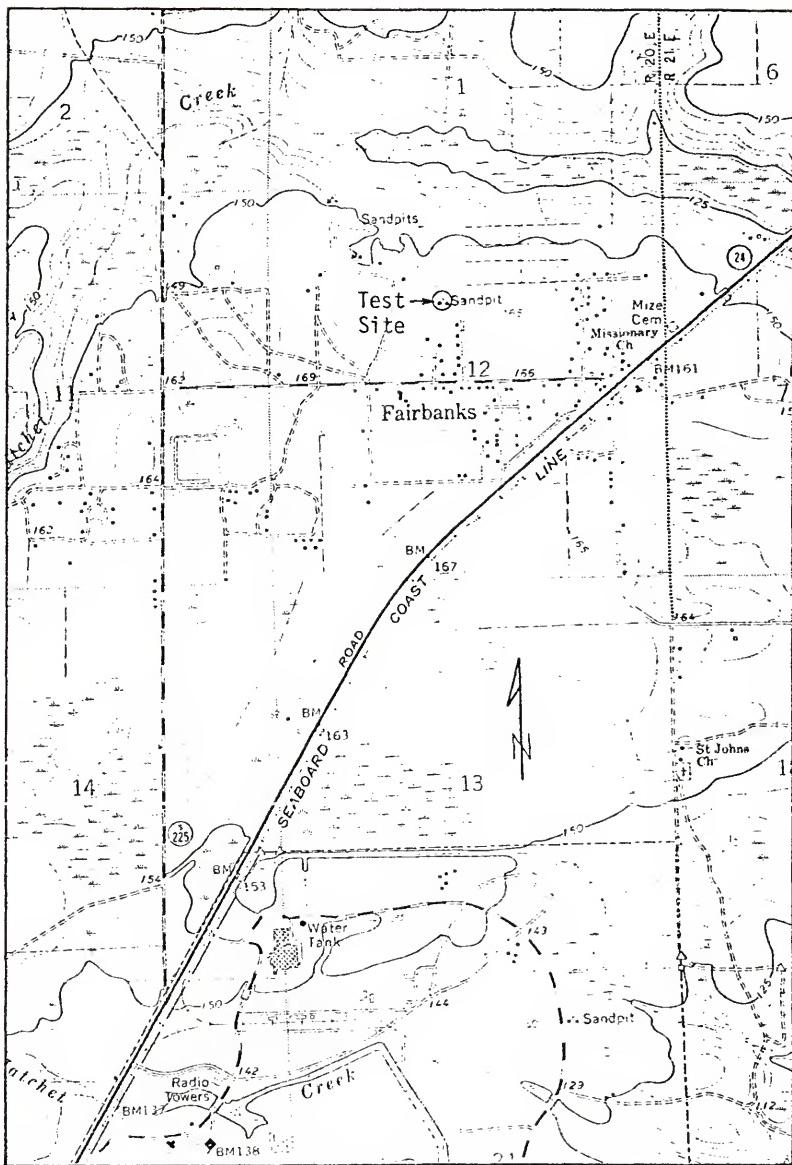
### MODEL PILE TEST SITES

Two sites were needed for the model pile testing program: one consisting of granular soils and the other of cohesive soils. Sites with reasonably uniform soil conditions were desired so that test data scatter due to natural soil variability could be minimized. In addition, accessibility to the cone penetrometer truck was necessary and the site had to be located within 10 to 15 miles of Gainesville since numerous trips to each site would be required. After considerable searching and exploration, three sites were located which appeared to be suitable for the testing program. Each of these sites is discussed in the following sections.

#### 3.1 Fairbanks Site

The Florida Department of Transportation (FDOT) has been operating a sand borrow pit at Fairbanks for a number of years. Preliminary CPT soundings and examination of the borrow pit walls indicated this site contained a relatively uniform deposit of clean sand to a depth of about 10 ft. Since the site appeared suitable for the model pile testing program, permission was obtained from the FDOT to conduct tests at this location. Fig 3.1 shows the location of this site.

The uniform sand deposit had been stripped from most of the FDOT property; however, an area located along the north boundary appeared to be undisturbed and was selected as the test site. The location of this



### FAIRBANKS SITE LOCATION

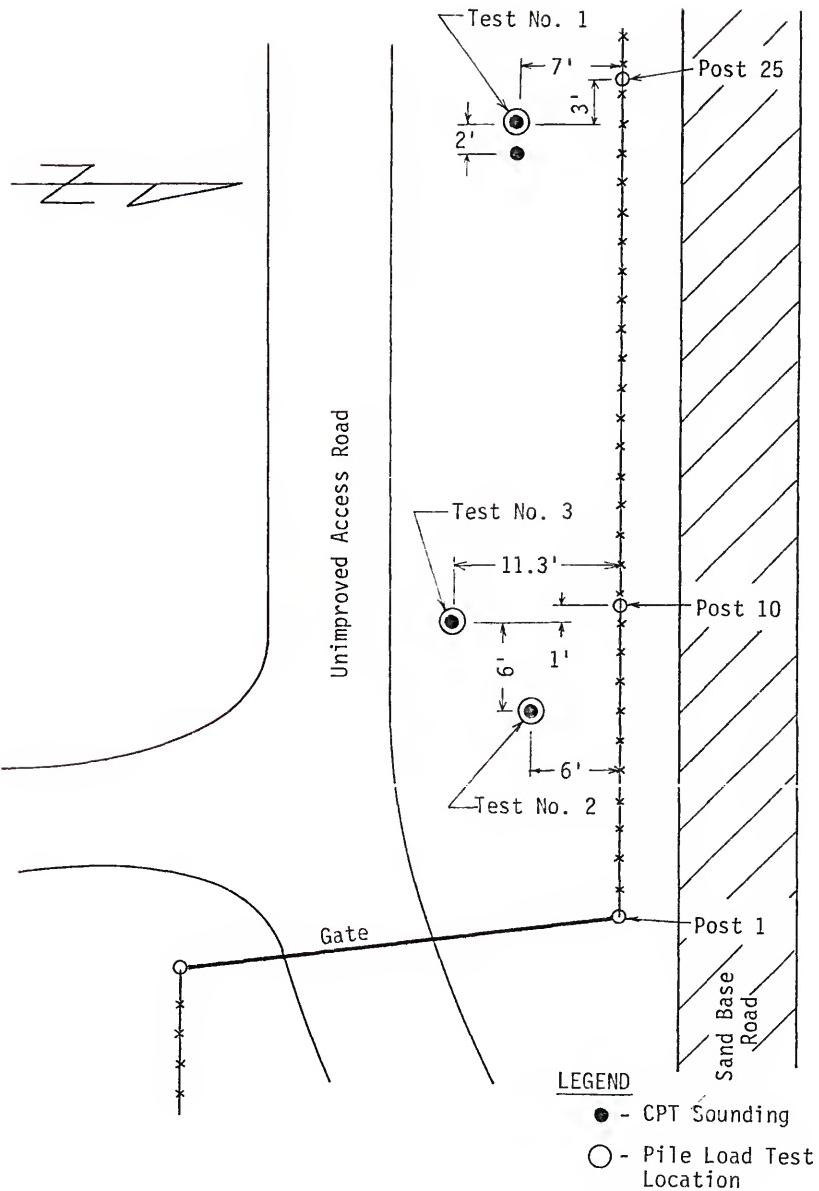
FIGURE 3.1

area is shown in Fig 3.2. CPT soundings were made at three locations within this area, and preliminary model pile tests were performed at each location to check the performance of the model pile testing equipment and to aid in developing test procedure guidelines. The results of these tests will be presented and discussed in the following chapter.

Fig 3.3 presents a typical CPT log from the test area which indicates a soil profile consisting almost entirely of sand. The upper 8 ft is loose to medium dense while the sand below 8 ft is medium dense to dense. Based on these data, it was decided to perform additional model pile tests at this site; however, cone soundings made at additional potential test locations revealed the presence of buried asphalt and debris. Personnel from the FDOT remembered that waste materials had been buried at various locations around the site but could not remember the exact locations; therefore, the borrow pit site was abandoned. Permission could not be obtained from the surrounding land-owners to test on their property; thus, a search was conducted for a new site.

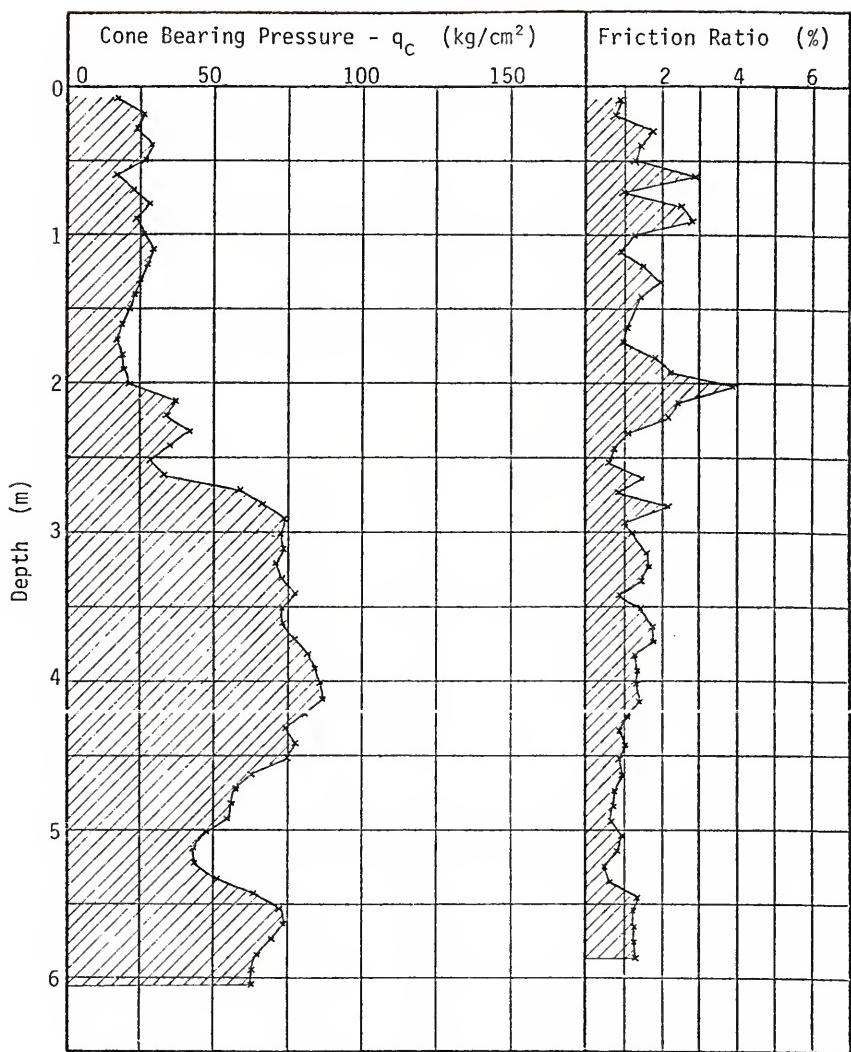
### 3.2 Beville Site

Several previous civil engineering graduate students conducted field research projects at a site located on S.W. 17th Avenue in Gainesville. Although exploration for these projects only extended to shallow depths, the data indicated that the site might be suitable for the model pile research. Nine preliminary cone soundings were made at locations scattered throughout the site to determine if this area would be suitable for the model pile testing program. The site location, the preliminary sounding locations, and one of the nine



FAIRBANKS SITE LAYOUT

FIGURE 3.2



FAIRBANKS SITE CPT LOG

FIGURE 3.3

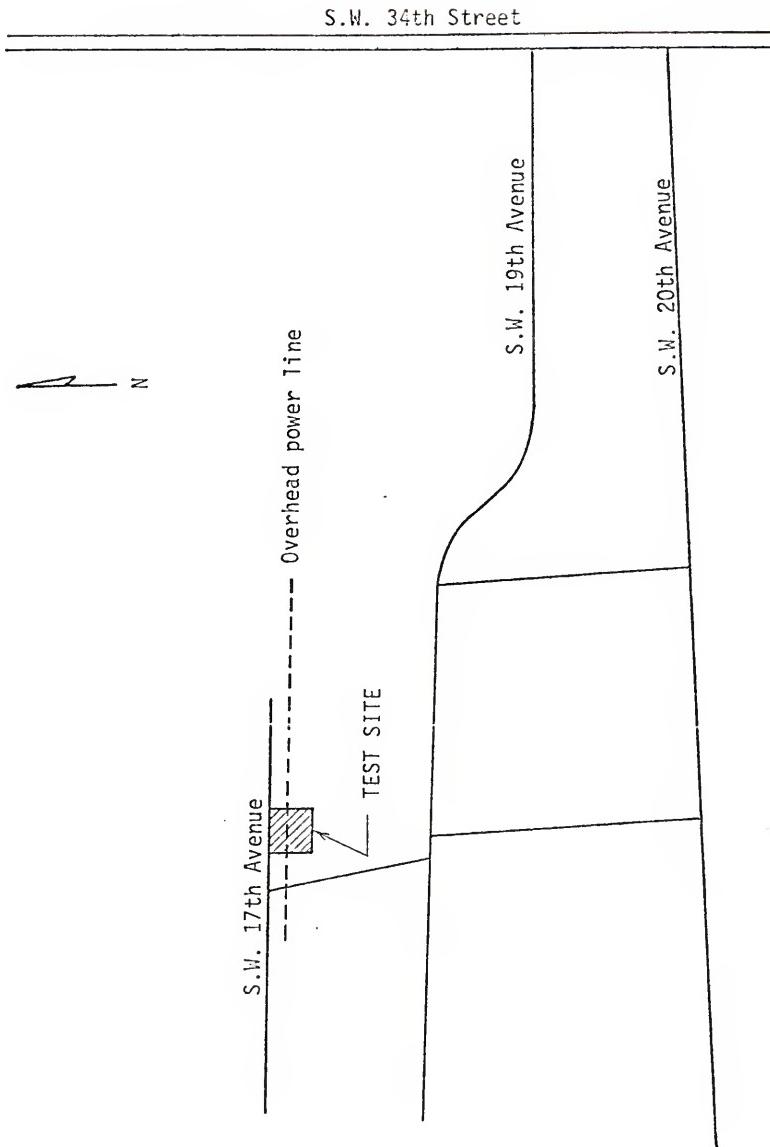
preliminary CPT logs are presented in Figs 3.4, 3.5, and 3.6. Appendix B contains logs of all the preliminary soundings.

Based on CPT data interpretation guidelines developed by Schmertmann (1974c) the preliminary soundings indicated that the soil profile consisted of 7 to 10 ft of loose to medium dense sand underlain by a layer of clayey sand to sandy clay. This site was suitable in all respects except for the thickness of the sand deposit which was slightly less than was desired. Since a thicker deposit of surface sand could not be located, the site selected as a test area, and permission for testing was obtained from Mr. Jack Beville, the property owner.

### 3.2.1 Site Layout and Exploration

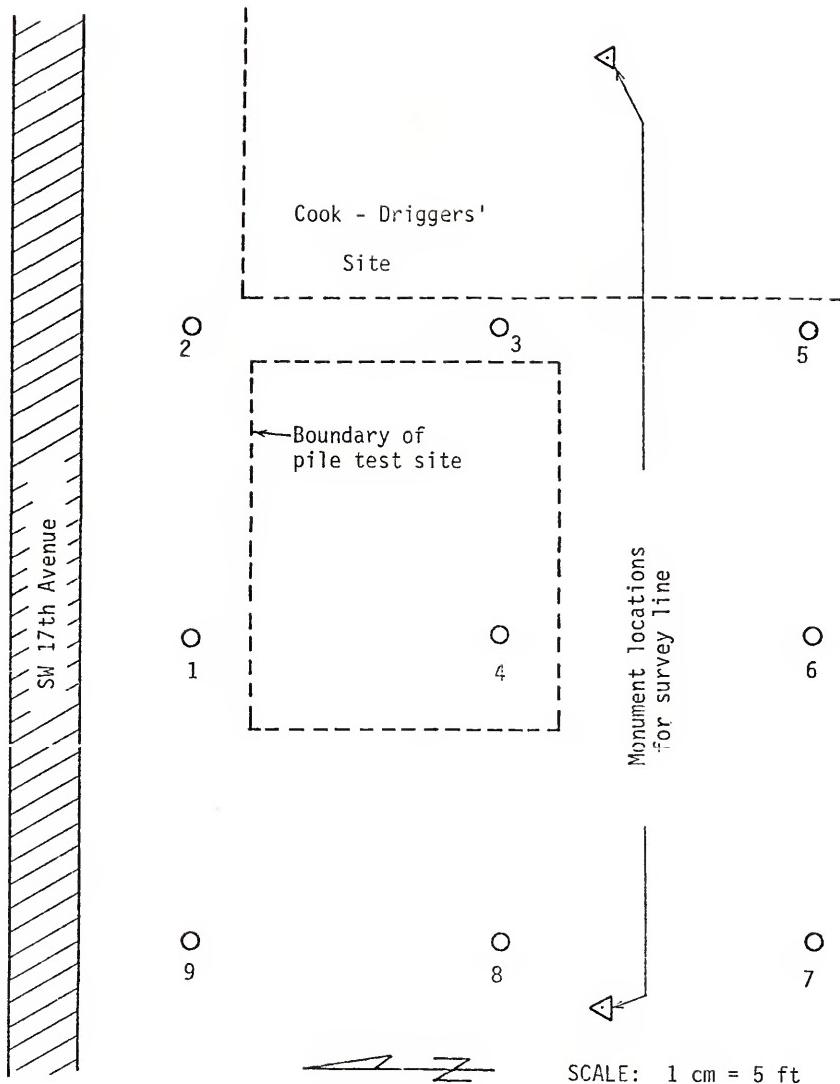
Thirty-two pile test locations were established in the vicinity of preliminary CPT Sounding Nos 1, 2, 3, and 4. The test locations were referenced to two steel pins set in concrete just beyond the east and west boundaries of the test area. The steel pins' locations were established with reference to surrounding landmarks as shown in Fig 3.7.

Cone penetrometer soundings were conducted at 28 of the 32 test locations. Two electrical and two mechanical penetrometer soundings were made at each of the 28 locations, with the exception of the Test No 25 location where only mechanical penetrometer soundings were made. Each sounding was located 1.5 ft from the pile test location. Mechanical penetrometer soundings were located on opposite sides of each test location along a north-south line through the location. Electrical soundings were also made on opposite sides of each test location along an east-west line. The sounding locations are shown in Fig 3.7



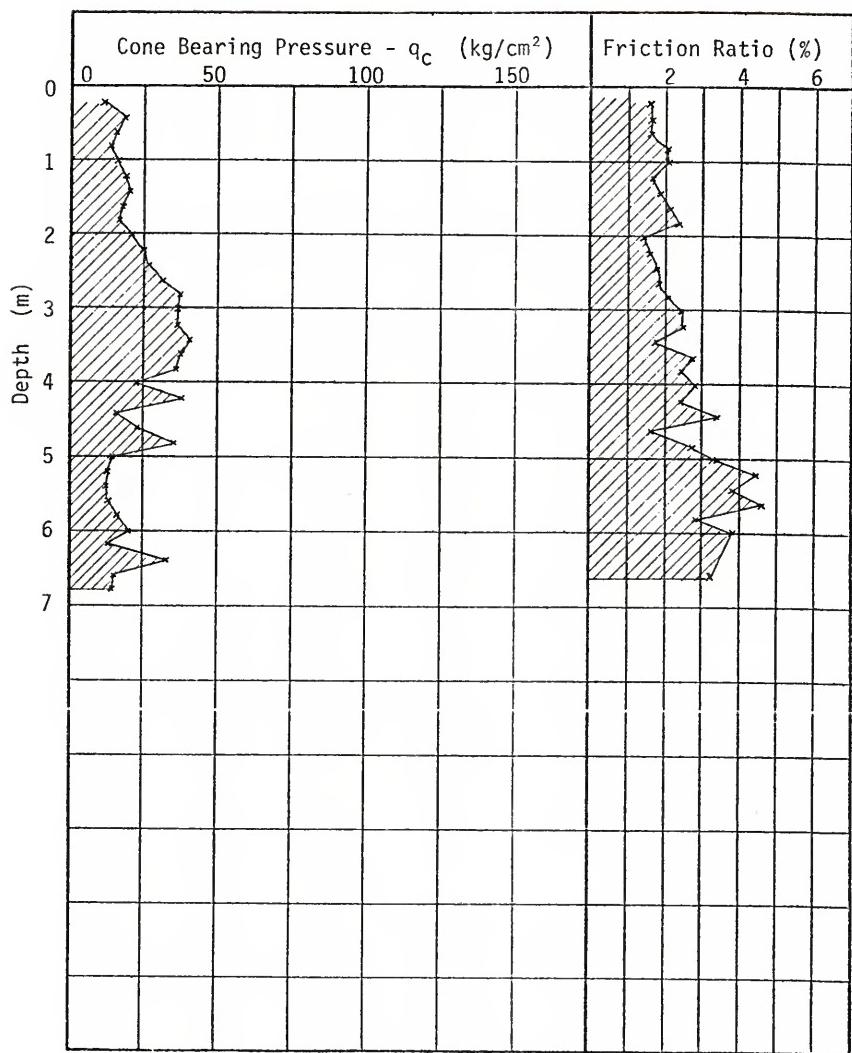
BEVILLE SITE LOCATION

FIGURE 3.4



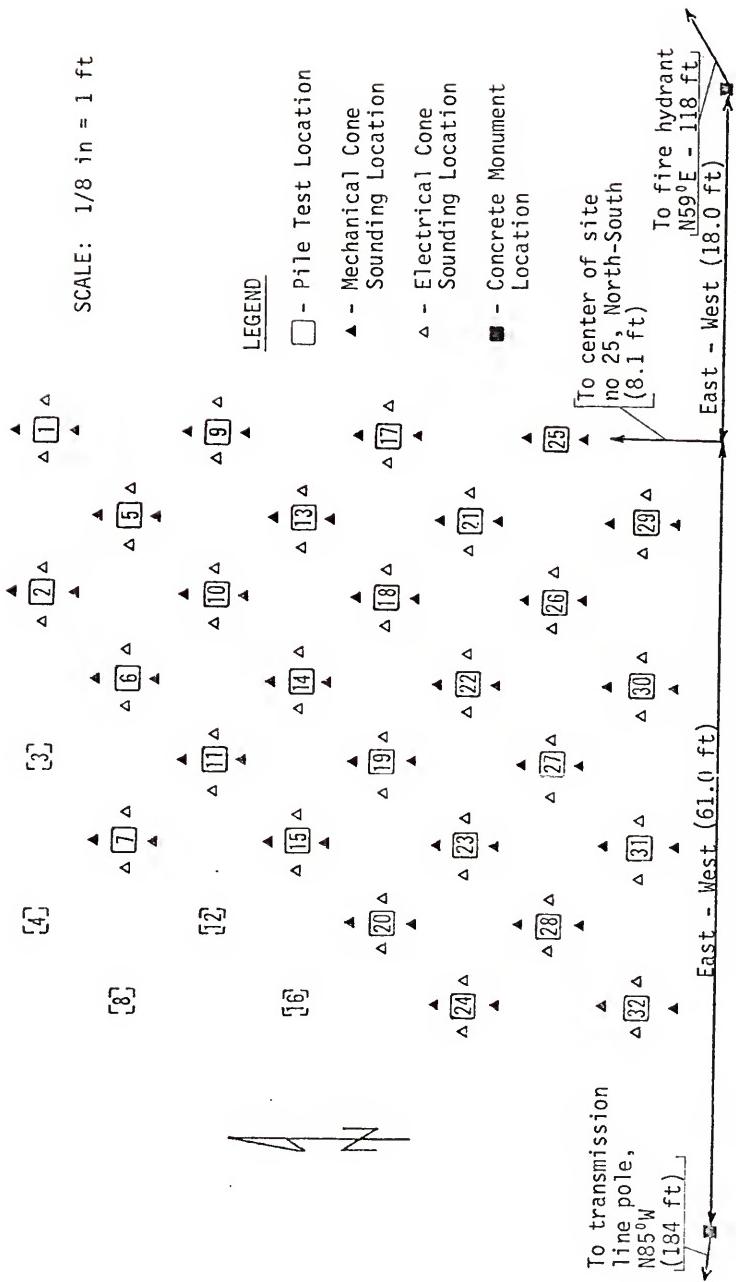
LOCATION OF PRELIMINARY BEVILLE SITE CPT SOUNDINGS

FIGURE 3.5



PRELIMINARY BEVILLE SITE CPT LOG

FIGURE 3.6



FAIRBANKS SITE LAYOUT

FIGURE 3.7

and all sounding logs are presented in Appendix B. The numbering system used to identify each sounding is explained by the following:

Sounding No 21E2

21 - Test location where the sounding was made.

E - Denotes electrical sounding (M denotes a mechanical sounding).

2 - Indicates that the sounding was located on the east side of the test location. For a mechanical sounding, the number 2 would indicate a sounding to the south of the test location. Sounding Nos 21E1 and 21M1 would indicate electrical and mechanical soundings to the west and north of Test Site No 21, respectively.

Cone point and friction sleeve resistance data were recorded at 10 cm depth increments during each mechanical penetrometer sounding. Data were recorded continuously during each electrical sounding; however, the electrical CPT logs in Appendix B only present data at 10 cm depth intervals. A penetration rate of approximately 2 cm/sec was used for all soundings.

### 3.2.2 Soil Properties

#### 3.2.2.1 General conditions

All penetrometer soundings indicate that the site contains a loose to medium dense sand layer to a depth varying from about 7 to 10 ft below ground surface. The cone point resistance ( $q_c$ ) in this layer was either approximately constant or increased slightly with depth at most locations and did not vary greatly from location to location which indicates that the deposit is relatively uniform both vertically and laterally. A layer of clayey sand to sandy clay was encountered beneath the sand deposit at most sounding locations.

Recorded variations in  $q_c$  and friction ratio (FR) data in the clayey

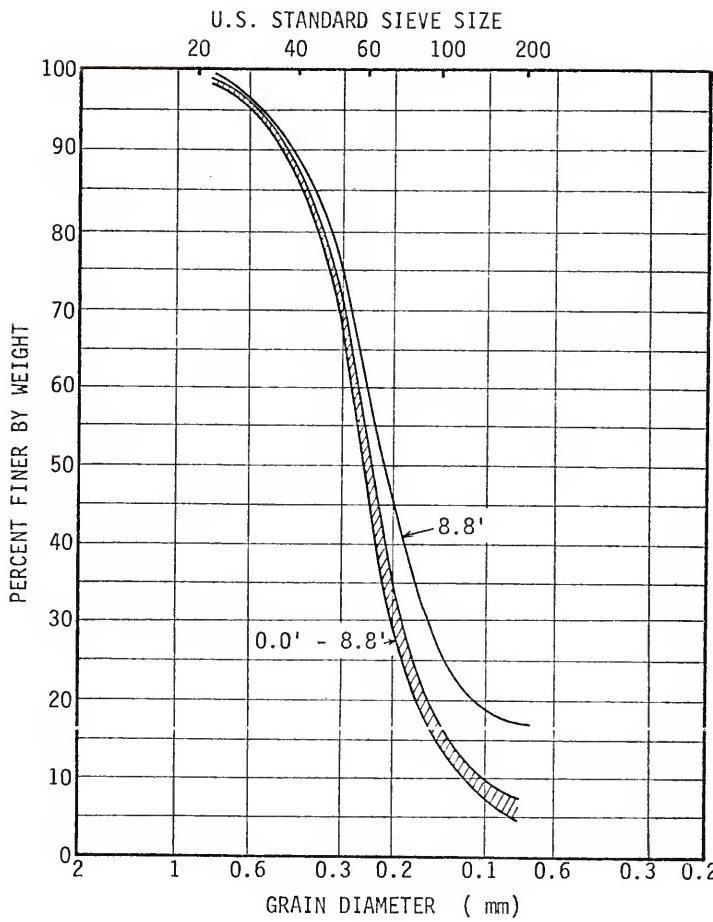
layer indicate a high degree of variability in both relative density or consistency and clay content. This clayey layer was generally 2 to 4 ft thick and was underlain by a deposit of medium dense to dense sand at most sounding locations. Observations made at various times throughout the course of testing at this site showed that the ground-water level varied from 9 to 11 ft below ground surface.

### 3.2.2.2 Soil composition

Visual examination of samples of soil from the upper 6 to 10 ft showed it to be a relatively clean fine to medium quartz sand. The grain size and shape of this sand was investigated by both Driggers (1971) and Freed (1973). Freed's gradation curve ranges are presented in Fig 3.8. These curves show that the sand is uniformly graded and slightly silty. Freed's data showed the gradation to be very consistent with depth to about 8.5 ft. The percent of soil passing the No 200 sieve increased significantly below 8.5 ft. Both Freed and Driggers also presented photomicrographs of the sand grains which showed that the soil is composed of subangular grains.

### 3.2.2.3 Natural and relative density

Drigger (1971) performed natural and relative density tests on the sand from an area immediately adjacent to the test area used for this research, and Freed (1973) performed similar tests on sand from the pile test site while assisting with this research. Driggers' work resulted in average maximum and minimum densities of 119.6 and 89.4pcf and an average natural density of 93.6pcf. These values resulted in an average relative density of 18.5%. All of Driggers' testing was performed on samples taken from a depth of 3.0 ft.



GRAIN SIZE CURVES FOR BEVILLE SAND

FIGURE 3.8

Freed performed tests on nine samples taken from depths ranging from 0.6 to 8.9 ft. He did not report maximum and minimum density values for the individual tests but reported that the average values were 116 and 91 pcf, respectively. In situ dry density, field moisture content, and relative density values reported by Freed are summarized in Table 3.1. Results of four in-place densities performed by Freed using a Rainhart volumemeter gave natural dry densities very close to those reported in Table 3.1.

TABLE 3.1  
SUMMARY OF BEVILLE SITE DENSITY AND MOISTURE CONTENT DATA

Sample Depth (ft)	w (%)	$\gamma_{nat}$ (pcf)	$D_r$ (%)
0.62 - 1.12	2.3	103.7	56.8
1.12 - 1.67	3.0	105.5	63.3
3.31 - 3.74	2.6	102.5	52.1
4.02 - 4.30	3.1	104.4	59.5
5.58 - 6.14	4.8	103.8	57.3
6.14 - 6.41	7.0	105.8	65.0
7.76 - 8.04	16.6	100.4	43.4
8.04 - 8.60	14.9	113.6	----
8.60 - 8.87	14.1	116.4	----

The in situ dry densities determined by Freed are considerably higher than those determined by Driggers. This is not surprising since static cone penetrometer soundings in the vicinity of Driggers' tests gave  $q_c$  values in the range of 10 to 20 kg/cm<sup>2</sup> while soundings in the vicinity

of Freed's tests gave values ranging from 20 to 50 kg/cm<sup>2</sup>. The minimum densities reported by both investigators agree well, but there is a considerable difference in the maximum densities (Driggers' 119.6pcf vs. Freed's 116.0 pcf). This difference is surprising since grain size curves and photomicrographs of the sand presented by both investigators are very similar. Driggers' maximum density tests were performed using a vibrating table in accordance with ASTM D-2049 while Freed used a variety of methods in an attempt to duplicate Driggers' results. It is believed that Freed's data are more representative of the model pile test site conditions, primarily because his samples were taken directly from the test site.

#### 3.2.2.4 Shear strength

Drained triaxial compression tests were performed on reconstructed samples of sand by Driggers (1971) and Cook (1971). These samples were taken from an area adjacent to the model pile test site. However, gradation curves for sand from the test site and the adjacent area are almost identical; thus, the strength properties should be comparable. Driggers' samples were compacted to a relative density of 18% (using Freed's  $\gamma_{min}$  and  $\gamma_{max}$  values) and gave an angle of internal friction ( $\phi$ ) of 35.8 degrees. Cook's samples were compacted to a relative density of 74.5% and gave a  $\phi$  of 41.6 degrees. Using the average relative density (56.8%) for the test site and interpreting linearly between Cook's and Driggers'  $\phi$  -  $D_r$  data results in an estimated  $\phi$  of 39.8 degrees for the model pile test site sand.

#### 3.3 Paines Prairie Site

Locating a suitable clay site in the Gainesville area proved to

be a difficult problem. Most clays in this area are stiff and highly overconsolidated instead of soft or medium stiff as was desired. In addition, surface layers of clay of sufficient thickness for the testing program are rare in this area. After considerable searching, an area was located in Paines Prairie which appeared to meet the clay site requirements. This site and the properties of the site soils are discussed in the following sections.

### 3.3.1 General Conditions

Paines Prairie is a large flat area located southeast of Gainesville as shown in Fig 3.9. In the recent past, this area was a large lake. It is reported that the lake drained and refilled several times due to the formation and plugging of sinkholes in the lakebed. Refilling has been prevented in recent years by means of artificial drainage and pumping.

Deposits of highly plastic soft green clay were encountered in the old lakebed during construction of I-75 across Paines Prairie. Attempts were made to locate the test site in an area containing this clay, but this proved impossible for two reasons:

1. Areas containing these soils were soft and marshy, thus inaccessible to the testing equipment.
2. The State of Florida recently purchased the prairie and turned it over to the Department of Natural Resources (DNR) which is maintaining it as a wildlife refuge. Permission could not be obtained to conduct tests in the main prairie basin where the soft green clays are located.

Although testing was prohibited in the prairie basin, DNR personnel did grant permission to conduct tests along the northeast edge of the prairie. After making numerous CPT soundings in the region outlined by DNR personnel, an area was located which appeared to meet the



site requirements. The logs of six mechanical CPT soundings made in this area are contained in Appendix C, and a typical log is presented in Fig 3.10. The location of the area and the six preliminary penetrometer soundings are shown in Fig 3.11.

The preliminary CPT data show a soil profile consisting of 2 to 3 ft of surface sand underlain by a 10 to 12 ft thick deposit of medium stiff cohesive material. The cone penetrometer friction ratios in this deposit generally varied between 3.0 and 5.0%, indicating a sandy clay to clayey sand. This was confirmed by visual examination of soil samples obtained from the area. On the basis of these findings, it was decided to use the area as a test site.

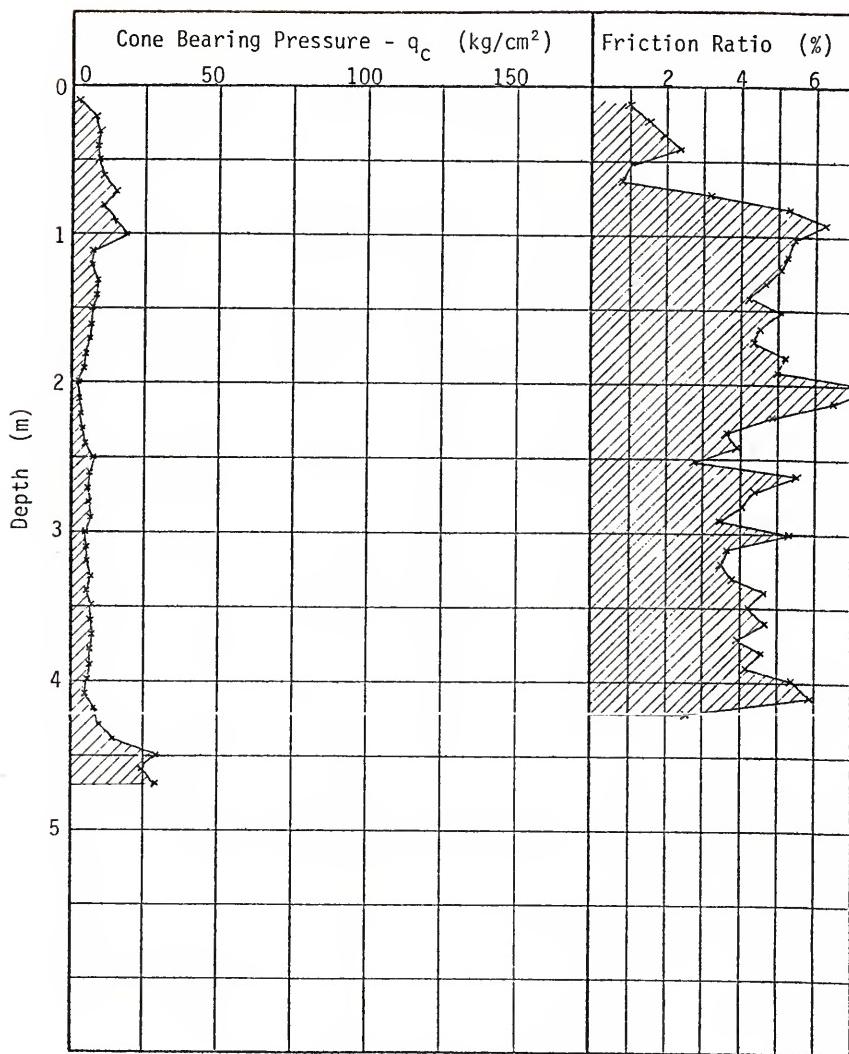
### 3.3.2 Site Layout and Exploration

The test area was located between preliminary Sounding Nos 1A and 2A because the cohesive soil appeared to be more uniform and slightly more clayey in this area. Two steel pins were driven on either side of the selected area, and six test locations were established and referenced to the steel pins. Two electrical penetrometer and two mechanical penetrometer soundings were made at each test location in exactly the same manner as at the Beville site. A site layout sketch is shown in Fig 3.12, and logs of all penetrometer soundings are presented in Appendix C.

### 3.3.3 Soil Properties

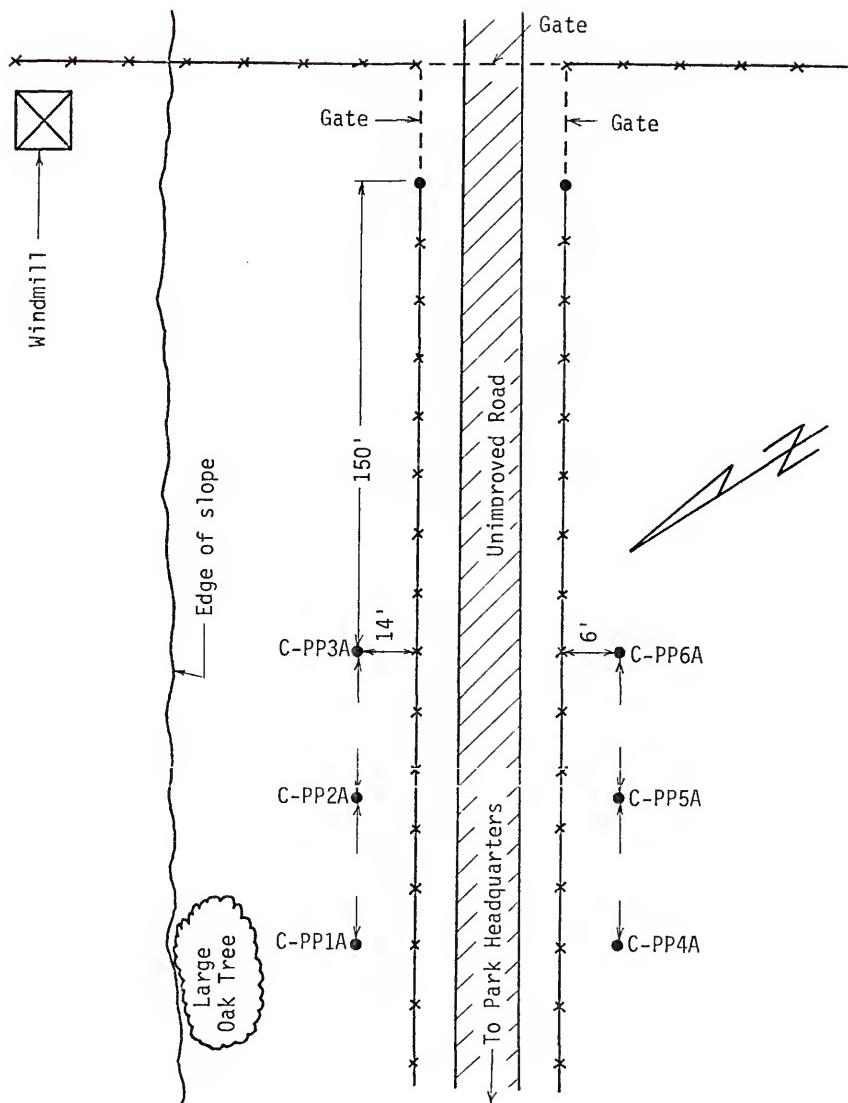
#### 3.3.3.1 Undisturbed sampling

Continuous undisturbed sampling was conducted at the location shown in Fig 3.12 using a Standard Swedish piston sampler. This



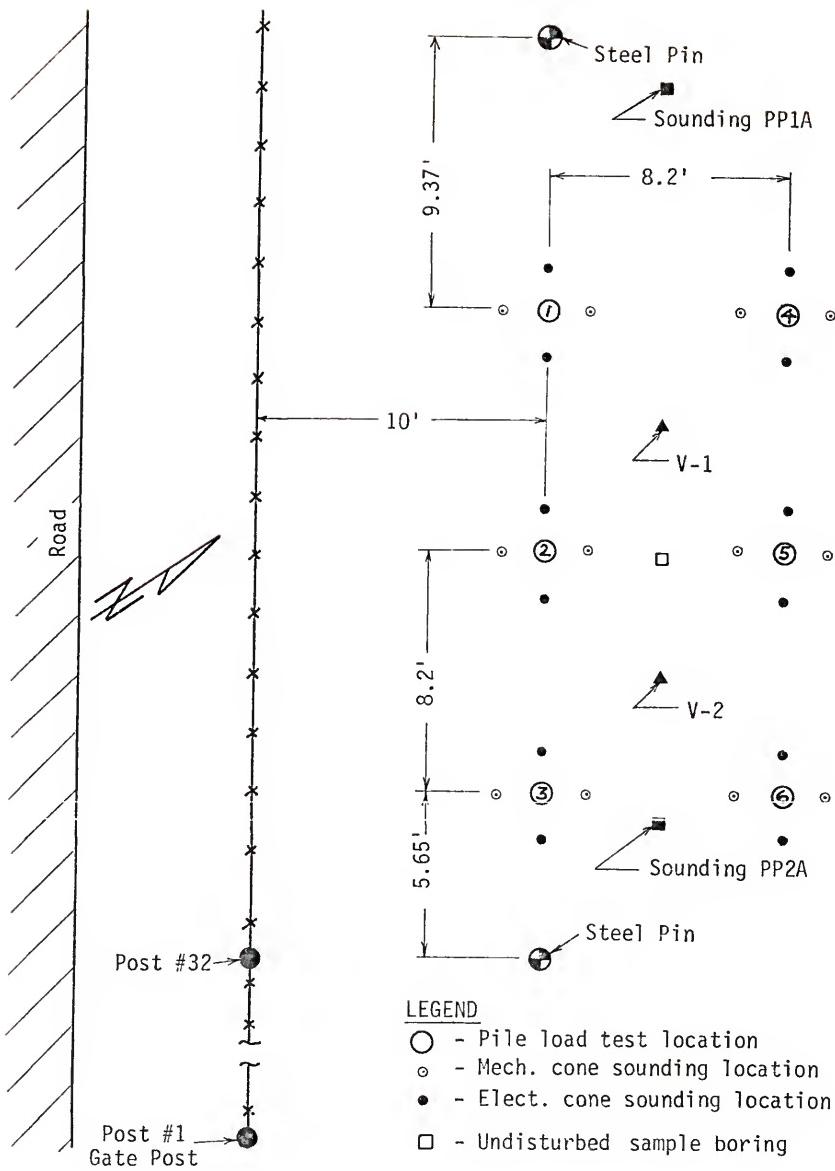
PRELIMINARY CPT LOG FROM PAINES PRAIRIE SITE

FIGURE 3.10



PAINES PRAIRIE PRELIMINARY CONE SOUNING LOCATIONS

FIGURE 3.11



PAINES PRAIRIE TEST SITE LAYOUT

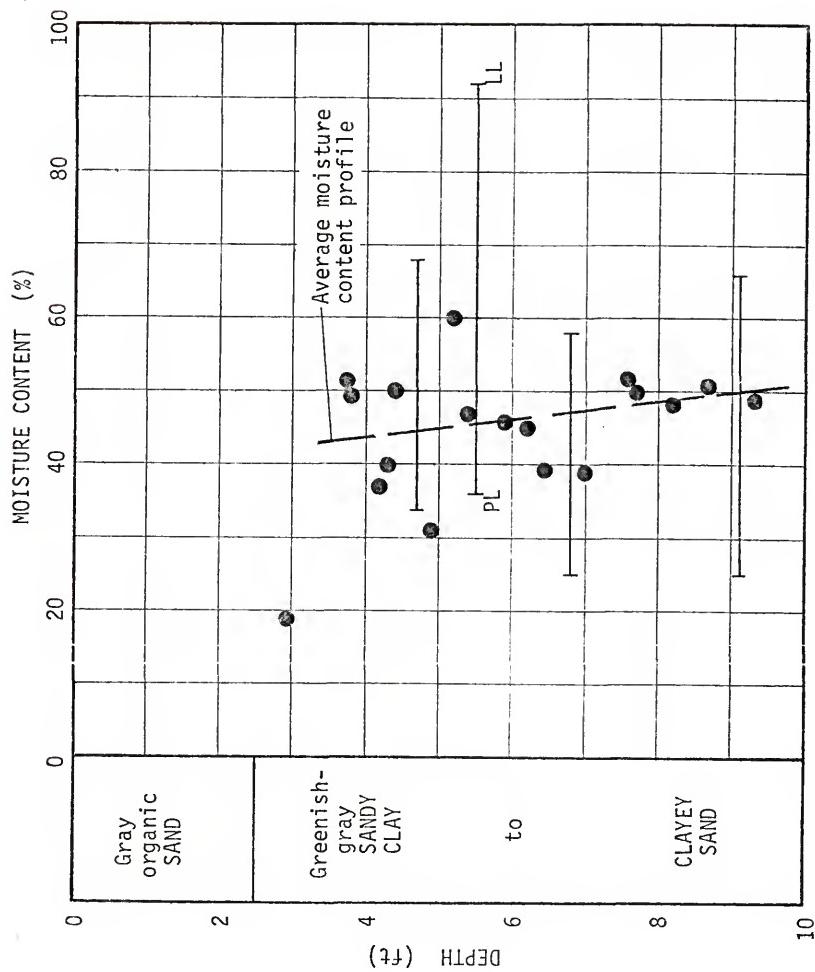
FIGURE 3.12

sampler provides a high quality, undisturbed sample 5.0 cm diameter by 70 cm long. The samples are retained in a series of 20 cm long fiberglass tubes which fit inside the main sampling apparatus. After each sampler thrust, the fiberglass tubes are removed from the sampler, a cut is made through the soil between each tube section, and the tubes are immediately sealed with rubber end caps. The sampler worked well at this site and full sample recovery was achieved during each sampling operation.

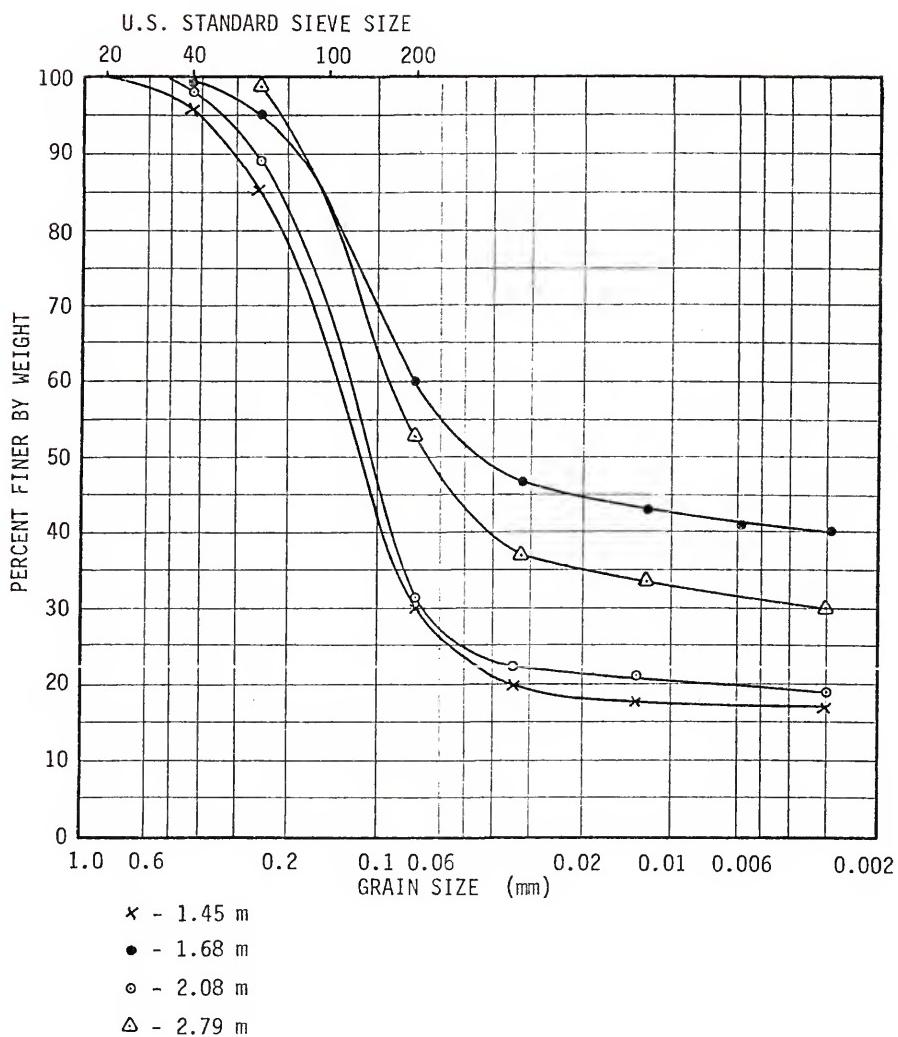
### 3.3.3.2 Index properties

Twelve natural moisture content tests were performed on portions of the undisturbed samples to provide a depth-moisture content profile for the cohesive soil layer. Moisture content data were also obtained for samples subjected to consolidation and triaxial shear tests. Four samples were selected from various depths for Atterberg limit and grain size determination tests. These tests were performed in accordance with ASTM specifications. Moisture content and Atterberg limit test results are presented graphically in Fig 3.13, and grain size curves are shown in Fig 3.14.

According to these data, the soil layer is composed of highly plastic sandy clay (CH) which grades into clayey sand (SC) with depth. The lower plasticity of the two deeper samples is probably the result of a higher percentage of fine sand in these samples rather than to differences in the clay fraction between the shallower and deeper samples. The grain size curves show that the fine portion of all the samples consists mainly of very fine clay particles, the majority of which have an effective diameter less than 0.0012 mm.



MOISTURE CONTENT AND ATTERBERG LIMIT DATA - PINES PRAIRIE SITE  
FIGURE 3.13



PAINES PRAIRIE GRAIN SIZE CURVES

FIGURE 3.14

### 3.3.3.3 Consolidation testing

One-dimensional consolidation tests were performed on two undisturbed samples taken from the clayey layer. The test samples were 5.02 cm diameter by 1.91 cm high. One sample was taken from a depth of 4.2 ft and was representative of the more clayey portion of the layer while the other, from a depth of 7.6 ft, was representative of the more sandy material. The initial vertical pressure applied to the 4.2 and 7.6 ft samples were 0.25 and 0.0625 tsf, respectively. The vertical pressure on each sample was doubled during each successive load increment until a pressure of 16 tsf was attained. Two additional samples from approximately the same depth were remolded and subjected to consolidation testing using the same procedure as for the undisturbed samples.

Void ratio versus logarithm of pressure ( $e - \log \sigma'_v$ ) curves from the consolidation tests are presented in Figs 3.15 and 3.16. These data show that the upper portion of the clay layer is highly overconsolidated ( $OCR \approx 15$ ) and highly compressible once the applied pressure exceeds the preconsolidation pressure. The lower portion of the layer is only slightly overconsolidated ( $OCR \approx 1.5$ ) and moderately compressible.

### 3.3.3.4 Permeability tests

Constant head permeability tests were performed on samples from three different depths. These tests were performed in a triaxial chamber on 5.0 cm diameter by 7.6 cm high samples which had been reconsolidated to a confining pressure approximately equal to the effective

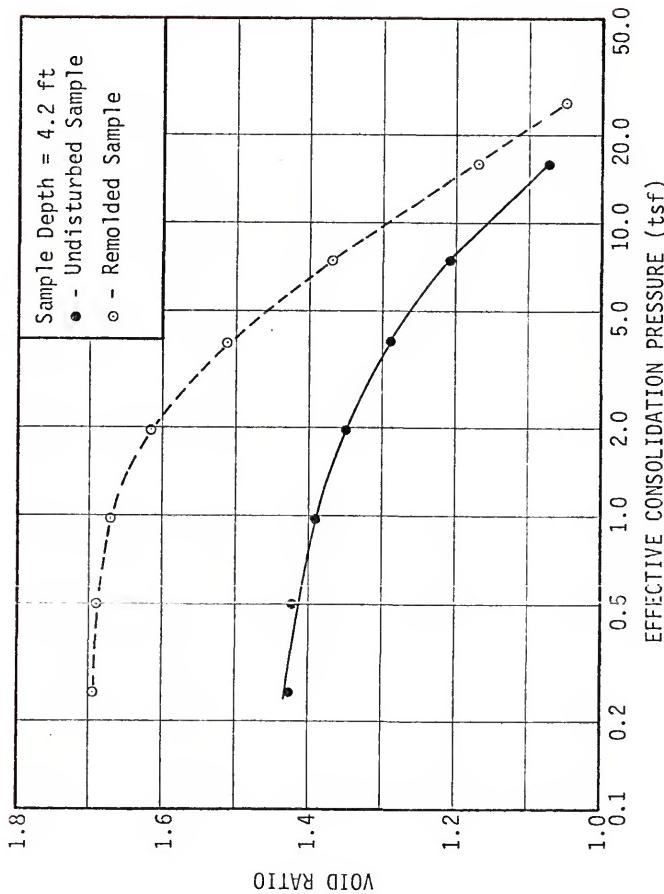
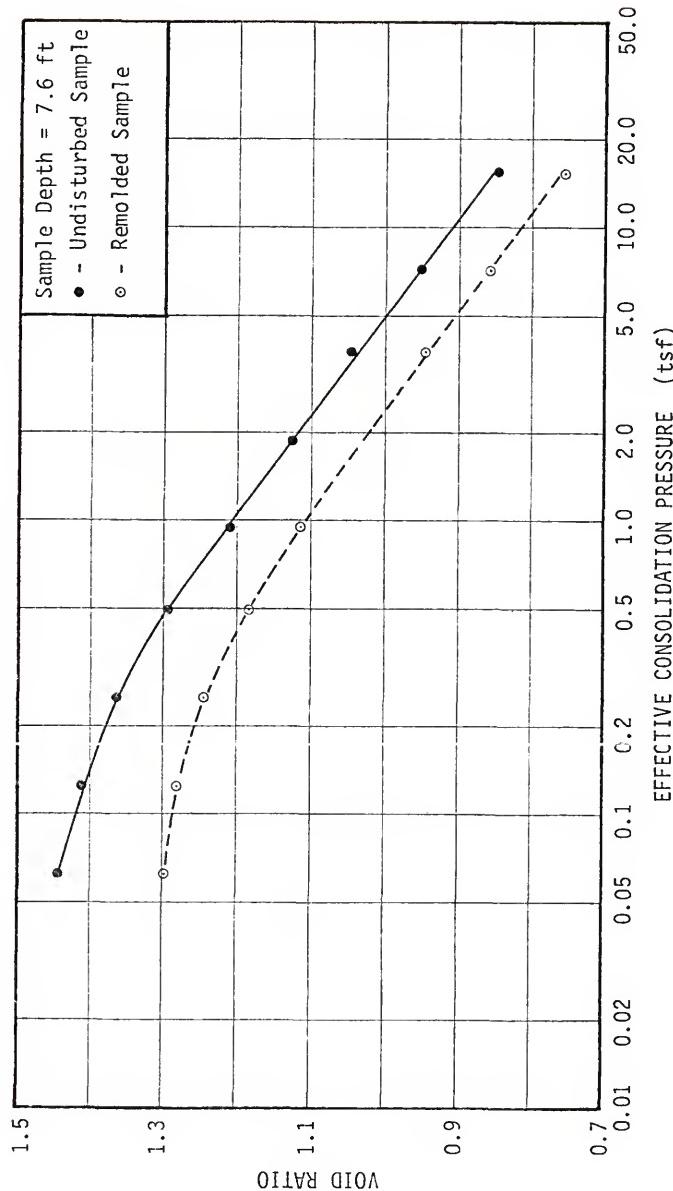


FIGURE 3.15



CONSOLIDATION CURVES FOR PAINES PRAIRIE CLAY

FIGURE 3.16

overburden stress. Flow through each sample was maintained until a constant flow rate was attained. Permeability values ( $k_v$ ) were computed using the final constant flow rates. Results of these tests are summarized in Table 3.2, and permeability values computed from the consolidation test data are contained in Table 3.3.

TABLE 3.2  
PAINES PRAIRIE PERMEABILITY TEST DATA

Sample Depth (ft)	$k_v$ (cm/sec)
4.3	$4.8 \times 10^{-7}$
6.2	$2.1 \times 10^{-6}$
8.2	$1.1 \times 10^{-4}$

As would be expected, the permeability test data show a consistent increase in permeability with depth and the values are consistent with the soil types indicated by the index property tests. Consolidation test data from the 7.6 ft sample give considerably higher  $k_v$  values than the permeability tests on samples from 6.2 and 8.2 ft. Possible reasons for this difference are:

1. The thin (1.91 cm) consolidation test sample may have been more clayey than the permeability test samples, although visual examination did not indicate a significant difference in the composition of the samples.
2. Sample smear resulting from trimming the sample ends may have affected the test results. End smear effects would have more influence on the much thinner consolidation test sample.
3. The consolidation test only provides an indirect measure of permeability and is generally not as accurate as a carefully performed permeability test.

TABLE 3.3  
PERMEABILITY DATA FROM PAINES PRAIRIE  
CONSOLIDATION TESTS

Sample Depth (ft)	Vertical Pressure (tsf)	$k_v$ (cm/sec)	
		Undisturbed	Remolded
4.2	0.25	$2.3 \times 10^{-8}$	
	0.50	$2.1 \times 10^{-8}$	
	1.0	$3.0 \times 10^{-7}$	
	2.0	$2.3 \times 10^{-7}$	
	4.0	$1.2 \times 10^{-7}$	$5.5 \times 10^{-9}$
	8.0	$7.8 \times 10^{-8}$	$1.3 \times 10^{-9}$
	16.0	$4.5 \times 10^{-8}$	$8.1 \times 10^{-10}$
7.6	0.0625	$1.0 \times 10^{-7}$	
	0.125	$1.3 \times 10^{-7}$	
	0.25	$1.0 \times 10^{-7}$	
	0.50	$5.3 \times 10^{-8}$	$6.0 \times 10^{-8}$
	1.0	$1.0 \times 10^{-7}$	$4.7 \times 10^{-7}$
	2.0	$6.7 \times 10^{-8}$	$1.2 \times 10^{-7}$
	4.0	$3.1 \times 10^{-8}$	$5.5 \times 10^{-8}$
	8.0	$2.0 \times 10^{-8}$	$2.8 \times 10^{-8}$
	16.0	$1.7 \times 10^{-8}$	$1.2 \times 10^{-8}$

The permeability test results are thought to be more representative of actual conditions.

### 3.3.3.5 Shear strength tests

Tests performed to evaluate the shear strength of Paines Prairie soils included consolidated-undrained (CU) and unconsolidated-undrained (UU) triaxial compression tests and in situ vane shear tests. Three CU triaxial shear tests were conducted on the same samples used for the previously discussed permeability tests. Two UU triaxial shear tests were performed on samples taken from depths of 3.8 and 5.2 ft. Lubricated end platens were used for the UU tests, and all samples were sheared at a strain rate of 0.27% per minute. The results of these tests, presented in Table 3.4, show an undrained shear strength decreasing with depth from about 1200 psf near the top of the layer to about 1000 psf near the bottom.

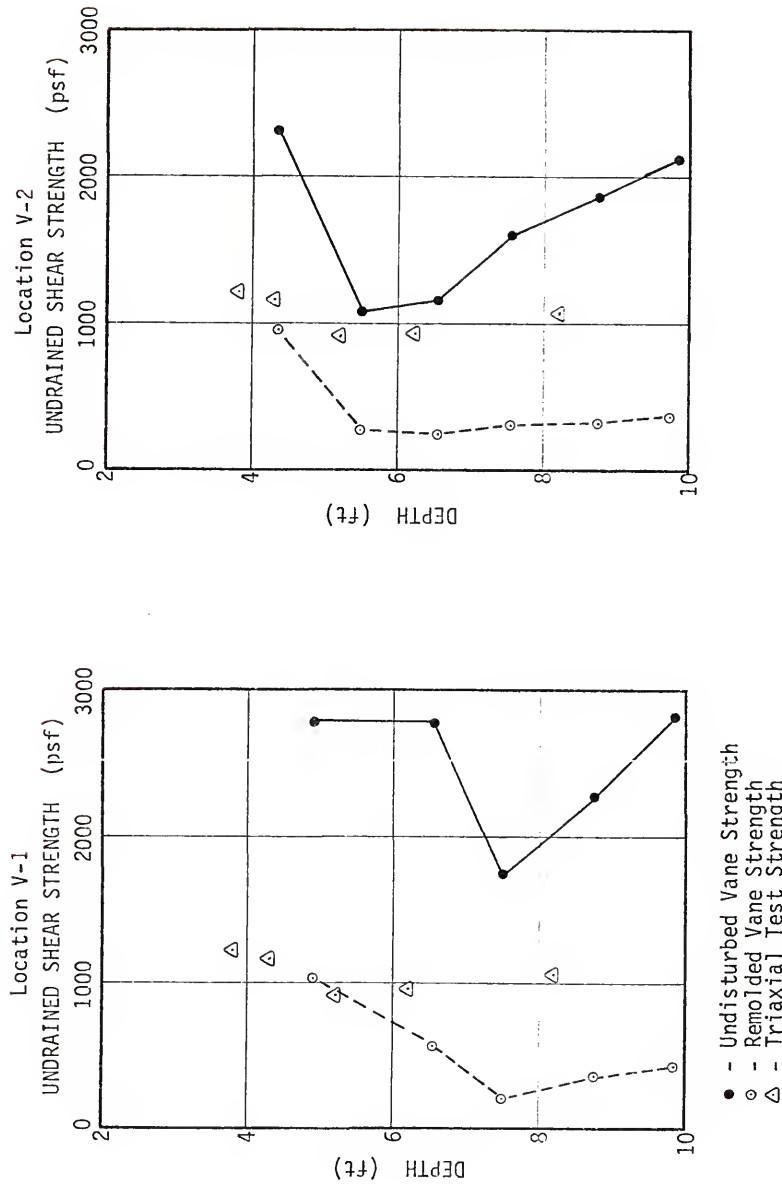
TABLE 3.4  
SUMMARY OF PAINES PRAIRIE TRIAXIAL SHEAR TEST RESULTS

Sample Depth (ft)	Type of Test	w (%)	$\gamma_{nat}$ (pcf)	$s_u$ (psf)	$\epsilon$ at failure (%)
3.8	UU	58.2	101.2	1220	2.5
4.3	CU	49.9	107.0	1163	10.7
5.2	UU	44.6	108.7	925	8.3
6.2	CU	62.0	100.0	945	6.8
8.2	CU	48.7	107.1	1062	10.0

In situ vane shear tests were performed at two locations using a manually operated Jonell and Nilsson vane borer. Tests were performed at depth intervals ranging from 0.33 to 0.50 m using a shear vane 6.5 cm diameter by 13.0 cm high. After thrusting the vane to the desired depth, an undisturbed strength test was conducted by rotating the vane at a rate of about 5 degrees per minute. The vane was then rapidly rotated through ten complete revolutions, and a second test was conducted to determine the undrained strength of the remolded soil. The results of these tests are presented graphically in Fig 3.17. For comparison, the triaxial compression test results are also presented in this figure.

The vane shear tests gave undrained strength values considerably higher than the triaxial tests and the vane data were scattered over a wider range of values. Bjerrum (1972) and others have noted that the field vane test generally gives higher undrained strength values for cohesive soils than does the triaxial test, and Bjerrum suggested that a reduction factor be applied to vane strength data. The magnitude of his suggested reduction is dependent on the plasticity index of the soil tested. Applying this correction to the Paines Prairie vane data accounts for about 35% of the difference between the vane and triaxial data. Some drainage may have occurred in the soil surrounding the vane since these soils contain a large amount of sand. This could account for the remaining difference between the vane and triaxial strength data.

The ratio of the remolded strength to the undisturbed strength, defined as sensitivity, provides a measure of the sensitivity of a soil to disturbance. Sensitivity data computed from the undisturbed



UNDRAINED SHEAR STRENGTH TEST RESULTS - PAINES PRAIRIE CLAY

FIGURE 3.17

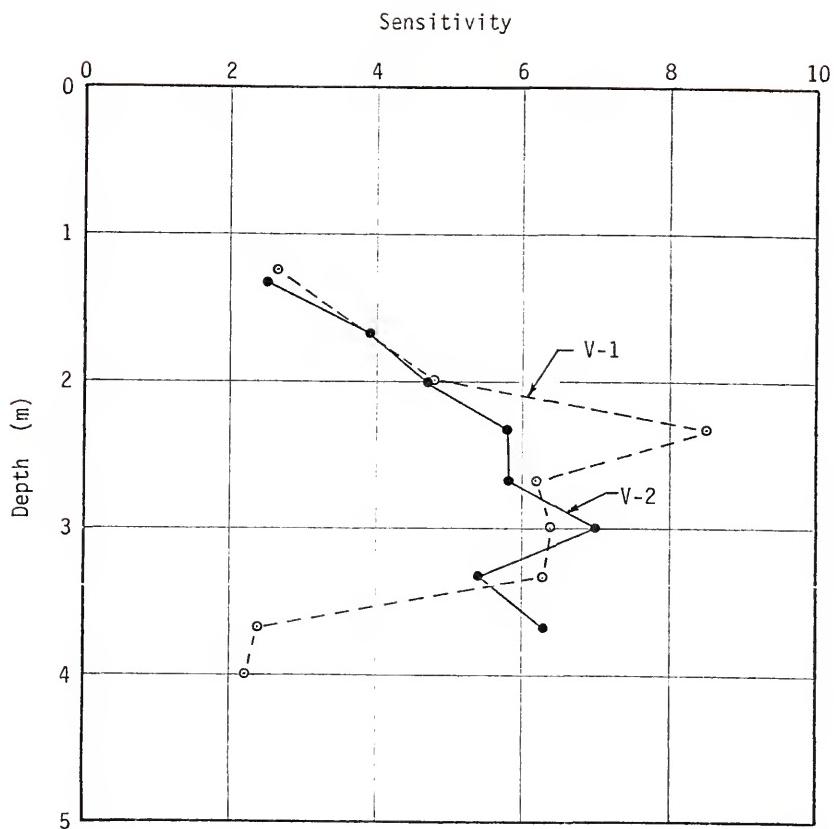
and remolded vane strength data are plotted in Fig 3.18. These values, ranging from 2.2 to 8.5 and averaging 5.0 indicate that this soil ranges from slightly to highly sensitive according to the criteria suggested in Leonards (1962). These values also indicate that considerable disturbance could occur during "undisturbed" sampling and sample trimming operations. Such disturbance could be responsible for some of the difference between the vane and triaxial shear test results.

#### 3.4 Pile-Soil Friction Tests

Laboratory direct shear tests were conducted to evaluate the effect of pile and penetrometer sleeve roughness on the friction acting on the pile and cone friction sleeve. These tests were performed by replacing the bottom half of the direct shear sample with steel or concrete blocks to simulate the pile or penetrometer sleeve surface.

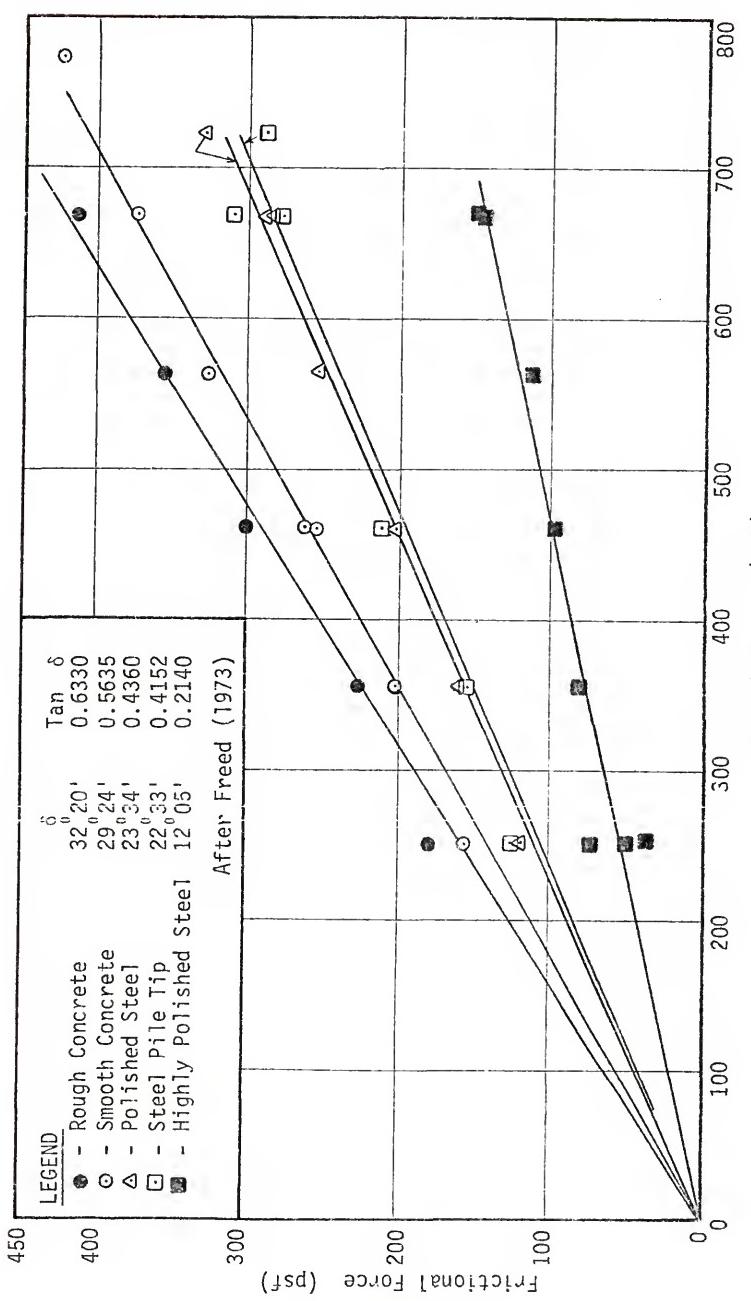
The friction tests for the Beville site sand were conducted by Freed (1973) and are described in detail in his thesis. He determined friction coefficients for five different surfaces varying from rough concrete to highly polished steel. The results of these tests are presented in Fig 3.19. The smooth and rough concrete friction tests were performed directly on the model pile surfaces, and the highly polished steel surface was machined to simulate the penetrometer friction sleeve surface. Surface roughness tests were performed to assure that polished steel and penetrometer surfaces were comparable. These surface roughness measurements were also described in detail by Freed.

Similar tests were performed by the author using samples of Paines Prairie clay. These tests were performed on remolded samples under consolidated-drained conditions in order to simulate the shear



PAINES PRAIRIE CLAY SENSITIVITY DATA

FIGURE 3.18



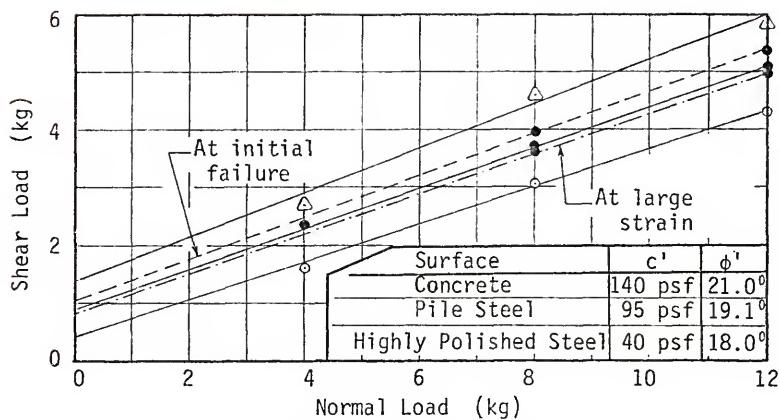
SUMMARY OF FREED'S DIRECT SHEAR TESTS  
FIGURE 3.19

that occurs at the surface of a pile driven into clay. Tests were conducted on a rough concrete surface and on Freed's polished and highly polished steel surfaces. The test results are shown as solid lines in Fig 3.20.

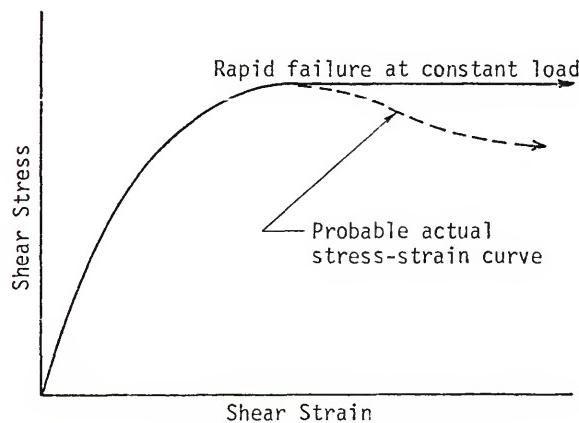
These tests were performed using controlled stress equipment; thus, it was impossible to define the stress-strain curve beyond the point of peak strength. Because of the large strains that occur when a pile is driven into a soil, it was thought that residual rather than peak remolded strength might be the controlling factor in pile friction behavior. One additional test was performed on the polished steel surface to investigate this effect. This test was conducted in the same manner as the previous tests until the initial failure occurred, at which time the shear load was removed and the sample was manually moved back and forth across the steel surface to induce much higher magnitudes of shear strain. This was continued until a total movement of about 2 ft had been attained. The shear load was then gradually reapplied until failure again occurred. The resulting failure envelopes for this test, shown as dashed lines in Fig 3.20, show that the additional sliding strain had little effect on the interface shear strength.

The shear surface that developed during the rough concrete friction tests occurred in the soil just above the concrete surface and not at the surface. Because of this, the results of these tests probably represent the remolded drained strength of the clay.

Similar soil-pile shear tests have been performed by Potyondy (1961) and Lingo (1962). The results of their tests cannot be directly related to this research because different soils were used



(a) RESULTS OF CLAY-PILE SHEAR TESTS



(b) TYPICAL STRESS-STRAIN CURVE

FIGURE 3.20

and qualitative surface roughness measurements were not made for their simulated pile materials. However, their results can be generally compared to the previously discussed tests and are useful in evaluating the full-scale pile tests presented in Chapter 9. Lingo and Potyondy's results, along with Freed's data, are summarized in Table 3.5 as ratios of  $\tan \delta$  for smooth steel to  $\tan \delta$  for the other materials tested.

TABLE 3.5

## SUMMARY OF SAND-PILE LABORATORY FRICTION TESTS

		Tan $\delta$ Ratios		
	Rough steel Smooth steel	Smooth concrete Smooth steel	Rough concrete Smooth steel	Wood Smooth steel
Freed	--	1.29	1.45	--
Potyondy	1.45	1.78	2.07	1.50
Lingo	1.37	1.27	1.45	1.32

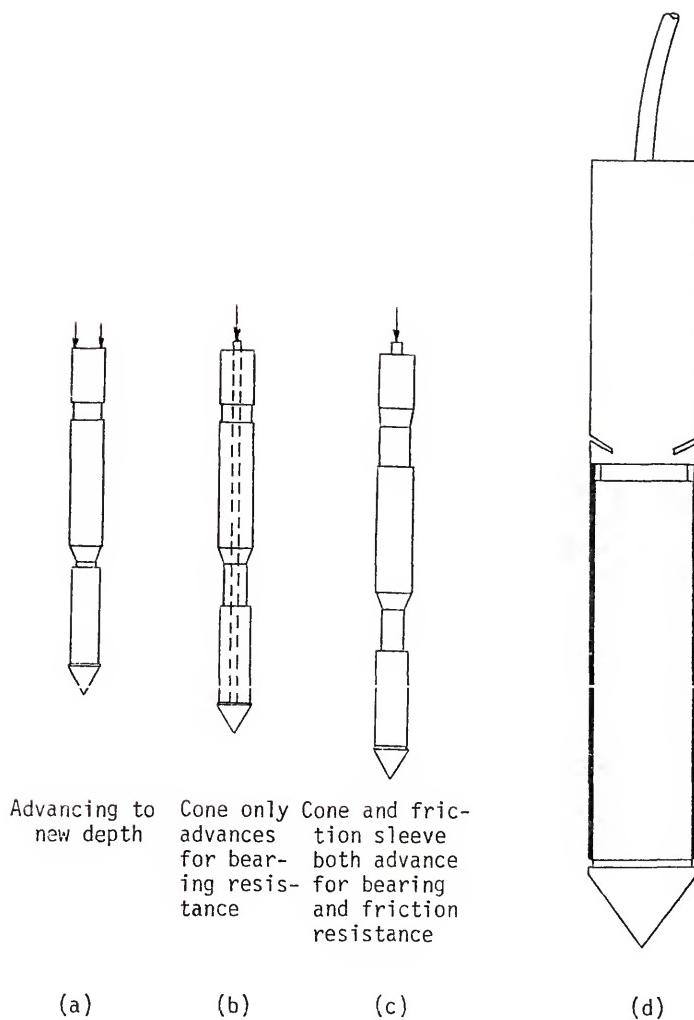
## CHAPTER 4

### EQUIPMENT FOR MODEL PILE RESEARCH

#### 4.1 Penetrometer Equipment

Two types of penetrometers were used during this research: a Begemann mechanical friction sleeve penetrometer and a Fugro electrical friction sleeve penetrometer. A 10 t hydraulic ram, designed and constructed especially for cone sounding by NV Goudsche Machinefabriek, was used to force the penetrometers into the ground. This equipment is mounted on a heavy-duty truck which provides the reaction weight for the penetrometer thrust load.

The mechanical penetrometer tip is equipped with a cone point having a projected area of  $10 \text{ cm}^2$  and an apex angle of 60 degrees. The friction sleeve, slightly larger in diameter than the tip, has a surface area of  $150 \text{ cm}^2$ . The center of the friction sleeve is located 20 cm above the base of the point. This tip is operated by a double push-rod system as shown in Fig 4.1. The tip is thrust to the test depth by pushing on the outer rods, and the test is then conducted by transferring the thrust to the inner rods. Thrusting on the inner rods causes the cone point to advance while the outer rods remain stationary. After the point advances approximately 3.5 cm (Fig 4.1b), the friction sleeve engages and moves simultaneously with the tip (Fig 4.1c). The tip is then advanced to the next test depth by again thrusting on the outer rods, which also causes the point and friction sleeve to return to their original position (Fig 4.1a). Two thrust



BEGEMANN MECHANICAL AND FUGRO ELECTRICAL FRICTION SLEEVE PENETROMETERS

FIGURE 4.1

load measurements are recorded during each penetration test: one during the point advance and the other while both the tip and friction sleeve are moving. The cone penetration resistance ( $q_c$ ) is determined from the first reading and the friction sleeve resistance ( $f_s$ ) is computed using the difference between the first and second readings.

The electrical penetrometer, shown in Fig 4.1d, is different from the mechanical penetrometer in both design and method of operation. The point of this penetrometer has the same dimensions as those of the mechanical tip, but the friction sleeve is located immediately above the point and no relative movement occurs between the point and tip during operation. Point and friction sleeve loads are measured simultaneously by two independent strain gauge load cells contained in the penetrometer body. An electrical cable, which replaces the inner push-rods in the mechanical penetrometer system, transmits the electrical signals from the load cells to the ground surface where they are monitored by a voltmeter or chart recorder. This penetrometer is pushed into the ground by a continuous thrust as opposed to the intermittent thrusting used with the mechanical system. The point and friction sleeve resistance can be recorded continuously with depth or at selected depth intervals.

One significant deficiency in the design of the electrical penetrometer furnished for this research was noted. The diameter of the cone point was found to be slightly larger than the diameter of the friction sleeve. This results in the point creating a hole slightly larger than the friction sleeve and could cause greatly reduced values of sleeve friction to be recorded. This deficiency was eliminated by having the point machined to a diameter 0.002 in smaller than that of the friction sleeve.

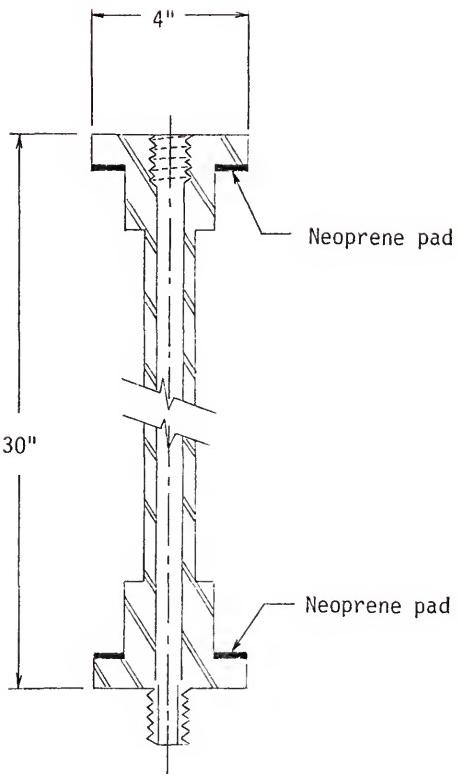
#### 4.2 Model Piles

Three model piles had been constructed by a previous investigator at the University of Florida during a pile capacity research project which was never completed. These included a constant diameter pipe pile, a square precast concrete pile, and a round step-taper pile. These piles were used for this research project since they represented a good cross section of the types of piles in common use today.

The model pipe pile had a diameter of 4.0 in and was constructed in 2.5 ft sections so that the pile length could be varied. Later modifications changed the length of the tip section to 2.25 ft. The apex angle of the point for this pile was 120 degrees. Five pile sections were available, permitting fabrication of a pile 12.25 ft long.

The concrete pile, with a side dimension of 4.0 in, was also constructed in 2.5 ft sections. Addition of a load cell to the first section of this pile extended its length to 3.67 ft. This section was fitted with a point having a 90-degree apex angle. Four additional sections were available, permitting assembly of a pile 13.67 ft long. Each section of the concrete pile contained a central hollow steel core and steel end plates as shown in Fig 4.2. Piles with both rough and smooth surface textures were constructed by using forms of different roughness to cast concrete around the steel core section.

The step-taper pile consisted of four sections of different diameter as detailed in Table 4.1. This permitted assembly of a pile 10.1 ft long. This pile also had a 90-degree point apex angle.



INNER CORE OF MODEL CONCRETE PILE

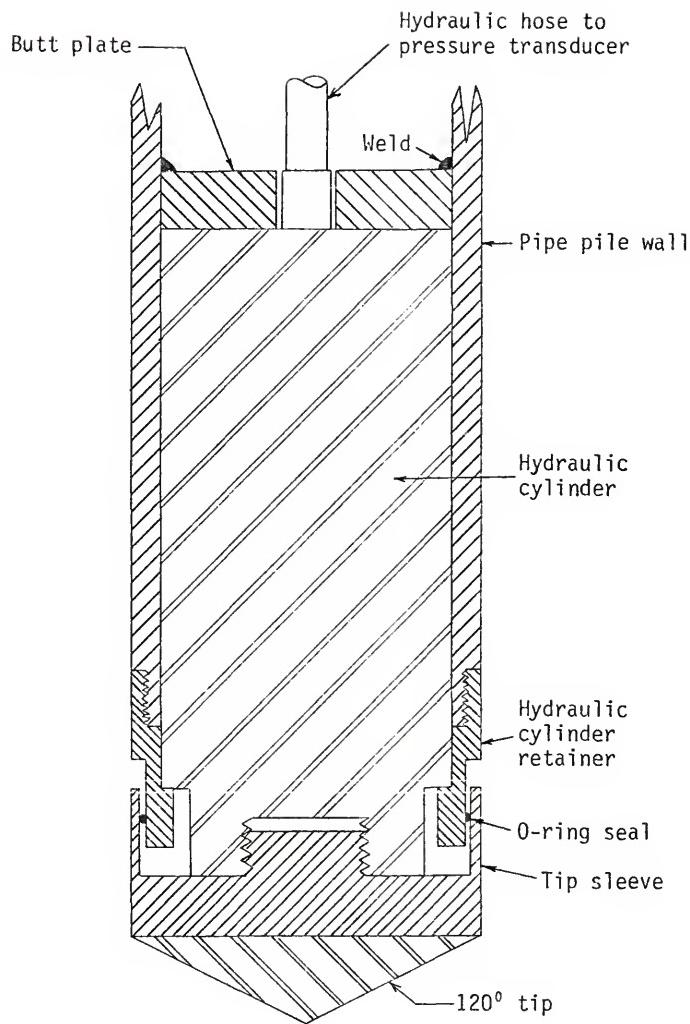
FIGURE 4.2

TABLE 4.1  
STEP-TAPER PILE SECTION DIMENSIONS

Section No.	Diameter (in)	Length (ft)
1	2.875	2.60
2	3.520	2.50
3	4.020	2.50
4	4.520	2.50

Since any static pile capacity analysis methods which could be imagined would require separate evaluation of point and side friction resistance, it was considered important that a means be provided for separating total pile resistance into these two components. Previous attempts had been made to place electrical strain gauge load cells in the tips of the model piles, but these load cells could not withstand pile driving stresses. While evaluating other methods of measuring the pile tip load, this investigator was impressed with the reliability and durability of the hydraulic load cell used with the cone penetrometer sounding equipment. After evaluating a hydraulic load cell system and discussing the problem with a hydraulics equipment engineer, it was decided to construct a load cell of this type, place it on a model pile, and test it under field conditions.

Fig 4.3 shows the basic design for the first load cell constructed. This cell consisted of a 25 t capacity Enerpac Model RC-256 hydraulic cylinder fitted into the pile end. The pile tip was designed to thread into the ram of the hydraulic cylinder, and a rubber O-ring seal was placed between the pile point sleeve and the shaft of the pile. A



MODEL PIPE PILE LOAD CELL

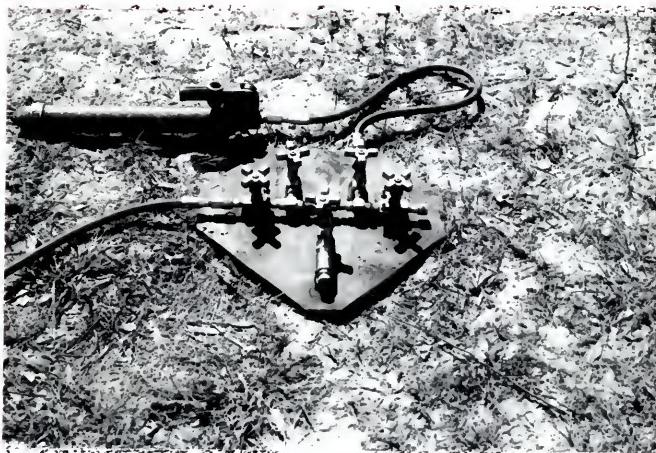
FIGURE 4.3

high-pressure hydraulic hose connected to the cylinder extended through the center of the pile and connected to a pressure measuring system at the ground surface. The pressure measuring system consisted of a MB/Alinco Model 151 high precision 5000 psi transducer and a strip chart recorder. This transducer was connected to a valve manifold, as shown in Fig 4.4, which permitted the transducer to be isolated during pile driving.

This system performed flawlessly during several load tests on the pipe pile driven at three different locations at the Fairbanks site; thus, the other two model piles were fitted with similar load cells. A hydraulic cylinder identical to that used in the pipe pile was placed in the concrete pile load cell. It was necessary to place this cylinder in a steel housing attached which attached to the end of the pile as shown in Fig 4.5. The difference in surface texture between the steel housing and the remainder of the concrete pile presented some difficulties in evaluating the side friction data from this pile. A carefully machined Teflon seal was placed in the tip assembly to prevent soil contaminants from entering the tip and to provide a low-friction connection between the point sleeve and the pile shaft. Exploded and fully assembled views of this load cell are shown in Fig 4.6. An Enerpac Model RC-102 10-ton hydraulic cylinder was used for the step-taper pile load cell; otherwise, this unit, shown in Fig 4.7, was identical in design to the pipe pile load cell.

#### 4.3 Pile Driving and Load Testing Equipment

An Acker portable aluminum tripod and motorized cathead was used with a 140 lb standard penetration test hammer to drive the model piles. Driving was accomplished using a 1.0 in diameter manila rope wrapped

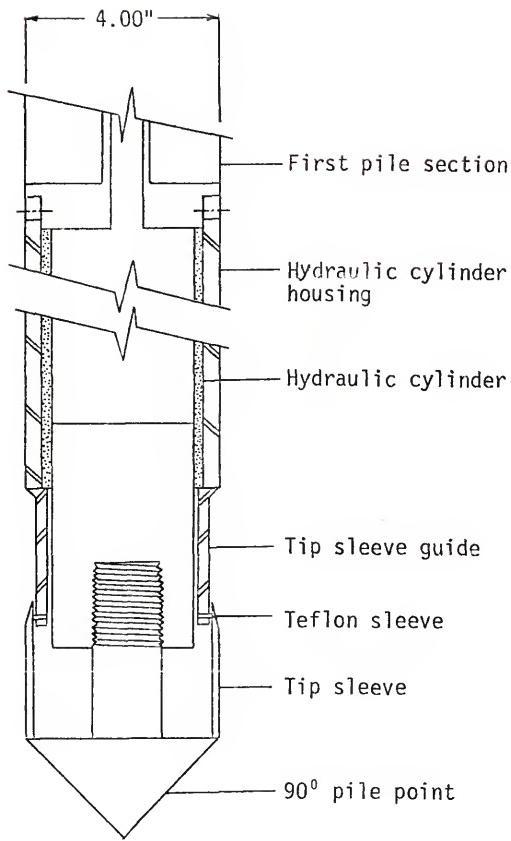


#### List of Components

- a - Auxilliary hydraulic pump
- b - Electronic pressure transducer
- c - Hydraulic hose to tip load cell

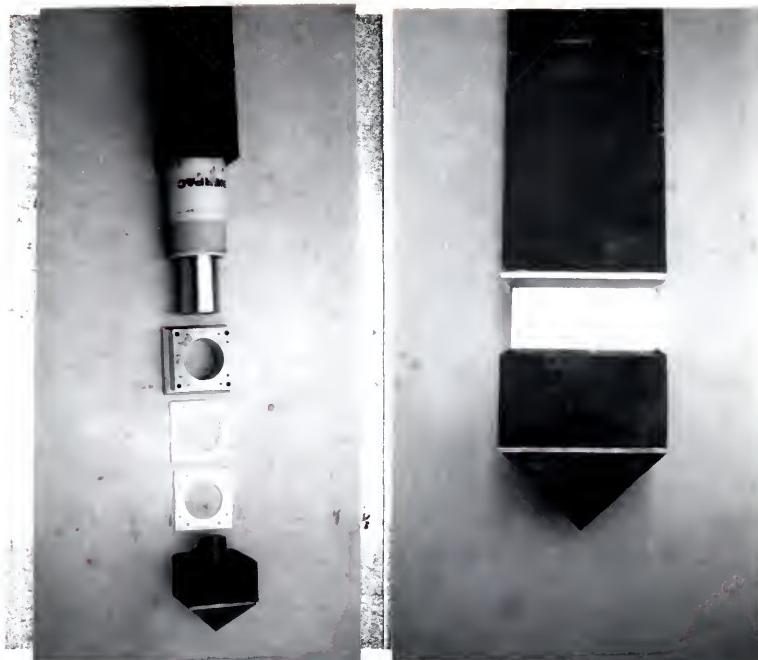
TRANSDUCER VALVE MANIFOLD

FIGURE 4.4



CONCRETE PILE LOAD CELL DETAILS

FIGURE 4.5



#### List of Components

- a - Pile tip
- b - Teflon bushing retainer
- c - Teflon bushing
- d - Hydraulic cylinder retainer
- e - Hydraulic cylinder
- f - Concrete pile tip section

EXPLODED AND ASSEMBLED VIEWS OF CONCRETE PILE LOAD CELL

FIGURE 4.6



Exploded  
View

Assembled  
View

List of Equipment

- a - Pile tip
- b - Rubber O-ring
- c - Cylinder retainer
- d - Hydraulic cylinder
- e - Pile

EXPLODED AND ASSEMBLED VIEWS OF STEP-TAPER PILE LOAD CELL

FIGURE 4.7

four turns around the 4.5 in diameter cathead. A pile driving head containing a 9.5 in diameter by 1.0 in thick Mikarta cushion block was fabricated for use with this system. Fig 4.8 shows the pile driving equipment in operation.

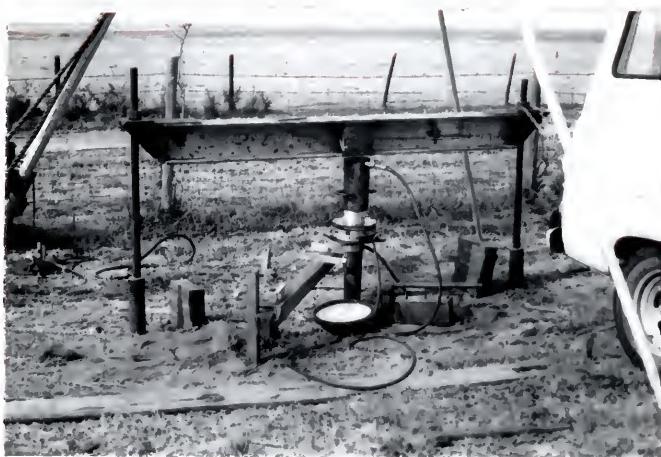
Reaction for the pile load was obtained through a beam and reaction pile system as shown in Fig 4.9. Standard 3.5 in OD (NW) flush-joint drill casing was used for reaction piles. These reaction piles were driven open ended to minimize soil displacement and compaction around the piles. Two 8WF30 steel beams fitted with special end connections were attached to the reaction piles by threaded AW drill rods. Two beams and four reaction piles were normally used for tests in sand, while one beam and two reaction piles were used for testing in clays. This system was designed such that the reaction piles would be located 4.1 ft from the center of the test pile location to minimize the effect of the reaction piles on the load test results and to provide a beam system that would supply adequate reaction capacity with beams that could be handled manually by two persons.

Two methods were used to evaluate the possible effect of the reaction piles on the load test results. One method, proposed by Hansen (1968), uses conventional soil mechanics theory to account for the changes in horizontal stress causes load transfer between the pile and surrounding soil. The second theory, presented by Banerjee (1970), examines the effect of the reaction piles on the observed settlement of the test pile. In this analysis, the piles were assumed to be rigid bodies and the soil is treated as an elastic half-space. Solutions to both of these methods for various test pile-reaction pile spacing are presented graphically in Fig 4.10. These solutions are based on four



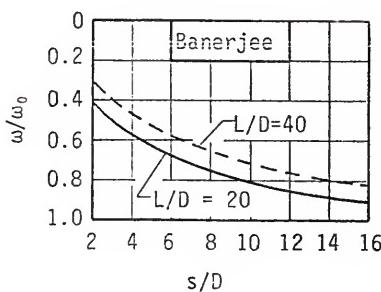
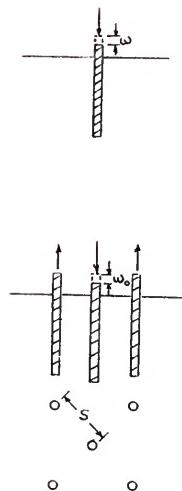
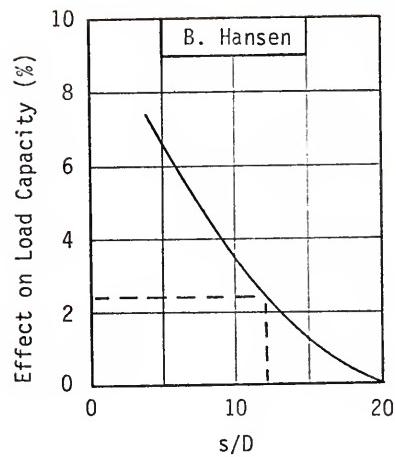
MODEL PILE DRIVING EQUIPMENT

FIGURE 4.8



LOAD REACTION BEAM AND PILES

FIGURE 4.9



GRAPHS OF POSSIBLE REACTION EFFECTS

FIGURE 4.10

reaction piles equally spaced around the test pile. They indicate that the reaction piles should not cause a difference of more than 5% in the side friction capacity and that the observed settlement should not be more than 20% in error since the L/D ratio for the test piles was generally 30 or less. Effects of these magnitudes were considered permissible and are much less than would occur during a typical pile load test, where the test pile-reaction pile spacing is generally on the order of 5 to 7 test pile diameters as opposed to the spacing of about 12 diameters for the model pile set-up.

Difficulties were encountered in preventing pile wobble during driving in sands. In some cases, this causes an enlarged hole to form around the upper part of the piles and almost certainly was affecting the side friction resistance of the piles. A driving guide securely positioned between the anchor piles by chains and turn-buckles eliminated this problem. Fig 4.11 shows a pile being held in position for driving by the driving guide.

A 50 t hydraulic ram and remote pump were used to load the piles driven in sand, and a 10 t ram was used for piles driven in clay. The applied butt load was measured using a Martin-Decker 30,000 lb hydraulic load cell placed on top of the pile. This loading equipment is shown in place on a test pile in Fig 4.12. Deflection of the test pile was measured using two 0.001 in dial gauges mounted on an 8 ft long laminated wood reference beam. Fig 4.13 shows the dial gauge set-up, and Fig 4.14 shows a completed load test assembly.

The load testing apparatus was sheltered during each test with a canvas cover to minimize the effect of temperature changes. The tip load cell was found to be sensitive to changes in ambient temperature,



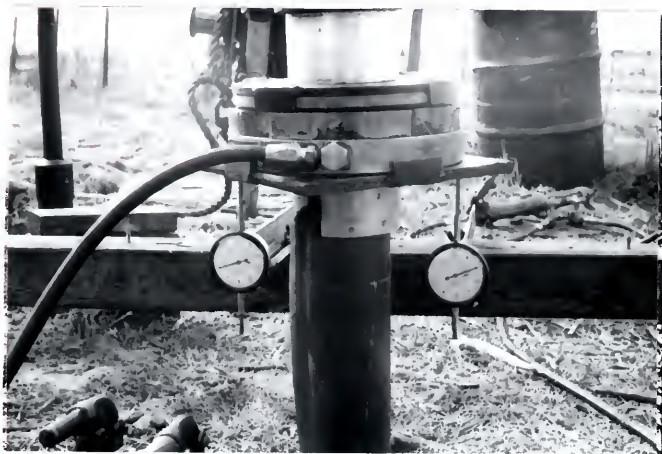
MODEL PILE DRIVING GUIDE

FIGURE 4.11



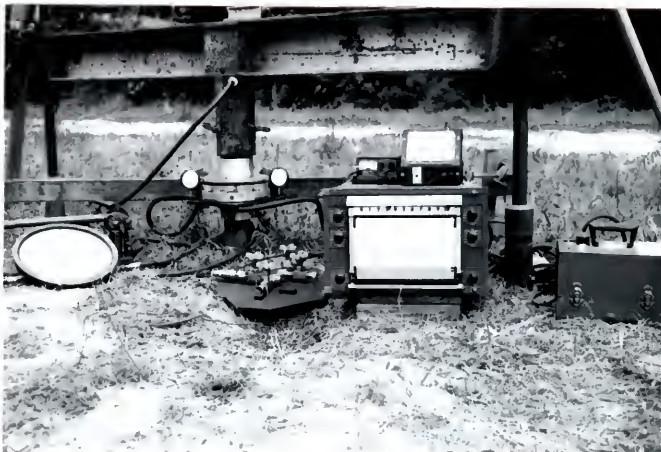
MODEL PILE LOADING EQUIPMENT

FIGURE 4.12



MODEL PILE SETTLEMENT GAUGES

FIGURE 4.13



COMPLETE MODEL PILE LOAD TEST SET-UP

FIGURE 4.14

even when the canvas cover was in place. Exposure of a portion of the black hydraulic hose leading to the load cell was found to be responsible for this problem. This was eliminated by burying the exposed hydraulic hose a short distance below ground surface.

## CHAPTER 5

### MODEL PILE TESTING TECHNIQUES

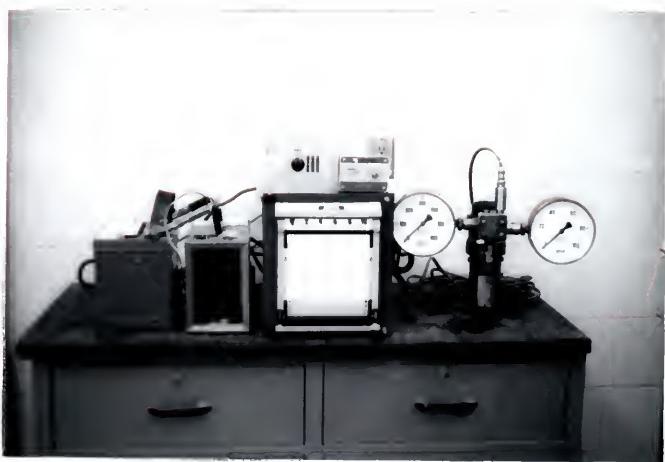
Chapter 4 described the basic equipment used in the model pile testing program and discussed the design and operation of this equipment. This chapter describes the manner in which the tests were performed and presents the results of supplementary research conducted to assist in establishing test procedures.

#### 5.1 Penetration Testing

##### 5.1.1 Mechanical Penetrometer Soundings

A hydraulic load cell equipped with Bourdon gauges is normally used to measure penetration resistance during mechanical CPT soundings. An alternate means of measuring penetration resistance is to use electronic pressure transducers mounted in the hydraulic load cell in conjunction with a strip chart recorder. The pressure transducer method was used for all soundings at the model pile test sites because it permits obtaining more accurate and consistent data. Fig 5.1 shows the load cell which attaches to the hydraulic ram used for penetrometer thrusting along with the transducers, recorder, and other necessary electronic equipment.

A typical record of a mechanical CPT test and the manner in which these data are interpreted are shown in Fig 5.2. The resistance curve generally rises rapidly at the beginning of a test as point resistance is mobilized. The curve then flattens out and usually maintains a

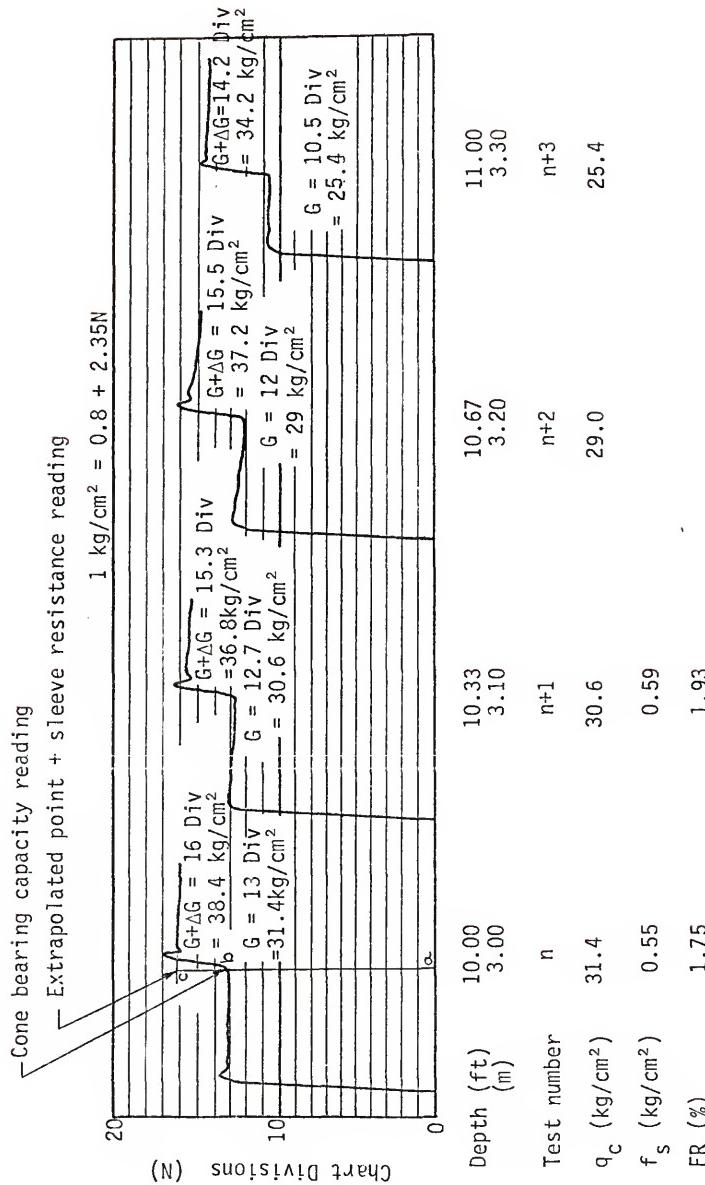


#### List of Equipment

- a - Storage battery
- b - DC to AC power converter
- c - Chart recorder
- d - DC power supply for transducer
- e - Hydraulic load cell
- f - Pressure transducer

MECHANICAL PENETROMETER LOADING HEAD AND RECORDING EQUIPMENT

FIGURE 5.1



TYPICAL MECHANICAL PENETROMETER SOUNDING RECORD

FIGURE 5.2

constant slope throughout the remainder of the point-only penetration. This slope may reflect an increasing, decreasing, or constant penetration resistance with depth, depending on the type and condition of the soil being penetrated. A second sharp rise in the penetration resistance record occurs at the point where the friction sleeve engages and begins to move with the point. This portion of the curve also tends to flatten out and approach a constant slope reflecting the resistance to both the point and friction sleeve movement. The overshoot, which usually occurs at the beginning of the friction sleeve movement, is thought to be caused partly by the added force necessary to accelerate the friction sleeve, partially by the change from static to moving friction, and partially by inertia of the recording system. This small portion of the curve is ignored when interpreting the data.

The penetrometer point resistance ( $q_c$ ) is determined from the abscissa of the penetration resistance curve at the point where the friction sleeve is engaged (distance a-b from Fig 5.2). To determine the friction sleeve resistance, the second straight line portion of the penetration resistance curve is projected back to intersect an extension of line a-b. Since a-c equals the combined point and friction sleeve resistance, b-c represents the sleeve resistance. Because of the design of the Begemann mechanical friction cone, the sleeve resistance measured with the tip at a certain depth corresponds to a depth 20 cm less than that of the point.

The following equations were used to compute  $q_c$ ,  $f_s$ , and friction ratios (FR) from the strip chart records:

$$(q_c)_n = C (G)_n \quad (5.1)$$

$$(f_s)_n = C (\Delta G)_{n+2} \quad (5.2)$$

$$(FR)_n = \frac{(q_c)_n}{(f_s)_n} (100\%) \quad (5.3)$$

where

$n$  = the CPT test number where the tests are numbered consecutively from top to bottom of a sounding

$c$  = calibration constant for the load cell-transducer-recorder assembly

$G$  = distance a-b

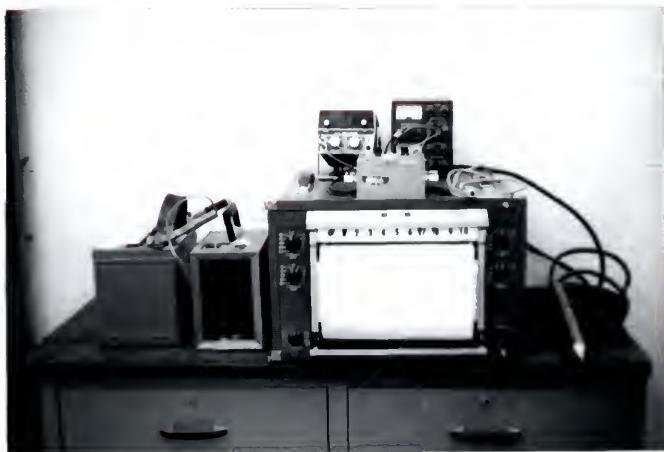
$\Delta G$  = distance b-c

The use of  $(\Delta G)_{n+2}$  in Eq 5.2 is necessary to account for the 20 cm separation between the point and friction sleeve since tests were performed at 10 cm depth intervals in all soundings conducted at model pile test sites. The constant (C) was determined by carefully calibrating the load cell and recording equipment in the laboratory before performing CPT soundings. This calibration was checked periodically during the course of the sounding work.

The cone penetration rate during each test was controlled at about 2 cm/sec in accordance with ASTM Tentative Specifications for Quasi-Static Cone Penetration Testing (1974). A penetration rate of about 6 cm/sec was used to advance the cone between sounding depths.

#### 5.1.2 Electrical Penetrometer Soundings

Electrical penetrometer resistance measurements were made using a multi-channel strip chart recorder which permitted recording separate plots for point and sleeve friction resistance. The penetrometer and complete recording system are shown in Fig 5.3. This penetrometer tip was advanced continuously at a rate of 2 cm/sec during each sounding, except for short delays to add 1.0 m long sections of push rods. Penetration resistance was recorded continuously during each sounding,



#### List of Equipment

- a - DC storage battery
- b - DC to AC power converter
- c - Chart recorder
- d - Digital voltmeter
- e - DC power supplies for penetrometer load cells
- f - Balance circuitry for penetrometer load cells
- g - Electrical penetrometer

#### ELECTRICAL PENETROMETER AND RECORDING EQUIPMENT

FIGURE 5.3

and a depth record was maintained on the chart paper by use of a recorder event marker. Fig 5.4 presents a portion of a typical electrical sounding record.

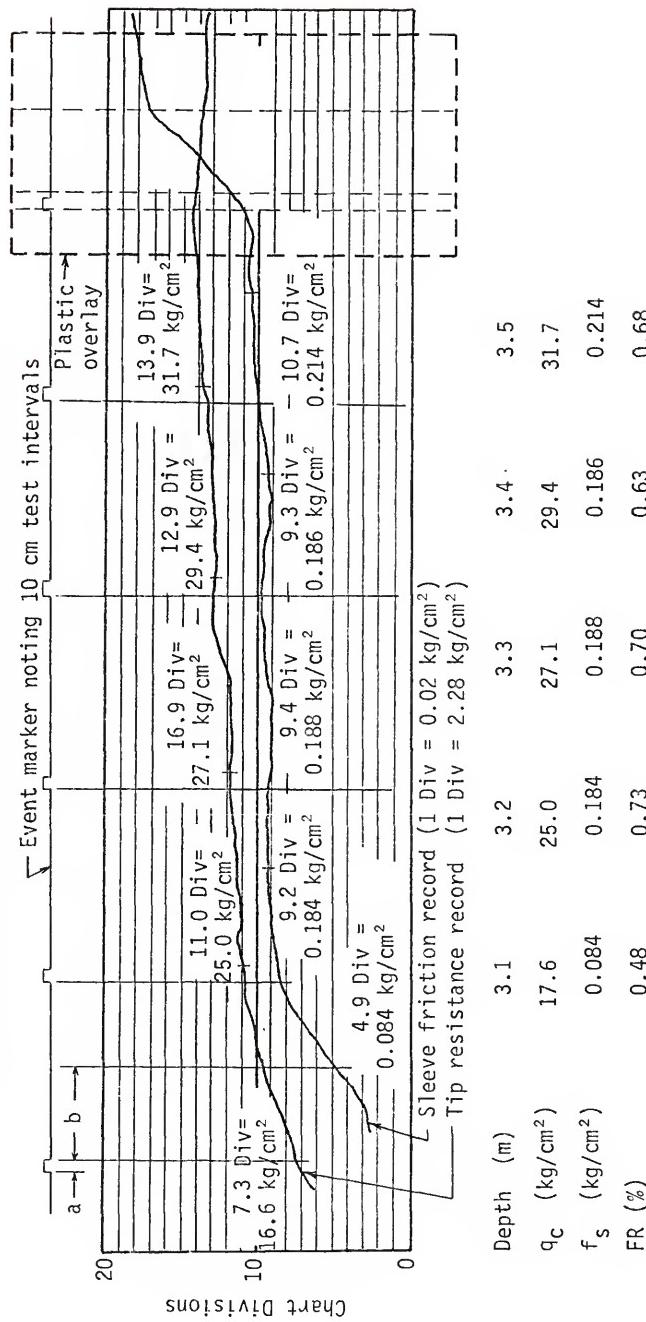
Although penetration resistance was recorded continuously during the electrical CPT soundings, only data at 10 cm depth intervals were analyzed and presented on CPT logs. When analyzing the data in this manner, it was necessary to account for the position offset of the recorder pens and the 6.5 cm distance between the cone point and the center of the friction sleeve. These factors resulted in the sleeve resistance record for a particular depth lagging behind the point resistance record for the same depth. A transparent plastic overlay with guidelines drawn at appropriate spacing was used to simplify transferring data from the chart records. Using this overlay, the abscissas of the point and friction sleeve resistance plots were determined for each depth interval, and the corresponding  $q_c$  and  $f_s$  values were determined by multiplying the abscissas by calibration factors for the point and friction sleeve load cells.

The electrical penetrometer was calibrated before and at periodic intervals during the sounding programs. A calibration study was also performed to determine the amount of load transfer that occurs between the two load cells. This was accomplished by loading the point while maintaining zero load on the friction sleeve and vice versa, while recording the output of both load cells. This study showed the effect of load transfer to be negligible.

## 5.2 Pile Load Testing in Sand

A number of methods for conducting pile load tests have been used. The most common method consists of applying load to the pile in

- a = lag distance between event marker pen and cone point pen on chart recorder  
 b = distance between point resistance and sleeve friction pens to account for vertical distance between point and center of friction sleeve



TYPICAL ELECTRICAL PENETROMETER SOUNDING RECORD

FIGURE 5.4

increments, with each load increment being maintained at a constant level until a certain period of time has elapsed or until the rate of pile settlement reaches some minimum specified value. This type of test is usually referred to as a maintained load (ML) test. A second test method that has been used frequently in recent years is the constant rate of penetration (CRP) test. In this test, the pile is forced into the ground at a constant rate, with load and settlement data being recorded continuously or at specified settlement intervals. A third method of load testing was considered for use during this study. In this method, the load is increased to a certain level and the pile is allowed to "relax". During the relaxation period, the pile settlement gradually increases while the applied load decreases. This relaxation process is continued until the time rate of change of both settlement and applied load approaches zero, at which time the load is increased to a higher value. This method of testing will be referred to as the load relaxation (LR) test.

Each of these three methods was considered for load testing the model piles driven in sand and each offered certain advantages and disadvantages. The MLT appeared to be the best model of the manner in which load is applied to an actual service pile and should provide the most realistic load-settlement data. The main disadvantage of this test is the amount of time normally required to complete a load test.

The CRP test is not a good model of actual pile load application; however, Fuller and Hoy (1970) report that tests completed in 30 to 60 min using this method provide ultimate pile capacities which are generally within 5% of those determined by the ML test method. The time required to complete a CRP test made this method attractive; however,

the ability of the method to provide realistic load-settlement data was questioned. The CRP test method was rejected for this reason.

The main advantage offered by the LR test method was the ease of performing the test since constant attention would not be required to maintain the pile load at a constant value. The disadvantages of this test were:

1. Insufficient data were available in the literature to ascertain that data obtained using this method correlated well with data obtained using the standard ML test.
2. Condition of the loading equipment for performing this test was more critical than for the other test methods. Any volume changes in the hydraulic loading system (leaking seals and fittings, thermal expansion and contraction, etc.) would cause errors in the test data.

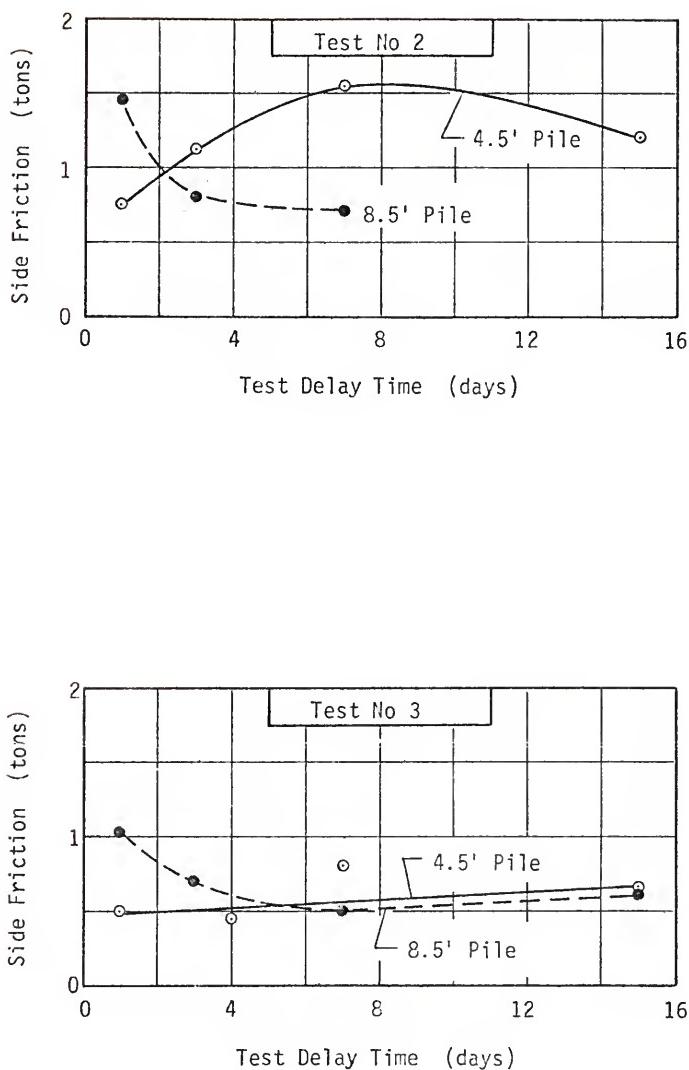
Because of these disadvantages, this test method was also rejected and the ML test was selected as the best available method for obtaining reliable data.

Another factor which was considered important in the model testing program was the delay time between driving and testing each pile. Although excess pore pressures generated during pile driving should dissipate rapidly in sands, it was thought that corrosion of the pile and chemical bonding at the pile-soil interface might cause a significant change in side friction resistance with time. Load tests were performed on piles driven at two locations at the Fairbanks site to evaluate this effect. The steel pipe pile was used for these tests because any corrosion or chemical bonding effect should be more pronounced for steel than for concrete. Each of these piles was driven to depths of 4.5 and 8.5 ft and tested after delay times of 1, 3, and 7 days. In addition, the 4.5 ft pile at one location and the 8.5 ft pile at the other location were tested after a 15-day delay time. Delay

time was defined as the time between driving and testing or between successive tests.

The results of these tests, shown in Fig 5.5, were inconclusive. The 4.5 ft pile at Location No 2 showed an increase in side friction with time to a delay time of 7 days and a decrease between delay times of 7 and 15 days. The data for a pile of the same length tested at Location No 3 did not exhibit any definite trends but indicated a slight increase in friction with time. Tests at both locations performed on 8.5 ft piles resulted in a decrease in side friction with time to a delay time of 7 days; however, the test at Location No 3 showed a slight friction increase between set times of 7 and 15 days. Because these data were inconclusive, a decision was made to perform subsequent tests in sand one day after driving. It was thought that this would allow sufficient time for dissipation of any excess pore pressure which might be generated but would not allow time for a significant amount of chemical action to occur at the pile-soil interface. Additional data on the time-side friction behavior of piles in sands would be valuable but could not be gathered during this project without reducing the scope of other project phases. Time-friction behavior would provide a good topic for an independent research project.

The Fairbanks site test data presented in Fig 5.5 also presented another interesting problem concerning load test procedures. The model piles were built in sections so that piles of different lengths could be driven and tested at the same location to provide shaft friction distribution data. A number of piles were to be tested at the same location by driving the pile to a greater depth after each test rather than driving piles of different lengths at different locations. This



EFFECT OF TEST DELAY TIME ON SIDE FRICTION

FIGURE 5.5

procedure was questioned because the Fairbanks data showed a decrease in total side friction capacity with an increase in pile length.

Although this phenomenon appeared to be caused by pile wobble during driving, creating an enlarged hole around the pile, it was thought that the process of driving, load testing, adding additional pile sections, and redriving might be influencing the results. Because of this, some tests on model concrete piles were performed at the Beville site on piles of different lengths driven at the same location and some were performed on piles of different lengths driven at different locations. The guide sleeve described in Chapter 4 was used to eliminate wobble during driving of these piles. Data from these tests, presented in Chapters 6 and 7, did not show a significant difference between the two test procedures; thus, subsequent tests on the pipe and step-taper pile were performed on piles of increasing length driven at the same location.

The size of load increments used for each test was selected to provide 7 to 10 data points well spaced along the load-settlement curve. Each load test was continued until pile settlement was at least equal to 20% of the pile diameter on side dimension, with each load increment being maintained on the pile until the rate of settlement was equal to or less than 0.010 in for a 5 min period. This settlement criterion was usually met very quickly (5 to 10 min) for the first few load increments, but often required a 30 to 60 min period for load increments which fell on the failure portion of the load-settlement curve. After completion of load testing, the piles were generally unloaded by reducing the butt load in four to five equally spaced increments.

Before the start of each test, the zero setting for the pile tip load cell and recording apparatus was checked and adjusted and a reading was taken to determine the residual pile forces resulting from pile driving. The pile tip load was recorded continuously during each test, and pile settlement and butt load were recorded at frequent time intervals. After unloading, a final tip load cell reading was made to determine the after-test residual pile loads.

### 5.3 Pile Load Testing in Clay

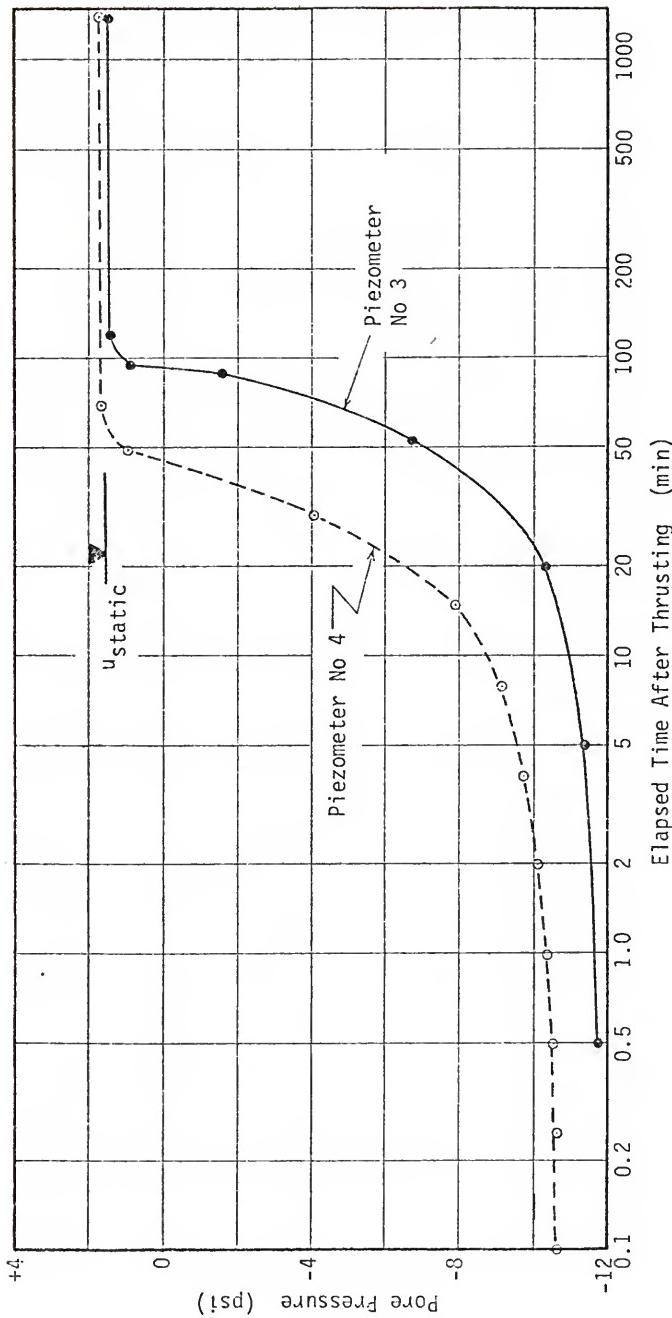
Since actual foundation piles driven in clay are generally loaded slowly and are required to support relatively constant loads for long periods of time, the soil which provides pile support behaves in a drained manner. It was considered important that the model pile load tests for this study also be performed under drained soil conditions to properly model actual pile behavior. To assure that this criterion was met, it became necessary to define a minimum delay time between driving and load testing that would assure full dissipation of excess pore pressures generated during driving.

A study was conducted at the Paines Prairie site to define the required delay time using two Geonor vibrating wire piezometers. The Geonor piezometer tip is 3.2 cm in diameter and has a conical point; thus, it is a good model of both the cone penetrometer and the model pipe pile. A porous bronze pore-pressure sensing element is located 2.3 cm above the base of the piezometer point. Two series of tests were performed using these piezometers. In the first series, the piezometers were thrust into the ground and the time-rate of pore pressure decay after completion of the thrusting operation was measured. In

the second test series, the model pile was driven between the piezometers, and both the generation of pore pressure during driving and the rate of pore pressure dissipation after driving were measured.

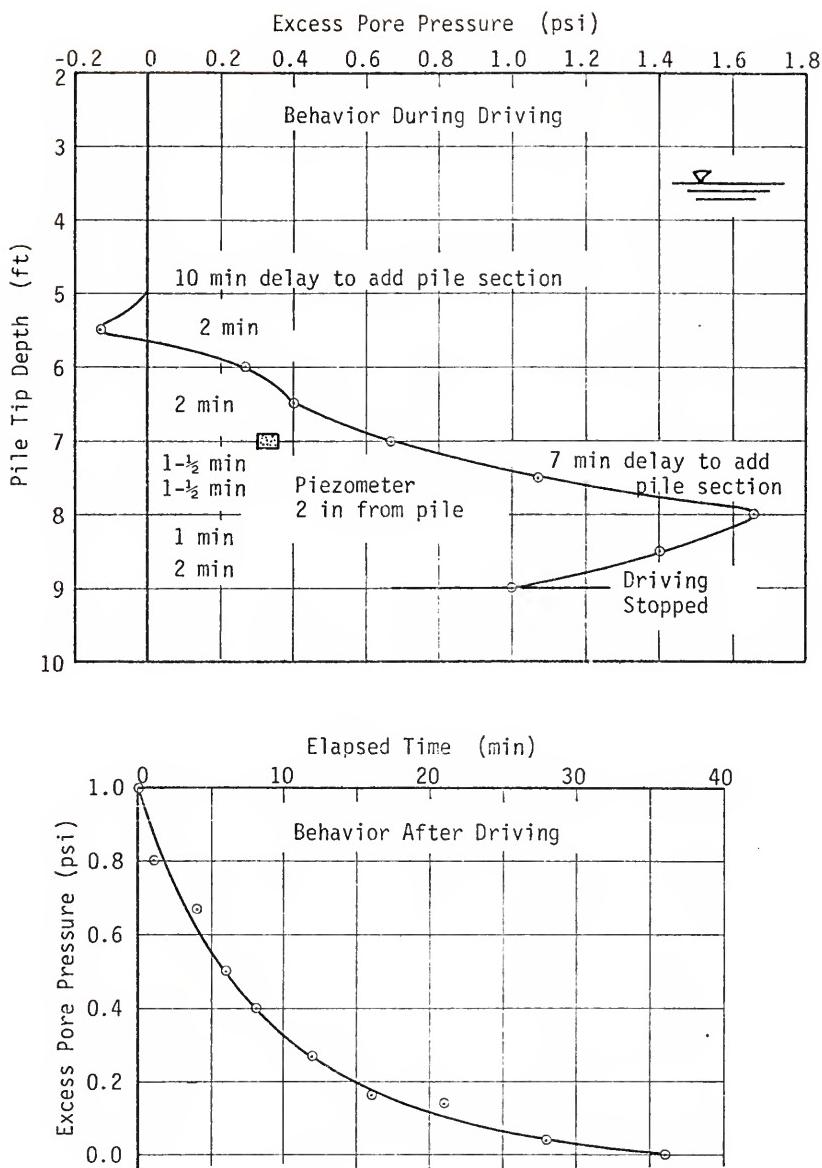
Fig 5.6 shows the results of the first series of tests. Both piezometers, placed at a depth of 7 ft, showed an initial negative excess pore pressure of about -13 psi. Time for complete dissipation of this excess pore pressure varied from 70 to 120 min. The negative excess pore pressures were surprising since the soil at this site did not appear sufficiently stiff and overconsolidated to produce strong dilatant behavior. It was thought that the negative pore pressures might be caused by the design of the piezometer tip rather than by dilatant behavior of the soil. This seemed possible because the pore pressure sensing element is located just above the piezometer point, a region which is shown to be in tension by the solution to Mindlin's equation for a pile embedded in an elastic soil. This solution indicates a zone of negative pore pressure could develop just above the point as a result of soil tension, even though positive pore pressures were created below the point. The second piezometer test was performed to investigate this possibility.

The second test was conducted using the piezometers installed during the first test series. The 4 in diameter model pipe pile was driven between the piezometers, at a distance of 2 in from Piezometer No 3 and 4.0 ft from Piezometer No 4. The pore pressure generated at Piezometer No 3 during driving and the time-rate of pore pressure decay are shown in Fig 5.7. No change in pore pressure occurred at Piezometer No 4. These data confirm that the pore pressure generated below the tip of a penetrating object is positive in the Paines Prairie clay.



PORE PRESSURE DECAY AFTER PIEZOMETER THRUSTING

FIGURE 5.6



PORE PRESSURE BEHAVIOR DURING AND AFTER PILE DRIVING

FIGURE 5.7

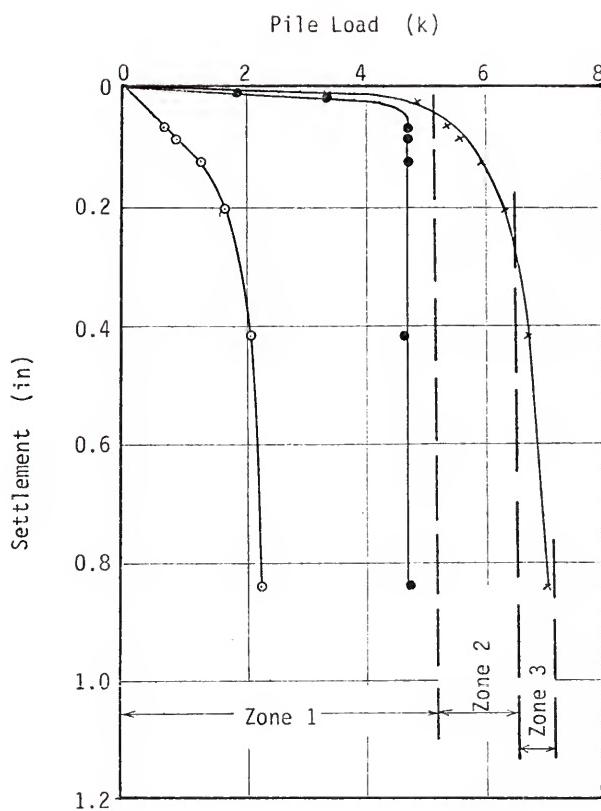
A change in pore pressure did not occur until the pile tip was within 2 ft of the piezometer depth which, coupled with the fact that no pore pressure change occurred at a lateral distance of 4 ft from the pile, shows that the region of pore pressure change around the driven pile was very limited. The excess pore pressure generated during pile driving completely dissipated within 40 min after termination of driving.

The rate of excess pore pressure decay after piezometer insertion and pile driving indicated that fully drained soil conditions should exist around the pile within 2 hrs after pile driving; however, no pile load tests were started until two full days had elapsed since driving. The minimum 2-day waiting period was chosen to provide an ample safety factor with respect to the pore pressure delay time and for convenience in maintaining a testing schedule.

In addition to starting the load tests under fully drained soil conditions, it was desired to also perform the tests under drained conditions. Clark and Meyerhof (1972) and Airhart *et al.* (1967) have presented data indicating that excess pore pressures generated in clays during pile load testing are small in comparison to those generated during pile driving and that these pore pressures have little effect on the pile load capacity. To check the behavior in the Paines Prairie soils, the two Geonor piezometers were installed near a test pile location, and pore pressures were to be monitored during a load test. However, the piezometer readout equipment malfunctioned before the load test could be performed. Since the project could not be delayed while the piezometer equipment was repaired, it became necessary to infer pore pressure behavior from the measured behavior of

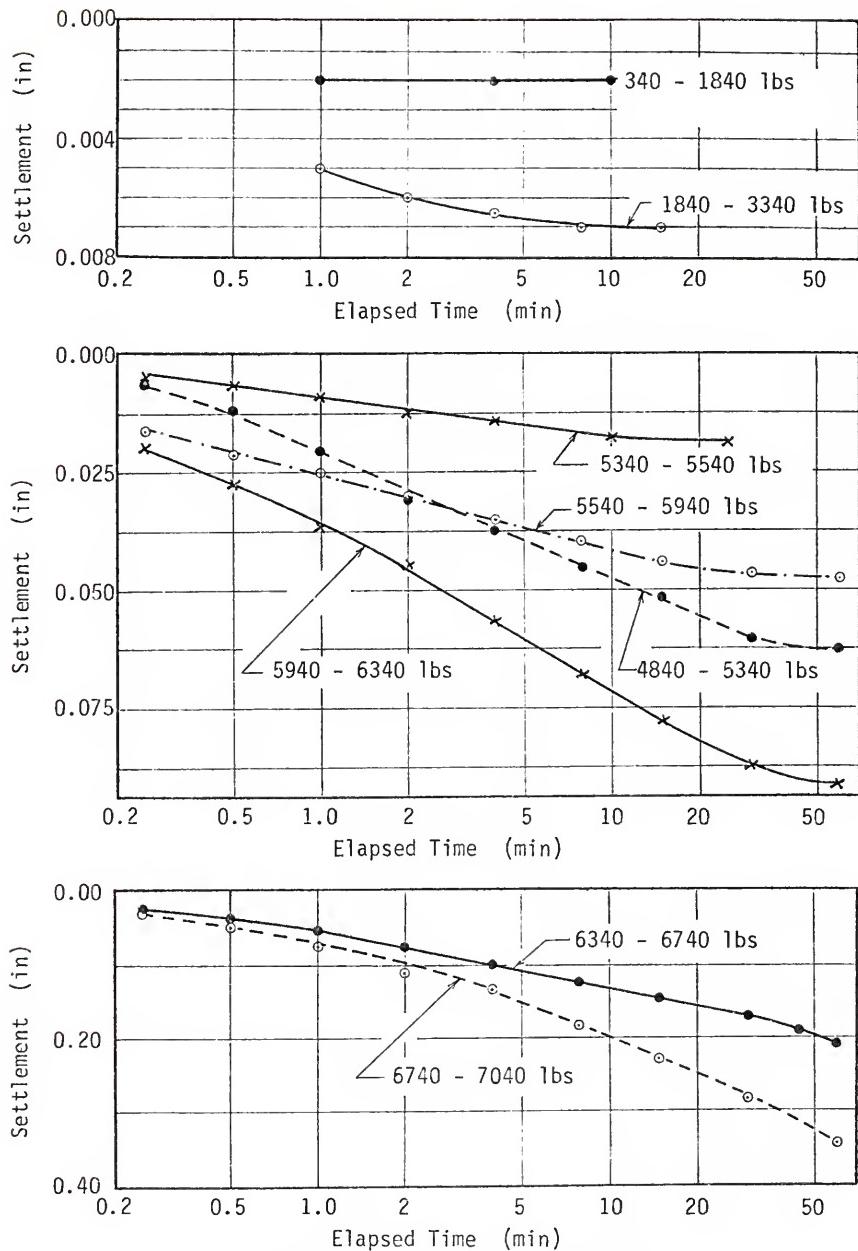
the pile during load testing.

A pile load-settlement curve, time-settlement data for each load increment, and pile point resistance-time curves from a typical load test are presented in Figs 5.8, 5.9, and 5.10, respectively. These data show that three distinctly different types of pore pressure behavior were occurring during each load test. For load increments falling on the initial linear portion of the load-settlement curve, the settlement occurred almost instantaneously with load application, and there was little variation of point and side friction resistance throughout the duration of the load increment. This indicates that the soil behaved elastically in this region of the load-settlement curve and that pore pressures generated during these increments were probably small. During the second portion of the load-settlement curve (Zone 2 in Fig 5.8), the shape of the pile time-settlement curves was very similar to that for a normally consolidated clay subjected to one-dimensional consolidation loading. During the primary settlement time period, the pile point resistance gradually increased and approached an asymptotic value. These data indicate that significant pore pressure was developed beneath the pile tip and that the tip capacity increased as the pore pressure dissipated. Both point and side friction resistance reached constant values at or before the time the load-settlement curve indicated primary settlement was complete. The time-settlement curves for load increments in the third portion of the load-settlement curve (Zone 3 in Fig 5.8) show that a plunging type failure occurred near the end of the test. It is doubtful that full pore pressure dissipation occurred beneath the point during the latter load increments; however, the point and side friction resistance remained relatively



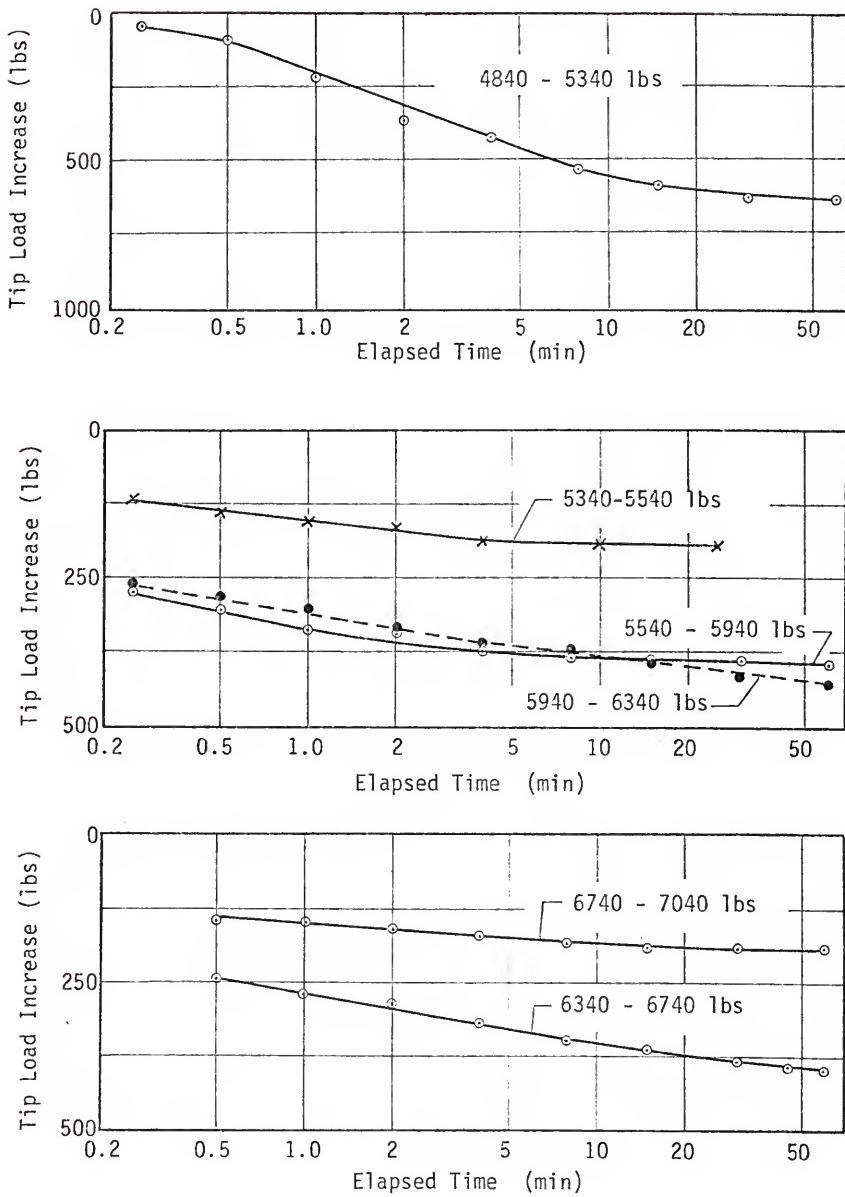
MODEL PILE LOAD-SETTLEMENT CURVES

FIGURE 5.8



MODEL PILE TIME SETTLEMENT CURVES

FIGURE 5.9



TIME INCREASE IN PILE TIP LOAD

FIGURE 5.10

constant throughout these increments. This indicates that either the excess pore pressure remained constant throughout these increments or that significant excess pore pressures were not generated.

Considering the pile behavior described in the preceding paragraph, the following procedure was adopted for load testing model piles driven in clay:

1. Initial load increments were maintained until both the point load and pile settlement attained constant values or for a period of 10 min, whichever was greater.
2. For load increments falling in Zone 2 of the load-settlement curve, the load was held constant on the pile until the "primary type" settlement was complete and the point resistance attained a constant value.
3. The final load increments were held until the point load reached a constant value and the rate of settlement was less than 0.010 in for a 10 min period.

Both time-settlement curves and a load-settlement curve were plotted during each test to assure that the load testing procedure was followed.

Except for the loading time criteria, the procedures for load testing model piles in clay were identical to the procedures described for piles driven in sand. The influence of the thin layer of surface sand at the Paines Prairie site was eliminated by driving the piles through sleeves set in holes excavated through the sand as shown in Fig 5.11.

#### 5.4 Pile Tip Load Cell Operation

Each pile tip hydraulic load cell was filled with hydraulic oil by first using a vacuum pump to evacuate the entire system and then permitting oil to enter the desired hydraulic cylinder and hose. This procedure was repeated several times throughout the project to assure that air in the system was not affecting the performance of the load cells.



MODEL PILE IN SLEEVE THROUGH SAND LAYER

FIGURE 5.11

Each pile tip was extended about 0.75 in before the piles were driven, and the tip position remained constant throughout the driving and testing operation. This procedure was followed to prevent relative movement between the pile tip and shaft, which could affect the load test results. The transducer manifold valve, shown in Fig 4.4, was closed during driving to prevent possible transducer damage due to impulse loading.

## CHAPTER 6

### MODEL PILE TEST DATA

#### 6.1 Cone Penetrometer Soundings

The equipment and procedures used for obtaining penetrometer data were described in Chapters 4 and 5. Data from these soundings are presented in the appendices in the form of graphs of unit cone bearing capacity ( $q_c$ ) and friction ratio (FR) versus depth. Only one mechanical penetrometer sounding was made at each pile test location at the Fairbanks site. These sounding logs are presented in Figs A-1 through A-3 in Appendix A.

Two electrical and two mechanical penetrometer soundings were made at each Beville site test location, with the exception of Location No 25 where only mechanical soundings were made. Figs B-5 through B-32 in Appendix B contain graphical logs of these soundings. All soundings from each test location have been presented on a single page to show the uniformity (or variability) of soil conditions at each test location. In addition to the graphical logs, each figure contains a tabulation of the average  $q_c$  and  $f_s$  values for both the electrical and mechanical penetrometers.

Penetrometer soundings at the Paines Prairie site were made in the same manner as at the Beville site. Logs of these soundings are presented in Figs C-4 through C-9 in Appendix C.

## 6.2 Model Pile Driving Data

Although the objectives of this research project did not include evaluation of pile driving resistance or correlation of driving resistance and pile load capacity, driving resistance records were maintained for each pile driven at the Beville and Paines Prairie sites. These records are summarized in Tables B-1 and C-1 in Appendices B and C.

## 6.3 Fairbanks Site Pile Load Tests

Eighteen individual load tests were performed on 4.0 in diameter model pipe piles driven at three separate locations. At Location No 1, the model pile was driven incrementally to depths of 4.0, 6.5, and 9.0 ft and a load test was performed at each depth. Data from these tests are presented in Figs A-4 through A-6 in the form of load-settlement curves for total pile load, tip load, and side friction load.

The pile was driven incrementally to depths of 4.5 and 8.9 ft at Location No 2. Several load tests were performed on the pile at each depth after various 'set' times as were described in Chapter 5. Load-settlement curves from these tests are presented in Figs A-7 through A-13. At Location No 3, the pile was driven incrementally to 4.5 and 8.5 ft and tested in the same manner as at Location No 2. Figs A-14 through A-19 contain the results of these tests.

## 6.4 Beville Site Pile Load Tests

### 6.4.1 Pipe Pile Tests

Twenty-six load tests were performed on 4.0 in diameter model pipe piles at six different test locations. The piles were driven incrementally to depths varying from 2.0 to 12.0 ft at Location Nos 2, 7, 13, and 24 with a load test being performed at each depth increment as

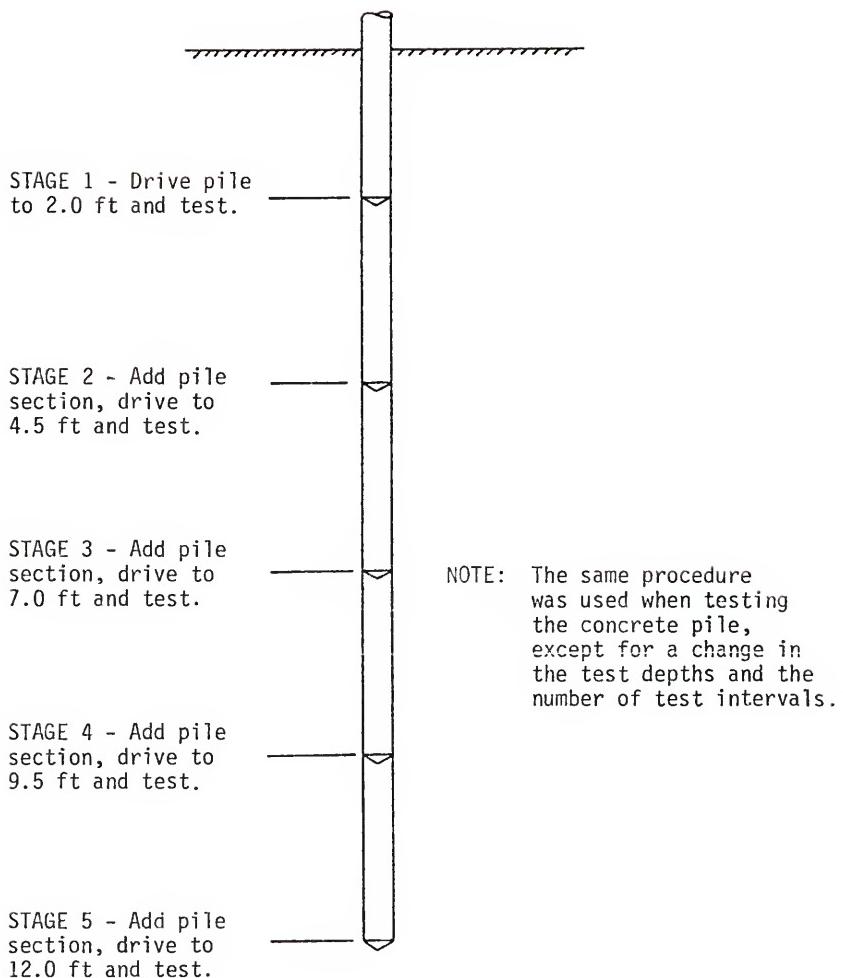
shown in Fig 6.1. Load-settlement curves for these tests are presented in Figs B-33 through B-50.

The pipe pile was incrementally jacked-in to depths of 2.0, 4.5, 7.0, and 9.5 ft at Location Nos 28 and 31. Total pile resistance, tip load and side friction resistance were monitored continuously during the jacking-in process, and a conventional pile load test was performed at each of the above four depth increments. Jack-in resistance curves are contained in Figs B-51 and B-56, and the load-settlement curves from the load tests are presented in Figs B-52 through B-55 and B-57 through B-60.

#### 6.4.2 Concrete Pile Tests

A total of 26 load tests were performed on model concrete piles driven at 18 different locations. Sixteen tests were performed on smooth concrete piles and the remaining 10 were on rough concrete piles. Both types of piles were installed by both driving and jacking-in.

Tests on driven smooth concrete piles were performed at Location Nos 1, 6, 9, 10, 11, 14, 18, and 25. Load-settlement curves for these tests are presented in Figs B-61 through B-70, B-73, and B-84. A smooth concrete pile was jacked-in to a depth of 3.0 ft at Location No 17. Fig B-72 presents the results of a load test performed at this depth. Attempts were made to jack this pile to a greater depth, but lateral movement of the pile could not be controlled and further testing at this location was abandoned. The jack-in procedure was more successful at Location No 21 where the smooth concrete pile was incrementally installed to depths of 3.0, 6.0, and 8.5 ft. Fig B-75 presents the jack-in resistance curves for this pile, and the results of



TYPICAL DRIVING AND TESTING SEQUENCE FOR MODEL PILE PILES

FIGURE 6.1

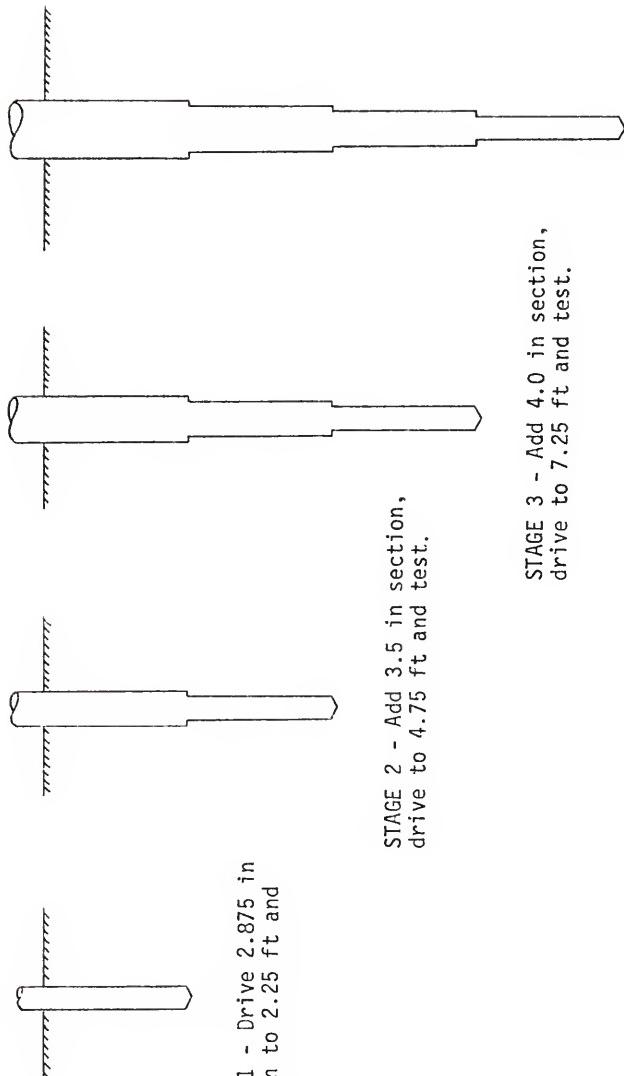
load tests performed at each depth increment are contained in Figs B-76 through B-79.

The results of load tests performed on driven rough concrete piles are presented in Figs B-71, B-74, B-79, and B-85 through B-88. These tests were performed at Location Nos 15, 19, 22, 26, 27, 29, and 30. A rough concrete pile was jacked in to a depth of 3.0 ft at Location No 27; however, this pile also began to move laterally when attempts were made to jack it in to greater depths. The results of a load test performed on the 3.0 ft pile at this location are contained in Fig B-86. The rough concrete pile was successfully jacked in to depths of 3.0, 6.0, and 8.0 ft at Location No 23. The jack-in resistance curves for this pile and the results of the individual load tests are presented in Figs B-80 through B-83.

#### 6.4.3 Step-Taper Pile Tests

Sixteen load tests were conducted on model step-taper piles driven at four locations. The piles were driven and tested in a manner that would permit as much information as possible to be obtained concerning the development of shaft resistance with depth. Fig 6.2 shows the driving and testing sequence used at each test location.

The pile was driven to test depths of 2.25, 4.75, 7.25, and 9.75 ft at Location Nos 5, 12, and 32. Load-settlement curves for tests at these locations are shown in Figs B-89 through B-96, and B-102 through B-105. This pile was jacked in to the same test depths at Location No 20. Fig B-97 contains the jack-in resistance curves and load-settlement curves from the conventional load tests are presented in Figs B-98 through B-101.



TYPICAL DRIVING AND TESTING SEQUENCE FOR MODEL STEP-TAPER PILES

FIGURE 6.2

## 6.5 Paines Prairie Pile Tests

### 6.5.1 Pipe Pile Tests

The 4.0 in diameter pipe pile was driven to depths of 6.0 and 9.5 ft at Location Nos 1 and 2 with load tests being conducted at each depth. A sleeve was placed to a depth of 2.67 ft at Location No 1 and 2.50 ft at Location No 2 to eliminate the influence of the surface sand layer. Load-settlement curves for these tests are presented in Figs C-10 through C-13. Two additional tests were performed on the 9.5 ft pile at Location No 2 after set times of 18 and 30 days to evaluate the effect of set time on pile capacity. The results of these tests are presented in Figs C-14 and C-15.

### 6.5.2 Concrete Pile Tests

The rough concrete pile was driven and tested at Location Nos 3 and 5. Smooth concrete piles were not tested at the Paines Prairie site. This pile was driven to depths of 6.5 and 9.0 ft at Location No 3, where a sleeve had been set to a depth of 2.67 ft. The results of load tests performed at these depths are presented in Figs C-16 and C-17.

At Location No 5, the sleeve was set to a depth of 2.75 ft and the pile driven to depths of 5.5 and 8.5 ft. One load test was performed on the 5.5 ft pile and four tests were performed on the 8.5 ft pile after set times of 3, 9, 15, and 29 days. The results of these tests are presented in Figs C-24 through C-28.

### 6.5.3 Step-Taper Pile Tests

The step-taper pile was driven and tested at Location Nos 4 and 6 in a three-stage sequence as shown in Fig 6.2. The pile was sleeved to

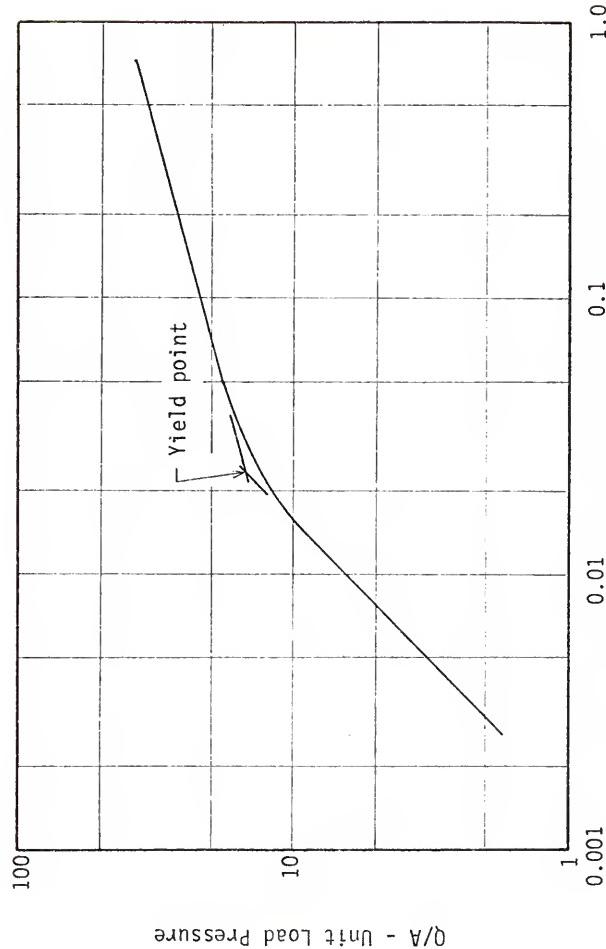
2.58 ft at Location No 4 and driven to depths of 5.0, 7.5, and 10.0 ft. One test was performed at 5.0 and 7.5 ft, and four tests were conducted on the 10.0 ft pile after set times of 2, 7, 15, and 35 days. These test results are shown in Figs C-18 through C-23.

At Location No 6, the pile was sleeved to 2.83 ft and driven to depths of 5.0, 7.5, and 10.0 ft with a load test being performed at each depth. Figs C-29 through C-31 show the results of these tests.

#### 6.6 Definition of Failure Loads

In order to rationally evaluate the pile load test results, it was necessary to define a point on the load-settlement curves corresponding to either ultimate failure or a maximum working load. Chellis (1951) summarizes 16 different methods which have been used for selecting this point, and the more recent literature contains numerous other methods. None of these methods seemed satisfactory because the defined failure points either had no physical significance with respect to the actual pile behavior or the location of the failure point was not consistent for load-settlement curves with different shapes.

Osterberg (1947) presented a procedure for evaluating plate load test data which appeared to be more rational than any of the methods which have been used for pile load test data. In this method, the load-settlement data are normalized and plotted in log-log form as shown in Fig 6.3. Osterberg showed experimentally that when plate load test data are plotted in this manner, the data points form two straight line segments. He also showed theoretically that the intersection of the straight line segments defines the load at which plastic flow or local bearing capacity failure begins to occur. Thus, this procedure defines a point that is unique and has some physical significance.



EXAMPLE OF OSTERBERG'S LOG-LOG LOAD-SETTLEMENT PLOT

FIGURE 6.3

Since load-settlement curves for plate and pile load tests generally have the same shape, it appeared that Osterberg's method could also be applied to pile load test data. The method was applied to several Beville site tests and found to work well; therefore, it was selected for use in this research program.

Log-log graphs of settlement versus total pile resistance have been included with each of the previously referenced pile load-settlement curves. These log-log photos have not been normalized for the sake of convenience, but the point defined by the straight line segments has the same significance as the similar point on a normalized plot. Examination of the log-log load-settlement curves shows that the intersection point occurs where the arithmetic load-settlement curves begin to deviate significantly from the initial straight line slope. The total pile settlement is generally small at this point; thus, the load at this point is called the 'yield load' rather than the failure load.

Although Osterberg's method provided a good definition of failure, it was difficult to relate the defined load to  $q_c$  values from cone penetration tests because  $q_c$  values correspond to a settlement or deformation that is large with respect to the cone dimension, while the yield load occurs at a settlement that is small with respect to the pile base dimension. In other words,  $q_c$  represents an ultimate failure load as opposed to the yield load obtained from Osterberg's criteria. Because of this problem, a second pile failure load, called the ultimate load, was defined as the load causing a settlement equal to 20% of the pile width or diameter. While this definition is arbitrary, it always resulted in a point that was well along the final failure

portion of the load-settlement curve and, therefore, corresponds more closely to the condition represented by  $q_c$  tests. Both the yield load-settlement ( $\delta_y$ ) and ultimate load-settlement ( $\delta_u$ ) are indicated on all pile load-settlement curves.

While Osterberg's failure criteria worked reasonably well for all model pile tests, it generally gave better results for tests in sand than in clay. This would be expected because the criteria were developed for sands, but the difference appears to be more the result of the magnitude of settlement at which yield occurs rather than to the differences in soil type. The piles tested in the Paines Prairie clay reached the yield point at very small settlements, generally in the range of 0.01 to 0.02 in. Because of this, relatively few points were available to define the initial straight line portion of the log-log curve. In addition, seating of the pile loading components and the accuracy of the pile settlement gauges can have a significant effect on the accuracy of measurement for the first 0.01 to 0.02 in of pile movement.

#### 6.7 Side Friction and Tip Resistance Corrections

Because of the configuration of the model pile tip load cells as described in Chapter 4, it was necessary to make corrections to the measured end bearing and side friction components in order to obtain the actual values of these components. Each of the load cells had a small sleeve section connected to the pile tip, which resulted in a portion of the side friction resistance being registered as tip resistance.

In addition, the load cell housing for the concrete pile resulted in the first 14.5 in of this pile having a steel surface. Since the

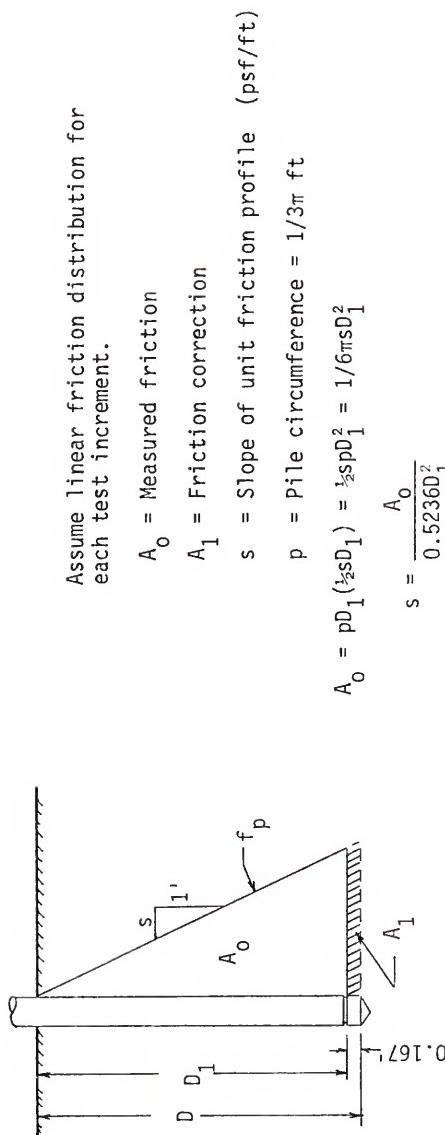
coefficient of friction between the steel housing and soil was less than that between concrete and soil, this resulted in the side friction measured on the concrete pile being less than what would have been measured had the entire pile surface been composed of concrete. The following sections describe the corrections made to account for these effects.

#### 6.7.1 Pipe Pile Corrections

For pipe piles in sand, the tip resistance and side friction corrections were computed assuming a linearly increasing distribution of unit side friction as shown in Fig 6.4. Combining this assumption with the measured total side friction and the actual pile length over which the measured friction occurred permitted computation of the rate of increase in side friction with depth. This value was then used to compute the side friction acting on the tip sleeve, which was added to the measured side friction and subtracted from the measured tip resistance.

The computed corrections along with the corrected values both of ultimate and yield side friction and tip resistance for pipe pile tests at the Fairbanks and Beville sites are presented in Tables 6.1 and 6.2. The maximum side friction correction amounted to 16% of the corrected side friction. The change in tip resistance resulting from this correction was less than 2%.

The same procedure was used for correcting the results of tests in clay except that unit side friction was assumed constant with depth. Corrected ultimate and yield pile resistance components for the pipe pile tests at Paines Prairie are summarized in Table 6.3.



PIPE PILE SIDE FRICTION CORRECTION METHOD

FIGURE 6.4

TABLE 6.1  
SUMMARY OF ULTIMATE CAPACITY DATA FOR  
BEVILLE AND FAIRBANKS SITE PIPE PILES

Test No	Pile Length (ft)	Installation Method	$F'_s$ (lbs)	$Q_t^i$ (lbs)	$\Delta F_s = \Delta Q_t$ (lbs)	$F_s$ (lbs)	$Q_t$ (lbs)
2	4.0	Driven*	765	3600	68	833	3532
	7.0	Driven*	880	5670	44	924	5626
	9.5	Driven*	2200	11,500	79	2279	11,421
	12.0	Driven*	3820	11,650	109	3929	11,541
7	2.0	Driven*	550	2600	105	655	2495
	4.5	Driven*	1090	3740	86	1176	3654
	7.0	Driven*	1140	4100	57	1197	4043
	9.0	Driven*	2060	7420	78	2138	7342
13	2.0	Driven	540	2620	103	643	2517
	4.5	Driven	650	3405	51	701	3354
	7.0	Driven	1200	5420	59	1259	5361
	9.5	Driven	2570	10,610	97	2667	10,513
	11.5	Driven	4470	14,450	133	4603	14,317
24	2.0	Driven	900	4220	172	1072	4048
	4.25	Driven	1870	4240	147	2017	4093
	6.75	Driven	3930	5290	193	4123	5097
	9.25	Driven	3820	8210	144	3964	8066
	11.75	Driven	4200	4400	125	4325	4075
28	2.0	Jacked-In	850	3650	162	1012	3488
	4.5	Jacked-In	1500	5780	118	1618	5662
	7.0	Jacked-In	2500	8480	123	2623	8357
	9.5	Jacked-In	5300	14,490	191	5491	14,299
31	2.0	Jacked-In	800	3030	153	953	2877
	4.5	Jacked-In	1310	5810	103	1413	5707
	7.0	Jacked-In	2810	11,920	139	3849	11,781
	9.5	Jacked-In	5800	13,820	209	6009	13,611

\*Guide sleeve not used

TABLE 6.2

SUMMARY OF YIELD CAPACITY DATA FOR  
BEVILLE AND FAIRBANKS SITE PIPE PILES

Test No	Pile Length (ft)	$F_s$ (lbs)	$Q_t$ (lbs)	$\Delta F_s = \Delta Q_t$ (lbs)	$F_s$ (lbs)	$Q_t$ (lbs)
2	4.0	740	2710	66	806	2644
	7.0	805	4460	40	845	4420
	9.5	1830	9700	66	1896	9634
	12.0	3400	9650	97	3373	9553
7	2.0	510	2000	97	607	1903
	4.5	1000	2470	79	1079	2391
	7.0	1250	2860	62	1312	2823
	9.0	2070	5700	79	2149	5621
13	2.0	540	2120	103	643	2017
	4.5	600	2500	47	647	2453
	7.0	1010	4180	50	1060	4130
	9.5	2190	8500	83	2273	8417
	11.5	4600	11,800	137	4737	11,663
24	2.0	1020	3360	194	1214	3165
	4.25	1770	2750	148	1918	2611
	6.75	3880	3090	199	4073	2771
	9.25	4090	5010	152	4242	4855
	11.75	3650	2900	109	3759	2791
28	2.0	930	2770	177	1107	2593
	4.5	1530	4440	120	1650	4320
	7.0	2630	6810	130	2760	6680
	9.5	5300	11,600	195	5585	11,409
31	2.0	880	2200	168	1048	2032
	4.5	1370	4320	108	1478	4213
	7.0	2850	9550	141	2991	9409
	9.5	5600	8950	202	5802	8748

TABLE 6-3  
MODEL PILE SIDE FRICTION CORRECTIONS IN CLAY

Test No	Pile Type	Pile Length (ft)	$F_s^i$ (lbs)	At Peak Friction $F_s$ (lbs)	$F_s^i$ (lbs)	$Q_t^i$ (lbs)	At Ultimate Capacity $F_s$ (lbs)	$Q_t$ (lbs)
1-1	Pipe	3.33	2580	140	2720	2070	1930	110
1-2	Pipe	6.83	4700	120	4820	4700	2060	120
2-1	Pipe	3.50	1600	80	1680	1590	1570	80
2-2	Pipe	7.00	3880	95	3975	3830	1655	95
4-1	Pipe	2.42	1020		1120	965	1030	90
6-1	Pipe	2.17	1070	115	1185	1070	885	115
3-1	Concrete	3.75	3500	570	4070	3500	1825	155
3-2	Concrete	6.34	4770	430	5200	4770	2065	115
5-1	Concrete	2.75	2280	540	2820	2280	1655	145
5-2	Concrete	5.75	5390	540	5930	5390	1455	145
4-2	Step-Taper	4.92	3225	115	3340	2820	1120	100
4-3	Step-Taper	7.42	4675	100	4775	4450	1105	95
6-2	Step-Taper	4.67	3050	105	3155	2870	750	100
6-3	Step-Taper	7.17	5750	120	5870	4970	655	105
							5075	550

TABLE 6.4  
SUMMARY OF ULTIMATE CAPACITY DATA FOR CONCRETE PILES AT BEVILLE SITE

Test No	Pile Length (ft)	Installation Method	$F'_S$ (1bs)	$Q'_t$ (1bs)	$\Delta F_S$ (1bs)	$\Delta Q_t$ (1bs)	$F_S$ (1bs)	$Q_t$ (1bs)
1-S	3.0	Driven	400	4320	142	-53	542	4267
1-S	6.0	Driven	1890	6330	317	-111	2207	6219
1-S	8.5	Driven	4700	7230	547	-188	5247	7042
6-S	8.5	Driven	3370	7190	343	-117	3713	7073
9-S	3.0	Driven	800	4600	287	-106	1087	4494
9-S	6.5	Driven	1670	6110	259	-89	1929	6021
9-S	8.5	Driven	5350	9090	621	-213	5971	8877
10-S	6.0	Driven	1840	3600	310	-108	2150	3492
11-S	8.0	Driven	4310	8110	565	-185	4875	7925
14-S	6.0	Driven	1820	3300	307	-107	2127	3193
15-R	3.0	Driven	1060	3520	500	-133	1560	3387
17-S	3.0	Jacked-In	605	7550	216	-79	821	7471
18-S	3.0	Driven	830	3380	295	-109	1125	3271
19-R	3.0	Driven	1320	4700	698	-165	2081	4535
21-S	3.0	Jacked-In	600	5090	213	-79	813	5011
21-S	6.0	Jacked-In	2190	7510	369	-129	2559	7381
21-S	8.5	Jacked-In	5300	11,150	613	-211	5913	10,939
22-R	6.0	Driven	1610	5880	334	-85	1944	5795
23-R	3.0	Jacked-In	650	5300	305	-81	955	5219
23-R	6.0	Jacked-In	2900	7610	604	-154	3504	7456
23-R	8.0	Jacked-In	4590	12,790	701	-160	5291	12,614
25-S	3.0	Driven	--	--	--	--	--	--
26-R	6.0	Driven	3010	6080	628	-160	3638	5920
27-R	3.0	Jacked-In	980	4750	461	-123	1441	4627
29-R	8.0	Driven	7620	5300	1164	-292	8784	5008
30-R	8.33	Driven	4300	12,650	627	-158	4927	12,492

TABLE 6.5  
SUMMARY OF YIELD CAPACITY DATA FOR CONCRETE PILES AT BEVILLE SITE

Test No	Pile Length (ft)	Installation Method	$F'_s$ (lbs)	$Q'_t$ (lbs)	$\Delta F_s$ (1bs)	$\Delta Q_t$ (1bs)	$F_s$ (1bs)	$Q_t$ (1bs)
1-S	3.0	Driven	395	3190	140	-17	535	3173
1-S	6.0	Driven	2030	4400	341	-119	2371	4281
1-S	8.5	Driven	3520	5205	410	-141	3930	5064
6-S	8.5	Driven	3220	4770	373	-129	3593	4641
9-S	3.0	Driven	800	3490	287	-106	1087	3384
9-S	6.5	Driven	1535	4460	238	-82	1773	4378
9-S	8.5	Driven	4540	7390	527	-181	5067	7209
10-S	6.0	Driven	1615	2710	272	-95	1887	2615
11-S	8.0	Driven	3875	6100	508	-166	4383	5934
14-S	6.0	Driven	1430	2630	241	-84	1671	2546
15-R	3.0	Driven	700	2540	330	-88	1030	2452
17-S	3.0	Jacked-In	670	5790	239	-88	909	5672
18-S	3.0	Driven	665	2410	236	-87	901	2323
19-R	3.0	Driven	1505	3370	796	-188	2301	3182
21-S	3.0	Jacked-In	495	4280	176	-65	671	4215
21-S	6.0	Jacked-In	1700	6140	286	-100	1986	6040
21-S	8.5	Jacked-In	3810	9200	441	-152	4251	9048
22-R	6.0	Driven	1685	4040	350	-89	2035	3951
23-R	3.0	Jacked-In	635	4080	298	-79	933	4001
23-R	6.0	Jacked-In	2630	6000	548	-140	3178	5860
23-R	8.0	Jacked-In	3890	9500	594	-149	4484	9351
25-S	3.0	Driven	2600	4760	927	-343	3527	4417
26-R	6.0	Driven	2685	4550	560	-143	3245	4407
27-R	3.0	Jacked-In	980	3370	461	-123	1441	3247
29-R	8.0	Driven	5800	2880	884	-222	6684	2658
30-R	8.33	Driven	5020	7830	733	-184	5753	7646

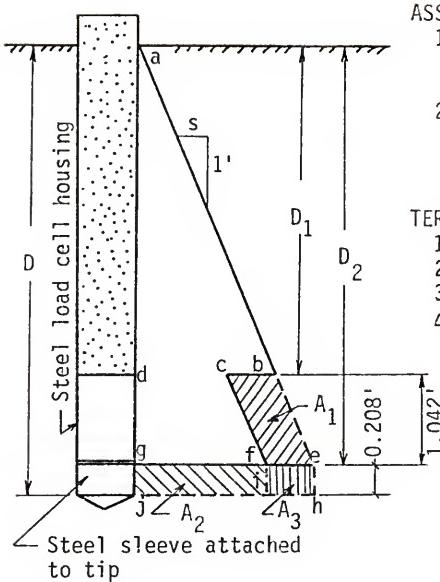
### 6.7.2 Concrete Pile Corrections

The correction procedure used for the concrete piles was the same as that described for the pipe piles, except that it was necessary to account for the effect of the steel load cell housing. This was accomplished using the pile-soil friction coefficients presented in Chapter 3. The details of this correction procedure for tests in sand are shown in Fig 6.5. The procedure for tests in clay was identical except for the assumed constant distribution of side friction with depth. The computed corrections and the corrected pile resistance components for tests performed at the Beville and Paines Prairie sites are summarized in Tables 6.3 through 6.5.

It should be noted that the concrete pile corrections resulted in an increase in total pile capacity, while the total pipe pile capacity remained the same before and after corrections.

### 6.7.3 Step-Taper Pile Corrections

The correction procedure used for tests performed on the first section of the step-taper pile was the same as that used for the pipe pile since this section forms a small diameter pipe pile. The correction procedure became more difficult when sections of different diameter were embedded. In this case, the pipe pile correction procedure could not be used because a portion of the measured shaft resistance resulted from bearing on the diameter step areas. Corrections for these piles were made using penetrometer sleeve friction values at the pile tip level, in conjunction with computed ratios of pile friction to sleeve friction to be described in a later chapter. The resulting corrections, along with corrected values of shaft and tip resistance, for the Beville site are contained in Tables 6.6 and 6.7, and those



## ASSUMPTIONS

1. Linear distribution of unit side friction
2.  $\left(\frac{f_{\text{steel}}}{f_{\text{conc.}}}\right)_{\text{pile}} = \left(\frac{f_{\text{steel}}}{f_{\text{conc.}}}\right)_{\text{Freed lab test}}$

## TERMINOLOGY

1.  $s$  = slope of unit friction profile
2.  $p$  = pile perimeter
3.  $A_0$  = total measured side friction
4.  $A_1$  = side friction correction for steel housing
5.  $A_2$  = estimated actual friction on tip sleeve
6.  $A_3$  =  $A_2$  corrected to a concrete surface
7.  $m$  = material correction factor  
= 0.749 (smooth concrete)  
= 0.656 (rough concrete)

DETERMINING  $s$ 

From assumption 2,  $dc = m(db)$   
and  $gf = m(ge)$

$$\begin{aligned} A_0 &= \text{Area}(abd) + \text{Area}(dcfg) \\ &= pD_1\left(\frac{1}{2}sD_1\right) + 1.042p\left(\frac{1}{2}\right)(msD_1 + msD_2) \\ &= \left\{\frac{1}{2}pD_1^2 + mp(D_1 + D_2)\right\}s \end{aligned}$$

Since  $p = 1.333$  ft

$$\begin{aligned} s &= \frac{A_0}{0.667D_1^2 + 0.52(D_1 + D_2)} \text{ smooth concrete} \\ &= \frac{A_0}{0.667D_1^2 + 0.455(D_1 + D_2)} \text{ rough concrete} \end{aligned}$$

SUMMARY

$$\text{Total side friction correction} = A_1 + A_2 + A_3$$

$$\text{Tip resistance correction} = -A_2$$

DETERMINING  $A_2$ 

$$\begin{aligned} gf &= m(ge) \\ &= m(sD_2) \end{aligned}$$

$$\begin{aligned} A_2 &= 0.208p(msD_2) \\ A_2 &= 0.208sD_2 \text{ sm. conc.} \\ &= 0.182sD_2 \text{ rgh. conc.} \end{aligned}$$

DETERMINING  $A_3$ 

$$\begin{aligned} A_3 &= A_2/m - A_2 = A_2(1/m - 1) \\ A_3 &= 0.335A_2 \text{ sm. conc.} \\ A_3 &= 0.524A_2 \text{ rgh. conc.} \end{aligned}$$

DETERMINING  $A_1$ 

$$\begin{aligned} A_1 &= (A_0 + A_1) - A_0 \\ &= \frac{1}{2}spD_1^2 - A_0 \\ &= 0.667sD_1^2 - A_0 \end{aligned}$$

## CONCRETE PILE SIDE FRICTION CORRECTION METHOD

FIGURE 6.5

TABLE 6.6  
SUMMARY OF ULTIMATE CAPACITY DATA FOR  
STEP-TAPER PILE AT BEVILLE SITE

Test No	Pile Length (ft)	Installation Method	$Q_s'$ (lbs)	$Q_t'$ (lbs)	$\Delta Q_s = \Delta Q_t$ (lbs)	$Q_s$ (lbs)	$Q_t$ (lbs)
5	2.50	Driven	250	1410	39	299	1371
	4.75	Driven	1980	1980	46	2026	1934
	7.25	Driven	5120	3540	184	5304	3356
	9.75	Driven	14,080	4800	124	14,204	4676
12	2.25	Driven	460	1740	78	538	1662
	4.75	Driven	2640	2990	53	2693	2937
	7.25	Driven	7520	2480	100	7620	2380
	9.75	Driven	12,790	3010	265	13,055	2745
20	2.25	Jacked-In	540	2170	91	631	2079
	4.75	Jacked-In	3700	4680	68	3768	4612
	7.25	Jacked-In	10,900	4950	108	11,008	4842
	9.75	Jacked-In	21,000	5100	308	21,300	4800
32	2.25	Driven	620	1390	105	725	1285
	4.75	Driven	2900	3980	92	2992	3888
	7.25	Driven	9210	2720	118	9328	2602
	9.75	Driven	11,450	4390	298	11,748	4092

TABLE 6.7

SUMMARY OF YIELD CAPACITY DATA FOR  
STEP-TAPER PILE AT BEVILLE SITE

Test No	Pile Length (ft)	Installation Method	$Q_s'$ (lbs)	$Q_t'$ (lbs)	$\Delta Q_s = \Delta Q_t$ (lbs)	$Q_s$ (lbs)	$Q_t$ (lbs)
5	2.50	Driven	260	1250	39	299	1211
	4.75	Driven	1740	1560	40	1780	1520
	7.25	Driven	4000	2640	144	4144	2496
	9.75	Driven	10,180	3220	90	10,270	3130
12	2.25	Driven	460	1630	78	538	1552
	4.75	Driven	2200	2340	44	2244	2296
	7.25	Driven	6120	1120	81	6201	1039
	9.75	Driven	10,000	2100	207	10,207	1893
20	2.25	Jacked-In	540	2160	91	631	2069
	4.75	Jacked-In	3790	2590	70	3860	2520
	7.25	Jacked-In	10,180	1550	101	10,281	1449
	9.75	Jacked-In	19,650	2400	300	19,950	2100
32	2.25	Driven	600	1340	102	702	1238
	4.75	Driven	2700	3120	86	2786	3034
	7.25	Driven	7920	1000	101	8021	899
	9.75	Driven	8150	3000	206	8356	2794

for the Paines Prairie tests are in Table 6.3.

The corrected values of side friction, tip resistance, and total pile resistance were used for all calculations described in subsequent chapters of this paper. It should be noted, however, that the load-settlement curves contained in the appendices are plots of uncorrected (field) data.

## CHAPTER 7

### MODEL PILE CAPACITY PREDICTIONS IN SAND

#### 7.1 Data Summary

Data on capacity of model piles driven in sands were provided by tests performed at both the Fairbanks and Beville sites. These data have been presented in detail in Chapter 6. Some of the longer piles at the Beville site extended into layers of clayey soil and cannot be used for the sand correlation studies. Also, the side friction data obtained from the Fairbanks tests will not be considered because the pile-driving guide was not used and because the data may have been affected by debris buried at the site. Tables 7.1 through 7.3 summarize all the model pile data available for use in the sand correlation studies after tests in clay and the Fairbanks side friction data were eliminated.

#### 7.2 Pile Tip Resistance

##### 7.2.1 General

As detailed in Chapter 2, the method currently in use in The Netherlands for predicting pile tip resistance is the result of research efforts and data correlations extending over a period of about forty years. Although there are some questions regarding the assumptions on which this method is based, primarily the assumed rupture surface, data available at present indicate that this method gives reasonable predictions and closely approximates reported variations

TABLE 7.1  
PILE CAPACITY DATA SUMMARY  
MODEL CONCRETE PILE DRIVEN IN SAND

Test No	Pile Length (ft)	Installation Method	Yield Capacity $F_s$ (lbs)	Capacity $Q_t$ (lbs)	Ultimate Capacity $F_s$ (lbs)	Capacity $Q_t$ (lbs)
1-S	3.0	Driven	535	3173	542	4267
	6.0	Driven	2371	4281	2207	6219
6-S	8.5	Driven	3593	--	3713	--
9-S	3.0	Driven	1087	3384	1087	4494
	6.5	Driven	1773	4378	1929	6021
10-S	6.0	Driven	1887	2615	2150	3492
11-S	8.0	Driven	4383	5934	4875	7925
14-S	6.0	Driven	1671	2546	2127	3193
15-R	3.0	Driven	1030	2452	1560	3387
17-S	3.0	Jacked-In	909	5672	821	7471
18-S	3.0	Driven	901	2323	1125	3271
19-R	3.0	Driven	2301	3182	2081	4535
21-S	3.0	Jacked-In	671	4215	813	5011
	6.0	Jacked-In	1986	6040	2559	7381
22-R	6.0	Driven	2035	3951	1944	5795
23-R	3.0	Jacked-In	933	4001	955	5219
	6.0	Jacked-In	3178	5860	3504	7456
	8.5	Jacked-In	4484	9351	5291	12,614
25-S	3.0	Driven	3527	4417	--	--
26-R	6.0	Driven	3245	4407	3638	5920
27-R	3.0	Jacked-In	1441	3247	1441	4627
30-R	8.33	Driven	5753	7646	4927	12,492

TABLE 7.2  
PILE CAPACITY DATA SUMMARY  
MODEL PIPE PILES DRIVEN IN SAND

Test No	Pile Length (ft)	Pile Dia (in)	Installation Method	Yield F <sub>s</sub> (lbs)	Capacity Q <sub>t</sub> (lbs)	Ultimate F <sub>s</sub> (lbs)	Capacity Q <sub>t</sub> (lbs)
2	4.0	4.00	Driven**	806	2644	833	3532
	7.0	4.00		845	4420	924	5626
	9.5	4.00		--	9634	--	11,421
5	2.50	2.875	Driven	299	1211	299	1371
	4.75	2.875		--	1520	--	1934
	9.75	2.875		--	3130	--	4676
7	2.0	4.00	Driven**	607	1903	655	2495
	4.5	4.00		1079	2391	1176	3654
	7.0	4.00		1312	2823	1197	4043
	9.0	4.00		--	5621	--	7342
12	2.25	2.875	Driven	538	1552	538	1662
	4.75	2.875		--	2296	--	2937
	7.25	2.875		--	1039	--	2380
13	2.0	4.00	Driven	643	2017	643	2517
	4.5	4.00		647	2453	701	3354
	7.0	4.00		1060	4130	1259	5361
20	2.25	2.875	Jacked-In	631	2069	631	2079
	4.75	2.875		--	2520	--	4612
	7.25	2.875		--	1449	--	4842
24	2.0	4.00	Driven	1214	3165	1072	4048
	4.25	4.00		1918	2611	2017	4093
	6.75	4.00		4079	2771	4123	5097
	9.25	4.00		4242	4855	3964	8066
28	2.0	4.00	Jacked-In	1107	2593	1012	3488
	4.5	4.00		1650	4320	1618	5662
	7.0	4.00		2760	6680	2623	8357
	9.5	4.00		5585	11,409	5491	14,299
31	2.0	4.00	Jacked-In	1048	2032	953	2877
	4.5	4.00		1478	4213	1413	5707
	7.0	4.00		2991	9409	3849	11,781
	9.5	4.00		5802	8748	6009	13,611

TABLE 7.2 (Continued)

Test No	Pile Length (ft)	Pile Dia (in)	Installation Method	Yield Capacity $F_s$ (lbs)	Capacity $Q_t$ (lbs)	Ultimate Capacity $F_s$ (lbs)	Capacity $Q_t$ (lbs)
32	2.25	2.875	Driven	702	1238	725	1285
	4.75	2.875	Driven	--	3034	--	3888
	7.25	2.875	Driven	--	899	--	2602
	9.75	2.875	Driven	--	2794	--	4092
F-1*	4.0	4.00	Driven**	--	--	--	3120
	6.5	4.00	Driven**	--	2830	--	3960
F-2*	4.5	4.00	Driven**	--	3790	--	4650
	8.9	4.00	Driven**	--	13,400	--	17,600
F-3*	4.4	4.00	Driven**	--	5810	--	7380
	8.0	4.00	Driven**	--	7750	--	10,000

\*Fairbanks Site test

\*\*Guide sleeve not used

TABLE 7.3

PILE CAPACITY DATA SUMMARY  
MODEL STEP-TAPER PILES DRIVEN IN SAND

Test No	Pile Length (ft)	Yield Capacity Q <sub>s</sub> (lbs)	Capacity Q <sub>t</sub> (lbs)	Ultimate Capacity Q <sub>s</sub> (lbs)	Capacity Q <sub>t</sub> (lbs)
5	4.75	1780	1210	2030	1370
	7.25	4140	1520	5300	1930
	9.75	10,270	3130	14,200	4680
12	4.25	2240	2300	2690	2940
	7.25	6200	1040	7600	2380
	9.75	10,210	--	13,060	--
20	4.75	3860	2520	3770	4610
	7.25	10,280	1450	11,010	4840
	9.75	19,950	--	21,300	--
32	4.75	2790	3030	2990	3890
	7.25	8020	900	9330	2600
	9.75	8360	2790	11,750	4090

in tip resistance with depth in the vicinity of soil layer interfaces. For these reasons, it was decided to evaluate the model pile data using this method and to attempt to modify the method or develop a new approach only if the predicted values did not correlate well with the field data.

#### 7.2.2 Predictions Using Electrical Penetrometer Data

A computer program was written and used to predict the point capacity of model piles using the Begemann method described in Chapter 2. Several example problems were analyzed by both the computer program and hand calculations to assure that the program gave correct answers.

Predicted ultimate and yield pile point capacities, along with the corresponding measured capacities for model pipe piles in sand, are presented in Table 7.4. Note that the step-taper pile point data have been included in this table since it is reasonable to assume that the point resistance of this pile will not be affected by the small shaft step located 2.6 ft above the tip. Also listed in Table 7.4 are prediction errors for each test, computed using the following equation:

$$E = \frac{Q(\text{predicted}) - Q(\text{measured})}{Q(\text{measured})} \times 100\% \quad (7.1)$$

The prediction error ( $E$ ) expresses the percent deviation of the predicted value from the actual value. A positive value of  $E$  represents an overprediction and a negative value an underprediction.

The Begemann method provides an ultimate capacity prediction since  $q_c$  values used in this method are obtained during continuous penetration or at penetrations that are large in relation to the cone diameter. Therefore, only pile point resistances measured at large settlements should be expected to correlate with predictions made using this method.

TABLE 7.4

SUMMARY OF PIPE PILE TIP CAPACITY AND  
ELECTRICAL PENETROMETER PREDICTIONS FOR TESTS IN SAND

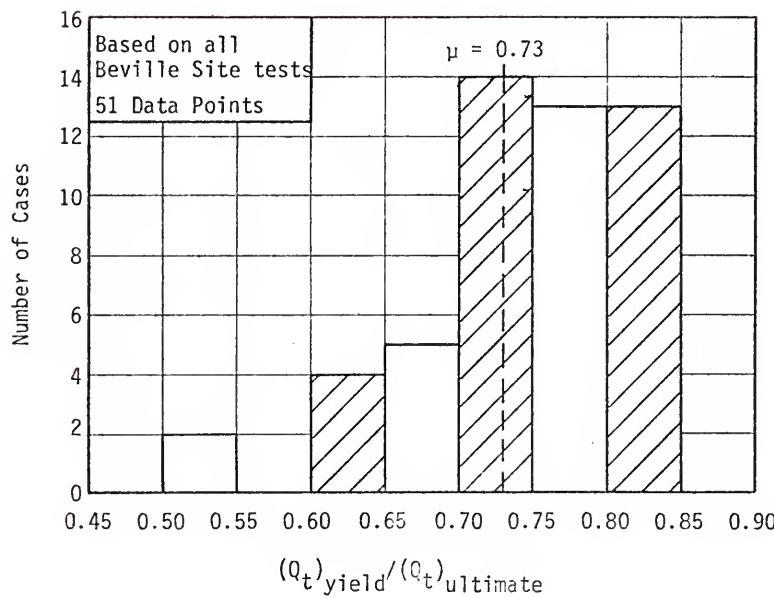
Test No	Pile Length (ft)	Pile Dia (in)	Ultimate Capacity			Yield Capacity		
			Actual (k)	Predicted (k)	Error (%)	Actual (k)	Predicted (k)	Error (%)
2	4.0	4.0	3.53	3.70	4.8	2.64	2.66	0.7
	7.0	4.0	5.63	5.68	0.9	4.42	4.09	- 7.5
	9.5	4.0	11.42	9.07	-20.6	9.63	6.53	-32.2
5	2.50	2.875	1.37	1.84	34.3	1.21	1.32	9.1
	4.75	2.875	1.93	2.49	29.0	1.52	1.79	17.8
	9.75	2.875	4.68	5.85	25.0	3.13	4.21	34.5
7	2.0	4.0	2.50	3.81	52.4	1.90	2.74	44.2
	4.5	4.0	3.65	5.41	48.2	2.39	3.90	63.2
	7.0	4.0	4.04	6.83	69.0	2.82	4.92	74.5
	9.0	4.0	7.34	7.40	0.8	5.62	5.33	- 5.2
12	2.25	2.875	1.66	1.67	0.6	1.55	1.20	-22.6
	4.75	2.875	2.94	2.75	- 6.5	2.30	1.98	-13.9
	7.25	2.875	2.38	4.44	86.5	1.04	3.20	207.8
13	2.0	4.0	2.52	2.87	13.9	2.02	2.07	2.5
	4.5	4.0	3.35	3.47	3.6	2.45	2.50	2.0
	7.0	4.0	5.36	5.14	- 4.1	4.13	3.70	-10.4
20	2.25	2.875	2.08	2.35	13.0	2.07	1.69	-18.4
	4.75	2.875	4.61	3.28	-48.4	2.52	2.36	- 6.3
	7.25	2.875	4.82	3.06	-36.5	1.45	2.20	51.7
24	2.00	4.0	4.05	4.11	1.5	3.16	2.96	- 6.3
	4.25	4.0	4.09	4.09	0.0	2.61	2.94	12.6
	6.75	4.0	5.10	6.20	21.6	2.77	4.46	61.0
	9.25	4.0	8.07	8.64	7.1	4.86	6.22	28.0
28	2.0	4.0	3.49	3.52	0.8	2.59	2.53	- 2.3
	4.5	4.0	5.66	5.16	- 8.8	4.32	3.72	-13.9
	7.0	4.0	8.36	6.55	-21.6	6.68	4.72	-29.3
	9.5	4.0	14.30	12.55	-12.2	11.41	9.04	-20.8
31	2.0	4.0	2.88	2.74	- 4.9	2.03	1.97	- 3.0
	4.5	4.0	5.71	3.95	-30.8	4.21	2.84	-32.5
	7.0	4.0	11.78	9.42	-20.0	9.41	6.78	-27.9
	9.5	4.0	13.61	14.11	3.7	8.75	10.16	16.1
32	2.25	2.875	1.29	2.04	58.1	1.24	1.47	18.5
	4.75	2.875	3.89	4.78	22.9	3.03	3.44	13.5
	7.25	2.875	2.60	4.81	85.0	0.90	3.46	284.4
	9.75	2.875	4.09	7.03	71.9	2.79	5.06	81.4

This presented a problem in predicting yield capacities since conventional CPT techniques and equipment do not permit measuring yield  $q_c$  values. Since the yield capacity concept is useless if yield capacities cannot be predicted, the model pile data were analyzed to determine if there was a relationship between measured yield and ultimate capacity. This was done by computing a ratio of ultimate to yield tip capacity for each model pile test performed at the Beville site. The computed ratios are presented graphically in Fig 7.1. This histogram shows that, while there was a large scatter in the ratios, most values fell within the range of 0.70 to 0.85, which indicated that it might be possible to make reasonably accurate yield capacity predictions by using the average ultimate to yield capacity ratio and the computed ultimate capacity. The resulting equation is

$$(Q_t)_{yield} = 0.73(Q_t)_{ult}. \quad (7.2)$$

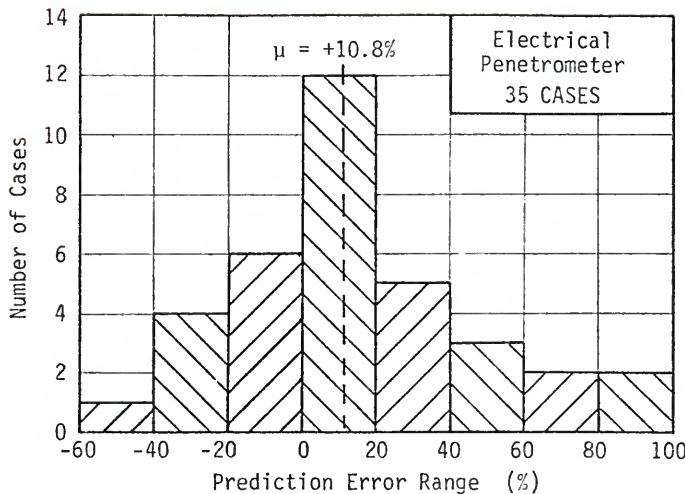
where  $(Q_t)_{ult}$ . is the capacity predicted by the Begemann method. Yield capacities computed using Eq 7.2 were then compared to measured values to determine the accuracy with which yield capacities could be predicted.

Histograms of the ultimate prediction errors for all pipe piles are shown in Fig 7.2, and a similar graph showing only data from the 4.0 in diameter piles is presented in Fig 7.3. Similar histograms for the yield capacity predictions are shown in Figs 7.4 and 7.5. The ultimate capacity correlations show that, on the average, the Begemann method slightly overpredicted the pipe pile point capacity with the overprediction being less for the 4.0 in diameter piles than for the 2.875 in diameter piles. In addition, the histograms are approximately normally distributed about the mean. The yield capacity histograms show the same tendencies, but with a larger amount of scatter about the



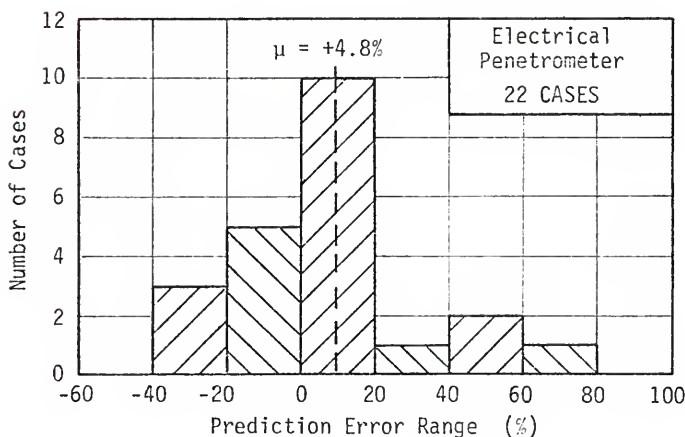
DISTRIBUTION OF ULTIMATE TO YIELD TIP CAPACITY RATIOS IN SAND

FIGURE 7.1



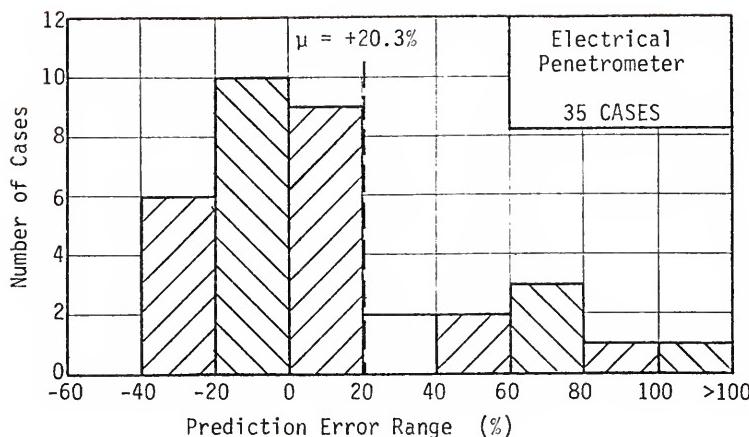
ULTIMATE TIP CAPACITY PREDICTION ERROR DISTRIBUTION  
FOR ALL PIPE PILES IN SAND

FIGURE 7.2



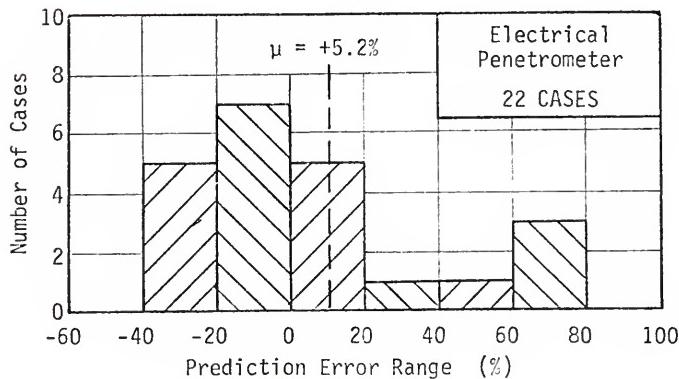
ULTIMATE TIP CAPACITY PREDICTION ERROR DISTRIBUTION  
FOR 4.0 IN PIPE PILES IN SAND

FIGURE 7.3



YIELD TIP CAPACITY PREDICTION ERROR DISTRIBUTION  
FOR ALL PIPE PILES IN SAND

FIGURE 7.4



YIELD TIP CAPACITY PREDICTION ERROR DISTRIBUTION  
FOR 4.0 IN DIAMETER PIPE PILES IN SAND

FIGURE 7.5

mean. Possible reasons for the prediction errors and their significance will be discussed in a later section of this chapter.

Measured and predicted tip capacities for the 4.0 in square concrete pile are summarized in Table 7.5. Yield capacities were estimated using Eq 7.2. Histograms of the prediction errors are shown in Figs 7.6 and 7.7. These graphs also show a tendency to overpredict both ultimate and yield capacities and, surprisingly, the yield capacity correlation was slightly better than that for ultimate capacity.

#### 7.2.3 Predictions Using Mechanical Penetrometer Data

Ultimate and yield capacities were predicted for each pile using mechanical penetrometer data and the same prediction method as was used with the electrical cone data. Tables 7.6 and 7.7 summarize the predicted and measured pipe and concrete pile predictions. Data from the six Fairbanks site pipe pile tests have been included in this summary.

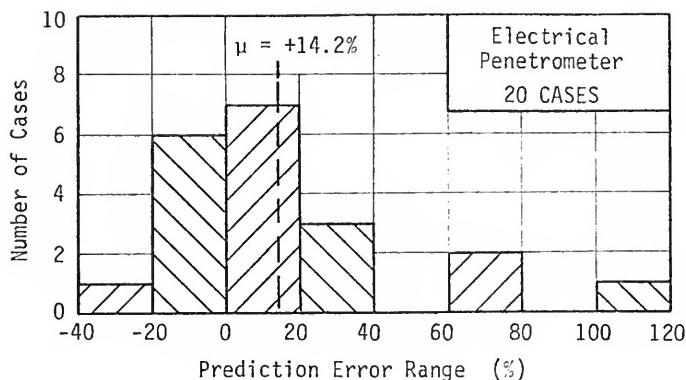
Tip resistance prediction error distributions for all pipe piles, 4.0 in diameter pipe piles, and concrete piles determined from the mechanical penetrometer predictions are shown in Figs 7.8 through 7.13. In general, these prediction errors show the same tendencies as those for the electrical penetrometer; however, there is more scatter in the mechanical cone predictions, particularly for the concrete piles. These data also show that the prediction error was greater for 2.875 in diameter pipe piles than for the 4.0 in diameter piles.

#### 7.2.4 Possible Causes of the Prediction Errors

Data presented in the preceding section show that the average capacity prediction is approximately equal to the average measured tip capacity. The histograms approximately indicate a normal or bell-shaped

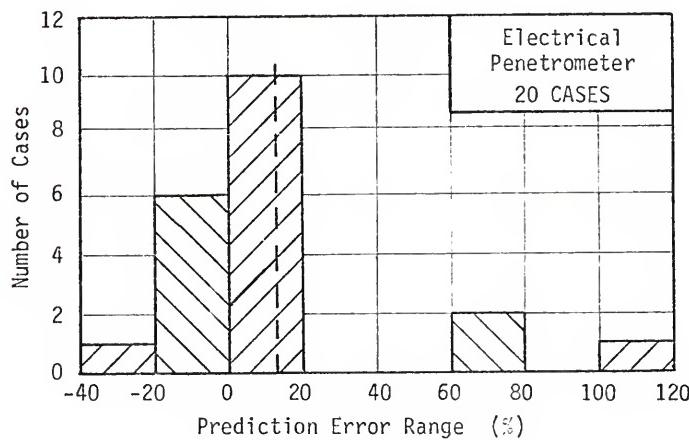
TABLE 7.5  
SUMMARY OF CONCRETE PILE TIP CAPACITY AND  
ELECTRICAL PENETROMETER PREDICTIONS FOR TESTS IN SAND

Test No.	Pile length (ft)	Actual (k)	Ultimate Predicted (k)	Error (%)	Actual (k)	Yield Predicted (k)	Error (%)
1	3.0	4.27	5.10	19.5	3.17	3.74	18.0
	6.0	6.22	6.73	8.2	4.28	4.94	15.4
9	3.0	4.49	4.54	1.0	3.38	3.33	-1.5
	6.5	6.02	5.00	-16.9	4.38	3.67	-16.2
10	6.0	3.49	5.78	65.5	2.61	4.24	62.2
	8.0	7.92	9.61	21.3	5.93	7.05	19.0
11	6.0	3.19	7.10	122.4	2.55	5.21	104.7
	14	6.0	3.39	5.43	60.3	2.45	3.99
15	3.0	7.47	8.00	7.1	5.67	5.87	3.5
	17	3.0	3.27	3.65	11.6	2.32	2.68
18	3.0	4.53	4.84	6.7	3.18	3.55	15.3
	19	3.0	5.01	6.33	26.3	4.21	3.55
21	3.0	7.38	5.49	-25.6	6.04	4.03	-33.3
	6.0	5.79	5.67	-2.2	3.95	4.16	5.3
22	6.0	5.22	5.43	4.0	4.00	3.99	-0.4
	3.0	7.46	9.11	22.2	5.86	6.69	14.1
23	6.0	12.64	10.25	-18.9	9.35	7.52	-19.5
	8.0	5.92	5.69	-3.9	4.41	4.18	-5.2
26	6.0	4.63	4.03	-12.9	3.25	2.95	-8.9
	3.0	12.49	10.94	-12.4	7.65	8.03	5.0
30	8.0						



ULTIMATE TIP CAPACITY PREDICTION ERROR DISTRIBUTION FOR CONCRETE  
PILES IN SAND COMPUTED FROM ELECTRICAL PENETROMETER DATA

FIGURE 7.6



YIELD TIP CAPACITY PREDICTION ERROR DISTRIBUTION FOR CONCRETE  
PILES IN SAND COMPUTED FROM ELECTRICAL PENETROMETER DATA

FIGURE 7.7

TABLE 7.6  
SUMMARY OF PIPE PILE TIP CAPACITY AND  
MECHANICAL PENETROMETER PREDICTIONS FOR TESTS IN SAND

Test No	Pile Length (ft)	Pile Dia (in)	Ultimate Capacity			Yield Capacity		
			Actual (k)	Predicted (k)	Error (%)	Actual (k)	Predicted (k)	Error (%)
2	4.0	4.0	3.53	6.02	70.5	2.64	4.33	64.0
	7.0	4.0	5.63	6.79	20.6	4.42	4.89	10.6
	9.5	4.0	11.42	14.42	26.3	9.63	10.38	7.8
5	2.50	2.875	1.37	2.62	91.2	1.21	1.89	56.2
	4.75	2.875	1.93	3.22	66.8	1.52	2.32	52.6
	9.75	2.875	4.68	9.10	94.4	3.13	6.55	109.3
7	2.0	4.0	2.50	3.43	41.2	1.90	2.47	30.0
	4.5	4.0	3.65	4.58	25.5	2.39	3.30	38.1
	7.0	4.0	4.04	4.73	17.1	2.82	3.41	20.9
	9.0	4.0	7.34	8.96	22.1	5.62	6.45	14.7
12	2.25	2.875	1.66	1.70	2.4	1.55	1.22	-21.3
	4.75	2.875	2.94	2.44	-17.0	2.30	1.76	-23.5
	7.25	2.875	2.38	2.92	22.7	1.04	2.10	101.9
13	2.0	4.0	2.52	4.17	65.5	2.02	3.00	48.5
	4.5	4.0	3.35	4.90	46.3	2.45	3.53	44.1
	7.0	4.0	5.36	7.81	45.7	4.13	5.62	36.1
20	2.25	2.875	2.08	1.90	-8.7	2.07	1.37	-33.8
	4.75	2.875	4.61	1.85	-60.0	2.52	1.33	-47.2
	7.25	2.875	4.82	2.11	-56.2	1.45	1.52	4.8
24	2.00	4.0	4.05	4.16	2.7	3.16	3.00	-5.1
	4.25	4.0	4.09	5.42	32.5	2.61	3.90	49.4
	6.75	4.0	5.10	6.51	27.6	2.77	4.69	69.3
	9.25	4.0	8.07	9.35	15.9	4.86	6.73	38.5
28	2.0	4.0	3.49	3.28	-6.0	2.59	2.36	-8.9
	4.5	4.0	5.66	4.73	-16.4	4.32	3.41	-21.1
	7.0	4.0	8.36	5.43	-35.0	6.68	3.91	-41.5
	9.5	4.0	14.30	11.76	-17.8	11.41	8.47	-25.8
31	2.0	4.0	2.88	2.95	2.4	2.03	2.12	4.4
	4.5	4.0	5.71	4.63	-18.9	4.21	3.33	-20.9
	7.0	4.0	11.78	9.00	-23.6	9.41	6.48	-31.1
	9.5	4.0	13.61	16.19	19.0	8.75	11.66	33.2

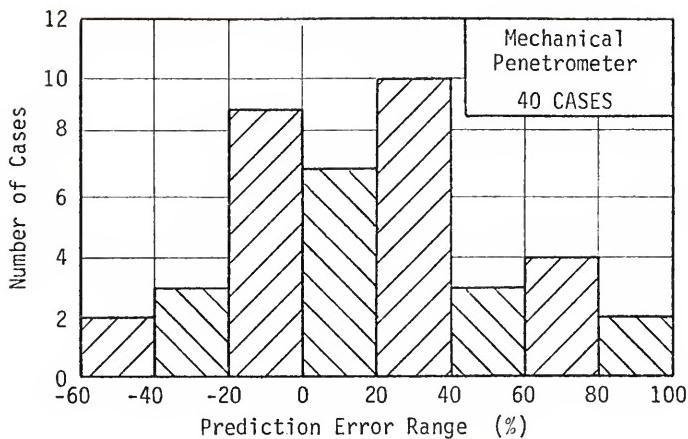
TABLE 7.6 (Continued)

Test No	Pile Length (ft)	Pile Dia (in)	Ultimate Capacity			Yield Capacity		
			Actual (k)	Predicted (k)	Error (%)	Actual (k)	Predicted (k)	Error (%)
32	2.25	2.875	1.29	1.45	12.4	1.24	1.04	-16.1
	4.75	2.875	3.89	2.49	-36.0	3.03	1.79	-40.9
	7.25	2.875	2.60	3.16	21.5	0.90	2.28	153.3
	9.75	2.875	4.09	6.73	64.5	2.79	4.85	73.8
F-1	4.0	4.0	3.12	3.77	20.8	--	--	--
	6.5	4.0	3.96	5.02	26.8	2.83	3.71	31.0
F-2	4.5	4.0	4.65	6.28	35.1	3.79	4.65	32.3
	8.9	4.0	17.60	15.06	-14.4	13.40	11.14	-16.8
F-3	4.4	4.0	7.38	6.38	-13.6	5.81	4.72	-18.7
	8.0	4.0	10.00	8.44	-15.6	7.75	6.25	-19.3

TABLE 7.7

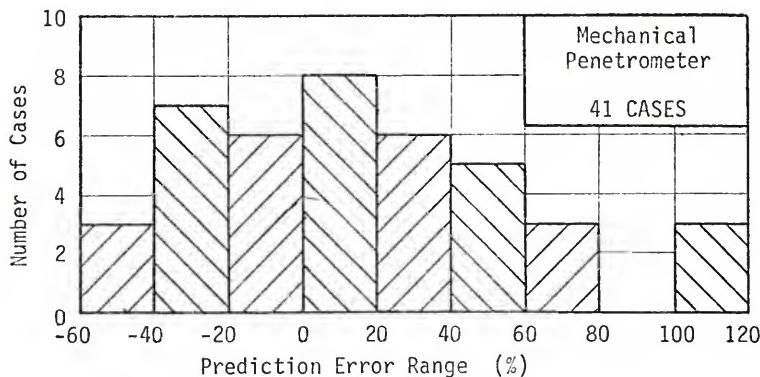
SUMMARY OF CONCRETE PILE TIP CAPACITY AND  
MECHANICAL PENETROMETER PREDICTIONS FOR TESTS IN SAND

Test No	Pile Length (ft)	Ultimate Capacity			Yield Capacity		
		Actual (k)	Predicted (k)	Error (%)	Actual (k)	Predicted (k)	Error (%)
1	3.0	4.27	5.08	19.1	3.17	3.73	17.5
	6.0	6.22	5.57	-10.4	4.28	4.09	- 4.5
9	3.0	4.49	8.03	78.7	3.38	5.89	74.2
	6.5	6.02	7.80	29.5	4.38	5.72	30.8
10	6.0	3.49	7.08	102.7	2.61	5.20	98.7
11	8.0	7.92	11.59	46.2	5.93	8.51	43.4
14	6.0	3.19	6.93	117.0	2.55	5.09	99.8
15	3.0	3.39	4.83	42.6	2.45	3.54	44.6
17	3.0	7.47	9.32	24.7	5.67	6.84	20.6
18	3.0	3.27	5.23	59.9	2.32	3.84	65.3
19	3.0	4.53	4.97	9.6	3.18	3.65	14.6
21	3.0	5.01	5.20	3.8	4.21	3.82	- 9.4
	6.0	7.38	6.21	-15.9	6.04	4.56	-24.5
22	6.0	5.79	6.55	13.0	3.95	4.81	21.7
23	3.0	5.22	5.08	- 2.6	4.00	3.73	- 6.8
	6.0	7.46	5.39	-27.7	5.86	3.96	-32.5
	8.0	12.64	7.21	-43.0	9.35	5.29	-43.4
25	3.0	--	--	--	4.42	8.51	92.6
26	6.0	5.92	5.09	-14.0	4.41	3.76	-15.2
27	3.0	4.63	5.18	12.0	3.25	3.80	17.1
30	8.0	12.49	7.16	-42.7	7.65	5.25	-31.3



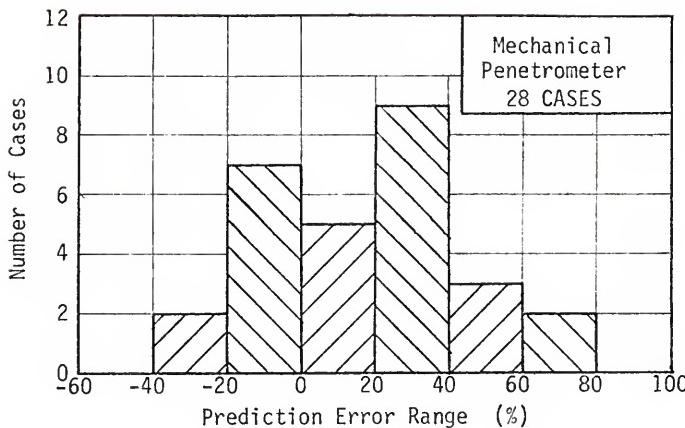
ULTIMATE TIP CAPACITY PREDICTION ERROR DISTRIBUTION FOR PIPE PILES IN SAND COMPUTED FROM MECHANICAL PENETROMETER DATA

FIGURE 7.8



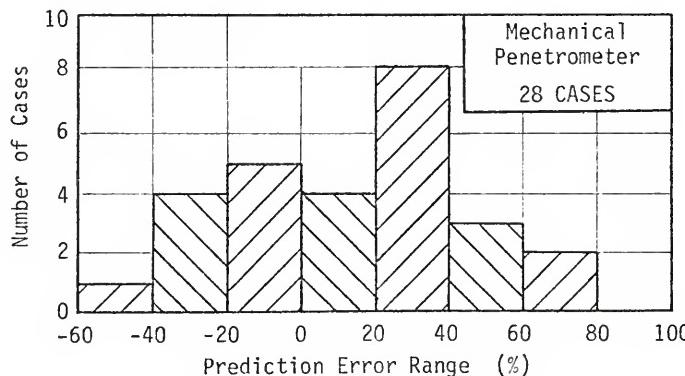
YIELD TIP CAPACITY PREDICTION ERROR DISTRIBUTION FOR PIPE PILES IN SAND COMPUTED FROM MECHANICAL PENETROMETER DATA

FIGURE 7.9



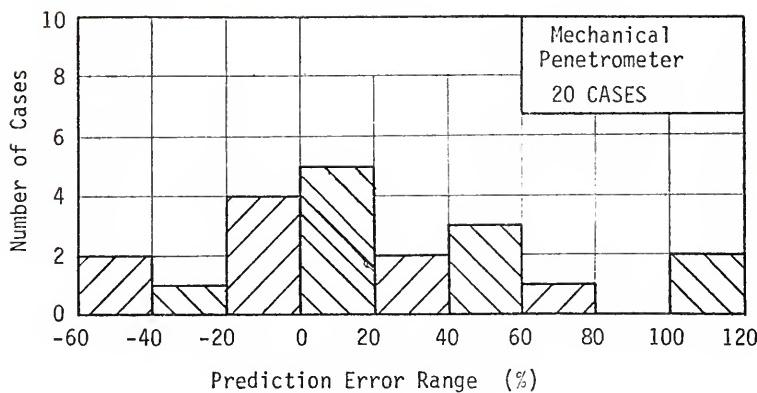
ULTIMATE TIP CAPACITY PREDICTION ERROR DISTRIBUTION FOR 4.0 IN DIAMETER PIPE PILES IN SAND COMPUTED FROM MECHANICAL PENETROMETER DATA

FIGURE 7.10



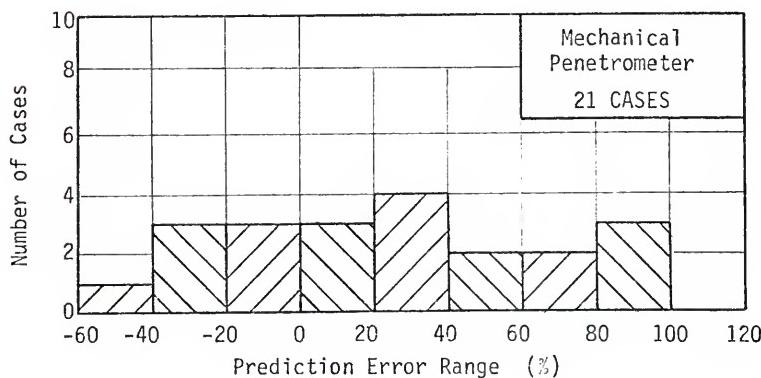
YIELD TIP CAPACITY PREDICTION ERROR DISTRIBUTION FOR 4.0 IN DIAMETER PIPE PILES IN SAND COMPUTED FROM MECHANICAL PENETROMETER DATA

FIGURE 7.11



ULTIMATE TIP CAPACITY PREDICTION ERROR DISTRIBUTION FOR CONCRETE  
PILES IN SAND COMPUTED FROM MECHANICAL PENETROMETER DATA

FIGURE 7.12



YIELD TIP CAPACITY PREDICTION ERROR DISTRIBUTION FOR CONCRETE  
PILES IN SAND COMPUTED FROM MECHANICAL PENETROMETER DATA

FIGURE 7.13

distribution around the mean prediction error. This indicates that, on the average, the predicted tip resistance will be approximately equal to the actual value, but the question remains as to why the prediction errors occur. The two most obvious possible causes are

1. Variations in the sand deposits could result in the bearing capacity at the pile location being different from that at the cone sounding locations.
2. The Begemann prediction method may not properly model actual pile behavior in soils, particularly where there is a considerable  $q_c$  variation with depth.

The tip capacity predictions on which the preceding correlations are based were determined by averaging predictions computed from two cone soundings located on opposite sides of the test pile. The effects of natural soil variability, as indicated by  $q_c$  data, can be evaluated by examining the range in predicted capacities determined from each individual sounding at each test site. These ranges for electrical cone ultimate capacity predictions for the concrete and 4.0 in pipe piles are plotted versus the actual capacities in Fig 7.14. The vertical lines on these graphs show the range in predicted tip capacity determined by considering each sounding individually. These graphs show that, with few exceptions, the actual capacity falls within or very close to the range of capacities predicted from the two soundings and indicates that soil variability is probably responsible for a large amount of the prediction error scatter.

The jacked-in pile tests, for which tip capacity was measured at frequent depth intervals, provide a means of checking the adequacy of the Begemann method in accounting for  $q_c$  variations with depth. If the variations in the predicted capacity with depth follow the same trend as the variations in actual capacity, this would indicate that the

VARIATION IN ULTIMATE PILE TIP CAPACITY COMPUTED FROM ELECTRICAL CONE SOUNDINGS LOCATED ON OPPOSITE SIDES OF THE TEST PILE

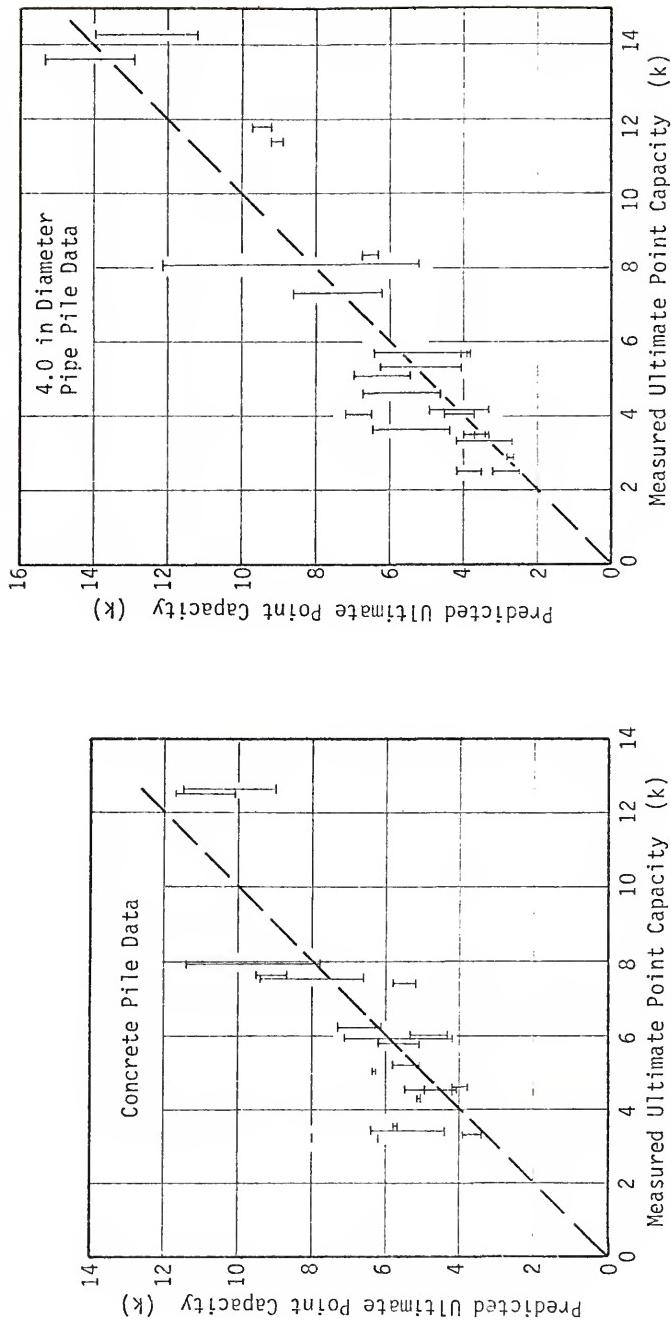


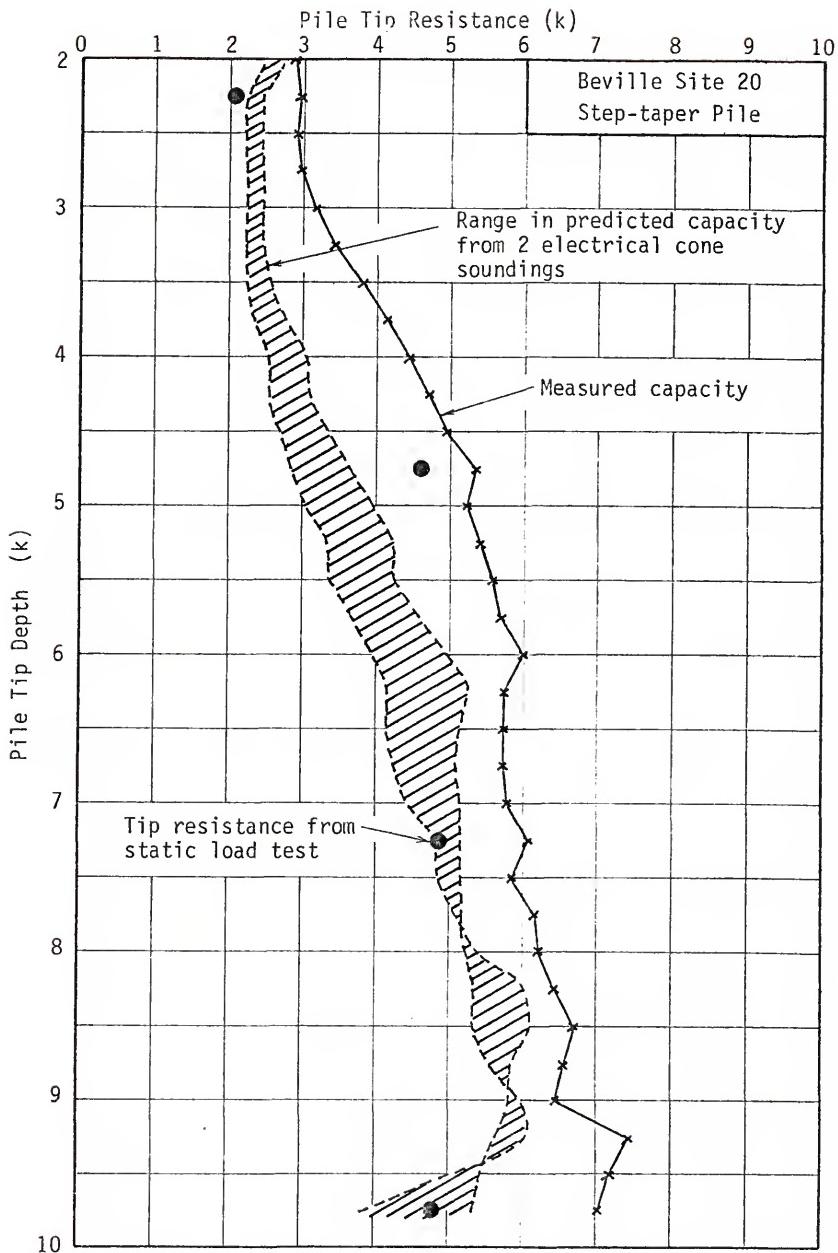
FIGURE 7.14

manner in which the  $q_c$  values are averaged in the prediction method is adequate. Curves showing measured tip capacity during the jack-in tests for both pipe and concrete piles, along with predicted capacity curves, are presented in Figs 7.15 through 7.19. These curves show that the predicted capacity curves generally parallel the actual capacity curves except for the upper 3 to 4 ft at Test Site No 21. The variation between the predicted and measured curves above the 3 ft level at this site may be due to placing the pile in a hole predrilled to a depth of about 1.5 ft. This predrilling should cause a reduction in tip capacity during the initial penetration; however, this effect was not noted for the jacked-in pipe piles which were set in 0.5 ft deep predrilled holes. The variation below 6.5 ft at Site No 23 is caused by the large variation in  $q_c$  values from the two soundings below this level. Note that the curve from one sounding closely follows the actual capacity curve.

Based on these evaluations, it seems likely that the prediction errors were primarily caused by natural variations in the soils at the test sites and that the Begemann prediction method adequately accounts for  $q_c$  variations with depth (scale effects) and provides reasonably accurate predictions of pile tip capacity. The latter conclusion is based on the following:

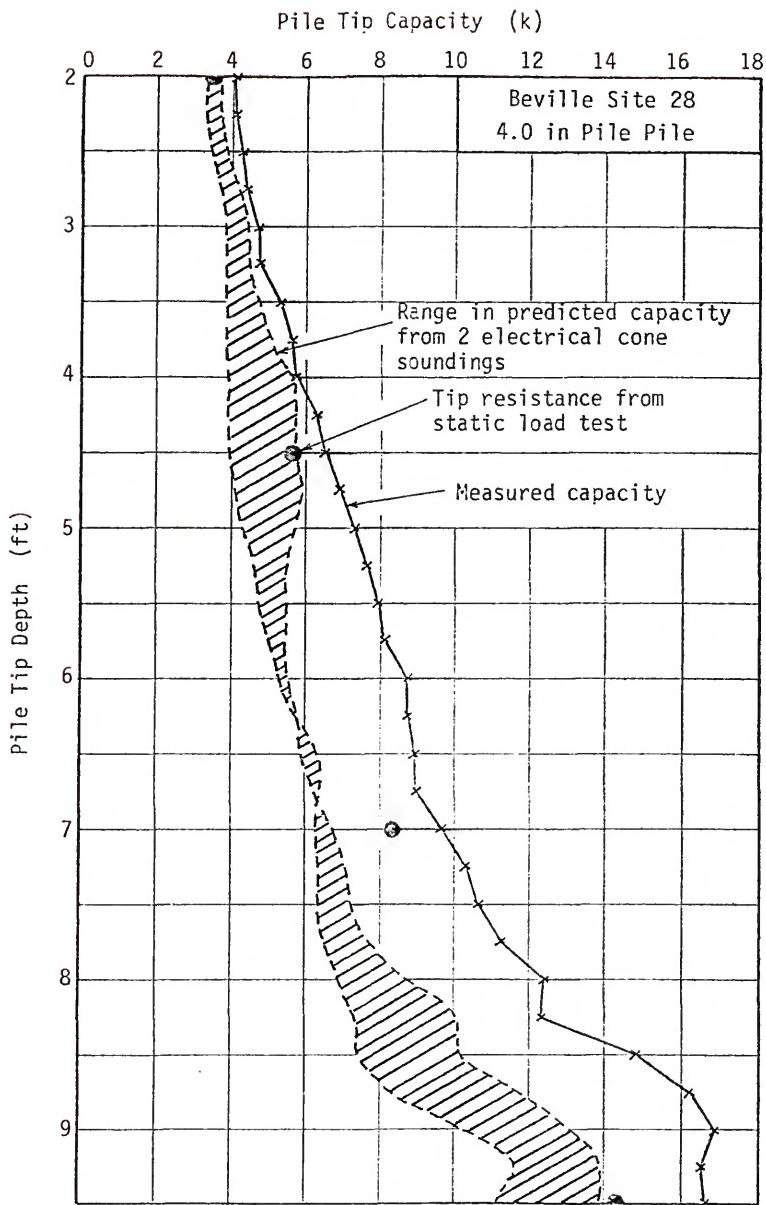
1. Since the predicted capacity curves for the jacked-in piles approximately parallel the actual capacity curves, scale effects must have been reasonably accounted for.
2. The average prediction error was close to zero (10 to 20%), and the individual test errors showed an approximately normal distribution about the mean, indicating a strong tendency to predict the correct value.

As a result of the good correlation between measured and predicted tip capacities, Begemann's method was judged to be sufficiently accurate



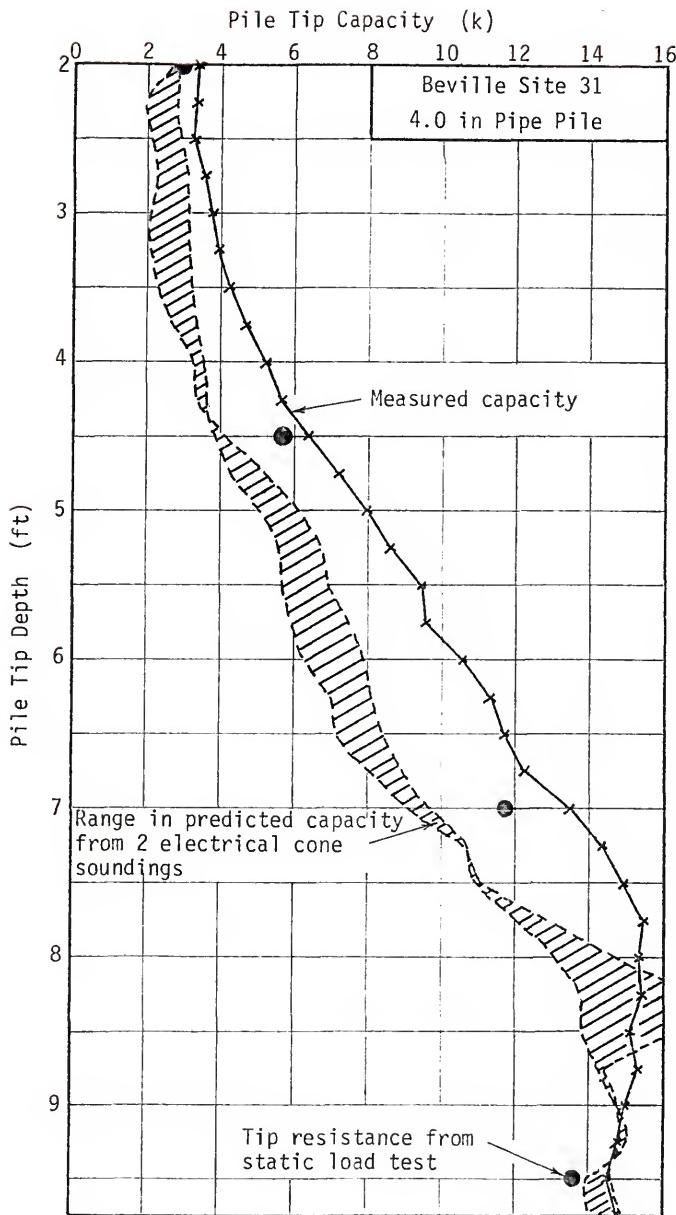
PREDICTED AND MEASURED TIP CAPACITY FOR A JACKED-IN PILE

FIGURE 7.15



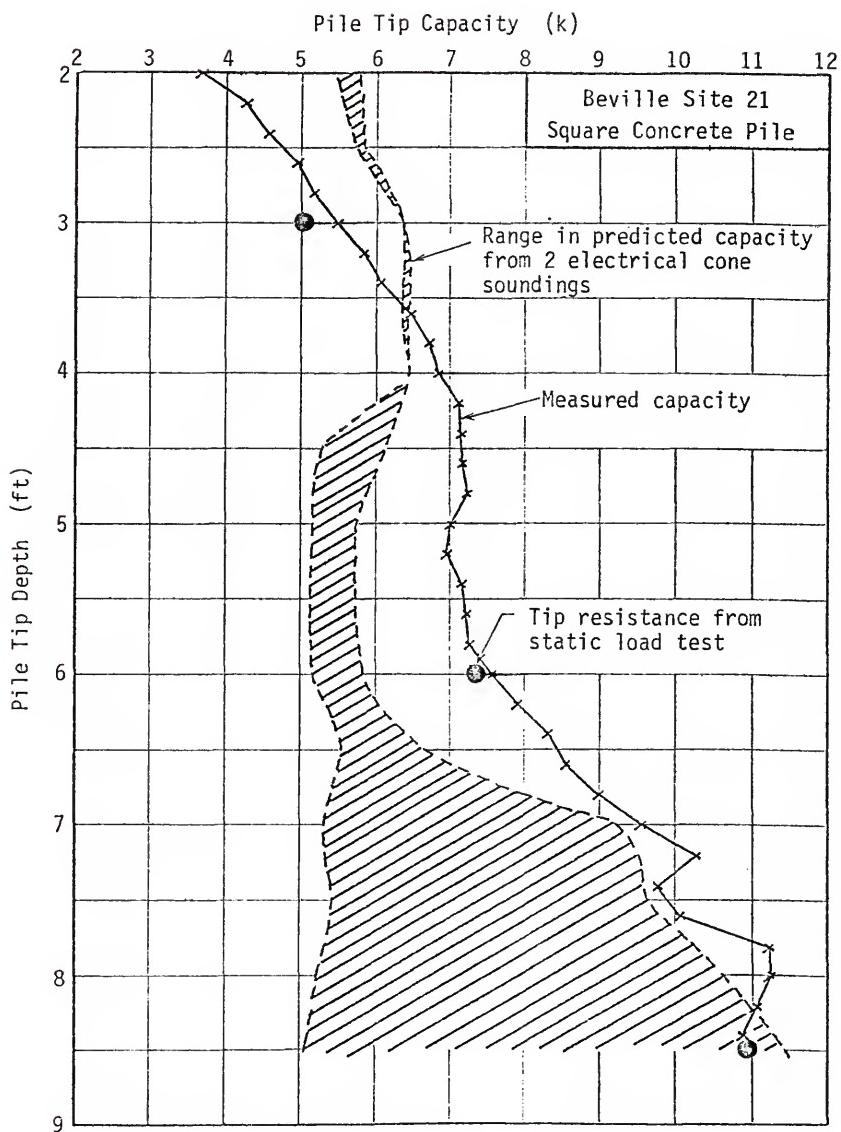
PREDICTED AND MEASURED CAPACITY FOR A JACKED IN PILE

FIGURE 7.16



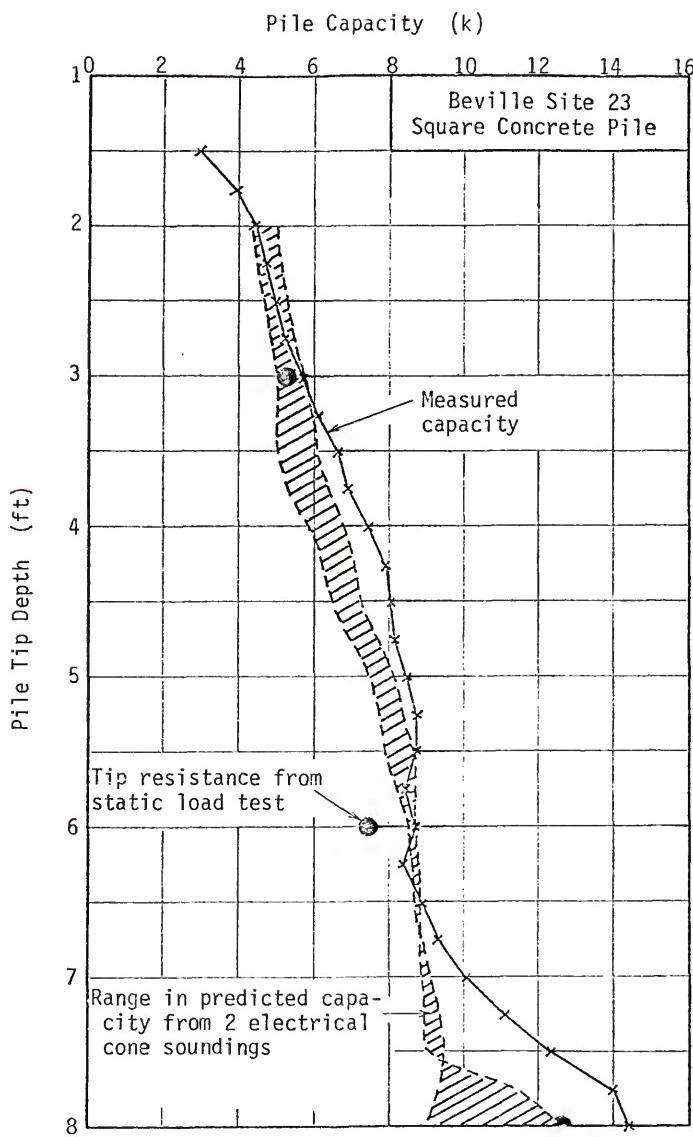
PREDICTED AND MEASURED TIP CAPACITY FOR A JACKED-IN PILE

FIGURE 7.17



PREDICTED AND MEASURED CAPACITY FOR A JACKED-IN PILE

FIGURE 7.18



PREDICTED AND MEASURED CAPACITY FOR A JACKED-IN PILE

FIGURE 7.19

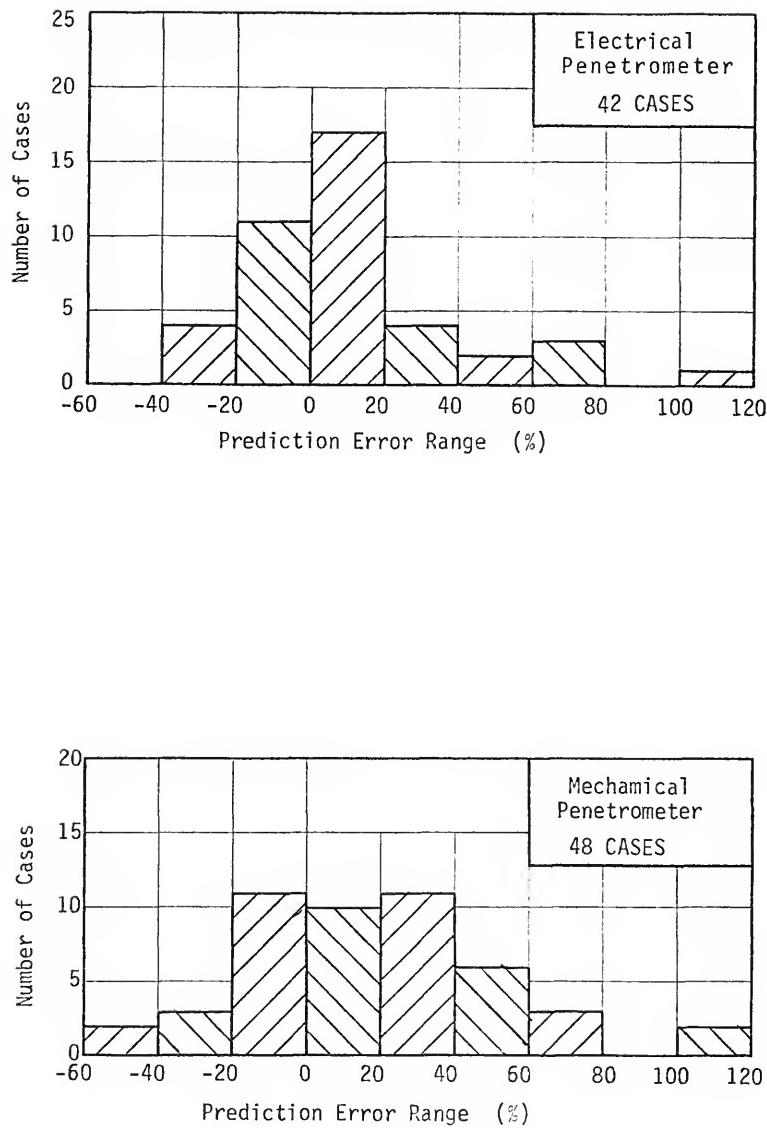
in sands above the water table.

#### 7.2.5 Electrical vs. Mechanical Cone Tip Capacity Predictions

Predicted and measured tip capacity data for the 4.0 in pipe and concrete piles have been combined into composite histograms in Fig 7.20 in order to evaluate the relative accuracy of predictions computed from electrical and mechanical penetrometer data. These graphs show that using mechanical cone data results in a greater average overprediction and a greater range in prediction error.

The greater average prediction error for the mechanical cone data is the result of this cone producing slightly higher  $q_c$  values in the Beville site sands. Since the ratio of mechanical to electrical cone resistance ( $q_{cm}/q_{ce}$ ) is not a constant, the Beville site trend could not be expected to occur in all sands. Mechanical cone  $q_c$  values would probably be lower than electrical cone values in dense sands because of the stress relief provided by the recessed mantle above the mechanical cone point. It would be desirable to correct  $q_{cm}$  data to equivalent  $q_{ce}$  data for the purpose of estimating pile capacities because the electrical cone is a better physical model of a pile; however, sufficient data are not presently available to make such corrections.

Reasons for the greater amount of scatter in the mechanical cone tip capacity predictions are not fully understood, but they are probably associated with the design and operation of this cone. Stress release above the tip, variable friction on the tip mantle, and the incremental pushing procedure would be expected to result in more variability in  $q_{cm}$  than  $q_{ce}$ . Even greater variations probably occur in normally gathered  $q_{cm}$  data due to the use of Bourdon gauge readings instead of the more accurate electrical readout equipment used for this research.



COMPOSITE TIP CAPACITY PREDICTION ERROR DISTRIBUTION GRAPH  
FOR MODEL PIPE AND CONCRETE PILES IN SAND

FIGURE 7.20

#### 7.2.6 Effect of Pile Installation Method

Figs 7.21 and 7.22 show plots of measured tip capacity and predictions based on electrical CPT data for both driven piles (open dots) and jacked-in piles (solid dots). Using the predicted capacity as a basis of comparison, these graphs show that there was little difference between the tip capacity of driven and jacked-in concrete piles, but the capacity of jacked-in pipe piles was noticeably higher than that of driven pipe piles. The data presented in Figs 7.15 through 7.19 also show that pile tip resistance during continuous penetration is considerably higher than that determined from static load tests on the jacked-in piles.

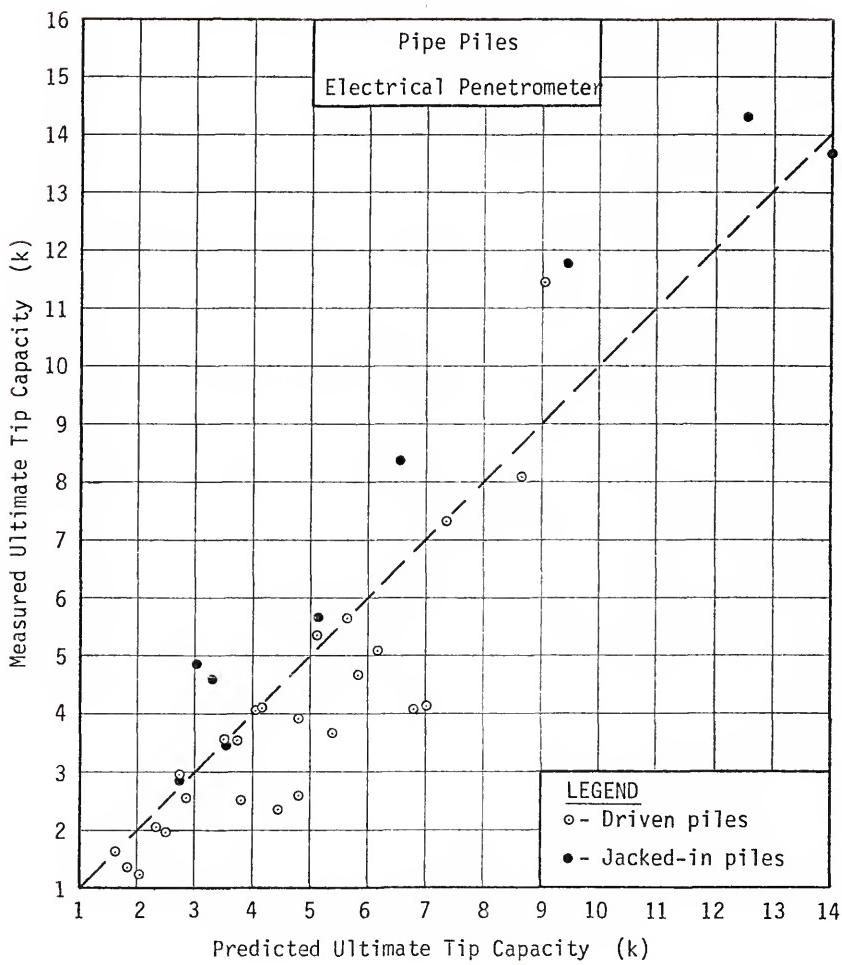
There are two probable reasons for the continuous jack-in resistance being greater than the static load test resistance:

1. The penetration rate is significantly higher during the jack-in procedure.
2. The pile was jacked in using 3 to 4 in strokes; thus, the resistance measurements were made at greater deflections than those obtained from the static load tests. The importance of this effect is shown schematically in Fig 7.23.

The comparative static load test data for driven and jacked-in piles indicate that steady continuous penetration is more effective in compacting soil beneath the pile tip than dynamic driving. This could be responsible for the tendency to overpredict tip capacity since the penetrometer is forced into the soil using a steady continuous thrust.

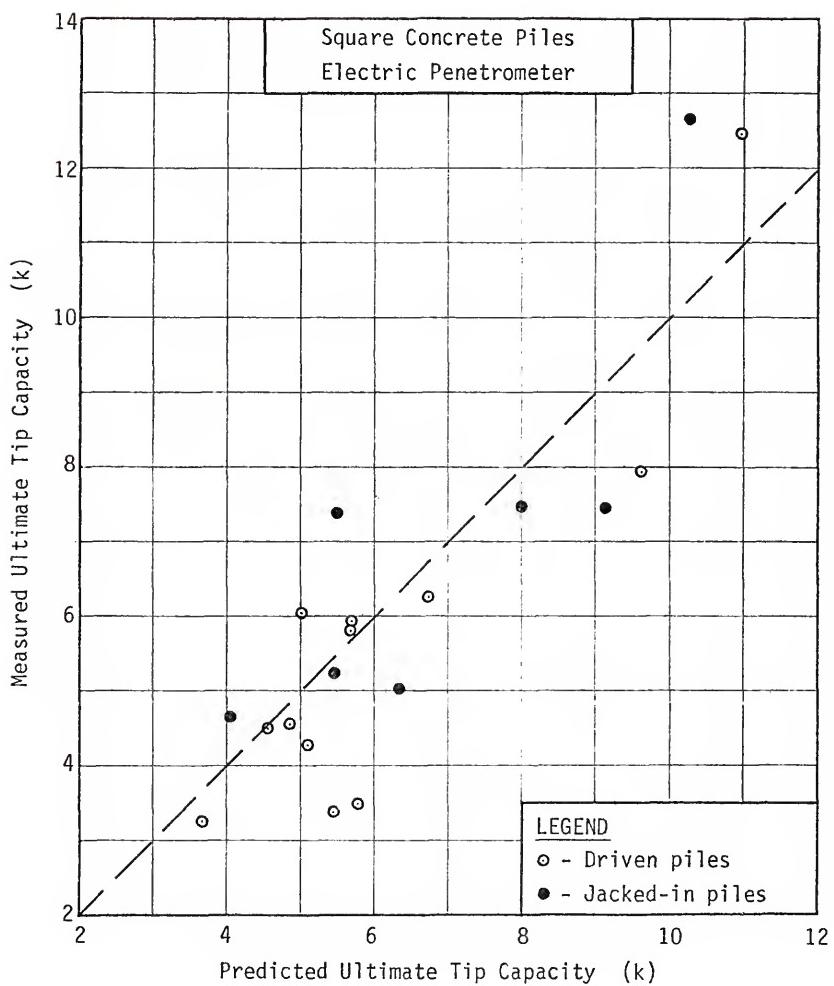
#### 7.2.7 Effect of Pile Point Size, Shape, and Angle

Since the predicted point capacities computed from CPT data represent a measure of the average soil strength in the vicinity of the pile tip, it is possible to roughly evaluate the effects of pile size, shape



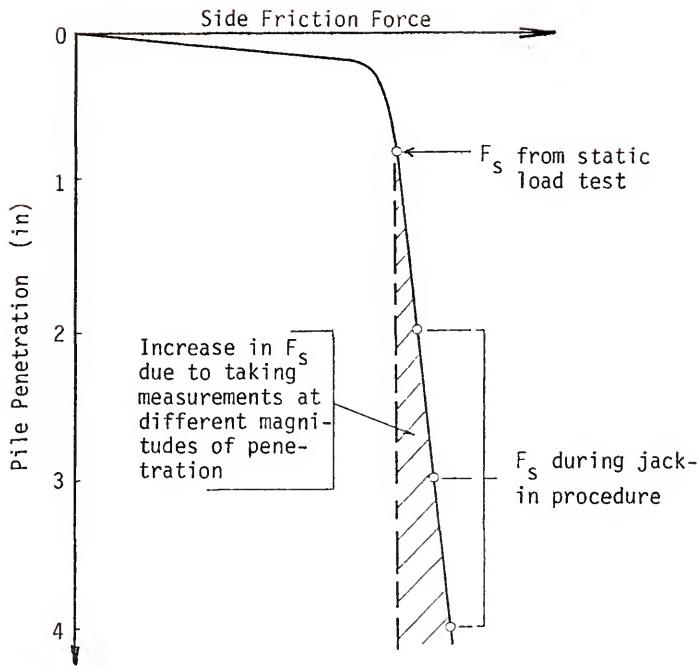
CORRELATION OF MEASURED AND PREDICTED  
ULTIMATE TIP CAPACITY FOR PILES IN SAND

FIGURE 7.21



CORRELATION OF MEASURED AND PREDICTED  
ULTIMATE TIP CAPACITY FOR PILES IN SAND

FIGURE 7.22



POSSIBLE EFFECTS OF CONTINUOUS PILE PENETRATION ON MEASURED PILE FRICTION

FIGURE 7.23

and point angle on tip bearing capacity by comparing predicted to actual capacities for the different size and shape piles. This has been done in Table 7.8.

TABLE 7.8

RATIOS OF PREDICTED TO  
ACTUAL POINT CAPACITY IN SAND

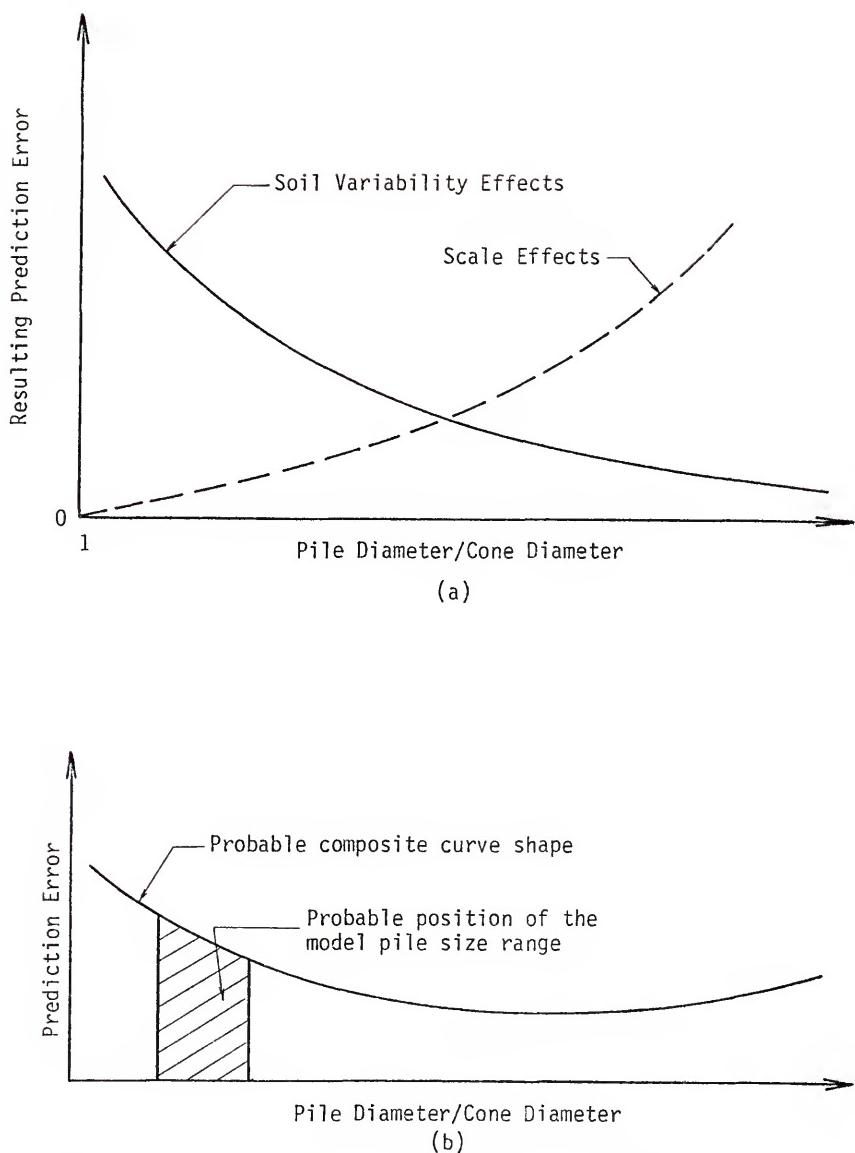
Pile Type	Point Angle	$\frac{Q_{actual}}{Q_{predict.}}$
4.0 in pipe	120°	0.954
2.875 in pipe	90°	0.800
4.0 in concrete	90°	0.876

The ratios for the two pipe piles show that the highest tip capacity was produced by the largest tip angle (flatter tip). The ratios for the 2.875 in pipe pile and the concrete pile indicate a square cross section will produce higher tip capacities than a round section. Since the differences in the ratios are small relative to factors of safety normally used and may be influenced by factors other than tip shape or angle, these effects can be neglected for practical purposes. It should also be noted that the ratios in Table 7.8 were computed using data for piles of different sizes and shapes and may also reflect the influence of these factors. Therefore, the ratios should be considered only as general indicators of the tip angle effect.

Two factors which must be considered when evaluating the effect of pile size (width or diameter) on tip capacity prediction accuracy are natural soil variability and prediction model scale effect errors. If

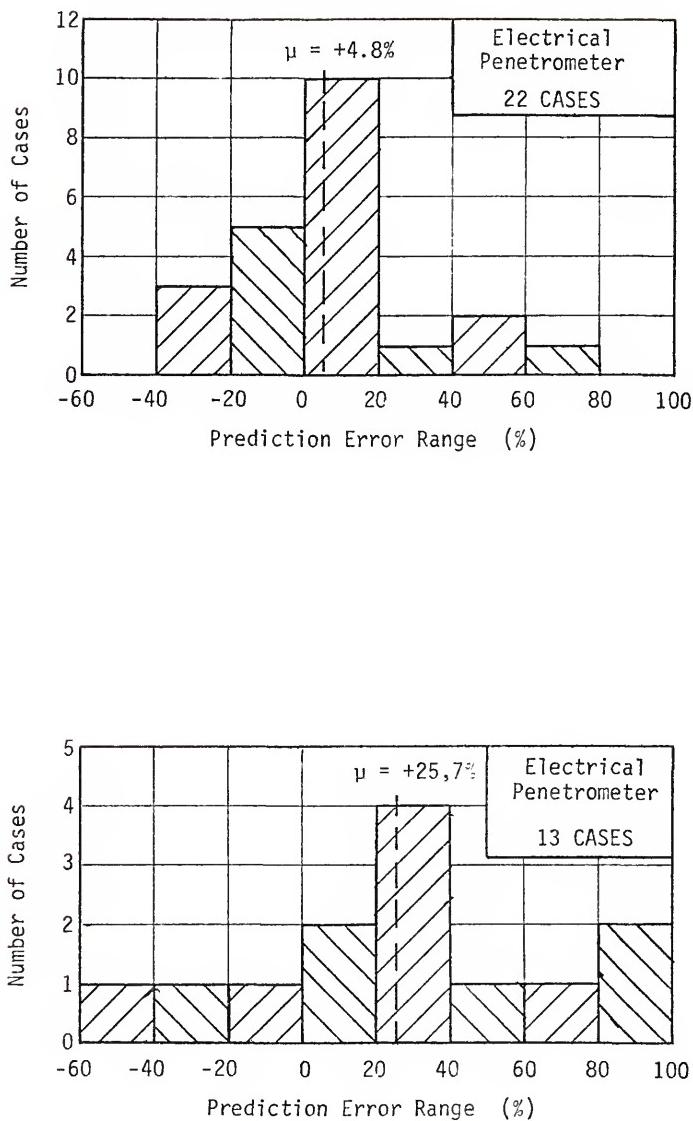
a CPT sounding was made at the exact pile location or if there were no variations in the soil between the sounding and pile location, prediction accuracy should increase with decreasing pile size since the cone becomes a better model as the pile size approaches the cone size. However, if there are natural variations in the soil deposit, prediction accuracy should increase with increasing pile size because minor irregularities in the soil profile have less effect on the capacity of a larger pile. The opposite effects of these two factors are shown qualitatively in Fig 7.24a.

Whether better capacity predictions can be made for large or small piles will depend on the position of the curve representing the algebraic sum of the two curves shown in Fig 7.24a. Although it is impossible to determine the exact position of the composite error curve, its general shape can be deduced from the capacity prediction data for the model piles. The curves shown in Figs 7.15 through 7.19 indicate that the prediction model used reasonably accounted for scale effects over the range of pile sizes tested, while Fig 7.14 shows that soil variability had a large effect on capacity predictions. Therefore, it appears that the soil variability errors should be predominant and the composite error curve should take the shape shown in Fig 7.24b. This curve indicates that capacity predictions for large piles (to some limiting size) should be more accurate than those for small piles. Prediction error histograms for the 2.875 and 4.0 in diameter pipe piles shown in Fig 7.25 support this theory. Additional data on the tip capacity of larger piles would be required to determine the pile size at which scale effect errors become more significant than errors caused by soil heterogeneity.



EFFECT OF PILE SIZE AND SOIL VARIABILITY ON PREDICTION ACCURACY

FIGURE 7.24



ULTIMATE TIP CAPACITY PREDICTION ERROR  
DISTRIBUTION FOR PILE PILES IN SAND

FIGURE 7.25

### 7.3 Pile Side Friction

#### 7.3.1 General Considerations

The most obvious approach to predicting pile side friction from CPT data is to make direct use of local friction sleeve data since these data provide a measure of unit friction acting on the side of the penetrometer rods. Using this approach, the problem becomes one of determining the ratio between unit pile friction ( $f_p$ ) and penetrometer sleeve friction ( $f_s$ ). A number of factors probably influence this ratio, the more important of which are believed to be:

1. Relative roughness of the pile and friction sleeve.
2. Shape and position of the friction sleeve. Because of this factor, the pile to penetrometer friction ratio will probably be different for the electrical and mechanical cone tips.
3. The effect of additional sliding strain on unit friction. This may be important because sleeve friction is always measured near the point (at small sliding strains). Unit friction farther up along the pile shaft may be reduced because of larger amounts of sliding strain.
4. Difference in pile and cone point angles. Begemann (1965) indicated that sharper point angles produce higher  $f_p$  values.
5. Differences in pile and cone shape. Leonards (1962) indicated that  $f_p$  for round piles is approximately 30% higher than  $f_p$  for comparable square piles.
6. Difference in pile and cone size. The lateral expansion caused by the penetrating cone is thought to be great enough to develop full passive resistance; therefore, this effect should be negligible in uniform soil layers. However, scale effects may be important at soil layer interfaces.
7. The manner in which total pile friction is determined from load test data. Use of the yield point failure criteria will normally result in lower  $f_p$  values than would be obtained by using ultimate failure criteria.

If the possible effects of Item 3 are neglected and the scale effects mentioned in Item 6 are properly accounted for, the  $f_p/f_s$

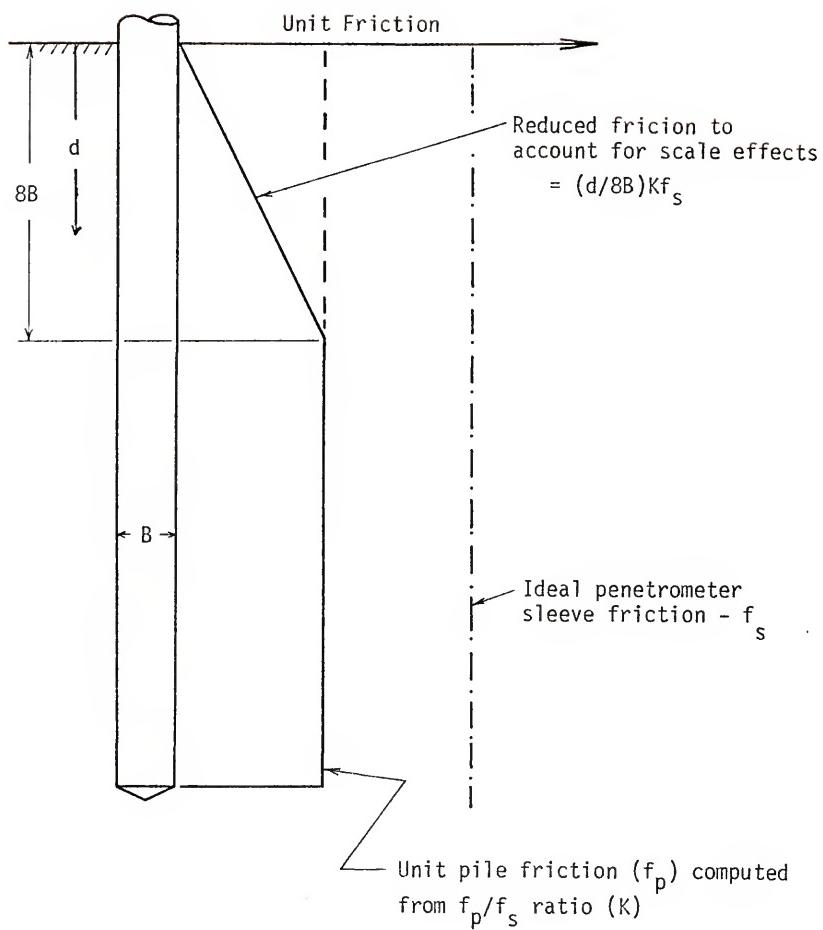
ratio should be constant for a particular pile and penetrometer. This theory was the starting point for developing a side friction prediction method.

Scale effects at the ground surface were accounted for by assuming that  $f_p$  between the surface and a depth of  $8B$  varies linearly with  $d/B$  from zero at the surface to  $f_s$  ( $f_p/f_s$ ) at a depth of  $8B$ . The effect of this correction for an idealized soil profile is shown in Fig 7.26. Depth of embedment corrections for side friction at layer interfaces will be discussed in more detail in Chapters 10 and 11.

The depth of embedment correction for  $f_p$  is similar to that made when computing pile point resistance near the ground surface or at layer interfaces and indirectly assumes that the penetrometer (or pile) friction ratio remains constant while both  $q_c$  and  $f_s$  vary linearly. This assumption is indirectly justified by CPT logs obtained in deep sand deposits which show almost constant FR values even when  $q_c$  varies over wide ranges. For example, see Schmertmann (1969). Practically no systematic research data exist to confirm or contradict this assumption, and studies directed toward clarification of this point are needed. In view of a lack of supporting data, this assumption can be justified by noting that it will either result in little or no error, or a conservative error, depending on what actually happens near the ground surface.

### 7.3.2 Pile Friction Distribution Studies

Several model piles were tested at different depths at the same location, providing a profile of total pile friction with respect to depth. By assuming that total friction over each depth interval remained constant with continued pile penetration,  $f_p$  distribution



DEPTH OF EMBEDMENT FRICTION REDUCTION CONCEPT

FIGURE 7.26

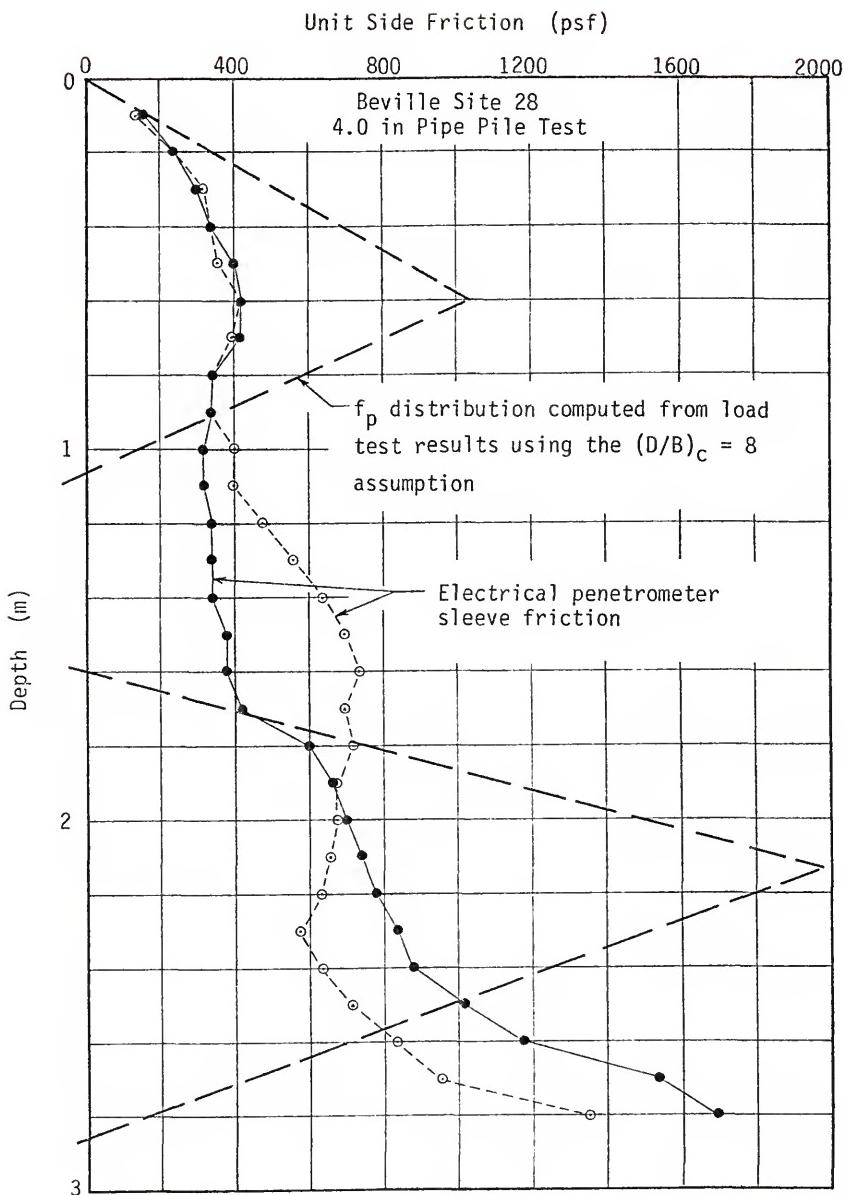
curves could be computed from these data. It was thought that the relationship between computed  $f_p$  curves and  $f_s$  depth curves would provide some insight into the  $f_p/f_s$  ratio.

Representative unit pile friction profiles computed from total friction measurements on incrementally tested pipe and concrete piles are presented in Figs 7.27 and 7.28. The computed  $f_p$  profiles, which show negative values at some depths, prove that assuming unit friction remains constant with additional pile penetration over each depth interval cannot be correct and that  $f_p$  must decrease as additional lengths of pile are driven past a certain point. As discussed in Chapter 2, Begemann (1969a) arrived at a similar conclusion several years ago by noting that total penetrometer rod friction sometimes decreased with depth. The same conclusion was reached by Vijayvergiya (1971), who analyzed pile load test data presented by Vesic (1970) and showed that unit pile friction probably decreased as the test piles were lengthened and driven deeper into a sand deposit.

### 7.3.3 Pile Friction Reduction Studies

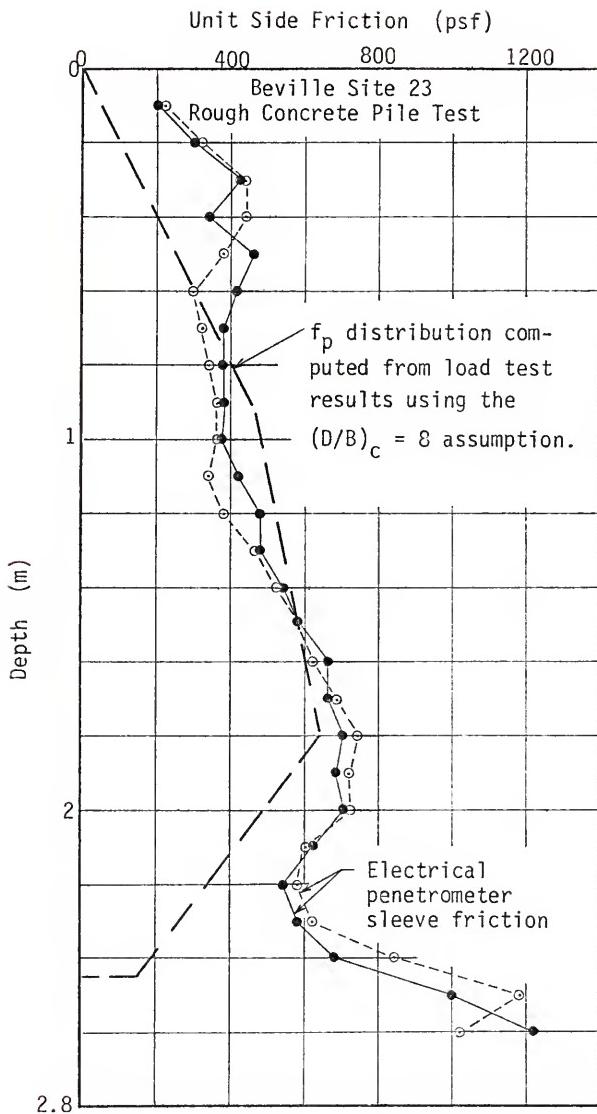
Typical stress-strain behavior of soils indicates that sliding resistance at the pile-soil interface should be a maximum for very small values of sliding strain and should decrease to some final residual value at large strains. This concept is illustrated in Fig 7.29. Also, the peak  $f_p$  value should be related to  $f_s$  since  $f_s$  is representative of penetrometer friction at small strains.

By applying these two concepts, it should be possible to correctly predict total pile friction distribution curves from  $f_s$  data if the correct ratio of peak  $f_p$  to  $f_s$  and the shape of the  $f_p$ -strain reduction curve were known. An analysis of this type was performed



COMPUTED UNIT SIDE FRICTION DISTRIBUTION FOR PIPE PILE IN SAND

FIGURE 7.27



COMPUTED UNIT SIDE FRICTION DISTRIBUTION FOR CONCRETE PILE IN SAND

FIGURE 7.28

using the following equation to estimate total pile friction:

$$F_s = \sum_{d=0}^{8B} \frac{d}{8B} k R_f f_s A'_s + \sum_{d=8B}^L k R_f f_s A'_s \quad (7.3)$$

in which

$F_s$  = total pile friction

$B$  = pile width or diameter

$k$  = ratio or maximum  $f_p$  to  $f_s$

$R_f$  = friction reduction factor

$A'_s$  = pile surface area between  $f_s$  measuring intervals

$d$  = depth from ground surface

$L$  = total length of embedded pile

In general terms, this equation states that the friction acting on the pile at any depth is equal to the unit friction at that depth times the pile area over which the unit friction acts. Unit friction is assumed equal to the product of penetrometer sleeve friction ( $f_s$ ), the ratio of penetrometer to peak pile friction ( $k$ ), and a reduction factor ( $R_f$ ).

The value of  $R_f$  is dependent on the length of pile that has been driven past the point in question. Values of  $R_f$  were determined using the following equation:

$$R_f = \frac{(R_f)_{\min} - 1}{n \epsilon ((R_f)_{\min} - 1) - 1} + (R_f)_{\min} \quad (7.4)$$

in which

$(R_f)_{\min}$  = final or residual  $f_p/f_s$  value

$\epsilon$  = sliding strain computed as  $(L - d)/B$

$n$  = dimensionless parameter which controls the shape of the friction reduction curve

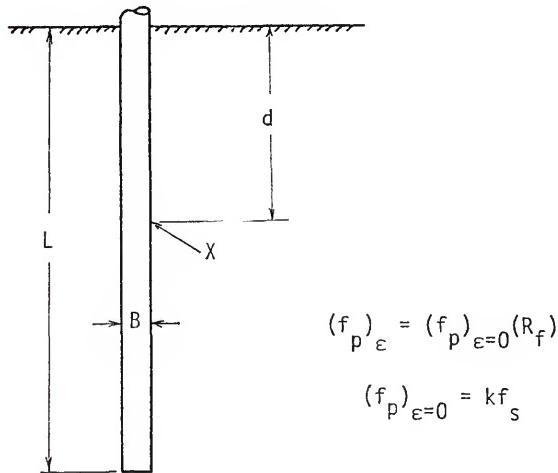
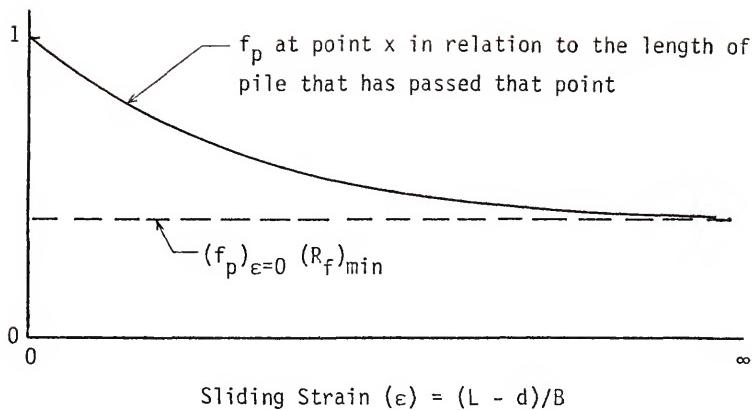
Eqs 7.3 and 7.4 and their physical significance are further detailed in

in Fig 7.29, which illustrates the basic concept, and Fig 7.30, which is a graphical presentation of Eq 7.4 for an assumed  $(R_f)_{min}$  value of 0.5.

A parametric study was performed using Eqs 7.3 and 7.4 with various values of the unknown variables  $k$ ,  $(R_f)_{min}$ , and  $n$  that fell within reasonable limits. This analysis was performed for two pipe and two concrete piles tested at the Beville site. The computed total friction resistance curves obtained from use of these equations were then compared to the actual resistance curves to determine the combination of variables that gave predicted curves which corresponded most closely to the actual curves. Examples of the comparison curves for one pipe pile and one concrete pile are shown in Figs 7.31 and 7.32.

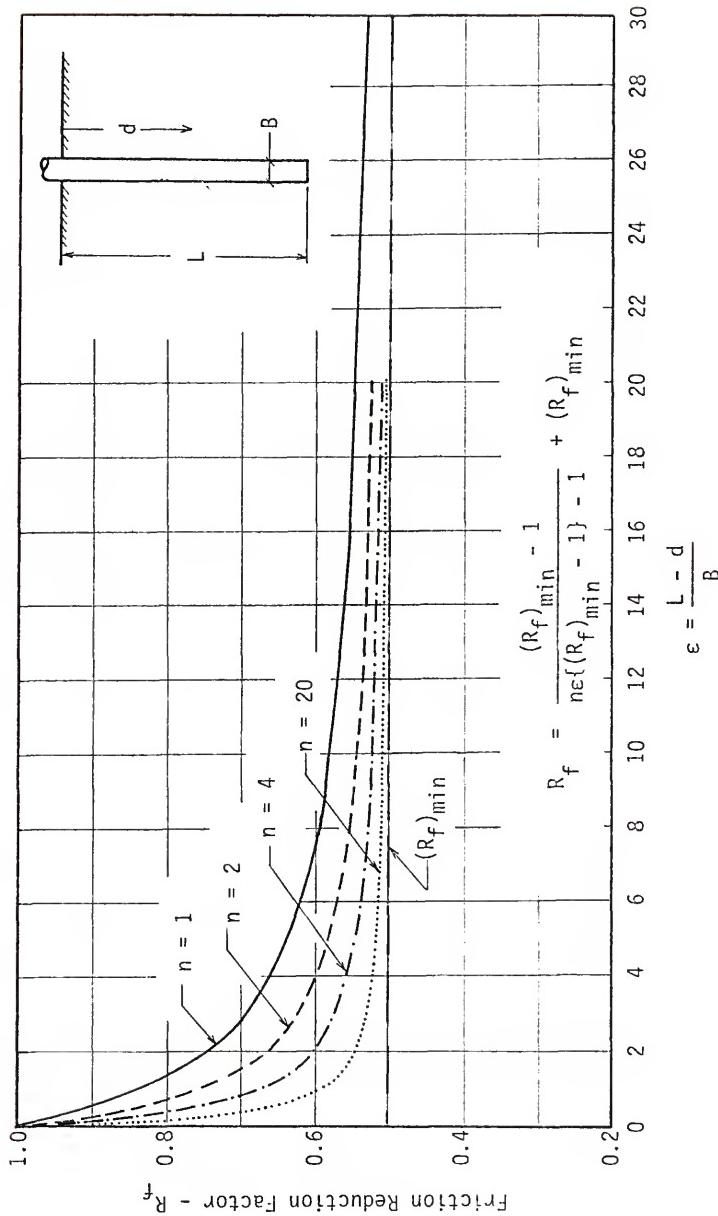
The parametric study results showed that the best fit between measured and predicted total friction curves was obtained by using large  $n$  values which, as shown in Fig 7.30, is approximately equivalent to assuming that  $f_p$  is independent of sliding strain and  $R_f$  is constant at the  $(R_f)_{min}$  value. In addition, practically the same results were obtained by using large  $n$  values with different combinations of  $k$  and  $(R_f)_{min}$ . This resulted in approximately the same  $k(R_f)_{min}$  (and therefore  $kR_f$ ) product and indicated that  $k$  and  $R_f$  could be combined into a single factor, herein designated as  $K$ .

The curves for large  $n$  values, presented in Figs 7.31 and 7.32, show good agreement between measured and computed friction values except for the data points at shallow depths. Data for the other two piles which were evaluated showed the same trend, indicating that the assumed constant  $f_p/f_s$  ratio is reasonable except when very short piles are considered.



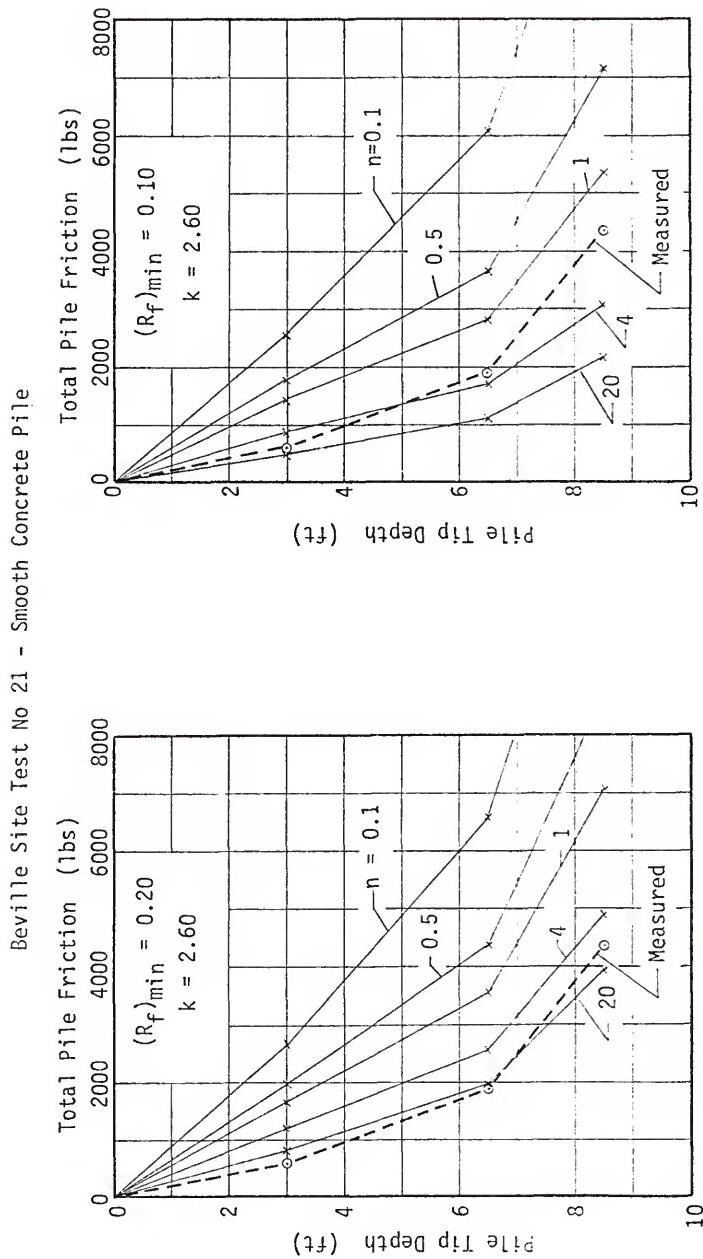
EXPERIMENTAL PILE SIDE FRICTION REDUCTION CONCEPT

FIGURE 7.29



EXAMPLE OF EXPERIMENTAL PILE SIDE FRICTION REDUCTION CURVES

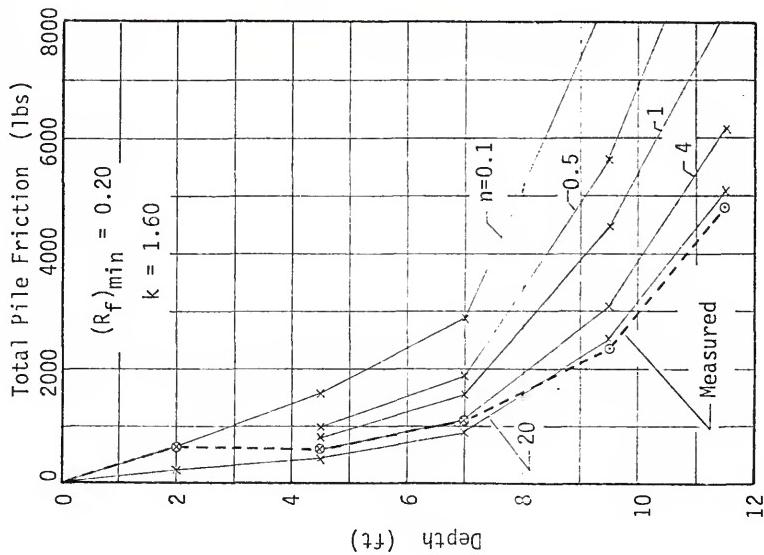
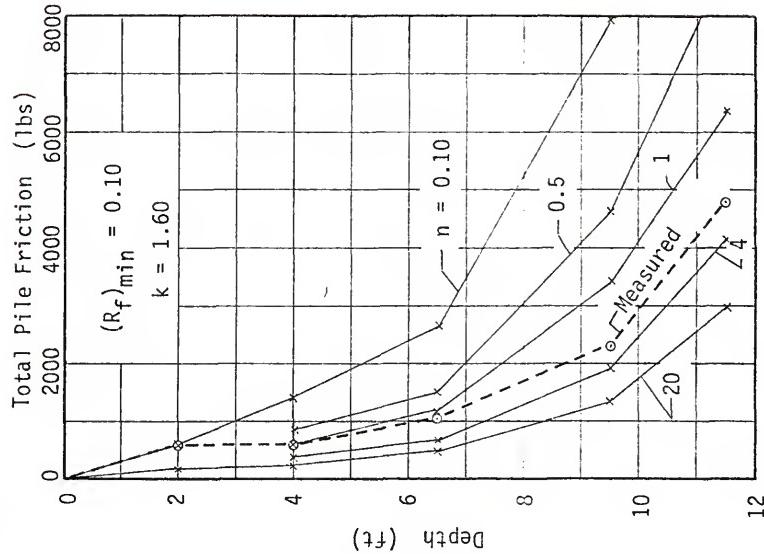
FIGURE 7.30



TRIAL CURVES USING PILE FRICTION REDUCTION CONCEPT

FIGURE 7.31

Bevill Site Test No 13 - 4.0 in Pipe Pile



TRIAL CURVES USING PILE FRICTION REDUCTION CONCEPT

FIGURE 7.32

The higher than expected friction on very short piles may be the result of a different failure mode for these piles as compared to longer piles. Fig 7.33 illustrates a possible explanation for this phenomenon. If the classic shallow foundation-type failure occurs at the tip of the short piles, as shown in Fig 7.33a, the soil adjacent to the pile shaft would be displaced upward and inward, tending to produce passive lateral pressure against the shaft.

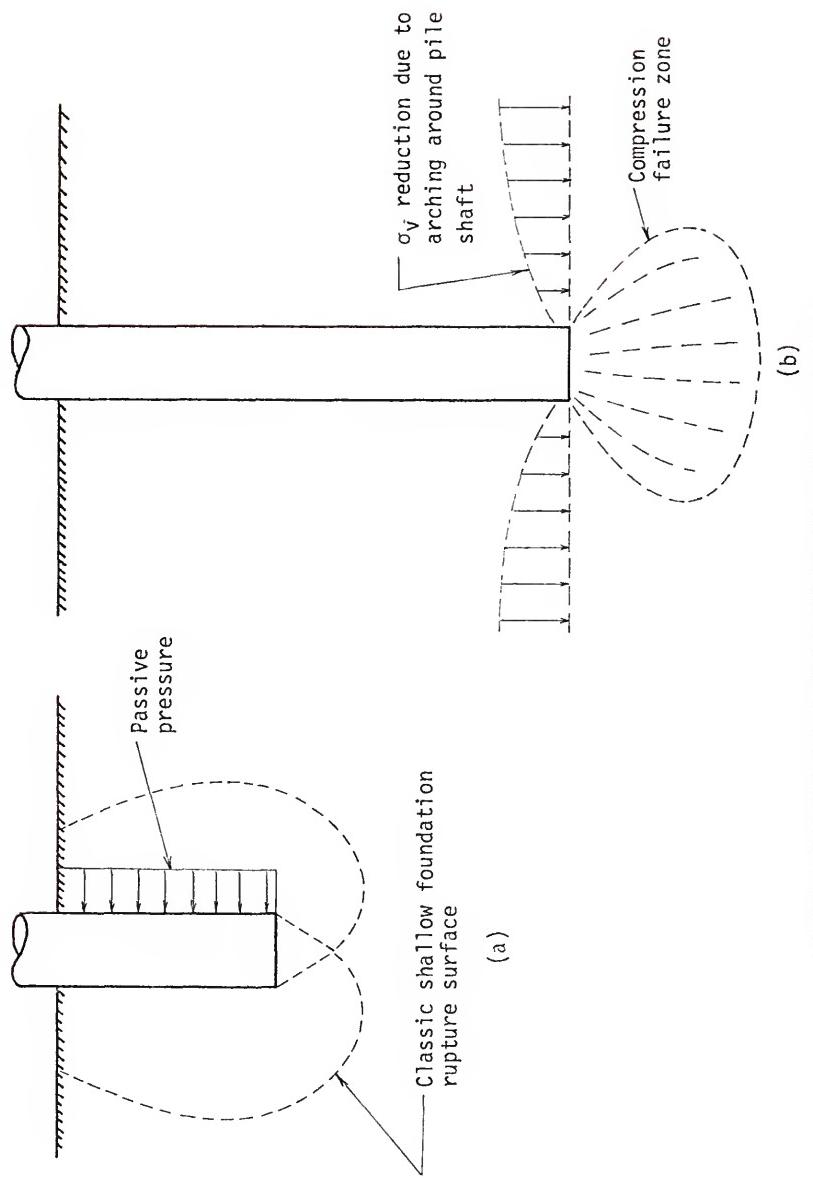
For longer piles, a compression-type tip failure, as shown in Fig 7.33b, is more likely, and the increase in lateral shaft pressure would not occur. There is some evidence, Awkati (1974) and Vesic (1970), which shows that the lateral pressure near the tips of long piles or penetrometers actually decreases for some distance above the pile tip. Vesic attributes this to arching around the pile base. Regardless of the cause of this phenomenon, it should be accounted for in any prediction model for estimating pile side friction.

#### 7.3.4 Development of the Prediction Equation

Based on the results of the studies described in the preceding two sections, it appeared that Eq 7.3 should be modified to take the following form for piles driven into a reasonably uniform deposit of sand:

$$F_s = \sum_{d=0}^{8B} \frac{d}{8B} K f_s A_s' + \sum_{d=8B}^L K f_s A_s'. \quad (7.5)$$

The  $K$  factor in Eq 7.5, which relates penetrometer sleeve friction to pile friction, includes the effects of all variables which affect this relationship and is not the same as the  $k$  factor in Eq 7.4. Note that the first term in Eq 7.5 accounts for scale effects at the ground



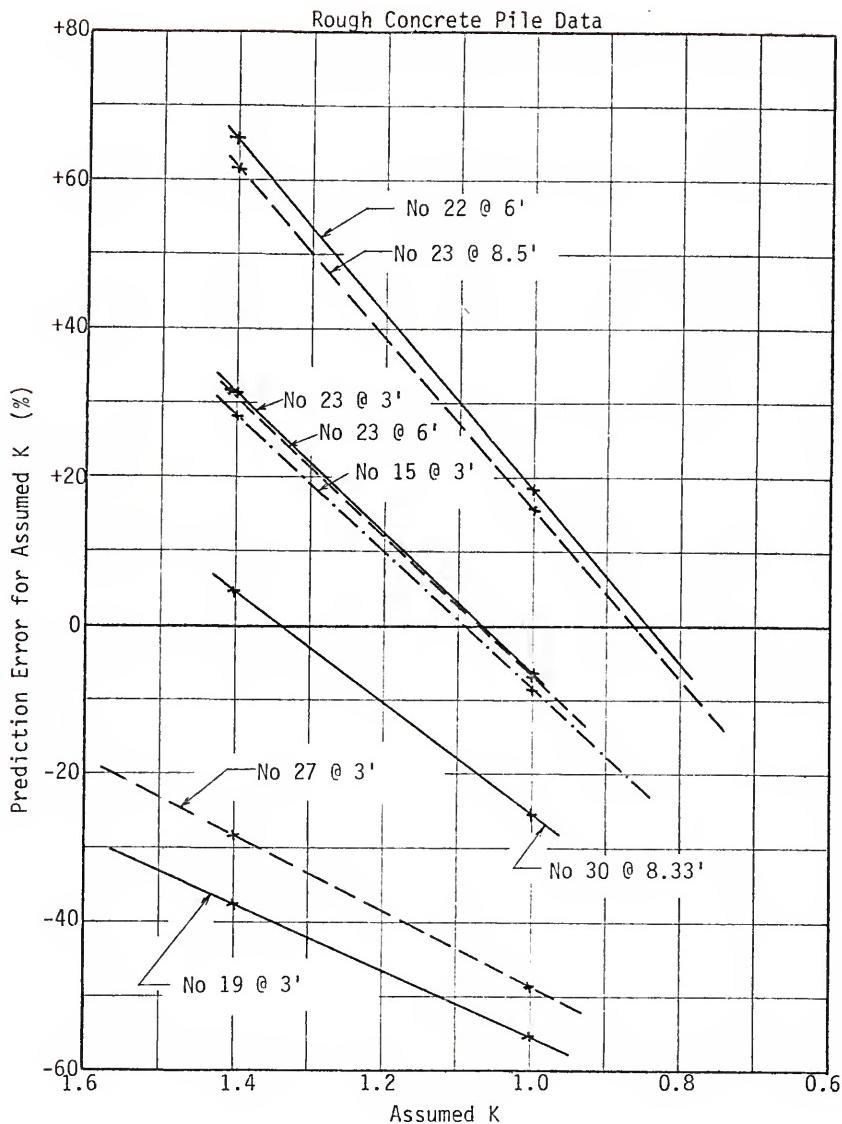
POSSIBLE FAILURE MODES FOR SHALLOW AND DEEP FOUNDATIONS  
FIGURE 7.33

surface as described in the preceding section.

A trial-and-error analysis was conducted using measured  $F_s$  and  $f_{se}$  data from the model tests to determine values of the unknown K factor. Fig 7.34 illustrates the manner in which this analysis was carried out. For each pile test, different values of K were substituted into Eq 7.5, and a value of  $F_s$  was predicted from the electrical cone sleeve friction data. A prediction error was then computed and a point plotted on a graph of prediction error versus assumed K. A prediction error versus K curve was developed in this manner for each pile test, and the correct K value was determined from the intersection of this curve with the zero prediction error line.

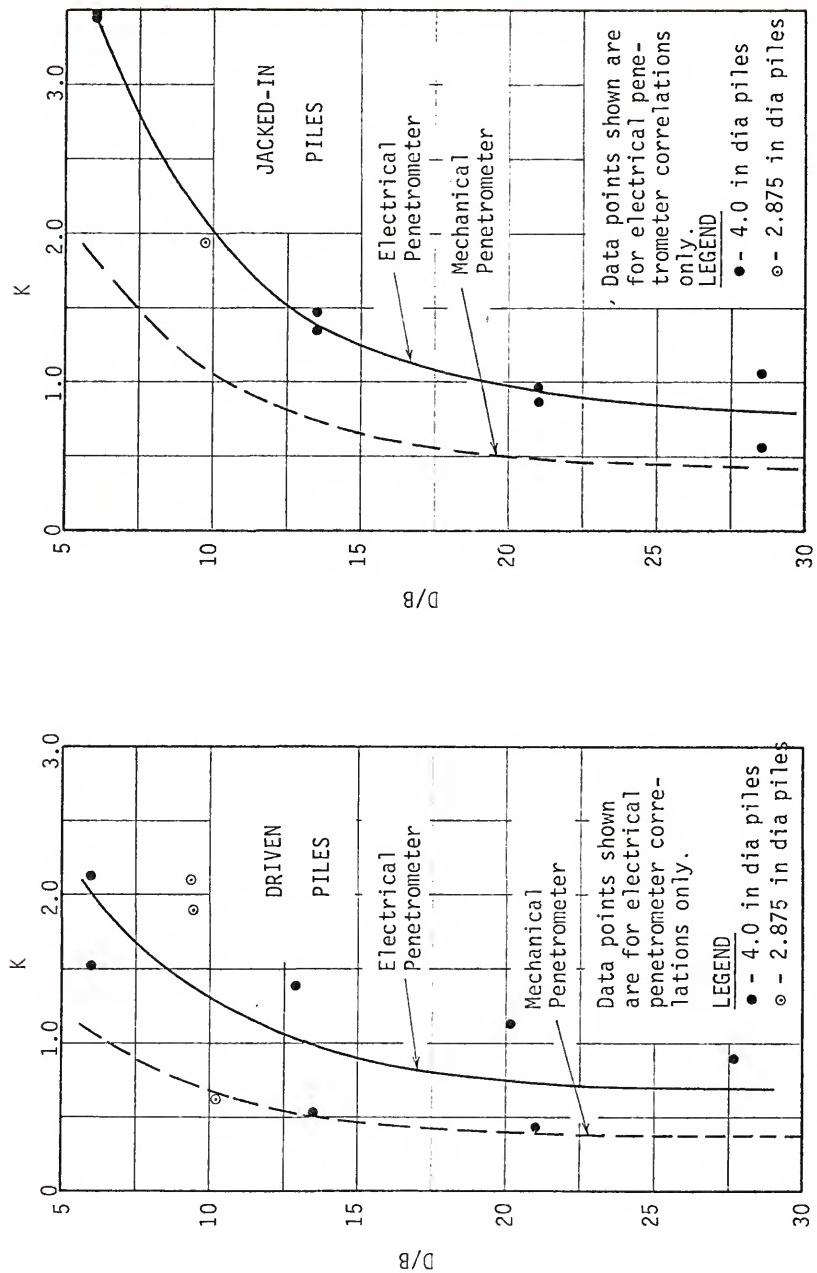
The K values determined from this analysis were plotted as a function of D/B for each pile type and installation method in order to develop K curves for design use. These curves are presented in Figs 7.35 and 7.36. Although the data points on these graphs show a considerable amount of scatter, they exhibited a definite trend which enabled 'eyeball' average curves to be drawn. All the curves show that K is approximately constant for piles 20B or greater in length, but increases with decreasing pile length for piles shorter than 20B. This indirectly accounts for the higher measured friction on the shorter piles.

Design curves for mechanical penetrometer data were developed from electrical penetrometer curves using the ratio of average  $f_{sm}$  to  $f_{se}$  of 0.52, computed using all Beville site cone sounding data. These curves are also shown in Figs 7.35 and 7.36.

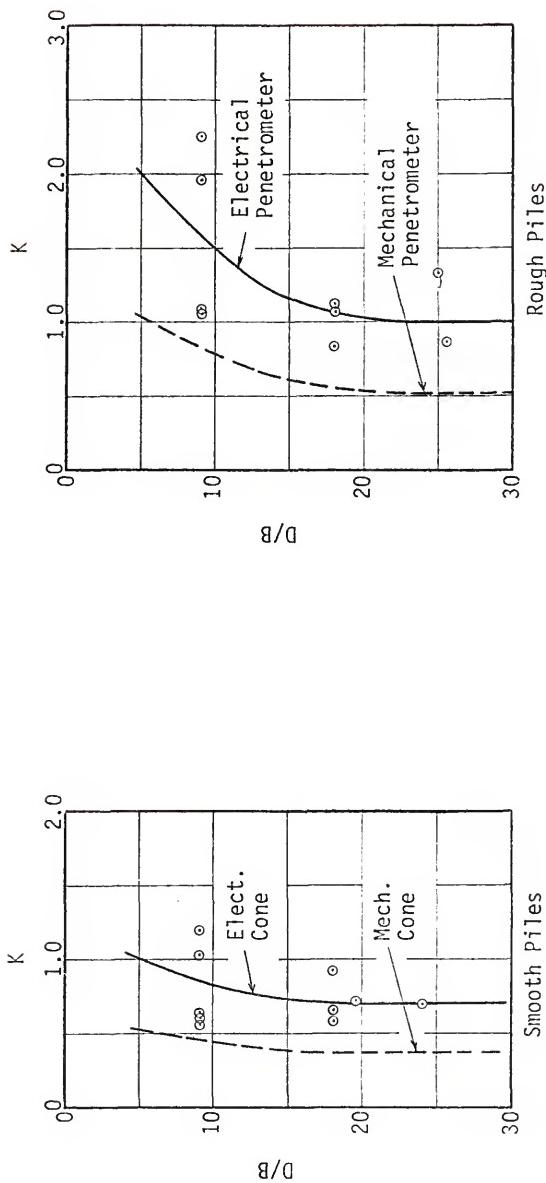


TRIAL AND ERROR METHOD OF DETERMINING  $K$  VALUES

FIGURE 7.34



K-FACTOR CURVES FOR 4.0 IN DIAMETER PIPE PILES IN SAND  
FIGURE 7.35



K-FACTOR CURVES FOR MODEL SQUARE CONCRETE PILES IN SAND

FIGURE 7.36

### 7.3.5 Pile Friction Predictions Using Electrical Cone Data

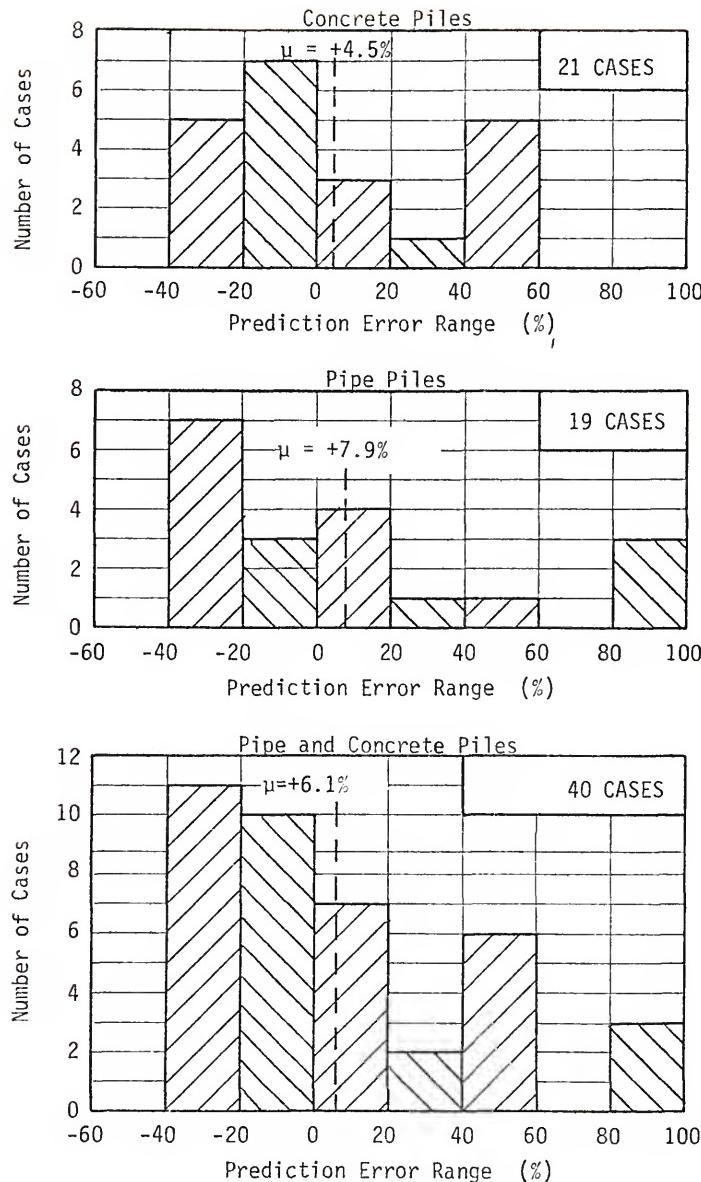
A side friction prediction was made for each model pile tested in sand using electrical cone data, Eq 7.5, and the appropriate curve from Figs 7.35 and 7.36 to evaluate the accuracy of the prediction equation. The results of this analysis are summarized in Tables 7.9 and 7.10 and Fig 7.37. Ultimate side friction resistance values were used to compute the prediction errors, but approximately the same results would be obtained by using yield capacity friction since the average yield capacity friction was only 6% lower than the average ultimate value.

The histograms in Fig 7.37 show a greater range in prediction errors than would be desirable; however, the average errors are small and the histogram combining both pipe and concrete pile data shows a skewed distribution with a peak falling in the conservative prediction error range. This becomes significant when the predicted side friction and tip bearing values are combined to predict total pile capacity.

The range in side friction prediction errors could probably be reduced by modifying Eq 7.5 to account for the reduction in side friction that probably occurs with additional sliding strain; however, carefully performed tests on fully instrumented piles would be required before such a correction could be made. Until data of this type become available, Eq 7.5 can be used to make reasonably accurate side friction estimates.

### 7.3.6 Pile Friction Predictions Using Mechanical Cone Data

Comparisons of measured friction resistance and values predicted using Eq 7.5, Figs 7.35 and 7.36, and mechanical cone sleeve friction data are presented in Tables 7.9 and 7.10 and Fig 7.38. The mechanical



DISTRIBUTIONS OF ELECTRICAL PENETROMETER SIDE FRICTION  
PREDICTION ERRORS FOR MODEL PILES IN SAND

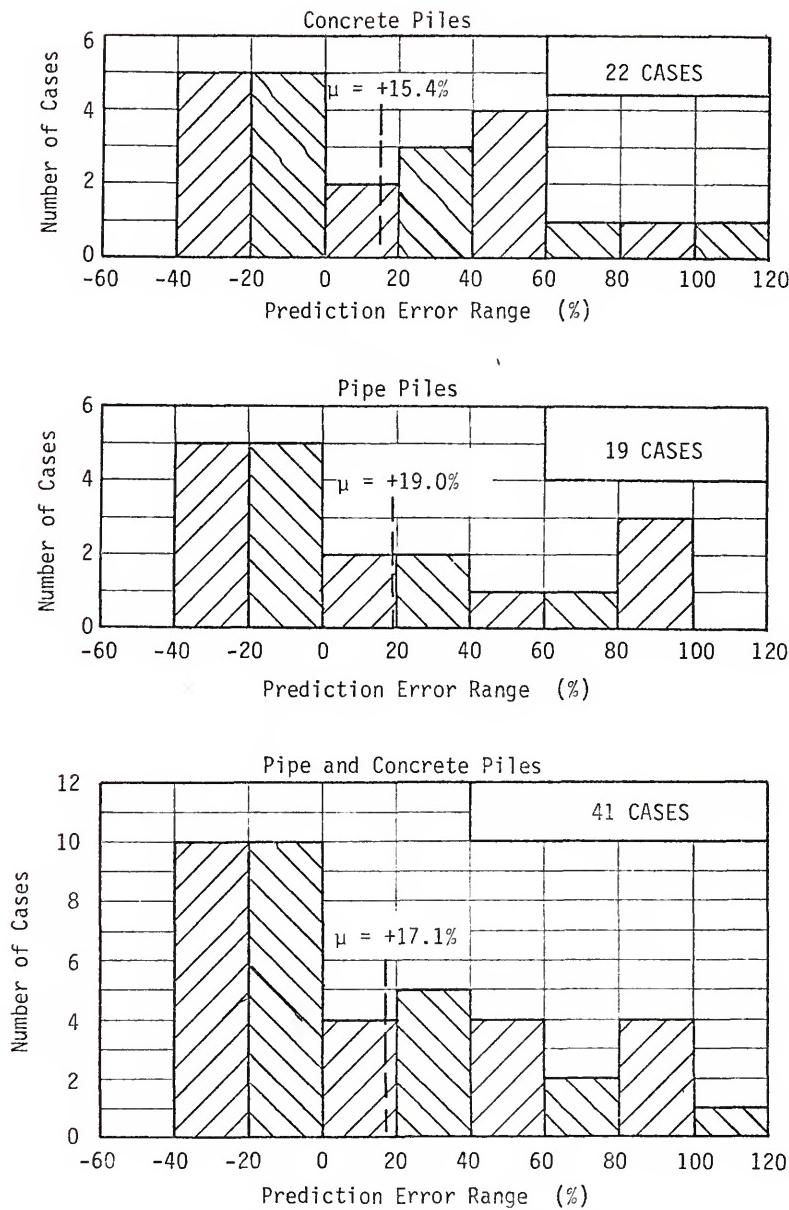
FIGURE 7.37

TABLE 7.9  
SUMMARY OF SIDE FRICTION PREDICTIONS FOR PIPE PILES IN SAND

Test No.	Pile Length (ft)	Electrical Penetrometer		Mechanical Penetrometer	
		Predicted $F_s$ (k)	Measured $F_s$ (k)	Error (%)	Predicted $F_s$ (k)
5	2.5	0.56	0.30	86.7	0.75
12	2.25	0.39	0.54	-27.8	0.50
13	2.0	0.85	0.64	32.8	1.05
	4.5	1.22	0.65	87.7	1.44
	7.0	1.82	1.06	77.3	2.19
20	2.25	0.69	0.63	9.5	0.90
24	2.0	0.93	1.21	-23.1	0.95
	4.25	1.46	1.92	-23.9	1.40
	6.75	2.14	3.28	-34.7	2.38
	9.25	3.32	4.24	-21.7	3.56
28	2.0	1.07	1.08	-0.9	1.41
	4.5	1.68	1.65	1.8	1.83
	7.0	2.71	2.76	-1.8	2.61
	9.5	4.20	5.58	-24.7	3.46
31	2.0	1.11	1.11	0.0	1.05
	4.5	1.39	1.48	-6.1	1.25
	7.0	2.76	2.53	9.1	2.57
	9.5	5.35	3.70	44.6	4.81
32	2.25	0.46	0.70	-34.3	0.51

TABLE 7.10  
SUMMARY OF SIDE FRICTION PREDICTIONS FOR CONCRETE PILES IN SAND

Test No	Pile Length (ft)	Electrical Penetrometer		Predicted $F_s$ (k)	Measured $F_s$ (k)	Error (%)	Predicted $F_s$ (k)	Measured $F_s$ (k)	Error (%)
		Predicted $F_s$ (k)	Measured $F_s$ (k)						
1-S	3.0	0.81	0.54	50.0	0.89	0.54	0.54	0.54	64.8
6-S	6.0	1.75	2.37	-26.2	2.08	2.37	3.55	2.37	-12.2
6-S	8.5	3.00	3.55	-15.5	4.14	3.55	1.09	4.14	16.6
9-S	3.0	0.89	1.09	-18.3	1.56	1.09	3.37	1.77	43.1
6.5	6.5	1.74	1.77	-1.7	5.8	2.34	1.89	1.77	90.4
10-S	6.0	2.00	1.89	-0.9	6.29	4.38	4.38	4.38	23.8
11-S	8.0	4.34	4.38	-0.9	6.29	1.18	1.67	1.18	43.6
11-S	6.0	1.27	1.67	-23.9	45.6	1.29	1.03	1.29	-29.3
14-S	6.0	1.50	1.03	40.6	1.86	0.91	0.91	0.91	25.2
15-R	3.0	1.28	0.91	-28.9	0.85	0.90	0.90	0.90	104.4
17-S	3.0	0.64	0.90	-29.1	1.64	2.30	2.30	2.30	-5.6
18-S	3.0	0.90	2.30	50.7	0.82	0.67	0.67	0.67	-28.7
19-R	3.0	1.65	0.67	19.1	1.92	1.99	1.99	1.99	22.4
21-S	3.0	1.01	2.37	24.0	2.92	2.04	2.04	2.04	-3.5
6.0	6.0	2.37	1.99	49.5	1.36	0.93	0.93	0.93	43.1
22-R	6.0	2.53	2.04	-1.9	2.78	3.18	3.18	3.18	46.2
23-R	3.0	1.39	0.93	15.6	3.60	4.48	4.48	4.48	-12.6
6.0	6.0	3.12	3.18	-1.9	3.53	--	2.41	3.53	-19.6
8.5	8.5	5.18	4.48	15.6	2.31	1.55	1.55	1.55	-31.7
25-S	3.0	--	3.24	-15.7	1.44	-18.7	1.44	1.44	-28.7
6.0	6.0	2.73	1.44	-25.4	5.75	5.75	5.75	5.75	7.6
3.0	3.0	1.17	4.29	3.63	--	--	--	--	-36.9
8.33	8.33	4.29	5.75	3.63	--	--	--	--	--



DISTRIBUTIONS OF MECHANICAL PENETROMETER SIDE FRICTION  
PREDICTION ERRORS FOR MODEL PILES IN SAND

FIGURE 7.38

cone prediction errors show the same trends as those for electrical cone but were scattered over a wider range. This shows that electrical cone data are also superior for estimating side friction.

#### 7.3.7 Effects of Pile Roughness and Shape

The relative position of the K design curves for smooth and rough concrete piles presented in Fig 7.36 shows the effect of pile roughness on side friction. The ratio of K values for smooth and rough concrete piles greater than 20B in length (0.70:1.00) indicates approximately 40% higher unit friction on the rough piles, while Freed's (1973) laboratory tests show the difference should be about 12%. The reason for the difference in the field and laboratory percentages is not fully understood but is probably partially due to experimental error and variable soil conditions at the field test site. Regardless of which value is accepted as being more correct, the data show that concrete pile capacity could be increased by casting piles in rough forms instead of the smooth steel forms that are normally used.

The K values for steel and smooth concrete piles greater than 20B in length are approximately equal, indicating that unit friction is the same for both surfaces. However, Freed's laboratory data show that friction on smooth concrete should be about 33% higher than that for the pile steel. The most logical explanation for the field tests not indicating this difference is that round piles produce a 33% higher friction than square piles with the same surface texture, which is in agreement with the value presented in Leonards (1962). This indicates that the greater friction, which should have occurred on the concrete piles, was just offset by the decrease in friction resulting from a difference in pile shape.

The effect of tip angle on side friction is difficult to evaluate because the effects of other interrelated variables such as pile surface roughness, pile shape, and size cannot be completely determined. The pipe pile design curves in Fig 7.35 show that the computed K values for 90° point angles (2.875 in pile) fall within the same range as the values for 120° point angles (4.0 in pile), indicating that point angle is not a significant variable. Additional research is needed to clarify this point since Begemann's (1963) work showed that pile point angle has a significant effect on tension pile friction.

#### 7.4 Shaft Resistance on Step-Taper Piles

##### 7.4.1 Formulating the Prediction Method

It is more difficult to rationally evaluate step-taper pile shaft resistance data than side friction data for constant section piles because step-taper pile shaft resistance is the sum of two components, friction along the constant diameter sections and end bearing on the step areas. The load test results provide total shaft resistance but no means of determining the relative contributions of the two components.

In order to develop a prediction equation, the following assumptions were made regarding side friction and step bearing:

1. Unit side friction on each constant diameter section will be equal to that on an equivalent constant section pile.
2. Unit step bearing ( $q_s$ ) will be proportional to  $q_c$  at the step depth.

The first assumption is probably slightly conservative since the wedge action of the tapered pile should produce soil compaction around the pile, causing higher lateral stresses than are produced by constant diameter sections. This effect would be more pronounced just below

each diameter step and is probably insignificant along the remainder of the pile.

With regard to the second assumption,  $q_s$  would be expected to exceed  $q_c$  at the same level because of soil compaction and higher lateral stresses caused by the pile wedge action near the pile step.

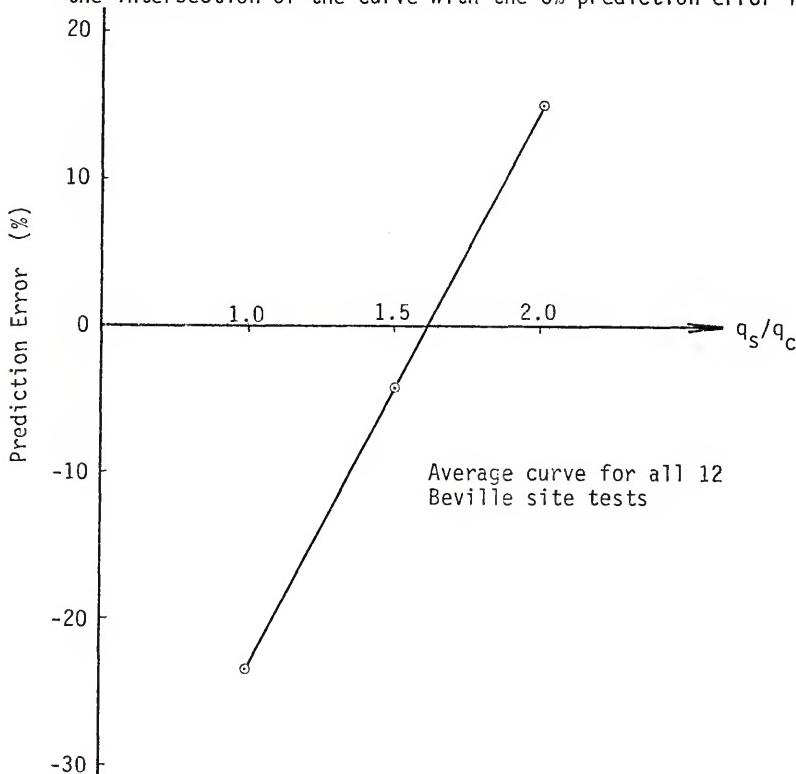
Schmertmann (1972) showed that the radial effective stress, is the main variable controlling  $q_c$  and it should have the same effect on pile step bearing or end bearing.

As a result of the first assumption, the design curves for constant section piles can be used to estimate side friction on the step-taper piles. This permitted computation of a  $q_s/q_c$  ratio for the step-taper pile load tests by using the trial-and-error procedure presented in Fig 7.39. The results of this analysis, also shown in Fig 7.39, give an average  $q_s/q_c$  ratio of 1.6. This value was determined by applying the trial-and-error procedure to all 12 step-taper tests simultaneously and plotting the results in terms of average values rather than plotting a separate curve for each test. Since the  $q_s/q_c$  value seemed reasonable, the following tentative design procedure was adopted for step-taper pile shaft resistance:

1. Compute the side friction contribution using the design method and curves developed for constant section pipe piles with the concept shown in Fig 7.40. Determine D/B values for each section using the section diameter and the depth to which that diameter section extends.
2. Compute the step bearing contribution from  $q_c$  data using a  $q_s/q_c$  ratio of 1.6. When the pile step falls between two cone sounding values, use the average of these two values as  $q_c$ . If the step is at a cone sounding level, use the average of that value and the values immediately above and below as  $q_c$ .

Trial and Error Procedure for Determining  $q_s/q_c$

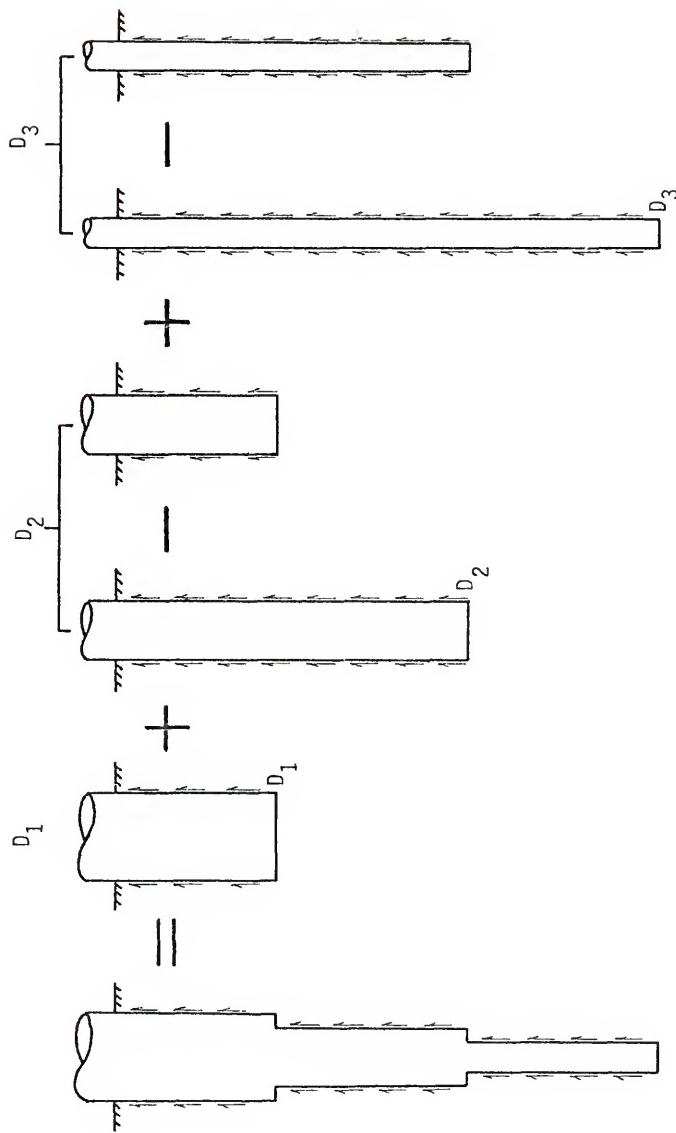
1. Compute side friction on each constant diameter section as if the entire pile were of that diameter.
2. Compute total step bearing using an assumed value for  $q_s/q_c$ .
3. Sum the components from steps 1 and 2 to determine the predicted capacity and compute a prediction error.
4. Repeat steps 1 through 3 for each step-taper pile test to determine an average prediction error for each assumed  $q_s/q_c$  value.
5. Plot the prediction error versus the assumed  $q_s/q_c$  and determine the intersection of the curve with the 0% prediction error line.



PROCEDURE FOR DETERMINING THE RATIO OF  
PILE STEP BEARING TO CONE BEARING RESISTANCE

FIGURE 7.39

Determine K from  $D/B$  value based on:



METHOD OF PREDICTING SIDE FRICTION COMPONENT  
OF SHAFT RESISTANCE FOR STEP-TAPER PILES

FIGURE 7.40

#### 7.4.2 Shaft Resistance Predictions for Step-Taper Piles

The design method outlined in the preceding section was used to make shaft resistance predictions for each step-taper pile tested. The results of analyses based on electrical penetrometer data are presented in Table 7.11. Similar results obtained using mechanical penetrometer data are contained in Table 7.12.

The shaft resistance prediction errors show that the design method was successful in predicting the correct value of shaft resistance. Electrical penetrometer data again provided slightly better predictions than mechanical penetrometer data and the results obtained by both are considered good.

Fig 7.41 shows that, although the average prediction obtained using  $q_s/q_c = 1.6$  was good, there was a tendency toward underprediction for piles with higher shaft resistance capacities. Since the high shaft resistance values were measured on longer piles, it is possible that the  $q_s/q_c$  ratio may increase with depth, at least to a certain point. If so, the ratio computed from the tests on short model piles probably represents a lower limit of  $q_s/q_c$  in sands.

### 7.5 Total Pile Capacity Predictions

#### 7.5.1 Prediction Accuracy for Constant Section Piles

Total ultimate pile capacity predictions, obtained by summing predicted point capacity and side friction, along with measured ultimate capacities and prediction errors for all model pipe and concrete piles tested in sands, are summarized in Tables 7.13 through 7.16. Histograms of the prediction errors are shown in Fig 7.42.

These tables and figures, when compared to similar data for point capacity and side friction predictions presented in Sections 7.2 and

TABLE 7.11

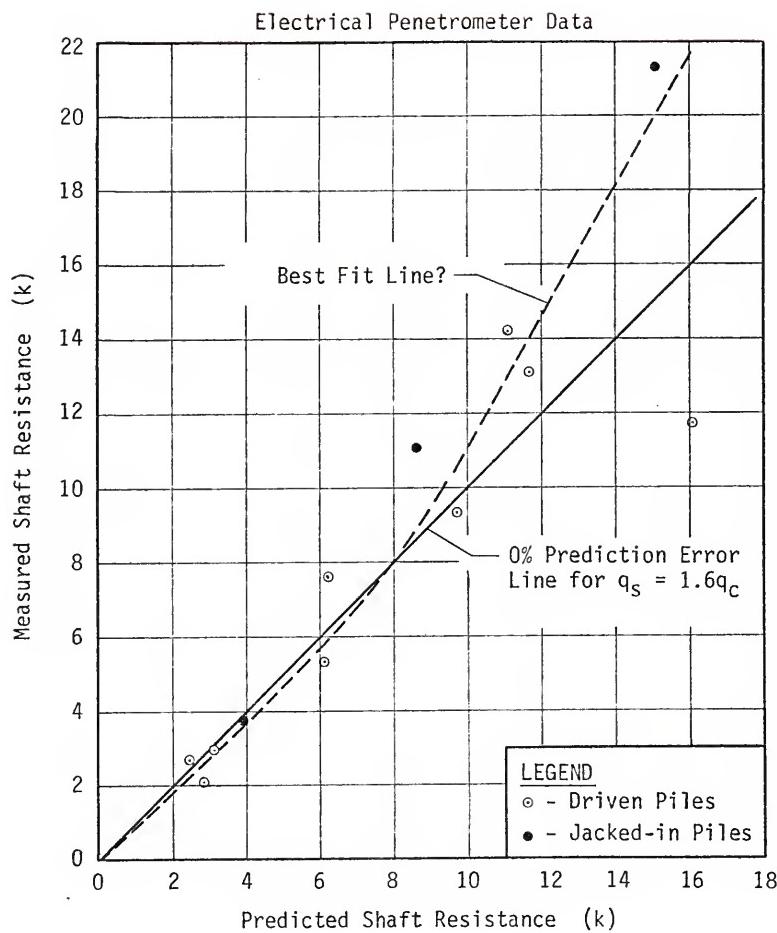
## ULTIMATE CAPACITY PREDICTIONS FOR STEP-TAPER PILE SHAFT RESISTANCE IN SANDS

Test No	Pile Length (ft)	Electrical Penetrometer			Mechanical Penetrometer		
		Pred Q <sub>s</sub> (k)	Meas Q <sub>s</sub> (k)	Error (%)	Pred Q <sub>s</sub> (k)	Meas Q <sub>s</sub> (k)	Error (%)
5	4.75	2.83	2.03	39.4	3.93	2.03	93.6
	7.25	6.15	5.30	16.0	8.39	5.30	58.3
	9.75	11.13	14.20	-21.6	14.57	14.20	2.6
12	4.75	2.43	2.69	- 9.0	2.72	2.69	1.1
	7.25	6.21	7.60	-18.3	5.78	7.60	-23.9
	9.75	11.72	13.06	-10.3	9.63	13.06	-26.3
20	4.25	3.95	3.77	4.8	3.93	3.77	4.2
	7.25	8.63	11.01	-21.6	6.63	11.01	-39.8
	9.75	15.09	21.30	-29.1	10.28	21.30	-51.7
32	4.75	3.16	2.99	5.7	2.84	2.99	- 5.0
	7.25	9.75	9.33	4.5	6.52	9.33	-30.1
	9.75	16.10	11.75	37.0	10.71	11.75	- 8.8

TABLE 7.12

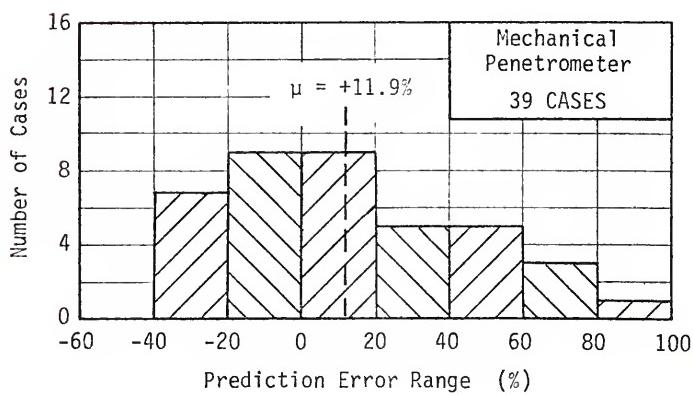
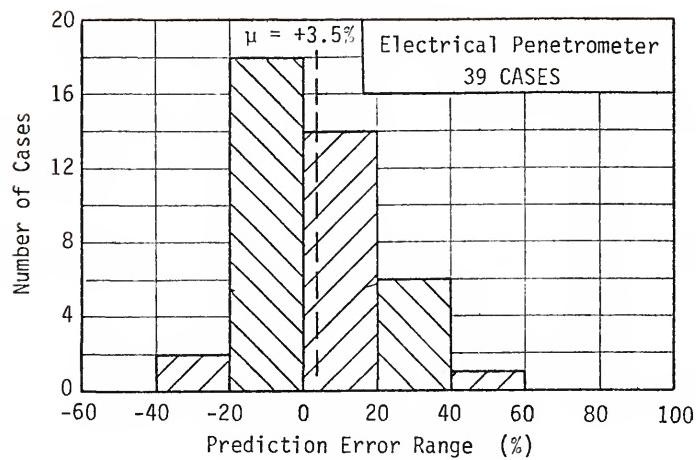
## YIELD CAPACITY PREDICTIONS FOR STEP-TAPER PILE SHAFT RESISTANCE IN SANDS

Test No	Pile Length (ft)	Electrical Penetrometer			Mechanical Penetrometer		
		Pred Q <sub>s</sub> (k)	Meas Q <sub>s</sub> (k)	Error (%)	Pred Q <sub>s</sub> (k)	Meas Q <sub>s</sub> (k)	Error (%)
5	4.75	2.38	1.78	33.7	3.30	1.78	85.4
	7.25	5.17	4.14	24.9	7.04	4.14	70.0
	9.75	9.35	10.27	- 8.9	12.23	10.27	19.1
12	4.75	2.04	2.24	- 8.9	2.28	2.24	1.8
	7.25	5.22	6.20	-15.8	4.85	6.20	-21.8
	9.75	9.84	10.21	- 3.6	8.08	10.21	-20.9
20	4.75	3.32	3.86	-14.0	3.30	3.86	-14.5
	7.25	7.25	10.28	-29.5	5.56	10.28	-45.9
	9.75	12.68	19.95	-36.4	8.63	19.95	-56.7
32	4.75	2.65	2.79	- 5.0	2.38	2.79	-14.7
	7.25	8.19	8.02	2.1	5.47	8.02	-31.8
	9.75	13.52	8.36	61.7	8.99	8.36	7.5



CORRELATION OF MEASURED AND PREDICTED  
SHAFT RESISTANCE OF STEP-TAPER PILES IN SAND

FIGURE 7.41



ULTIMATE CAPACITY PREDICTION ERROR DISTRIBUTIONS  
FOR PIPE AND CONCRETE PILES IN SAND

FIGURE 7.42

TABLE 7.13

## SUMMARY OF TOTAL CAPACITY ELECTRICAL PENETROMETER PREDICTIONS FOR PIPE PILES IN SAND

Test No.	Pile Length (ft)	$F_s$ (k)	Ultimate Capacity			$F_s$ (k)	Predicted $Q_t$ (k)	Predicted $P_{ult}$ (k)	Meas $P_{ult}$ (k)	Error (%)	Yield Capacity Meas		Yield Pyield (k)	Meas Pyield (k)	Error (%)
			Predicted $Q_t$ (k)	$P_{ult}$ (k)	Error (%)										
5	2.5	0.56	1.84	2.40	1.72	39.5	0.56	1.32	1.88	1.55	21.3				
12	2.25	0.39	1.67	2.06	2.21	-6.8	0.39	1.20	1.59	2.11	-24.6				
13	2.0	0.85	2.87	3.72	3.19	16.6	0.85	2.07	2.92	2.68	8.9				
	4.5	1.22	3.47	4.69	4.04	16.1	1.22	2.50	3.72	3.11	19.6				
	7.0	1.82	5.14	6.96	6.61	5.3	1.82	3.70	5.52	5.18	6.6				
20	2.25	0.69	2.35	3.04	2.97	2.4	0.69	1.69	2.38	2.70	-11.8				
24	2.0	0.93	4.11	5.04	5.15	-0.2	0.93	2.96	3.89	4.90	-20.6				
	4.25	1.46	4.09	5.55	6.09	-8.9	1.46	2.94	4.40	4.50	-2.2				
	6.75	2.14	6.20	8.34	9.55	-12.8	2.14	4.46	6.60	7.08	-6.8				
	9.25	3.32	8.64	11.96	12.00	-0.3	3.32	6.22	9.54	9.15	4.3				
28	2.0	1.07	3.52	4.59	4.50	-2.0	1.07	2.53	3.60	3.78	-4.8				
	4.5	1.68	5.16	6.84	7.29	-6.2	1.68	3.72	5.40	5.97	-9.5				
	7.0	2.71	6.55	9.26	10.98	-15.7	2.71	4.72	7.43	9.35	-20.5				
	9.5	4.20	12.55	16.75	19.75	-15.2	4.20	9.04	13.24	17.05	-22.3				
31	2.0	1.11	2.74	3.85	3.74	2.9	1.11	1.97	3.08	3.07	0.3				
	4.5	1.39	3.95	5.34	5.17	-25.5	1.39	2.84	4.23	5.68	-25.5				
	7.0	2.66	9.42	12.18	14.80	-17.7	2.76	6.78	9.54	12.40	-23.1				
	9.5	5.35	14.11	19.46	17.75	9.6	5.35	10.16	15.51	14.50	7.0				
32	2.25	0.46	2.04	2.50	2.09	19.6	0.46	1.47	1.93	1.97	-2.0				

TABLE 7.14

## SUMMARY OF TOTAL CAPACITY MECHANICAL PENETROMETER PREDICTIONS FOR PIPE PILES IN SAND

Test No.	Pile Length (ft)	$F_s$ (k)	Ultimate Capacity			$F_s$ (k)	Yield Capacity		
			Predicted $Q_t$ (k)	Pult (k)	Meas Pult (k)		Predicted $Q_t$ (k)	Meas Yield (k)	Error (%)
5	2.5	0.75	2.62	3.37	1.72	95.9	0.75	1.89	2.64
12	2.25	0.50	1.70	2.20	2.21	-0.4	0.50	1.22	1.72
13	2.0	1.05	4.17	5.22	3.19	63.6	1.05	3.00	4.05
4.0	1.44	4.90	6.34	4.04	56.9	1.44	3.53	4.97	3.11
7.5	2.19	7.81	10.00	6.61	51.3	2.19	5.62	7.81	5.18
20	2.25	0.90	1.90	2.80	2.97	-5.7	0.90	1.37	2.27
24	2.0	0.95	4.16	5.11	5.15	-7.7	0.95	3.00	3.95
4.25	1.40	5.42	6.82	6.09	12.0	1.40	3.90	5.30	4.50
6.75	2.18	6.51	8.69	9.55	-9.0	2.18	4.69	6.87	7.08
9.25	3.56	9.35	12.91	12.00	7.6	3.56	6.73	10.29	9.15
28	2.0	1.41	3.28	4.69	4.50	4.2	1.41	2.36	3.77
4.5	1.83	4.73	6.56	7.29	-10.0	1.83	3.41	5.24	5.97
7.0	2.61	5.43	7.84	10.98	-28.6	2.61	3.91	6.52	9.35
9.5	3.46	11.76	15.22	19.75	-22.9	3.46	8.47	11.93	17.05
31	2.0	1.05	2.95	4.00	3.74	6.9	1.05	2.12	3.17
4.5	1.25	4.63	5.88	7.17	-18.0	1.25	3.33	4.58	5.68
7.0	2.57	9.00	11.57	14.80	-21.8	2.57	6.48	9.05	12.40
9.5	4.81	16.19	21.00	17.75	18.3	4.81	11.66	16.47	14.50
32	2.25	0.51	1.45	1.96	2.09	-6.2	0.51	1.04	1.55
								1.97	-21.3

TABLE 7.15  
SUMMARY OF TOTAL CAPACITY MECHANICAL PENETROMETER  
PREDICTIONS FOR CONCRETE PILES IN SAND

Test No	Pile Length (ft)	$F_S$ (k)	Ultimate Capacity			$F_S$ (k)	Predicted $Q_t$ (k)	$P_{ult}$ (k)	Error (%)	Predicted $Q_t$ (k)	$P_{yield}$ (k)	Yield Capacity Meas	Yield Capacity Predicted	Error (%)
			Predicted $Q_t$ (k)	$P_{ult}$ (k)	Meas									
1-S	3.0	0.89	5.08	5.97	4.81	24.1	0.89	3.73	4.62	3.71	4.62	3.71	24.5	-
	6.0	2.08	5.57	7.65	8.43	-9.3	2.08	4.09	6.17	6.65	-	6.65	-7.2	-
9-S	3.0	1.56	8.03	9.59	5.58	71.9	1.56	5.89	7.45	4.47	6.15	4.47	66.7	47.8
	6.5	3.37	7.80	11.17	7.95	40.5	3.37	5.72	9.09	6.15	7.54	4.51	67.2	67.2
10-S	6.0	2.34	7.08	9.42	5.64	67.0	2.34	5.20	7.54	4.51	14.80	10.32	43.4	43.4
11-S	8.0	6.29	11.59	17.88	12.80	39.7	6.29	8.51	14.80	10.32	6.27	4.22	48.6	48.6
14-S	6.0	1.18	6.93	8.11	5.32	52.4	1.18	5.09	5.55	4.84	8.70	6.58	39.1	39.1
15-R	3.0	1.29	4.83	6.12	4.95	23.6	1.29	3.55	4.84	3.48	8.70	6.58	32.2	32.2
17-S	3.0	1.86	9.32	11.21	8.29	35.2	1.86	6.84	8.70	6.58	3.84	4.69	3.22	45.6
18-S	3.0	0.85	5.23	6.08	4.40	38.2	0.85	2.92	5.09	5.29	5.09	4.93	-3.5	-
19-R	3.0	1.64	4.97	6.61	6.61	0.0	1.64	3.65	5.48	4.64	4.89	4.89	-5.1	-
21-S	3.0	0.82	5.20	6.02	5.82	3.4	0.82	3.82	4.56	4.56	8.03	8.03	-19.3	-
	6.0	1.92	6.21	8.13	9.94	-18.2	1.92	4.81	7.73	5.99	29.0	29.0	-	-
22-R	6.0	2.92	6.55	9.47	7.74	22.3	2.92	4.81	7.73	5.99	3.22	3.22	-	-
23-R	3.0	1.36	5.08	6.44	6.18	4.2	1.36	3.73	5.09	4.93	3.2	3.2	-	-
	6.0	2.78	5.39	8.17	10.96	-25.5	2.78	3.96	6.74	9.04	25.4	25.4	-	-
	8.5	3.60	7.21	10.81	17.90	-39.6	3.60	5.29	8.89	13.83	35.7	35.7	-	-
25-S	3.0	--	--	--	--	--	2.41	8.51	10.92	7.73	41.3	41.3	-	-
26-R	6.0	2.31	5.09	7.40	9.56	-22.6	2.31	3.74	6.05	7.65	20.9	20.9	-	-
27-R	3.0	1.55	5.18	6.73	6.07	10.9	1.55	3.80	5.35	4.69	14.1	14.1	-	-
30-R	8.33	3.63	7.16	10.79	17.42	-38.1	3.63	5.26	8.89	13.40	33.6	33.6	-	-

TABLE 7.16  
SUMMARY OF TOTAL CAPACITY ELECTRICAL PENETROMETER  
PREDICTIONS FOR CONCRETE PILES IN SAND

Test No.	Pile Length (ft)	$F_S$ (k)	Ultimate Capacity			$F_S$ (k)	Predicted $Q_t$ (k)	Predicted $Q_{ult}$ (k)	Error (%)	Yield Capacity Meas (k)	Yield Capacity Predicted $Q_t$ (k)	Yield Capacity Predicted $Q_{ult}$ (k)	Error (%)
			Predicted	Meas	P <sub>ult</sub> (k)								
1-S	3.0	0.81	5.10	5.91	4.81	22.9	0.81	3.74	4.55	3.71	22.6	22.6	0.6
	6.0	1.75	6.73	8.48	8.43	0.6	1.75	4.94	6.69	6.65			
9-S	3.0	0.89	4.54	5.43	5.58	-2.7	0.89	3.33	4.22	4.47	-5.6		
	6.5	1.74	5.00	6.74	7.95	-15.2	1.74	3.67	5.41	6.15	-12.0		
10-S	6.0	2.00	5.78	7.78	5.64	37.9	2.00	4.24	6.24	4.51	38.3		
	8.0	4.34	9.61	13.95	12.80	9.0	4.34	7.05	11.39	10.32	10.4		
11-S	8.0	1.27	7.10	8.37	5.32	57.3	1.27	5.21	6.48	4.22	53.5		
	14-S	3.0	1.50	5.43	6.93	4.95	40.0	1.50	3.99	5.49	3.48		
15-R	3.0	1.28	8.00	9.28	8.29	11.9	1.28	5.87	7.15	6.58	57.7		
17-S	3.0	0.64	3.65	4.29	4.40	-2.5	0.64	2.68	3.32	3.22	8.7		
18-S	3.0	1.63	4.84	6.47	6.61	-2.1	1.63	3.55	5.18	5.48	-5.5		
19-R	3.0	1.01	6.33	7.34	5.82	26.1	1.01	4.65	5.66	4.89	15.7		
21-S	6.0	2.37	5.49	7.86	9.94	-20.9	2.37	4.03	6.40	8.03	-20.3		
	6.0	2.53	5.67	8.20	7.74	5.9	2.53	4.16	6.69	5.99	11.7		
22-R	3.0	1.39	5.43	6.82	6.18	10.3	1.39	3.99	5.38	4.93	9.1		
23-R	6.0	3.12	9.11	12.23	10.96	11.6	3.12	6.69	9.81	9.04	8.5		
	8.5	5.18	10.25	15.43	17.90	-13.8	5.18	7.52	12.70	13.83	8.2		
26-R	6.0	2.73	5.69	8.42	9.56	-11.9	2.73	4.18	6.91	7.65	-9.7		
27-R	3.0	1.17	4.03	5.20	6.07	-14.3	1.17	2.96	4.13	4.69	-11.9		
	8.33	4.29	10.94	15.23	17.42	-12.6	4.29	8.03	12.32	13.40	-8.1		

7.3, show that there is better correlation between measured and predicted total ultimate capacity than for either side friction or tip resistance. This occurs because the prediction methods used tended to overpredict tip resistance and underpredict side friction; thus, the errors tend to cancel each other. Note that while the average side friction errors indicated a general overprediction, the shape of the error distribution curves indicates that statistically an underprediction is more likely.

Tables 7.13 through 7.16 also present predicted and measured yield capacities for the pipe and concrete piles and the prediction errors are summarized graphically in Fig 7.43. These data indicate that the yield capacity of the model piles was predicted with about the same degree of accuracy as the ultimate capacity.

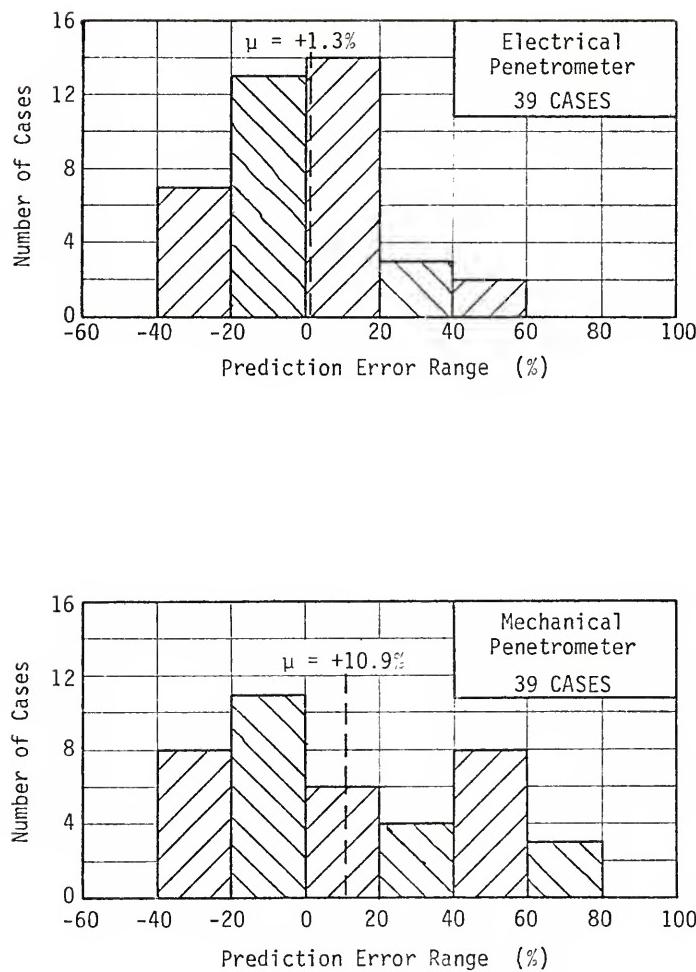
#### 7.5.2 Prediction Accuracy for Step-Taper Piles

Measured and predicted ultimate total capacity for the step-taper piles, along with prediction errors, is presented in Table 7.17, and the prediction error scatter is illustrated graphically in Fig 7.44. Similar yield capacity data summaries are contained in Fig 7.45 and Table 7.18. According to the graphs in Figs 7.44 and 7.45, the accuracy of the step-taper pile capacity predictions is comparable to that for constant section piles. These graphs also show that significantly better capacity predictions can be made from electrical penetrometer data, as was the case for the other piles analyzed and tested.

### 7.6 Design Safety Factors for Piles in Sand

#### 7.6.1 General Considerations

Safety factors used to determine allowable working loads from



YIELD CAPACITY PREDICTION ERROR DISTRIBUTIONS FOR  
4.0 IN PIPE AND CONCRETE PILES IN SAND

FIGURE 7.43

TABLE 7.17

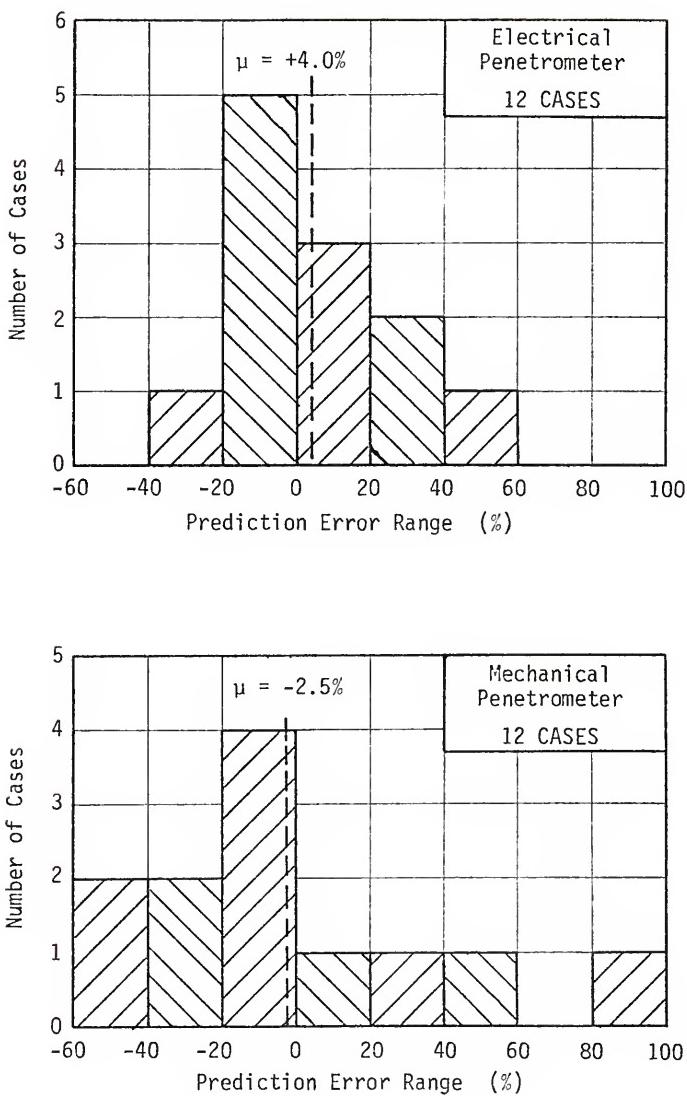
## ULTIMATE CAPACITY PREDICTIONS FOR STEP-TAPER PILES IN SAND

Test No	Pile Length (ft)	Electrical Penetrometer			Mechanical Penetrometer		
		Pred Pult (k)	Meas Pult (k)	Error (%)	Pred Pult (k)	Meas Pult (k)	Error (%)
5	4.75	5.02	3.96	26.8	7.15	3.96	80.5
	7.25	9.35	8.66	8.0	12.90	8.66	49.0
	9.75	16.98	18.88	-10.1	23.67	18.88	25.4
12	4.75	5.18	5.63	-8.0	5.16	5.63	-8.3
	7.25	10.65	9.98	6.7	8.70	9.98	-12.8
	9.75	14.84	15.81	-6.3	13.88	15.81	-12.2
20	4.75	7.23	8.38	-13.7	5.78	8.38	-31.0
	7.25	13.60	15.85	-14.2	8.74	15.85	-44.8
	9.75	19.65	26.10	-24.7	14.34	26.10	-45.0
32	4.75	7.94	6.88	15.4	5.33	6.88	-22.5
	7.25	14.56	11.93	22.0	9.68	11.93	-18.9
	9.75	23.13	15.84	46.0	17.44	15.84	10.1

TABLE 7.18

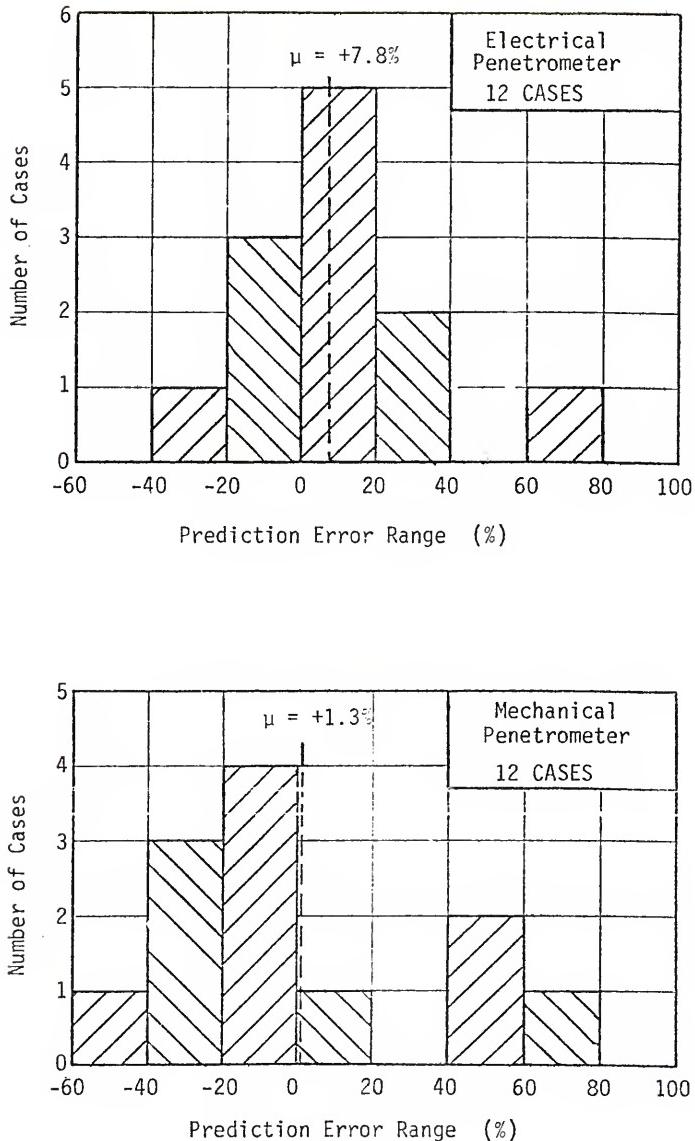
## YIELD CAPACITY PREDICTIONS FOR STEP-TAPER PILES IN SAND

Test No	Pile Length (ft)	Electrical Penetrometer			Mechanical Penetrometer		
		Pred $P_y$ (k)	Meas $P_y$ (k)	Error (%)	Pred $P_y$ (k)	Meas $P_y$ (k)	Error (%)
5	4.75	3.31	3.30	0.3	5.65	3.30	71.2
	7.25	7.51	6.64	13.1	10.33	6.64	55.6
	9.75	13.62	13.40	1.6	18.87	13.40	40.8
12	4.75	4.35	4.54	-4.2	4.06	4.54	-10.6
	7.25	8.95	7.24	23.6	6.98	7.24	-3.6
	9.75	12.12	12.10	0.2	11.18	12.10	-7.6
20	4.75	5.71	6.38	-10.5	4.65	6.38	-27.1
	7.25	10.88	11.73	-7.2	7.10	11.73	-39.5
	9.75	16.05	22.05	-27.2	11.59	22.05	-47.4
32	4.75	6.14	5.82	5.5	4.19	5.82	-28.0
	7.25	11.70	8.92	31.2	7.77	8.92	-12.9
	9.75	18.65	11.15	67.3	13.90	11.15	24.7



ULTIMATE CAPACITY PREDICTION ERROR DISTRIBUTION  
FOR STEP-TAPER PILES IN SAND

FIGURE 7.44



YIELD CAPACITY PREDICTION ERROR DISTRIBUTIONS  
FOR STEP-TAPER PILES IN SAND

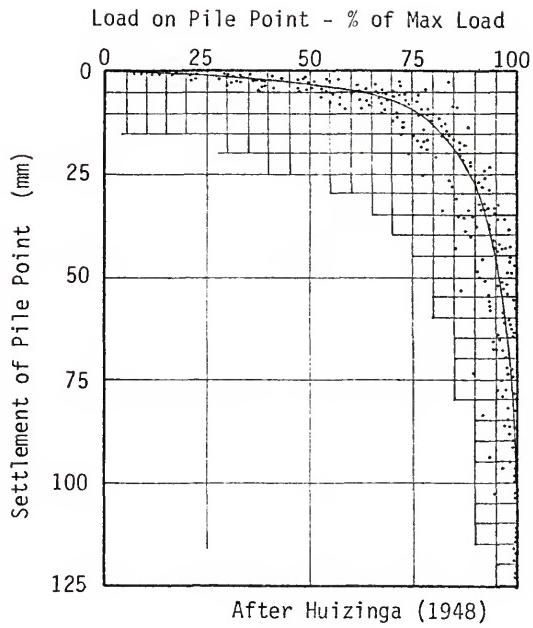
FIGURE 7.45

predicted pile capacities should be based on a number of factors, the more important of which are: accuracy of the prediction method used, the number of piles to be used for structural support, the consequences of a failure, group action effects, and the effects of possible foundation settlement. The data contained in this chapter permit determining safety factors to account for the accuracy of the CPT prediction method.

There are a number of ways which safety factors can be applied during pile capacity design studies. In this country, the most commonly used method is to apply a single safety factor to the total predicted pile capacity. In some European countries, partial safety factors are sometimes used to compute allowable end bearing and side friction resistance, and the sum of these components is used as the allowable pile load.

As discussed in Chapter 2, it is important to remember that any safety factor based on capacity prediction accuracy must be increased to assure that the actual pile load will not exceed a certain percentage of the ultimate load; otherwise, large long-term settlements are likely to occur. Data contained in the literature- (for example, see Fig 7.46) indicate that the maximum allowable working load should not exceed about 2/3 of the ultimate capacity.

Use of yield capacity failure criteria provides an alternate approach which eliminates the necessity of using a maximum allowable load to ultimate load ratio. The yield capacity can be used as the maximum allowable load since it represents the load at which local bearing capacity or plastic yield begins to occur, i.e., the point at which large and continuing settlement could be expected.



PILE SETTLEMENT AS A FUNCTION OF THE  
PERCENT OF ULTIMATE LOAD ACTING ON A PILE

FIGURE 7.46

The following sections present a summary of statistical analyses of the model pile predictions, from which design safety factors are developed. Both partial and total safety factor concepts are considered, using both ultimate and yield failure criteria.

#### 7.6.2 Safety Factors Based on Model Pile Capacity Predictions

The concept used in the statistical analyses of the model pile capacity prediction data to determine safety factors is illustrated in Fig 7.47. Capacity prediction errors were assumed to be normally distributed about the mean, and a safety factor was computed which would provide 95% assurance that the design load will be equal to or less than the actual allowable pile capacity. The equation used to compute the safety factor is as follows:

$$FS = \frac{\mu + t_{\alpha/2} \sigma_D}{100} + 1.00 \quad (7.6)$$

where

$\mu$  = average prediction error

$\sigma_D$  = standard deviation of the prediction errors

$t_{\alpha/2}$  = student's t-value for the desired confidence limit

For this problem,  $t_{\alpha/2}$  was taken as  $t_{0.05}$  since protecting against underdesign only requires consideration of one tail of the distribution curve.

It would be possible to compute safety factors for each of the pile types considered, but for the sake of simplicity, the piles were considered in two groups: constant-section piles and step-taper piles. Only data for 4.0 in pipe and concrete piles were used in the end bearing analysis since the prediction errors for these piles are believed to be more representative of what could be expected of actual

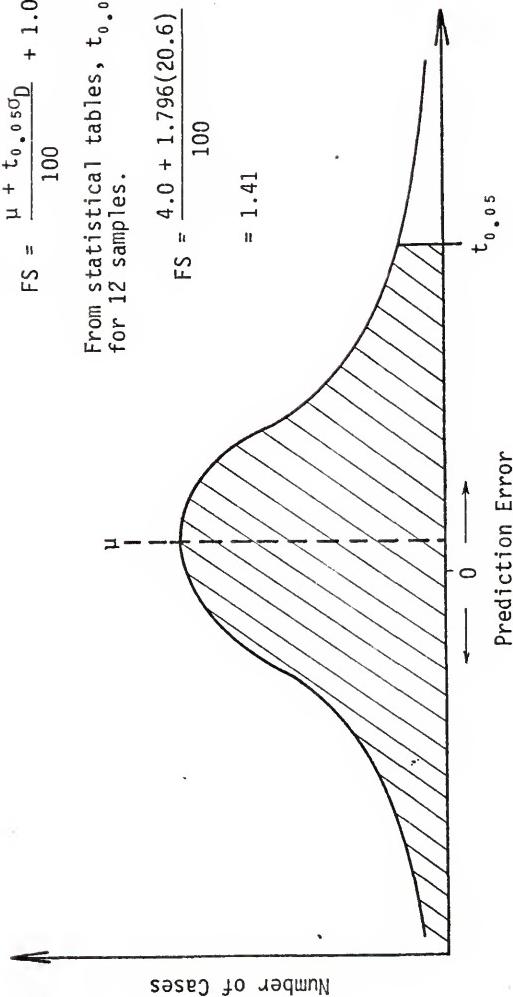
Example Calculation

Evaluate the step-taper pile ultimate capacity safety factor for electrical penetrometer data.

$$FS = \frac{\mu + t_{0.05} \sigma_D}{100} + 1.00$$

From statistical tables,  $t_{0.05} = 1.796$   
for 12 samples.

$$FS = \frac{4.0 + 1.796(20.6)}{100} + 1.00 \\ = 1.41$$



STATISTICAL CONCEPT FOR COMPUTING SAFETY FACTORS

FIGURE 7.47

piles than the 2.875 in pipe pile data.

Table 7.19 presents  $\mu$  and  $\sigma_D$  values for each pile group along with the computed safety factor (FS) to account for capacity prediction errors. The data in this table show that, for a particular penetrometer, ultimate and yield capacities can be estimated with about the same degree of confidence. The same is true for end bearing and side friction predictions. The computed safety factors also show that using electrical penetrometer data will permit use of safety factors about 20% lower than those required for use with mechanical cone data.

These safety factors were determined by applying a prediction method to pile load test data from which the prediction method was developed and are, therefore, representative of an ideal situation. Safety factors used for actual design problems at different sites should probably be somewhat higher. Comparison of these ideal safety factors with those determined from capacity prediction errors for full-scale piles, to be presented in Chapter 10, will permit further evaluation of the applicability of the safety factors in Table 7.19.

TABLE 7.19

## SUMMARY OF SAFETY FACTORS COMPUTED FROM MODEL PILE CAPACITY PREDICTION ERRORS

Pile Type	Case*	No of Samples	$\mu$	End Bearing $\sigma_D$	FS	$\mu$	Side Friction $\sigma_D$	FS	$\mu$	Total Capacity	FS $\sigma_D$
Constant Section	1	42	8.5	29.2	1.57	5.9	32.2	1.59	3.2	18.3	1.33
	2	42	8.9	31.2	1.60	5.9	32.2	1.59	1.4	19.4	1.33
	3	43	18.2	36.4	1.78	14.2	43.4	1.86	10.9	31.3	1.62
	4	43	19.3	38.0	1.82	14.2	43.4	1.86	11.6	31.8	1.64
Step-Taper	1	12			-0.2	22.5	1.40	4.0	20.6	1.41	
	2	12	Same as above		-8.2	25.5	1.38	7.8	24.2	1.51	
	3	12			-1.3	40.5	1.71	-2.5	37.9	1.66	
	4	12			-1.9	42.9	1.75	1.3	38.2	1.70	

\* Case 1: Electrical Penetrometer - Ultimate Capacity

Case 2: Electrical Penetrometer - Yield Capacity

Case 3: Mechanical Penetrometer - Ultimate Capacity

Case 4: Mechanical Penetrometer - Yield Capacity

CHAPTER 8  
MODEL PILE CAPACITY PREDICTIONS IN CLAY

8.1 Currently Available Prediction Methods

8.1.1 Pile Tip Capacity

The ultimate tip bearing capacity of a pile embedded in clay is normally calculated from the classic Terzaghi bearing capacity formula or some modification thereof. The problem is usually considered as a  $\phi = 0$  case for which the bearing capacity equation reduces to:

$$(Q_t)_{ult} = A_t(s_u N_c + \gamma D) \quad (8.1)$$

where

$A_t$  = pile tip area

$s_u$  = undrained shear strength

$N_c$  = bearing capacity factor

$\gamma$  = total unit weight of soil

$D$  = pile tip depth

The  $N_c$  factor in this equation is usually assumed equal to 9.0, although recent research by Ladanyi (1967) shows that  $N_c$  can vary over a wide range, depending on the stress-strain properties of the clay. Another factor which should cause concern when using this method is the wide range in undrained strength values that can be obtained for the same clay, depending on the type of test performed. As illustrated in Fig 3.17, field vane and undrained triaxial shear tests gave  $s_u$  values differing by a factor of about two.

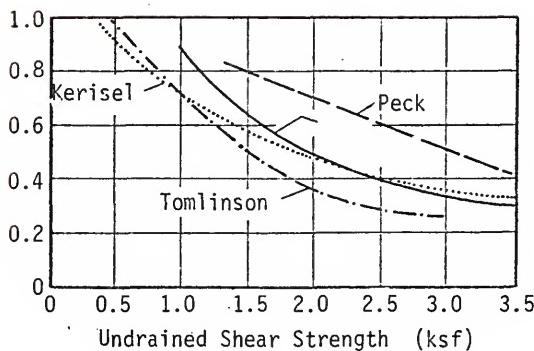
Results obtained using Eq 8.1 have usually been satisfactory, even though possible variations in  $N_c$  and  $s_u$  leave much room for error. This is probably more the result of tip bearing capacity in clays being an insignificant part of the total bearing capacity than to accurate predictions.

#### 8.1.2 Side Friction Estimates Using Undrained Strength Data

Traditionally, friction on piles in clay is estimated using undrained strength data and empirical factors relating unit pile friction (or adhesion) to undrained strength. The  $s_u$  to adhesion ratio, commonly referred to as  $\alpha$ , has been the subject of a great deal of study. Tomlinson (1957 and 1970), Woodward *et al.* (1961), Peck (1958), and Kerisel (1964) have presented  $s_u$ - $\alpha$  curves determined from empirical correlations using pile load test data. These curves are presented in Fig 8.1. All these investigators agree that  $\alpha$  is equal to or slightly greater than 1.0 for soft clays and decreases to as little as 0.25 for very stiff clays. While all of the design curves in Fig 8.1 have the same general shape, they show extreme values of  $\alpha$ , varying by a factor of about two at certain levels of  $s_u$ . The differences in reported  $\alpha$  values could be due to experimental error, different tests for  $s_u$ , and use of data from different types and lengths of piles to develop the different curves. However, a more likely reason is that pile friction is not a simple function of undrained shear strength.

#### 8.1.3 Drained Friction Concepts for Estimating Side Friction

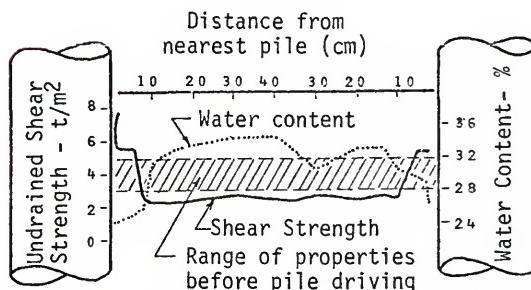
Tomlinson (1957) attributed the decrease in  $\alpha$  with increasing  $s_u$  to imperfect pile-soil contact caused by pile wobble and vibrations during driving. He reasoned that soft clays would squeeze and close



After McClelland (1974)

#### CORRELATION OF $\alpha$ WITH UNDRAINED SHEAR STRENGTH

FIGURE 8.1



Depth of observation = 6.7 m

Pile diameter = 25 cm

After Flatte (1972)

#### SHEAR STRENGTH AND WATER CONTENT VARIATION BETWEEN TWO DRIVEN PILES

FIGURE 8.2

back around the pile while stiff clays would have sufficient strength to maintain an enlarged hole. Although imperfect pile-soil contact may be partially responsible for the  $\alpha$  decrease, a more reasonable and probably more correct explanation of this phenomenon can be made in terms of drained friction.

When a pile is driven into a soft clay, the soil around the pile is remolded and displaced, primarily in the outward radial direction. This displacement causes an increase in both pore pressure and total horizontal pressure around the pile, setting up a consolidation process. The final effective octahedral stress after pile driving will be greater than that which existed before driving; therefore, the soil will be consolidated to a greater all-around pressure and should have a greater undrained strength and a decreased moisture content. Fig 8.2, from Flatté (1972), provides vivid evidence of the effects of radial consolidation around driven piles. The increase in strength that occurs due to consolidation around the pile is partially offset by a loss in strength caused by remolding, but for very soft clays ( $s_u \leq 500$  psf) the strength increase is usually predominant and results in  $\alpha$  values greater than 1.0.

In contrast, negative pore pressures could, and probably do, develop around a pile driven into very stiff clay. Dissipation of these negative pore pressures would cause water to be drawn into the soil around the pile, causing a strength decrease. An additional strength decrease would occur due to remolding; thus, small  $\alpha$  values would be expected.

In recent years, several engineers have recognized that the long-term load capacity of piles driven in clay is controlled by drained

friction at the soil-pile interface and have attempted to deal with the problem in more basic terms. The basic equation for friction on a pile in terms of effective stresses is:

$$f_p = \sigma'_{rf} \tan \delta' \quad (8.2)$$

where

$\sigma'_{rf}$  = final effective radial stress acting on the pile

$\delta'$  = drained friction angle between the soil and pile material

An alternate form of this equation is:

$$f_p = K_f \sigma'_v \tan \delta' \quad (8.3)$$

where

$K_f$  = ratio of final horizontal to initial vertical effective stress

$\sigma'_v$  = vertical effective stress

The main problem in applying this approach is determining the final effective radial stress.

Bozozuk (1972) used an effective stress approach to estimate down drag on piles driven through soft to medium clay beneath a highway embankment. He considered  $\sigma'_{rf}$  to be the sum of two components, the initial  $\sigma'_h$ , as determined from  $\sigma'_v$  and  $K_0$ , and the increase in  $\sigma'_h$ , resulting from embankment loading as determined from elastic theory. It is surprising that negative friction forces estimated in this manner agreed well with measured forces since he ignored the increase in effective radial stress caused by driving the pile into the clay layer. The reasons Bozozuk did not significantly underpredict pile friction are probably that he was dealing with a cemented, very sensitive, slightly overconsolidated clay and was estimating negative, rather than positive, friction.

Burland (1973) proposed a simplified effective stress approach in which pile friction is directly related to vertical effective stress. He replaced  $K_f' \tan \delta'$  in Eq 8.2 with a single term  $\beta$  and showed theoretically that if  $K_f'$  is assumed equal to  $K_0$ ,  $\beta$  for normally consolidated clays should only vary over a small range of about 0.24 to 0.29, as shown in Fig 8.3. He also evaluated the results of several pile load tests and found  $\beta$  values varying from 0.25 to 0.4. This approach appears to have merit for normally consolidated clays but is difficult to apply to overconsolidated soils because  $\beta$  varies over a much wider range, and there is no simple reliable method of determining  $K_f'$  or  $K_0$  for this type of soil.

Vijayvergiya and Focht (1972) assumed that  $\sigma_{rf}'$  is proportional to the Rankine passive pressure and expressed the relationship as follows:

$$f_p = \lambda (\bar{\sigma}_v' + 2\bar{s}_u) \quad (8.4)$$

where

$\lambda$  = empirical correlation coefficient

$\bar{\sigma}_v'$  = mean effective vertical stress along the pile shaft

$\bar{s}_u$  = average undrained shear strength along the pile shaft

This equation does not represent a true effective stress approach but recognizes that  $\sigma_{rf}'$  should be proportional to the total radial stress immediately after pile driving. This approach will be referred to hereafter as the  $\lambda$  method.

A large number of pile load tests were evaluated by Vijayvergiya and Focht in order to determine the range in  $\lambda$  values that should be considered for design purposes. From these correlations, the design curve shown in Fig 8.4 was developed. These authors suggested that use of this method be limited to pipe piles and that  $s_u$  should be determined

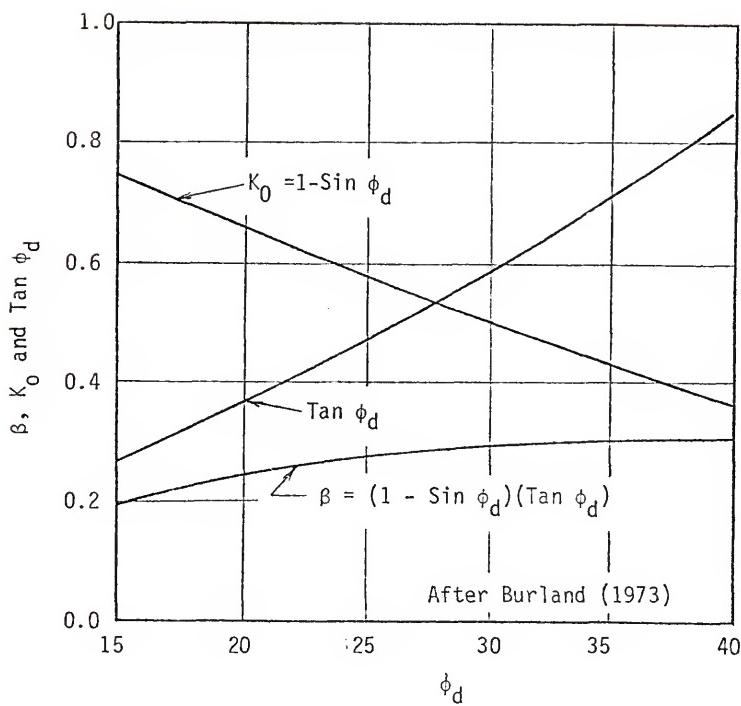
GRAPH OF  $\beta - \phi_d$  RELATIONSHIP

FIGURE 8.3

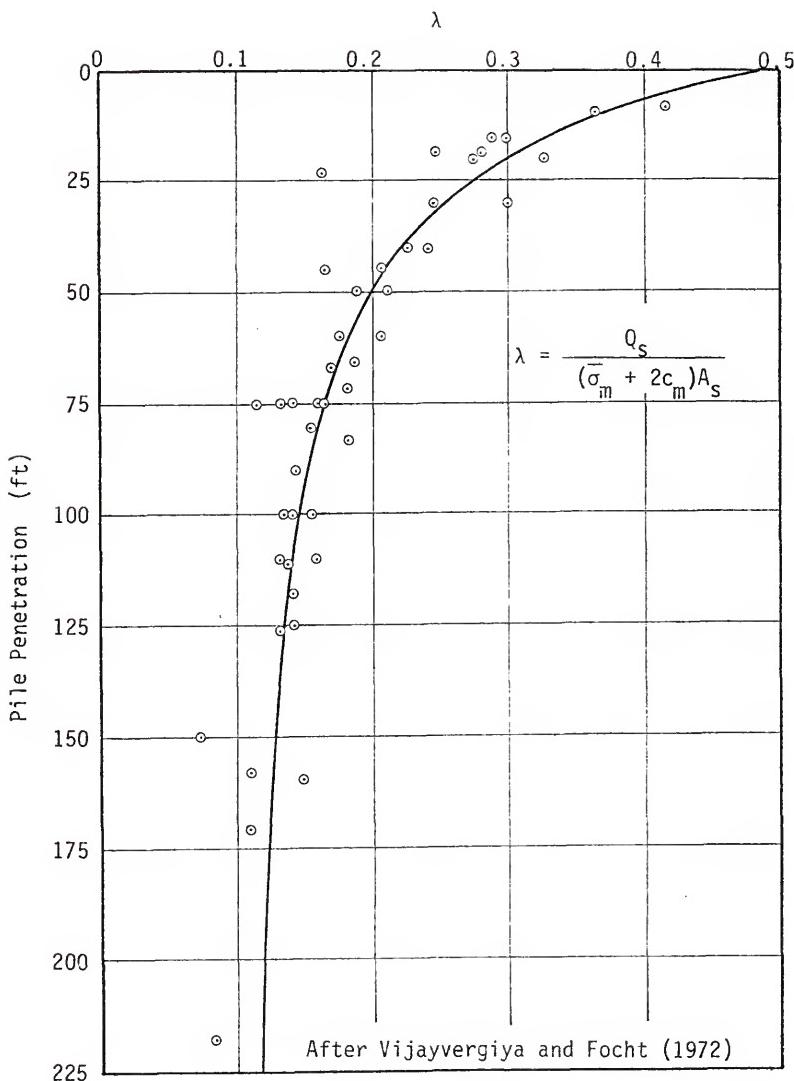
FRICTIONAL CAPACITY COEFFICIENT ( $\lambda$ ) VS PILE PENETRATION

FIGURE 8.4

by unconfined compression or miniature laboratory vane shear tests since these were the types of data used to develop the  $\lambda$  curve. Note that there are no restrictions placed on the strength or condition of the clay for which this method is applicable. The empirically determined  $\lambda$  curve apparently accounts for such factors as  $\tan \delta'$ , degree of overconsolidation, etc.

#### 8.1.4 Schmertmann's Method for Estimating $\sigma'_{rf}$

Empirical effective stress methods such as those proposed by Burland and Vijayvergiya and Focht are improvements over the undrained strength approach but still do not represent a rigorous solution to the problem. Bozozuk's method is fundamentally sound but his assumption that  $\sigma'_{rf}$  is equal to the initial horizontal effective stress plus embankment surcharge effects is questionable.

Schmertmann (1973) suggested a possible method for estimating  $\sigma'_{rf}$  based on cavity expansion theory. The method is based on the assumption that the pressuremeter limit pressure ( $p_L$ ) can be used to approximate the total radial stress acting on a pile immediately after driving. With this as a starting point, he evaluated the radial consolidation process that occurs due to the excess pore pressures generated during driving and arrived at the following equation for the final vertical to radial effective stress ratio:

$$\frac{\sigma'_{rf}}{\sigma'_v} = \frac{\frac{1}{(E/3)a_r} \left[ K_0 + \left( \frac{s_u}{p'_u} \right) \left( 1 + \ln \frac{E}{3s_{uu}} \right) \right] + \left( \frac{s_u/p'}{s_u/p'} \right)_u \left( \frac{1}{S_t} \right)}{1 + \frac{1}{(E/3)a_r}} \quad (8.5)$$

in which

$E$  = pressuremeter modulus

$a_r$  = coefficient of compressibility for the remolded clay

$(s_u/p')_u$  = ratio of undrained strength to effective consolidation pressure for undisturbed samples

$(s_u/p')_r$  = ratio of undrained strength to effective consolidation pressure for remolded samples

$s_{uu}$  = undisturbed undrained shear strength

$s_t$  = soil sensitivity

This stress ratio can be used in conjunction with  $\tan \delta'$  to estimate pile friction since  $\sigma'_{rf}$  is easily determined.

Schmertmann shows theoretically that the remolding which occurs around the pile can have a large influence on the value of  $\sigma'_{rf}$  and suggests that this effect can be evaluated by using both undisturbed and remolded E values in Eq 8.5. Use of  $E_u$  gives a lower bound solution while using  $E_r$  provides an upper bound. He also suggests that the actual  $\sigma'_{rf}$  value will probably be close to the average of the lower and upper bound values.

One of the main variables in Eq 8.5 is the undisturbed undrained shear strength. As explained in Section 8.1.1, widely varying  $s_u$  values can be determined, depending on the type of test performed. Schmertmann recommends using CPT data to estimate  $s_u$ , since the cone produces a cylindrical expansion of the clay as does the pressuremeter and pile.

## 8.2 Possible Methods of Using CPT Data

### 8.2.1 Tip Capacity Predictions

The quasi-static cone penetrometer is the most logical tool to use for an undrained shear strength analysis of pile tip capacity, since it provides a direct measure of unit bearing capacity of a small deep foundation. Using CPT data eliminates the need for selecting appropriate values of  $s_u$  and  $N_c$  as are required for conventional analysis but

retains the characteristics of empirical extrapolation of undrained strength data.

Rate of penetration may influence results obtained from CPT data; however, it is generally thought that the penetration rate effect does not exceed about 10% for the standard 1-2 cm/sec penetration rate in most soils, and this effect can usually be neglected. A scale effect correction will also be necessary when estimating pile tip capacity in clays from  $q_c$  data. For the sake of simplicity, the same  $q_c$  averaging intervals above and below the pile tip will be used for clays as were used for sands. The clay intervals should be somewhat smaller since the critical depth is less for clays. However, use of the larger sand averaging intervals should not produce significant errors in most cases. The sand interval method, as presented in Fig 2.9, will be applied to the model and full-scale piles tested in clays and modified if the results are not satisfactory.

### 8.2.2 Side Friction Predictions

Undrained shear strength controls both  $q_c$  and  $f_s$  in clays so these data should be directly applicable in side friction analysis methods based on undrained strength. Ratios of  $s_u$  to  $q_c$  have been reported by many investigators, for example, Sanglerat (1972, p. 162), Norwegian Geotechnical Institute (1973) and others. Reported  $q_c/s_u$  ratios usually fall within the range of 10 to 25 for mechanical cone data, with an average of about 15 to 18. Only a limited number of data are available for electrical penetrometers, but the ratio is believed to be approximately 30% lower. This ratio will be discussed in more detail in Section 8.4.1.

Use of the  $q_c/s_u$  ratio permits estimating  $s_u$  for clays which can be used in the  $\alpha$  method to predict pile side friction. Shear strength data obtained in this manner could also be used with the semi-effective stress  $\lambda$  method.

It should also be possible to use sleeve friction resistance as a measure of undrained shear strength for estimating pile capacity; however, little work has been done to relate  $f_s$  and  $s_u$  for clays. This problem will be investigated in this chapter, and it will be shown that  $f_s$  data are probably superior to  $q_c$  data for making side friction predictions from undrained strength data.

Schmertmann's drained friction method was developed with the cone penetrometer in mind and can easily be used in conjunction with CPT data. In general, this requires use of the  $q_c/s_u$  ratio and correlations between CPT data and other soil properties. This method will be applied to an actual problem for the first time in this chapter and the applicability of the method will be evaluated.

### 8.3 Model Pile Point Capacity Predictions

Table 8.1 shows a comparison of measured ultimate tip capacities for the Paines Prairie model piles with capacities predicted using the same procedure detailed for sands and both electrical and mechanical CPT data. The average electrical penetrometer prediction error (+9%) and error range (about -25 to +45%) are comparable to those for piles in sand, indicating that Begemann tip capacity prediction method is also applicable to piles in clay.

Direct use of mechanical cone data resulted in large overpredictions, as indicated by the average prediction error of +70% and the error range of +23 to +130%. This overprediction is caused by

TABLE 8.1  
SUMMARY OF ULTIMATE TIP CAPACITY PREDICTIONS FOR MODEL PILES IN CLAY

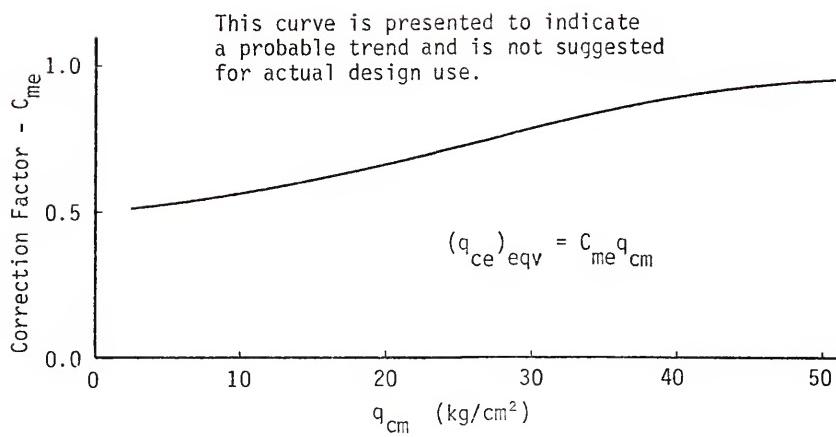
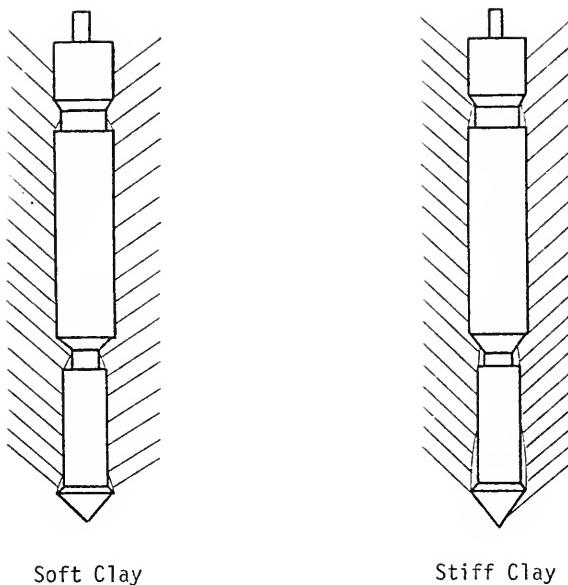
Test No	Pile Type	Tip Depth (ft)	Measured Qt (k)	Electrical Cone			Mechanical Cone			Mechanical Cone - Modified*		
				Pred Qt (k)	Error (%)	Pred Qt (k)	Error (%)	Pred Qt (k)	Error (%)	Pred Qt (k)	Error (%)	Pred Qt (k)
1	Pipe	6.0	1.82	1.60	-12.1	2.93	61.0	1.75	-3.8			
		9.5	1.94	2.68	38.1	3.21	65.5	1.92	-1.0			
2	Pipe	6.0	1.49	1.29	-13.4	2.67	79.2	1.60	7.3			
		9.5	1.56	1.61	3.2	3.24	107.7	1.94	24.3			
3	Conc	6.4	1.67	1.93	15.6	2.18	30.5	1.30	-22.1			
		9.0	1.95	2.20	12.8	2.40	23.1	1.44	-26.1			
4	Step-Taper	5.0	0.74	0.74	0.0	1.53	62.8	0.92	24.3			
		7.5	1.02	0.74	-27.4	1.57	53.9	0.94	-7.8			
		10.0	1.01	0.98	-3.0	2.04	102.0	1.22	20.7			
5	Conc	5.5	1.51	2.20	45.7	3.21	112.6	1.92	27.1			
		8.5	1.31	1.92	46.6	3.02	130.5	1.81	38.1			
6	Step-Taper	5.0	0.77	0.79	3.6	1.11	44.1	0.66	-14.2			
		7.5	0.65	0.71	9.2	1.00	53.8	0.60	-7.6			
		10.0	0.55	0.59	7.3	0.88	60.0	0.53	-3.6			

\*Mechanical cone prediction reduced by 1/1.67 since  $(\bar{q}_{cm}/\bar{q}_{ce}) = 1.67$  in the medium sandy clay below 4.5 ft.

increased  $q_{cm}$  values resulting from friction on the cone tip mantle and possible differences in excess pore pressures generated by the electrical and mechanical penetrometers as a result of the different penetrometer shapes and methods of advancement. The  $q_{cm}/q_{ce}$  ratio for the medium sandy clay to clayey sand in which the model pile tips were embedded was 1.67. Reducing the  $q_{cm}$  tip capacity predictions by this factor brings the mechanical cone predictions in line with those obtained using electrical cone data. This shows that the mechanical cone could also be used to predict pile tip capacity in clays if  $q_{cm}$  data could be converted to equivalent  $q_{ce}$  data.

Parez (1974) investigated the effect of tip mantle friction on  $q_c$  data by performing CPT tests in the same clay deposit using cones with mantle lengths 0.33, 1.0, and 3.0 times the tip diameter ( $D$ ). He reported no appreciable difference in  $q_c$  values measured using the 0.33D and 1.0D mantles, but  $q_c$  measured with the 3.0D mantle, the same as the Begemann mechanical penetrometer, was increased by 40% in medium clays and 20-35% in stiff clays. Sanglerat (1972) suggests that mantle friction for the Dutch-type mechanical penetrometers in clays can increase  $q_c$  by 80 to 100%.

The mantle friction effect trends indicated by Parez's data seem reasonable since stiff clays would be less likely to squeeze around the mantle and cause an appreciable increase in  $q_c$ . Therefore, a  $q_c$  correction curve would probably take the form shown in Fig 8.5. Additional research will be required to determine the true shape of this curve and the correction factor magnitudes. Until these data become available, use of a correction factor of 0.6 is suggested. This value is probably conservative for the types of clays in which piles would normally be founded.



POSSIBLE EFFECTS OF MANTLE FRICTION ON  $q_{cm}$

FIGURE 8.5

#### 8.4 Model Pile Side Friction Predictions

##### 8.4.1 $\alpha$ and $\lambda$ Methods Using $q_c$ Data

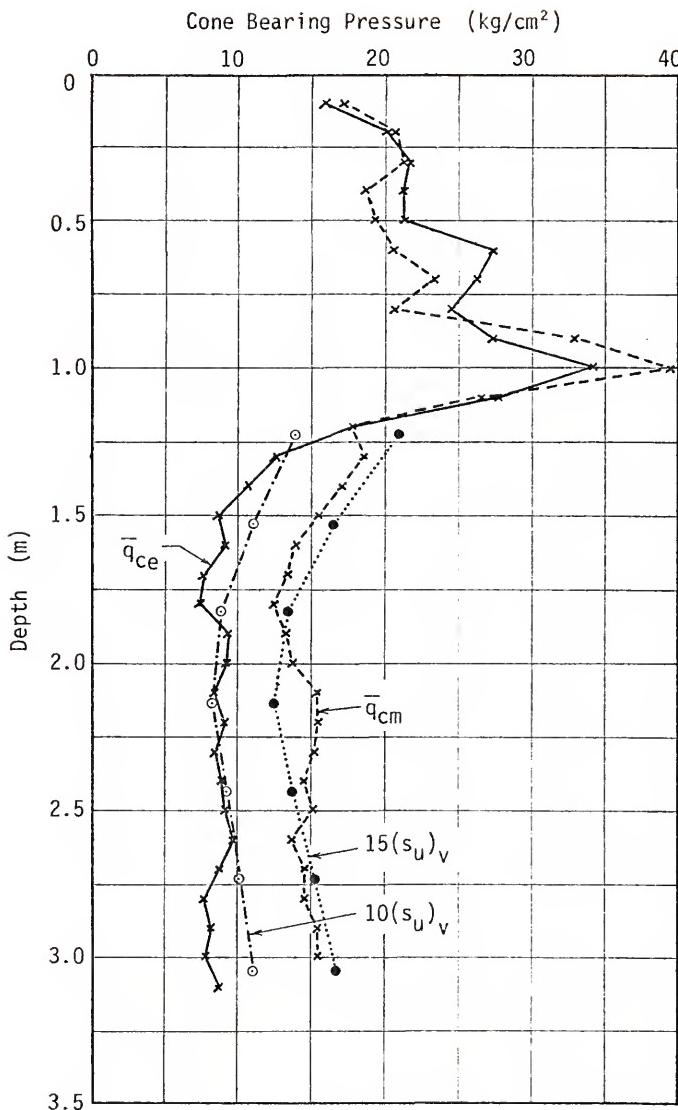
Typical reported  $q_c/s_u$  ratios for electrical and mechanical penetrometers are 10 and 15, respectively. These ratios were checked for the Paines Prairie clay using the average  $q_c$  profiles shown in Fig 8.6 and  $s_u$  data obtained from both field vane and undrained triaxial shear tests. The results are summarized in Table 8.2.

TABLE 8.2  
COMPUTED AND TYPICAL  $q_c/s_u$  RATIOS

	$s_u$ -Triaxial	$s_u$ -Field Vane	Typical
$q_{ce}/s_u$	18	10	10
$q_{cm}/s_u$	27	15	15

The calculated and typical reported values agree well if only field vane strength data are considered, but there is a large discrepancy between the ratios computed using field vane and triaxial data. The problem is determining which ratio should be used to estimate  $s_u$  for use in pile friction analysis. Correlations between  $q_c$  and triaxial  $s_u$  data should give better results since the  $\alpha$  and  $\lambda$  design curves were based on laboratory undrained strength data.

Comparisons of measured pile side friction and predictions made using both the  $\alpha$  and  $\lambda$  methods with the  $q_c/s_u$  ratios based on triaxial data are presented in Tables 8.4 and 8.5. Values for  $\alpha$  were determined from the curves and table presented in NAVDOCKS DM-7 (1962), reproduced

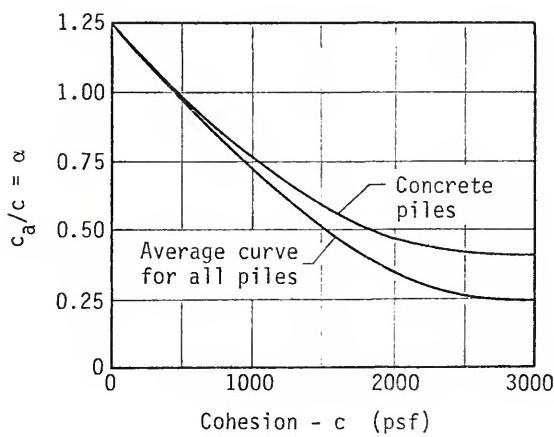


COMPARISON OF CONE BEARING PRESSURE AND FIELD VANE STRENGTH

FIGURE 8.6

TABLE 8.3  
NAVDOCKS DM-7 RECOMMENDED ADHESION VALUES

Pile Type	Consistency of Soil	Cohesion, $c$ (psf)	Adhesion, $c_a$ (psf)
Timber and Concrete	Very soft	0 - 250	0 - 250
	Soft	250 - 500	250 - 480
	Med. Stiff	500 - 1000	480 - 750
	Stiff	1000 - 2000	750 - 950
	Very stiff	2000 - 4000	950 - 1300
Steel	Very soft	0 - 250	0 - 250
	Soft	250 - 500	250 - 460
	Med. stiff	500 - 1000	460 - 700
	Stiff	1000 - 2000	700 - 720
	Very stiff	2000 - 4000	720 - 750



SIDE FRICTION DESIGN CURVES FOR PILES IN CLAY

FIGURE 8.7

herein as Table 8.3 and Fig 8.7, and  $\lambda$  values were obtained from Fig 8.4. The data in Tables 8.4 and 8.5 show the  $\alpha$  method was reasonably successful in predicting model pile friction but the  $\lambda$  method resulted in large overpredictions.

The discrepancy between answers provided by these two methods is not surprising when the methods are evaluated with respect to the special condition to which they were applied, i.e., very short piles in a relatively stiff clay. For this condition, the  $\bar{\sigma}_v^t$  term in the  $\lambda$  equation (Eq 8.4) becomes negligible and the  $\lambda$  and  $\alpha$  values are both approximately 0.4. The prediction equations for the two methods for this condition are:

$$f_p = \alpha s_u \approx 0.4 s_u \quad (8.6)$$

$$f_p = \lambda(\bar{\sigma}_v^t + 2\bar{s}_u) \approx 0.8 s_u \quad (8.7)$$

Obviously, one method will likely result in large prediction errors. The large  $\lambda$  method prediction errors may be the result of the  $\lambda$  design curve being positioned incorrectly for pile penetrations less than about 30 ft. This point will be discussed in more detail in the following section.

It is also important to note that the  $\alpha$  method predictions were based on computed  $q_c/s_u$  ratios that are quite different from those normally reported and used. This method would have also resulted in larger overpredictions if typical  $q_c/s_u$  ratios had been used. Because of this,  $s_u$  values estimated from  $q_c$  data should be based on correlations with laboratory test data whenever possible. If it is necessary to use  $q_c$  data for pile friction estimates when laboratory correlation data are not available, the  $s_u$  values obtained by using the typical

TABLE 8.4

MODEL PILE SIDE FRICTION PREDICTIONS IN CLAY  
USING  $q_c$  DATA AND THE  $\alpha$  METHOD

Test No	Pile Type	Embedded Length (ft)	Meas $F_s$ (k)	Elect. Cone		Mech. Cone	
				Pred $F_s$ (k)	Error (%)	Pred $F_s$ (k)	Error (%)
1-1	Pipe	3.33	2.72	2.49	- 8.4	2.48	- 8.8
1-2	Pipe	6.83	4.82	5.08	5.4	5.08	5.4
2-1	Pipe	3.50	1.67	2.61	56.3	2.62	56.9
2-2	Pipe	7.00	3.98	5.18	30.1	5.20	30.6
3-1	Conc	3.75	4.07	4.39	7.9	4.32	6.1
3-2	Conc	6.34	5.20	7.10	36.5	6.80	30.8
4	Pipe	2.42	1.12	1.30	16.1	1.29	15.2
5-1	Conc	2.75	2.82	3.84	36.2	3.17	12.4
5-2	Conc	5.75	5.93	6.88	16.0	6.11	3.0
6	Pipe	2.17	1.19	1.20	0.8	1.17	- 1.7

TABLE 8.5

MODEL PILE SIDE FRICTION PREDICTIONS IN CLAY  
USING  $q_c$  DATA AND THE  $\lambda$  METHOD

Test No	Pile Type	Embedded Length (ft)	Meas $F_s$ (k)	Elect. Cone		Mech. Cone	
				Pred $F_s$ (k)	Error (%)	Pred $F_s$ (k)	Error (%)
1-1	Pipe	3.33	2.72	5.66	108.1	5.15	89.3
1-2	Pipe	6.83	4.82	9.24	91.7	9.52	97.5
2-1	Pipe	3.50	1.67	5.99	258.7	5.97	257.5
2-2	Pipe	7.00	3.98	8.61	116.3	9.20	131.2
3-1	Conc	3.75	4.07	8.42	106.9	8.13	100.0
3-2	Conc	6.34	5.20	12.04	131.5	10.75	106.7
4	Pipe	2.42	1.12	3.29	193.7	2.83	152.7
5-1	Conc	2.75	2.82	9.34	231.2	6.00	112.8
5-2	Conc	5.75	5.93	12.83	116.3	9.55	61.0
6	Pipe	2.17	1.19	4.53	280.7	2.96	148.7

$q_c/s_u$  ratios should be corrected to reduce the estimated values to more nearly equal to the  $s_u$  values that would be obtained from conventional laboratory strength tests.

A general method for correlating field vane  $s_u$  data to laboratory  $s_u$  data is not available at this time; however, Bjerrum (1972) presented a field vane  $s_u$  correction curve for use in slope stability analysis which may be applicable to the pile friction case. This curve, shown in Fig 8.8, was developed by correlating field vane  $s_u$  data with  $s_u$  values backcalculated from landslide case history data and presents the correction factor in terms of the plasticity index of the clay. Although this correction curve is not directly applicable to the pile friction problem, it is suggested that the correction be applied to  $s_u$  values estimated using the typical  $q_c/s_u$  ratios before the data are used for pile friction analysis for the following reasons:

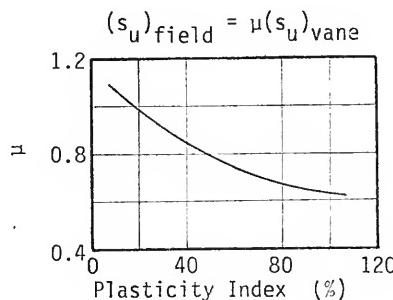
1. The typical  $q_c/s_u$  ratios provide an estimate of the field vane  $s_u$  since the  $q_c/s_u$  correlations are based primarily on field vane data.
2. Bjerrum suggested that the field vane test gives unconservative  $s_u$  values because of the much higher shear rate for this test as compared to a landslide where failure may develop slowly over a period of several years. The factors controlling the long-term stability of a slope are probably similar to those which control the long-term stability of a pile; therefore, the correction may be applicable to both situations.
3. Except for clays of very low plasticity, the Bjerrum correction results in an  $s_u$  reduction which will lead to more conservative pile friction estimates than if no correction was made.
4. Based on the Paines Prairie clay strength data, use of Bjerrum's curve would result in a correction in the right direction. This will probably also be the case for most clays, since field vane tests usually give higher  $s_u$  values than conventional undrained laboratory tests.

5. Alternate correction procedures are not available at this time. In the absence of a better correction method, it seems better to make a correction that is in the right direction and leads to more conservative friction predictions than to make no correction at all.

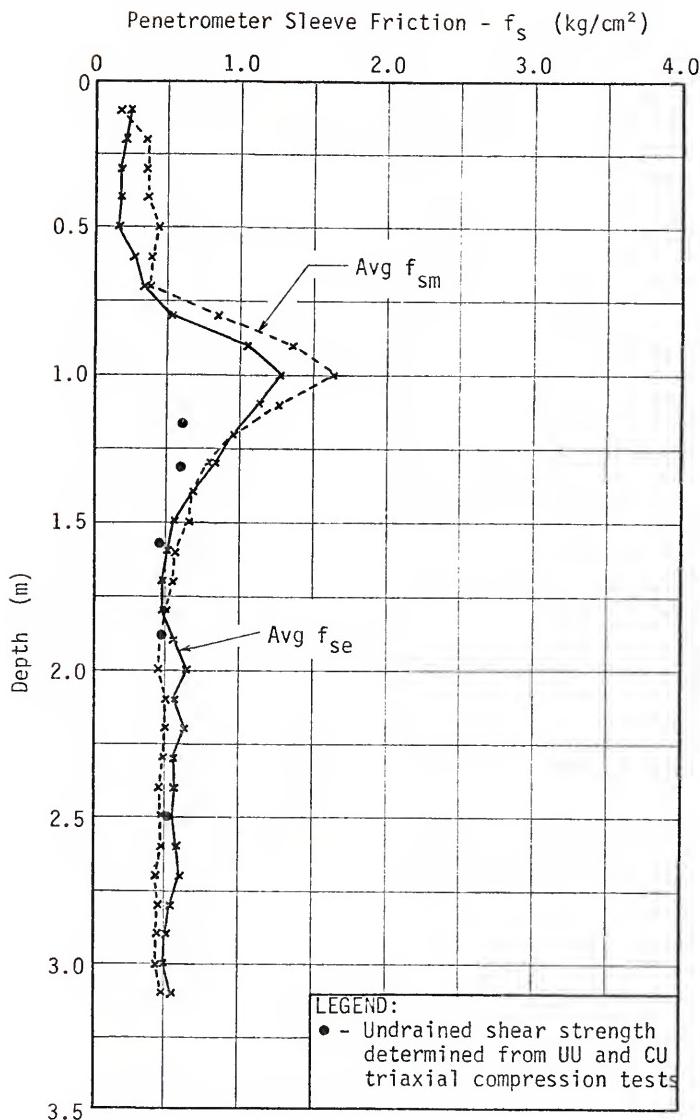
#### 8.4.2 $\alpha$ and $\lambda'$ Methods Using $f_s$ Data

Average  $f_s$  profiles for both the electrical and mechanical penetrometers are shown in Fig 8.9. These curves show that while the mechanical penetrometer produced slightly higher  $f_s$  values in the stiff clay and slightly lower values in medium clay, the difference was generally negligible. Also, the  $f_s$  values were approximately equal to  $s_u$  as determined by triaxial compression tests, as shown by the laboratory  $s_u$  data superimposed on the average  $f_s$  curves in Fig 8.9.

The electrical penetrometer  $f_s$  data were used to estimate the model pile side friction, using the assumption that  $f_s/s_u = 1.0$ . The results are presented in Table 8.6. An analysis using mechanical penetrometer  $f_s$  data was not performed, since the curves in Fig 8.6 show that the results would be approximately the same for either penetrometer.



BJERRUM'S FIELD VANE SHEAR STRENGTH CORRECTION CURVE  
FIGURE 11.6



AVERAGE SLEEVE FRICTION CURVES FOR PAINES PRAIRIE CLAY

FIGURE 8.9

Using  $f_s$  values as  $s_u$  in the  $\alpha$  method resulted in prediction errors comparable to those resulting from use of  $q_c$  data, and both approaches gave reasonable predictions. Use of  $f_s$  data is more promising because  $f_s$  data from both penetrometers are approximately equal, while the  $q_c$  values differ greatly depending on the penetrometer used. Unfortunately, little research effort has been made to correlate  $f_s$  and  $s_u$  data, and it is difficult to judge whether or not the  $f_s/s_u$  ratio of about 1.0 for the Paines Prairie soil is generally representative of clays. Additional research in this area would be valuable.

The  $\lambda$  method was not used with  $f_s$  data since it was apparent that the results would be approximately the same as those obtained using  $q_c$  data. Instead, Vijayvergiya and Focht's (1972) data were analyzed to determine the variation of  $\lambda$  with respect to relative penetration instead of the absolute penetration values used by Vijayvergiya and Focht. The results of this analysis are shown in Fig 8.10 and a new design curve, herein referred to as the  $\lambda'$  curve, was established. Data points for the 6.5 in model pile tests used by Vijayvergiya and Focht were not considered when the  $\lambda'$  curve was drawn. The  $\lambda'$  value, which is considerably smaller than the corresponding  $\lambda$  value for short piles, can be used directly in place of  $\lambda$  in Eq 8.4.

The  $\lambda'$  method was used with electrical penetrometer data to estimate the model pile side friction. As shown in Table 8.7, this method also overpredicted by a considerable amount; however, the average prediction error was reduced from +163% for the  $\lambda$  method using  $q_c$  data to +48% for the  $\lambda'$  method using  $f_s$  data. The error decrease is primarily due to using  $\lambda'$  instead of  $\lambda$ . When only data from the longer model piles are considered, the average  $\lambda'$  prediction error is reduced to

TABLE 8.6

MODEL PILE SIDE FRICTION PREDICTIONS IN CLAY  
USING  $f_{se}$  DATA AND THE  $\alpha$  METHOD

Test No	Embedded Length (ft)	Meas $F_s$ (k)	Pred $F_s$ (k)	Error (%)
1-1	3.33	2.72	2.51	- 7.7
1-2	6.83	4.82	5.11	6.0
2-1	3.50	1.67	2.62	56.9
2-2	7.00	3.98	5.19	30.4
3-1	3.75	4.07	4.02	- 1.2
3-2	6.34	5.20	6.62	27.3
4	2.42	1.12	1.48	32.1
5-1	2.75	2.82	3.42	21.3
5-2	5.75	5.93	6.66	12.3
6	2.17	1.19	1.17	- 1.7

TABLE 8.7

MODEL PILE SIDE FRICTION PREDICTIONS IN CLAY  
USING  $f_s$  DATA AND THE  $\lambda'$  METHOD

Test No	Embedded Length (ft)	Meas $F_s$ (k)	Pred $F_s$ (k)	Error (%)
1-1	3.33	2.72	4.07	49.6
1-2	6.83	4.82	6.11	26.8
2-1	3.50	1.67	3.72	122.7
2-2	7.00	3.98	5.18	30.1
3-1	3.75	4.07	4.47	9.8
3-2	6.34	5.20	5.98	15.0
4	2.42	1.12	1.88	67.8
5-1	2.75	2.82	4.99	76.9
5-2	5.75	5.93	7.23	21.9
6	2.17	1.19	1.85	55.5

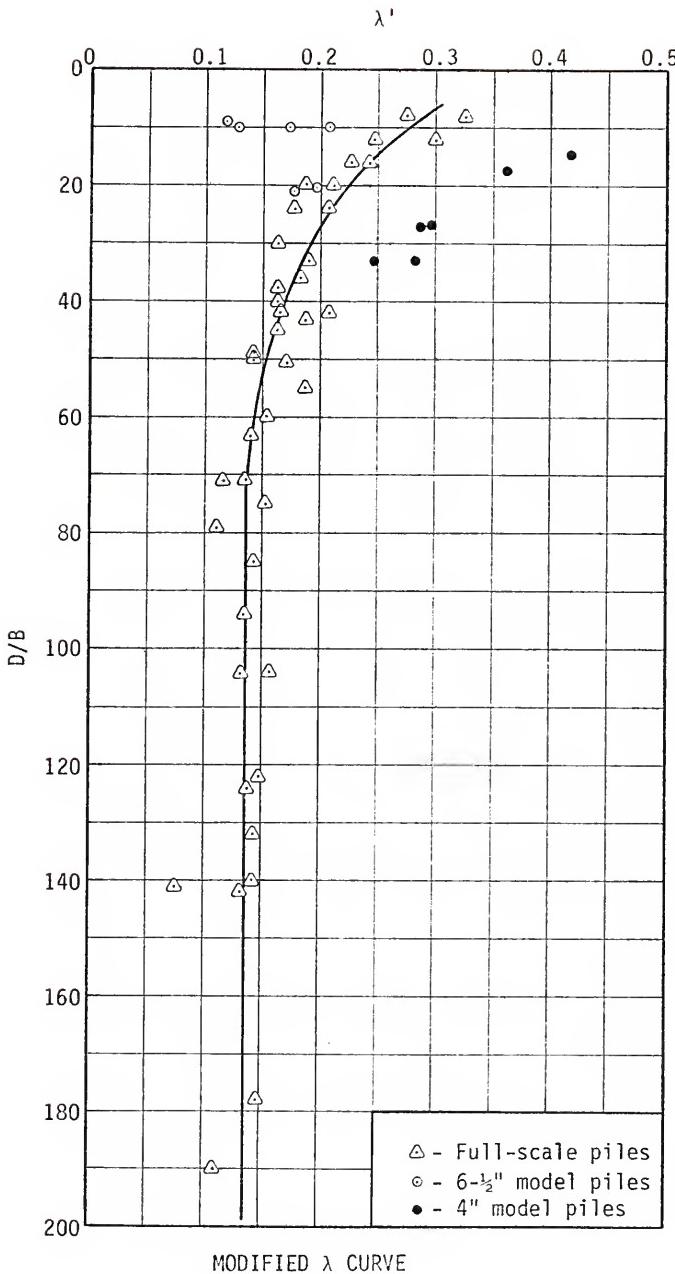


FIGURE 8.10

+23%, which is comparable to the +19%  $\alpha$  method error for the same piles. This indicates that the  $\lambda'$  method may be satisfactory for most practical situations; however, it probably should not be used for very short piles in stiff clay.

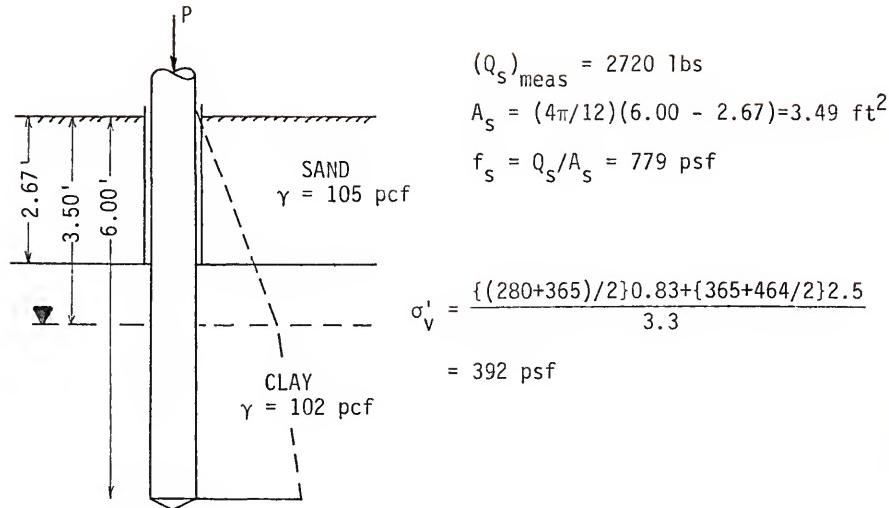
#### 8.4.3 Drained Friction Analysis of Model Pile Data

Both  $\tan \delta'$  and  $\sigma'_{rf}$  data are required before an effective stress analysis of pile friction can be made. The direct shear tests described in Chapter 3 provide the required  $\tan \delta'$  data; however, no proven method exists for accurately estimating  $\sigma'_{rf}$  on a pile driven in clay. Furthermore, Schmertmann's proposed CPT pressuremeter theory is apparently the only suggested approach to this problem.

With measured  $\tan \delta'$  data, the accuracy with which friction capacity predictions can be made will be directly proportional to the accuracy with which  $\sigma'_{rf}$  can be estimated. Therefore, evaluating  $\sigma'_{rf}$  predictions was considered more important than evaluating  $F_s$  predictions. Comparisons of  $\sigma'_{rf}$  predicted using Schmertmann's method with values backcalculated from measured  $Q_s$  and  $\tan \delta'$  are presented in Table 8.8.

The 'actual'  $\sigma'_{rf}/\sigma'_{yi}$  ( $K_f$ ) ratios reported in Table 8.8 are average values computed from measured unit weights, groundwater levels, total pile friction forces and drained friction angles. An example calculation is shown in Fig 8.11. The predicted ratios were computed using Eq 8.5 and the following assumptions:

1. Coefficient of compressibility ( $a_r$ ) data from consolidation tests on remolded samples.
2. Values of  $(s_u/p')_u$  determined from electrical cone  $q_c$  data, a  $q_c/s_u$  ratio of 1/10, and measured soil unit weights.
3. An assumed  $(s_u/p')_u/(s_u/p')_r$  ratio of 1.0. According to Schmertmann (1957), this ratio is usually less than 1.0,



Compute  $\sigma'_{rf}$  using drained friction test data

For soil on pile steel,  $c'_a = 95 \text{ psf}$  and  $\tan \delta' = 0.346$

$$\text{Lower limit estimate: } \bar{f}_s = c'_a + \sigma'_{rf} \tan \delta'$$

$$(\sigma'_{rf})_{LL} = (\bar{f}_s - c'_a)/\tan \delta' = (779 - 95)/0.364 = 1879 \text{ psf}$$

$$\{\sigma'_{rf}/\sigma'_{vi}\}_{LL} = 1879/392 = 4.79$$

Upper limit estimate: Neglect  $c'_a$

$$(\sigma'_{rf})_{UL} = f_s/\tan \delta' = 779/0.364 = 2140 \text{ psf}$$

$$\{\sigma'_{rf}/\sigma'_{vi}\} = 2140/392 = 5.46$$

#### RADIAL EFFECTIVE STRESS COMPUTATION FOR PAINES PRAIRIE TEST 1-1

FIGURE 8.11

but not by a significant amount. It was also found that varying this ratio over reasonable limits did not have a significant effect on the computed  $\sigma'_{rf}/\sigma'_{Vi}$  ratio.

4. An average sensitivity value computed from the field vane shear test results.
5. Estimated  $K_0$  values based on the available soils data for the Paines Prairie clay and published data for other clays.
6. Modulus ( $E$ ) values determined using estimated  $E/q_c$  ratios and the relationship between  $p_L$  and  $s_u$  based on suggestions presented by Schmertmann (1974c).

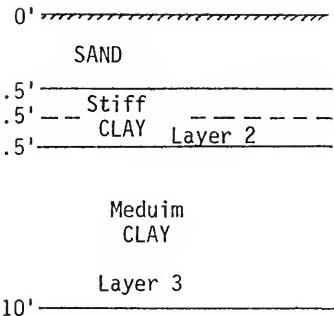
Figs 8.12 and 8.13 present typical calculations using both the assumed  $E/q_c$  ratio and the  $p_L-s_u$  relationship.

This analysis and the comparative data shown in Table 8.8 showed that the results obtained from Eq 8.5 are highly dependent on the input values for  $E$  and the  $s_u/p'$  ratio. This is reasonable since both the strength and stress-strain properties of the clay should have a large influence on the final effective radial stress acting on a pile. The problem in using this method in conjunction with  $q_c$  data is the empirical correlations that must be used to estimate soil properties from the CPT data. Additional research in this area would be useful, particularly in relating CPT data to  $E$  and  $p_L$ .

Considering the fact that Schmertmann's method represents a new and untried approach to the pile friction problem and that the method is in the developmental stage, the results in Table 8.8 are encouraging. With additional development, this method might provide the basis for a rational effective stress approach for evaluating friction on piles in clay.

#### 8.5 Step-Taper Pile Shaft Resistance

The approach used for estimating the shaft resistance of step-



	Soil Properties for	
	Layer 2	Layer 3
$\sigma'_c$	3.5 tsf	0.35 tsf
$K_o^*$	1.50	0.50
$a_r$	$0.050 \text{ ft}^2/\text{t}$	$0.068 \text{ ft}^2/\text{t}$
$s_{uu}^{**}$	2.39 tsf	0.90 tsf
$\bar{q}_{ce}$	23.9 tsf	9.0 tsf
$S_t$	5.0	5.0

\* - Assumed

\*\* - Computed from  $(s_u)_{fv}/\bar{q}_{ce} = 1/10$

Typical short pile length = 3.3 ft

Typical long pile length = 7.3 ft

#### Compute average soil properties for short pile case

$$\bar{K}_o = \{1.8(1.5) + 1.5(0.5)\}/3.30 = 1.04$$

$$a_r = \{1.8(0.054) + 1.5(0.068)\}/3.30 = 0.060 \text{ ft}^2/\text{t}$$

$$(s_u/p')_u = \{1.8(13.0) + 1.5(2.57)\}/3.30 = 8.26$$

$$E_u = \{1.8(239) + 1.5(90)\}/3.30 = 171 \text{ tsf} \quad (\text{Using } E = 10q_c)$$

$$E_r = E_u/S_t = 171/5 = 35 \text{ tsf}$$

$$s_{uu} = \{1.8(2.39) + 1.5(0.90)\} = 1.71 \text{ tsf}$$

From Eq 11.5

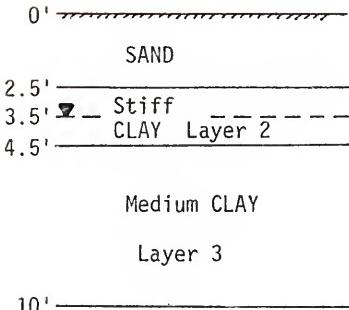
$$\frac{\sigma'_{rf}}{\sigma'_{vi}} = \frac{(1/3.42)\{1.04 + (8.26)(4.51)\} + 1.00(0.20)}{1 + 1/3.42} = 8.83$$

LL

For upper limit estimate, replace  $E_u$  with  $E_r$

$$\frac{\sigma'_{rf}}{\sigma'_{vi}} = \frac{(1/0.70)\{1.04 + (8.26)(1.92)\} + 0.20}{1 + 1/0.70} = 10.00$$

EXAMPLE CALCULATION OF SCHMERTMANN'S  $\sigma'_{rf}/\sigma'_{vi}$  RATIO  
FIGURE 8.12



The required soil properties for Layers 1 and 2 are presented in Fig 8.12

Compute average soil properties for long pile case

$$\begin{aligned}\bar{K}_o &= \{1.8(1.5) + 5.50(0.5)\} = 0.75 \\ a_r &= \{1.8(0.054) + 5.5(0.068)\} = 0.065 \text{ ft}^2/\text{t} \\ (s_u/p')_u &= \{1.8(13.0) + 5.5(2.57)\} = 5.14 \\ s_{uu} &= \{1.8(2.39) + 5.5(0.90)\} = 1.26 \text{ tsf}\end{aligned}$$

From Schmertmann (1973)

$$\begin{aligned}p_L &= p_o + s_u \{1 + \ln(E/3s_u)\} \approx p_o + 6s_u \\ s_u \{1 + \ln(E/3s_u)\} &\approx 6s_u \\ \ln(E/3s_u) &\approx 5 \\ E &\approx 3s_u e^5\end{aligned}$$

$$E_u = 3(1.26)(150) = 567 \text{ t}$$

$$E_r = E_u/S_t = 567/5 = 113 \text{ tsf}$$

$$\frac{\sigma'_{rf}}{\sigma'_{vi \text{ LL}}} = \frac{(1/12.3)\{0.75 + 5.14(6.01)\} + 1.00(0.20)}{1 + 1/12.3} = 2.56$$

EXAMPLE CALCULATION OF SCHMERTMANN'S  $\sigma'_{rf}/\sigma'_{vi}$  RATIO

FIGURE 8.13

TABLE 8.8  
PREDICTED AND ACTUAL  $\sigma'_{rf}/\sigma'_v$  ( $=K'_f$ ) RATIOS FOR MODEL FILES IN CLAY

Pile Case	Method of Estimating E	Predicted $(K'_f)_{LL}$	JHS Method $(K'_f)_{UL}$	Computed From Data $(K'_f)_{LL}$	Computed From Data $(K'_f)_{UL}$	$\frac{\text{Predicted}}{\text{Computed}}$
Short	$E = 10q_c$	10.00	8.83	9.41	4.07	4.46
Short	from $p_L$ est. (1)	9.32	6.10	7.71	4.07	5.85
Long	$E = 10q_c$	6.84	5.17	6.00	3.21	3.92
Long	from $p_L$ est.	6.89	2.56	4.73	3.21	3.92
						1.32

\* - Computed ignoring  $c'$  from drained friction tests.

\*\* - Computed using  $c'$  from drained friction tests.

$$(1) - \text{From } p_L = p_0 + s_u \{1 + \ln(E/s_u)\} \approx p_0 + 6.0s_u$$

taper piles in clay was similar to the method developed for sands. The friction on each constant diameter section was computed as if the entire pile was the same diameter and step-bearing resistance was estimated assuming  $q_s$  at each diameter step is proportional to  $q_c$  at that depth. In clays, the wedge action of the pile taper should not be as effective in increasing soil strength and density as in sands because the displacement caused by pile installation occurs primarily under undrained conditions. Therefore, the  $q_s/q_c$  ratio for clays should be less than that for sands.

Table 8.9 presents predicted shaft resistance values for the model step-taper piles tested at Paines Prairie. These predictions were made using the  $\alpha$  method and  $f_{se}$  data to compute side friction and a  $q_s/q_c$  ratio of 1.0 to compute step bearing. Although the number of comparisons are limited, the prediction errors indicate that the shaft resistance prediction accuracy is comparable to or better than that for side friction on constant section piles.

#### 8.6 Total Capacity Predictions

Table 8.10 presents measured values of total ultimate pile capacity along with predictions made using the Begemann method for estimating tip capacity and the  $\alpha$  method for estimating side friction. Undrained shear strength values required in the  $\alpha$  method were estimated from electrical penetrometer  $f_s$  data.

The resulting prediction errors are all positive (overprediction) and show that, on the average, total capacities were overpredicted by about 20%. However, the predictions are considered quite good since the range in prediction error was small. The prediction method could be made more conservative by applying an empirical reduction factor to

TABLE 8.9

PREDICTED AND MEASURED SHAFT RESISTANCE  
FOR MODEL STEP-TAPER PILES DRIVEN IN CLAY

Test No	Failure Criterion	Predicted Q <sub>s</sub> (lbs)	Measured Q <sub>s</sub> (lbs)	Error (%)
4-2	Peak	3268	3225	1.3
4-3	Peak	5493	4675	17.4
6-2	Peak	3134	3050	2.7
6-3	Peak	5220	5750	- 9.2
4-2	Ultimate	3268	2820	15.8
4-3	Ultimate	5493	4450	23.4
6-2	Ultimate	3134	2870	9.1
6-3	Ultimate	5220	4970	5.0

TABLE 8.10  
PREDICTED AND MEASURED TOTAL ULTIMATE CAPACITY OF MODEL PILES DRIVEN IN CLAY

Test No	Pile Type	Embedded Length (ft)	$Q_t$ (k)	Predicted $F_s$ (k)	$P_{ult}$ (k)	Measured $P_{ult}$ (k)	Error (%)
1-1	4.0" Pipe	3.33	1.60	2.51	4.11	3.96	3.8
1-2		6.83	2.68	5.11	7.79	6.71	16.1
2-1		3.50	1.29	2.62	3.91	3.12	25.3
2-2		7.00	1.61	5.19	6.80	5.45	24.8
3-1	4.0" Conc	3.75	1.93	4.02	5.95	5.65	5.3
3-2		6.34	2.20	6.62	8.82	6.83	29.1
4-1	Step-Taper	2.42	0.74	1.48	2.20	1.70	29.4
4-2		4.92	0.74	3.27	4.01	3.95	1.5
4-3		7.42	0.98	5.49	6.47	5.58	15.9
5-1	4.0" Conc	2.75	2.20	3.42	5.62	3.92	43.4
5-2		5.75	1.92	6.66	8.58	6.84	25.4
6-1	Step-Taper	2.17	0.79	1.17	1.96	1.75	12.0
6-2		4.67	0.71	3.13	3.84	3.69	4.1
6-3		7.17	0.59	5.22	5.81	5.64	3.0

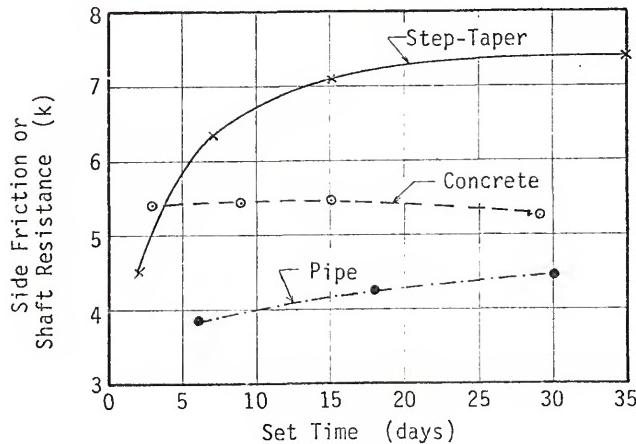
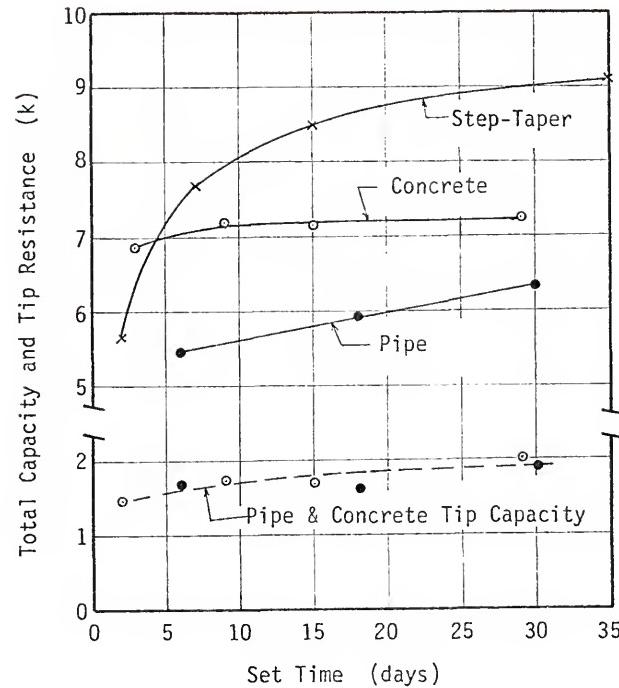
the predicted capacities; however, this may be undesirable since the total capacity may increase with time due to secondary consolidation effects. Data which indicate that a gradual increase in total capacity does occur will be presented in the following section.

### 8.7 Time Effects on Pile Capacity

The capacity of a pile driven in clay should increase with time as a result of secondary consolidation around the pile and possible chemical reactions at the soil-pile interface. A series of tests were conducted on each of the pile types tested at Paines Prairie to explore this effect. A typical test series consisted of driving the pile, waiting 2 days, performing a maintained load (ML) test to a butt settlement of about 0.8 in, leaving the pile in the residual settled position for an additional 7 days, performing another ML load test, and so on until the time between load tests reached approximately 30 days. Each ML load test was conducted as described in Chapter 4 and usually required 3 to 4 hrs to complete.

As described in Chapter 4, the regular model pile tests at Paines Prairie were performed 2 days after driving using the ML load test procedure. Each regular load test was continued to failure (butt settlement of about 0.8 in) normally using 5 to 8 load increments. Load increments falling within the initial linear portion of the load-settlement curve usually required only 10 to 15 min to complete, while the latter increments usually had to be maintained for 60 min or more before the settlement rate decreased to the desired level. The total time required to complete these tests usually varied from 3 to 5 hrs.

The results of the time study tests, presented in Fig 8.14, show that the increase in total capacity amounted to about 5% for the



PAINES PRAIRIE SET TIME-PILE CAPACITY GRAPHS

FIGURE 8.14

concrete pile, 15% for the pipe pile, and 60% for the step-taper pile. These graphs also show that the small increase in concrete pile capacity was totally due to an increase in tip bearing, while the increase in pipe pile capacity was mainly due to increased side friction. The fact that pipe pile friction increased with time while concrete pile friction did not may indicate that secondary consolidation effects were not significant at this site and that time increases in side friction are caused by chemical reactions at the pile-soil interface.

The step-taper pile load cell did not function properly during the time effect tests; thus, it was impossible to absolutely determine the percentage increase for tip bearing and shaft resistance. However, the tip capacity increase can be estimated using data from the pipe and concrete piles since the tip capacity behavior should be approximately the same for all three piles. The step-taper tip capacity curve in Fig 8.14 was drawn parallel to the curve for the pipe and concrete piles, and the estimated tip capacity and measured total capacity values were used to construct a shaft resistance-time curve for this pile. This curve indicates that a large increase in shaft resistance occurred, because of either time or reloading effects or a combination of both. Considering the time-capacity behavior of the constant section piles, it seems more likely that the shaft resistance increase was primarily due to performing multiple load tests on the same pile. A possible explanation for this occurring with the tapered pile and not with the constant section piles is that the wedge action of the tapered pile causes additional consolidation and strengthening of the soil around the pile during each load test.

Additional research is needed on the time-capacity behavior of

tapered piles. The results of tests performed two to three days after pile driving indicated that the efficiency of tapered piles in clay was only about 10% greater than constant section piles. On the other hand, tests performed after the piles had been in the ground for about sixty days and subjected to three to four load tests showed a much higher efficiency for the tapered piles. The questions which need answering are:

1. Will the capacity of a tapered pile initially tested a considerable time after driving be significantly higher than that of a pile tested a short time after driving?
2. How does the capacity of tapered piles in clay vary when the pile is loaded gradually and the final load is maintained for a long period of time?

Answers to these questions may show that tapered piles are very efficient in clays as well as sands and could permit use of higher design loads than would be indicated by load tests performed a short time after pile driving or by static analysis methods based on undrained shear strength.

### 8.8 Conclusions

Based on the data contained in this chapter and the current state-of-the-art with respect to estimating pile side friction in clays, the following procedures are suggested for predicting capacity of piles in clay from CPT data:

1. Compute the ultimate tip bearing capacity using the Begemann method described in Section 2.2.4 and illustrated in Fig 2.9. If mechanical penetrometer  $q_c$  data are used, apply a reduction factor of 0.6 to the computed capacity to account for penetrometer tip mantle friction.
2. Compute side friction using the  $\alpha$  method described in Section 8.1.2. Use  $f_s$  data as an estimate of undrained shear strength. If sleeve friction data are not available,  $s_u$  can be calculated from  $q_c$  data using  $q_c/s_u$

ratios. Whenever possible, the  $q_c/s_u$  ratio should be based on laboratory strength test results. If laboratory data are not available,  $q_c/q_s$  ratios of 10 and 16 can be used for the electrical and mechanical cones, respectively. In this case, it is recommended that the estimated  $s_u$  values be reduced by use of Bjerrum's field vane shear strength reduction curve.

These conclusions are based on the results of tests performed in a clay, in which positive excess pore pressures developed beneath the penetrometer and pile tips, as was shown in Section 3.4. The method should also provide satisfactory results in clays exhibiting different pore pressure behavior because the empirical design techniques on which the method is based presumably account for differing pore pressure behavior in an indirect manner. The full-scale pile test results, to be presented in Chapter 10, tend to support this conclusion. However, only a limited number of full-scale pile data are available for clays. The method is not recommended for use with very sensitive clays because  $f_s$  data are known to not be representative of  $s_u$  for this type of soil.

The suggested design method is recognized to be very empirical, particularly with respect to side friction predictions. Drained friction theories, such as the method proposed by Schmertmann, represent an approach to this problem which is fundamentally more correct, and future research should be directed toward use of an approach of this type.

## CHAPTER 9

### FULL-SCALE PILE TEST RESULTS

When theories or equations based on model tests are used to predict prototype behavior, there are always questions concerning the validity of the extrapolation. Therefore, the prediction equations developed in Chapters 7 and 8 were used to predict the capacity of several full-scale piles for which both CPT data and load test results were available. The pile load test results and the soil conditions at the test sites are presented in this chapter. Full-scale capacity predictions based on CPT data and a discussion of the correlation between predicted and measured capacities are presented in Chapter 10.

#### 9.1 West Palm Beach Tests

##### 9.1.1 Project and Site Description

Two 18 in square, precast concrete piles were load tested by the Florida Department of Transportation (FDOT) in conjunction with a research project on dynamic pile capacity prediction being conducted by Case Western Reserve University. The test piles were driven at the location of a bridge being constructed to carry Interstate Route 95 over Belvedere Road in West Palm Beach.

Four standard penetration tests (SPT) borings and four CPT soundings were made in the vicinity of the test pile locations, as shown in Fig D-1 in Appendix D. Logs of the SPT borings, showing both standard penetration resistance ( $N$ -values) and sample descriptions,

are presented in Figs D-2 and D-3. These borings were performed by a FDOT drilling crew under the direct field supervision of a soils engineer. The samples were described in the field by the supervising engineer and again in the laboratory by the author.

The CPT logs for this site are shown in Figs D-4 and D-5. These data were obtained using the Begemann mechanical friction sleeve penetrometer and electrical recording equipment as described in Chapters 4 and 5. Soundings C-1 and C-3 were made using 10 cm test intervals, while 20 cm intervals were used for soundings C-2 and C-4.

Based on visual examination of the SPT samples and evaluation of the CPT logs, the soil profile at this site is approximately as follows:

Layer No.	Depth (ft)	Soil Description
1	0-3	Brown to dark grey SAND, some organic matter
2	3-7	Tan fine to medium SAND, clean, medium dense
3	7-28	Tan fine to medium SAND, clean, loose to very loose
4	28-50	Tan to white, fine to coarse, medium dense SAND with varying amounts of shell, some cemented layers

The groundwater level was about 3.5 ft below the ground surface.

Zones of soil with very low penetration resistance were encountered between depths of 13 and 30 ft. The friction ratio data from CPT tests in this zone are in the range that would indicate clayey soils; however, the SPT samples showed these soils to be clean sands. It is doubtful that any significant clayey layers were missed since SPT sampling was conducted on 2.5 ft centers. Instead, it is believed that the low

penetration resistance values (both SPT and CPT) and unusually high friction ratios were caused by liquefaction of the sand during testing.

#### 9.1.2 Pile Load Test Program and Results

The two test piles were driven with a Fairchild 20 air hammer (modified Vulcan No 2) after the site had been excavated to a depth of about 3 ft. Test Pile No 1 was 35 ft long and was driven to a penetration of 26.5 ft, and Test Pile No 2, 45 ft long, was driven 37.2 ft. Driving records for both piles are presented in Fig D-6.

Maintained load tests were performed on each pile two days after driving. Load was applied to the pile with a hydraulic jack reacting against a steel beam attached to three 8 in steel H-piles driven at each end of the beam. The anchor piles were located 6 ft from the test pile at the ground surface and were battered away from the test pile to minimize their effects on the test pile performance. Pile settlement was measured with three dial gauges (0.001 in accuracy) mounted on an independent reference beam. The complete test assembly, shown in Fig 9.1, was covered with a tent during testing.

Load was applied to the piles in increments equal to one-half the pile design capacity ( $R$ ) until a load of  $2R$  was reached. Beyond  $2R$ , the load was increased in increments of  $0.25 R$  until failure occurred. The design capacity was computed from the pile driving resistance using the modified Engineering News Record equation. Each load increment was maintained until the increment settlement was less than  $0.01$  in in a 60 min period. The load test was terminated with the load increment that produced a settlement equal to or greater than  $0.02$  ( $\Delta P$ ) in, where  $\Delta P$  is the load increment size in tons.

A constant rate of penetration test was also performed on each



WEST PALM BEACH PILE LOAD TEST

FIGURE 9.1

pile one day after completion of the maintained load test. Load-settlement curves for both types of load tests are presented in Figs D-7 and D-8. After completion of the CRP tests, the piles were driven an additional few feet to determine if any change in driving resistance had occurred. Records of this redriving are also presented in Fig D-6.

## 9.2 Jefferson County Tests

### 9.2.1 Project and Site Description

Two 18 in square concrete piles were tested at a site near Monticello by the FDOT, also in conjunction with the Case Western Reserve research project. These piles were driven during construction of an overpass structure at the intersection of Interstate Route 10 and State Route 158.

Two SPT borings and two CPT soundings were made at the locations shown in Fig D-9. Boring logs are presented in Fig D-10 and the cone logs in Figs D-11 and D-12. Natural moisture content tests were performed on all SPT samples, and selected samples were tested to determine Atterberg limits and grain size distribution. Results of these tests are presented in Fig D-13.

Based on all the field and laboratory data, the soil profile at this site is approximately as follows:

Layer No.	Depth (ft)	Soil Description
1	0-3	Brown to grey fine silty sand, dense
2	3-20	Brown, yellow and red sandy clay to clayey sand (percent sand increases with depth), hard

Layer No.	Depth (ft)	Soil Description
3	20-32	Yellow to red fine silty sand with thin (1/16 in) clay lenses, medium dense to dense
4	32-68+	Light grey highly plastic clay with thin sandy lenses, stiff

Groundwater was encountered at a depth of about 30 ft in both borings.

#### 9.2.2 Pile Load Test Program and Results

The piles were driven in 13 ft deep pier excavations using equipment identical to that used at the West Palm Beach site. Test Pile No 1 (40 ft long) was driven to a penetration of 30 ft, and Test Pile No 2 (27 ft long) was driven 14 ft. Driving resistance records are presented in Fig D-14.

Load testing equipment and procedures were identical to those used at the West Palm Beach site and will not be further described. Results of the ML and CRP tests are presented in Figs D-15 and D-16.

### 9.3 Tarver, Georgia, Load Test

#### 9.3.1 Project and Site Description

A 14 in square concrete pile was driven and load tested by the Georgia Highway Department during design studies for a bridge on a small secondary road connecting SR-94 and SR-184 in south-central Georgia. The project site is located about 3.5 mi north of Tarver, Georgia.

Test borings made by the Georgia Highway Department showed a soil profile consisting of a 20 to 25 ft thick surface layer of medium dense to dense clayey sand underlain by a 55 ft layer of very loose silty sand. A plan of the proposed structure and boring logs are shown in Fig D-17.

Static cone soundings were attempted at three locations within the construction site; however, the dense upper crust could only be penetrated approximately 10 ft at two locations. Fig D-18 contains the log for Sounding No 1, which completely penetrated the dense layer. This sounding was made using the Begemann mechanical friction sleeve penetrometer with electronic readout equipment.

The CPT data correlate well with the test boring logs; however, the variation in SPT resistance in the upper layer should be noted, particularly between the two borings located in the test pile bent. Since Sounding No 1 was located 30 ft from the test pile, data from this sounding may not be truly representative of conditions at the pile location. Soundings could not be made closer to the test pile because it was located in the middle of a stream.

#### 9.3.2 Pile Testing Program and Results

Load was applied to the pile through a hydraulic jack-reaction beam-anchor pile system. Timber piles driven 7 ft from the test pile provided the load reaction. A wire, graduated scale, and mirror were used to measure pile settlement. The pile was loaded in increments of approximately 13 t to a load of 80 t, after which the increment size was decreased to 10 t. The load-settlement curve is shown in Fig D-19. The load test report stated that a plunging-type failure occurred at a load of 116 t.

### 9.4 Blount Island Tests

#### 9.4.1 Project and Site Description

An extensive pile load testing program was conducted on Blount Island in Jacksonville during design of the Offshore Power System

construction facility planned at that location. Tests were conducted on a variety of pile types and sizes, some of which were loaded in both tension and compression. This testing program was planned and supervised by Law Engineering Testing Company (LETCO), who obtained permission for the author to perform CPT soundings at each test site and furnished results of the pile load tests and boring logs for the site.

Two series of tests were conducted, one on the north side and one on the south side of the island. Piles were driven and tested at three sites at the north side location, but only data from two sites will be presented. The CPT sounding at the third site met refusal before reaching the depth to which the test pile was driven. Tests were conducted at four sites on the south side of the island.

The north-side test sites have been identified as Site Nos 215 and 230. Figs D-20 and D-21 contain logs of the borings made at these locations. Samples from these borings were not available for examination; thus, the soil descriptions in Figs D-20 and D-21 were taken directly from the LETCO logs. Logs of the CPT soundings made at these locations are shown in Figs D-22 and D-23. These soundings were made at least 15 ft away from the borings, using the Begemann mechanical friction sleeve penetrometer. Cone resistance was measured using the standard Bourdon gauge system.

In general, there was good agreement between the soil profiles indicated by the SPT borings and the CPT logs. Both show a profile consisting almost entirely of loose to medium dense sands to the depths penetrated. The boring logs show that the upper 25 ft of sand at Site No 230 was shelly, with the upper 9 to 10 ft being much denser than the underlying layers. According to LETCO engineers, this upper dense

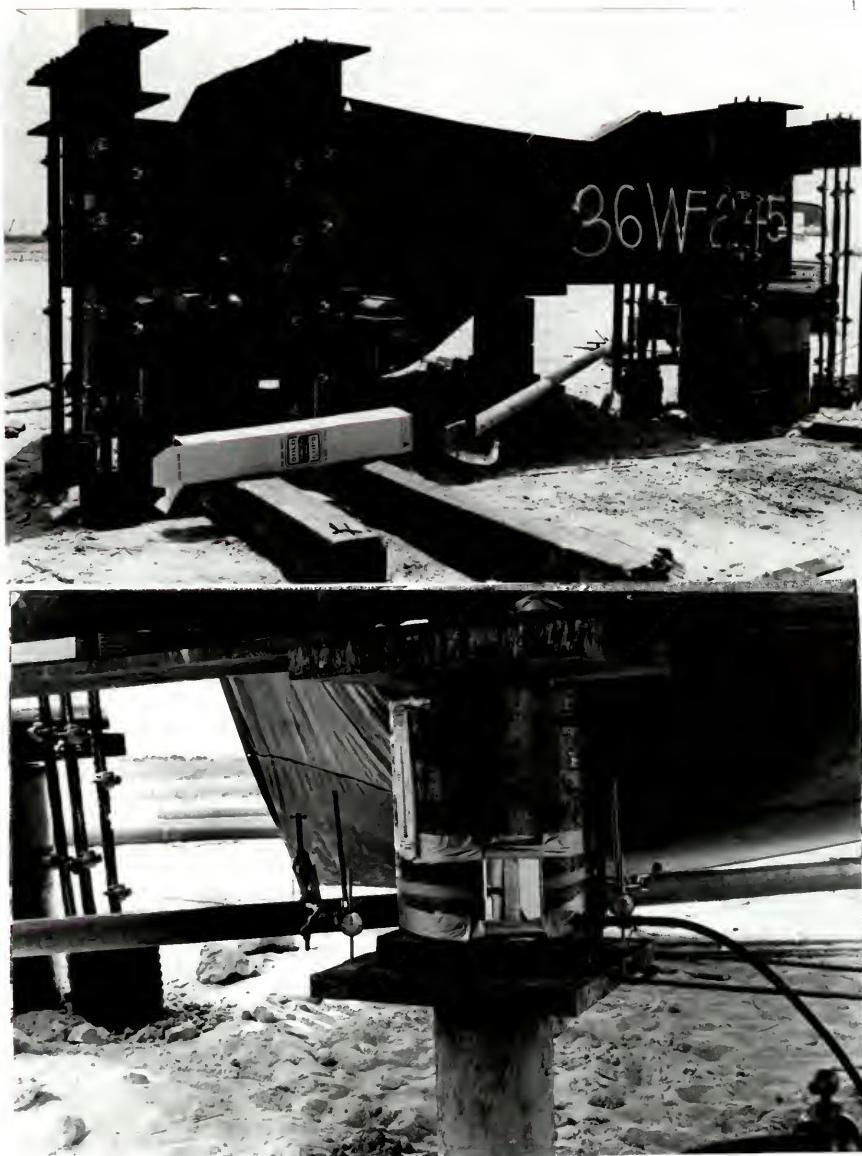
layer consists of dredged fill. Both the boring log and CPT data show a layer of soft clayey soil between depths of 43 and 55 ft at Site No 215.

Boring and CPT logs for the four south-side test sites (Site Nos 316, 322, 343, and 348) are presented in Figs D-24 through D-31. These logs show a soil profile consisting of loose to dense sands with occasional thin layers of clayey soil. The upper 10 to 15 ft are a dredged sand fill containing some shell and rock fragments. A thin layer of soft organic clay is usually present at the bottom of the dredged fill layer. The cone soundings were terminated in a dense sand layer at a depth of about 80 ft, except at Site No 343 where refusal was encountered on a limestone layer at a depth of 66 ft.

#### 9.4.2 Load Testing Program and Results

All piles were driven by Raymond International using a Model 65-C differential steam hammer. Driving resistance records are presented in Figs D-32 through D-34. Load was applied to the piles with a hydraulic jack acting against a steel reaction beam. Four Raymond step-taper piles were driven at each end of the beam to provide the necessary load reaction as shown in Fig 9.2. Pile settlement was measured with two dial gauges mounted on an independent reference beam. All piles were tested using the ML load test procedure.

Three piles were tested at Site No 215: a 70 ft long by 10 in square concrete pile, a 63 ft long pipe pile, and a 57 ft Raymond step-taper pile. These piles were tested to determine compression load capacity only, and the resulting load-settlement curves are shown in Figs D-35 through D-37.



BLOUNT ISLAND PILE LOAD TEST

FIGURE 9.2

Five piles were tested at Site No 227; however, thin limestone layers made it impossible to carry the cone soundings to the tip depths of four of the piles. Thus, it was only possible to analyze the results of one test performed on a 56 ft long by 10.75 in diameter pipe pile loaded in tension. The results of this test are presented in Fig D-38.

A 50 ft long by 14 in square concrete pile and a 50 ft long Raymond step-taper pile were tested at Site No 316. Both piles were tested in compression, and the test results are shown in Figs D-39 and D-40.

Tests were performed on three piles at Site No 322: a 42 ft timber pile, a 50 ft long pipe pile and a 74 ft long pipe pile. Both pipe piles were 10.75 in in diameter. The 74 ft pipe pile was tested in both tension and compression. Figs D-41 through D-44 contain the test results.

An 18 in square concrete pile, driven to a tip depth of 65 ft, was tested at Site No 343. This pile was driven through a 24 in diameter steel casing, set and washed out to a depth of 57 ft, and was tested in both compression and tension. Compression test results for this pile were not evaluated since the CPT sounding did not penetrate to a great enough depth to permit a tip resistance prediction to be made. The results of the tension test are presented in Chapter 10.

An 18 in square concrete pile was also tested at Site No 348. This pile was driven to a penetration of 49 ft and tested in compression only. The test results are shown in Fig D-45.

## CHAPTER 10

### FULL-SCALE PILE CAPACITY PREDICTIONS

#### 10.1 Description of Prediction Methods Used

All full-scale pile capacity predictions were made using mechanical penetrometer data. Predictions based on electrical CPT data would have been desirable since the model pile analyses showed that these types of data permit more accurate predictions; however, an electrical penetrometer suitable for making deep soundings was not available.

The methods used to predict full-scale pile capacity were those developed in Chapters 7 and 8 using the model pile load test results. These methods are summarized in the following sections, and the step-taper pile shaft resistance prediction method is extended to the case of a continuously tapered pile.

#### 10.1.1 Tip Bearing Capacity

The ultimate tip bearing capacity of all full-scale piles was estimated using the Begemann prediction method illustrated in Fig 11.1. For piles bearing in clay, the tip capacity computed using this method was multiplied by 0.6 to account for friction on the tip mantle of the mechanical penetrometer. The necessity of making this correction was discussed in Section 8.4.3.

The predicted yield tip capacity was determined by multiplying the predicted ultimate capacity by 0.73, the average ultimate to yield tip capacity ratio for the model pile tests.

### 10.1.2 Side Friction on Constant Section Piles

Side friction predictions for piles in sand were made using Eq 2.1 and the mechanical penetrometer K curves presented in Figs 7.35 and 7.36. The K value for full-scale concrete piles was determined by averaging the Fig 7.36 values for smooth and rough model piles because the surface roughness of full-scale piles falls between these two cases. Depth-of-embedment corrections were made at the ground surface in the manner illustrated in Fig 7.26 but not at soil layer interfaces. This point will be discussed in more detail in Chapter 11.

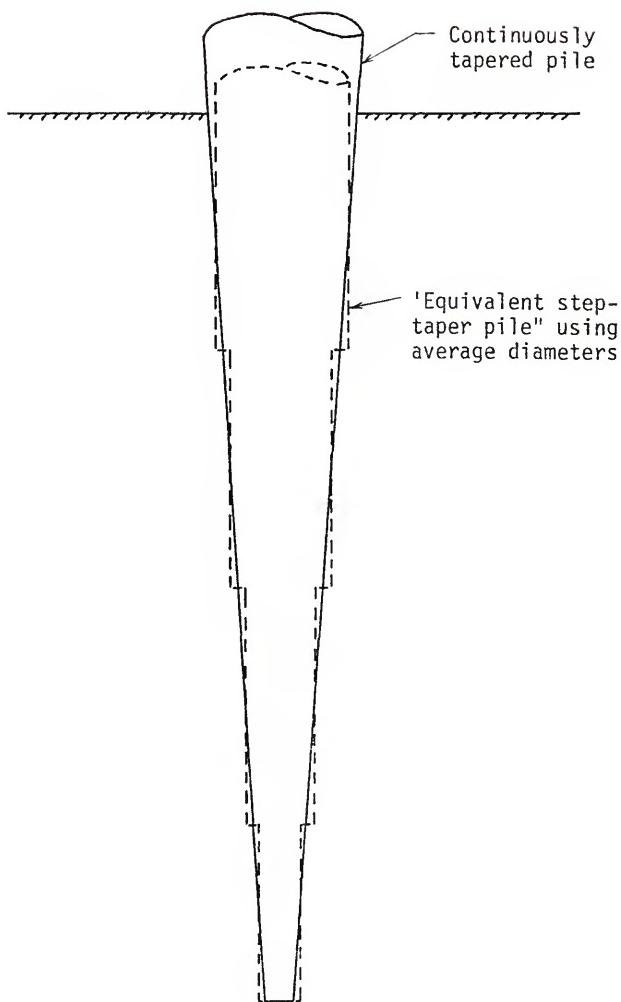
Predictions for piles in clay were made using the Tomlinson  $\alpha$  method based on  $s_u$  data as described in Chapter 8. Undrained shear strength was assumed to be equal to  $f_s$  except in the very stiff sandy clays at the Jefferson County site where a correction was made to account for probable end bearing on the mechanical penetrometer friction sleeve. This correction will be discussed in Section 10.2. Based on the model pile test results, yield and ultimate capacity side friction values were assumed to be equal.

### 10.1.3 Shaft Resistance of Tapered Piles

The ultimate shaft resistance of full-scale step-tapered piles was predicted by considering side friction on the constant diameter sections and end bearing at the steps in diameter independently as described in Sections 7.4 and 8.4. The side friction component on each constant diameter section was computed as if the entire pile was the same diameter, using the procedures described in Section 10.1.2. Step-bearing resistance was computed using  $q_s/q_c$  ratios of 1.6 and 1.0 for sands and clays, respectively.

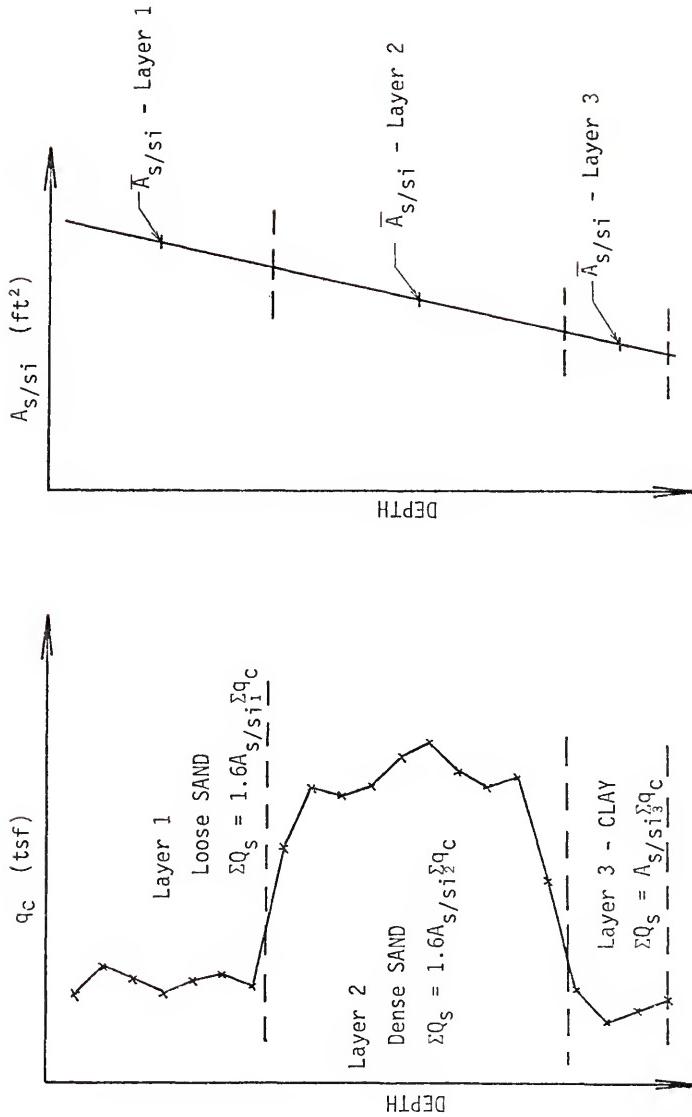
The side friction component of shaft resistance for the continuously tapered wood piles was estimated by determining an 'equivalent' step-taper pile and using the step-taper pile procedure. This concept is illustrated in Fig 10.1. For convenience, the steps were placed at depths that resulted in diameter steps of 1.0 in, which resulted in about five steps for the piles considered. The number of constant diameter sections which should be used to approximate the actual pile should be determined from the  $f_s$  profile. For a uniform soil, it would be adequate to base the calculations on the overall average pile diameter. For a layered soil profile, the average diameter through each layer should be used.

For computing the bearing component of shaft resistance, treating the continuously tapered piles as equivalent step-taper piles with a small number of diameter steps was considered too crude an approximation because of the large  $q_c$  variations which occurred with depth at the test sites. For this situation, the computed step bearing resistance would be highly dependent on the depths at which the equivalent pile diameter steps were placed. This problem can be essentially eliminated by placing a diameter step at each CPT sounding depth since  $q_c$  values are normally determined at small enough depth intervals to reflect the actual variation in bearing resistance with depth. The computations can be greatly simplified by constructing a curve of equivalent pile step area per cone sounding interval ( $A_s/s_i$ ) and considering the soil layering indicated by the CPT data as shown in Fig 10.2. Judgment must be used to determine whether a factor of 1.0, 1.6, or something between should be used with the  $q_c$  data to compute the equivalent step bearing in clay, sand, or mixed soils, respectively.



STEP-TAPER APPROXIMATION OF A CONTINUOUSLY TAPERED PILE

FIGURE 10.1



PROCEDURE FOR ESTIMATING BEARING COMPONENT OF SHAFT RESISTANCE ON CONTINUOUSLY TAPERED PILES

FIGURE 10.2

The yield capacity shaft resistance was computed using the ultimate to yield capacity shaft resistance ratio of 0.84 determined from the model pile tests in sands since the tapered piles considered were embedded almost totally in sands. This approach is not recommended in clays because the model pile tests indicate the yield capacity concept is not valid in cohesive soils.

#### 10.2 Comparison of Predicted and Measured Capacities

Full-scale pile capacity predictions, measured capacities, and prediction errors for the full-scale piles are summarized in Table 10.1. Actual ultimate capacity was determined from the pile load test data as the load causing a settlement equal to 10% of the pile width or diameter. In cases where a settlement of 0.10B was not attained during the load test, the maximum load applied to the pile was used as the ultimate capacity. Yield capacities were determined by plotting log-log load-settlement curves as explained in Section 6.6.

The prediction errors presented in Table 10.1 show that the full-scale ultimate pile capacity estimates were generally slightly conservative in contrast to the model pile predictions which were generally slightly unconservative. There are several possible reasons for these differences. One of the more important possible reasons is thought to be different pore pressure effects caused by the difference in groundwater conditions at the model and full-scale pile test sites.

Table 10.2 presents detailed information on the predicted ultimate capacity for the full-scale piles. The relative contributions of tip bearing, side friction, and shaft bearing to total capacity are shown, along with the percent of the total capacity which was predicted to occur in sand layers. These data show that, with the exception of

TABLE 10.1  
SUMMARY OF FULL-SCALE PILE CAPACITY PREDICTIONS

Test Location	Test or Site No.	Pile Type	Pile Length (ft)	Pred Pult (t)	Meas Pult (t)	Error (%)	Pred Py (t)	Meas Py (t)	Error (%)
W. P. Beach	1	18" Sq Conc	26.5	119	133	-10.5	102	83	22.9
	2	18" Sq Conc	37.2	64	96	-33.3	45	42	7.1
Jeff. Co.	1	18" Sq Conc	30	247	213	+16.0	199	--	--
	2	18" Sq Conc	14	202	171	+18.1	186	--	--
Tarver, Ga.	1	14" Sq Conc	14	73	116	-36.1	--	--	--
Blount Is.	215	10" Sq Conc	70	93	91	-2.2	86	77	11.7
	215	Timber	63	130	107	-21.4	107	54	98.1
Step-Taper	215	Step-Taper	57	97	145	-33.1	81	102	20.6
	227*	10.75" Pipe	56	39	46	-15.2	--	--	--
322	Timber	42	106	137	-22.6	87	105	-17.1	
	322	10.75" Pipe	50	62	74	-16.2	56	--	--
322	10.75" Pipe	74	180	181	-0.5	80	133	-39.8	
	322*	10.75" Pipe	74	85	82	-3.6	--	--	--
316	14" Sq Conc	52	116	168	-31.0	104	126	-17.5	
	316	Step-Taper	50	155	190	-18.4	128	143	-10.5
348	18" Sq Conc	49	153	196	-21.9	140	137	2.2	
	343*	18" Sq Conc	65**	77	80	-3.7	--	--	--

\*Tension Test

\*\*Cased to 57 ft

TABLE 10.2  
DETAILS OF THE PREDICTED ULTIMATE CAPACITY FOR THE FULL-SCALE PILES

Test Location	Test or Site No.	Pile Type	Pile Length (ft)	$Q_{ult}$ (t)	Resistance % End Bearing	Component % Side Friction	Contributions % Step Bearing	% Quilt In Sand
W. P. Beach	1	18" Sq Conc	26.5	119	58	42	--	100
	2	18" Sq Conc	37.2	64	45	55	--	100
Jeff Co.	1	18" Sq Conc	30	247	72	28	--	84
	2	18" Sq Conc	14	202	29	71	--	29
Tarver, Ga.	1	14" Sq Conc	14	73	60	40	--	100
Blount Is.	215	10" Sq Conc	70	93	25	75	--	93
	215	Timber	63	130	14	44	42	96
	215	Step-Taper	57	97	7	43	50	87
	222*	10.75" Pipe	56	39	--	100	--	100
	322	Timber	42	106	15	26	59	100
	322	10.75" Pipe	50	62	35	65	--	100
	322	10.75" Pipe	74	180	56	44	--	100
	322*	10.75" Pipe	74	85	--	100	--	100
	316	14" Sq Conc	52	116	44	56	--	100
	316	Step-Taper	50	155	11	26	63	100
348	18" Sq Conc	49	153	33	67	--	100	100
	343*	18" Sq Conc	65**	77	--	100	--	100

\*Tension Test

\*\*Cased to 57 ft

Test Pile No 2 at Jefferson County, all the piles developed their capacity primarily in sands. It is also interesting that the predictions indicate shaft bearing accounts for about 50% of the total capacity for all four tapered piles.

Twelve of the 17 full-scale piles tested were embedded entirely in sands, the exceptions being the two piles tested in Jefferson County and three piles tested at Blount Island Site No 215 where layers of both sand and clay were penetrated. Of the 12 piles driven in sands, nine were loaded in compression and three in tension. Predictions for all nine compression piles were conservative and capacities of two of the three tension piles were underestimated. The groundwater level was near the ground surface at all full-scale test sites where piles were driven in sands; thus, most of the CPT tests were performed in saturated soils where excess pore pressures could affect the test results. Significant excess pore pressures probably did not develop during pile load testing because of the high permeability of the granular soils and the slow loading rates used. Therefore, it is expected that CPT data obtained in a normal manner would tend to overestimate or underestimate pile capacity, depending on whether positive or negative pore pressures developed during the CPT testing.

Schmertmann (1974b) evaluated the effects of excess pore pressure development during CPT testing and concluded that data gathered using the normal penetration rate of 1.0 to 2.0 cm/sec would probably lead to conservative results in loose and medium dense sands due to positive excess pore pressure generation and could cause unconservative results in very dense sands due to negative pore pressure development. Positive pore pressure probably developed during CPT testing in sands at

the West Palm Beach and Blount Island sites since these sands generally ranged from very loose to medium dense; therefore, the cone data should result in conservative pile capacity predictions. The same effect would not occur at the model pile test sites since the testing was performed above the groundwater table.

The average underprediction for compression piles in sand was 21%, while that for tension piles was only 5%. This difference is probably the result of assuming that friction capacity in tension is equal to that in compression, as was done in making the friction predictions. Tension pile friction should be somewhat less because loading a pile in tension will reduce the effective vertical stress in the soil around the pile.

Overpredicting the capacity of the two piles tested in Jefferson County may have been caused by  $f_s$  values measured in the clays using the mechanical penetrometer being higher than the true sleeve friction. These clays were very hard and sandy and could have exerted considerable end bearing resistance on the lower beveled portion of the friction sleeve. An attempt was made to correct for this effect by comparing mechanical and electrical penetrometer friction sleeve data obtained in the upper layer of stiff clay at Paines Prairie. This comparison showed that the average  $f_{sm}$  was 12% higher than the average  $f_{se}$ ; therefore, the computed pile friction in the Jefferson County clay was reduced by a factor of 1.0/1.12. A larger reduction factor might be appropriate since the Jefferson County clay was much harder and sandier than the upper clay layer at Paines Prairie. It is also possible that negative pore pressures developed in the dense Jefferson County soils, which would result in unconservative CPT data.

The 36% underprediction for the Tarver, Georgia, test pile may be partially due to the CPT data not being representative of the soil conditions at the pile location. As explained in Section 9.3.1, the sounding on which the prediction was based was made a considerable distance from the pile location. In addition, only one of three soundings attempted penetrated the dense soils; therefore, the results of this sounding are probably more representative of the minimum soil strength at the site than the actual strength at the pile location.

Capacity predictions for three of the four full-scale tapered piles were also conservative. This could be the result of the  $q_s/q_c$  ratio used for the shaft resistance analysis being too low, since the data presented in Section 7.4.2 indicated that a value higher than 1.6 might be applicable to long tapered piles. However, it is also possible that the underpredictions for these piles were affected by pore pressure generation during the CPT tests. It appears likely that pore pressure effects may have been the main cause of the underprediction, since the average taper pile prediction error (-13%) was approximately equal to the average prediction error for constant section piles loaded in compression at the same site (-14%). Because of this, use of a  $q_s/q_c$  ratio higher than 1.6 is not recommended at this time; however, additional data on full-scale piles may justify revising this ratio upward.

### 10.3 Evaluation of Prediction Accuracy Safety Factors

#### 10.3.1 Comparison of Prediction Errors for Model and Full-Scale Piles

The validity of using the prediction methods developed from the model pile test results to predict the capacity of full-scale piles can be evaluated by comparing the prediction accuracy for the model and

full-scale piles. This comparison is presented in Table 10.3. The statistical parameters presented in this table were computed by lumping all model pile predictions in one group and all full-scale predictions in another. The statistical values are based on all 17 full-scale tests and 65 model pile tests.

TABLE 10.3  
COMPARISON OF PREDICTION ERRORS FOR  
MODEL AND FULL-SCALE PILES

Pile Type	Penetrometer	Prediction Error Statistic	
		Mean	Standard Deviation
Full-Scale	Mechanical	-10.7%	18.6%
Model	Mechanical	10.4%	31.1%
Model	Electrical	6.5%	18.7%

The difference in the mean prediction errors reflects the tendency to underpredict full-scale pile capacities and overpredict model pile capacities, as discussed in Section 10.2. The standard deviation of the prediction errors is probably a more meaningful statistic in that it is a measure of the prediction error scatter. It is significant that the standard deviation of the full-scale pile capacity prediction errors is considerably less than that of the model piles for the mechanical penetrometer. This reinforces the argument presented in Section 7.2.7 that it should be possible to make more accurate capacity predictions for larger piles because minor soil variations have less effect on the capacity of large piles.

If the error scatter for predictions based on electrical

penetrometer data reduces proportionally to that for the mechanical penetrometer when full-scale piles are considered, the data in Table 10.3 indicate that use of electrical penetrometer data should result in full-scale pile capacity predictions with a standard deviation of only about 11%.

These comparisons show that the prediction methods developed from the model pile studies can be used successfully to predict the capacity of full-scale piles with a width or diameter up to 18 in. Accurate predictions should be possible for even larger piles; however, from the available data, it is impossible to determine an upper limit of the pile size to which these methods are applicable.

#### 10.3.2 Safety Factor Analysis

Safety factors based on a statistical analysis of the model pile prediction errors were presented in Sections 7.6.2 and 8.5. A similar analysis based on data for full-scale piles contained in Table 10.3 indicates a safety factor of 1.22 should be applied to total ultimate capacity predictions to account for possible prediction errors. If an average prediction error of 0.0% is used instead of the -10.7% value contained in Table 10.3, the required safety factor is increased to 1.33. Safety factors applicable to electrical penetrometer predictions should be slightly smaller.

Partial safety factors applicable to end bearing and side friction cannot be determined from the full-scale pile data, since independent measurements of the two components were not made.

## CHAPTER 11

### RECOMMENDED CPT PILE CAPACITY DESIGN PROCEDURES

#### 11.1 Introduction

This chapter presents the author's recommendations for using quasi-static cone penetration data to estimate the load capacity of driven displacement piles. The recommendations are based on an evaluation of the model and full-scale pile studies described in the preceding chapters and are applicable to the types of piles, penetrometers, and soils considered in this study. The limitations of the recommended methods are further discussed in Section 11.6.

#### 11.2 Tip Bearing Capacity

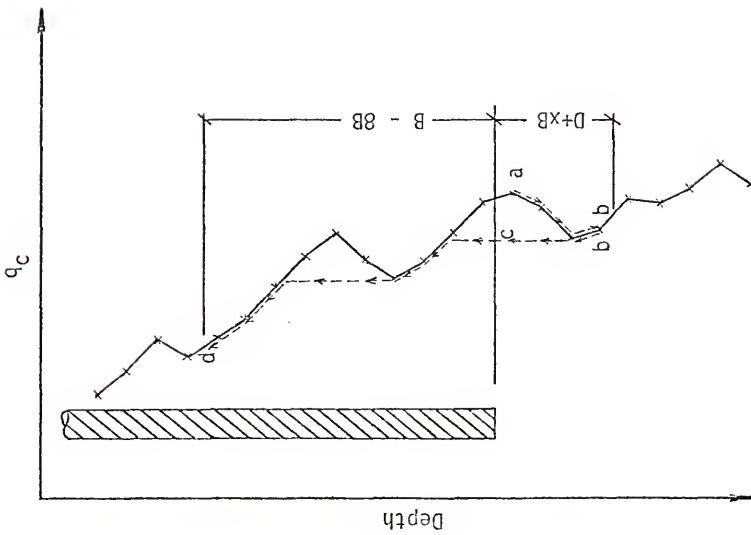
Use the Begemann procedure illustrated in Fig 11.1 to estimate the ultimate unit tip bearing capacity in both sands and clays. If the mechanical penetrometer is used in clays, the computed  $q_c$  value should be multiplied by 0.60 to account for the possible increase in  $q_c$  resulting from friction on the tip mantle. If the design is to be based on yield capacity criteria, multiply the computed ultimate tip resistance by 0.73.

Pile capacities computed using this procedure are greatly affected by isolated very low  $q_c$  values which may not be representative of actual soil conditions. Therefore, single  $q_c$  values which are very low in relation to the surrounding values should be ignored unless there is reason to believe that the values are representative of actual weak

$$q_p = \frac{q_{c1} + q_{c2}}{2}$$

$q_{c1}$  = Average  $q_c$  over a distance of  $x_B$  below the pile tip (path a-b-c). Sum  $q_c$  values in both the downward (path a-b) and upward (path b-c) directions. Use actual  $q_c$  values along path a-b and the minimum path rule along path b-c. Compute  $q_{c1}$  for  $x$ -values from 0.7 to 3.75 and use the minimum  $q_{c1}$  value obtained.

$q_{c2}$  = Average  $q_c$  over a distance of  $3B$  above the pile tip (path c-d). Use the minimum path rule as for path b-c in the  $q_{c1}$  computations.



BEGEMANN PROCEDURE FOR PREDICTING PILE TIP CAPACITY

FIGURE 11.1

soil layers, i.e., similar data from an adjacent sounding or soil samples which indicate thin layers of weak soil.

It is customary in The Netherlands to place an upper limit on allowable unit tip bearing capacity when CPT data are used for design. This limit, usually between 50 and 150 tsf, is intended to protect against grain crushing, long-term high-pressure creep, and other unknown factors affecting the behavior of soils subjected to extremely high-pressure loading. Schmertmann (1974c) has recommended using a maximum allowable tip bearing capacity of 100 tsf for onshore design. This recommendation should be followed unless data are available to show that higher contact pressures are permissible. It should be noted that this limitation applies to allowable unit bearing capacity and will seldom be a serious limitation since piles usually are not driven to such a high resistance.

### 11.3 Side Friction on Constant Section Piles

#### 11.3.1 Granular Soils

Compute the ultimate side friction on constant section piles using Eq 11.1 and the design curves in Fig 11.2.

$$F_s = K \left[ \sum_{d=0}^{8B} \frac{d}{8B} f_s A_s' + \sum_{d=8B}^L f_s A_s' \right] \quad (11.1)$$

where

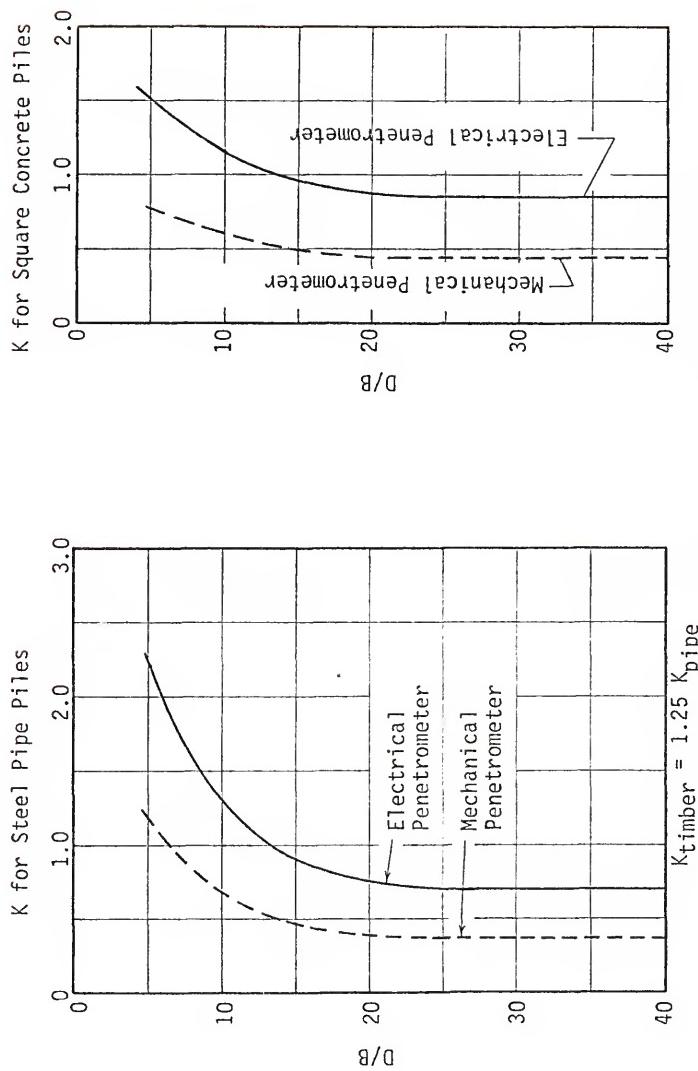
$F_s$  = total ultimate side friction resistance

$K$  = ratio of unit pile friction to unit sleeve friction from

Fig 11.2

$d$  = depth to the  $f_s$  value being considered

$B$  = pile width or diameter



PENETROMETER DESIGN CURVES FOR PILE SIDE FRICTION IN SAND

FIGURE 11.2

$f_s$  = unit sleeve friction resistance

$A'_s$  = pile-soil contact area per  $f_s$  depth interval

The design curves in Fig 11.2 are the curves developed from the model pile side friction analysis detailed in Section 7.3 and are the same as the curves presented in Figs 7.35 and 7.36. The K factor is the ratio between unit sleeve friction and unit pile friction. As pointed out in Section 7.3, the K factor should be determined by computing L/B using the total embedded pile length. A separate K factor should not be used for each  $f_s$  value.

Side friction calculations can be greatly simplified if sleeve friction resistance does not vary significantly with depth. For this case, Eq 11.1 can be simplified to Eq 11.2, provided the pile length is equal to or greater than 8B.

$$F_s = K \left[ \frac{1}{2} \left( \bar{f}_s A''_s \right)_{0-8B} + \left( \bar{f}_s A''_s \right)_{8B-L} \right] \quad (11.2)$$

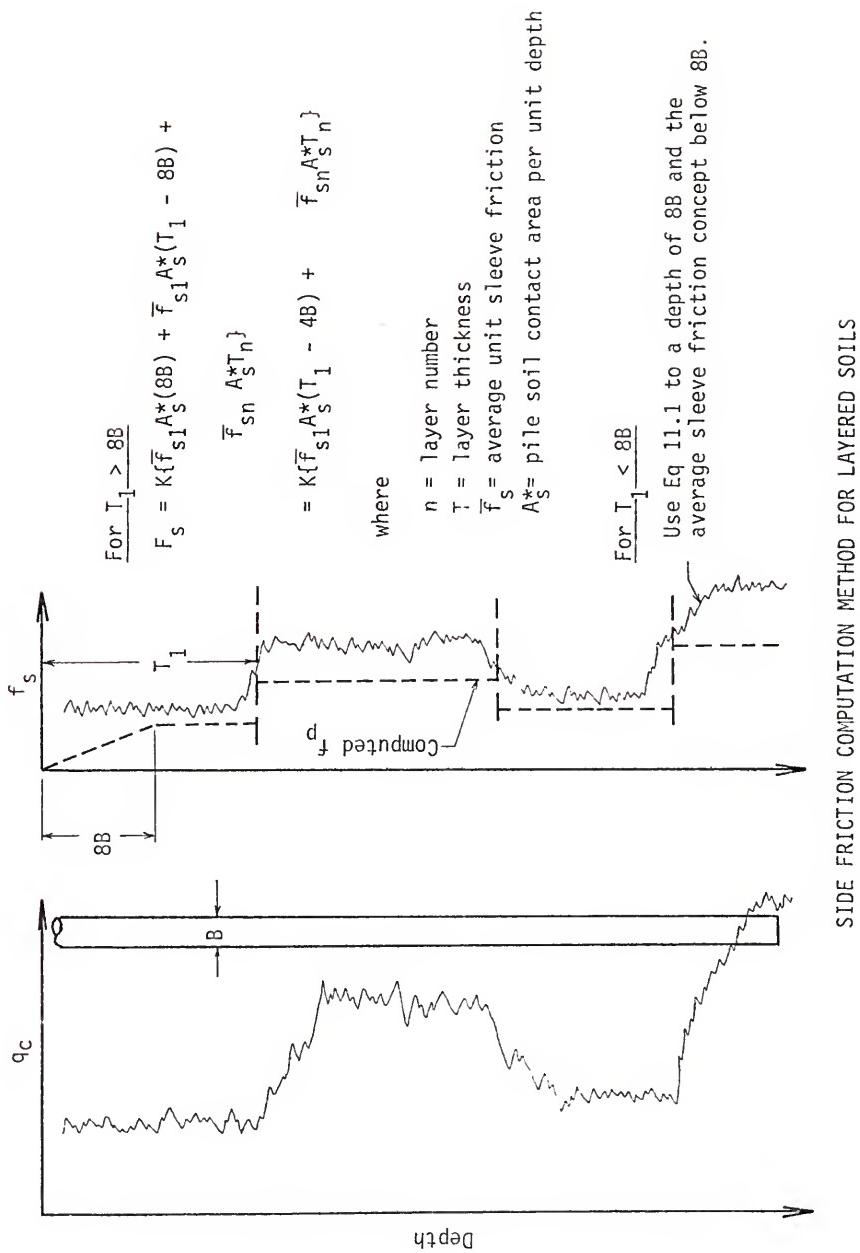
where

$\bar{f}_s$  = average unit sleeve resistance over the depth interval indicated by the subscript

$A''_s$  = pile-soil contact area over the above  $\bar{f}_s$  depth interval

If two or more sand layers are involved, Eq 11.2 can be used by considering each layer individually as shown in Fig 11.3. The K value used for a multi-layered system should be determined using the total pile length and will, therefore, be the same for each layer.

Note that Eqs 11.1 and 11.2 only incorporate a depth of embedment correction at the ground surface. Schmertmann (1967) and Freed (1972) recommended that a correction be made each time the pile enters a stronger soil layer. Their recommendations were based on the assumption

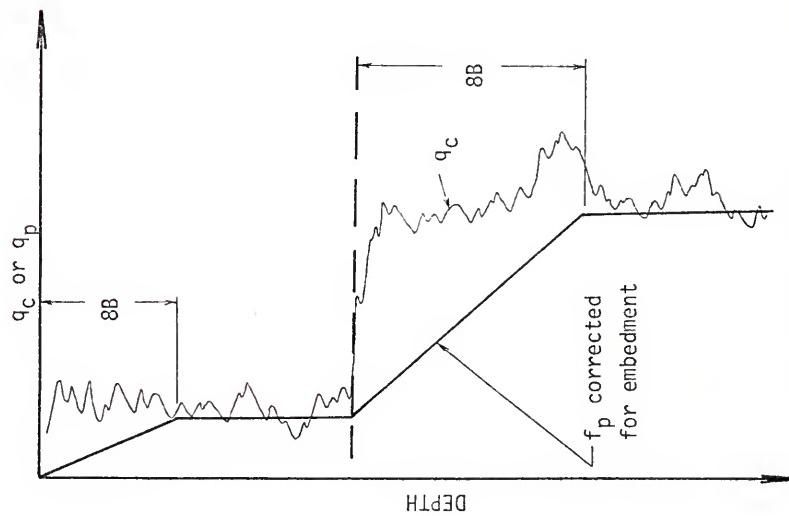
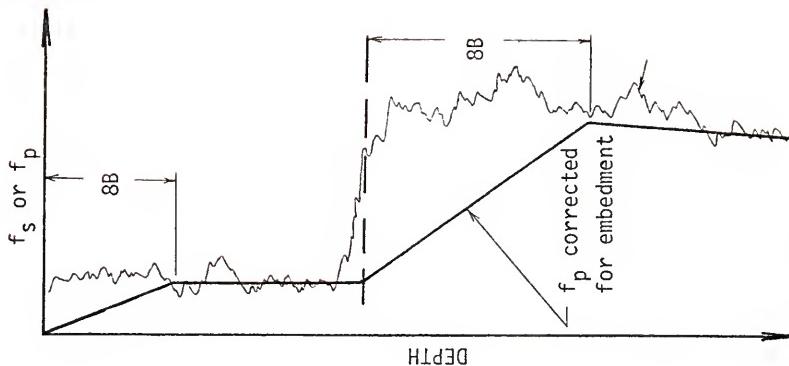


that the CPT friction ratio remains constant near layer interfaces and unit friction varies in proportion to unit tip resistance, as shown in Fig 11.4. Some CPT results are available, e.g., Schmertmann (1969), which tend to substantiate this assumption; however, it is difficult to draw any definite conclusions from these kinds of data, since the normally used 20 cm cone sounding interval is approximately equal to the 5 to 10B interval over which  $f_s$  would be expected to vary.

The recommendation that depth of embedment corrections not be made at layer interfaces when computing pile side friction is based on the following:

1. A lack of conclusive data to indicate such a correction should be made.
2. The fact that not making this correction did not result in any apparent large errors in the full-scale pile capacity predictions presented in Chapter 10.
3. The possibility that unit pile friction just below a layer interface may increase in the same manner as near the ground surface. The increase which occurs near the ground surface is reflected in the shape of the K curves in Fig 11.2.
4. Smear effects resulting from soil being carried down with the pile will mask layer boundary friction changes.
5. The desire to keep the prediction method simple and easy to apply. The existence of a distinct, significant interface is often difficult to decide and, in many cases, different engineers would disagree as to whether or not an interface actually exists. Eliminating the correction at layer interfaces eliminates these problems.

Pile friction predictions in sands can be based on  $q_c$  data when sleeve friction resistance information is not available. The calculations should be made by replacing  $f_s$  terms in Eq 11.1 (or 11.2) with 0.007  $q_c$  and using the electrical penetrometer design curves in Fig 11.2. This is equivalent to assuming an average electrical penetrometer friction ratio of 0.70%, which is a slightly conservative typical



SCHMIDTMANN & FREED METHOD FOR PILE FRICTION EMBEDMENT CORRECTION  
FIGURE 11.4

value for the sands in this study and in most other areas of Florida. The 0.70% FR value should be increased or decreased to better match experience in other areas.

### 11.3.2 Cohesive Soils

Total ultimate side friction in cohesive soils should be estimated using Eq 11.3 and the design curve in Fig 11.5.

$$F_s = \alpha' \bar{f}_s A_s \quad (11.3)$$

where

$\alpha'$  = ratio of pile to penetrometer sleeve friction in clay

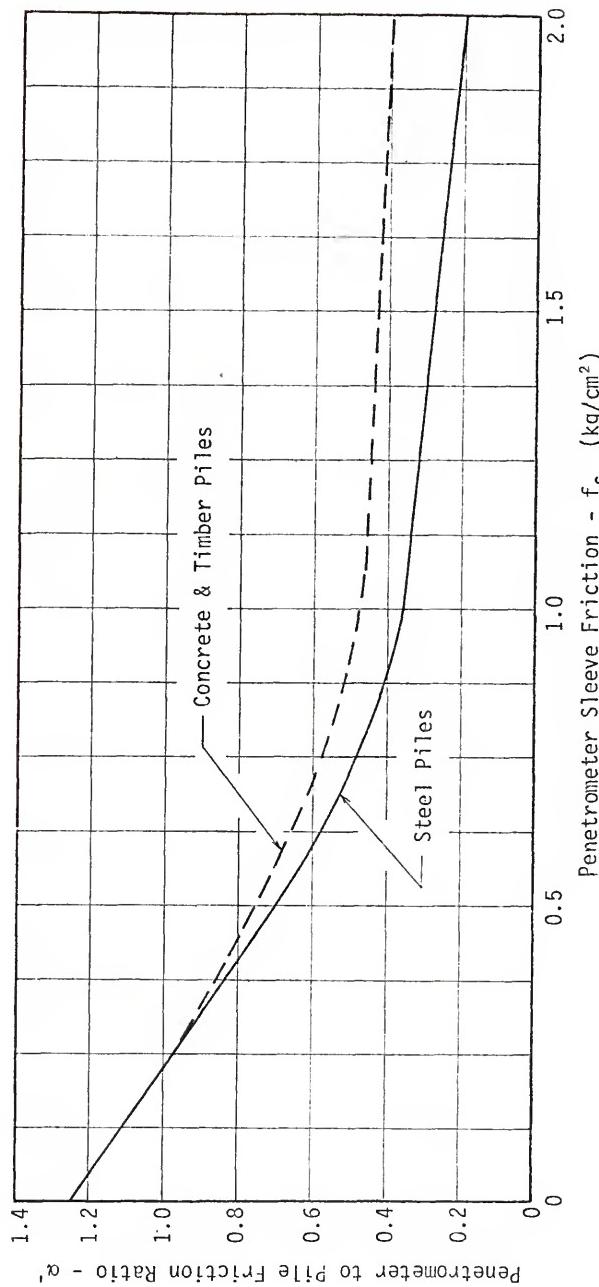
$\bar{f}_s$  = average undrained sleeve friction

$A_s$  = total soil-pile contact area

This recommendation is based primarily on the model pile studies which showed that, of the currently available clay-pile friction theories, Tomlinson's  $\alpha$ -method provided the best predictions.

The  $\alpha'$  curves shown in Fig 11.5 are identical to Tomlinson's  $\alpha$  curves as presented in tabular form in NAVDOCKS DM-7, except that the  $\alpha'$  curves are plotted as a function of  $f_s$ .

Additional full-scale pile capacity correlation studies may show that the  $\lambda$  (or  $\lambda'$ ) method described in Chapter 8 provides better predictions; however, this method is not recommended at this time because of the poor correlation obtained during the model pile studies. Ultimately, a drained friction approach to the clay-pile friction problem should be adopted, but it appears that at this time it is impossible to make sufficiently accurate predictions of the radial effective stress acting on a pile driven in clay. Schmertmann's suggested procedure for estimating radial effective stress, coupled with additional CPT and



PENETROMETER DESIGN CURVES FOR PILE SIDE FRICTION IN CLAY

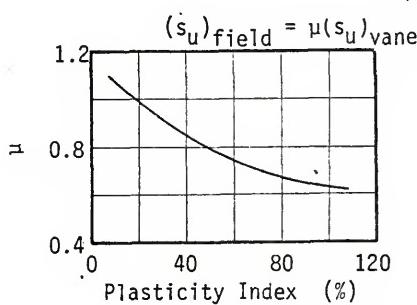
FIGURE 11.5

pressuremeter research, may provide the basis for an eventual solution to this problem.

Eq 11.3 is based on a limited number of data which indicate that  $f_s$  values obtained using either the electrical or mechanical penetrometer is a good approximation of undrained shear strength of clays. Since the relationship has not been proven for a wide variety of clays, undisturbed sampling and strength testing should be performed whenever possible to check the  $f_s - s_u$  ratio. This method should not be used for highly sensitive clays. Also, mechanical penetrometer  $f_s$  data should be reduced approximately 20% in hard clays to account for possible end bearing on the friction sleeve.

Eqs 11.4 or 11.5, applicable to electrical and mechanical penetrometer data, respectively, can be used to estimate pile friction in clays when  $f_s$  data are unavailable. The  $\mu$  term in these equations is Bjerrum's (1972) field vane shear strength correction factor, as shown in Fig 11.6.

$$F_s = 0.10 \mu \bar{q}_c A_s \quad (11.4)$$



BJERRUM'S FIELD VANE SHEAR STRENGTH CORRECTION CURVE

FIGURE 8.8

$$F_s = 0.067 \mu \bar{q}_c A_s \quad (11.5)$$

Whenever possible, pile friction should be estimated using both Eqs 11.3 and 11.4 or 11.5 to determine a range of possible friction resistance. If the predictions provided by each equation do not compare reasonably well, the undrained shear strength of the soil should be evaluated by other means.

#### 11.4 Tapered Pile Shaft Resistance

##### 11.4.1 Step-Taper Piles

Compute total ultimate shaft resistance as the sum of two independently determined components, friction on the constant diameter sections and end bearing at the diameter steps. The side friction component should be estimated using the procedures recommended for constant section piles in Section 11.3, with the following exception. In sands, the K term for each constant diameter section should be determined using the depth to which that diameter section extends. This point is illustrated by the example problem in Fig 11.7.

Use Eq 11.6 to estimate the end bearing component at the diameter steps.

$$Q_{step} = \sum_{steps} S q_c^* A_{step} \quad (11.6)$$

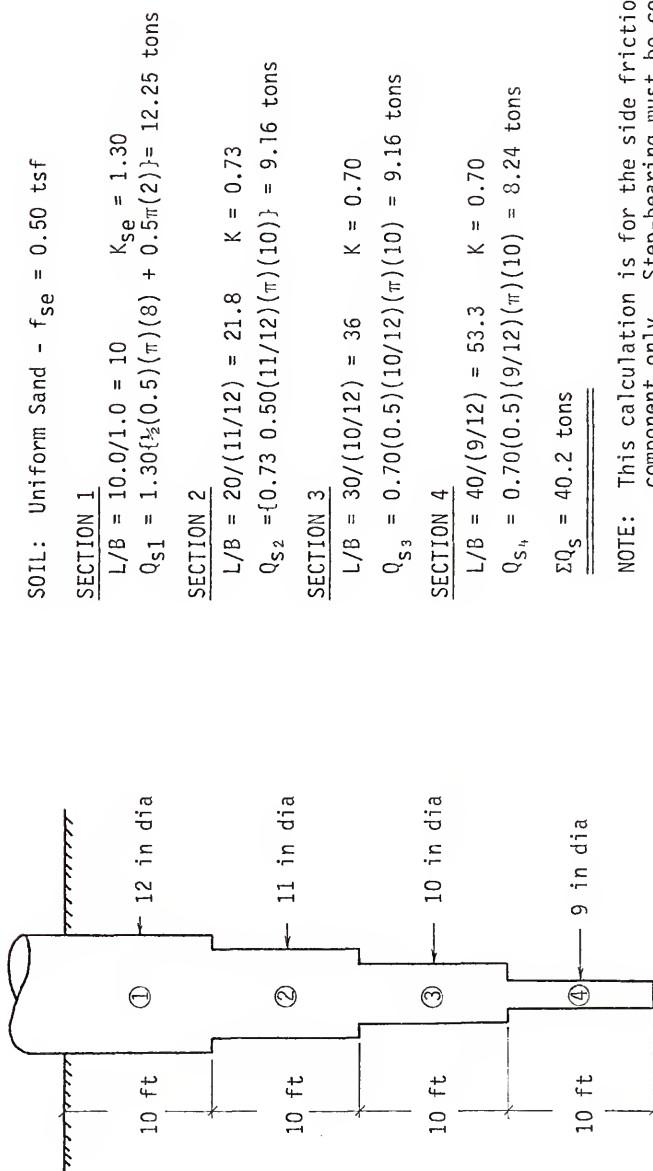
where

$Q_{step}$  = total end bearing component of shaft resistance over the entire tapered pile length

S = ratio of  $q_c$  to unit step bearing resistance

$A_{step}$  = bearing area at the diameter step

$q_c^*$  = average  $q_c$  value in the vicinity of the diameter step



EXAMPLE OF STEP-TAPER PILE FRICTION COMPUTATION

FIGURE 11.7

The values of S which should be used in Eq 11.6 are contained in Table 11.1. The mechanical penetrometer S value for clays incorporates the 0.60 correction factor recommended in Section 11.2 to account for tip mantle friction. The two  $q_c$  values occurring immediately above and below the step depth should be used to compute  $q_c^*$ ; however, unusually high or unusually low  $q_c$  values should be ignored.

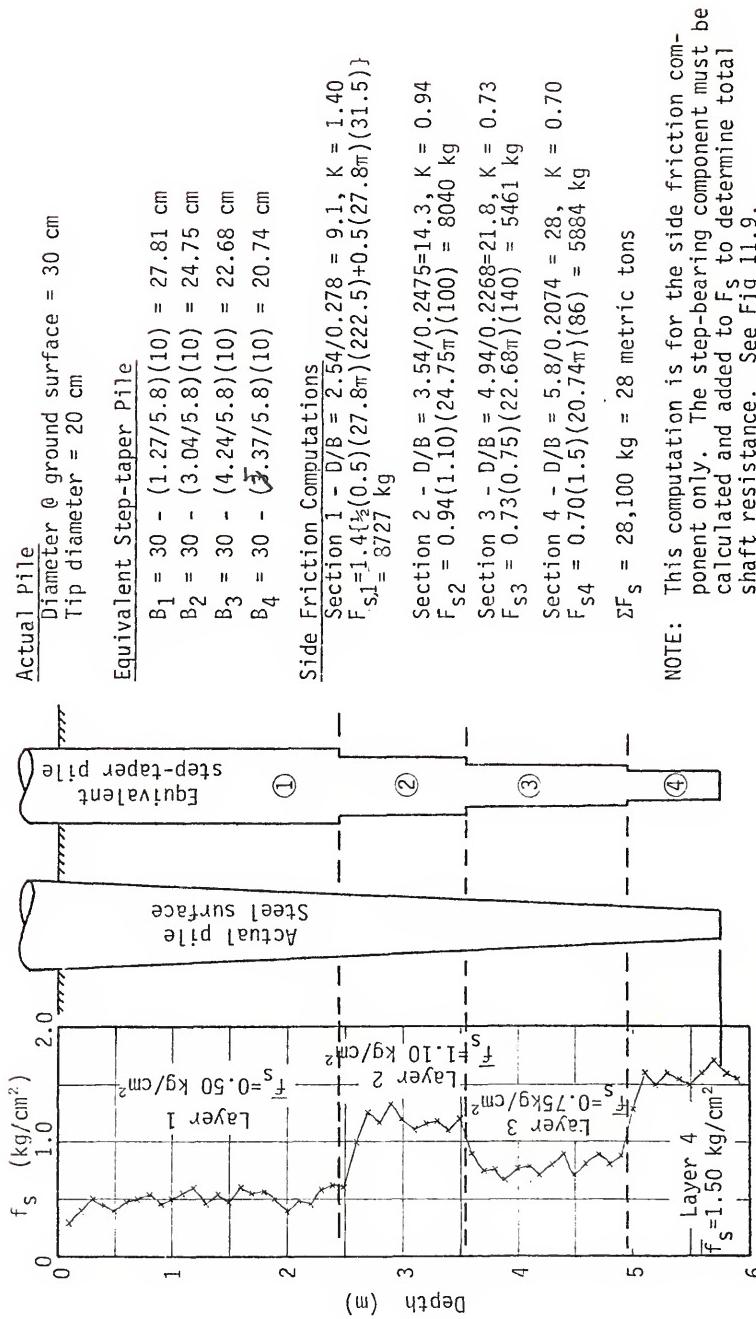
TABLE 11.1  
S VALUES FOR ESTIMATING TAPERED PILE SHAFT RESISTANCE

<u>Penetrometer</u>	<u>Soil Type</u>	<u>S</u>
Electrical	Sand	1.6
	Clay	1.0
Mechanical	Sand	1.6
	Clay	0.6

#### 11.4.2 Continuously Tapered Piles

The shaft resistance of piles with continuously tapered sections, such as timber or monotube piles, can be estimated by considering 'equivalent' step-taper piles and using the procedures in Section 11.4.1. In estimating the side friction components, diameter steps of the equivalent pile should be placed at layer interfaces as illustrated by the example problem in Fig 11.8.

Experimental K curves for timber piles could not be developed since model timber piles were not tested. The recommendation for timber pile K values presented in Fig 11.2 was developed using the friction test data presented in Table 3.5. The pipe pile K curve was used as



EXAMPLE COMPUTATION FOR CONTINUOUSLY TAPERED PILE SIDE FRICTION

FIGURE 11.8

a base for the timber pile because both types of piles have the same cross section shape. The results of Potyondy's and Lingo's tests, presented in Table 3.5, show that the timber friction coefficient is approximately the same as for smooth concrete. Freed's tests showed that the smooth concrete friction coefficient was 29% higher than that for the model pile steel. Combining Freed, Potyondy, and Lingo's results indicates that the timber friction coefficient should be approximately 1.3 times that for normal pile steel. The recommended ratio of 1.25 was chosen to be slightly conservative, since test data were not available to confirm the ratio inferred from the shear test data.

The step bearing component should be estimated by considering an 'equivalent' pile diameter step at each cone sounding depth. This procedure can be simplified by constructing a graph of pile step area per sounding interval ( $A_{s/si}$ ), noting the soil layering as indicated by the CPT data, and using the following equation:

$$Q_{\text{step}} = \sum_n S \bar{q}_{cn} \bar{A}_{s/si} \quad (11.7)$$

where

$n$  = soil layer number

$S$  = ratio of  $q_c$  to unit step bearing

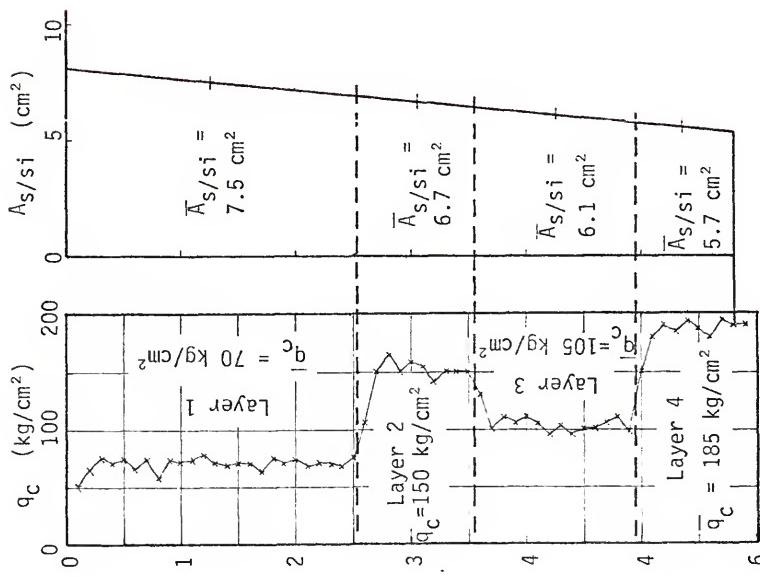
$\bar{q}_{cn}$  = average  $q_c$  for layer  $n$

$\bar{A}_{s/si}$  = average step area per sounding interval for layer  $n$

The step bearing component for the example problem in Fig 11.8 is computed in Fig 11.9 to illustrate this procedure.

### 11.5 Safety Factors

It is impossible to establish fixed safety factor criteria for pile capacity design since the degree of safety appropriate for each design depends on a large number of factors, including a large amount



From Fig 11.8, the pile taper is 0.01724 cm per cm of depth. The step-area curve was computed using this value.

#### Shaft Bearing Computation

##### Layer 1

$$\begin{aligned} Q_{s1} &= S\bar{q}_c \bar{A}_{s/s_i} \\ &= 1.6(70)(25.4)(7.5) = 21,340 \text{ kg} \end{aligned}$$

##### Layer 2

$$Q_{s2} = 1.6(150)(10.0)(6.7) = 16,080 \text{ kg}$$

##### Layer 3

$$Q_{s3} = 1.6(105)(14.0)(6.1) = 14,510 \text{ kg}$$

##### Layer 4

$$Q_{s4} = 1.6(185)(8.6)(5.7) = 14,510 \text{ kg}$$

$$\Sigma Q_s = 65.9 \text{ metric tons}$$

$$Q_{\text{shaft}} = \Sigma F_s + \Sigma Q_s = 28.1 + 65.9$$

$$Q_{\text{shaft}} = 94 \text{ metric tons}$$

EXAMPLE STEP BEARING COMPUTATION FOR A CONTINUOUSLY TAPERED PILE

FIGURE 11.9

of 'engineering judgment'. However, it is possible to use the capacity prediction results for the model and full-scale piles to determine the ranges within which design safety factors should fall.

Table 11.2 presents safety factors determined from a statistical analysis of the available pile test data. The statistical method used was described in Section 7.6. All the different pile types tested were analyzed as a group. The ultimate capacity safety factors were obtained by multiplying the safety factors computed from the prediction error data by 1.5 to provide a maximum design load equal to 2/3 of the ultimate pile capacity. The need for making this reduction was discussed in Section 7.6.

Based on the data in Table 11.2, recommended design safety factor ranges are presented in Table 11.3. These recommended ranges were developed by considering both the model and full-scale capacity prediction accuracy, with the minimum recommended values being approximately equal to the average of the computed safety factors for the model and full-scale piles. These values appear slightly conservative when only the full-scale pile data are considered. The upper limit values are based on the author's opinion that routinely gathered CPT data should not result in errors more than 20 to 30% greater than the prediction errors which resulted from using 'research quality' data.

Only composite safety factors applying to predicted total pile capacity have been presented, since the model pile studies showed that side friction and end bearing predictions were equally accurate; thus, there is no apparent advantage to be gained by using partial safety factors. Use of the yield capacity design method and safety factors eliminates the necessity of using the arbitrary ratio of 2/3 to

TABLE 11.2

Penetrometer Type	Failure Criteria	Soil Type	Full-Scale Piles			N	$\mu$	Model Piles	$\sigma_D$	FS
			N	$\mu$	$\sigma_D$					
Electrical	Ultimate	A11				(1.52)*		65	6.5	18.6
		Clay				14		17.1	12.8	2.10
		Sand				51		4.5	20.0	2.06
Mechanical	Yield	Sand				(1.46)*		51	2.9	20.6
	Ultimate	A11	17	-10.7	18.6	1.83				1.37
		Sand						51	8.5	34.4
	Yield	Sand	10	7.8	37.2	1.76		52	8.7	33.9
										1.64

NOTE:  $\mu$  &  $\sigma_D$  were determined from prediction error percentages  
 $N$  = No of tests analyzed

\* Computed from mechanical cone FS's using  $(FS)_{elect} \approx \frac{(FS)_{mech}}{1.2}$

determine maximum permissible working load from the estimated ultimate capacity; however, the yield capacity method is only applicable to piles in sands and should be used with caution in very loose sands.

TABLE 11.3  
RECOMMENDED SAFETY FACTORS FOR  
CPT PILE CAPACITY DESIGN

Penetrometer Type	Failure Criterion	Safety Factor Range
Electrical	Ultimate	1.75 to 2.25
	Yield	1.40 to 1.75
Mechanical	Ultimate	2.00 to 3.00
	Yield	1.75 to 2.25

#### 11.6 Limitations and Precautions

The design procedures presented in this chapter were developed from an extensive study relating the measured capacity of model and full-scale piles driven in sands and moderately sensitive clays to CPT data obtained using the Begemann mechanical friction sleeve penetrometer and the Fugro electrical friction sleeve penetrometer. The methods should be used with caution, or not used at all, when dealing with soils of a different type or when other kinds of penetrometers are used to obtain soils data.

The sand design procedures were developed mainly on the basis of pile and CPT tests in which fully drained conditions existed. Drained conditions will normally control pile behavior but may not be met during CPT testing in sands below the water table because of the relatively

fast rate of penetration normally used. Pile capacity predictions made using CPT data could, therefore, be either conservative or unconservative, depending on whether positive or negative pore pressures developed during CPT testing. When it is suspected that pore pressures are affecting CPT results, particularly in loose or very dense fine sands, the normal penetration rate should be decreased as recommended by Schmertmann (1974c) to obtain data on the magnitude of pore pressure effects. If the effects are found to be significant, the CPT data from sands should be adjusted according to the values estimated for zero excess pore pressure before being used for pile capacity predictions.

CHAPTER 12  
CONCLUSIONS AND RECOMMENDATIONS

12.1 Conclusions

This research resulted in a number of significant conclusions, both with respect to the use of CPT data for predicting pile capacity and to the performance of different types of penetrometers. These conclusions are as follows:

12.1.1 Penetrometer Performance

1. The Fugro electrical friction sleeve penetrometer provides data which are easier to interpret than does the Begemann mechanical friction sleeve penetrometer. This is primarily a result of the differences in design and operation of the penetrometer.
2. The tapered mantle attached to the mechanical penetrometer tip can affect measured  $q_c$  values in two ways. Soil which squeezes back around the mantle will exert a friction force on the tip, which causes measured  $q_c$  values to be higher than the true values. The reduced diameter of the tip mantle also causes a stress release just above the cone tip, which should cause measured  $q_c$  values to be lower than the true values. In some soils, the opposite effects caused by the tip mantle will approximately cancel each other, but in many soils, one of the effects becomes predominant and can

result in misleading  $q_c$  data. Based on currently available data, it appears that mantle friction is predominant in clays and very loose sands and the stress release effect controls in very dense sands. The effects are probably not highly significant in loose to dense sands.

3. End resistance on the beveled bearing area at the bottom of the mechanical penetrometer friction sleeve has a significant effect on sleeve friction resistance measurements in sand. Comparisons of the Beville site electrical and mechanical friction sleeve data, from medium dense sands above the groundwater table, indicate that end bearing accounts for about 50% of the measured mechanical penetrometer sleeve resistance.
4. Based on the Paines Prairie penetrometer data, end bearing on the mechanical penetrometer friction sleeve is not significant in soft to medium clays. However, the effect may be significant in stiff clays. Mechanical cone  $f_s$  values in the stiffer Paines Prairie clay was about 12% higher than electrical cone  $f_s$  values.

#### 12.1.2 Use of CPT Data to Estimate the Load Capacity of Driven Displacement Piles

1. Accurate pile capacity predictions can be made from either electrical or mechanical CPT data provided the data are carefully obtained, evaluated, and when necessary, corrected in accordance with the recommendations in Chapter 11.
2. Data obtained using the Fugro electrical penetrometer permit more accurate pile capacity predictions because the shape of

this penetrometer is a better pile model and provides more interpretable data.

3. The Begemann procedure for estimating pile tip bearing capacity, as illustrated in Fig 11.1, provides reasonably accurate predictions for piles bearing in sands. The model pile test results indicate that this method also provides accurate predictions for piles bearing in clay; however, a sufficient amount of full-scale pile load test data in clays were not obtained to fully verify this conclusion.
4. Mechanical penetrometer  $q_c$  values in clay should be reduced to about 60% of the measured values before being used to estimate pile end bearing capacity to account for possible friction on the tip mantle.
5. Side friction on piles in sand can be estimated with a reasonable degree of accuracy by using the penetrometer to pile friction ratios presented in Fig 11.2 and by making a simple depth of embedment correction at the ground surface only.
6. The ratio of penetrometer to pile friction in sand is larger for short piles ( $L/B < 20$ ) than for long piles.
7. The undrained friction approach of multiplying undrained shear strength by an empirically determined factor to estimate pile-soil friction provided the most accurate predictions of side friction on model piles driven in clay. Not enough data were available in clay to verify this conclusion for full-scale piles.
8. Unit sleeve friction appears to be a better measure of

undrained shear strength than  $q_c$  data for estimating pile friction. This conclusion is mainly based on the Paines Prairie penetrometer data which showed that penetrometer type had little effect on  $f_s$  in soft to medium clays, while  $q_c$  was highly dependent on the type of penetrometer used.

9. Unit sleeve friction resistance was approximately equal to undrained shear strength determined from undrained tri-axial compression tests for the Paines Prairie clay, but only about one half of the vane shear strength.
10. Normally used  $q_c/s_u$  ratios of 10 and 16 for the electrical and mechanical penetrometers were approximately equal to the measured ratios for the Paines Prairie clay when field vane  $s_u$  data were considered. However, use of these ratios would have considerably overestimated the laboratory determined undrained strength.
11. Future efforts to improve methods for predicting pile friction in clay should be directed toward the drained friction approach because the behavior of actual foundation piles is controlled by drained, rather than undrained, friction. Schmertmann's suggested procedure for estimating the final effective radial stress on a pile driven in clay, used herein for the first time, may provide the key to accurate drained friction predictions if procedures for estimating the necessary soil properties from CPT data can be adequately refined.
12. Reasonably accurate predictions of step-tapered pile

capacity can be made from CPT data by considering the total capacity, to be made up of three independent components computed as follows:

- a. End bearing resistance computed using the Begemann  $q_c$  averaging procedure for constant section piles.
  - b. Shaft friction computed by considering each constant diameter section as an equivalent part of a constant section pile.
  - c. Shaft bearing computed by multiplying the horizontal bearing area at each diameter step by the average  $q_c$  value in the vicinity of the step and an appropriate ratio of  $q_c$  to unit step bearing resistance.
13. The step-taper pile capacity prediction procedure can be used to estimate the capacity of continuously tapered piles by approximating the actual pile section with an 'equivalent' step-taper pile, as described in Chapter 11.
  14. Unit step bearing on the shaft of tapered piles is approximately 1.5 to 2.0  $q_c$  in sands and approximately equal to  $q_c$  in clays. A  $q_s/q_c$  value of 1.6 is recommended for sands, although it is realized that this value may be slightly conservative.
  15. The procedures developed during this study for estimating pile capacity in sands and clays can easily be used with soil profiles consisting of alternating sand and clay layers and is, therefore, applicable to a wide variety of geologic conditions.
  16. The CPT pile capacity design methods offer several

advantages over other currently available static analysis procedures. The more important advantages are:

- a. Pile capacities estimated from CPT are based on a large number of soil property measurements, since CPT tests are usually performed continuously or at 20 cm intervals. Pile capacity estimates made using other analysis methods are usually based on a limited number of strength tests. Because of the much larger number of tests on which the CPT predictions are based, the possibility of using nonrepresentative data is much less with this method.
- b. The CPT methods are based on in situ tests and are, therefore, not affected by the problems associated with obtaining and testing 'undisturbed' samples.
- c. The CPT methods eliminate the problem of choosing values for the bearing capacity factors required in a 'Terzaghi type' end bearing capacity analysis. These factors, whatever they may be, are automatically incorporated in the  $q_c$  data.
- d. CPT investigation is usually less expensive than conventional boring, sampling and laboratory testing investigations; therefore, a CPT design can be performed more economically, or more field investigation can be performed at the same cost. In the latter case, a better design would be possible as a result of increased knowledge of soil conditions.
- e. CPT design methods are believed to provide more

accurate pile capacity predictions in sands and predictions in clays which are comparable in accuracy to predictions obtained using other static analysis methods.

17. The main limitation to the CPT design methods is that some soils cannot be penetrated by commonly available cone penetration equipment. This problem is being overcome as equipment with higher thrust capabilities becomes available and by the development of wireline penetrometers which are used in conjunction with conventional drilling equipment.
18. Another possible limitation to using CPT data to estimate pile capacity, particularly in cohesive soils, is rate effects, which can include soil viscosity, long-term creep, progressive failure, and pore pressure behavior. Some of these factors have been discussed in this report; however, not enough is known about the rate effect at the present time to deal with it rationally.
19. The CPT design methods offer several advantages over dynamic pile capacity prediction methods. The more important of these are:
  - a. The accuracy and dependability of CPT predictions are much better than those provided by normally used dynamic equations such as the ENR and Hiley formulae.
  - b. The CPT methods are much simpler and easier to apply than the dynamic wave equation theory and are believed to provide comparable accuracy.

- c. The CPT methods can be used to evaluate pile capacities and design alternatives during the design stages of a project, while dynamic methods cannot be applied until some piles are driven.
- 20. Undrained shear strength analyses using Tomlinson's recommended  $\alpha$  values and  $f_s-s_u$  correlations provided the most accurate predictions of frictional capacity of model piles driven in clay.
- 21. Use of the Vijayvergiya and Focht (1972)  $\lambda$  method resulted in large overpredictions of friction on model piles in clay. Replotting the  $\lambda$  curve in terms of relative pile penetration and using the revised  $\lambda'$  curve significantly improved the predictions. It appears that this method may provide reasonable predictions for long piles ( $L/B>30$ ) but may not be applicable to short piles in stiff clay.
- 22. The recommended method for predicting pile friction in cohesive soils is not applicable to very sensitive clays and additional research is needed to define the limits of applicability of the method.
- 23. The recommended method for predicting pile friction in clays appears to be slightly unconservative when predictions from this method are compared to the measured friction capacity of model piles in clay. However, time effect tests performed on these model piles show that actual friction capacity increases with time. The predictions are more accurate and more conservative when compared to the long-term friction resistance measurements.

24. The pile point angle did not appear to significantly affect the friction capacity of compression piles driven in sands. This is in contrast with Begemann's findings concerning frictional resistance of tension piles in sands. Additional research on this effect would be valuable since the tests conducted during this research were not designed to study the tip angle effect and may not reflect the true magnitude of this effect.
25. Increasing pile surface roughness can significantly increase the frictional capacity of piles driven in both sands and clays.
26. Pile section shape appeared to have a significant effect on the frictional capacity of piles driven in sands. Unit friction on round sections appears to be considerably higher than that on square sections for piles with the same surface roughness.
27. Statistical analyses of the model and full-scale piles indicate that carefully gathered and evaluated CPT data will permit use of pile design safety factors of approximately 2.0 for electrical penetrometer data and 2.5 for mechanical penetrometer data.
28. Statistical analyses of the model pile prediction errors indicate that ultimate tip bearing and side friction capacity estimates were made with approximately equal accuracy; therefore, the results of this research do not justify using higher safety factors for pile side friction.

## 12.2 Significant Contributions of the Research

In the author's opinion, the significant contributions of this research project are as follows:

1. Development of a method for predicting side friction on driven constant section piles in sands from electrical or mechanical CPT friction sleeve data. The method can also be used when only  $q_c$  data are available, but with a lesser degree of confidence.
2. Development of a method for predicting side friction on driven constant section piles in clays from electrical or mechanical CPT friction sleeve data. This method can also be used with  $q_c$  data.
3. Development of a method for predicting shaft resistance for step-taper piles in both sands and clays from either electrical or mechanical CPT data.
4. Extension of the step-taper pile CPT design method for use with continuously tapered piles.
5. Generalization of the CPT design methods for sands and clays to permit predicting capacities of piles driven in layered soils.
6. Providing evidence that the Begemann method for estimating pile tip capacity in sands from CPT data is also valid for clays.
7. Demonstrating that use of undrained shear strength values for clays determined from 'typical'  $q_c/s_u$  ratios can result in large overestimates of pile capacity in some soils. It is recommended that  $s_u$  values determined in

this manner be corrected using Bjerrum's field vane shear strength reduction graph.

8. First application of a new method proposed by Schmertmann (1973) for estimating pile friction in clays in terms of effective stress. Although this method did not result in better predictions than methods based on undrained shear strength, the method is fundamentally more correct and should provide better predictions when improved correlations between CPT and pressuremeter data are developed.
9. Providing data on the comparative performance of the Begemann mechanical and Fugro electrical friction sleeve penetrometers. It is shown that the penetrometer design and method of operation can significantly affect measured  $q_c$  and  $f_s$  values and that the magnitude and direction of the effect is dependent on the type and condition of the soil being tested.
10. Demonstrating the validity of using the Begemann procedure for estimating pile tip capacity in sands from CPT data for a variety of pile sizes, shapes, and soil conditions.
11. Demonstrating that the Osterberg method for determining the yield capacity of plates bearing on sand can also be applied to piles driven in sand. The yield capacity concept provides a rational method of determining the maximum permissible working load on piles.

To the author's knowledge, Items 1 through 7 represent original contributions. Items 8 through 11, while not original, are significant contributions because they add to the understanding of pile and

penetrometer performance and permit CPT data interpretations and pile design studies to be performed with a greater degree of confidence.

### 12.3 Recommendations for Additional Research

In addition to improving our ability to make pile capacity predictions from CPT data, this research also indicated several areas in which additional research could significantly improve this ability.

The areas of needed research are:

1. Additional correlations between electrical and mechanical friction sleeve resistance in clays. Data from the Paines Prairie clay indicate that  $f_s$  is approximately independent of the penetrometer type. Determining the range of types and strengths of clays for which this is true would increase the usefulness of data from different types of penetrometers.
2. Additional correlations between  $f_s$  and  $s_u$  data in clays. The Paines Prairie correlations show that  $f_s$  measurements provide a good approximation of  $s_u$  for moderately sensitive clays and are, therefore, very useful in estimating pile friction. Additional correlations of this type will minimize the need for calibrating  $f_s$  data with respect to  $s_u$  measurements at each new site.
3. Studies on the long-term load carrying capability of tapered piles in clay. Analysis based on undrained shear strength and short-term load tests indicate that tapered piles do not offer any significant advantages over constant section piles in clay. However, reloading tests performed during this research indicate that the capacity of tapered

piles in clay will probably increase dramatically if the pile is subjected to long-term loads. This is thought to be the result of an increase in the effective stresses around the pile caused by the wedge action of tapered piles. Research is needed to provide data on the amount of load capacity increase which can be expected and the magnitude of settlement required to mobilize the increased capacity.

4. Studies to determine the effect of sliding strain on unit pile friction. The ability to predict both total side friction and friction distribution could be improved if the friction reduction effect discussed in Chapter 7 could be properly modeled. Tests on fully instrumented piles will be required to evaluate this effect.
5. Studies to improve our ability to estimate the soil parameters needed for an effective stress analysis of pile friction in clays. The effective stress approach is a significant improvement over the currently used undrained shear strength methods, but cannot be easily applied at this time because of our inability to correctly predict the controlling soil properties.
6. Studies to define unit pile friction behavior near an interface between a weak and strong soil layer. Unit friction reductions that may occur in this situation were neglected during development of the design methods presented in Chapter 10, apparently without causing serious capacity prediction errors. However, including these effects, if they do occur, should improve the predictions.

## LIST OF REFERENCES

- Airhart, T.P., Hirsch, T.J., and Coyle, H.M. (1967), "Pile-Soil System Response as a Function of Excess Pore Water Pressure and Other Soil Properties," Research Report 33-8, Study 2-5-62-33.
- Al-Awkat, Z. (1974), Personal correspondence with J. H. Schmertmann.
- American Society for Testing and Materials (1974), "Tentative Standard Method for Deep Quasi-Static Cone Penetration Test," In Committee D-18.06.02.
- Banerjee, P.K. (1970), Discussion, Proceedings of the Conference on Behavior of Piles, Institution of Civil Engineers, London, p. 207.
- Begemann, H.K.S. Ph. (1953), "Improved Method of Determining Resistance to Adhesion by Sounding Through a Loose Sleeve Placed Behind the Cone," Proceedings of the 3rd International Conference on Soil Mechanics and Foundation Engineering, Zurich, Vol. 1, p. 213.
- Begemann, H.K.S. Ph. (1963), "The Use of the Static Penetrometer in Holland," New Zealand Engineering, Vol. 18(2), p. 41.
- Begemann, H.K.S. Ph. (1965), "The Maximum Pulling Force on a Single Tension Pile Calculated on the Basis of Results of the Adhesion Jacket Cone," Proceedings of the 6th International Conference on Soil Mechanics and Foundation Engineering, Montreal, Vol. 2, p. 229.
- Begemann, H.K.S. Ph. (1969a), "The Dutch Static Penetration Test with the Adhesion Jacket Cone," Lab. Voor Grondmechanica, Delft, Medad., XII, No. 4, p. 69.
- Begemann, H.K.S. Ph. (1969b), "The Dutch Static Penetration Test with the Adhesion Jacket Cone," Lab. Voor Grondmechanica, Delft, Medad., XIII, No. 1, p. 1.
- Begemann, H.K.S. Ph. (1973), "Alternating Loading and Pulling Tests on Steel I-Beam Piles," Proceedings of the 8th International Conference on Soil Mechanics and Foundation Engineering, Moscow, Vol. 2, p. 13.
- Bjerrum, L. (1972), "Embankments on Soft Ground," Proceedings of the Specialty Conference on Performance of Earth and Earth-Supported Structures, ASCE, Purdue University, Vol. 2, p. 1.

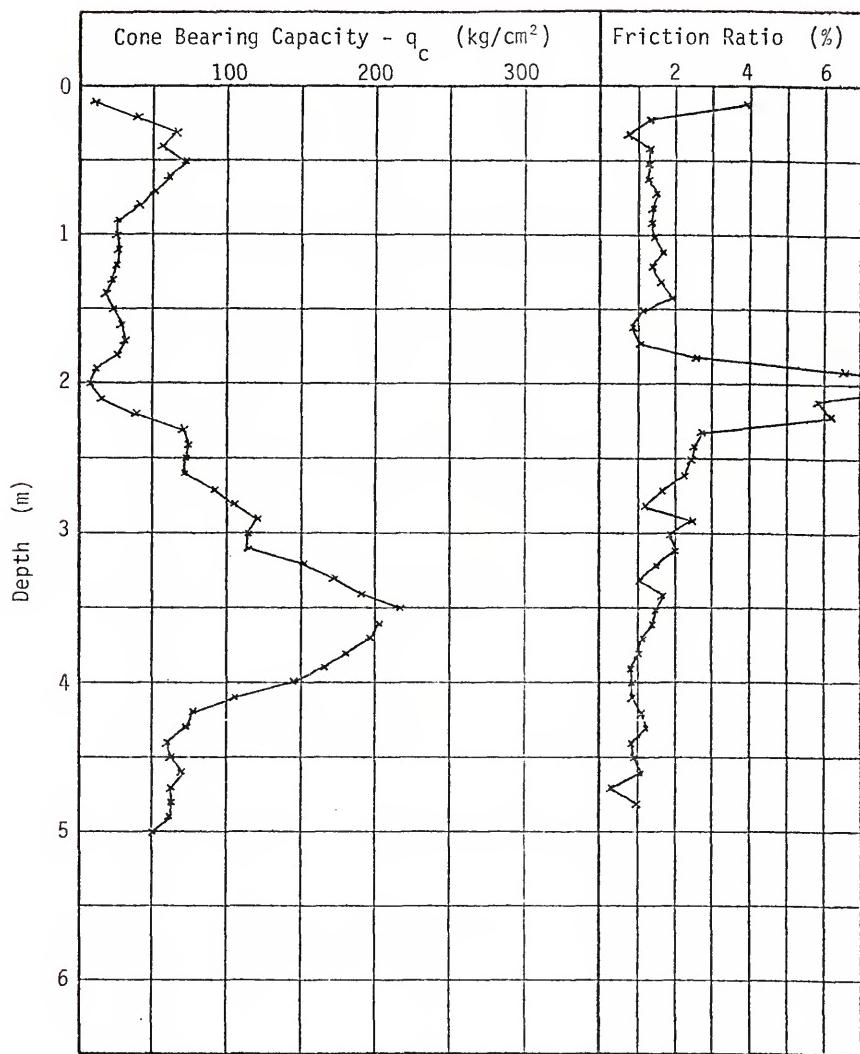
- Bogdanovic, L. (1961), "The Use of Penetration Tests for Determining the Bearing Capacity of Piles," Proceedings of the 5th International Conference on Soil Mechanics and Foundation Engineering, Paris, Vol. 2, p. 17.
- Bozozuk, M. (1972), "Downdrag Measurements on a 160-ft. Floating Pipe Test Pile in Marine Clay," Canadian Geotechnical Journal, Vol. 9, No. 2, p. 127.
- Burland, J. (1973), "Shaft Friction of Piles in Clay--A Simple Fundamental Approach," Ground Engineering, Vol. 6, No. 3, p. 30.
- Chellis, R.D. (1951), Pile Foundations, 1st Edition, McGraw-Hill Book Company, Inc., New York, N.Y.
- Clark, J.I. and Meyerhoff, G.G. (1972), "The Behavior of Piles Driven in Clay. I. An Investigation of Soil Stress and Pore Water Pressure as Related to Soil Properties," Canadian Geotechnical Journal, Vol. 9, p. 351.
- Cook, W.J. (1971), "A Field Study of Effect of Compaction and Changes in Lateral Stress on Buried Rigid Plate Load Tests in a Sand," Thesis presented to the University of Florida in partial fulfillment of the requirements for the degree of Master of Science.
- De Beer, E.E. (1963), "The Scale Effect in the Transposition of the Results of Deep Sounding Tests on the Ultimate Bearing Capacity of Piles and Caisson Foundations," Geotechnique, Vol. 8, p. 39.
- De Ruiter, J. (1971), "Electric Penetrometer for Site Investigations," Journal of the Soil Mechanics and Foundations Division, ASCE, Vol. 97, No. SM2, p. 457.
- Driggers, F.J. (1971), "A Field Study of Some Effects of Sand Overconsolidation on Static Cone and Pressuremeter Results," Thesis presented to the University of Florida in partial fulfillment of the requirements for the degree of Master of Science.
- Flatte, K. (1972), "Effects of Pile Driving in Clays," Canadian Geotechnical Journal, Vol. 9, No. 1, p. 81.
- Freed, D.L. (1973), "Prediction of Pile Side Resistance of Smooth and Rough 4-inch Square Concrete Model Piles Driven in Sand Using Static Cone Penetrometer Data," Thesis presented to the University of Florida in partial fulfillment of the requirements for the degree of Master of Science.
- Fuller, F.M. and Hoy, H.E. (1970), "Pile Load Tests Including Quick-Load Test Method, Conventional Methods and Interpretations," Highway Research Record No. 333, Highway Research Board, Washington, D.C., p. 74.

- Hansen, J.B. (1968), "A Theory for Skin Friction on Piles," Bulletin No. 25, Danish Geotechnical Institute.
- Heijnen, W.J. (1974), "Penetration Testing in Netherland," Proceedings of the European Symposium on Penetration Testing, Stockholm, Vol. 1, p. 79.
- Huizinga, T.K. (1951), "Application of Results of Deep Penetration Tests to Foundation Piles," Building Research Congress, London, Div. 1, Part 3, p. 173.
- Kerisel, J. (1961), "Foundations profondes en milieux sableux: variation de la force portante limite en fonction de la densite, de la profondeur, du diametre et de la vitesse d'enforcement," Proceedings of the 5th International Conference on Soil Mechanics and Foundation Engineering, Paris, Vol. 2, p. 73.
- Kerisel, J. (1964), "Deep Foundations Basic Experimental Facts," Proceedings of Conference on Deep Foundations, Mexico City, Vol. 1, p. 7.
- Ladanyi, B. (1967), "Deep Punching of Sensitive Clays," Proceedings of the 3rd Pan American Conference on Soil Mechanics and Foundation Engineering, Caracas, Vol. 1, p. 533.
- Lambe, T.W. and Whitman, R.V. (1969), Soil Mechanics, John Wiley & Sons, Inc., New York, N.Y.
- Leonards, G.A. (ed.) (1962), Foundation Engineering, McGraw-Hill Book Company, Inc., New York, N.Y.
- Lingo, E.W. (1962), "A Study of Friction and the Variations in 'Wall' Friction of Cohesionless Soils as Affected by Certain Physical Properties," Thesis presented to the University of Florida in partial fulfillment of the requirements for the degree of Master of Science.
- McClelland, B. (1964), "Design of Deep Penetration Piles for Ocean Structures," Journal of the Geotechnical Engineering Division, ASCE, Vol. 100, No. 677, p. 709.
- Menzenback, E. (1961), "The Determination of Permissible Point Loads of Piles by Means of Static Penetration Tests," Proceedings of the 5th International Conference on Soil Mechanics and Foundation Engineering, Paris, Vol. 2, p. 99.
- Meyerhoff, G.G. (1951), "The Ultimate Bearing Capacity of Foundations," Geotechnique, Vol. 2, No. 4, p. 301.
- Meyerhoff, G.G. (1956), "Penetration Tests and Bearing Capacity of Cohesionless Soils," Journal of the Soil Mechanics and Foundations Division, ASCE, Vol. 82, No. SM1, p. 866.

- Mohan, D., Jain, G.S., and Kumar, V. (1963), "Load-Bearing Capacity of Piles," Geotechnique, Vol. 13, No. 1, p. 76.
- Navdocks Design Manual DM-7 (1962), Soil Mechanics, Foundations, and Earth Structures, Chapter 13, Department of the Navy, Washington, D.C.
- Norwegian Geotechnical Institute (1973), "Internal Report on Use of CPT Data to Determine Undrained Shear Strength of Clay," Unpublished.
- Osterberg, J.O. (1947), Discussion, Symposium on Load Tests of Bearing Capacity of Soils, ASTM Special Technical Publication No. 79.
- Perez, L.A. (1974), "Static Penetrometer: The Importance of Skin Friction Associated with the Point Resistance," Proceedings of the European Symposium on Penetration Testing, Vol. 2, In press.
- Peck, R.B. (1958), "A Study of the Comparative Behavior of Friction Piles," Special Report No. 36, Highway Research Board, Washington, D.C.
- Plantema, G. (1948), "Results of a Special Loading Test on a Reinforced Concrete Pile, a So-Called Pile Sounding," Proceedings of the 2nd International Conference on Soil Mechanics and Foundation Engineering, Rotterdam, Vol. 2, p. 112.
- Potyondy, J.G. (1961), "Skin Friction Between Various Soils and Construction Materials," Geotechnique, Vol. 11, No. 4.
- Sanglerat, G. (1972), The Penetrometer and Soil Exploration, American Elsevier Publishing Company, Inc., New York, N.Y.
- Schmertmann, J.H. (1957), Discussion of "Effects of Sample Disturbance on the Shear Strength of a Clay," ASCE Separate Nos 570 and 718.
- Schmertmann, J.H. (1967), "Static Cone Penetrometers for Soil Exploration," Civil Engineering, Vol. 37, No. 6, p. 71.
- Schmertmann, J.H. (1969), "Dutch Friction Cone Penetrometer Exploration of Research Area at Field No. 5, Elgin AFB, Florida," Contract Report No. S-69-4, Waterways Experiment Station, Vicksburg, Miss.
- Schmertmann, J.H. (1972), "Effects of In Situ Lateral Stress on Friction Cone Penetrometer Data in Sands," Fugro Sondeer Symposium, Fugro-Cesco B.V., Leidschendam, The Netherlands, p. 37.
- Schmertmann, J.H. (1973), "Technical Note on Pile Friction in Clay," Prepared for Fugro, Inc., Unpublished.
- Schmertmann, J.H. (1974a), "Penetration Pore Pressure Effects on Quasi-Static Cone Bearing  $q_c$ ," Proceedings of the European Symposium on Penetration Testing, Stockholm, Vol. 2a, In press.

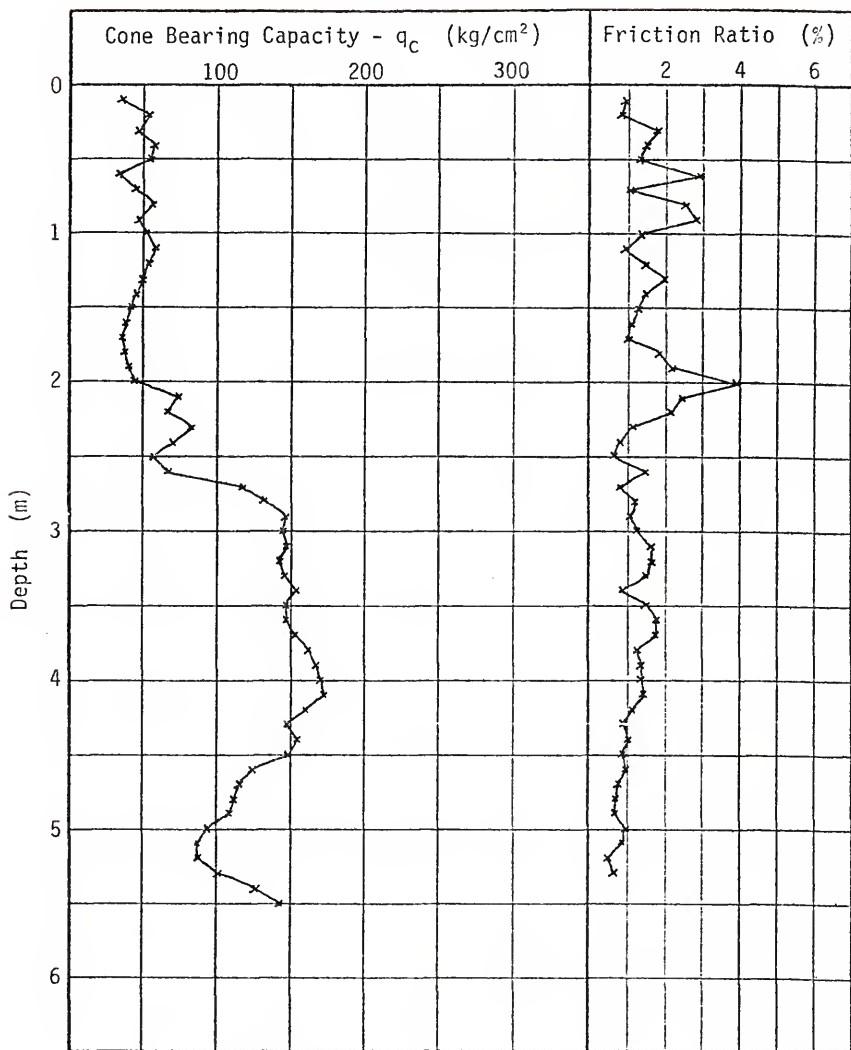
- Schmertmann, J.H. (1974b), Discussion, Proceedings of the European Symposium on Penetration Testing, Stockholm, Vol. 2b, In press.
- Schmertmann, J.H. (1974c), "Guidelines for Design Using CPT Data," Prepared for Fugro-Cesco B.V., Unpublished.
- Tomlinson, M.J. (1957), "The Adhesion of Piles Driven in Clay Soils," Proceedings of the 4th International Conference on Soil Mechanics and Foundation Engineering, London, Vol. 2, p. 66.
- Tomlinson, M.J. (1970), "Some Effects of Pile Driving on Skin Friction," Proceedings of the Conference on Behavior of Piles, Institution of Civil Engineers, London, p. 107.
- Van der Veen, C. and Boersma, L. (1957), "The Bearing Capacity of a Pile Predetermined by a Cone Penetration Test," Proceedings of the 4th International Conference on Soil Mechanics and Foundation Engineering, London, Vol. 2, p. 72.
- Vermeiden, J. (1948), "Improved Sounding Apparatus as Developed in Holland Since 1936," Proceedings of the 2nd International Conference on Soil Mechanics and Foundation Engineering, Rotterdam, Vol. 1, p. 280.
- Vesic, A.S. (1964), "Investigations of Bearing Capacity of Piles in Sand," Proceedings of the Conference on Deep Foundations, Mexico City, Vol. 1, p. 197.
- Vesic, A.S. (1970), "Load Transfer in Pile-Soil Systems," Proceedings of the Conference on Design and Installation of Pile Foundations and Cellular Structures, Lehigh University, Bethlehem, Pa, p. 47.
- Vijayvergiya, V.N. (1971), Discussion, Journal of the Soil Mechanics and Foundations Division, ASCE, Vol. 97, No. SM1, p. 252.
- Vijayvergiya, V.N. and Focht, J.A. (1972), "A New Way to Predict Capacity of Piles in Clays," Proceedings of the 4th Annual Offshore Technology Conference, Houston, Texas, p. 865.
- Woodward, R.J., Lundgren, R., and Boitano, J.D. (1961), "Pile Loading Tests in Stiff Clay," Proceedings of the 5th International Conference on Soil Mechanics and Foundation Engineering, Paris, Vol. 2, p. 177.

APPENDIX A  
FAIRBANKS SITE TEST RESULTS



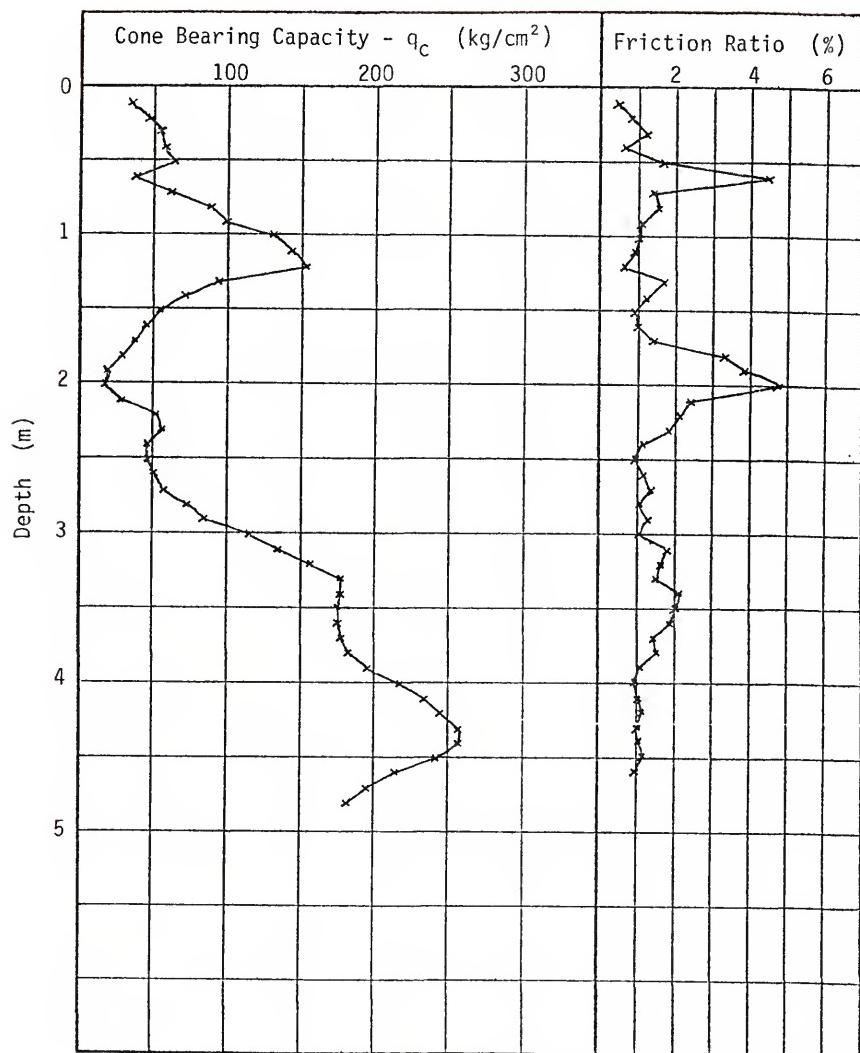
FAIRBANKS TEST NO 1 MECHANICAL CPT SOUNDING LOG

FIGURE A-1



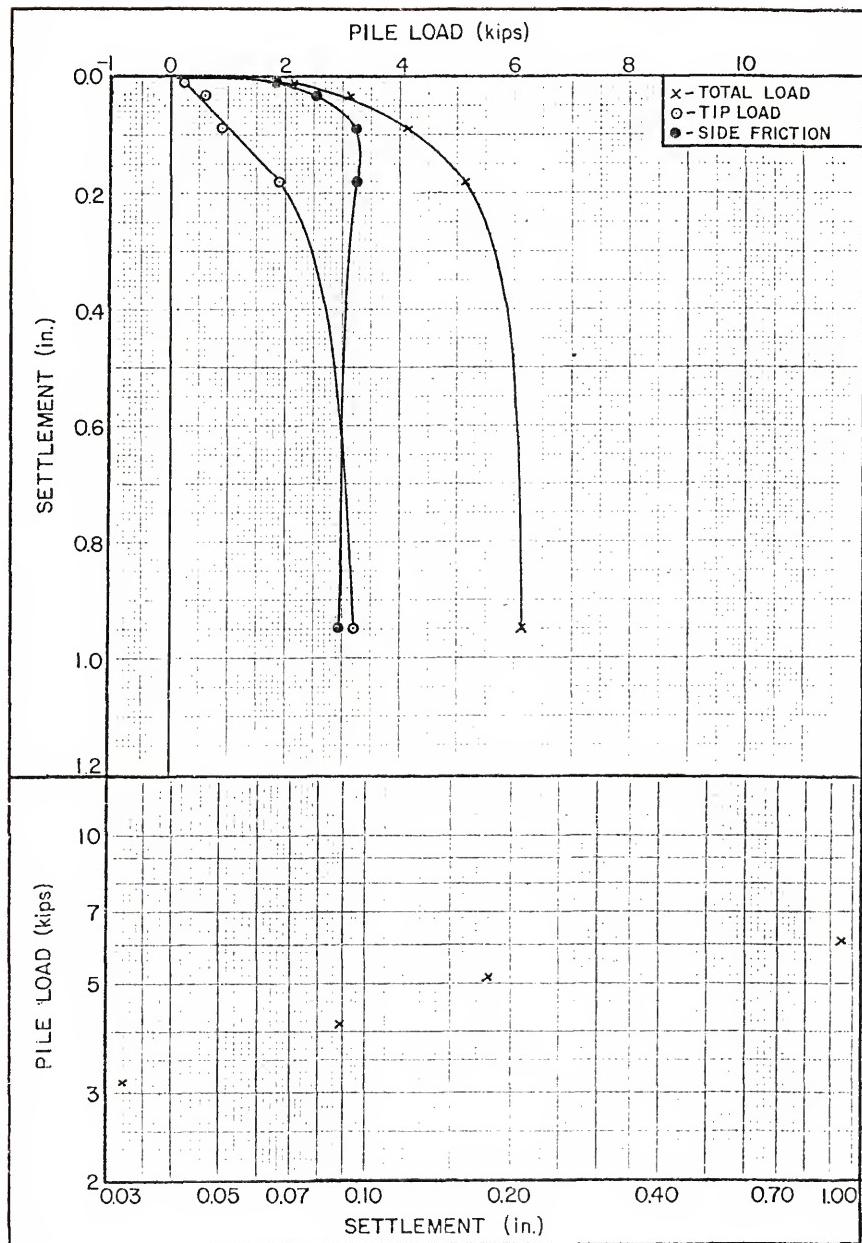
FAIRBANKS TEST NO 2 MECHANICAL CPT SOUNDING LOG

FIGURE A-2

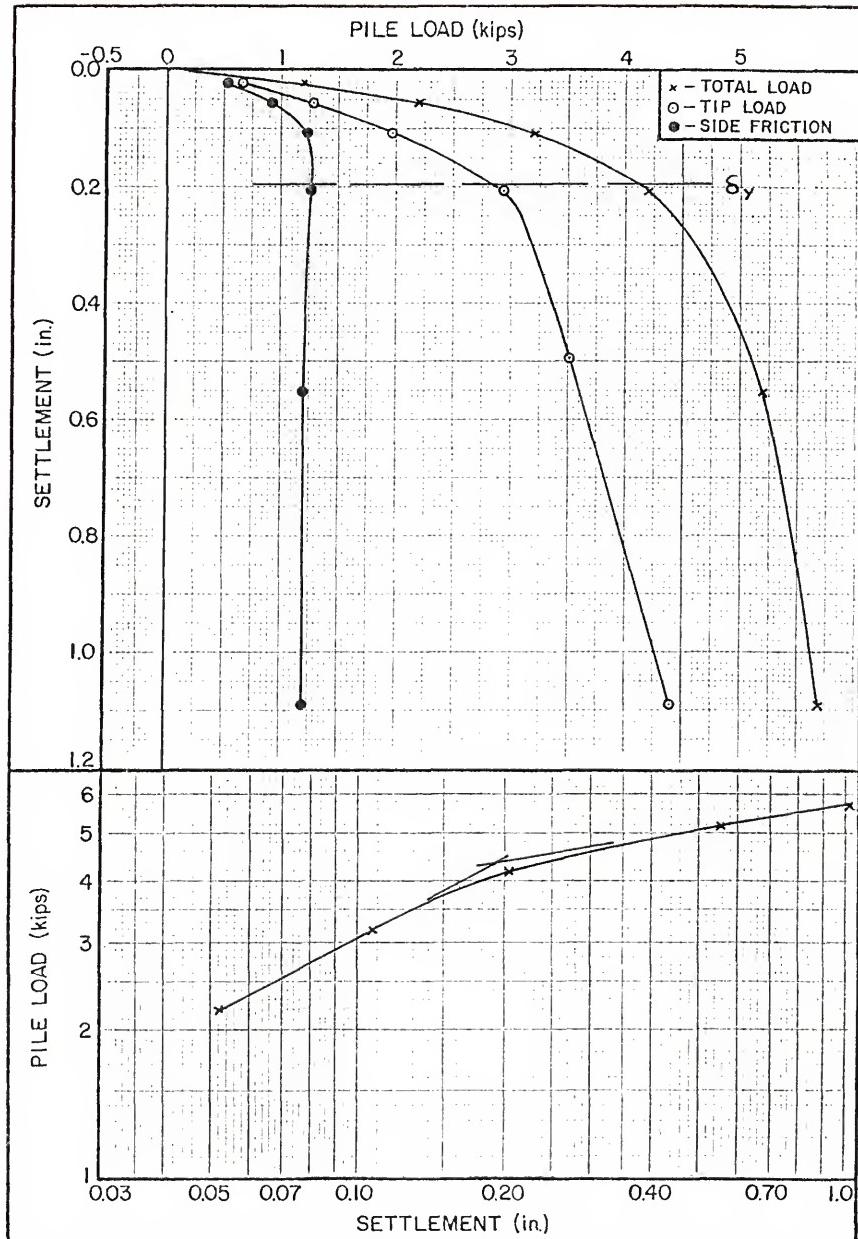


FAIRBANKS TEST NO 1 MECHANICAL CPT SOUNDING LOG

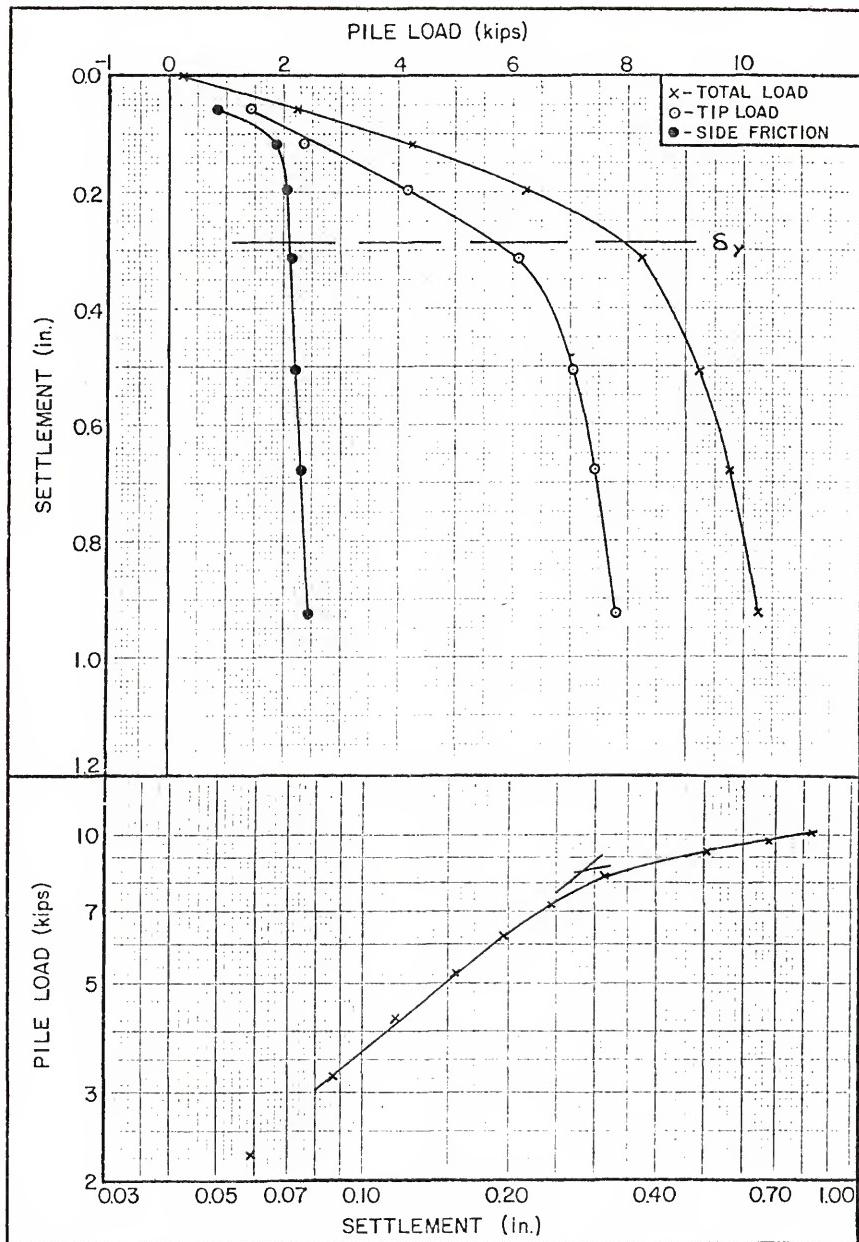
FIGURE A-3



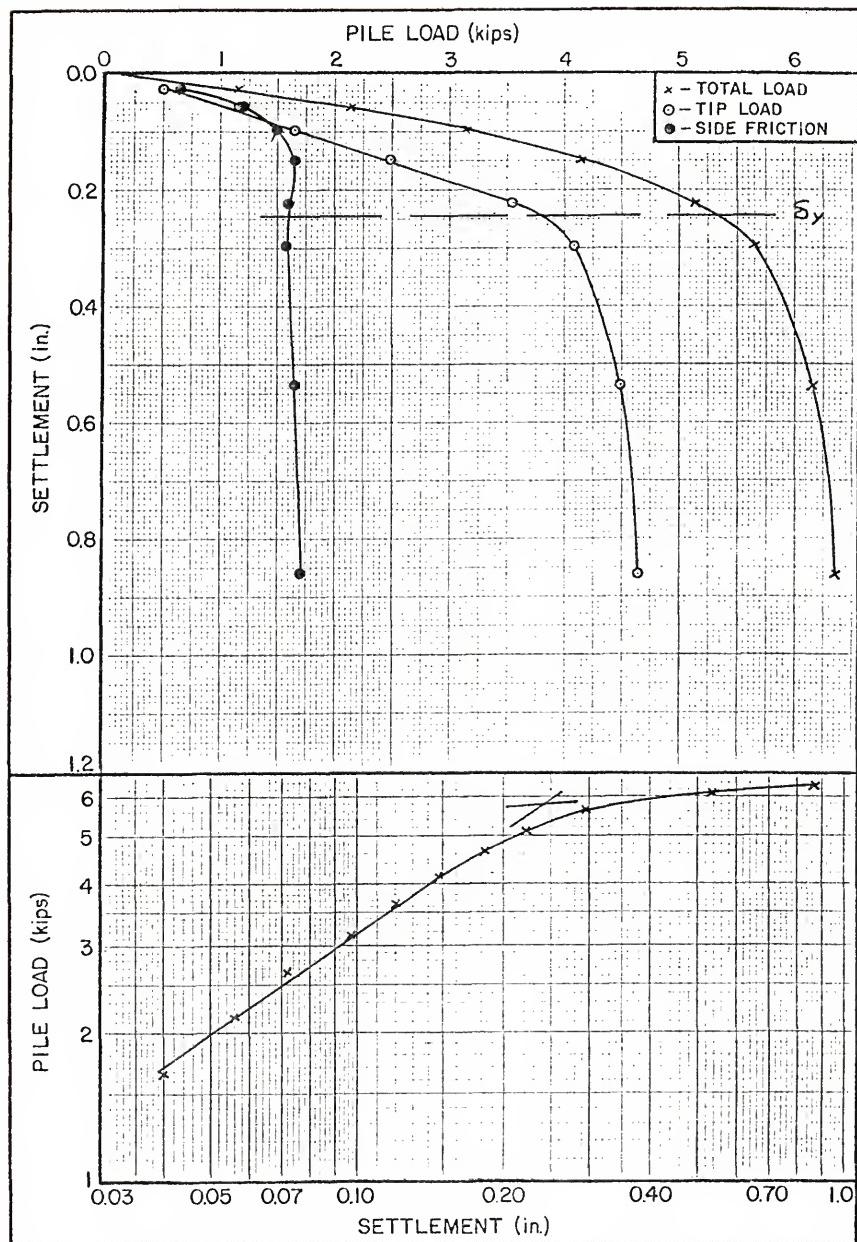
FAIRBANKS PILE LOAD TEST 1-1 RESULTS - 4.0 FT PIPE PILE  
FIGURE A-4



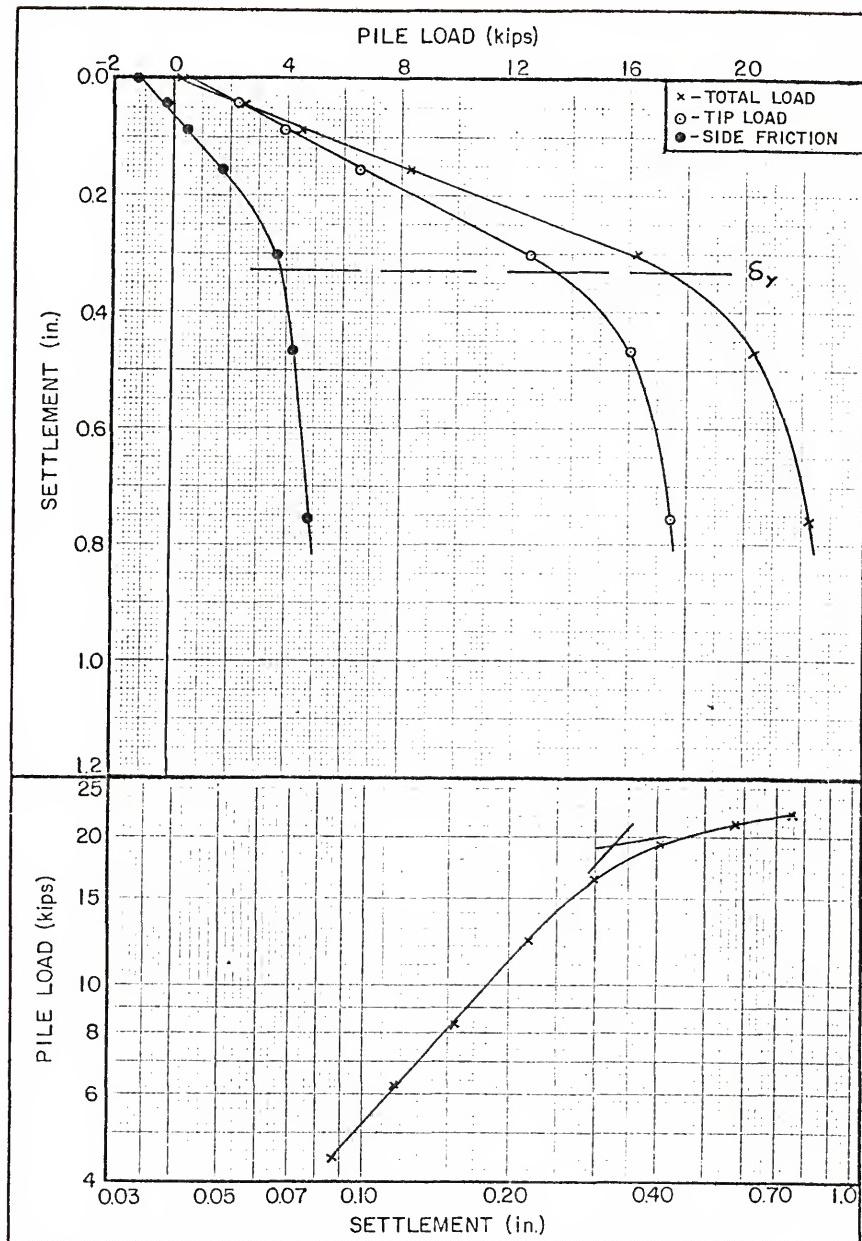
FAIRBANKS PILE LOAD TEST 1-2 RESULTS - 6.5 FT PIPE PILE  
 FIGURE A-5



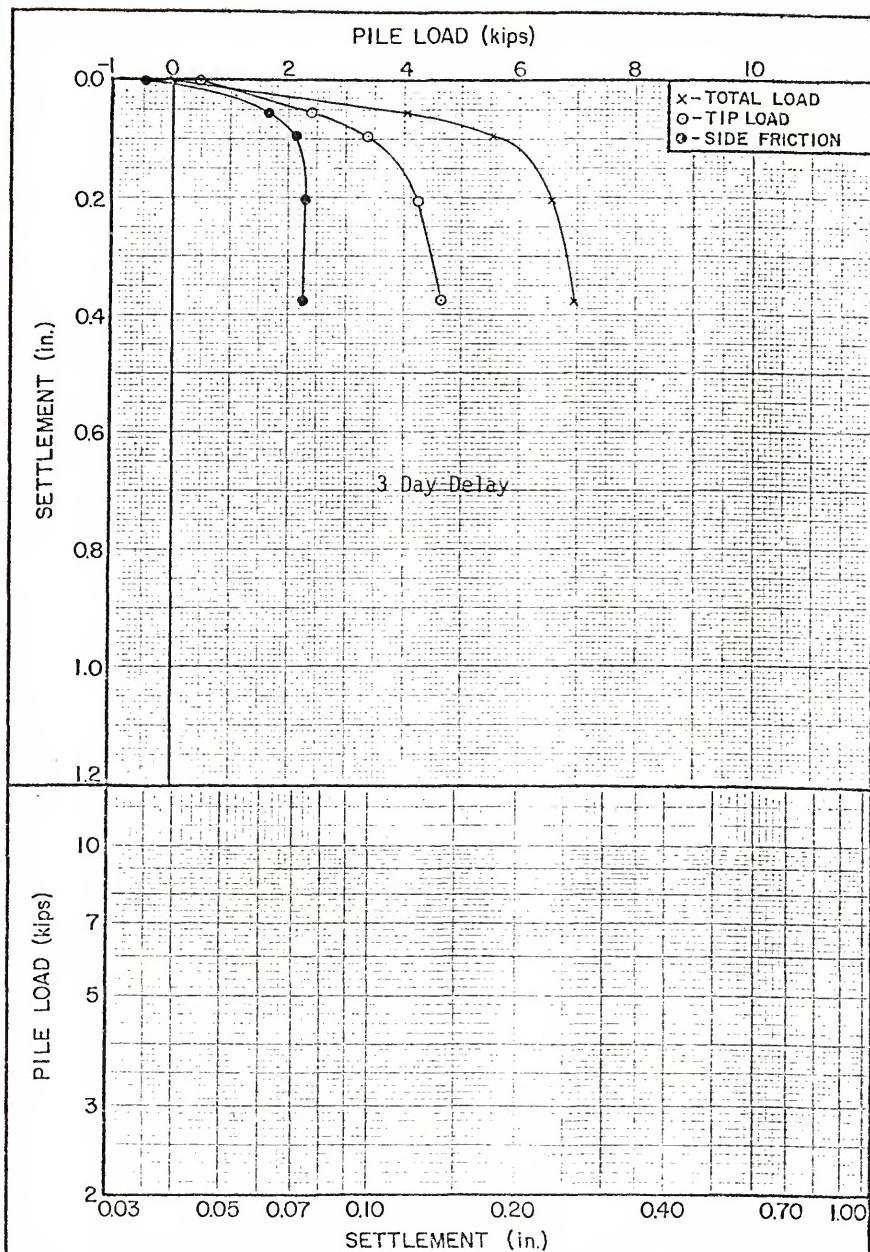
FAIRBANKS PILE LOAD TEST 1-3 RESULTS - 9.0 FT PIPE PILE  
FIGURE A-6



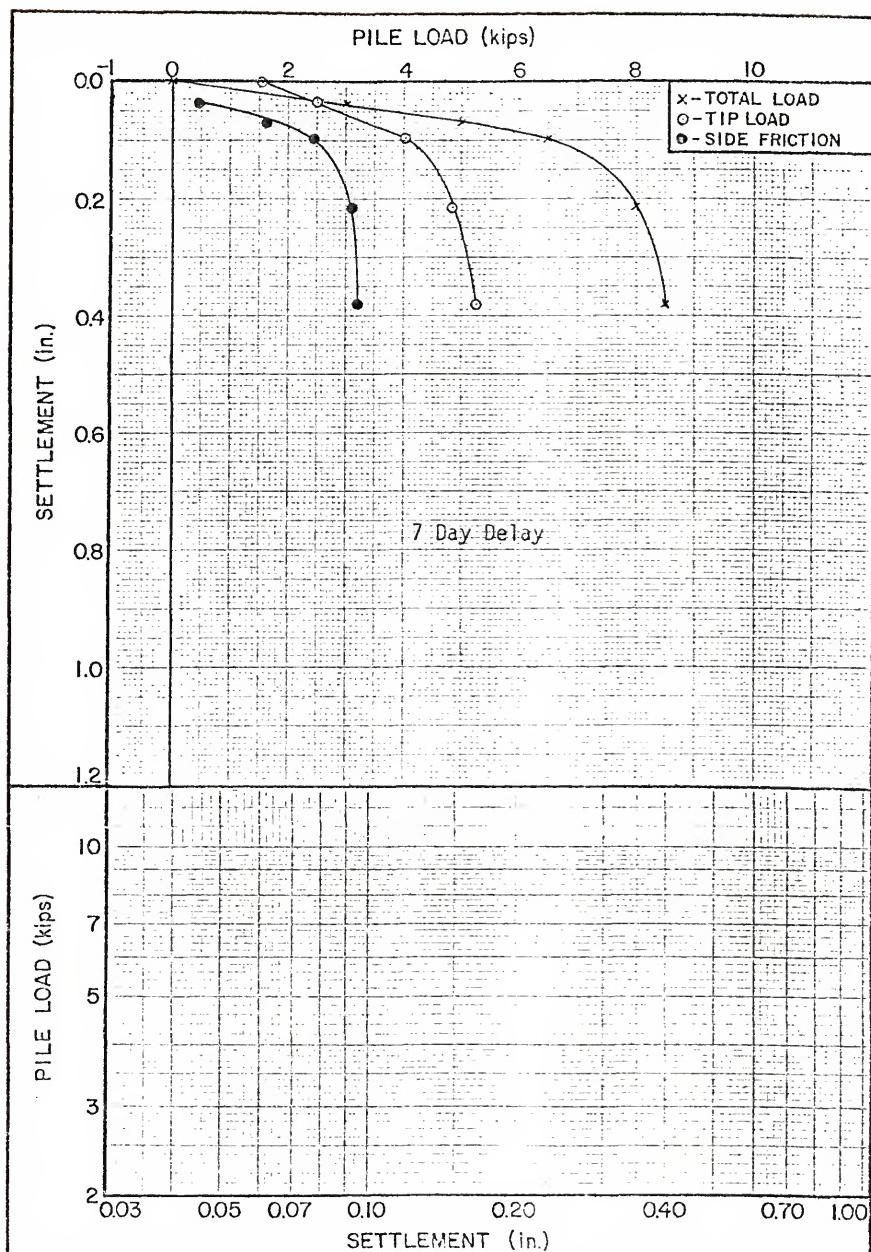
FAIRBANKS PILE LOAD TEST 2-1 RESULTS - 4.5 FT PIPE PILE  
FIGURE A-7



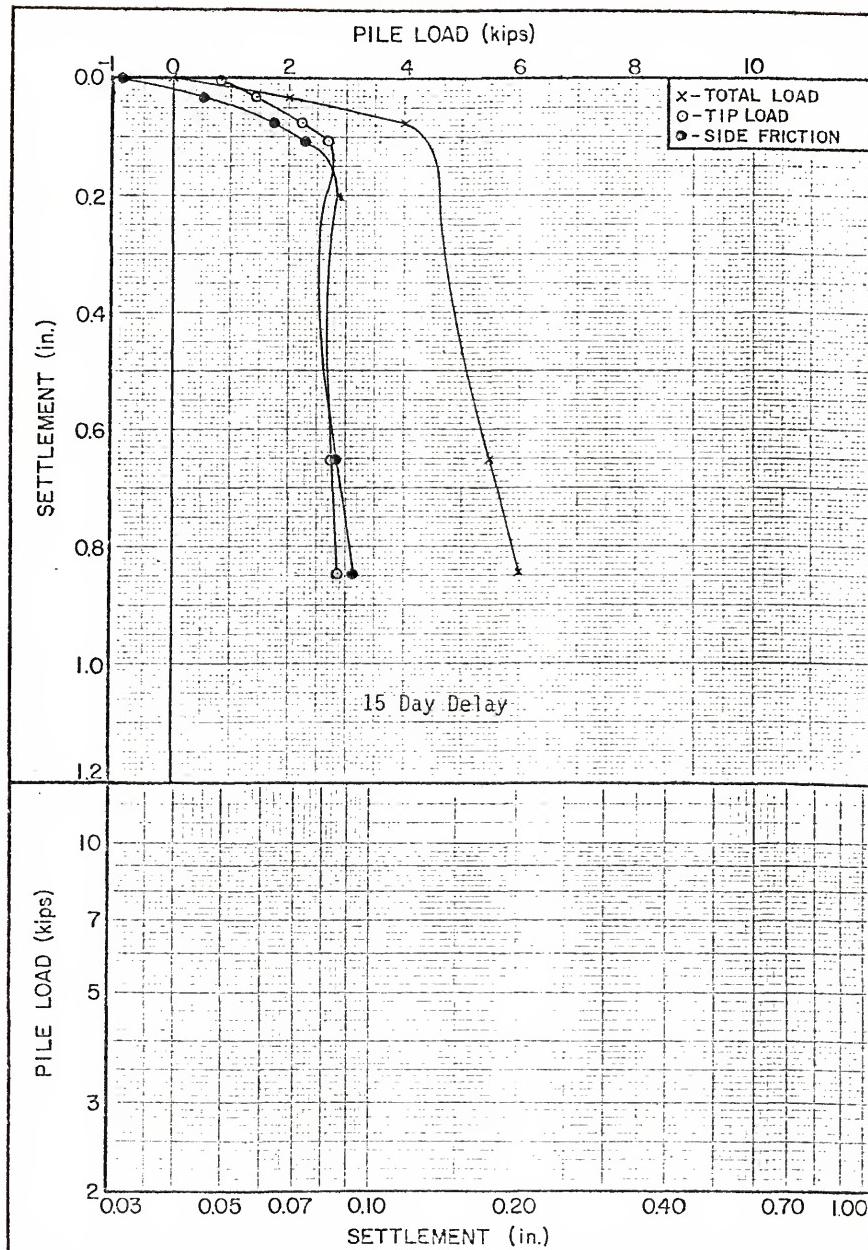
FAIRBANKS PILE LOAD TEST 2-2 RESULTS - 8.9 FT PIPE PILE  
FIGURE A-8



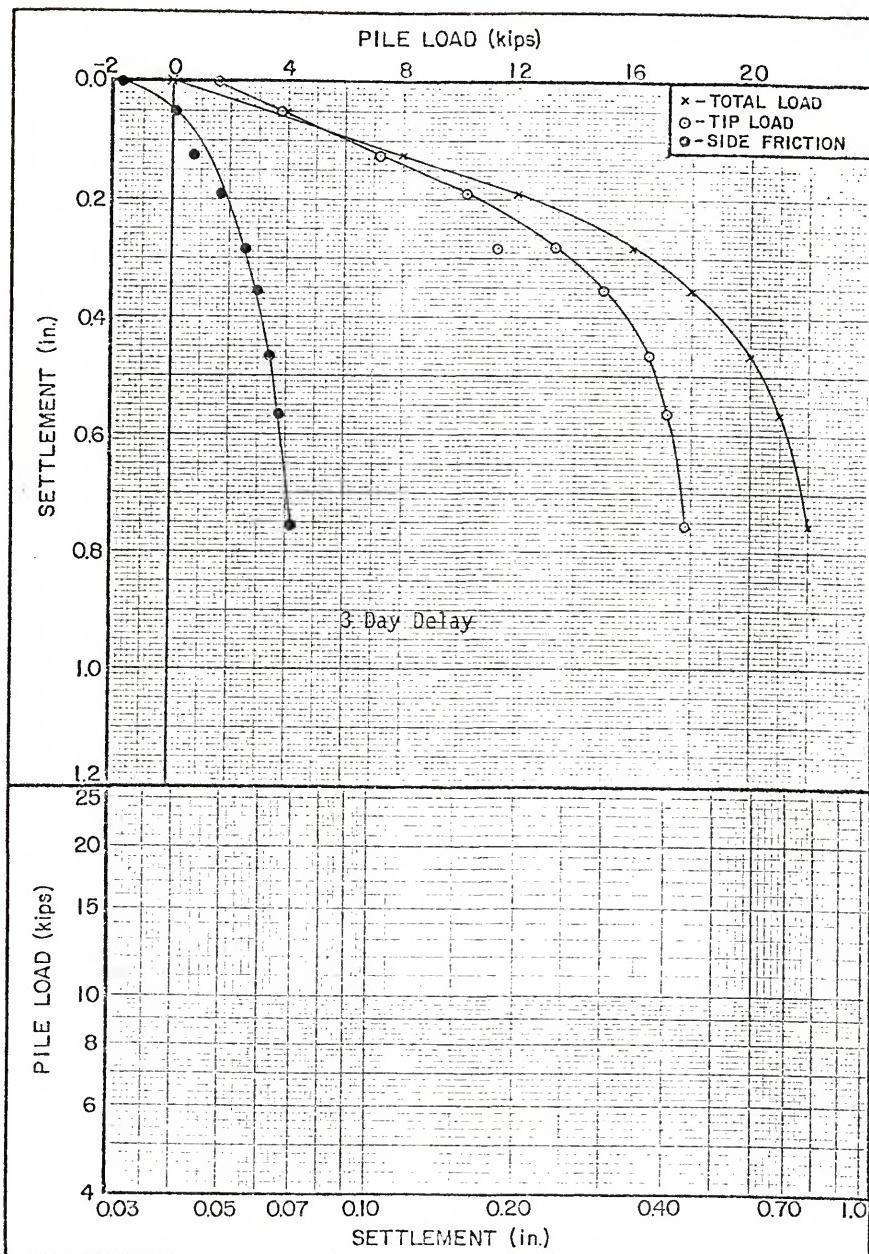
FAIRBANKS PILE LOAD TEST NO 2-1 RESULTS - 4.5 FT PIPE PILE  
FIGURE A-9



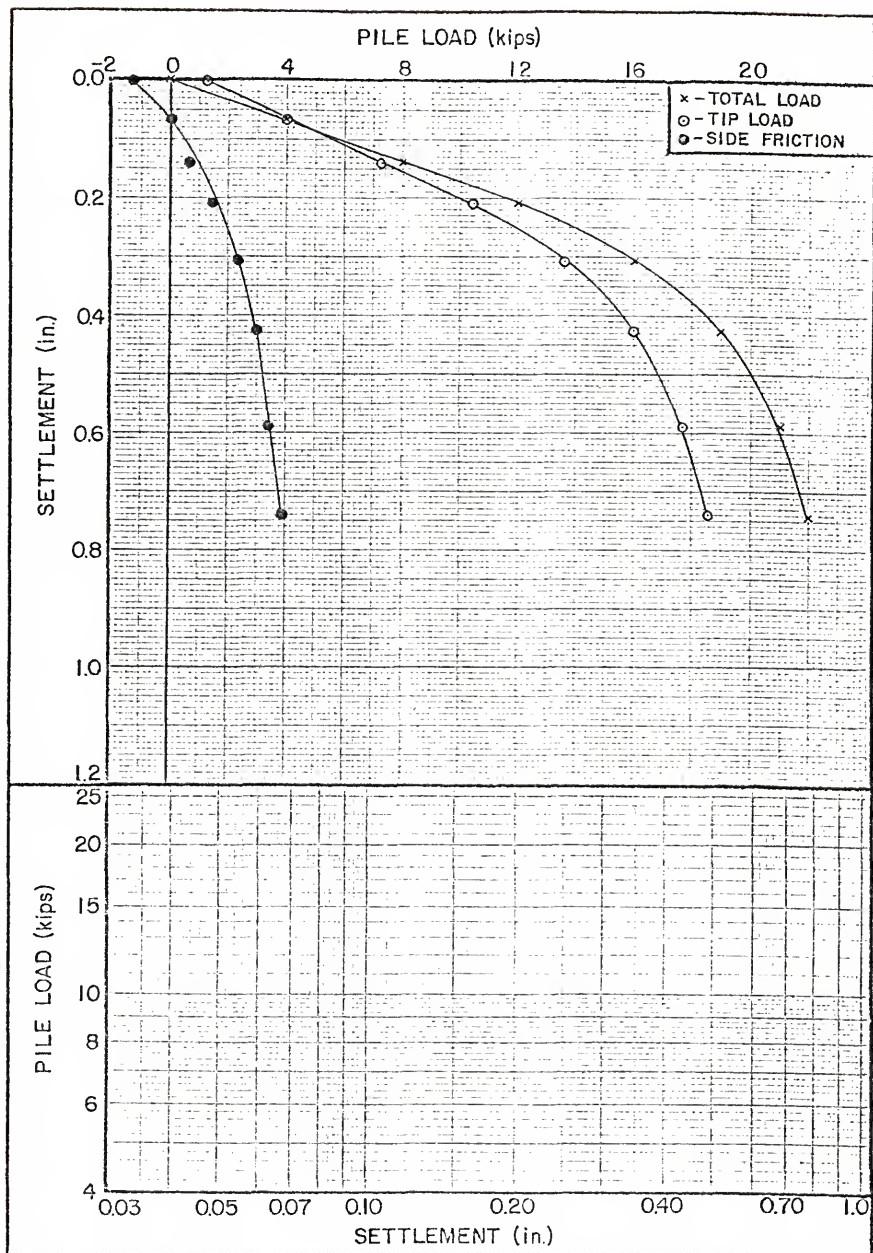
FAIRBANKS PILE LOAD TEST NO 2-1 RESULTS - 4.5 FT PIPE PILE  
FIGURE A-10



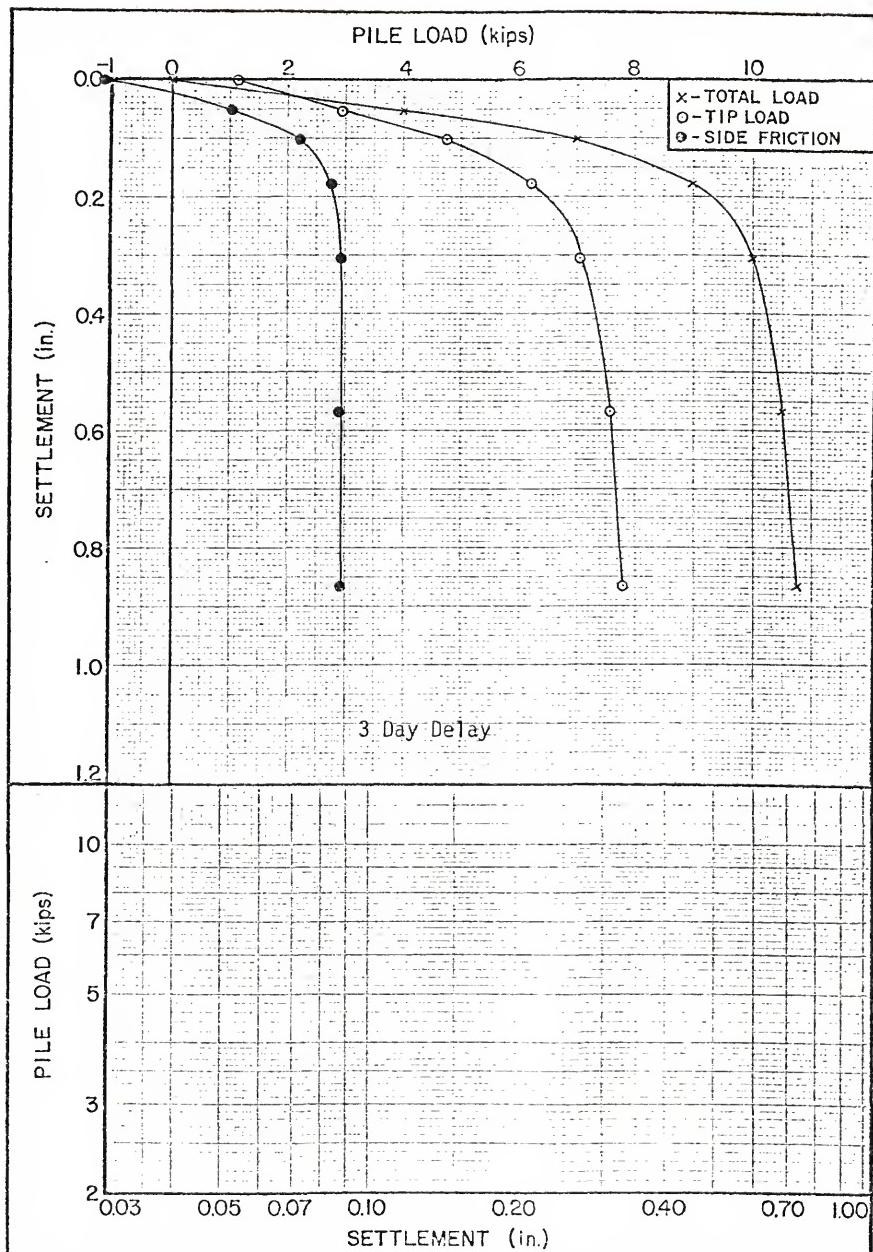
FAIRBANKS PILE LOAD TEST NO 2-1 RESULTS - 4.5 FT PIPE PILE  
FIGURE A-11



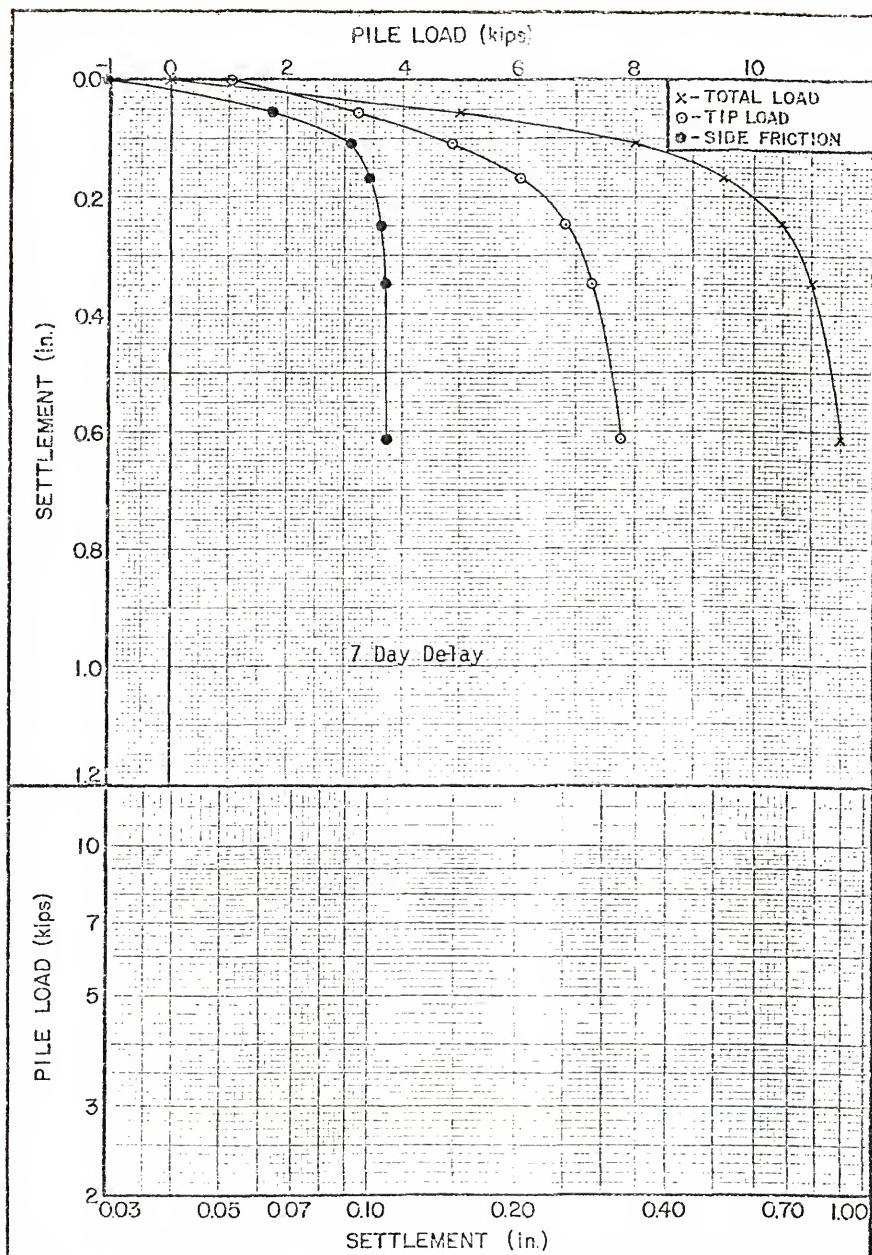
FAIRBANKS PILE LOAD TEST NO 2-2 RESULTS - 8.9 FT PIPE PILE  
FIGURE A-12



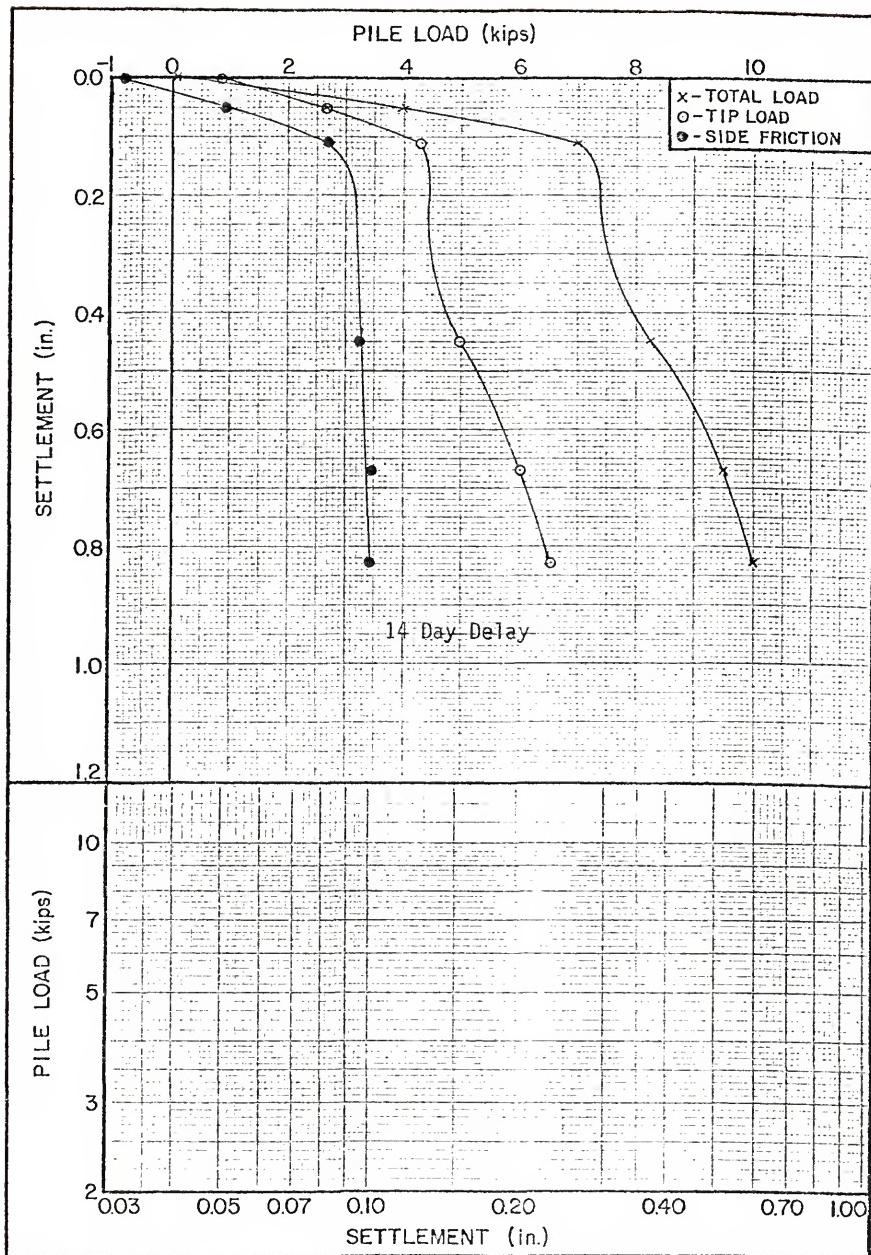
FAIRBANKS PILE LOAD TEST NO 2-2 RESULTS - 8.9 FT PIPE PILE  
FIGURE A-13



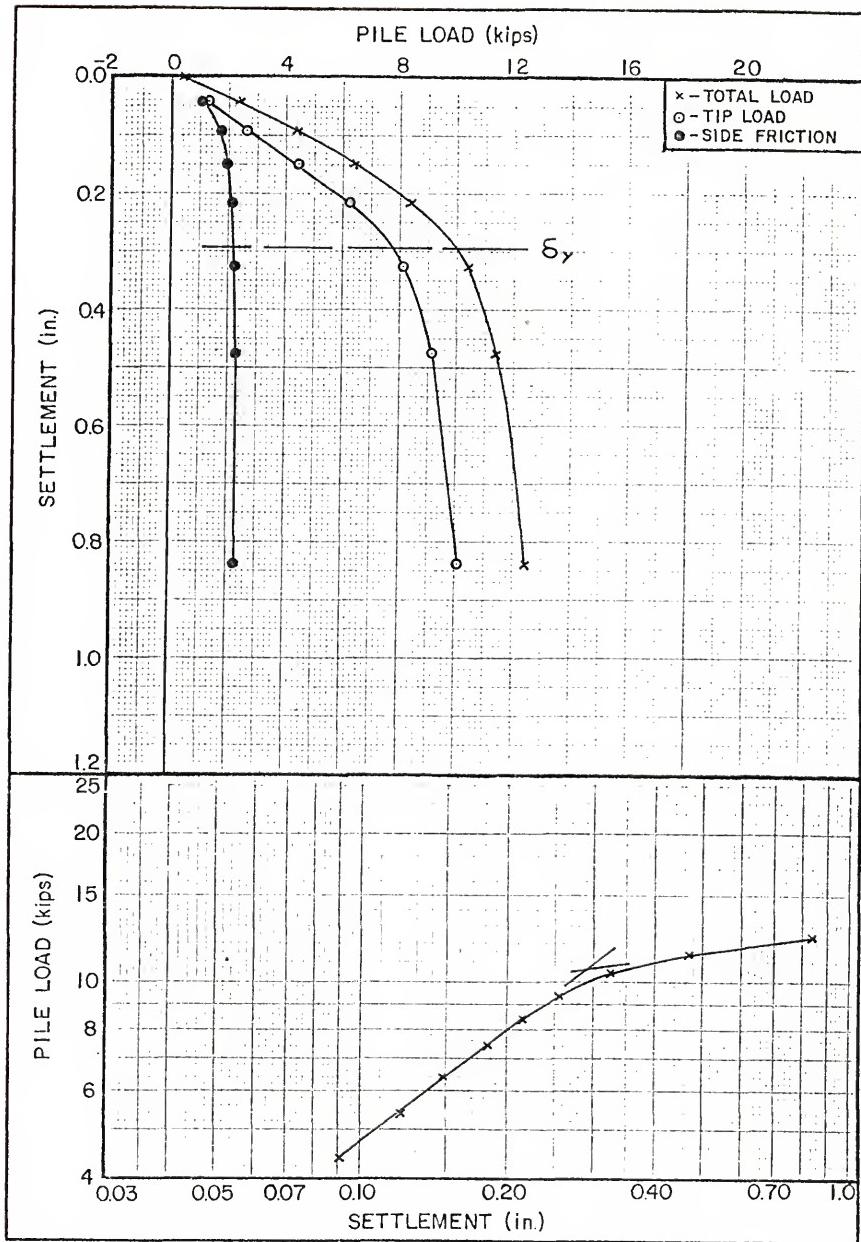
FAIRBANKS PILE LOAD TEST NO 3-1 RESULTS - 4.5 FT PIPE PILE  
FIGURE A-14



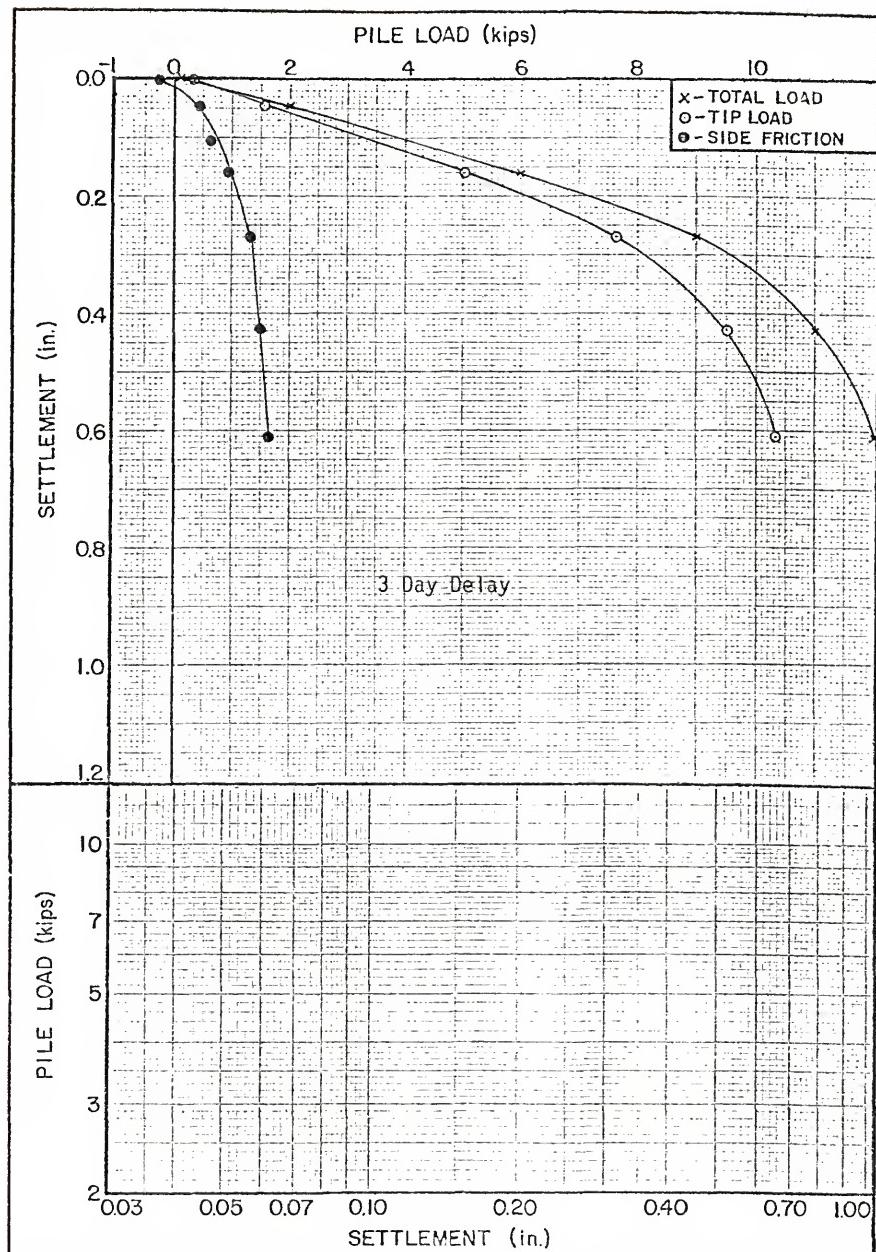
FAIRBANKS PILE LOAD TEST NO 3-1 RESULTS - 4.5 FT PIPE PILE  
FIGURE A-15



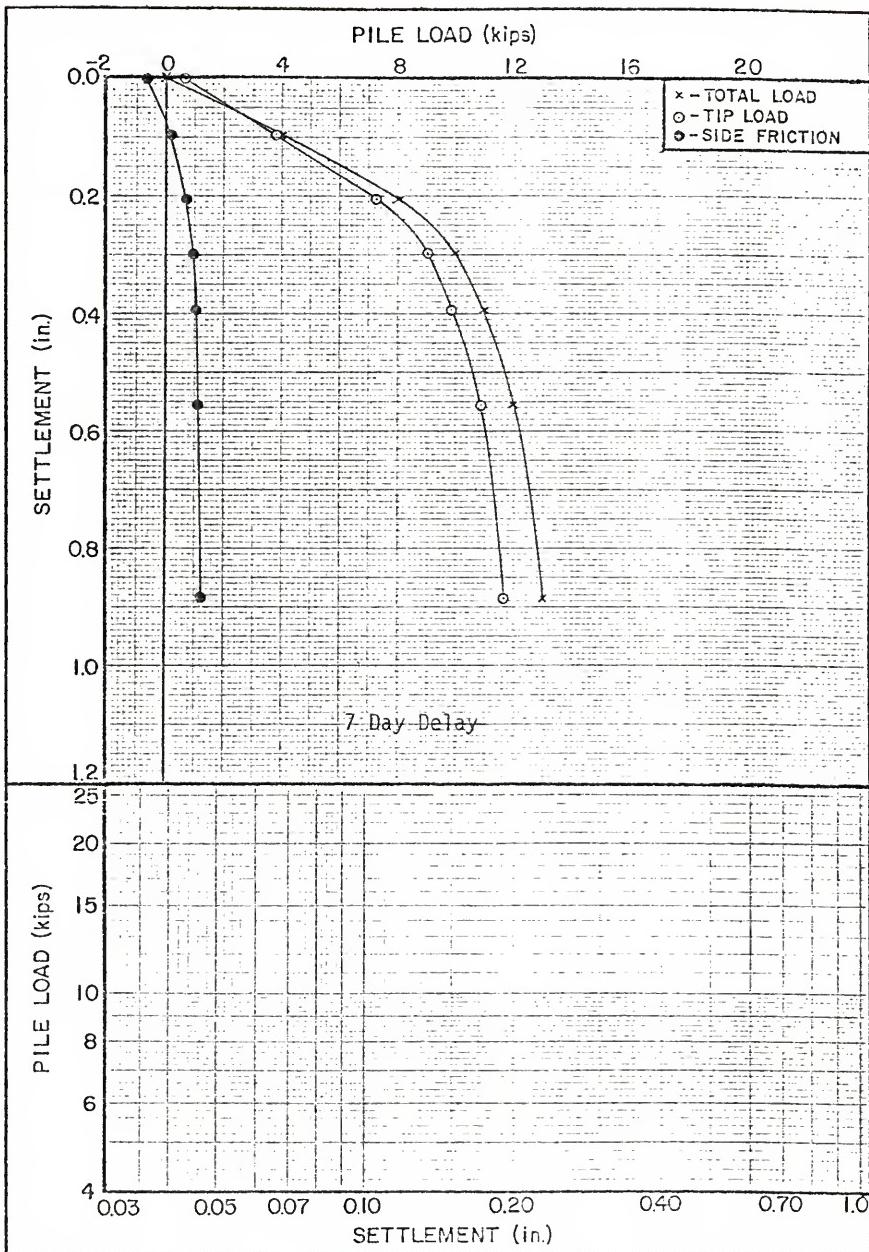
FAIRBANKS PILE LOAD TEST NO 3-1 RESULTS - 4.5 FT PIPE PILE  
FIGURE A-16



FAIRBANKS PILE LOAD TEST 3-2 RESULTS - 8.0 FT PIPE PILE  
FIGURE A-17



FAIRBANKS PILE LOAD TEST NO 3-2 RESULTS - 8.5 FT PIPE PILE  
FIGURE A-18



FAIRBANKS PILE LOAD TEST 3-2 RESULTS - 8.5 FT PIPE PILE  
FIGURE A-19

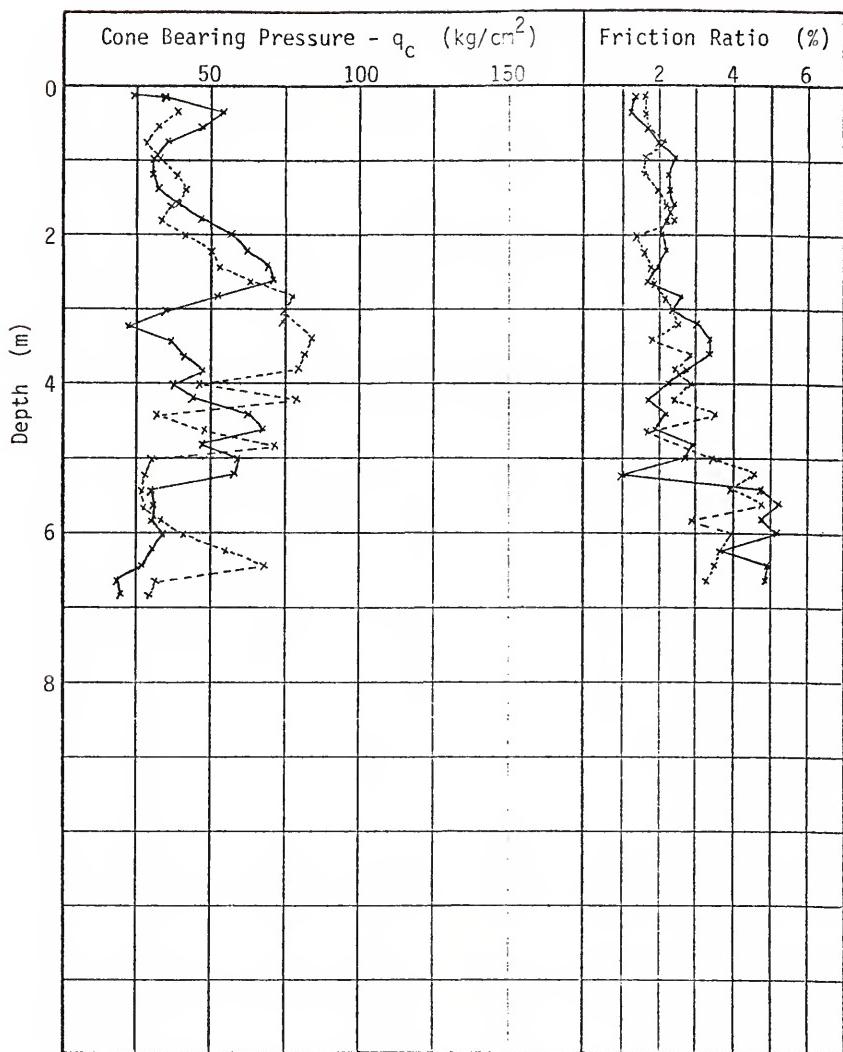
**APPENDIX B**  
**BEVILLE SITE TEST RESULTS**

TABLE B-1  
MODEL PILE DRIVING RESISTANCE DATA

Pile Number	Depth Interval (ft)	Hammer Drop (in)	Number of Blows
B- 1	2.67 - 3.00	12	36
	5.67 - 6.00	12	68
	8.33 - 8.50	12	29
B- 2	3.67 - 4.00	12	19
	6.67 - 7.00	12	48
	9.33 - 9.50	18	
B- 5	11.67 - 12.00	30	56
	2.33 - 2.50	12	5
	4.50 - 4.75	12	16
	7.00 - 7.25	12	49
B- 6	9.50 - 9.75	18	98
	8.33 - 8.50	12	36
B- 7	1.50 - 2.00	12	21
	4.33 - 4.50	12	11
	6.50 - 7.00	18	30
B- 9	8.33 - 8.50	18	32
	5.50 - 6.00	12	128
	5.67 - 6.00	18	23
B-10			
B-11	7.67 - 8.00	12	217
B-12	2.00 - 2.25	12	12
	4.50 - 4.75	18	13
	7.00 - 7.25	18	23
	9.50 - 9.75	18	39
B-13	1.67 - 2.00	12	20
	4.33 - 4.50	12	9
	6.67 - 7.00	18	48
	9.33 - 9.50	18	54
	11.00 - 11.50	18	306
B-14	5.67 - 6.00	12	30
B-15	2.67 - 3.00	12	25
B-18	2.67 - 3.00	12	23
B-19	2.67 - 3.00	12	52
B-22	5.67 - 6.00	12	72
B-24	1.75 - 2.00	12	21
	4.00 - 4.25	12	22
	6.50 - 6.75	12	45
	9.00 - 9.25	18	28
B-25	2.67 - 3.00	12	51
B-26	5.67 - 6.00	12	91
B-29	7.67 - 8.00	18	68
B-30	8.00 - 8.33	18	83
B-32	2.00 - 2.25	12	9
	4.50 - 4.75	18	23
	7.00 - 7.25	18	30
	9.50 - 9.75	18	48

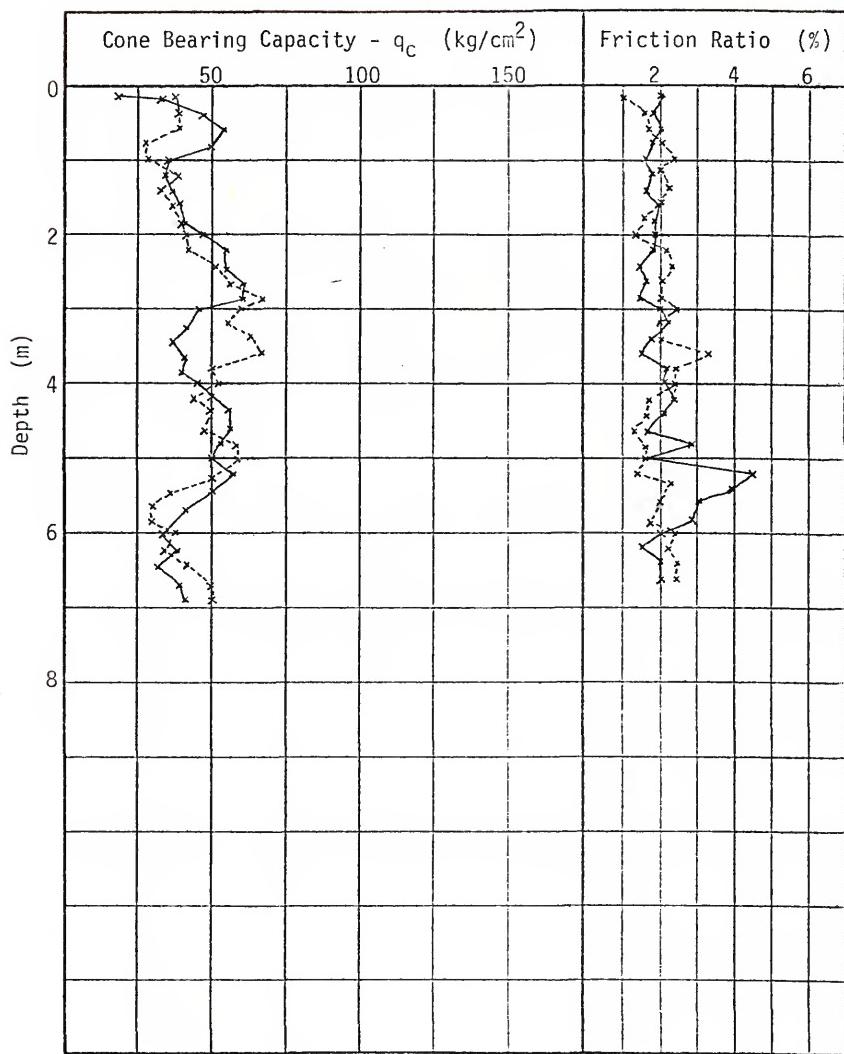
TABLE B-1 (Continued)

Pile Number	Depth Interval (ft)	Hammer Drop (in)	Number of Blows
PP-1	5.50 - 6.00	12	95
	9.00 - 9.50	30	42
PP-2	5.50 - 6.00	18	35
	9.00 - 9.50	18	43
PP-3	6.00 - 6.50	18	40
	8.50 - 9.00	18	146
PP-4	4.50 - 5.00	12	26
	7.00 - 7.50	18	45
	9.50 - 10.00	18	68
PP-5	5.00 - 5.50	18	76
	8.00 - 8.50	30	45
PP-6	4.50 - 5.00	12	23
	7.00 - 7.50	18	48
	9.50 - 10.00	18	55



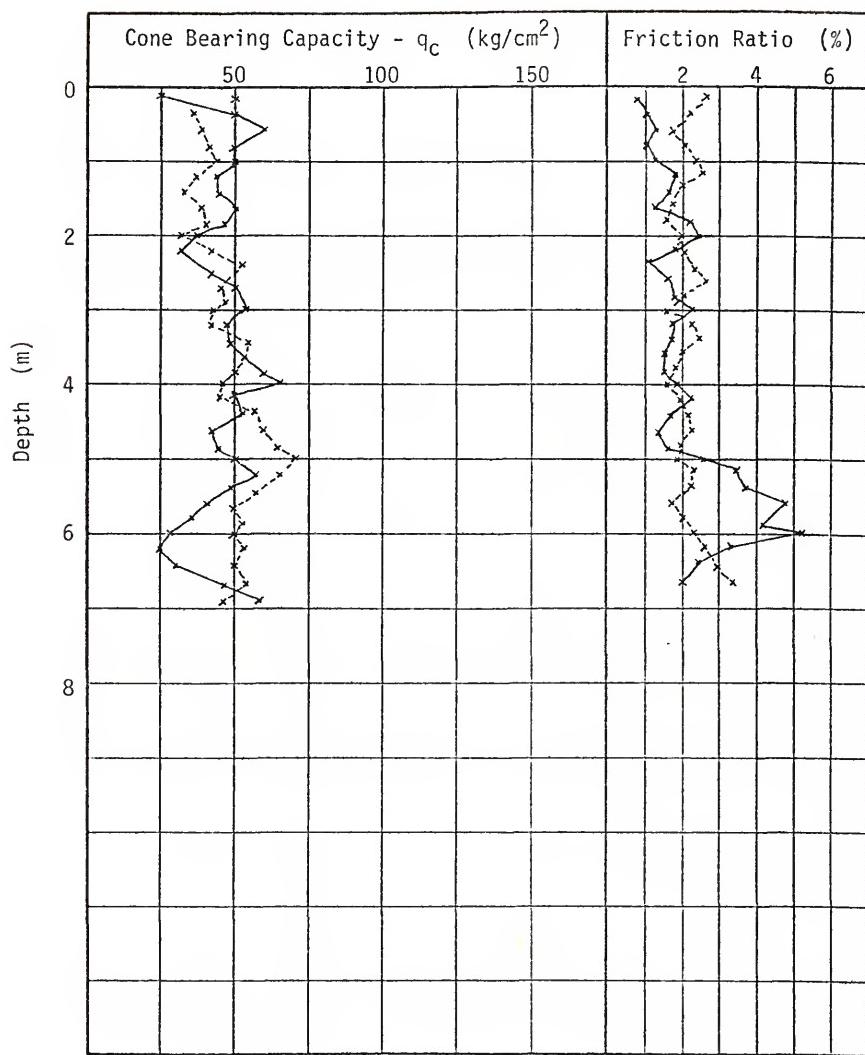
LOGS OF BEVILLE SITE PRELIMINARY CPT SOUNDINGS NO 1 AND 2

FIGURE B-1



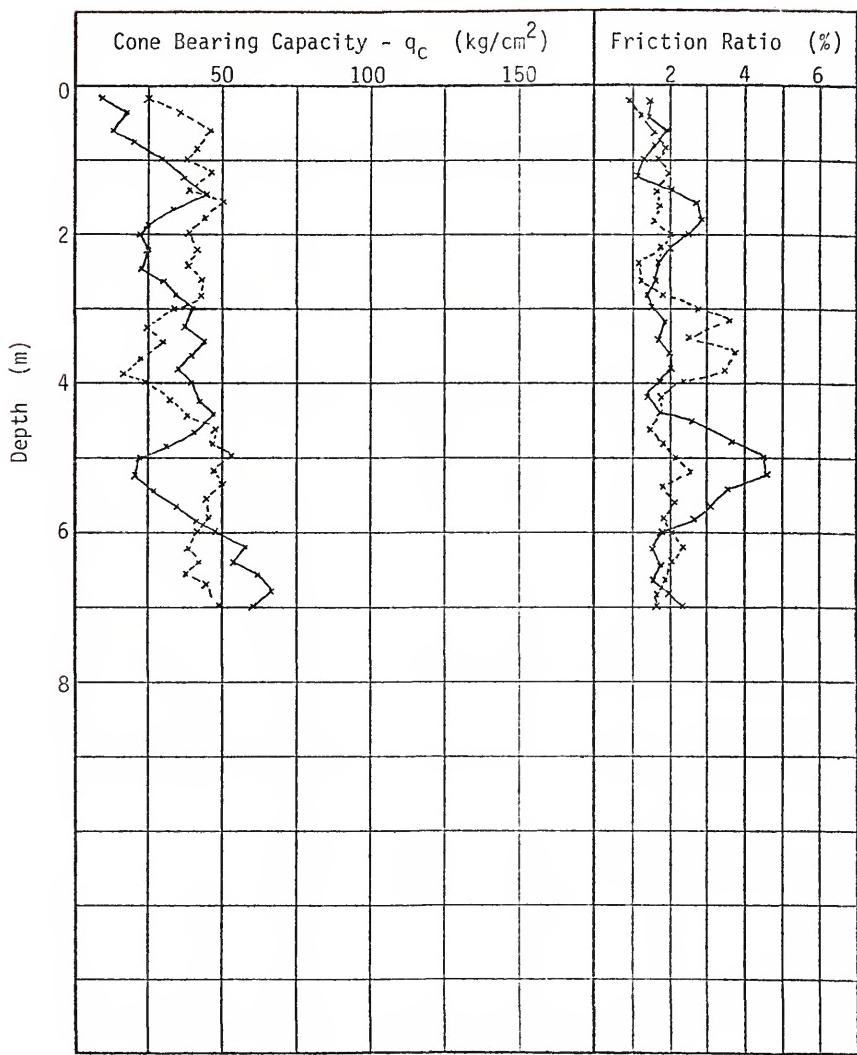
LOGS OF BEVILLE SITE PRELIMINARY CPT SOUNDINGS NO 3 AND 4

FIGURE B-2



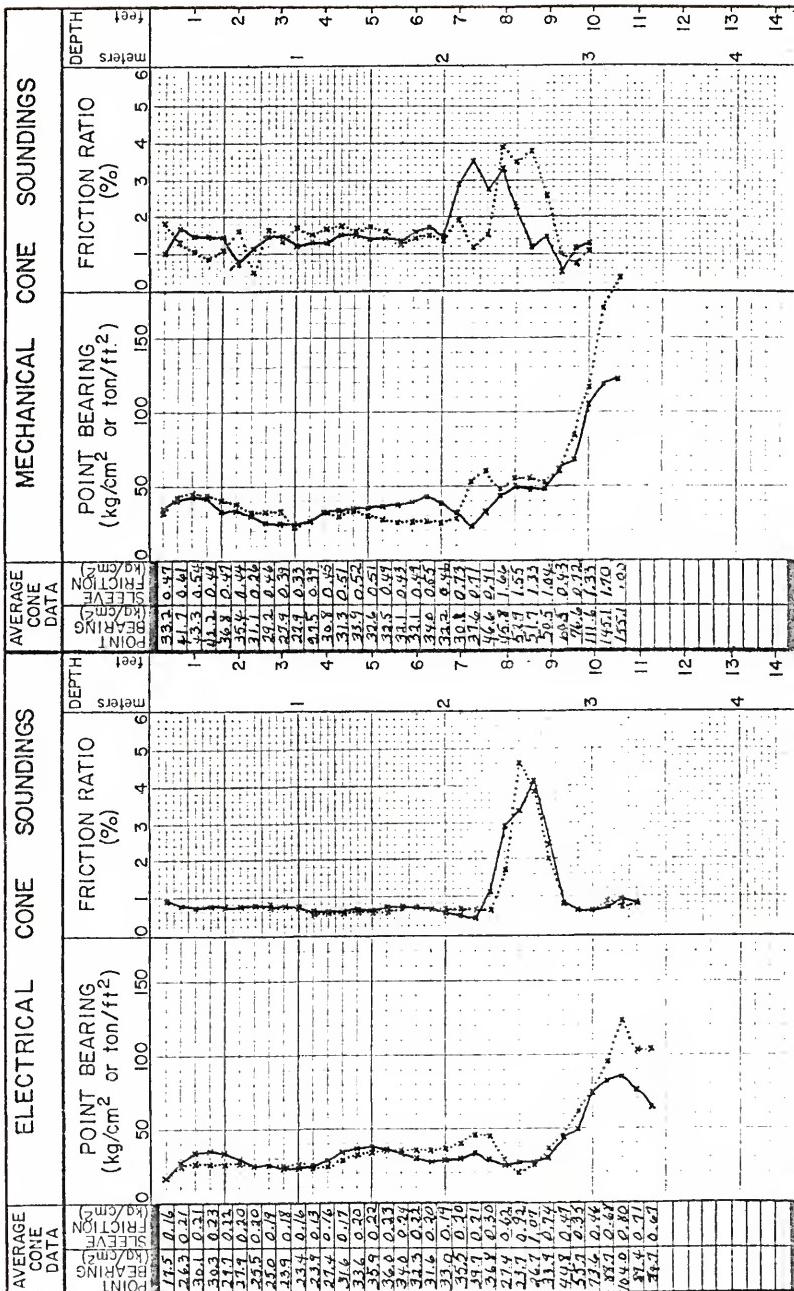
LOGS OF BEVILLE SITE PRELIMINARY CPT SOUNDINGS NO 5 AND 6

FIGURE B-3

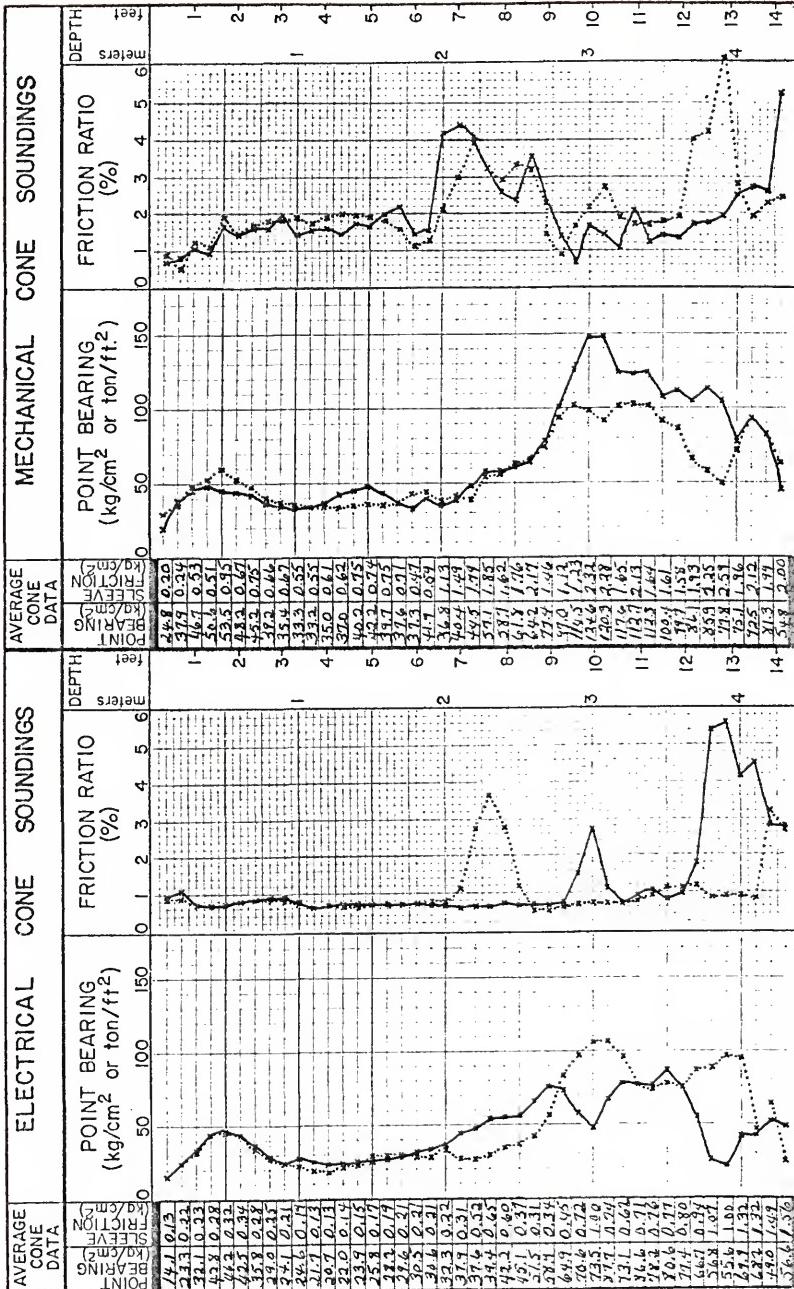


LOGS OF BEVILLE SITE PRELIMINARY CPT SOUNDINGS NO 7 AND 8

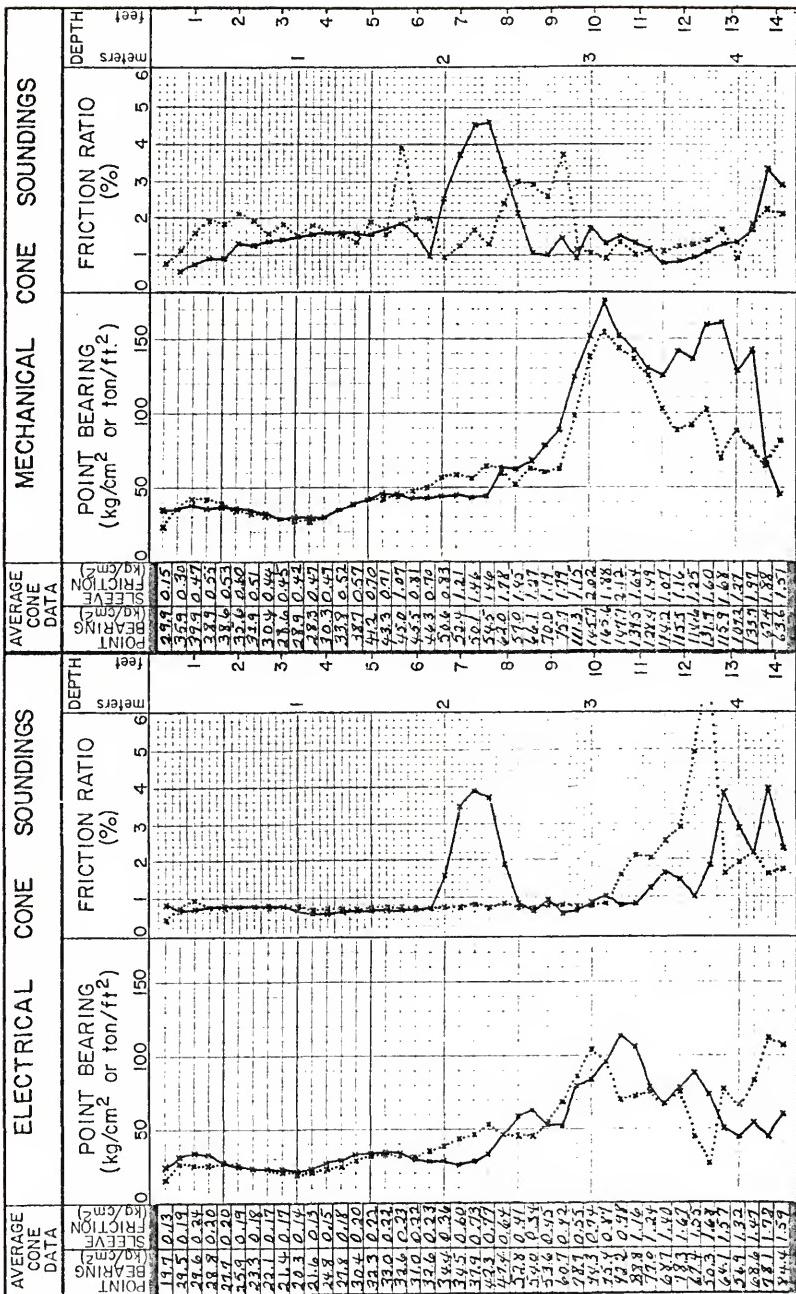
FIGURE B-4



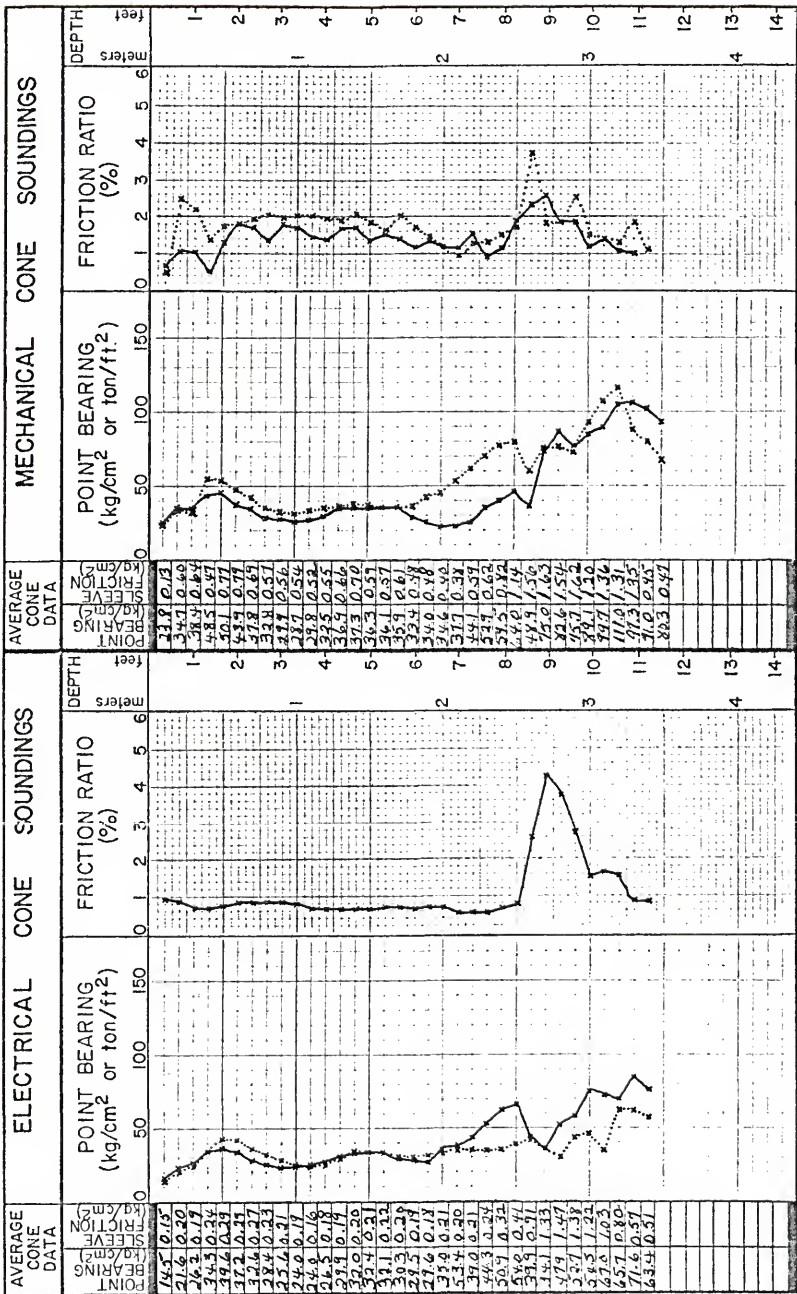
BEVILLE SITE NO 1 CPT LOGS  
FIGURE B-5



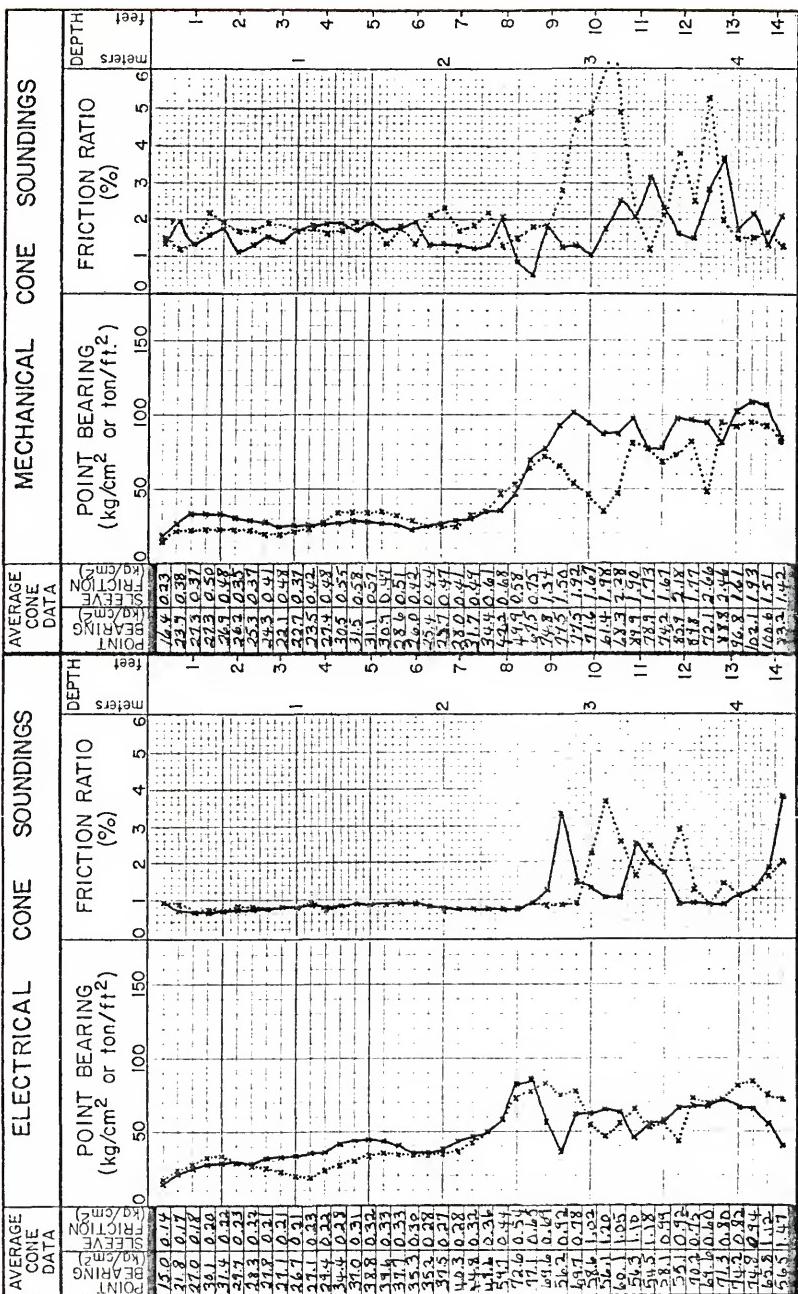
**BEVILLE SITE NO 2 CPT LOGS  
FIGURE B-6**



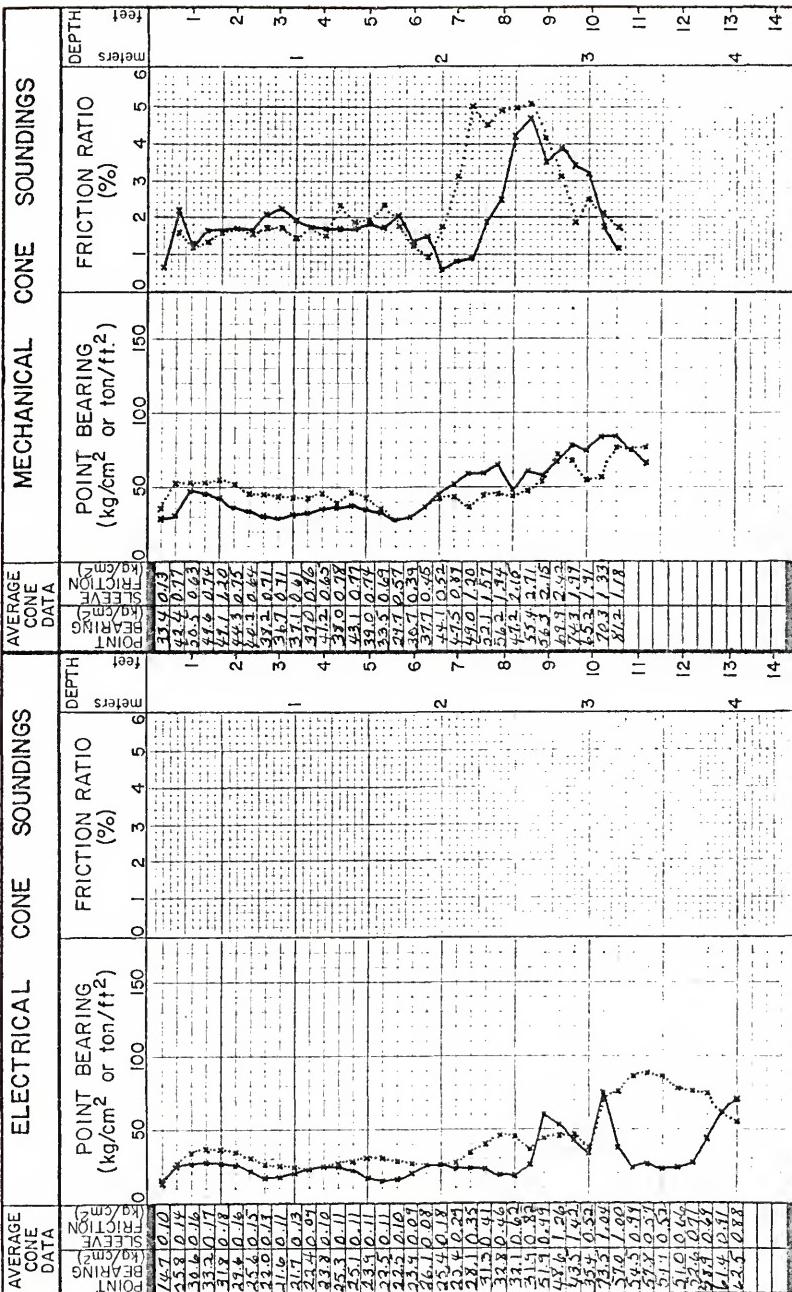
**BEVILLE SITE NO 5 CPT LOGS**  
**FIGURE B-7**



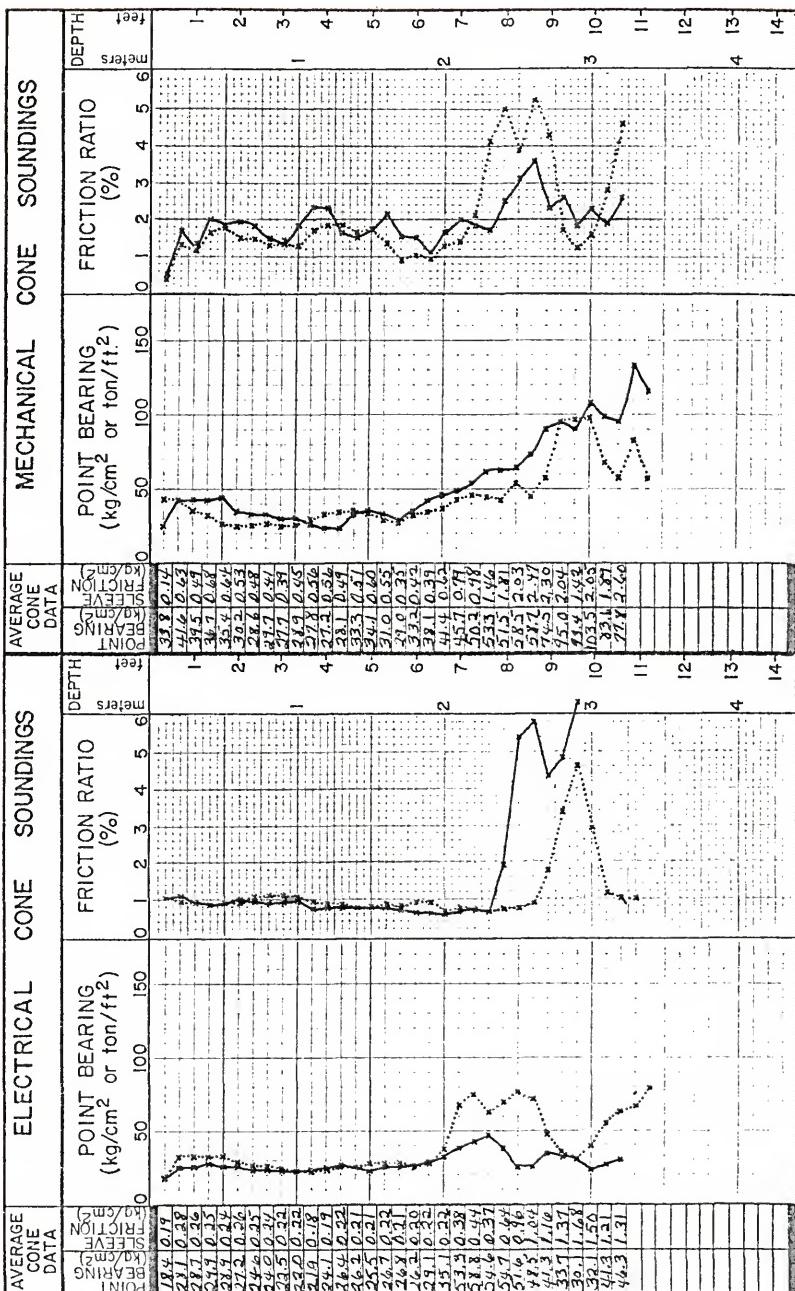
BEVILLE SITE NO 6 CPT LOGS  
FIGURE B-8



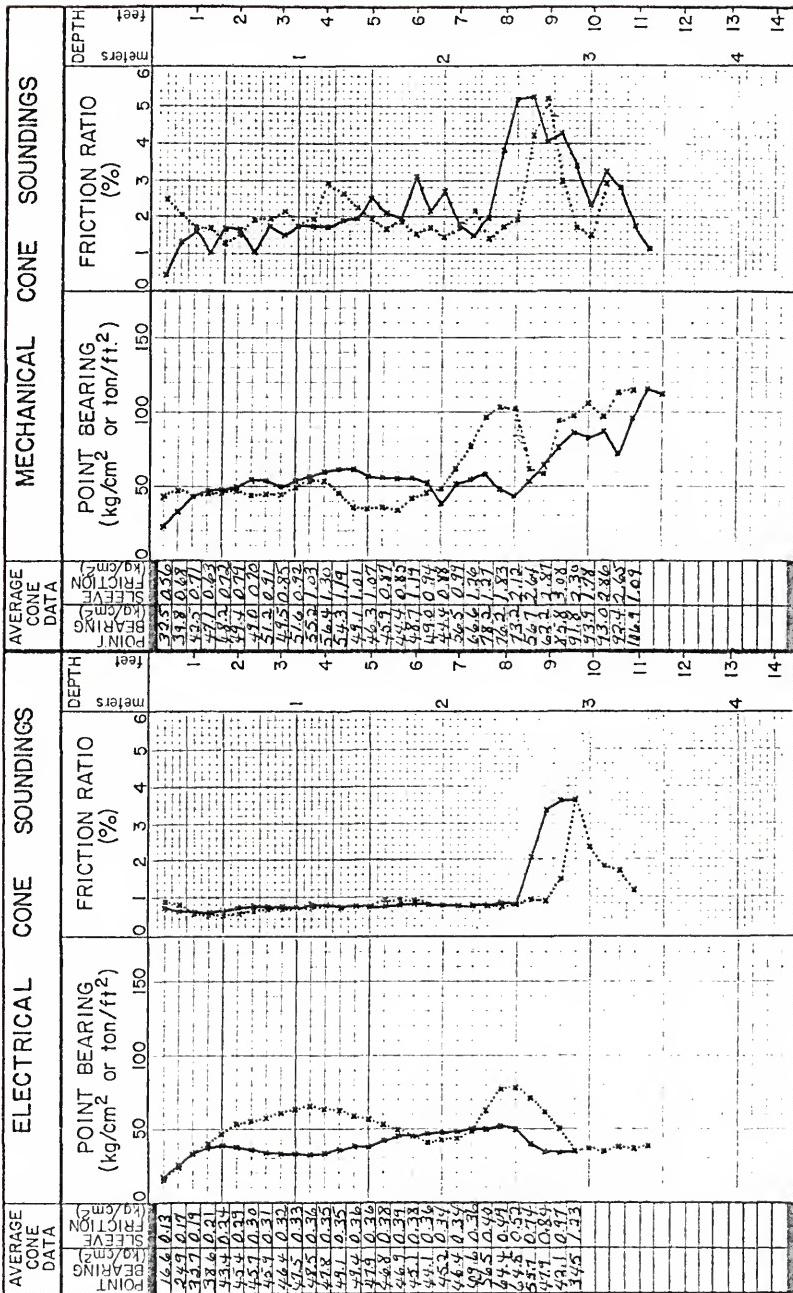
BEVILLE SITE NO 7 CPT LOGS  
FIGURE B-9



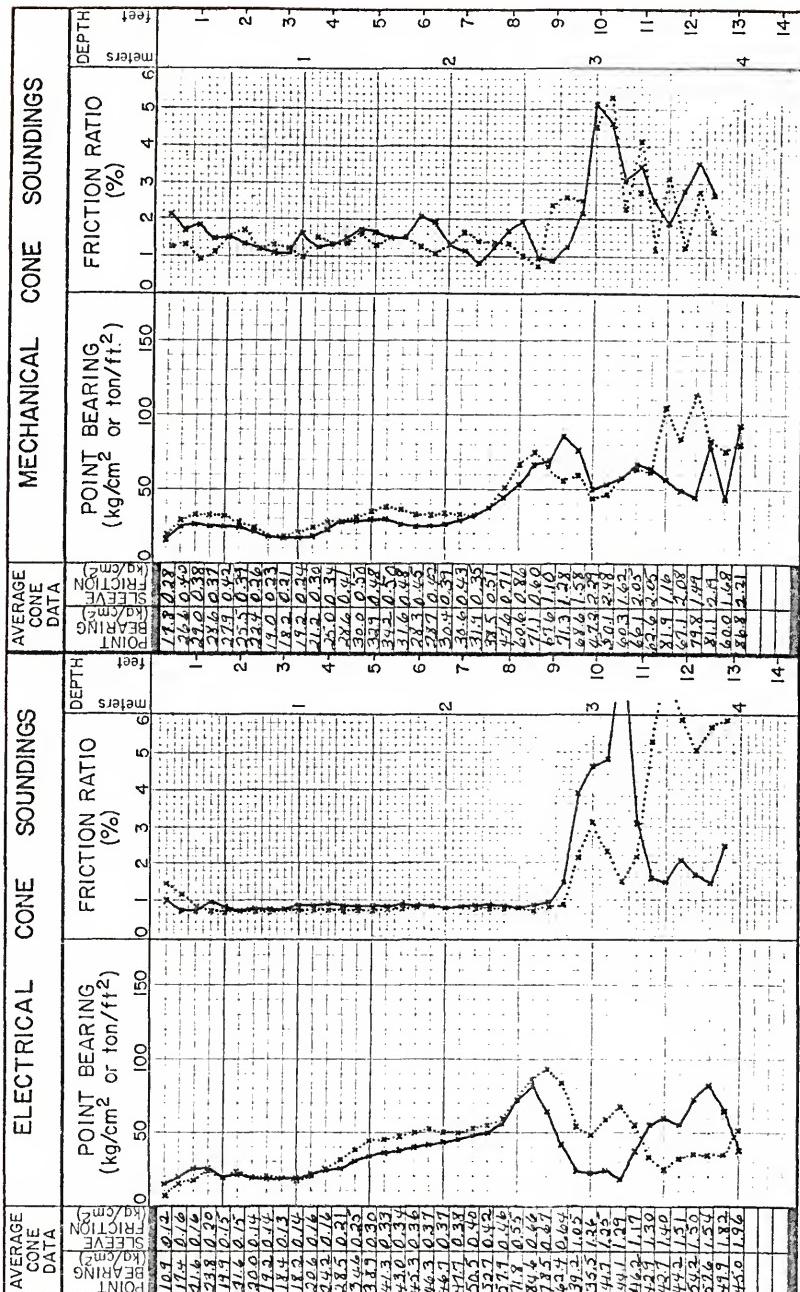
**BEVILLE SITE NO 9 CPT LOGS  
FIGURE B-10**



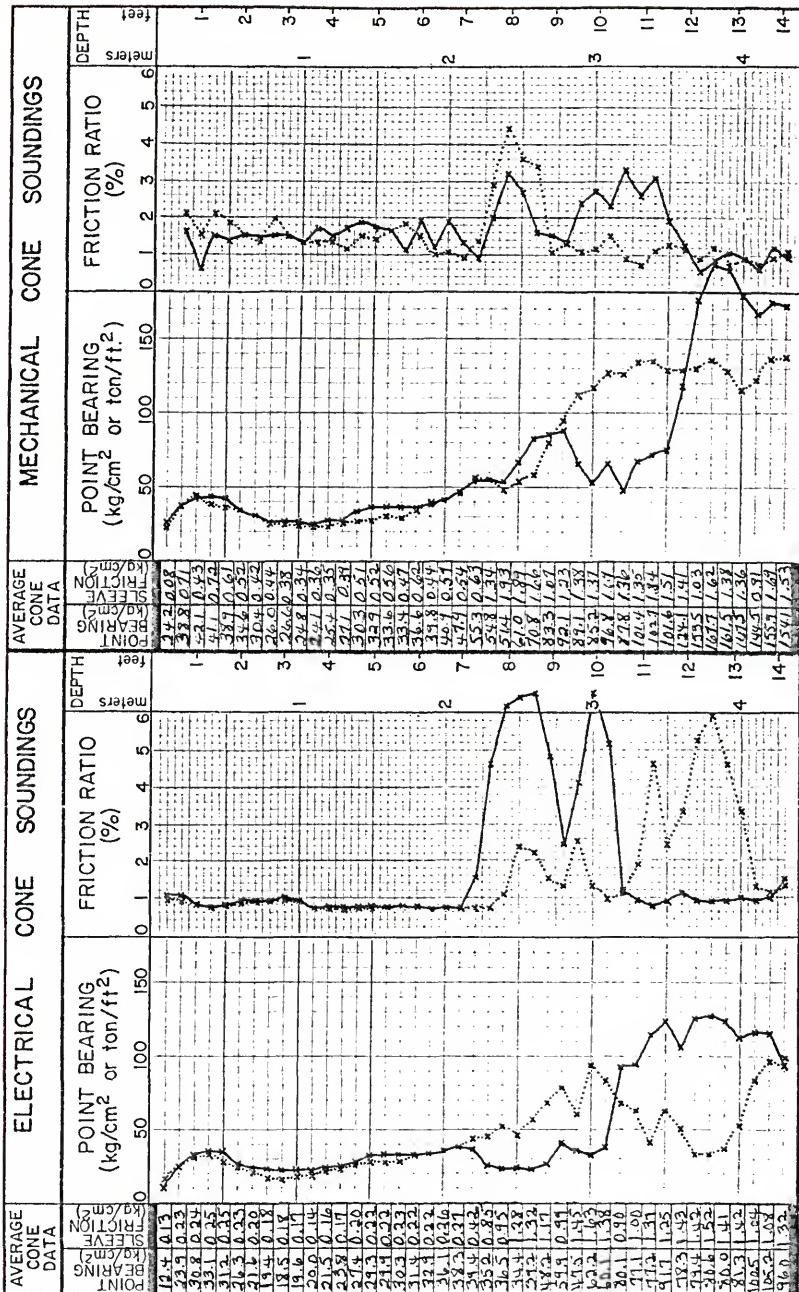
**BEVILLE SITE NO 10 CPT LOGS**  
**FIGURE B-11**

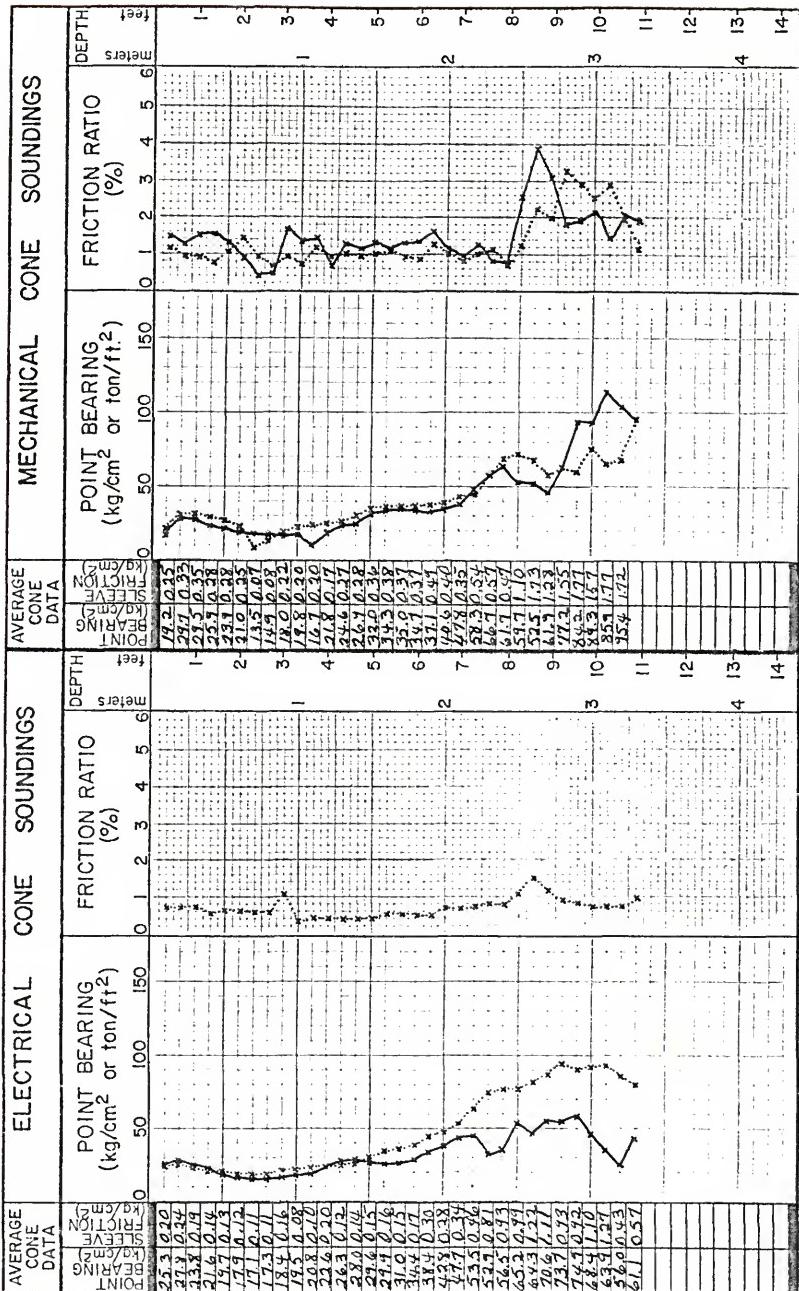


BEVILLE SITE NO 11 CPT LOGS  
FIGURE B-12

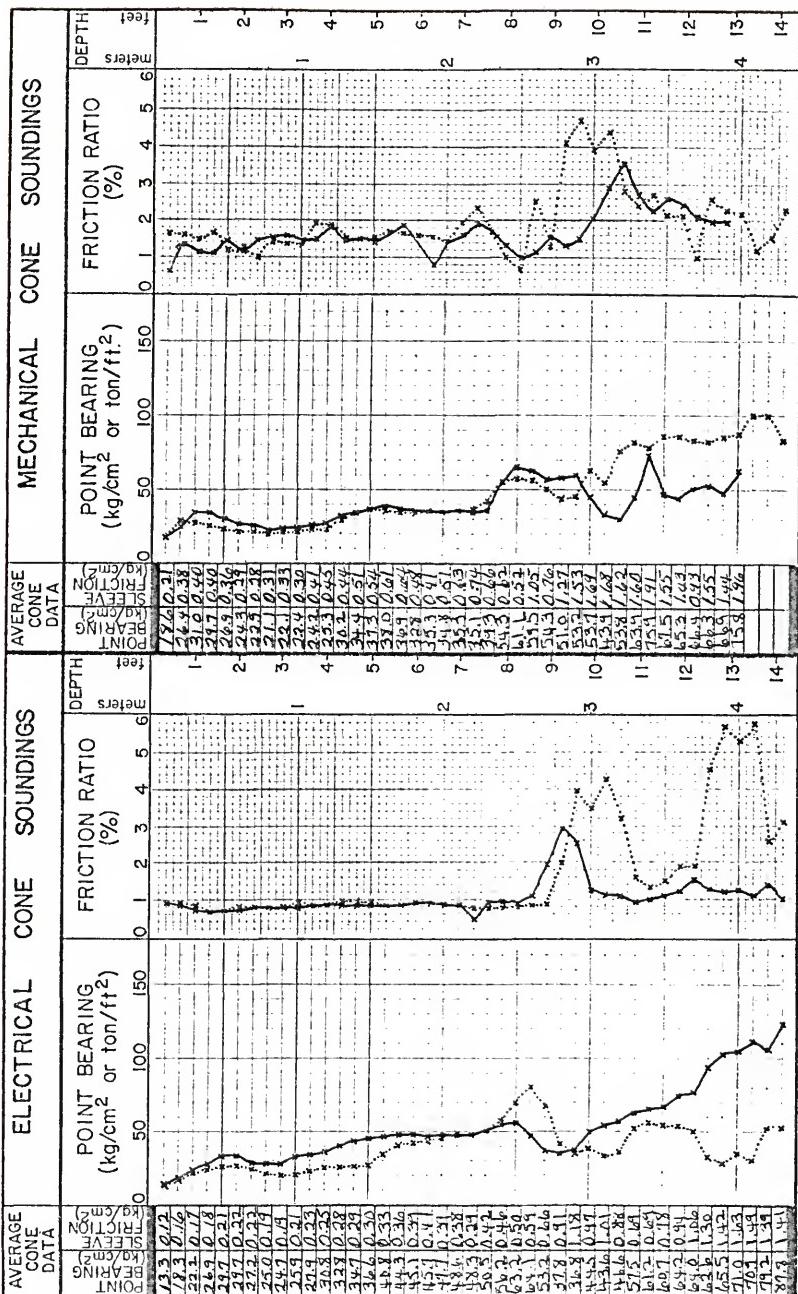


BEVILLE SITE NO 12 CPT LOGS  
FIGURE B-13

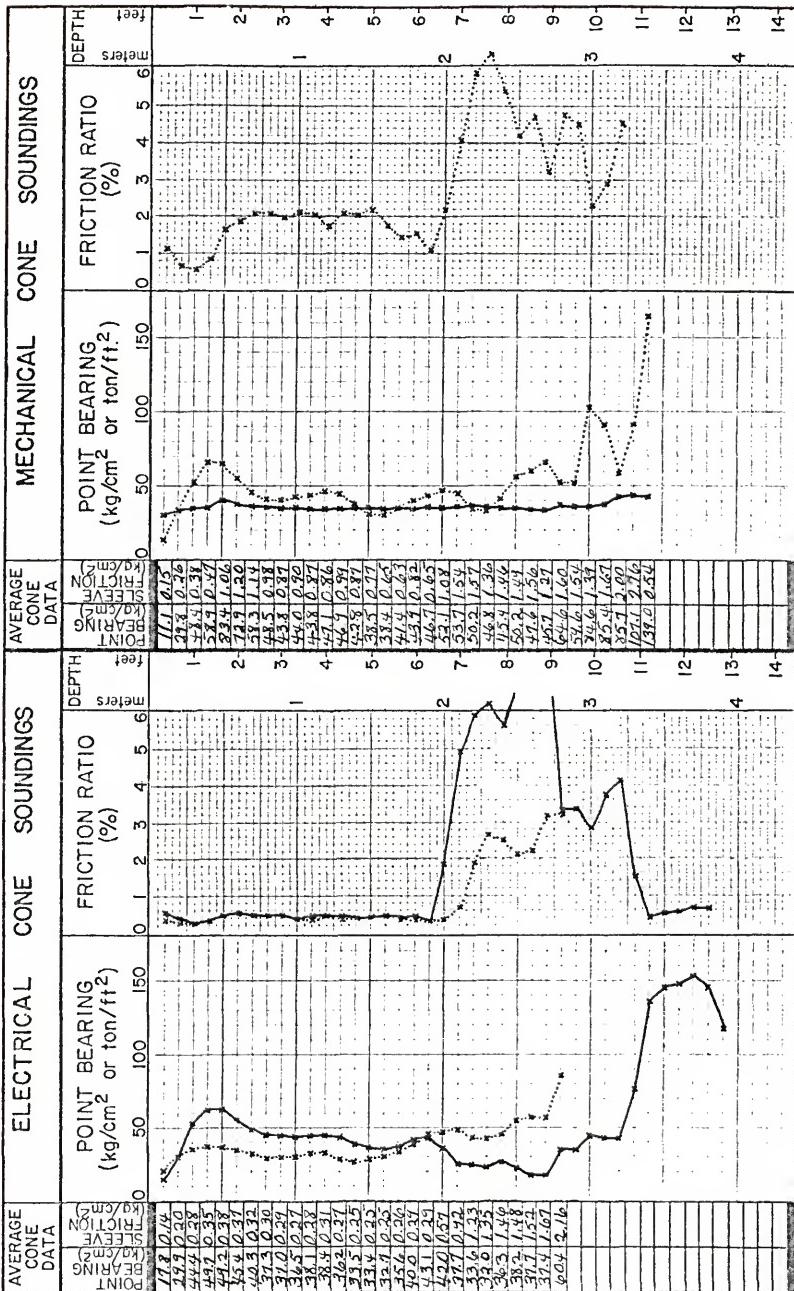




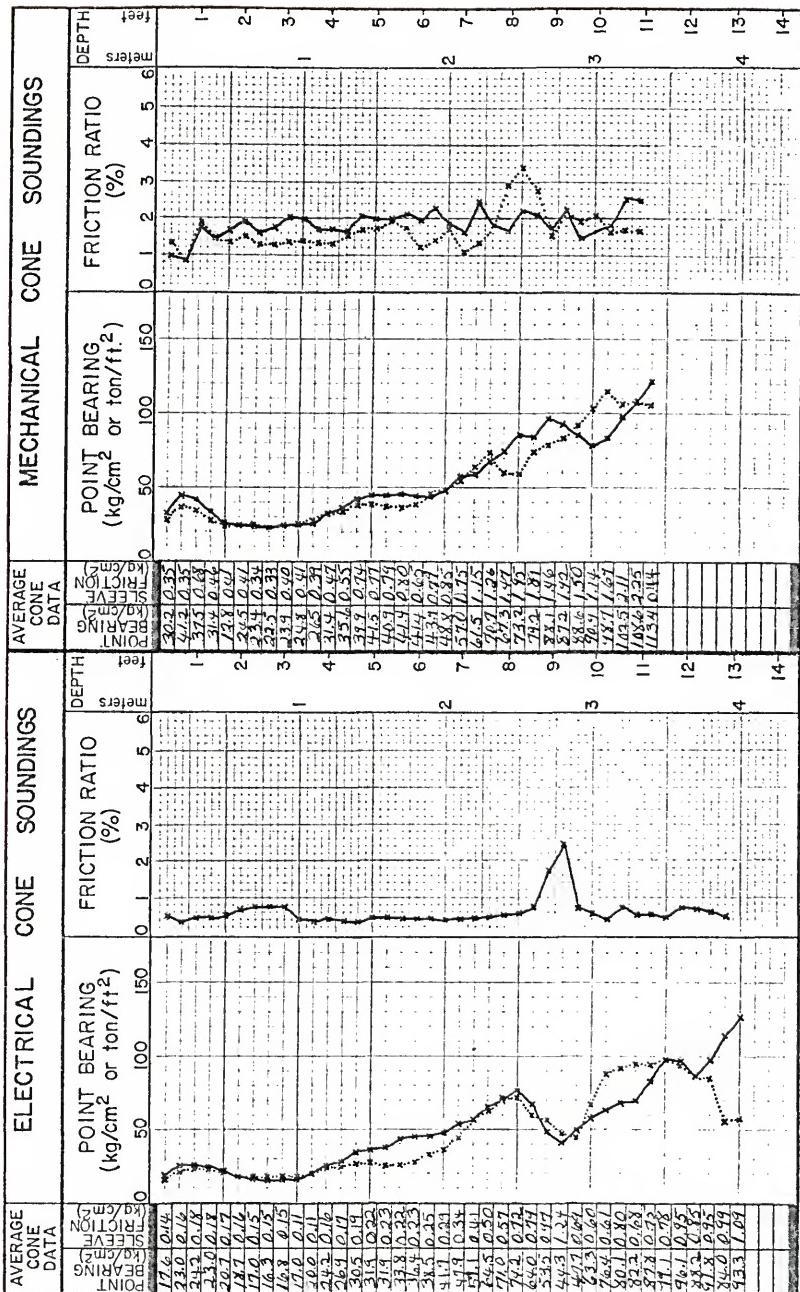
BEVILLE SITE NO 14 CPT LOGS  
FIGURE B-15



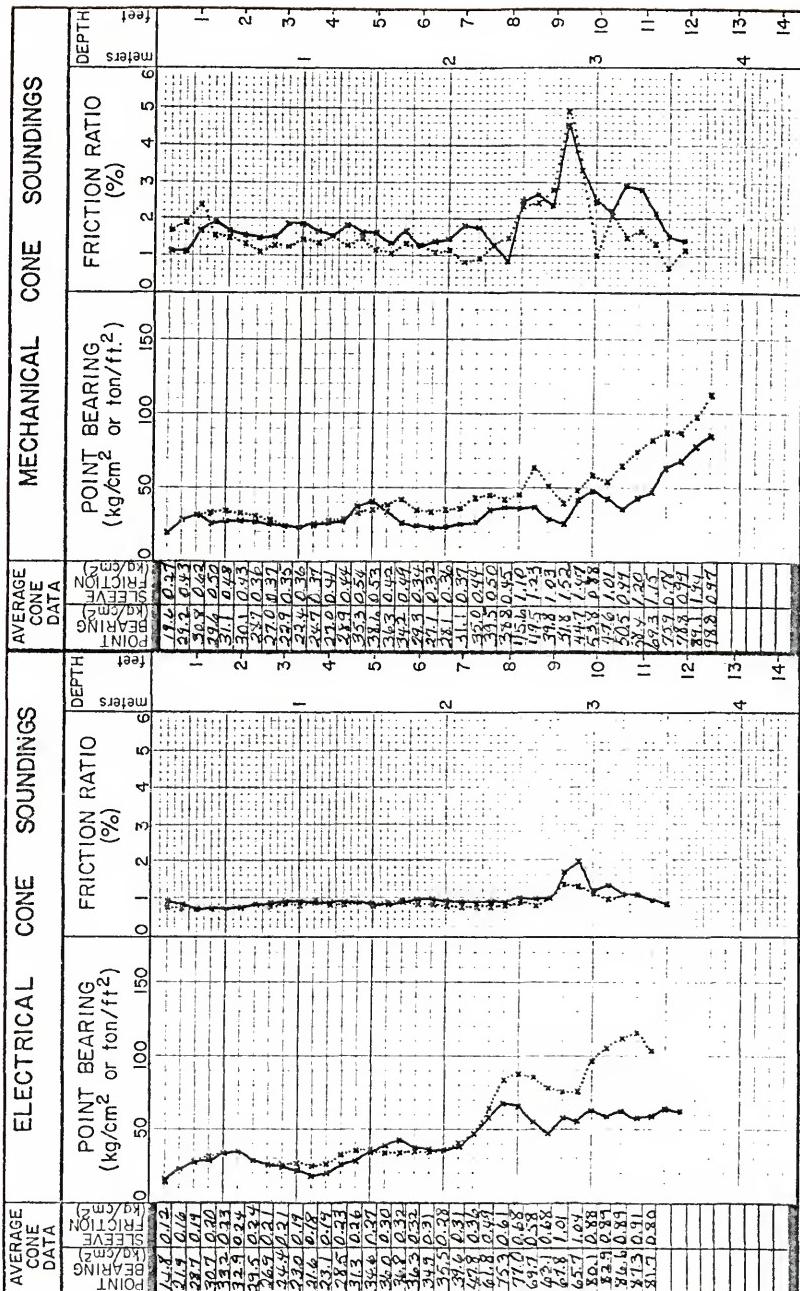
BEVILLE SITE NO 15 CPT LOGS  
FIGURE B-16



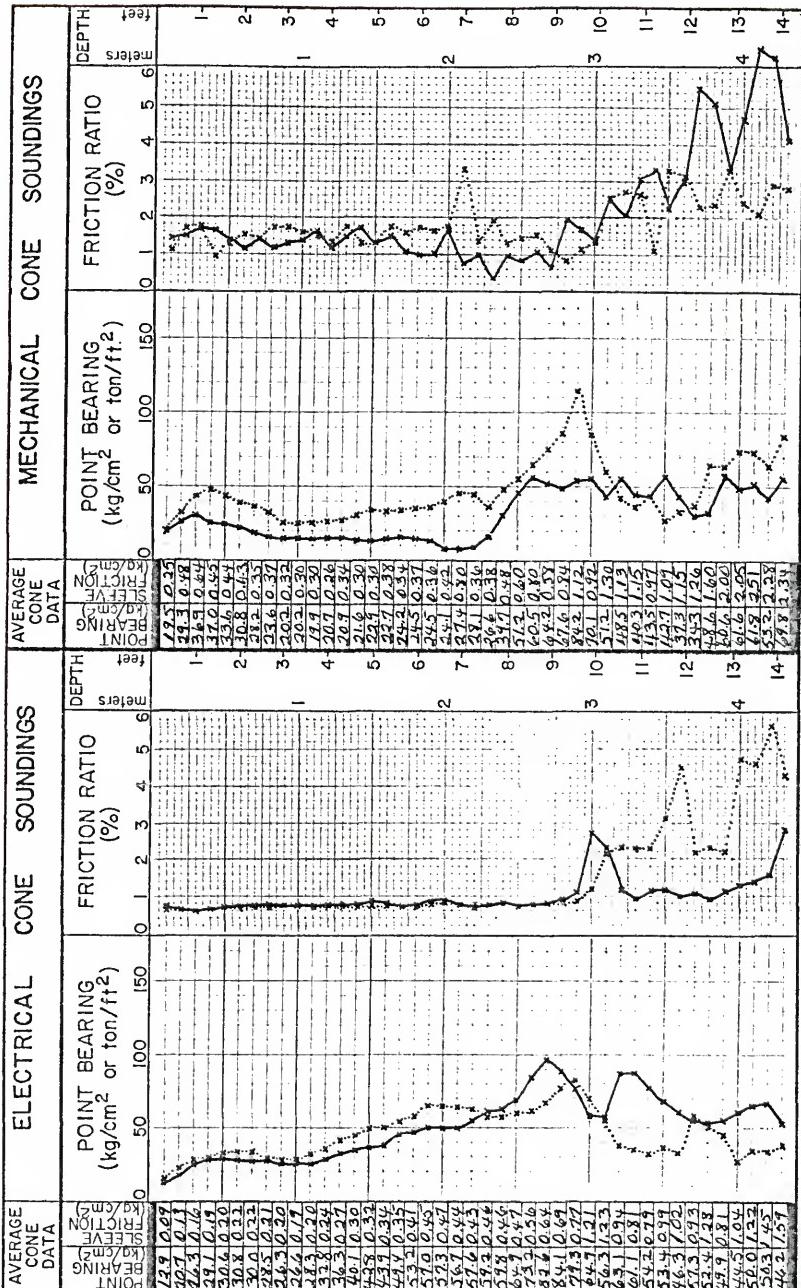
BEVILLE SITE NO 17 CPT LOGS  
FIGURE B-17



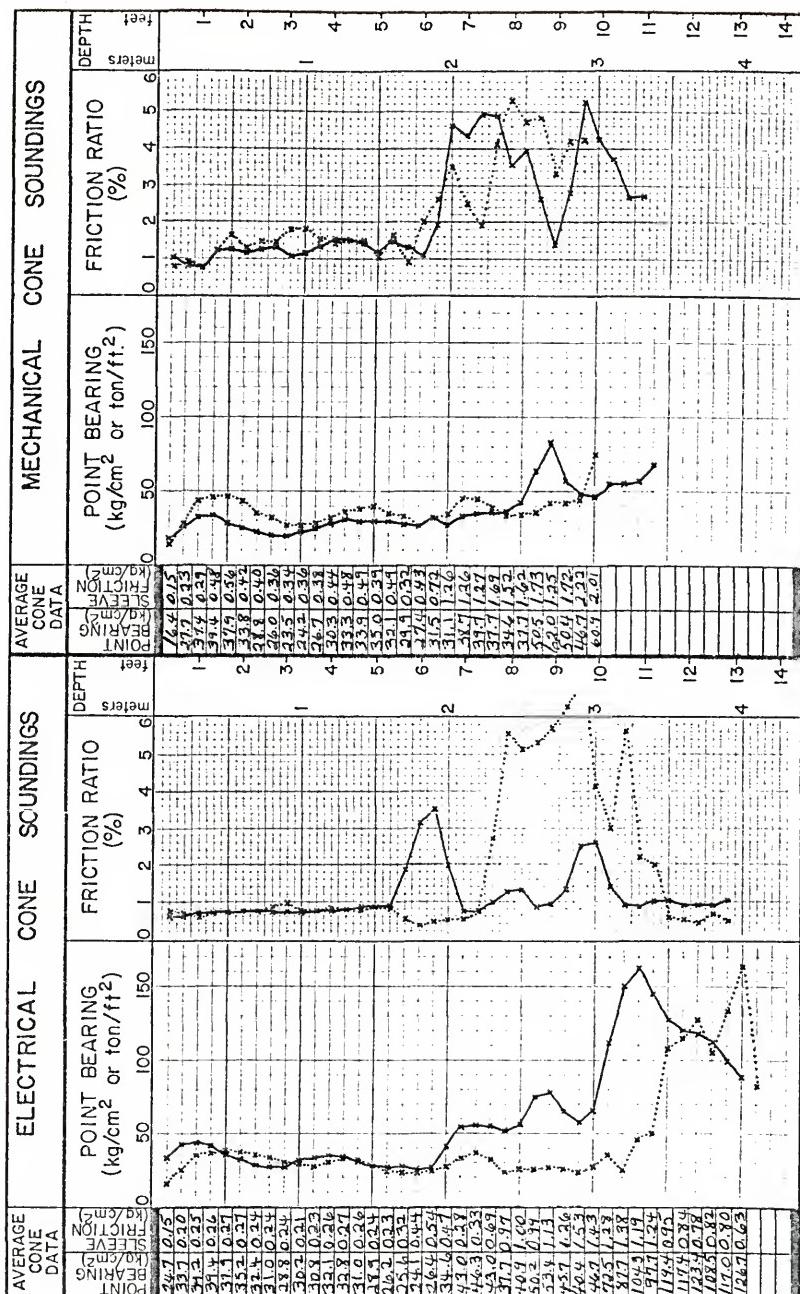
BEVILLE SITE NO 18 CPT LOGS  
FIGURE B-18



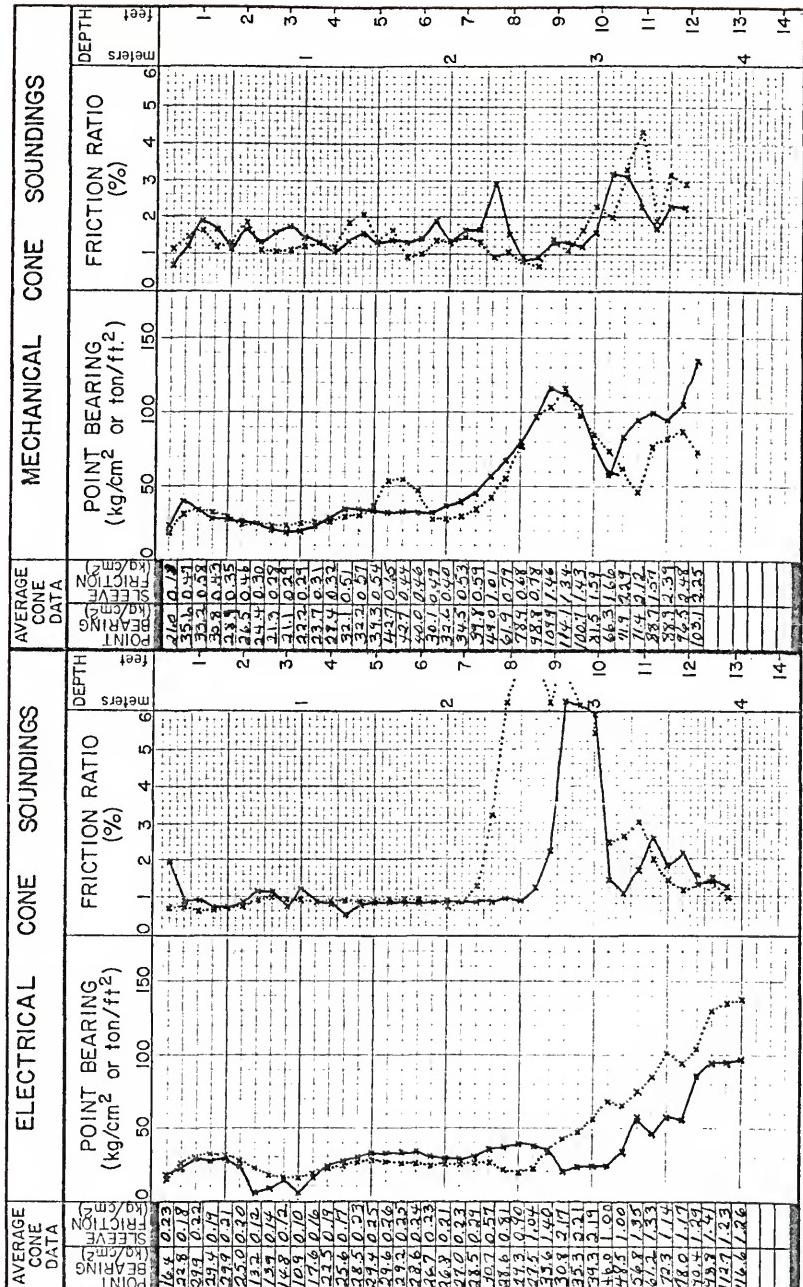
BEVILLE SITE NO 19 CPT LOGS  
FIGURE B-19



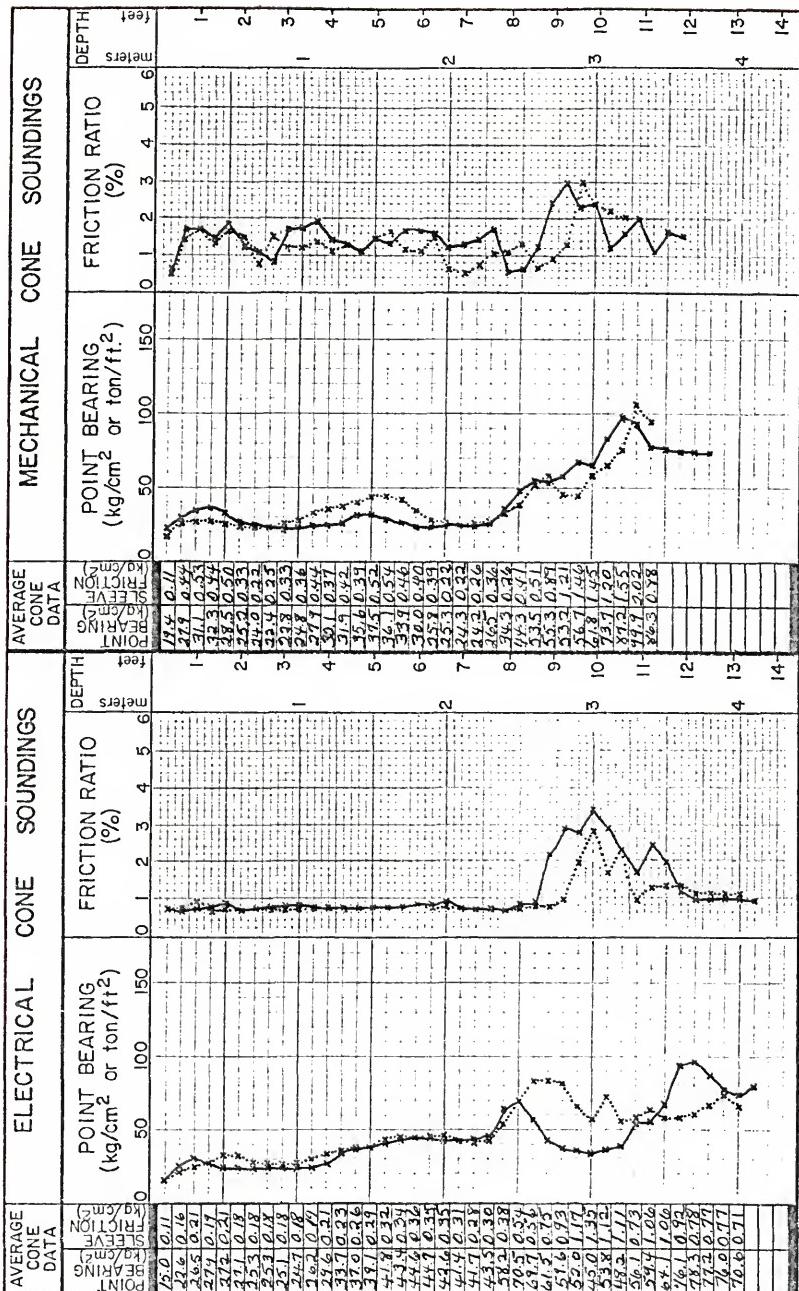
BEVILLE SITE NO 20 CPT LOGS  
FIGURE B-20



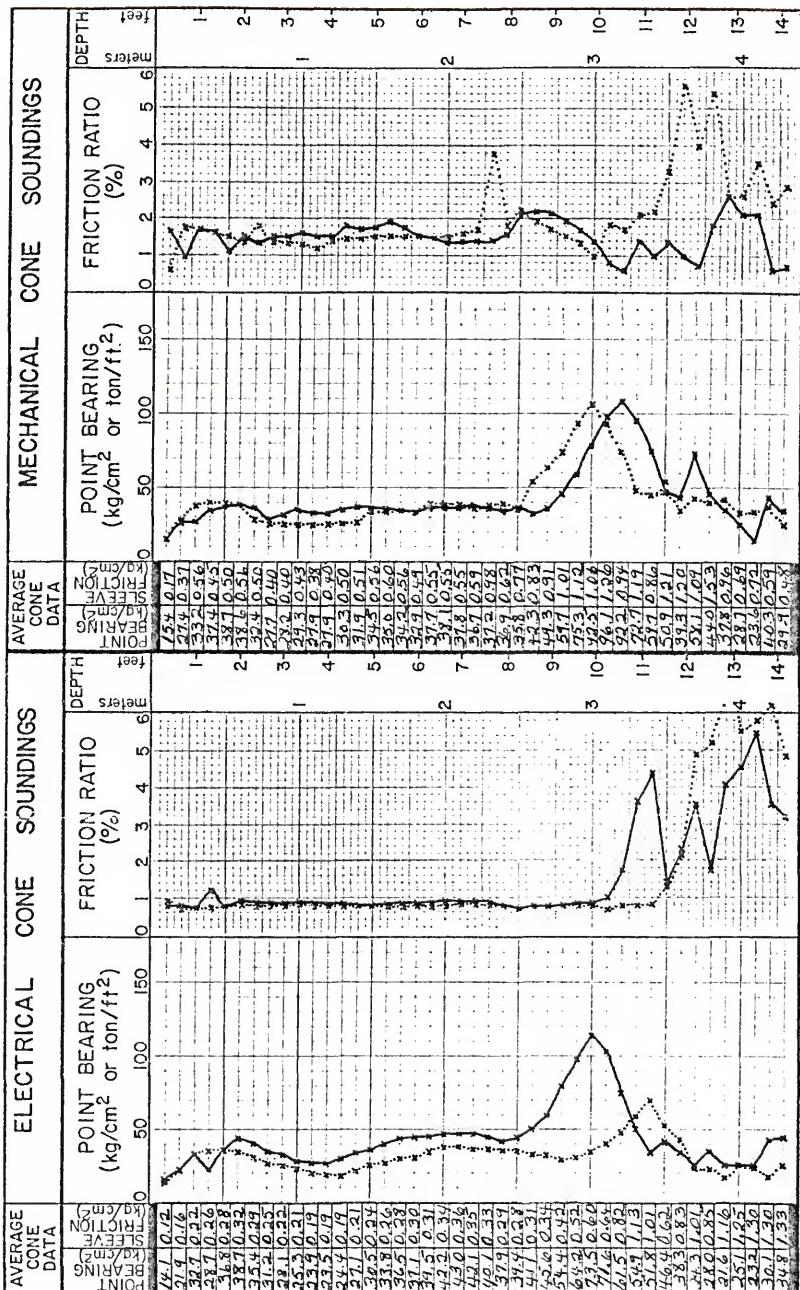
BEVILLE SITE NO 21 CPT LOGS  
FIGURE B-21

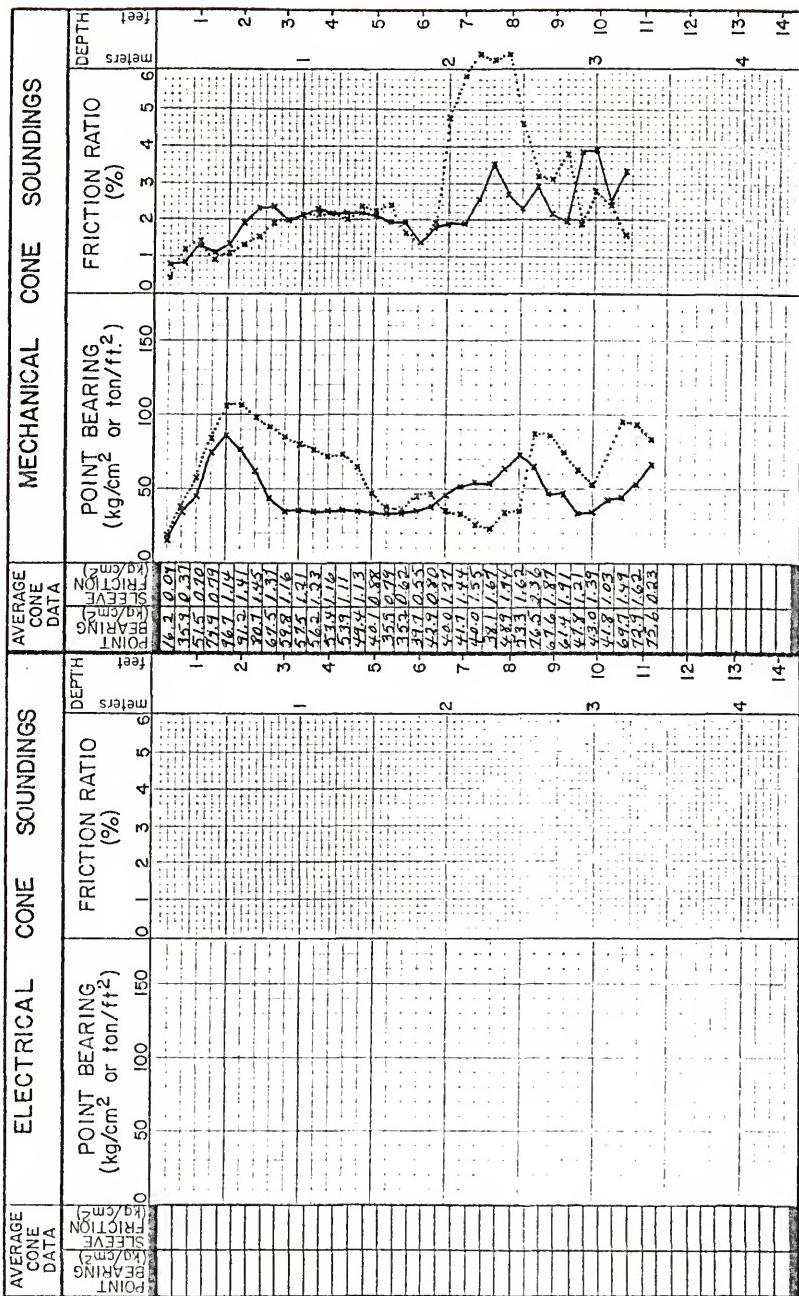


BEVILLE SITE NO. 22 CPT LOGS  
FIGURE B-22

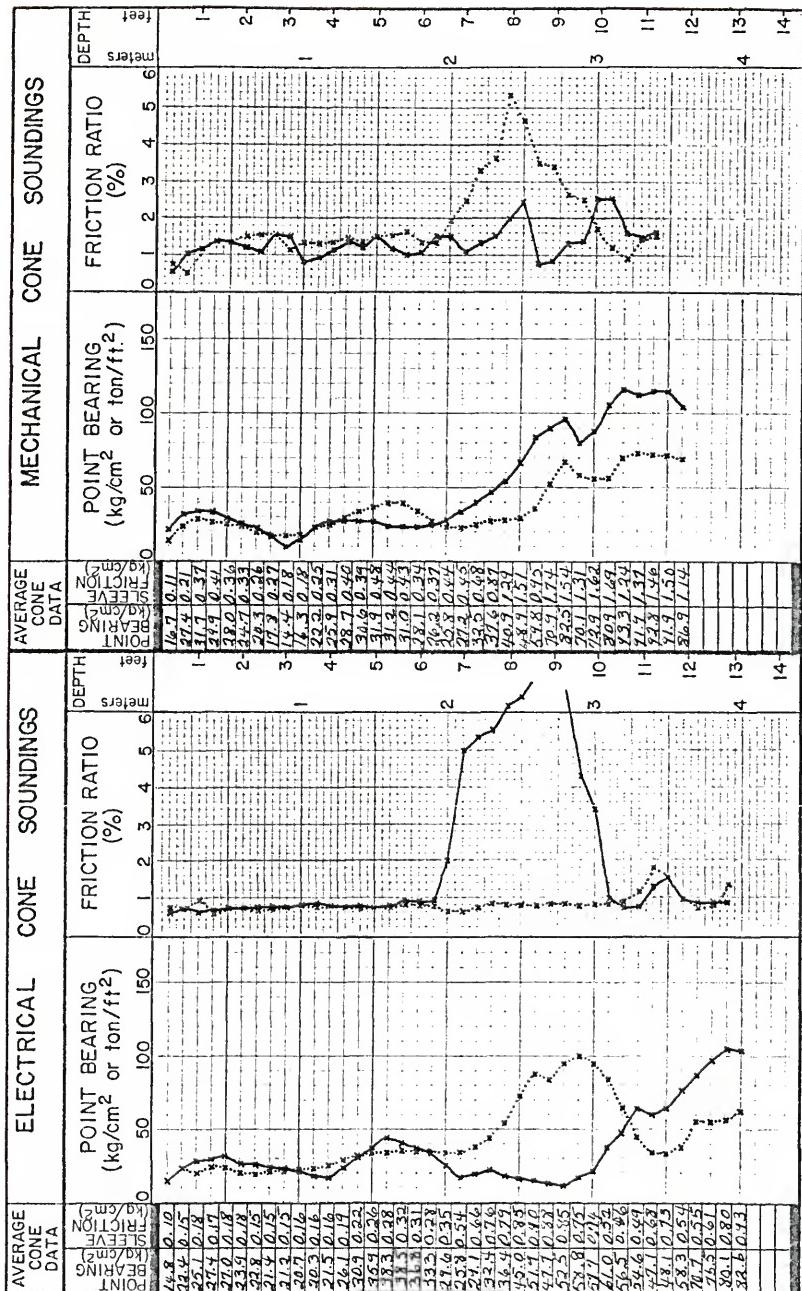


BEVILLE SITE NO 23 CPT LOGS  
FIGURE B-23

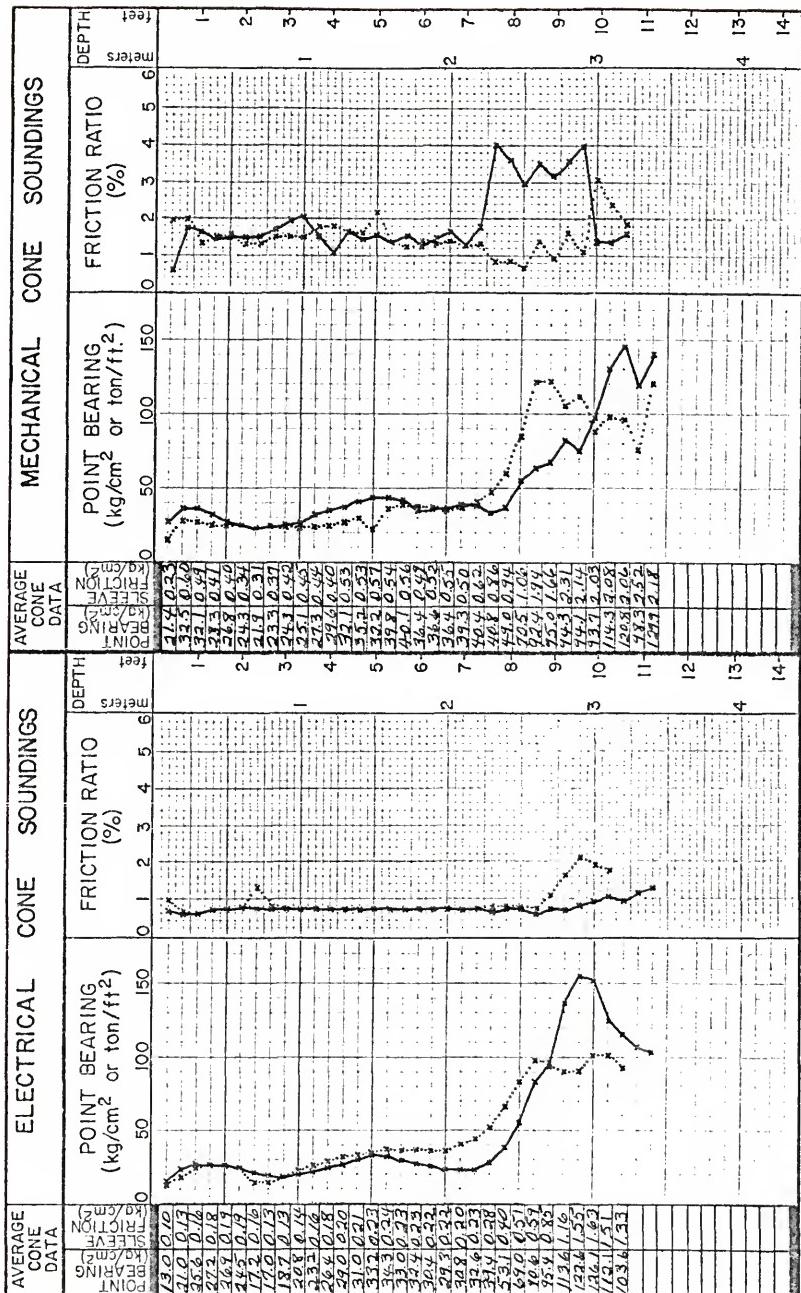


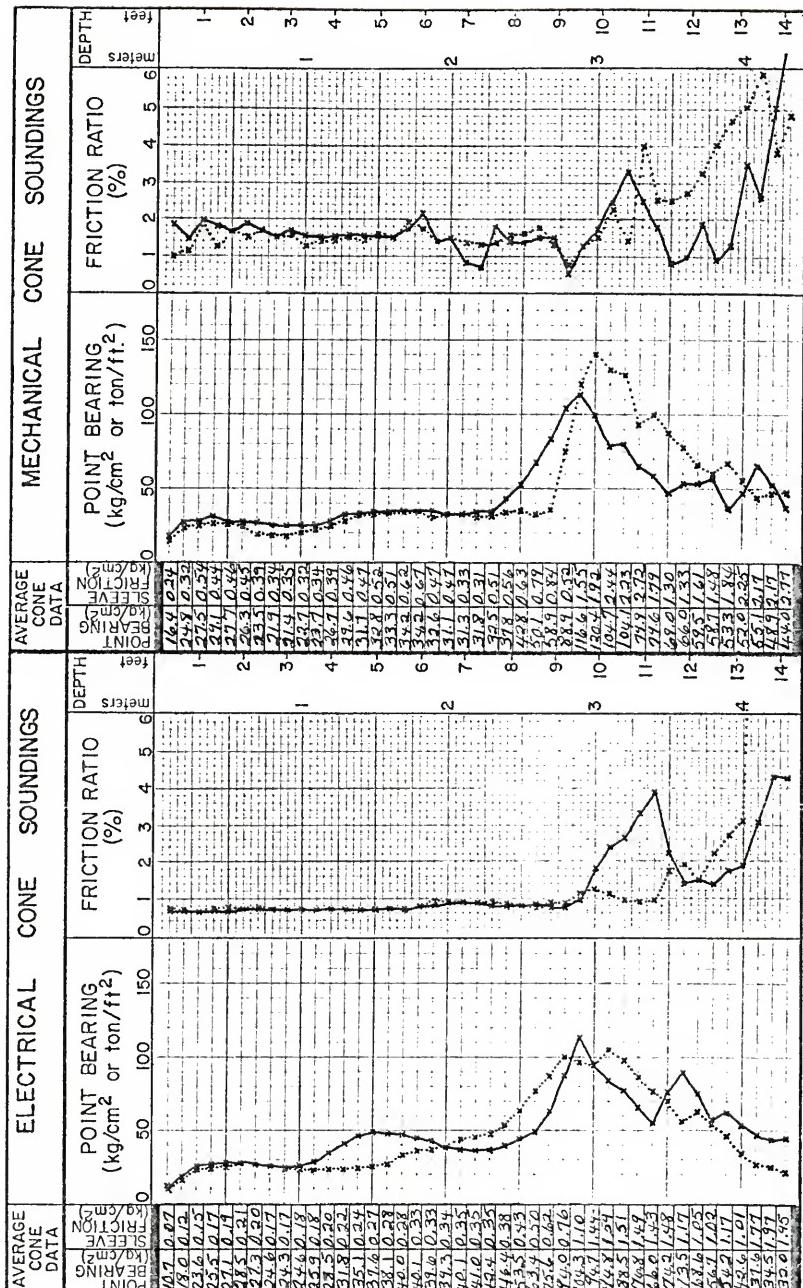


BEVILLE SITE NO 25 CPT LOGS  
FIGURE B-25

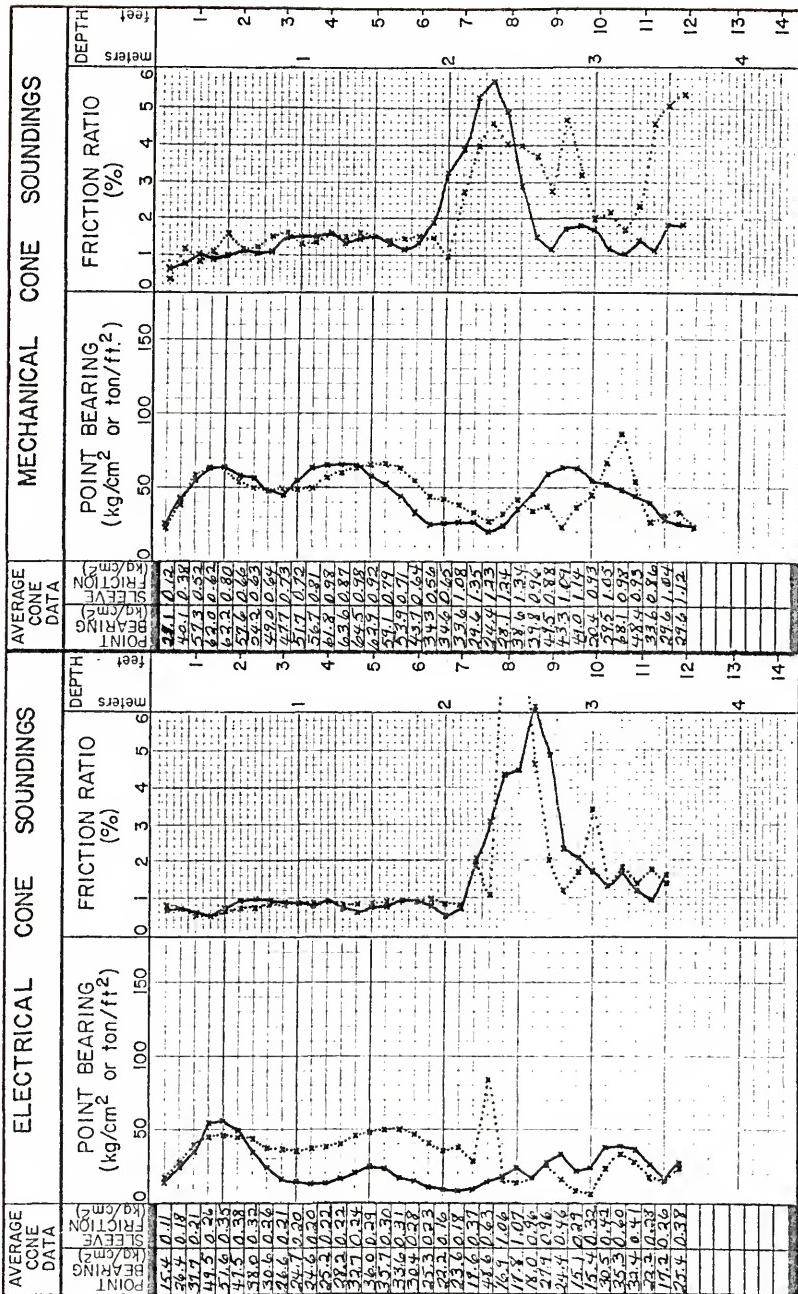


BEVILLE SITE NO 26 CPT LOGS  
FIGURE B-26

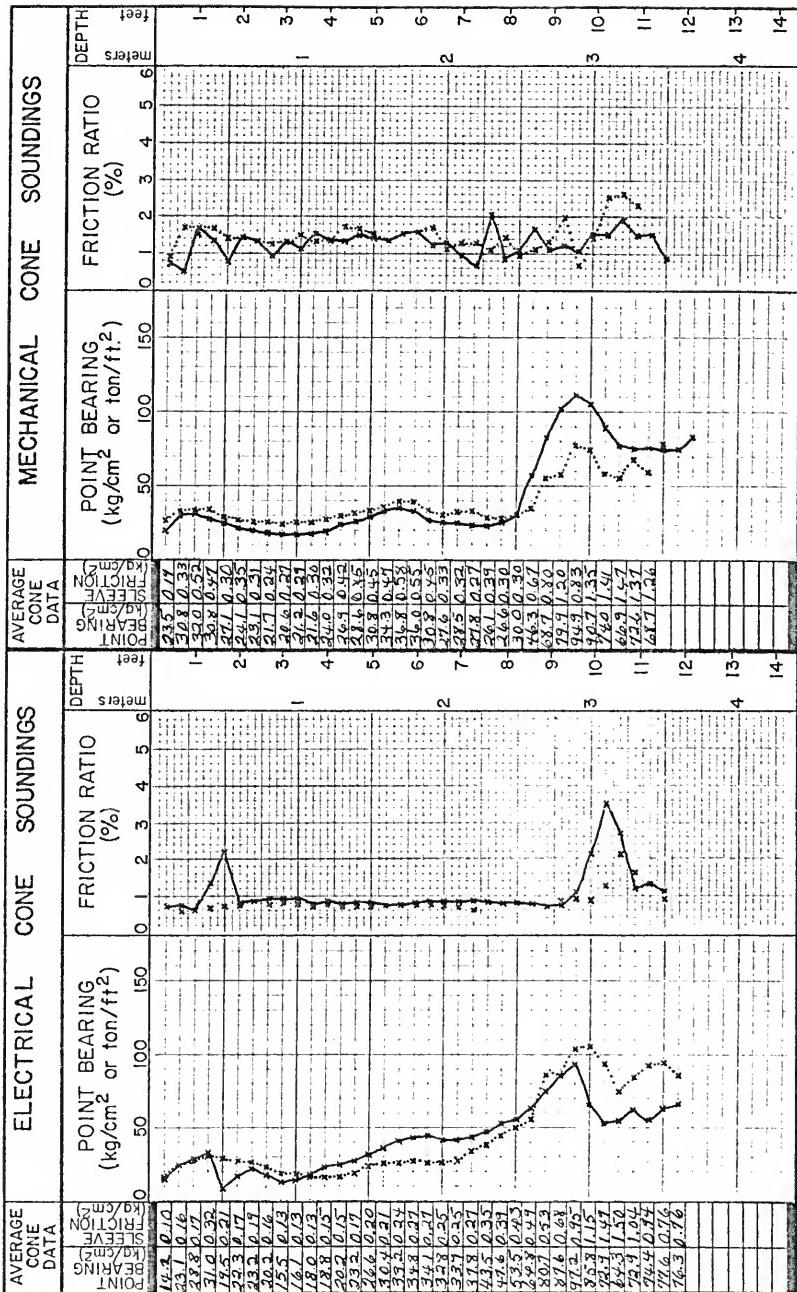




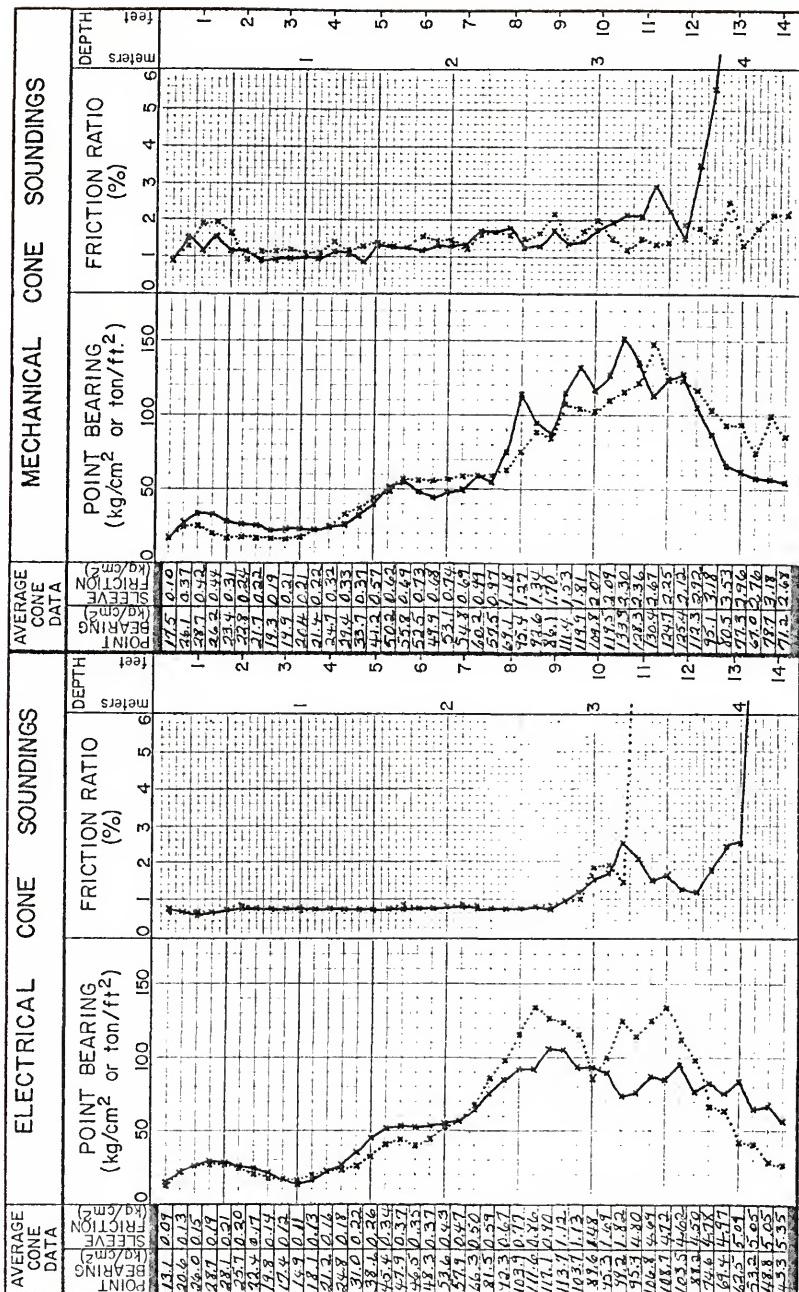
BEVILLE SITE NO. 28 CPT LOGS  
FIGURE B-28



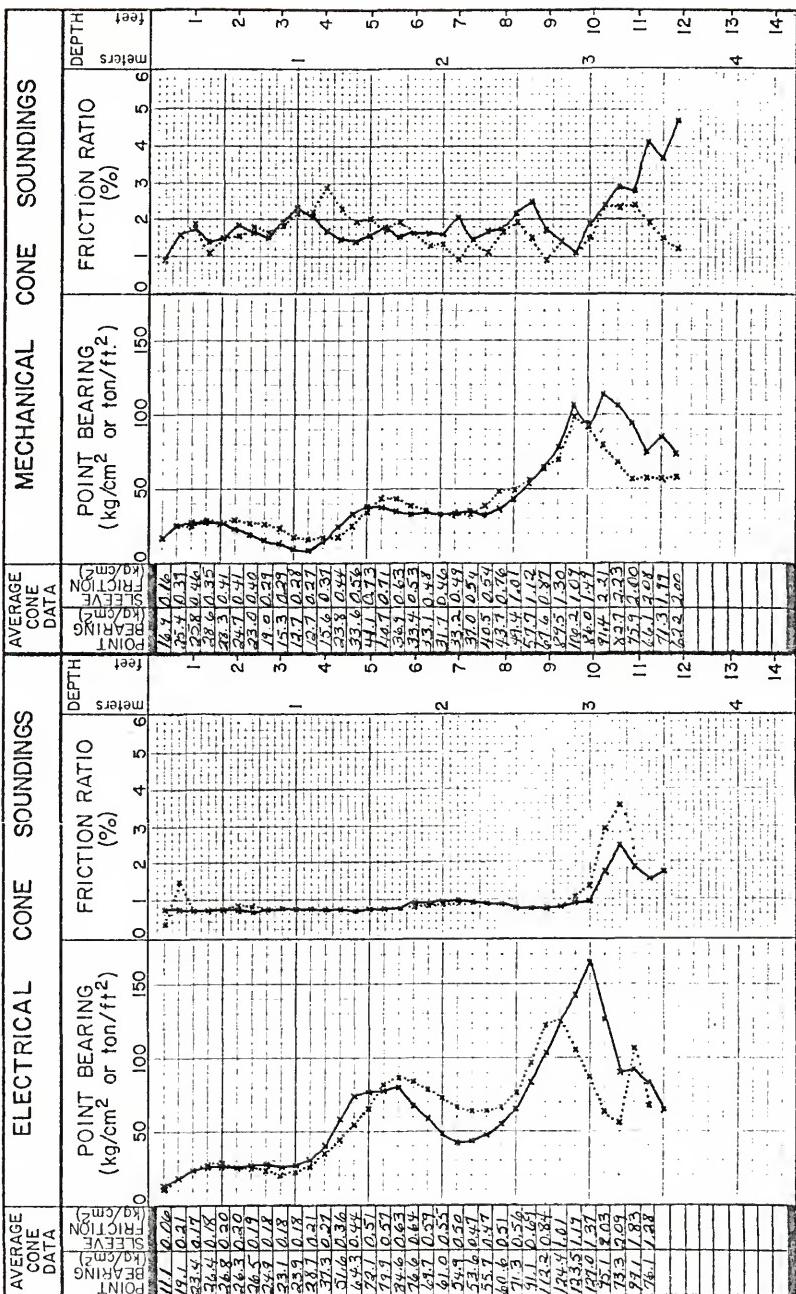
**BEVILLE SITE NO 29 CPT LOGS**  
**FIGURE B-29**



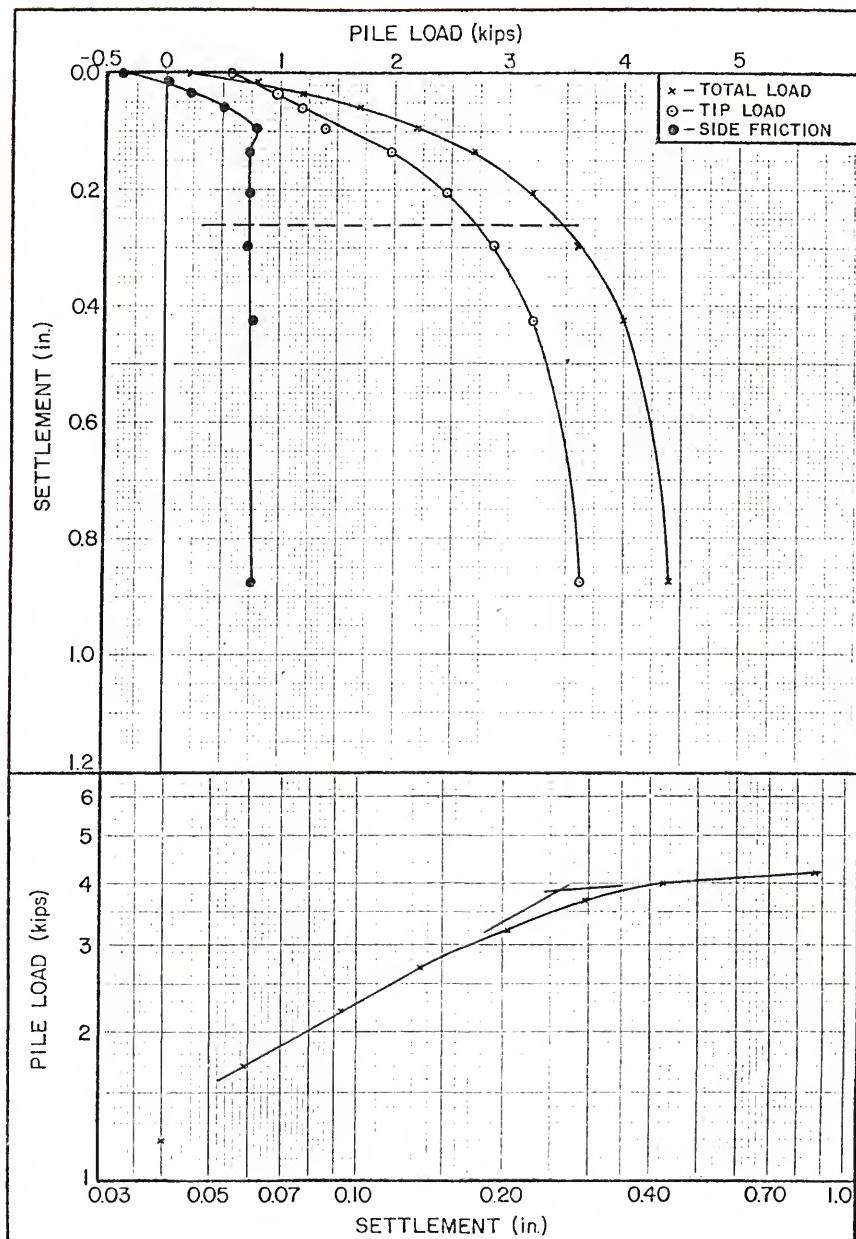
BEVILLE SITE NO 30 CPT LOGS  
FIGURE B-30



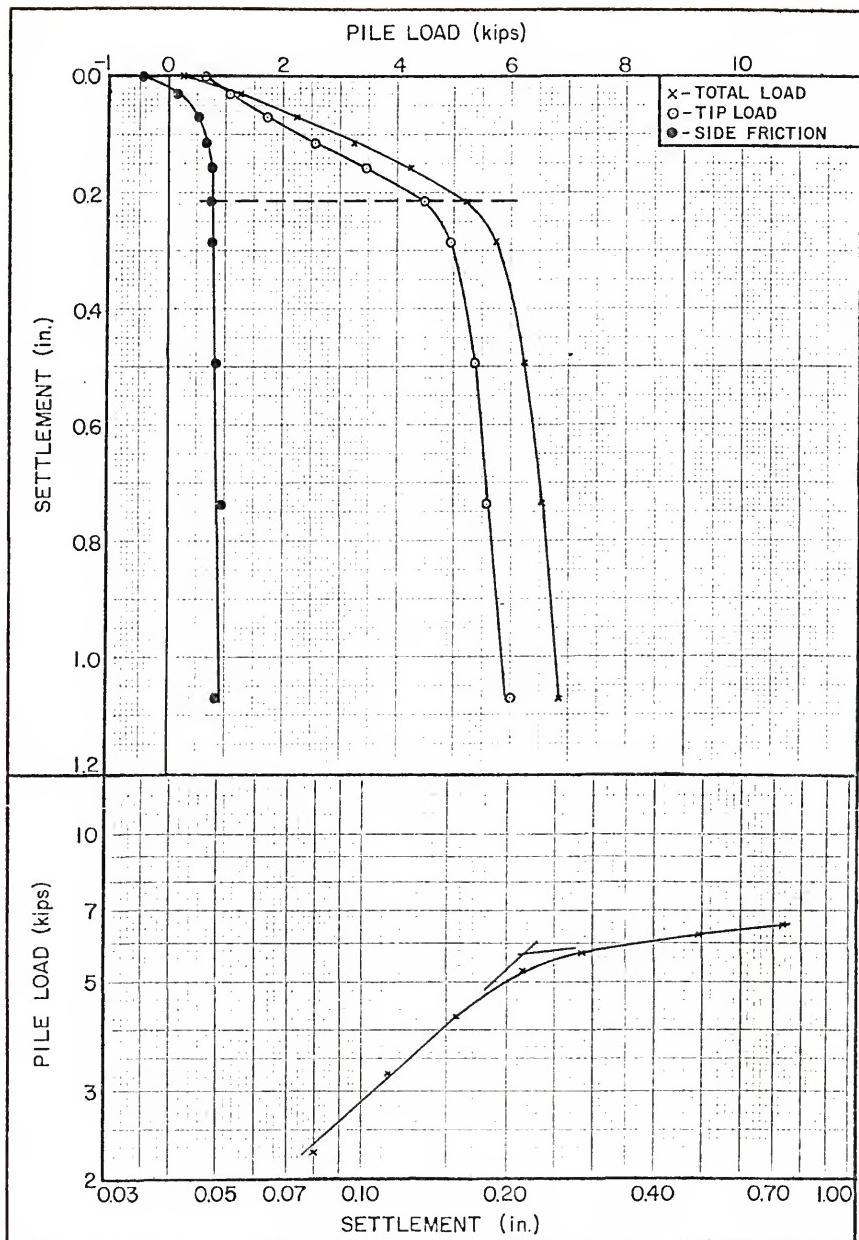
**BEVILLE SITE 31 CPT LOGS**  
**FIGURE B-31**



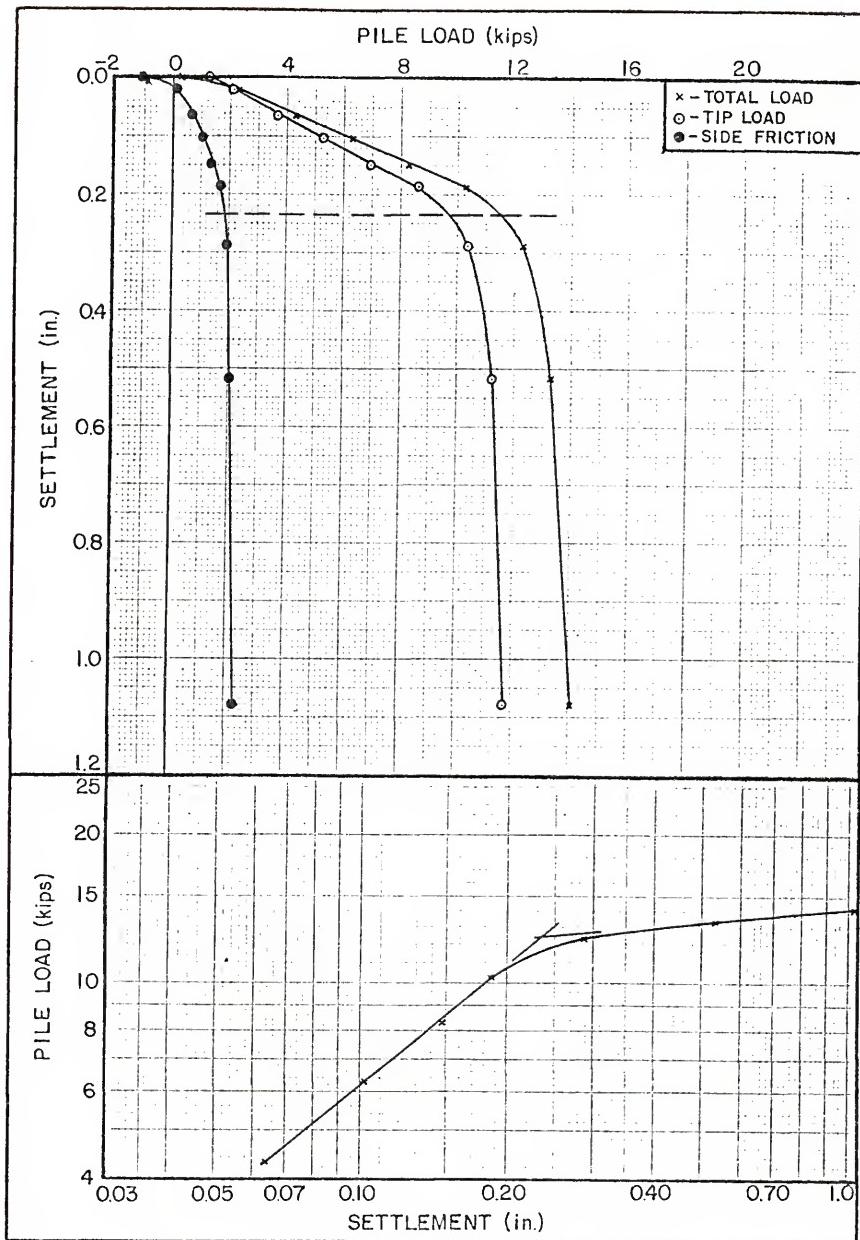
BEVILLE SITE NO 32 CPT LOGS  
FIGURE B-32



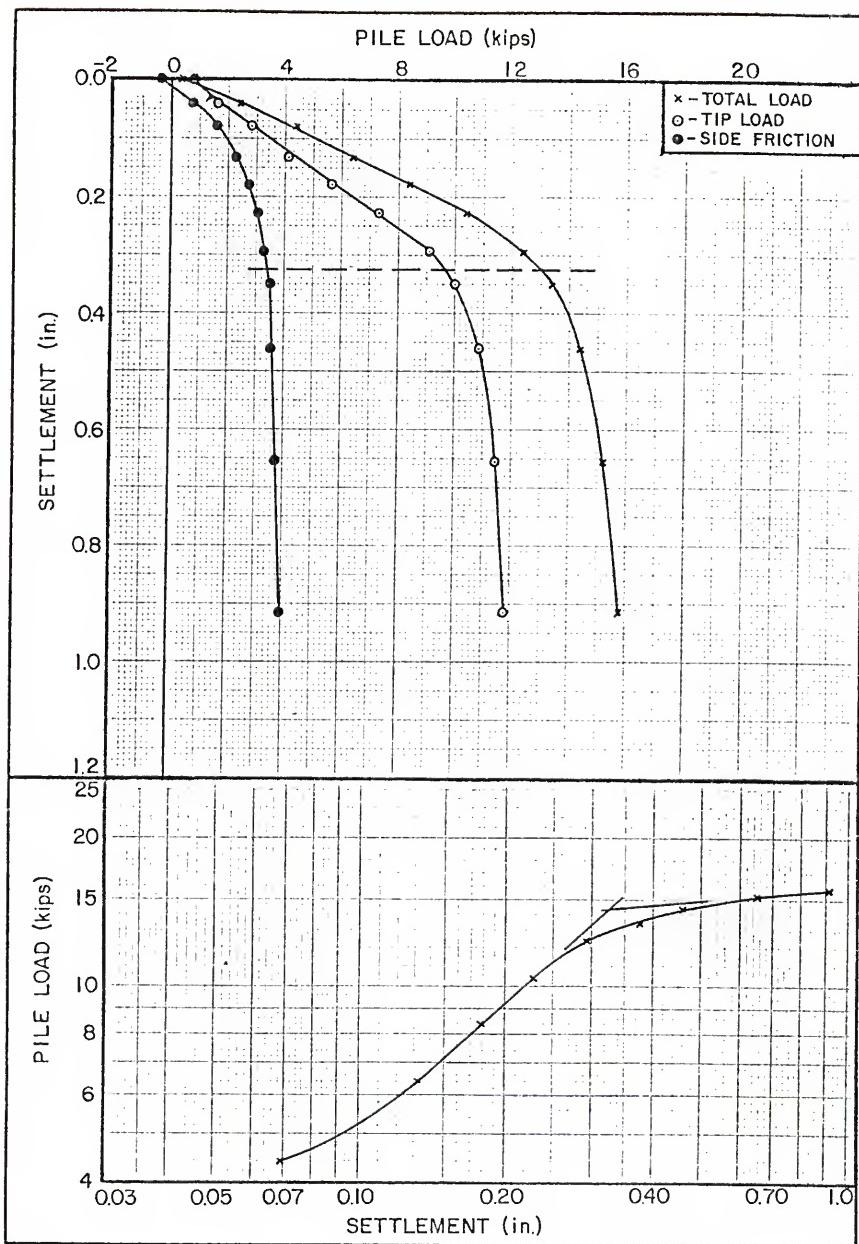
BEVILLE SITE NO 2 PILE LOAD TEST RESULTS - 4.0 FT PIPE PILE  
FIGURE B -33



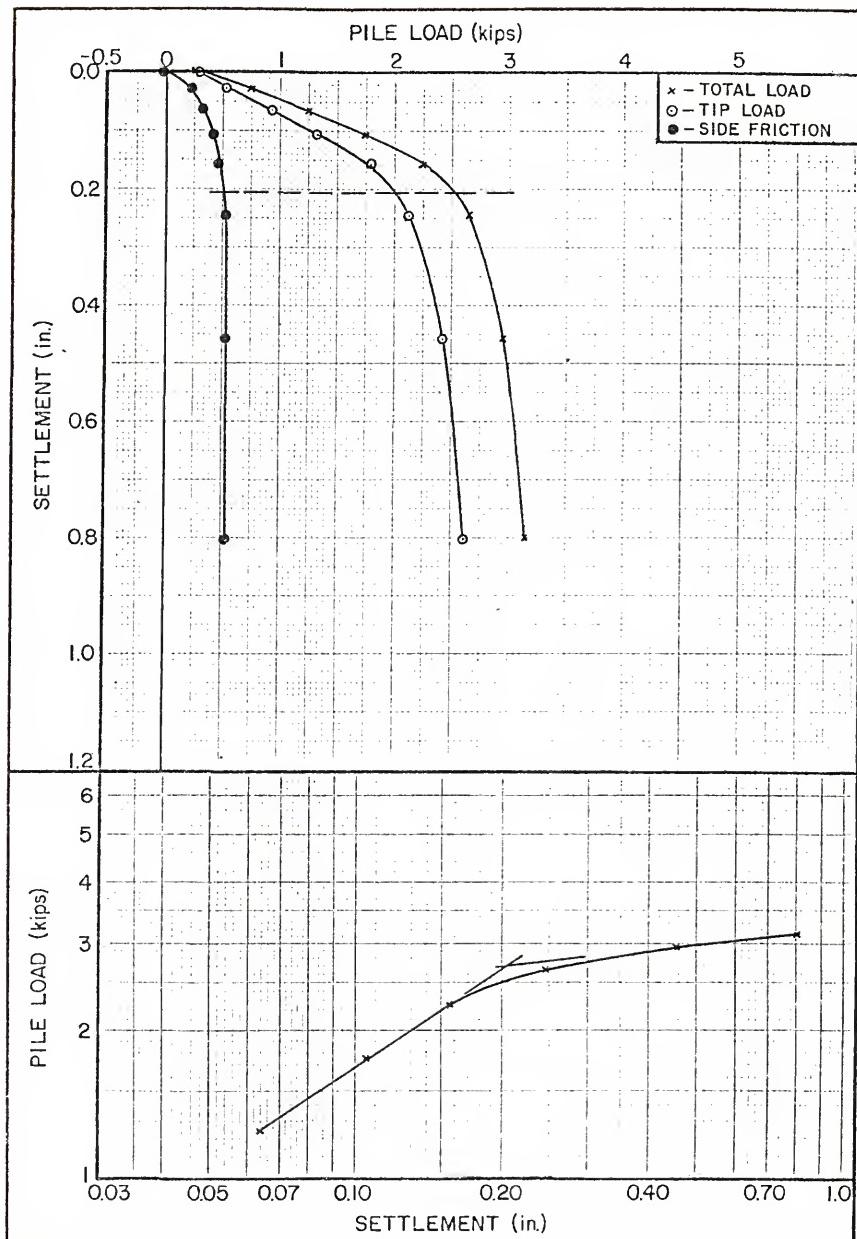
BEVILLE SITE NO 2 PILE LOAD TEST RESULTS - 7.0 FT PIPE PILE  
FIGURE B-34



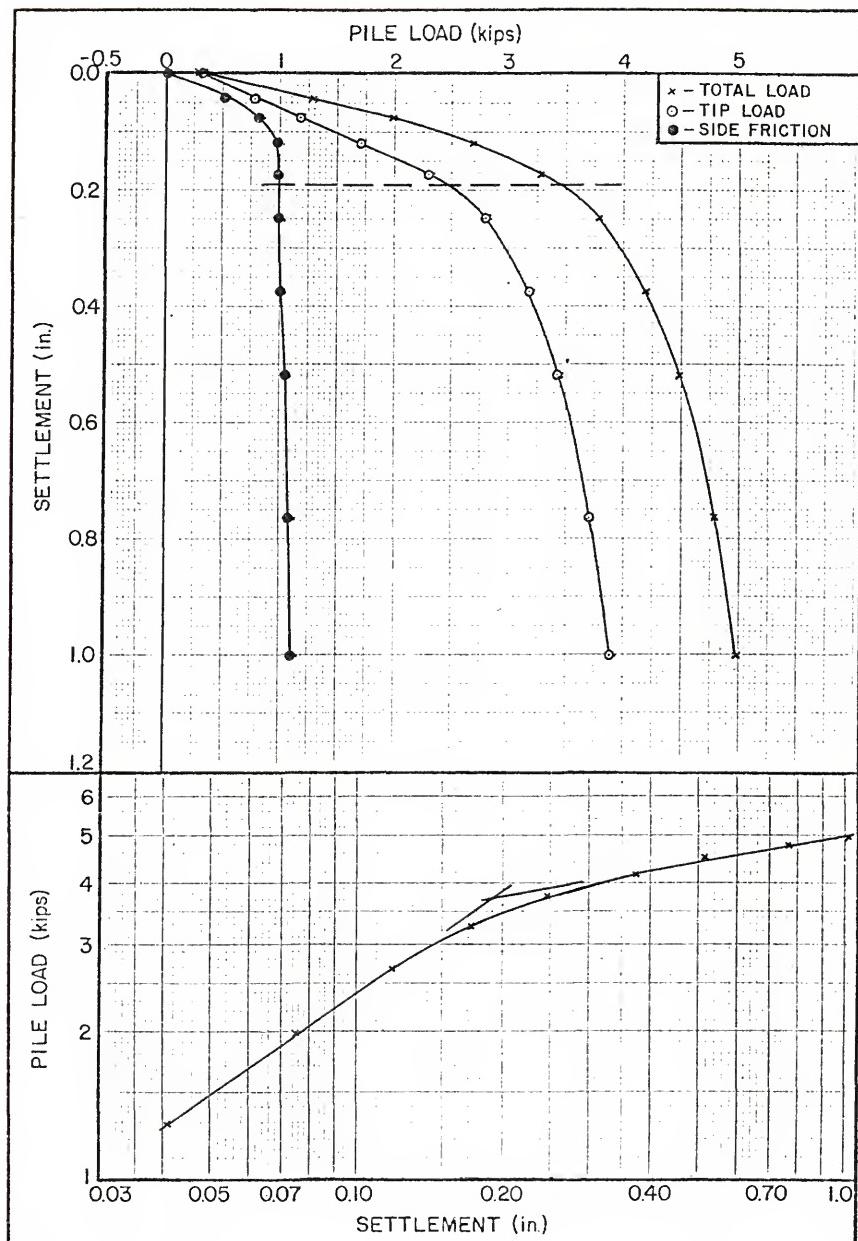
BEVILLE SITE NO 2 PILE LOAD TEST RESULTS - 9.5 FT PIPE PILE  
FIGURE B-35



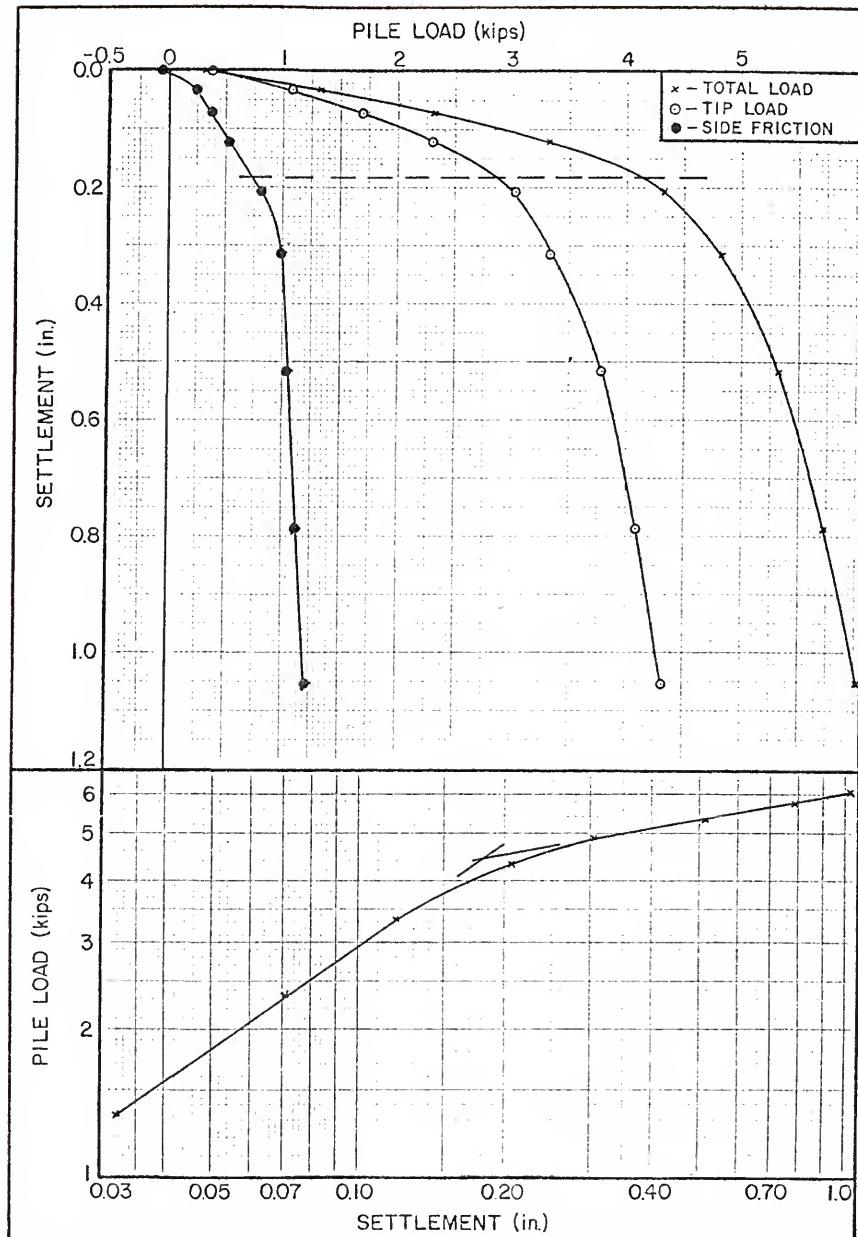
BEVILLE SITE NO 2 PILE LOAD TEST RESULTS - 12.0 FT PIPE PILE  
FIGURE B-36



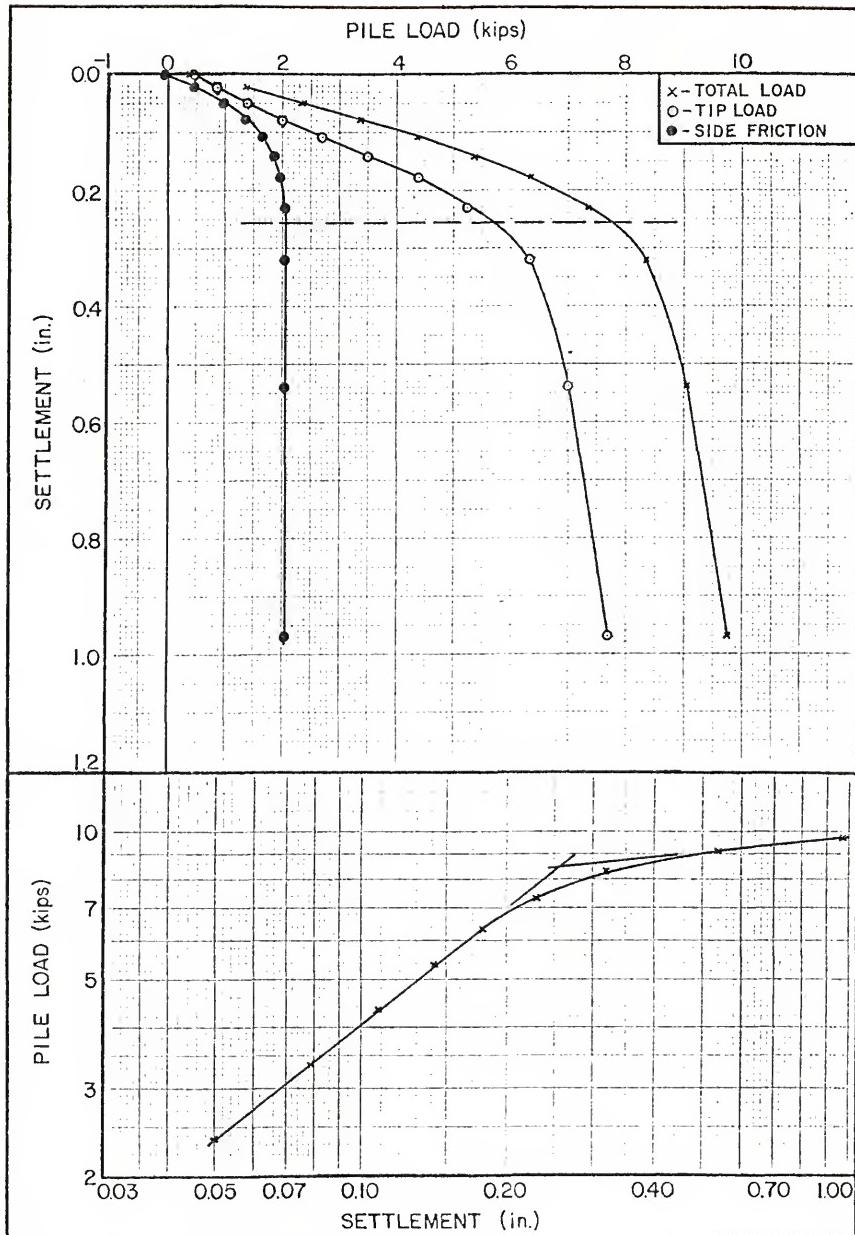
BEVILLE SITE NO 7 PILE LOAD TEST RESULTS - 2.0 FT PIPE PILE  
FIGURE B-37



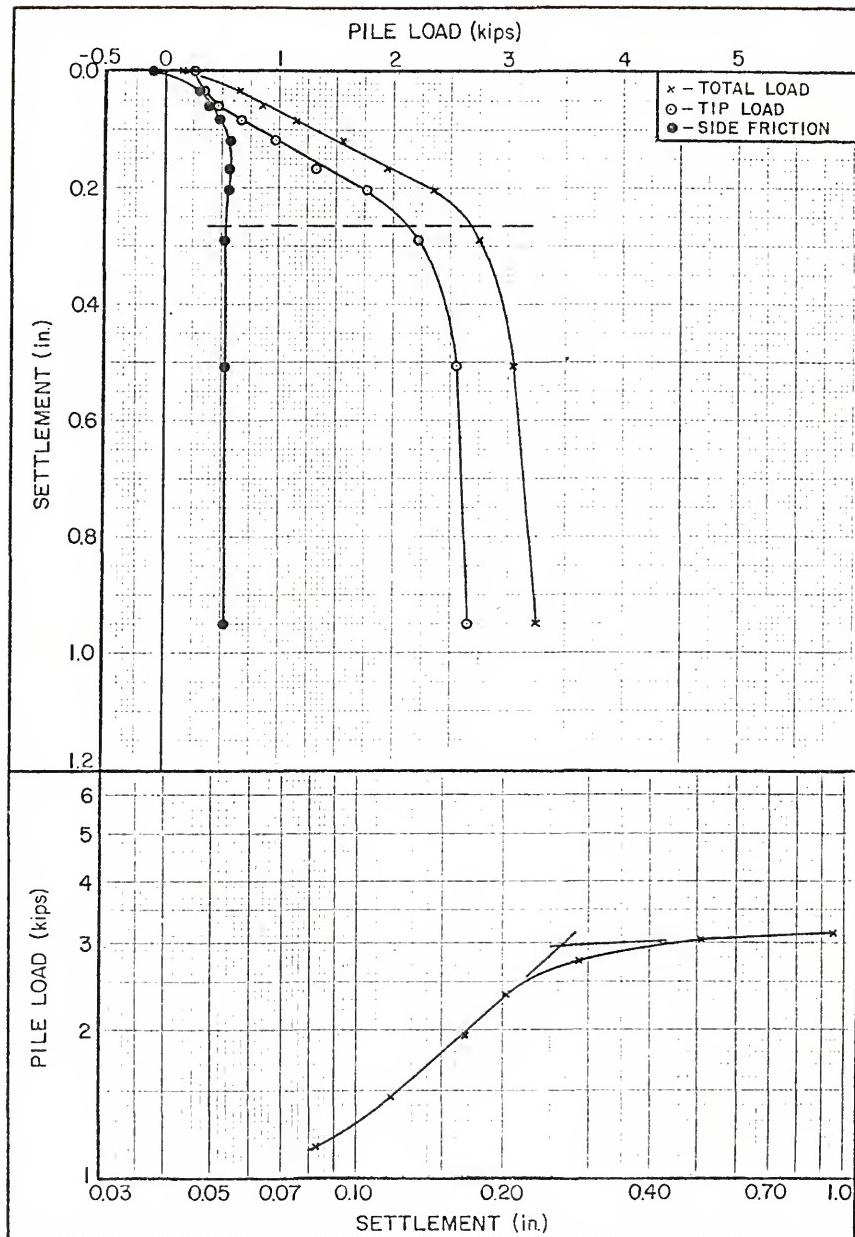
BEVILLE SITE NO 7 PILE LOAD TEST RESULTS - 4.5 FT PIPE PILE  
FIGURE B-38



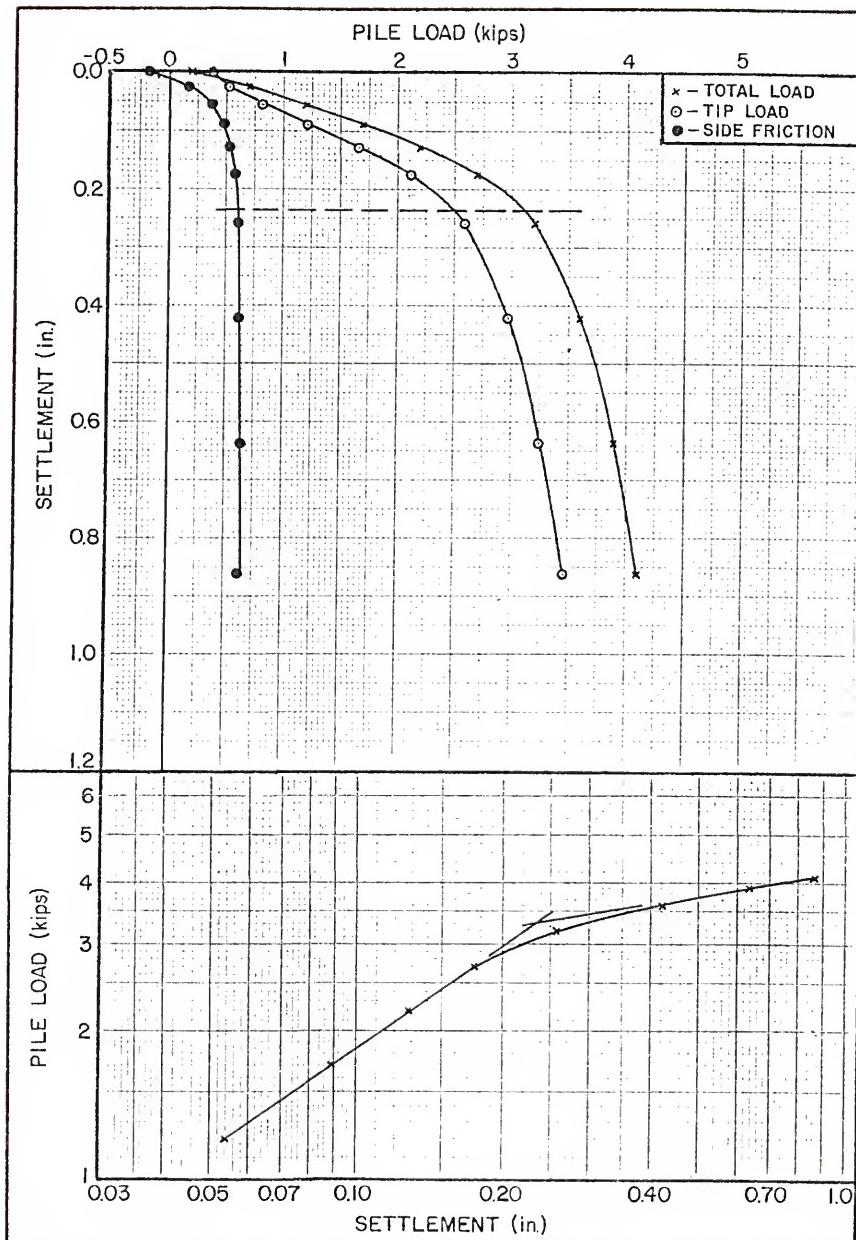
BEVILLE SITE NO 7 PILE LOAD TEST RESULTS - 7.0 FT PIPE PILE  
FIGURE B-39



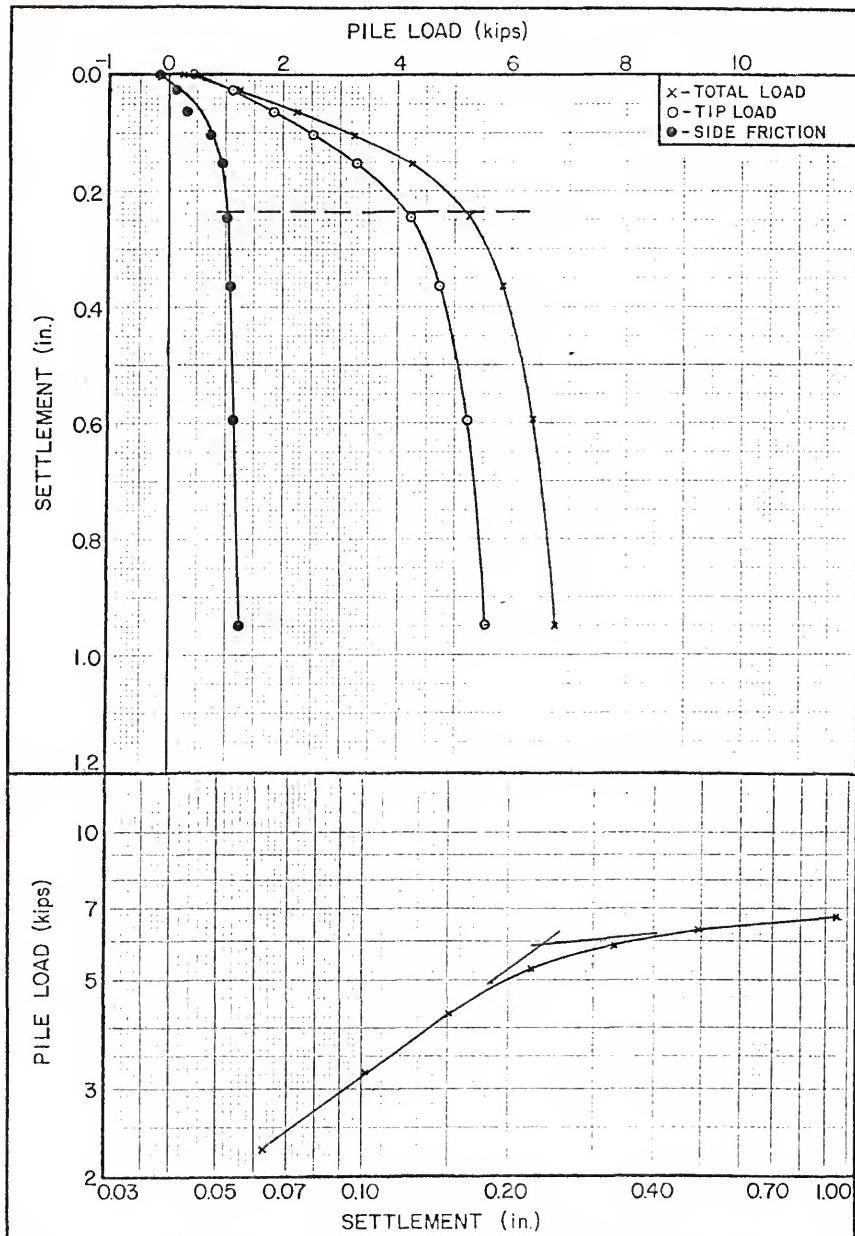
BEVILLE SITE NO 7 PILE LOAD TEST RESULTS - 9.0 FT PIPE PILE  
FIGURE B-40



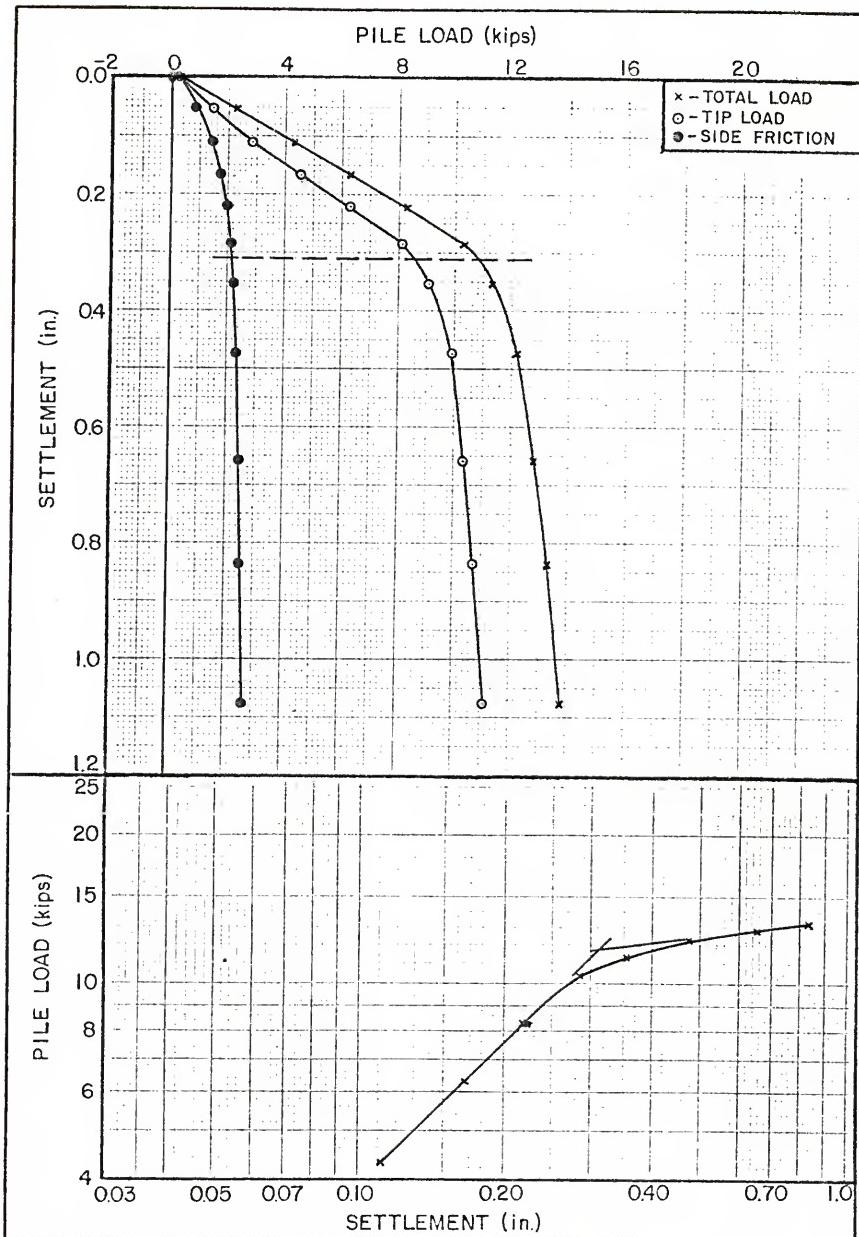
BEVILLE SITE NO 13 PILE LOAD TEST RESULTS - 2.0 FT PIPE PILE  
FIGURE B-41



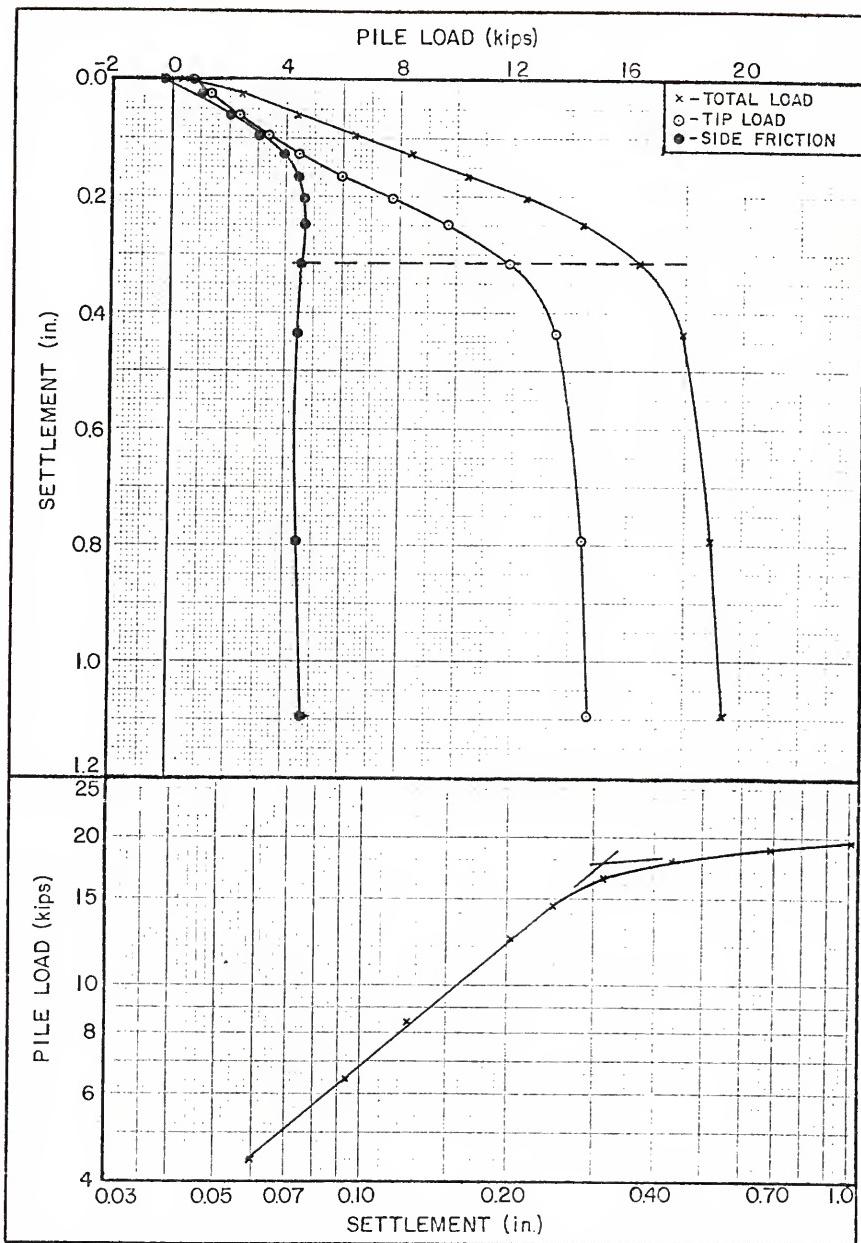
BEVILLE SITE NO 13 PILE LOAD TEST RESULTS - 4.5 FT PIPE PILE  
FIGURE B-42



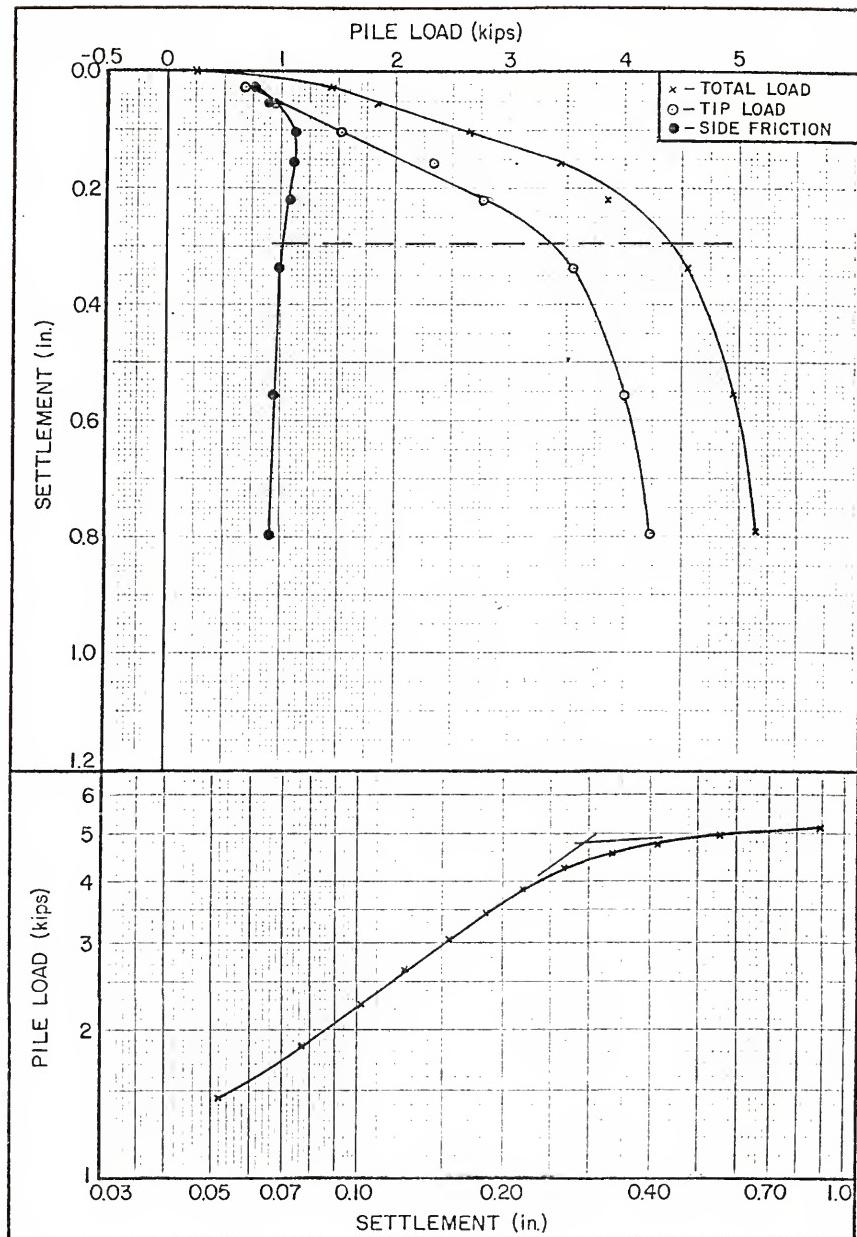
BEVILLE SITE NO 13 PILE LOAD TEST RESULTS - 7.0 FT PIPE PILE  
FIGURE B-43



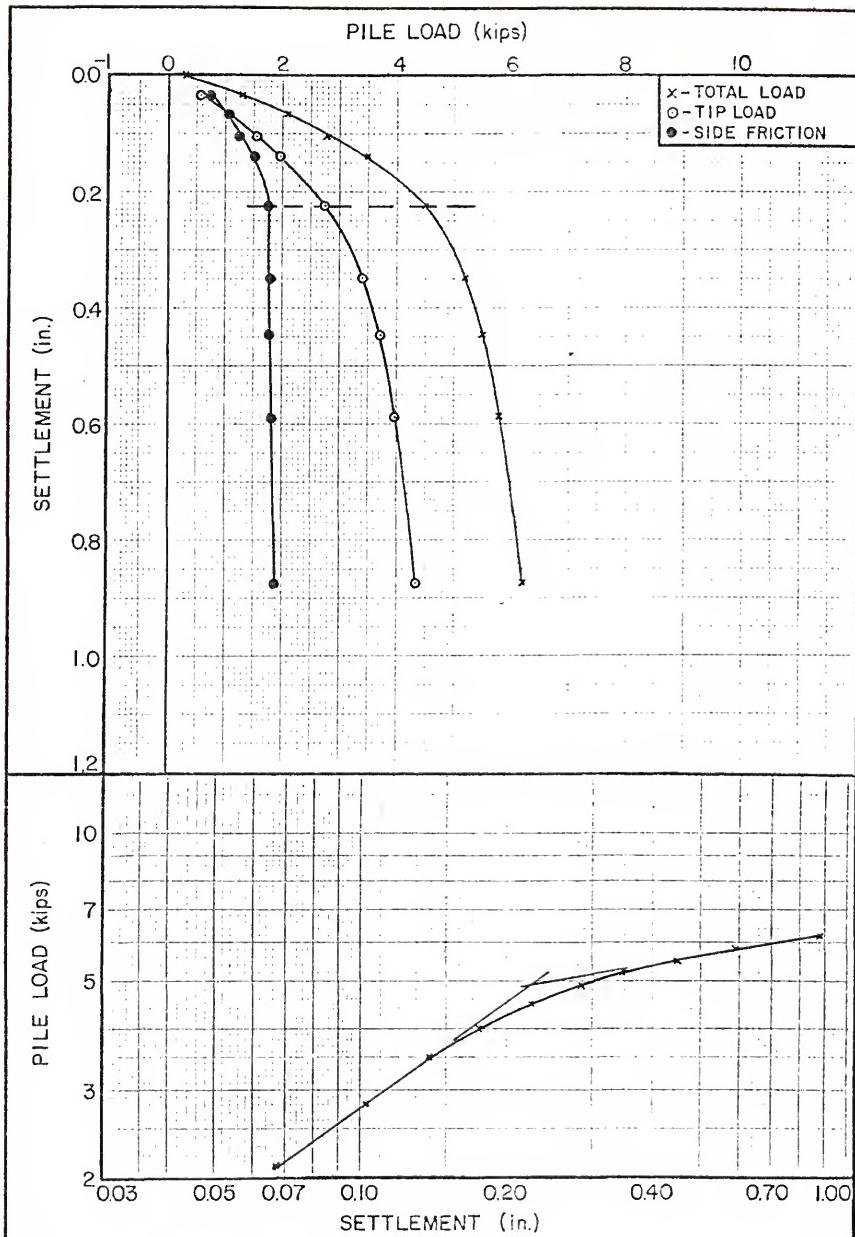
BEVILLE SITE NO 13 PILE LOAD TEST RESULTS - 9.5 FT PIPE PILE  
FIGURE B-44



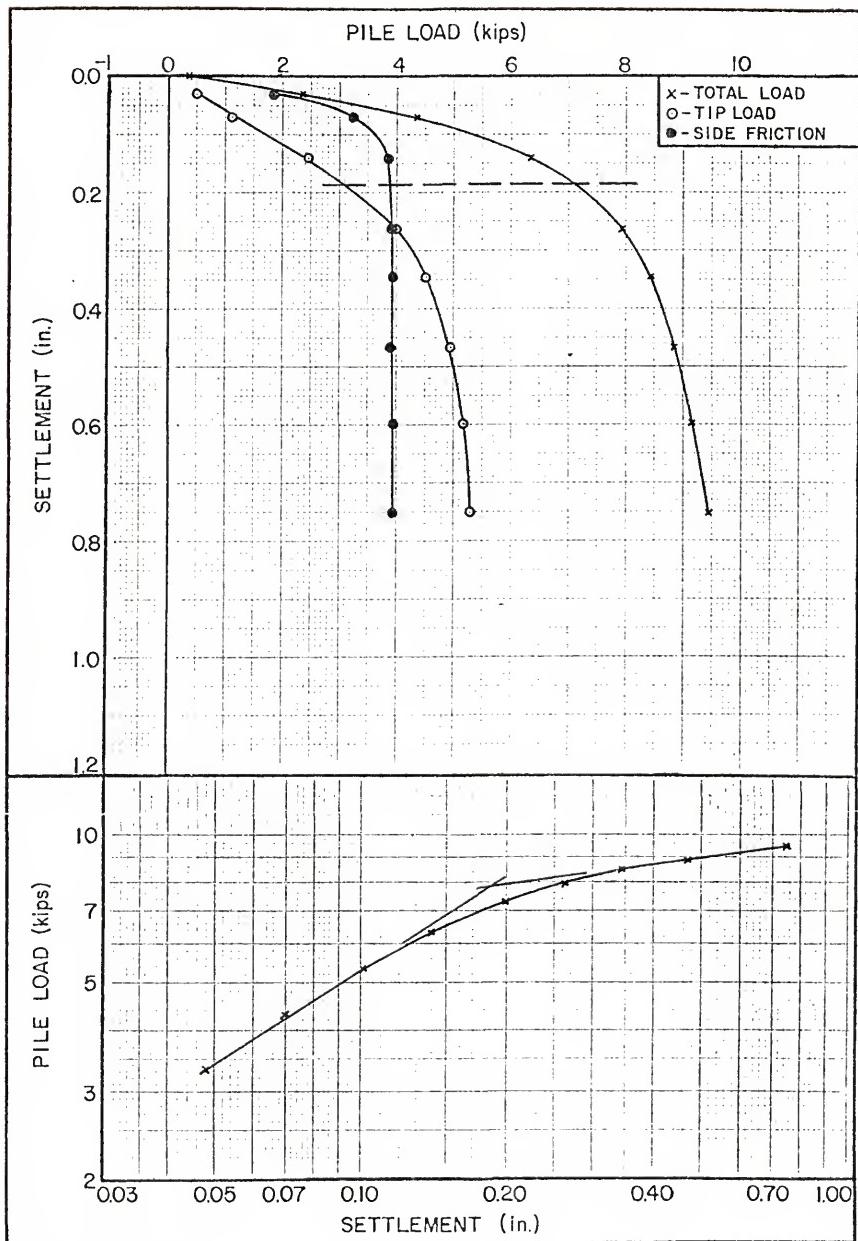
BEVILLE SITE NO 13 PILE LOAD TEST RESULTS - 11.5 FT PIPE PILE  
FIGURE B-45



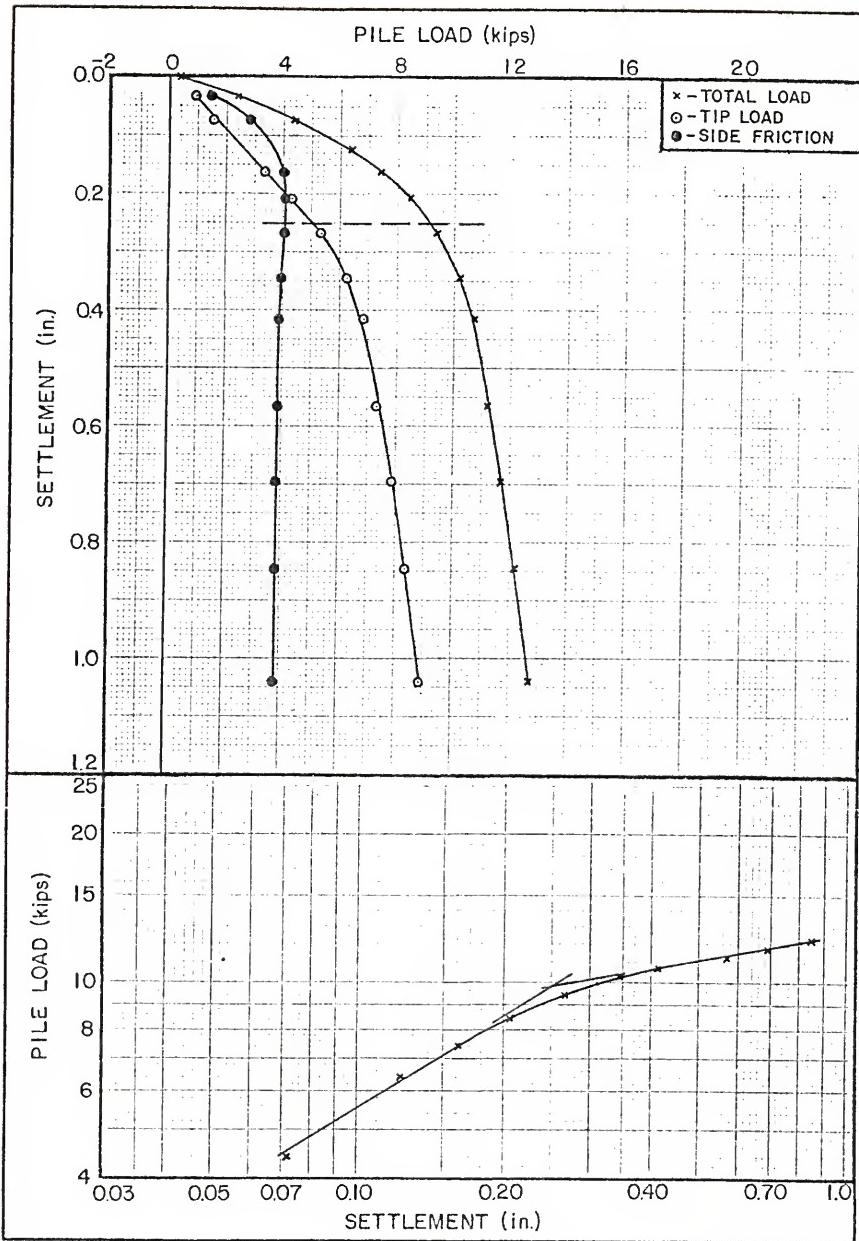
BEVILLE SITE NO 24 PILE LOAD TEST RESULTS - 2.0 FT PIPE PILE  
FIGURE B-46



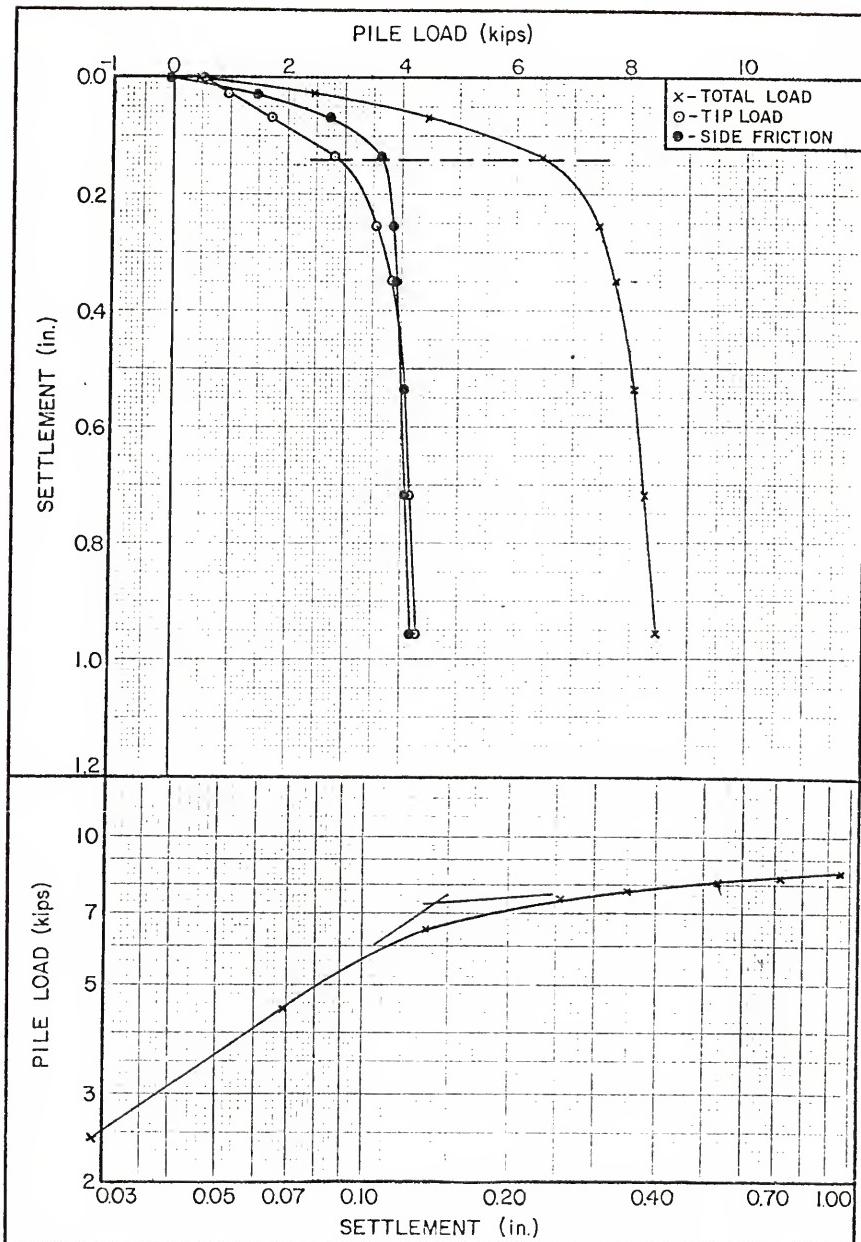
BEVILLE SITE NO 24 PILE LOAD TEST RESULTS - 4.25 FT PIPE PILE  
FIGURE B-47



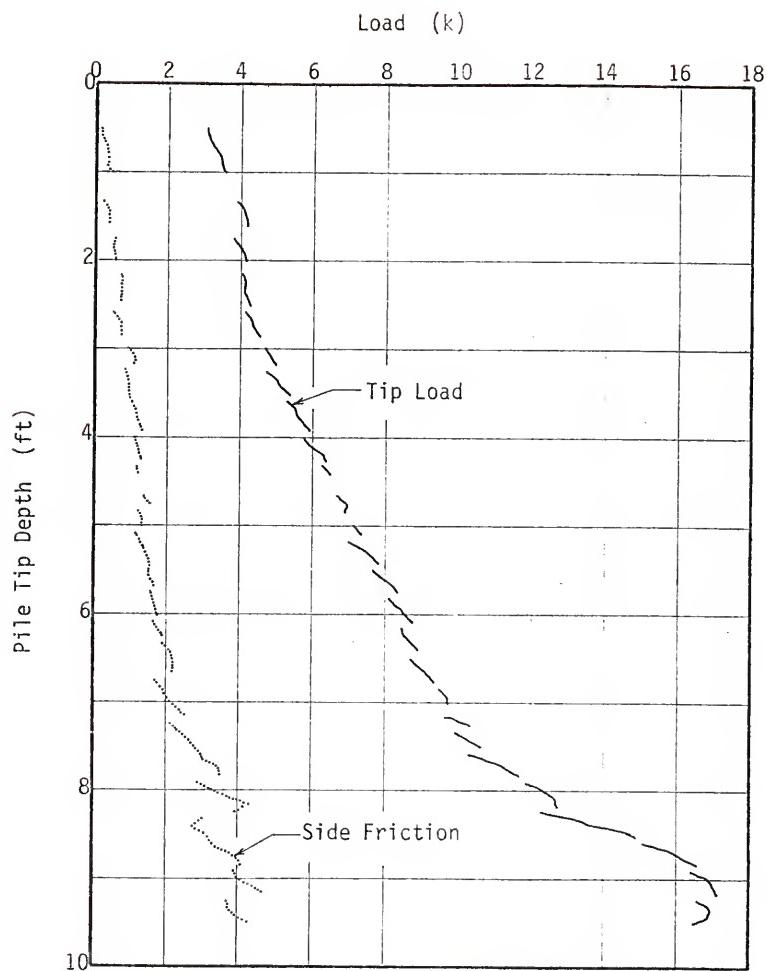
BEVILLE SITE NO 24 PILE LOAD TEST RESULTS - 6.75 FT PIPE PILE  
FIGURE B-48



BEVILLE SITE NO 24 PILE LOAD TEST RESULTS - 9.75 FT PIPE PILE  
FIGURE B-49

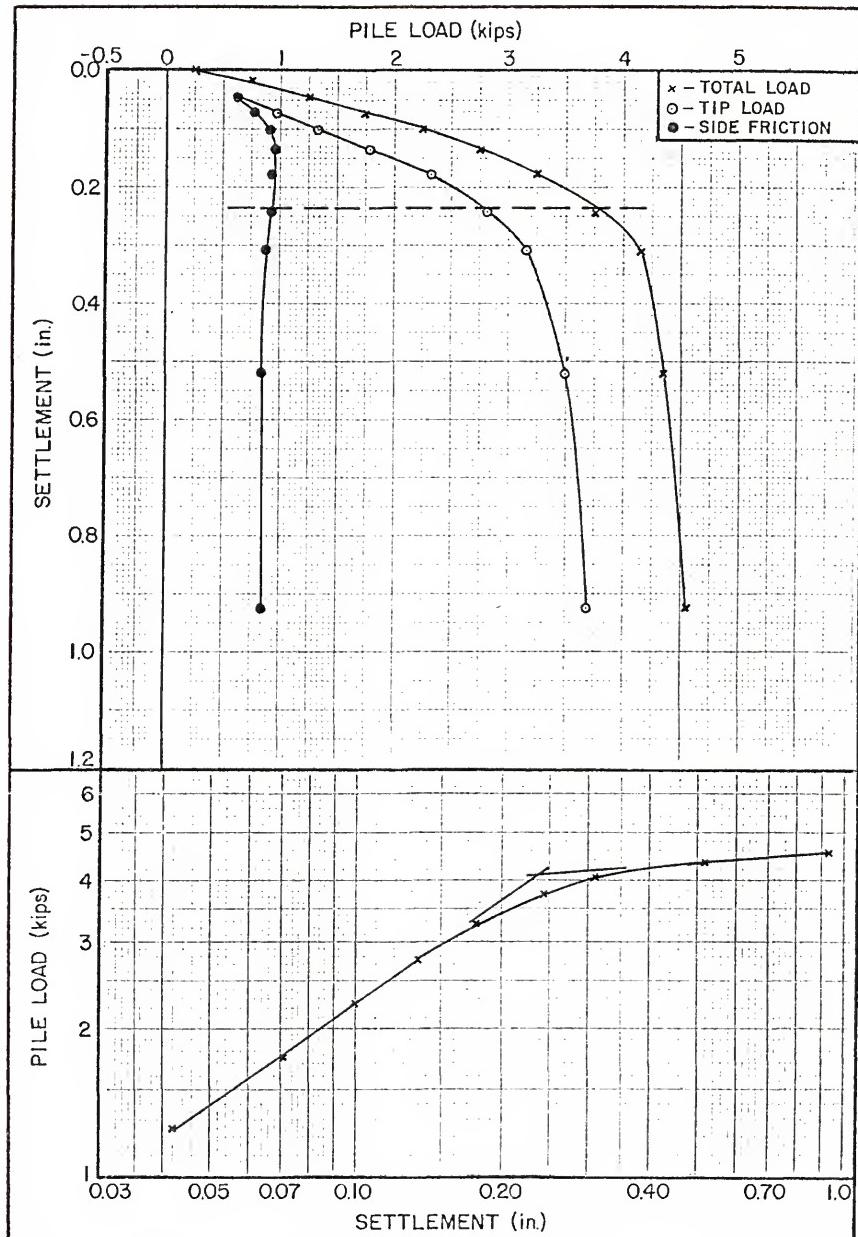


BEVILLE SITE NO 24 PILE LOAD TEST RESULTS - 11.75 FT PIPE PILE  
FIGURE B-50

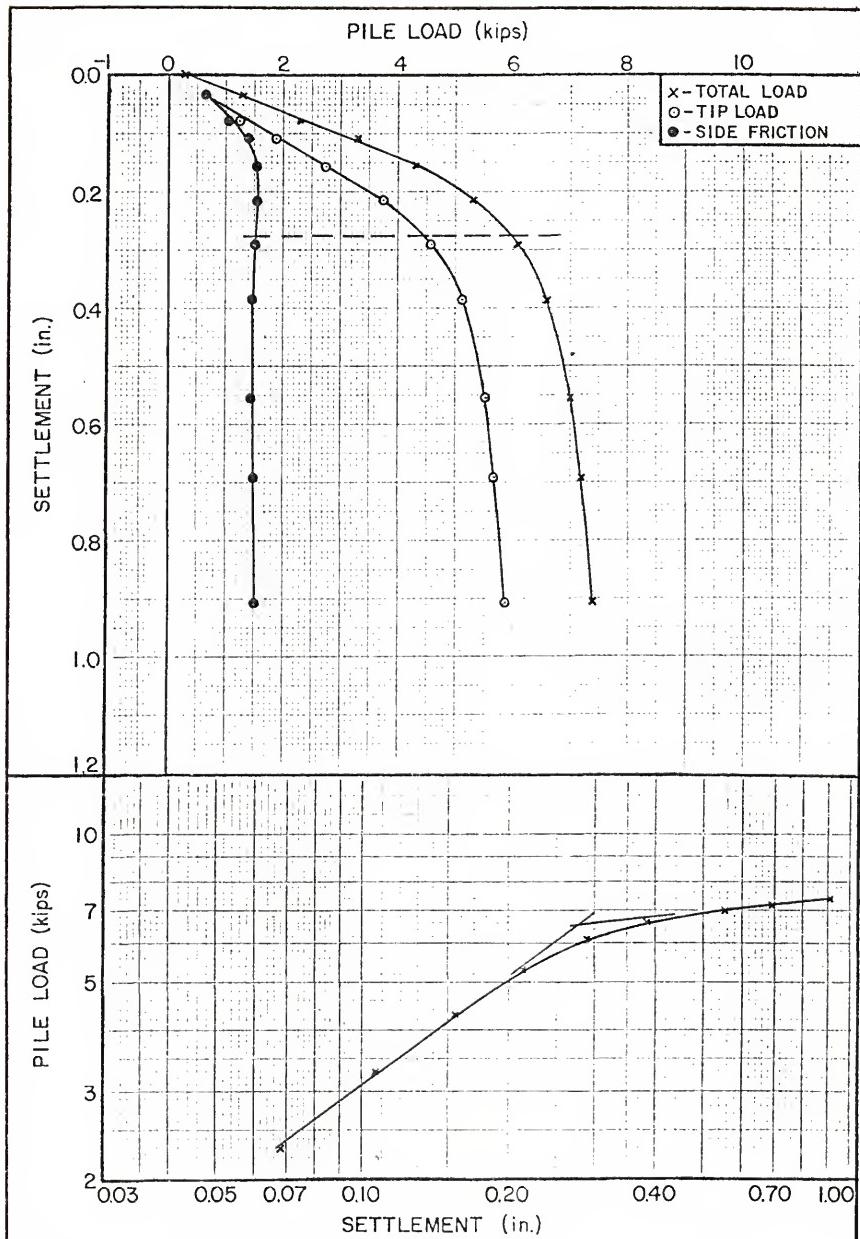


JACK-IN DATA FOR BEVILLE SITE 28 TEST

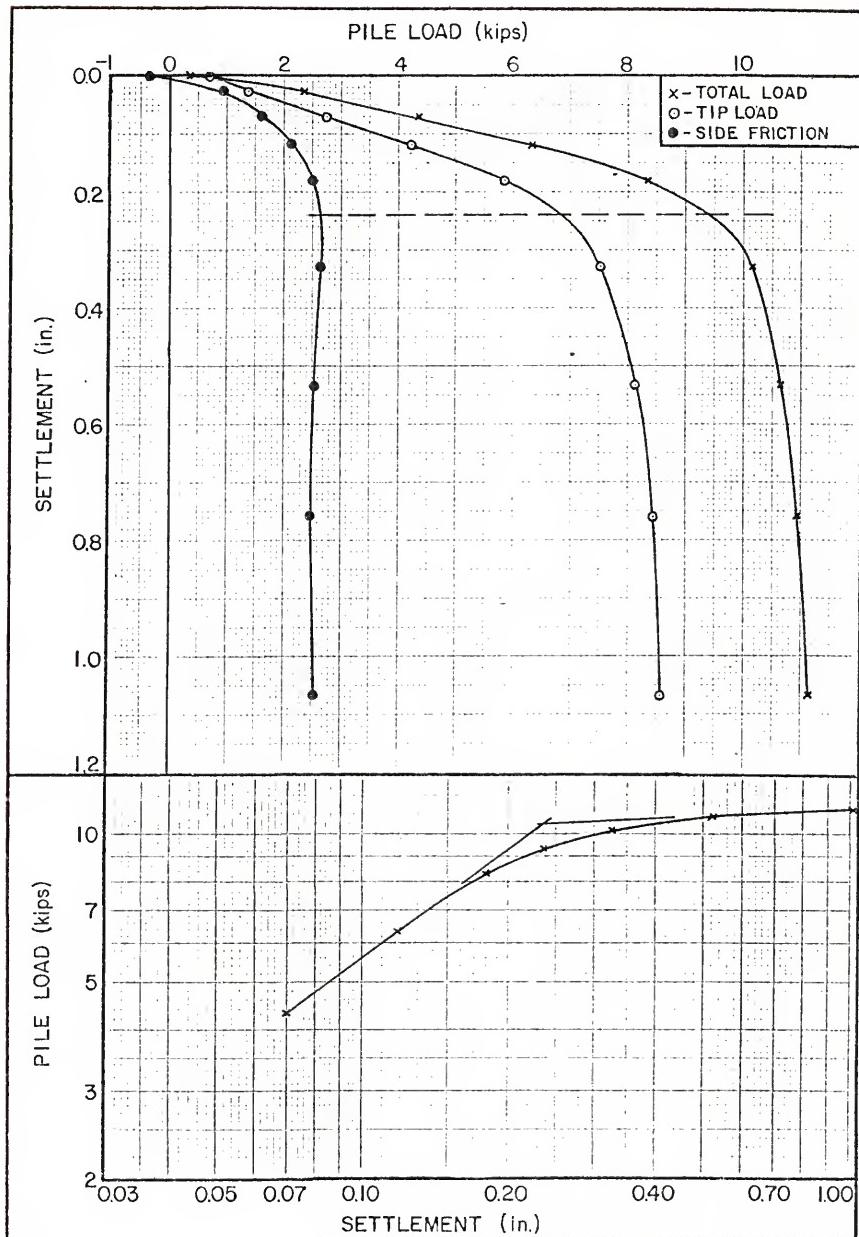
FIGURE B-51



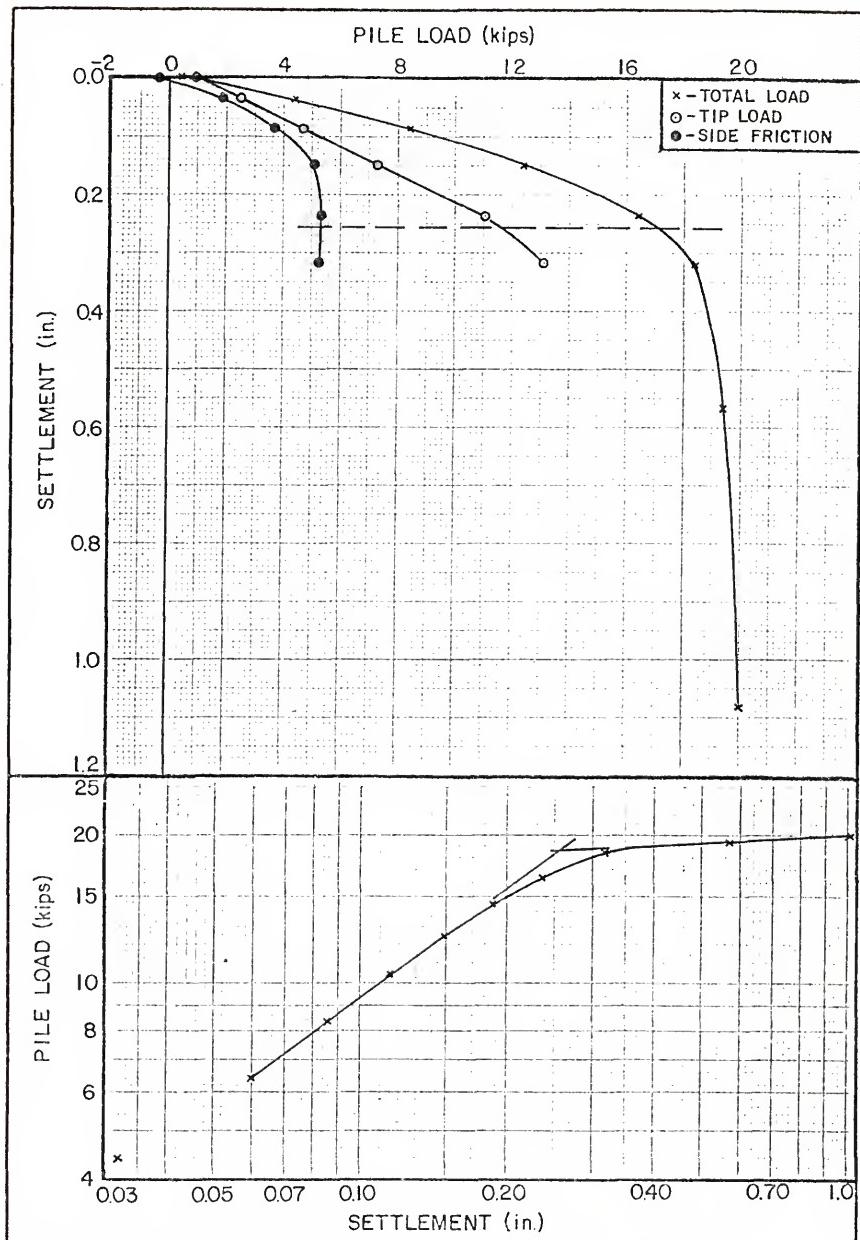
BEVILLE SITE NO 28 PILE LOAD TEST RESULTS - 2.0 FT PIPE PILE  
FIGURE B-52



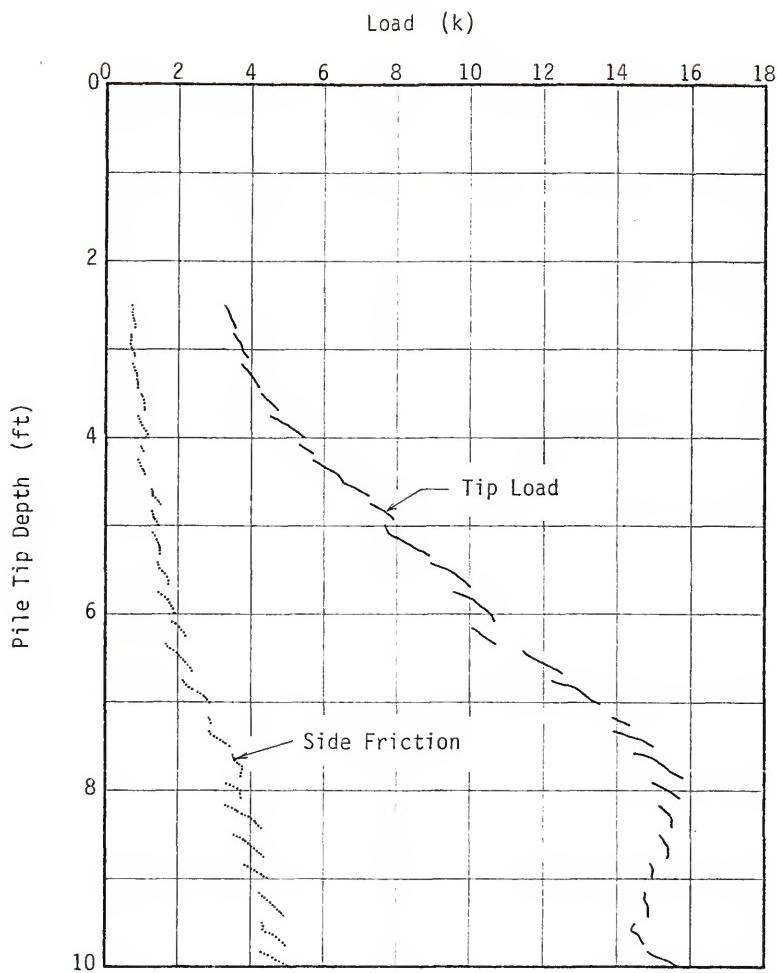
BEVILLE SITE NO 28 PILE LOAD TEST RESULTS - 4.5 FT PIPE PILE  
FIGURE B-53



BEVILLE SITE NO 28 PILE LOAD TEST RESULTS - 7.0 FT PIPE PILE  
FIGURE B-54

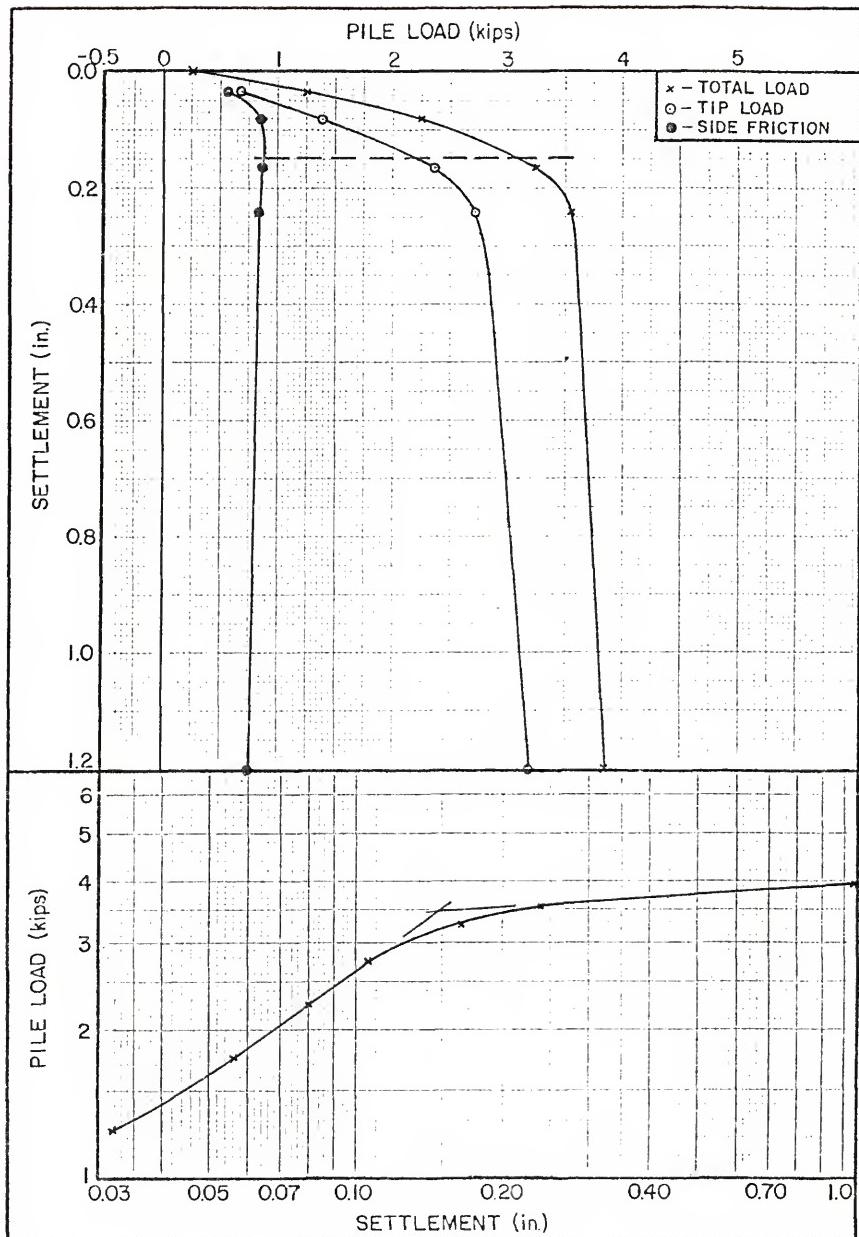


BEVILLE SITE NO 28 PILE LOAD TEST RESULTS - 9.5 FT PIPE PILE  
FIGURE B-55

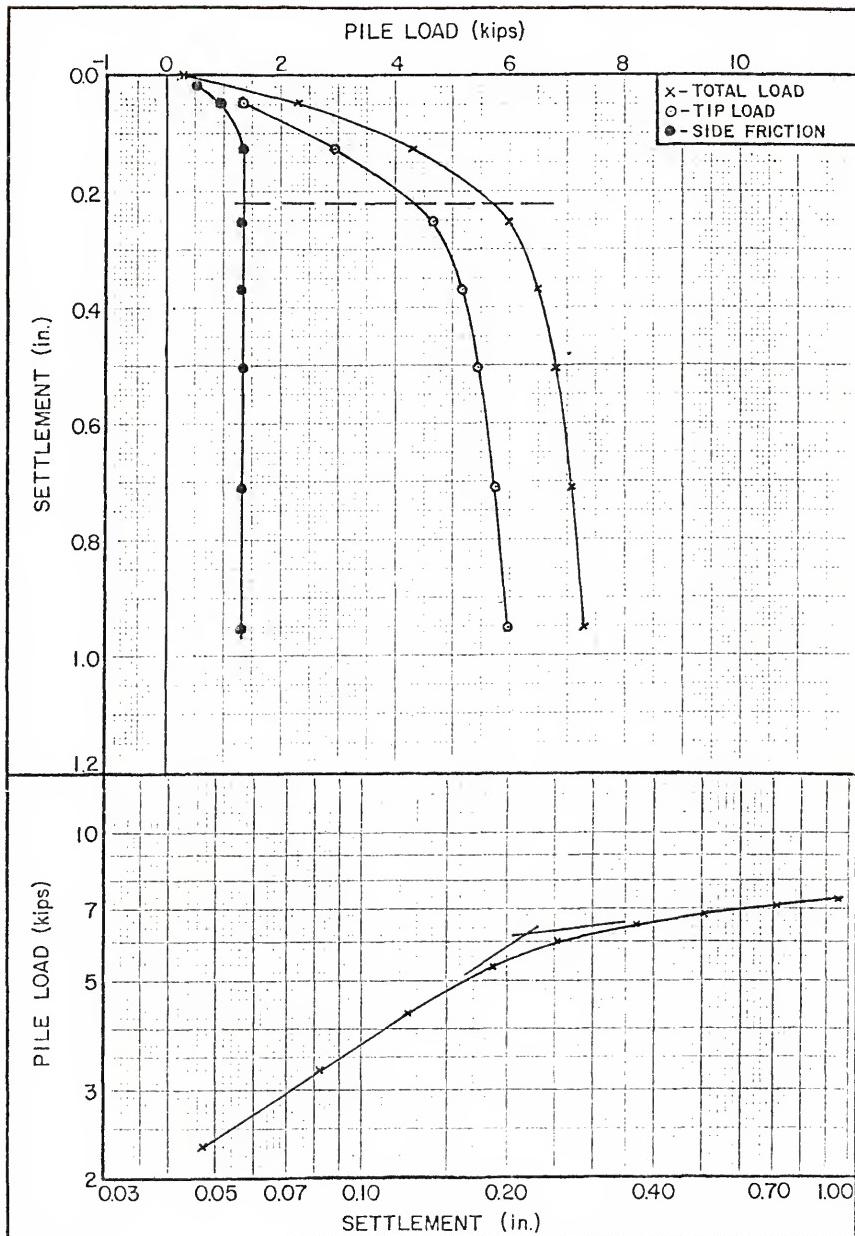


JACK-IN DATA FOR BEVILLE SITE 31 TEST

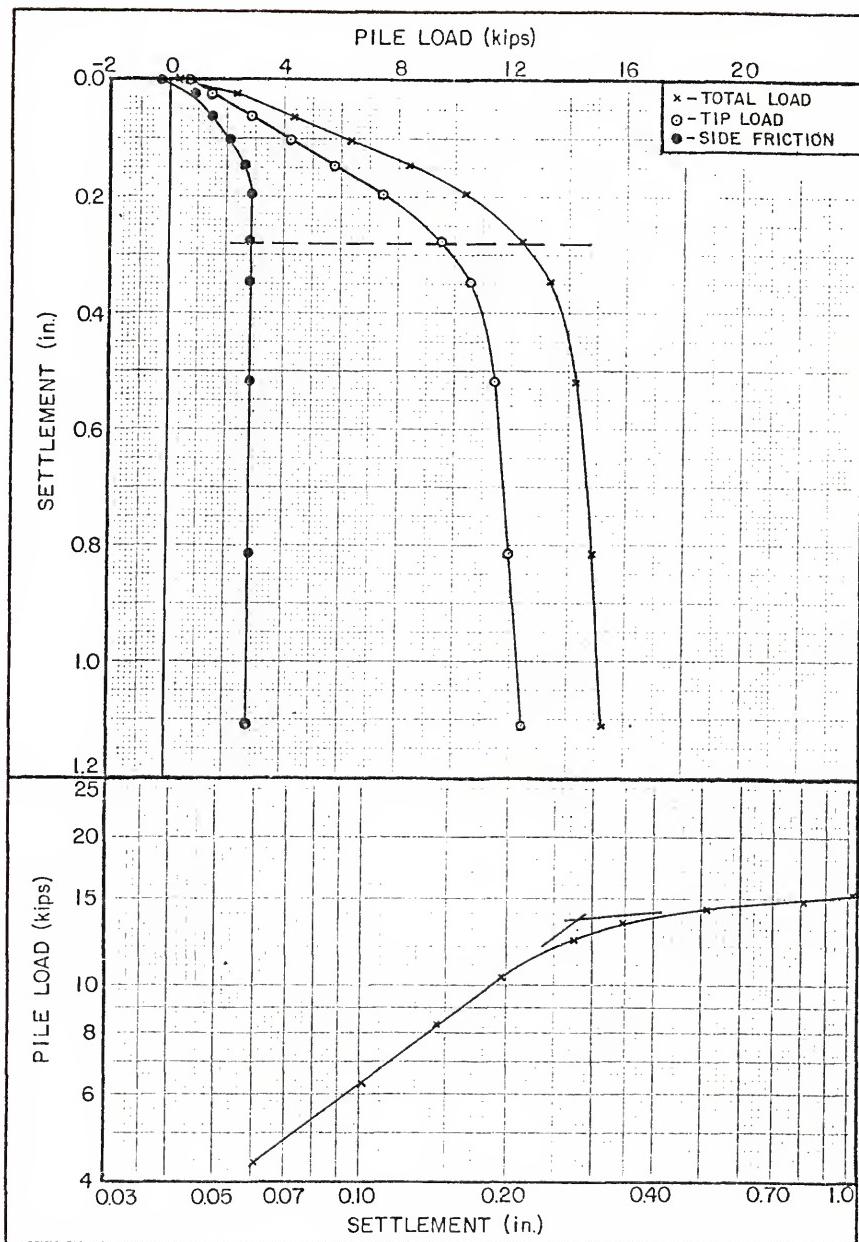
FIGURE B-56



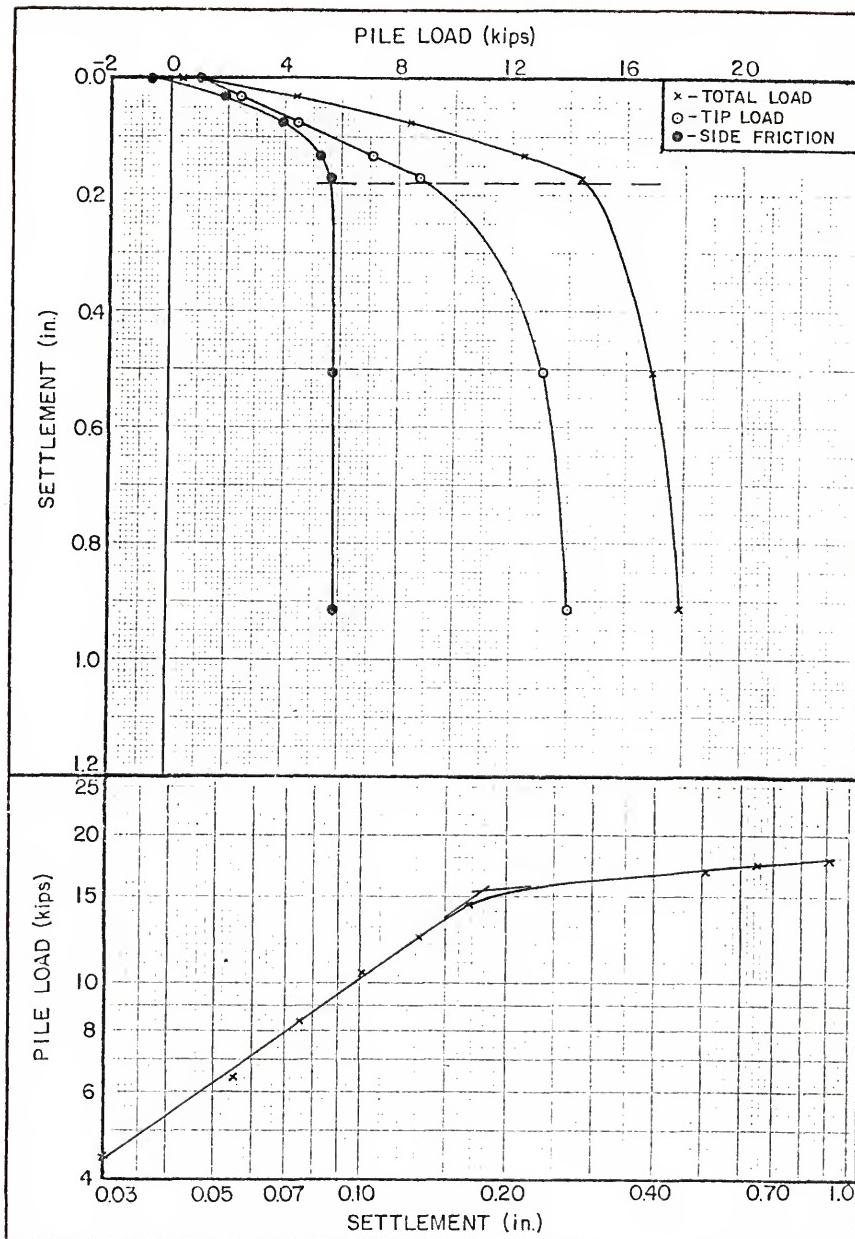
BEVILLE SITE NO 31 PILE LOAD TEST RESULTS - 2.0 FT PIPE PILE  
FIGURE B-57



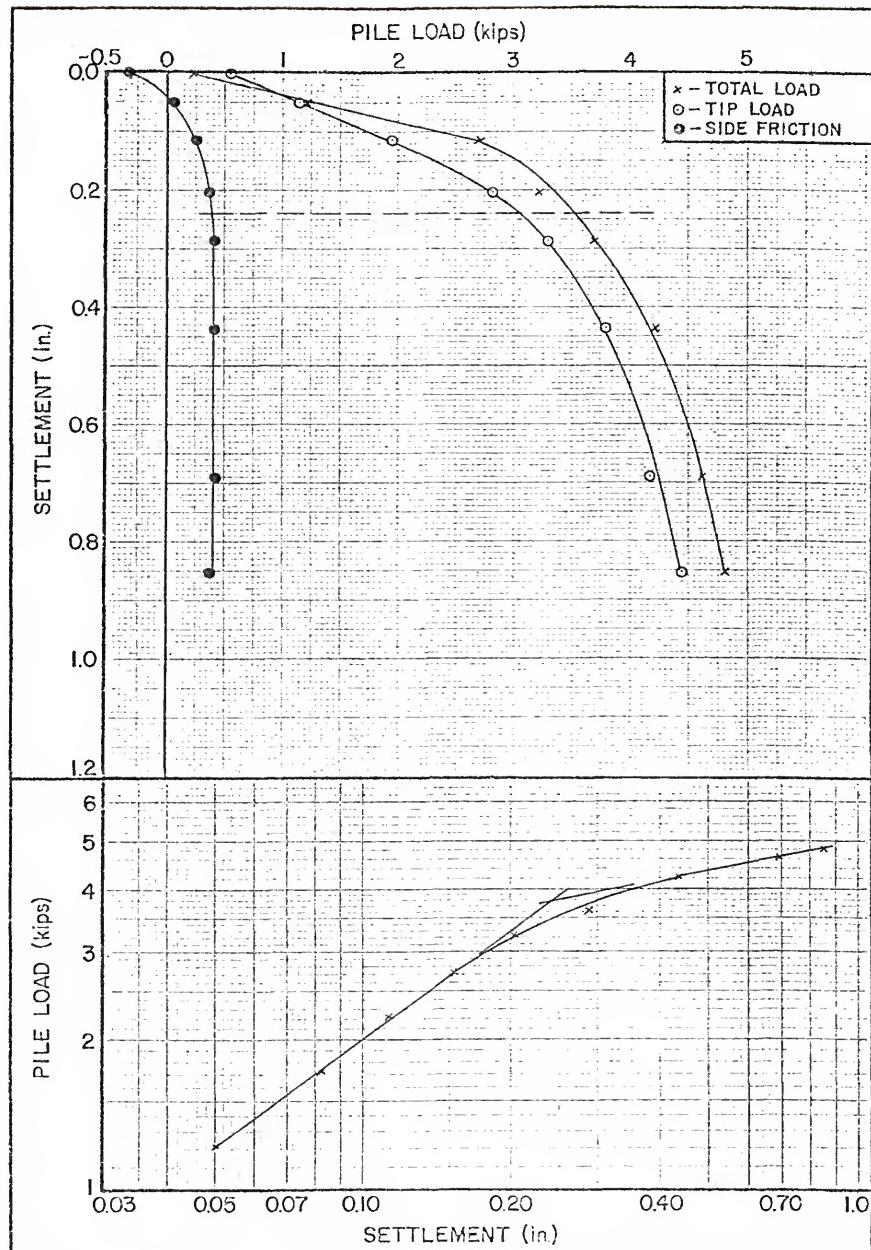
BEVILLE SITE NO 31 PILE LOAD TEST RESULTS - 4.5 FT PIPE PILE  
FIGURE B-58



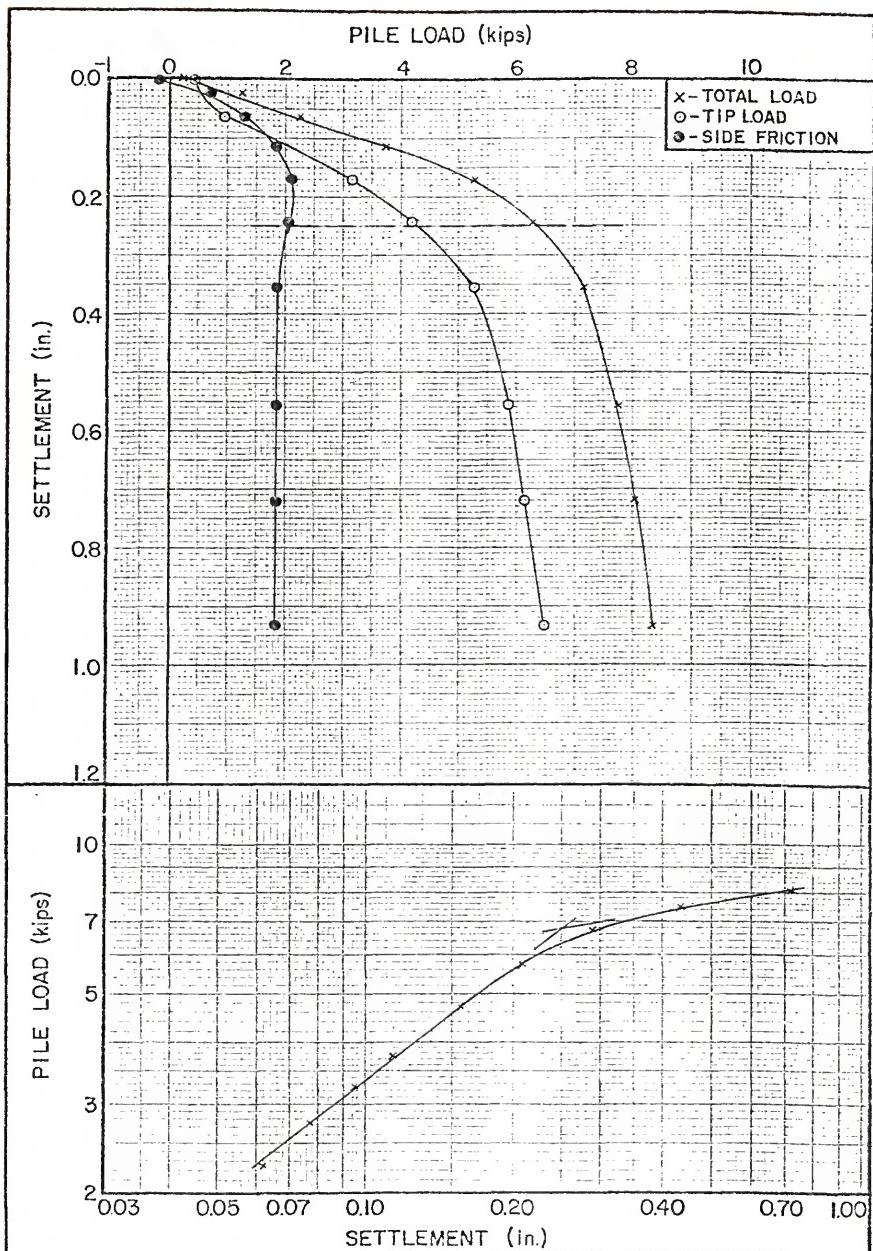
BEVILLE SITE NO 31 PILE LOAD TEST RESULTS - 7.0 FT PIPE PILE  
FIGURE B-59



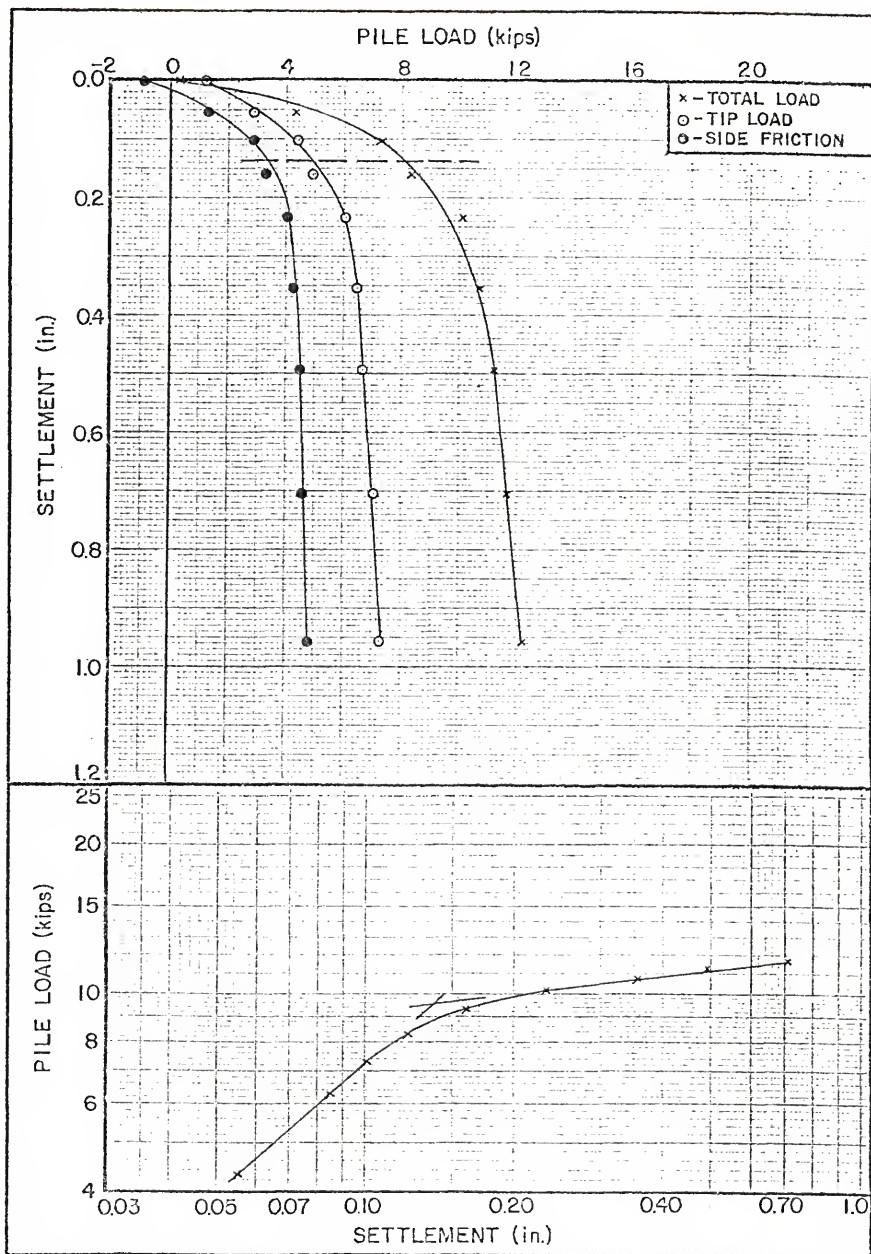
BEVILLE SITE NO 31 PILE LOAD TEST RESULTS - 9.5 FT PIPE PILE  
FIGURE B-60



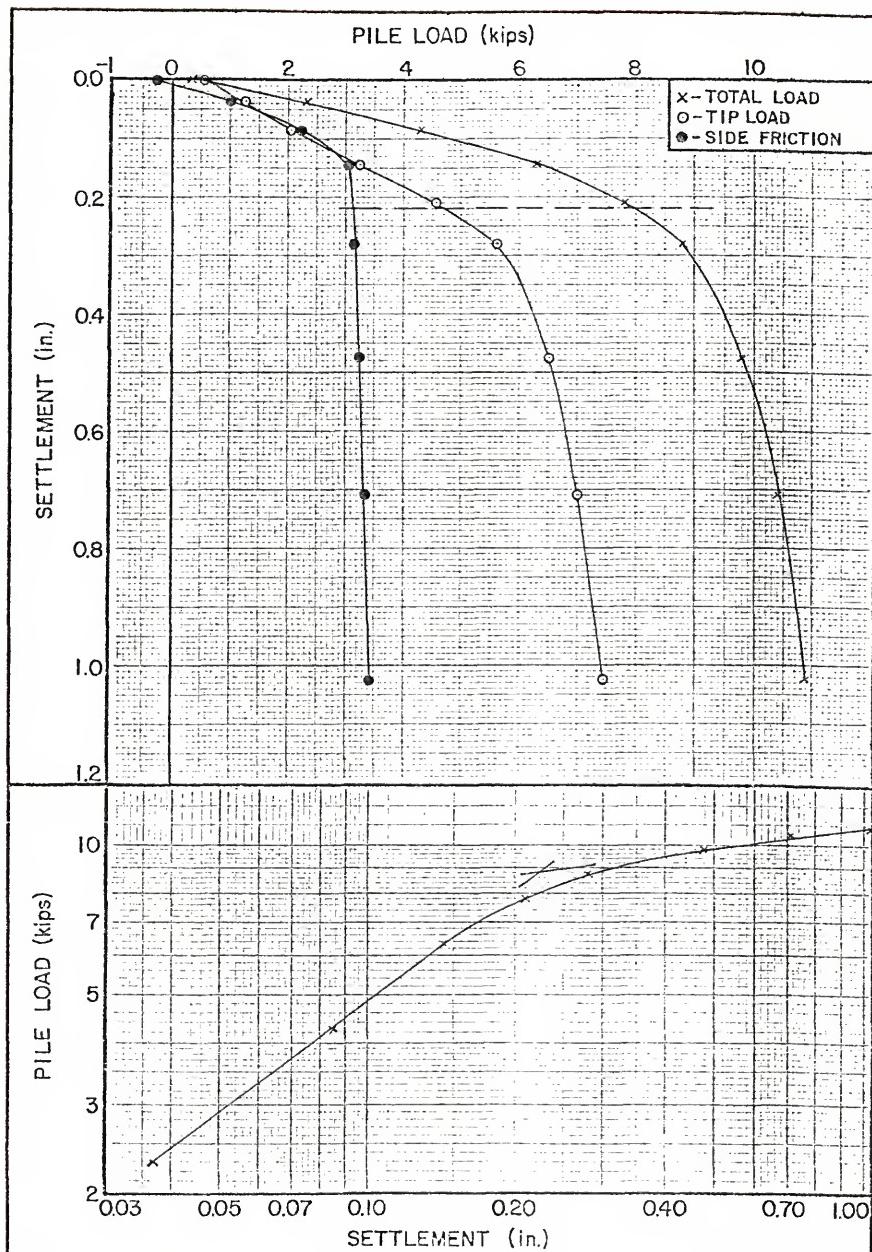
BEVILLE SITE NO 1 PILE LOAD TEST RESULTS - 3.0 FT CONCRETE PILE  
FIGURE B-61



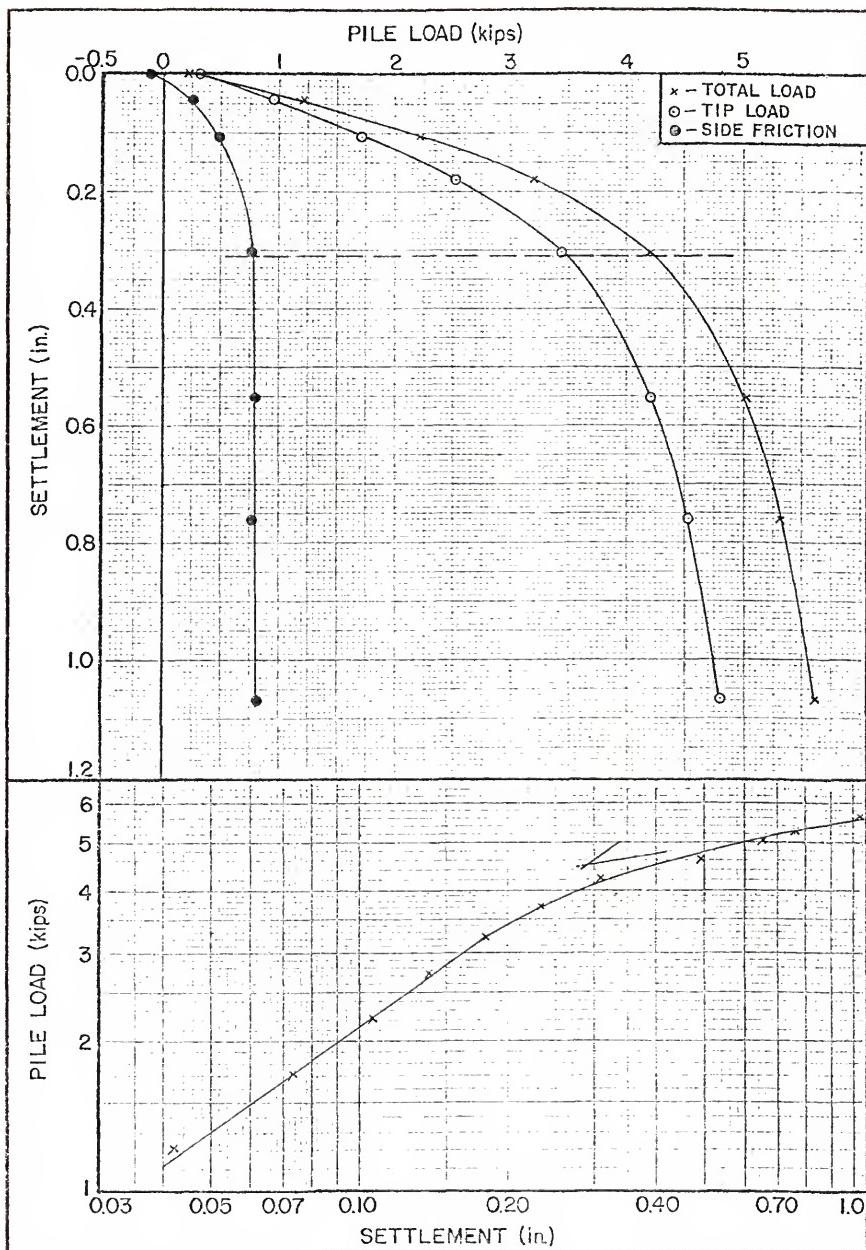
BEVILLE SITE NO 1 PILE LOAD TEST RESULTS - 6.0 FT CONCRETE PILE  
FIGURE B-62



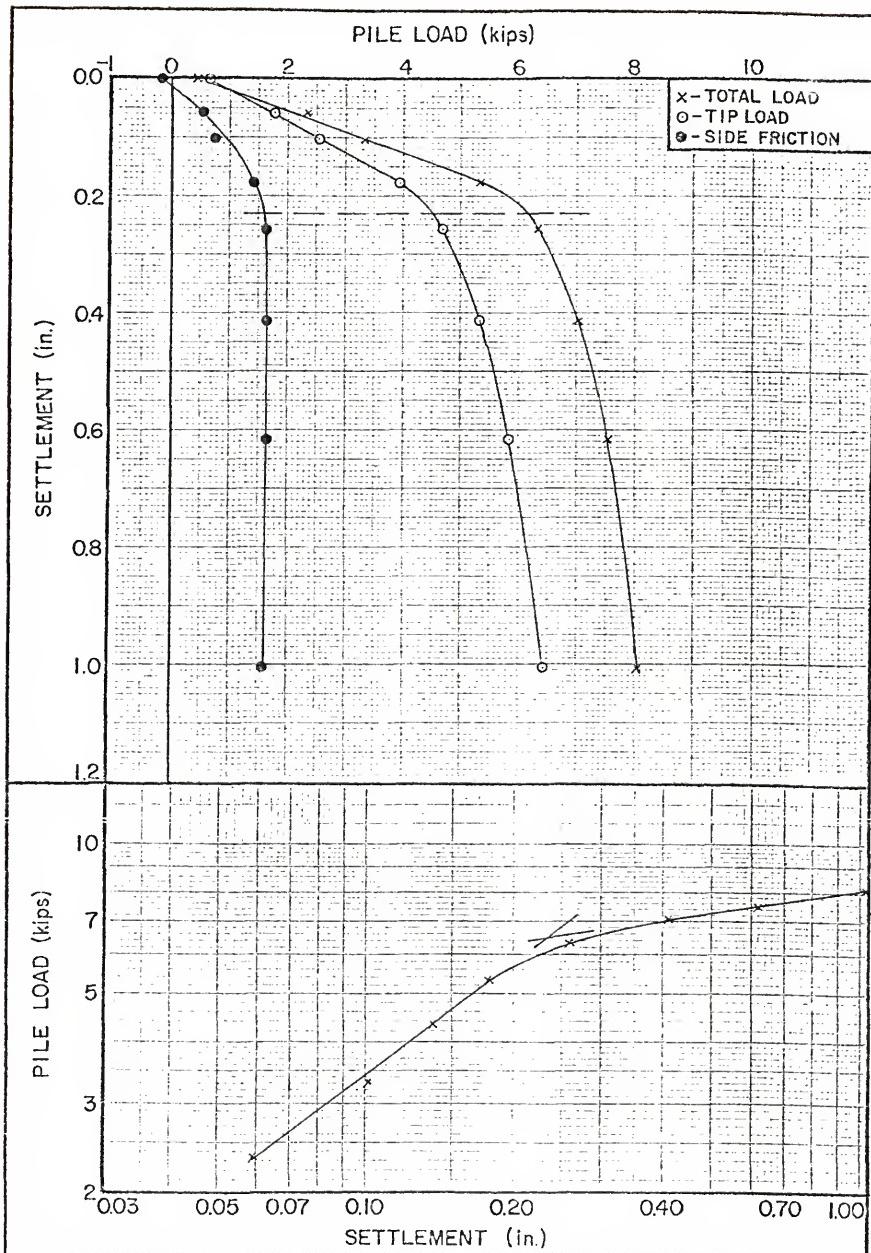
BEVILLE SITE NO 1 PILE LOAD TEST RESULTS - 8.5 FT CONCRETE PILE  
FIGURE B-63



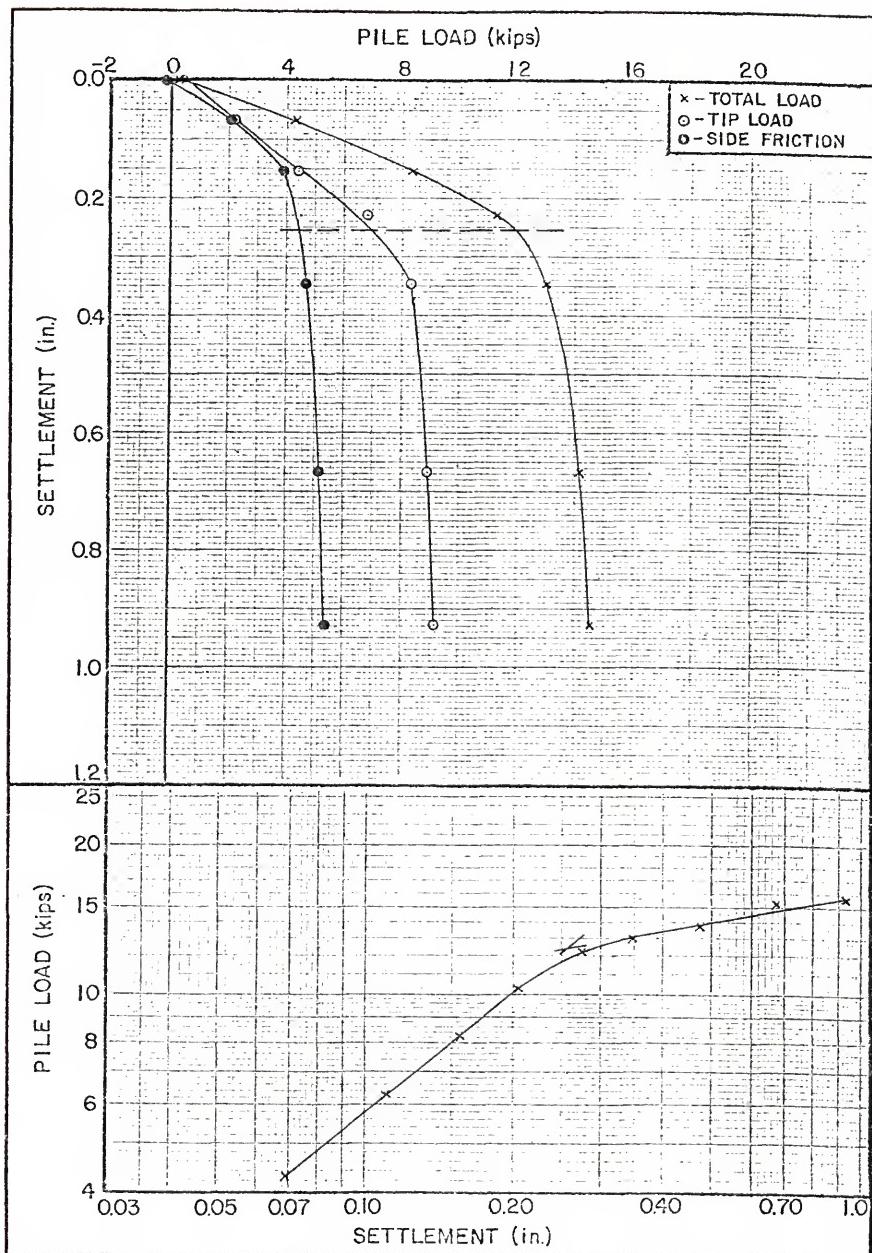
BEVILLE SITE NO 6 PILE LOAD TEST RESULTS - 9.7 FT CONCRETE PILE  
FIGURE B-64



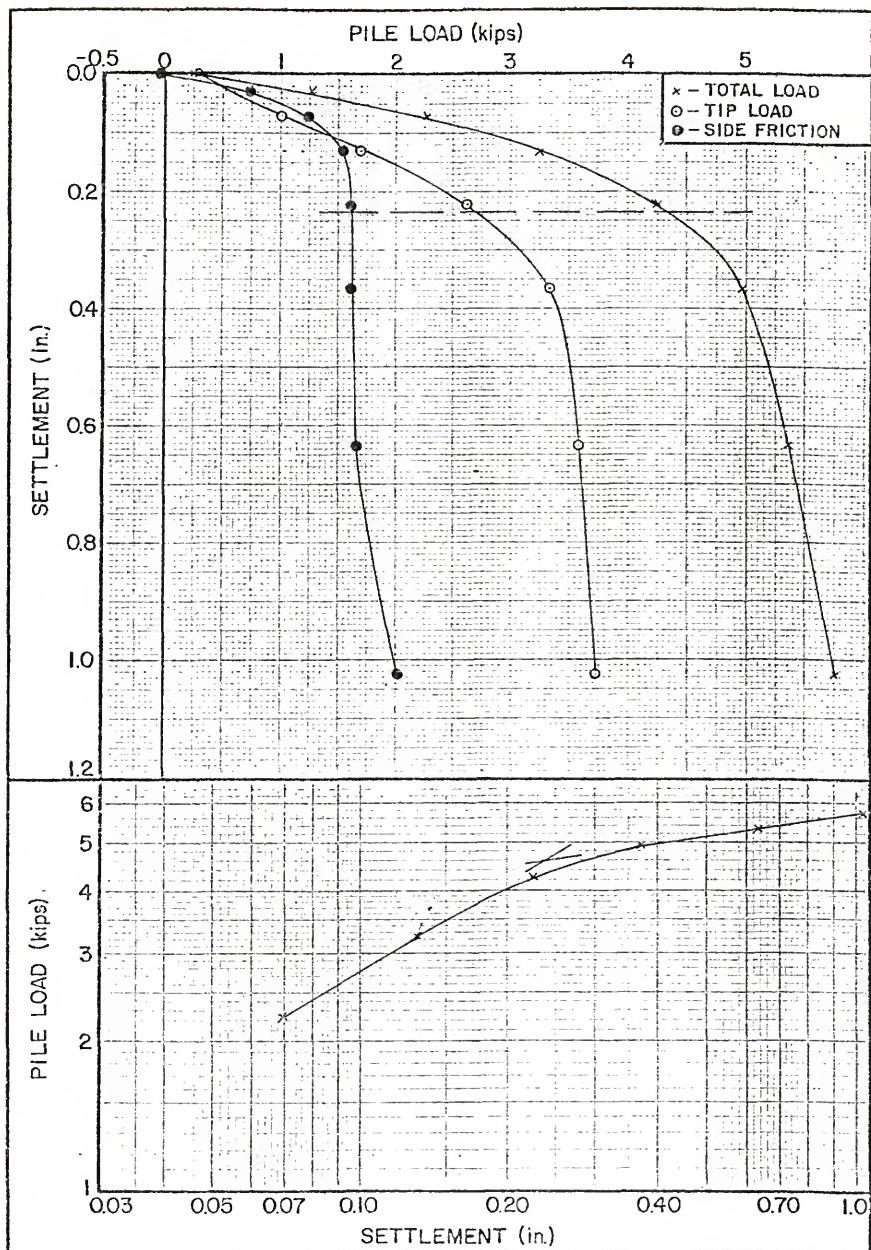
BEVILLE SITE NO 9 PILE LOAD TEST RESULTS - 3.0 FT CONCRETE PILE  
FIGURE B-65



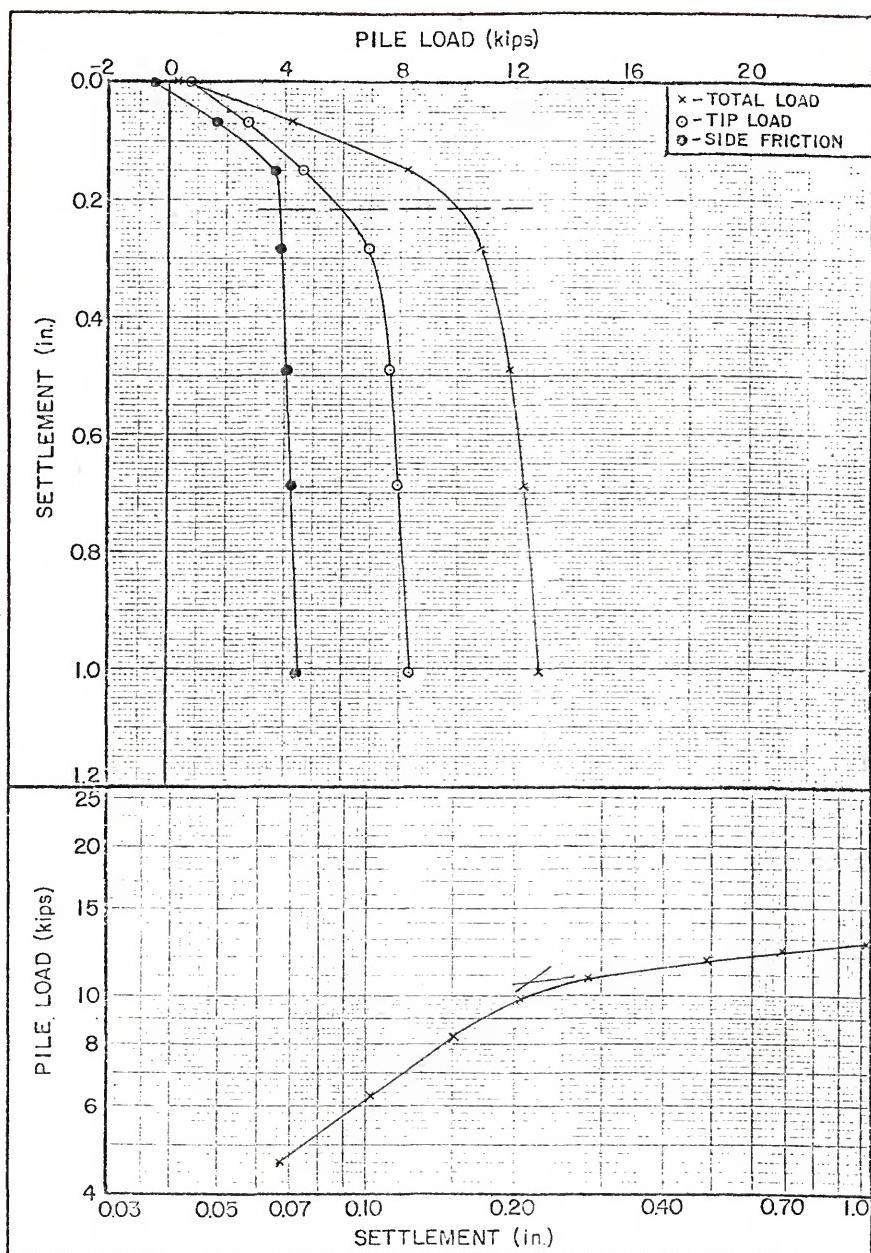
BEVILLE SITE NO 9 PILE LOAD TEST RESULTS - 6.5 FT CONCRETE PILE  
FIGURE B-66



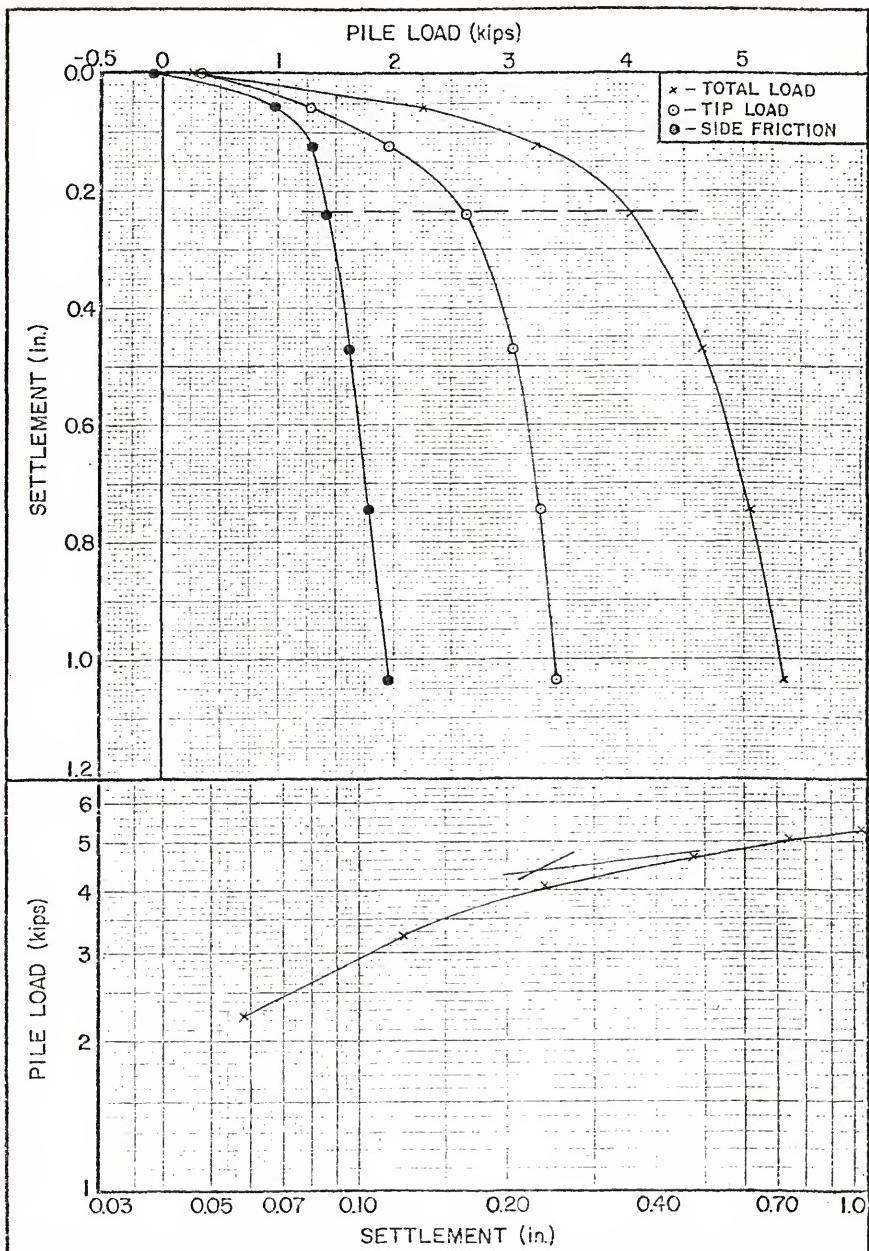
BEVILLE SITE NO 9 PILE LOAD TEST RESULTS - 8.5 FT CONCRETE PILE  
FIGURE B-67



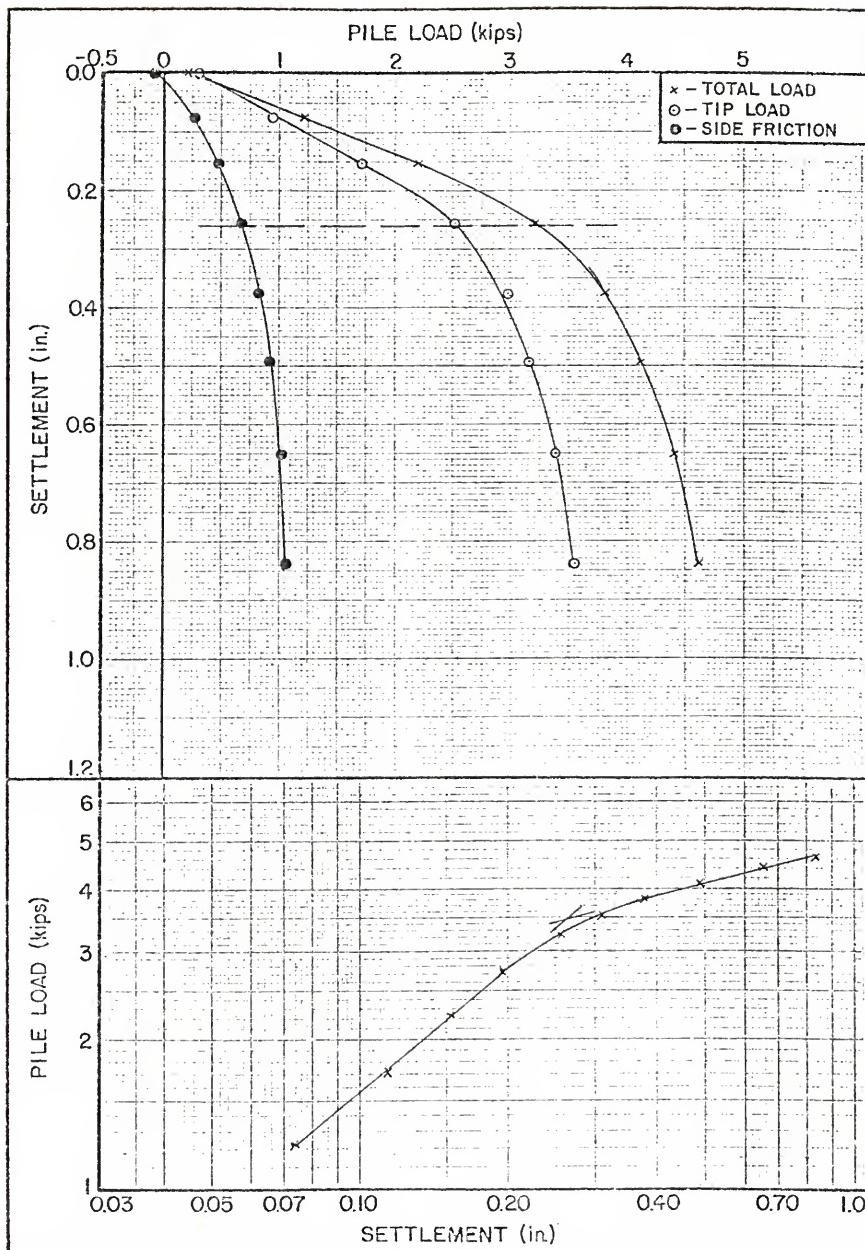
BEVILLE SITE NO 10 PILE LOAD TEST RESULTS - 6.0 FT CONCRETE PILE  
FIGURE B-68



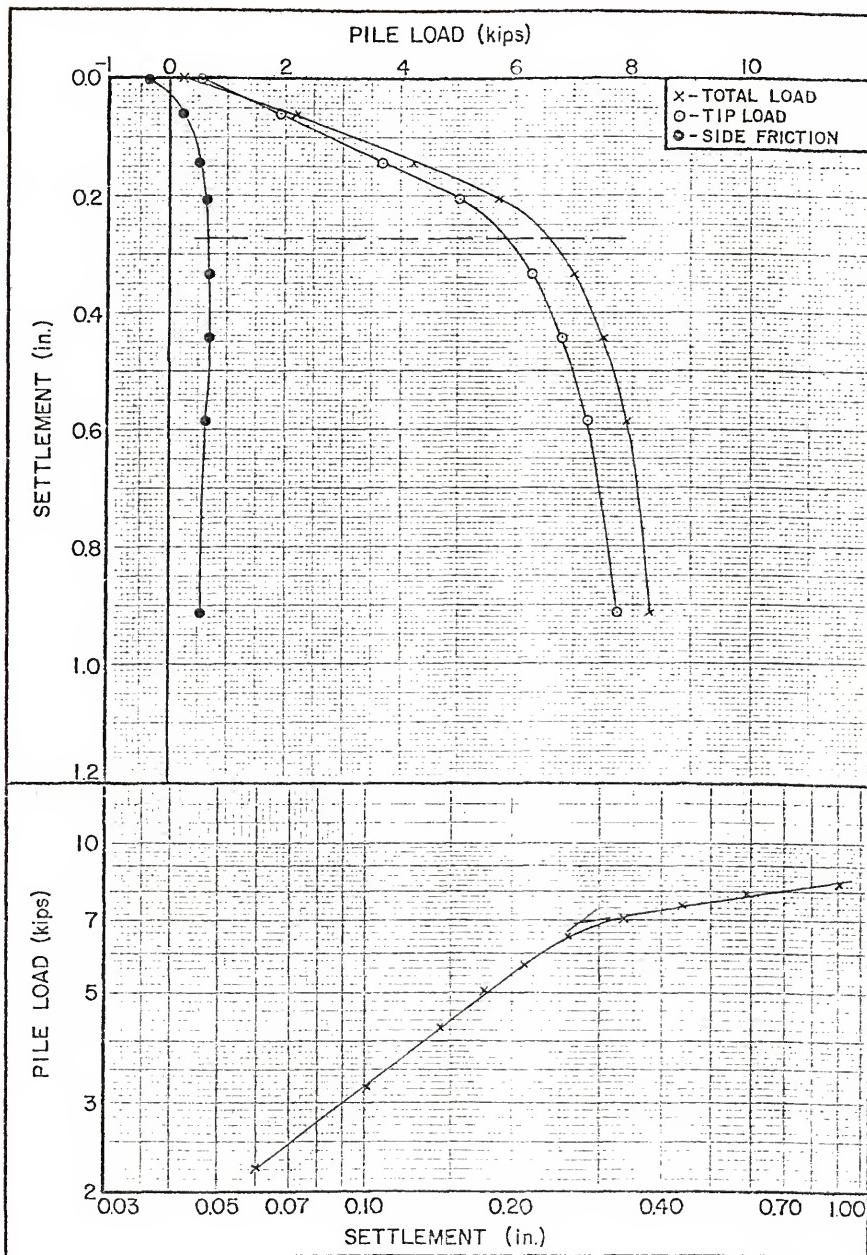
BEVILLE SITE NO 11 PILE LOAD TEST RESULTS - 8.0 FT CONCRETE PILE  
FIGURE B-69



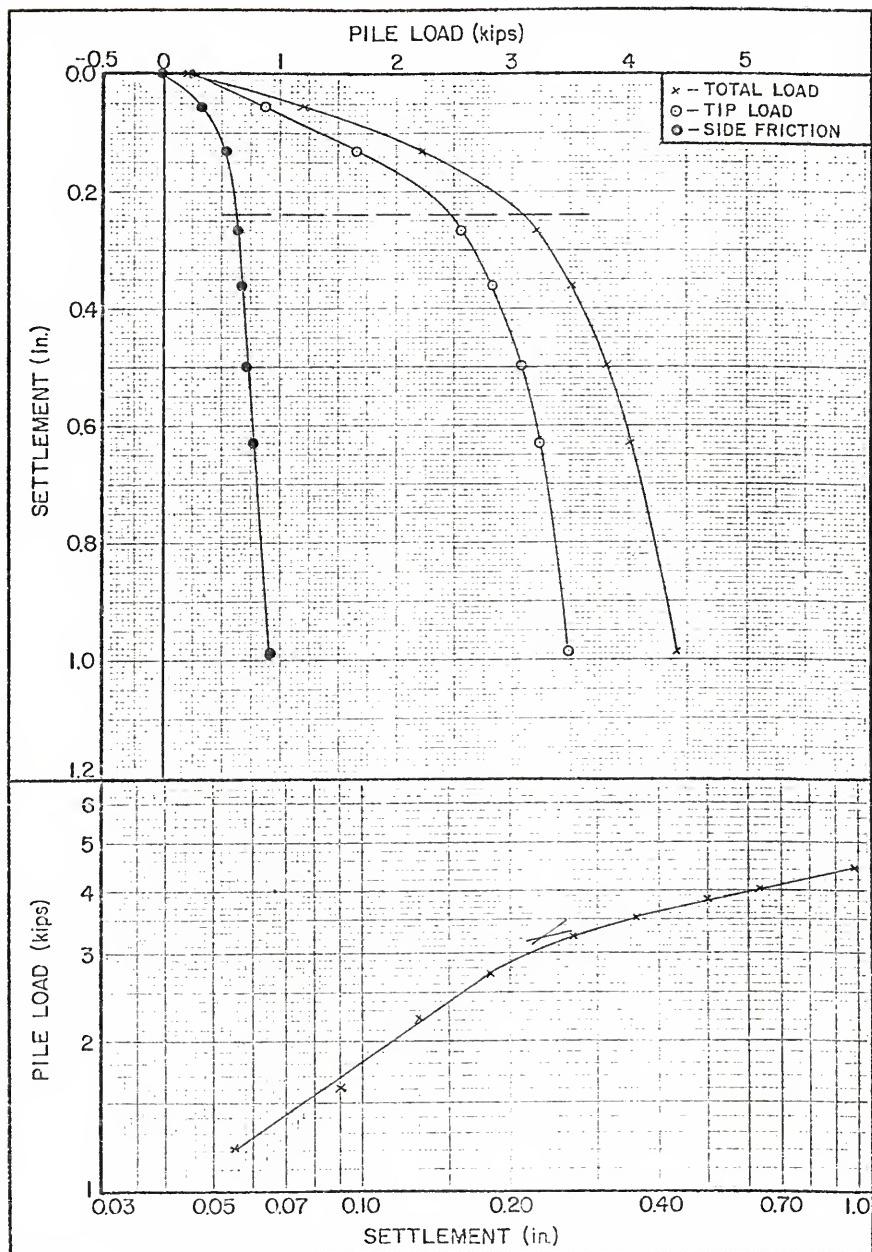
BEVILLE SITE NO 14 PILE LOAD TEST RESULTS - 6.0 FT CONCRETE PILE  
FIGURE B-70



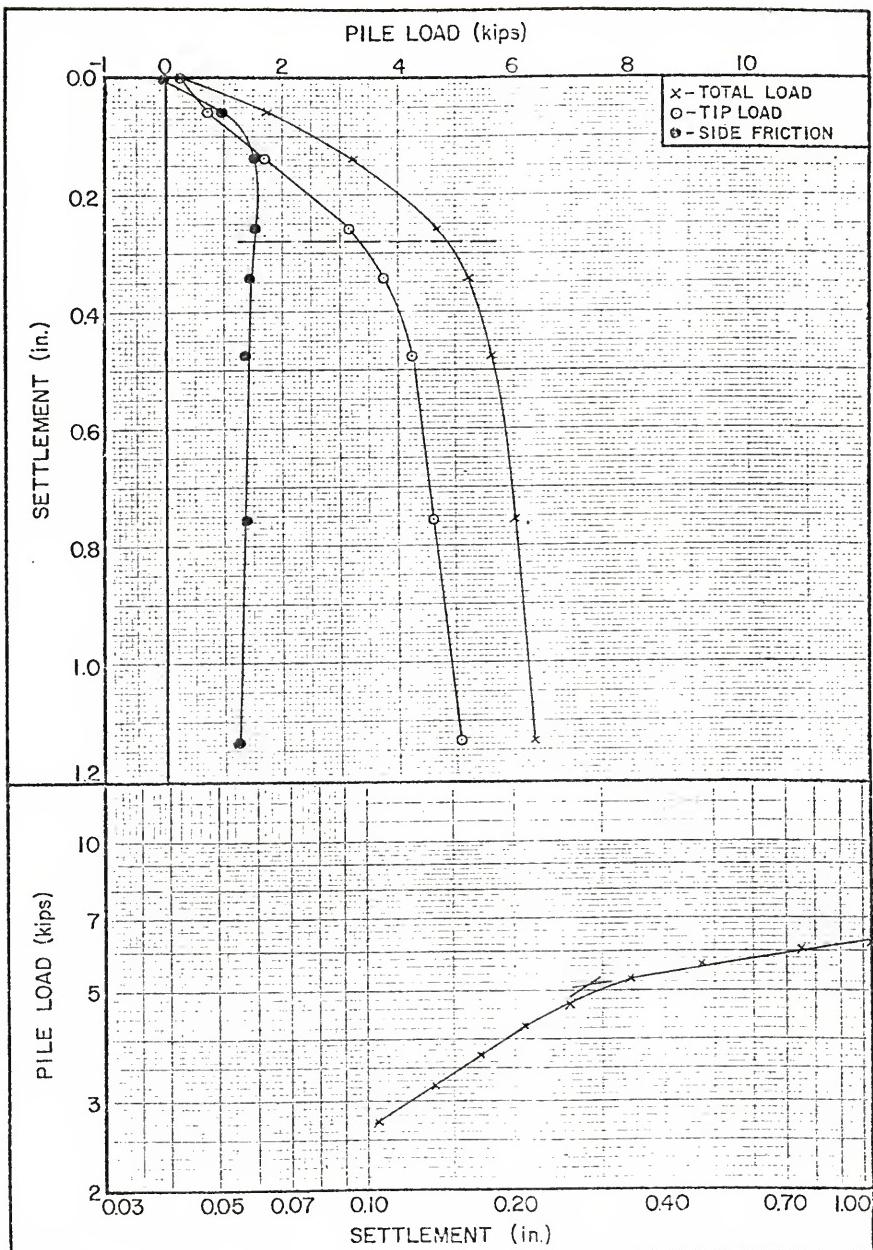
BEVILLE SITE NO 15 PILE LOAD TEST RESULTS - 3.0 FT CONCRETE PILE  
FIGURE B-71



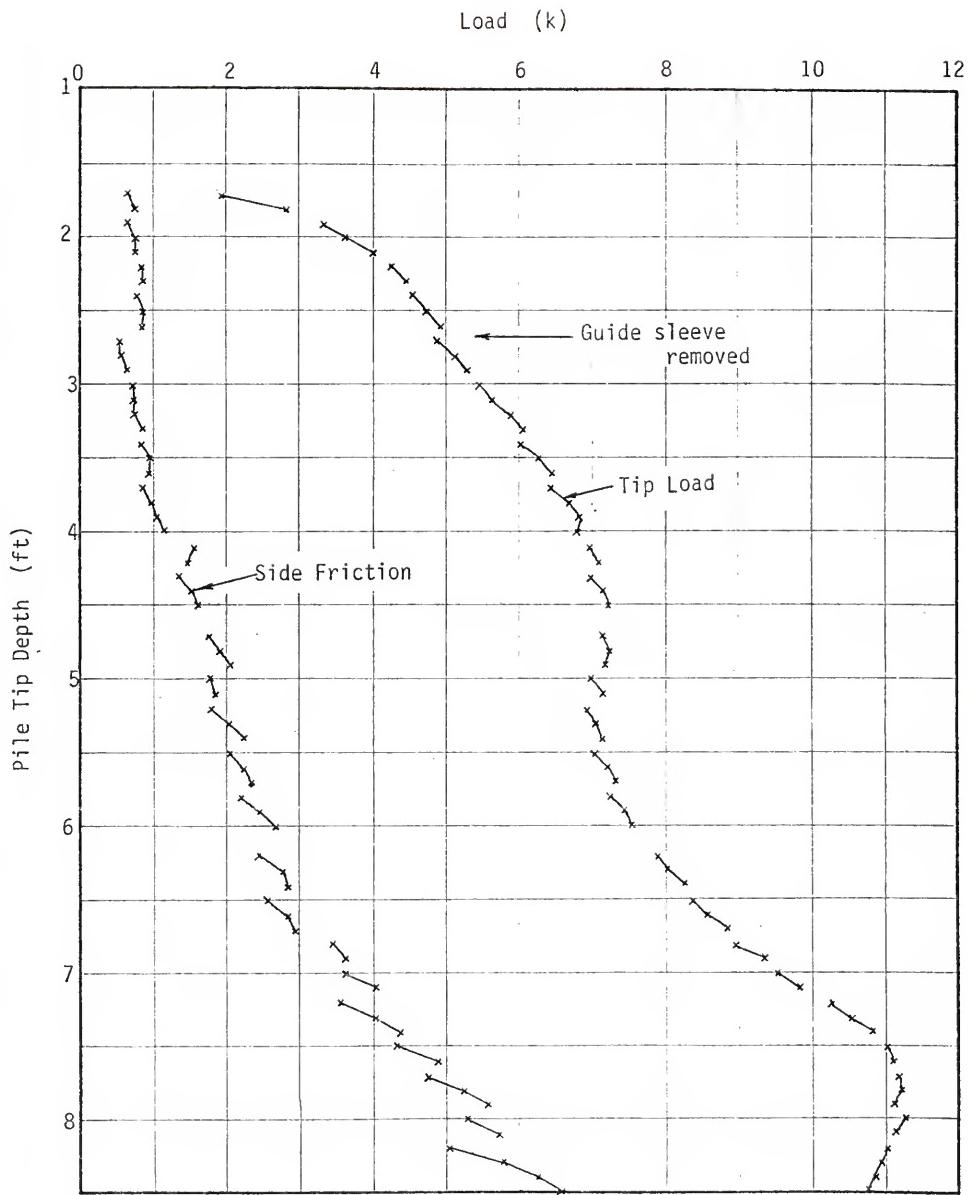
BEVILLE SITE NO 17 PILE LOAD TEST RESULTS - 3.0 FT CONCRETE PILE  
FIGURE B-72



BEVILLE SITE 18 PILE LOAD TEST RESULTS - 3.0 FT CONCRETE PILE  
FIGURE B-73

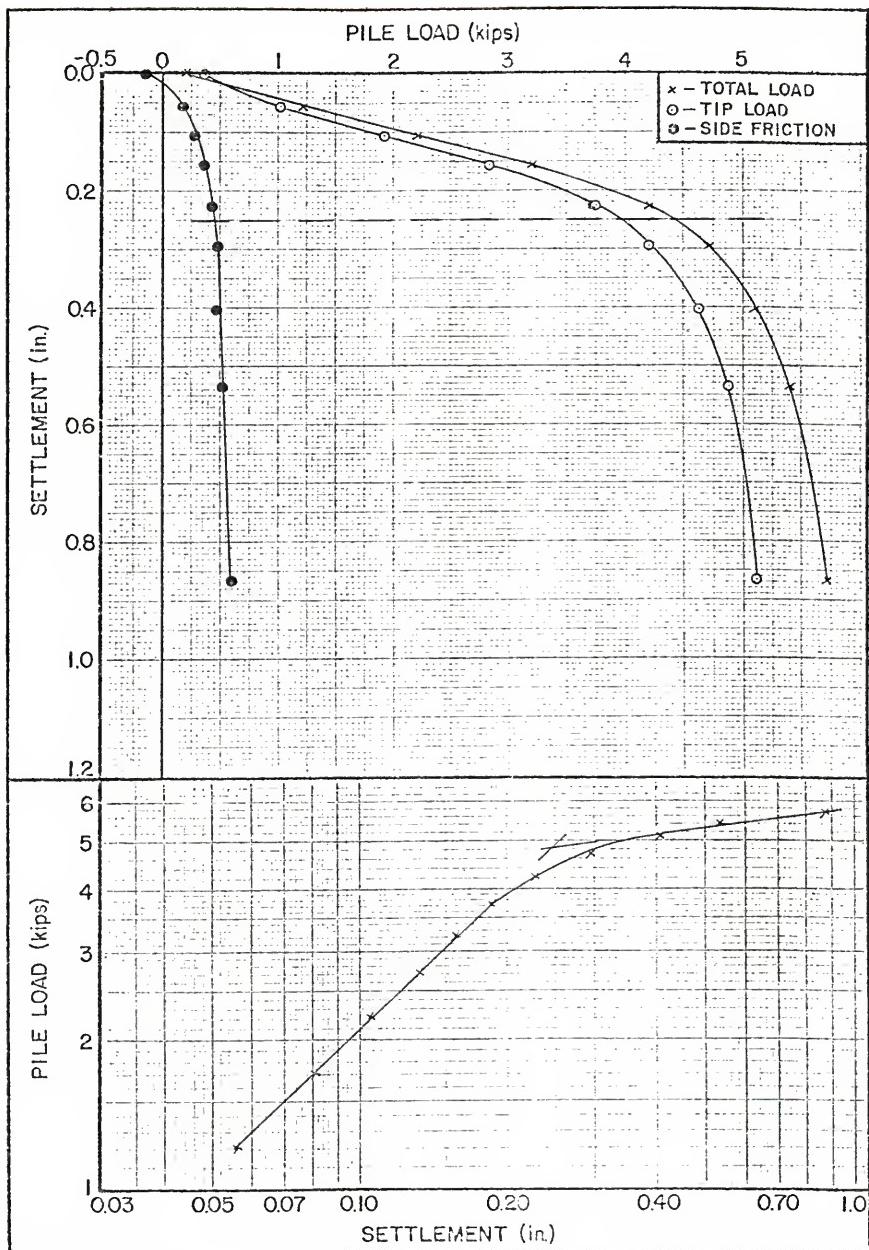


BEVILLE SITE NO 19 PILE LOAD TEST RESULTS - 3.0 FT CONCRETE PILE  
FIGURE B-74

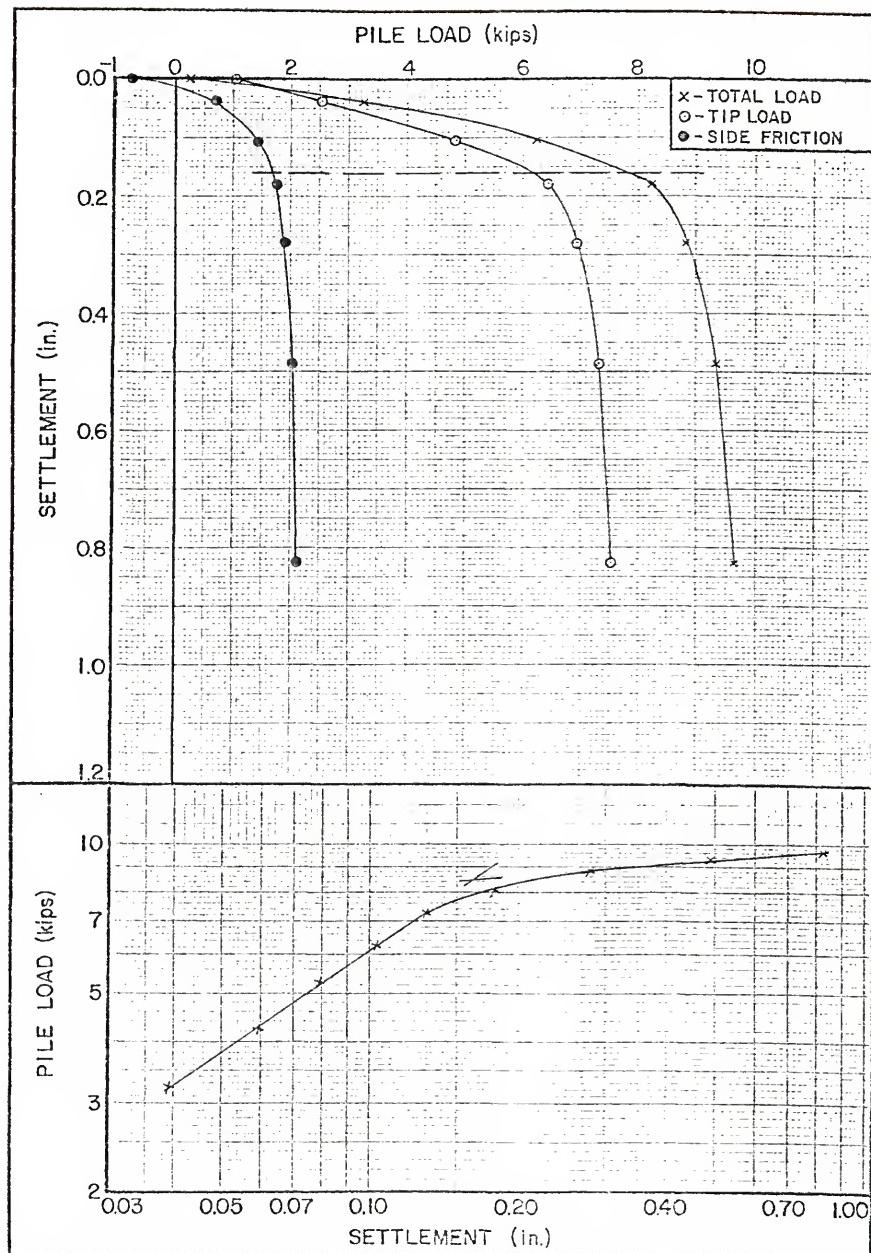


JACK-IN DATA FOR BEVILLE SITE 21 TEST

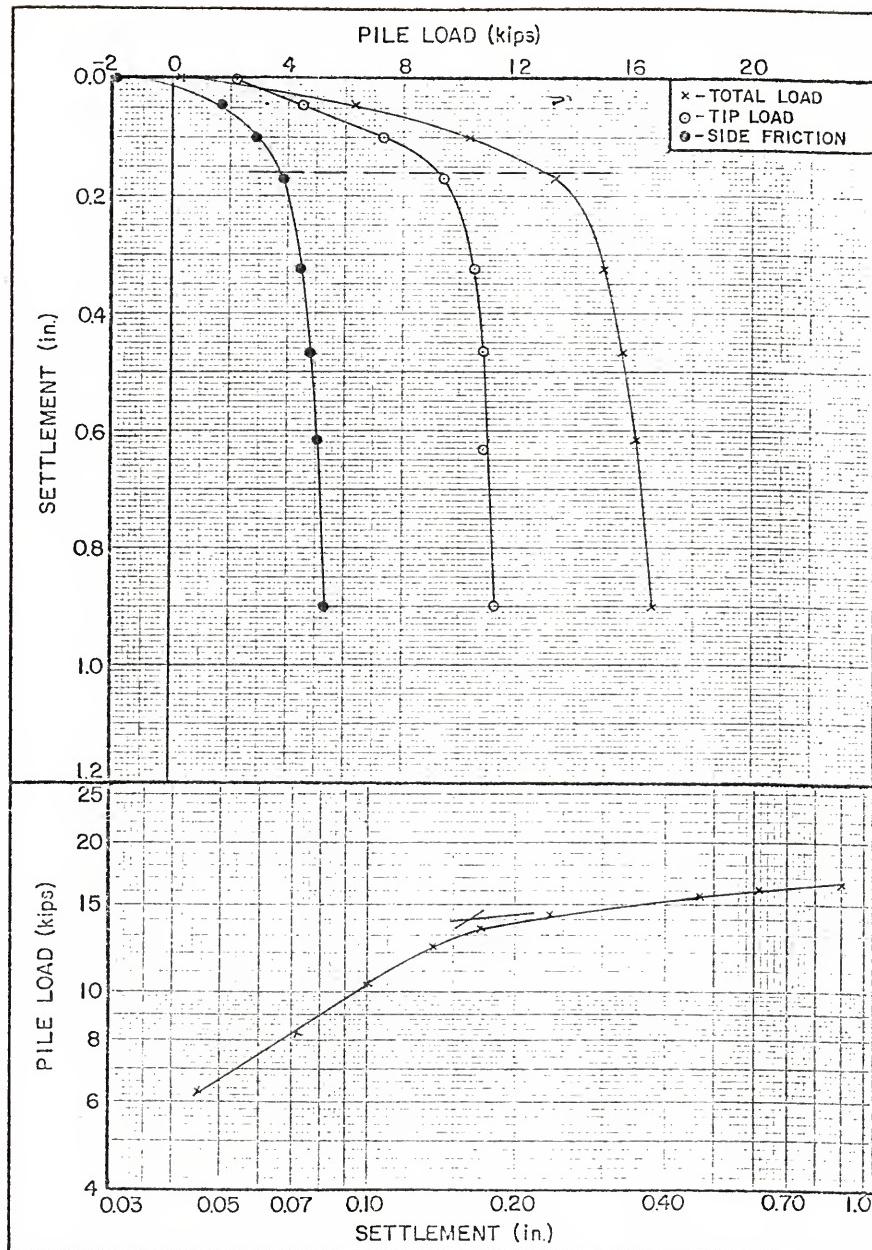
FIGURE B-75



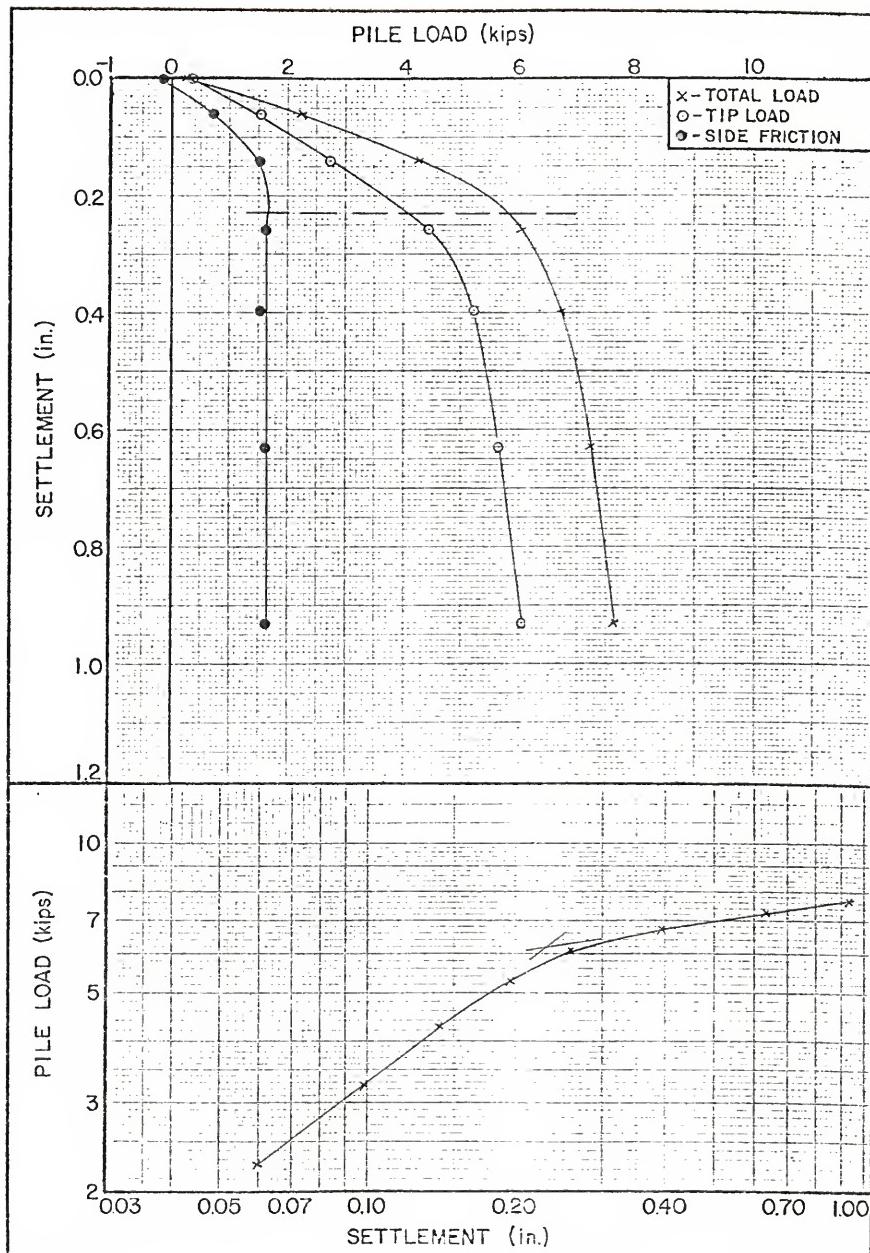
BEVILLE SITE NO 21 PILE LOAD TEST RESULTS - 3.0 FT CONCRETE PILE  
FIGURE B-76



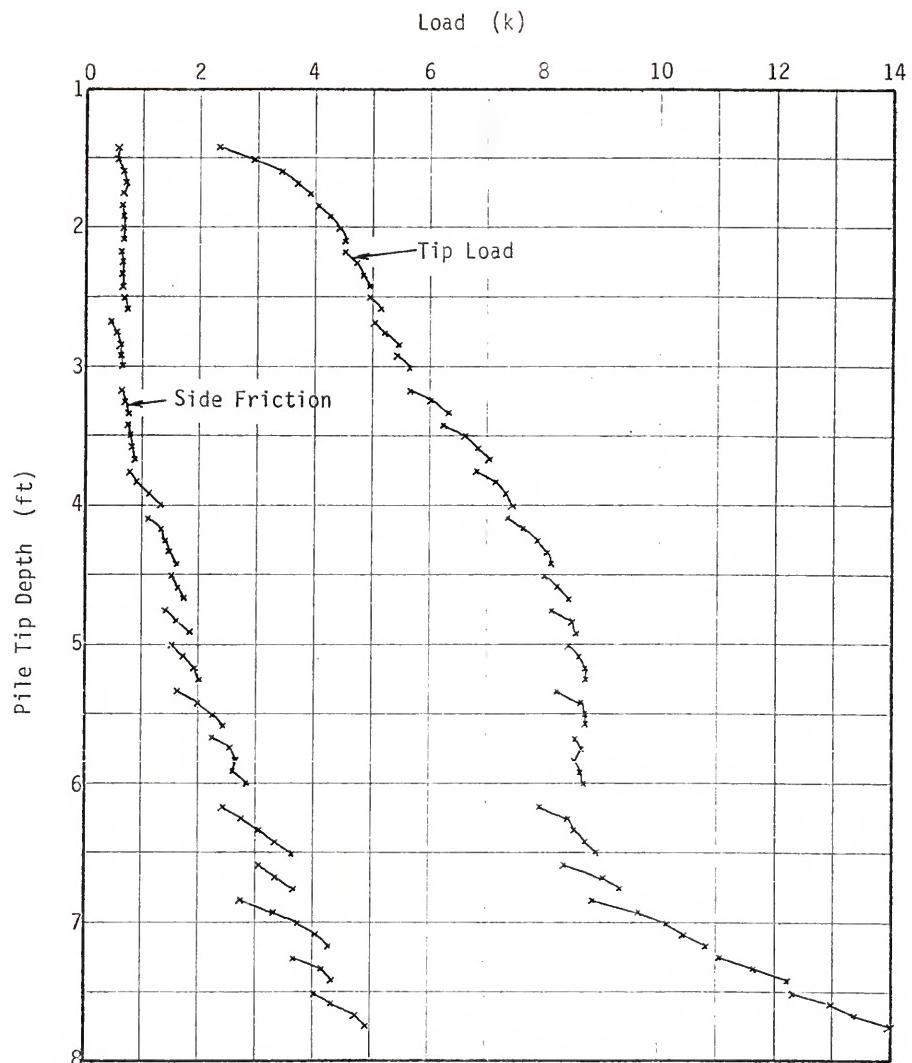
BEVILLE SITE NO 21 PILE LOAD TEST RESULTS - 6.0 FT CONCRETE PILE  
FIGURE B-77



BEVILLE SITE NO 21 PILE LOAD TEST RESULTS - 8.5 FT CONCRETE PILE  
FIGURE B-78

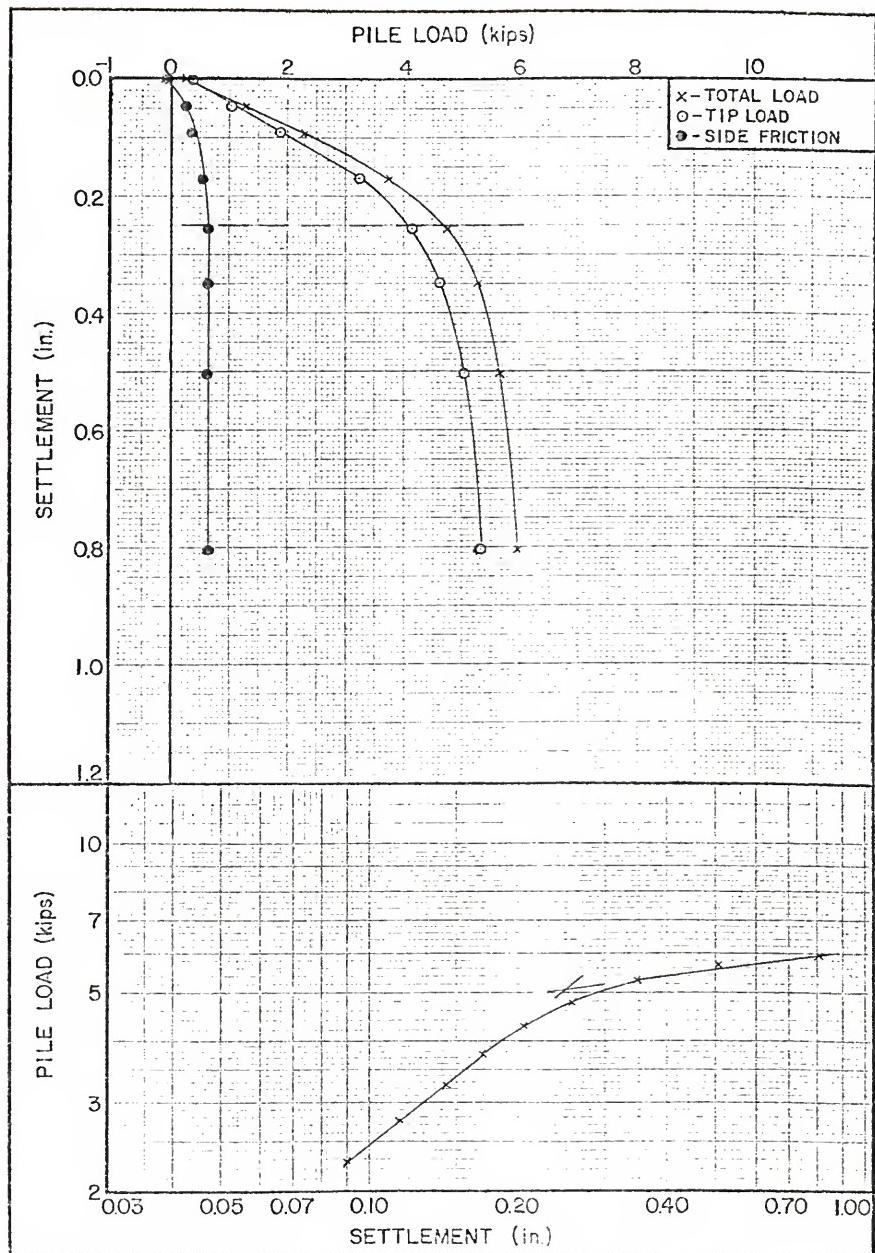


BEVILLE SITE NO 22 PILE LOAD TEST RESULTS - 6.0 FT CONCRETE PILE  
FIGURE B-79

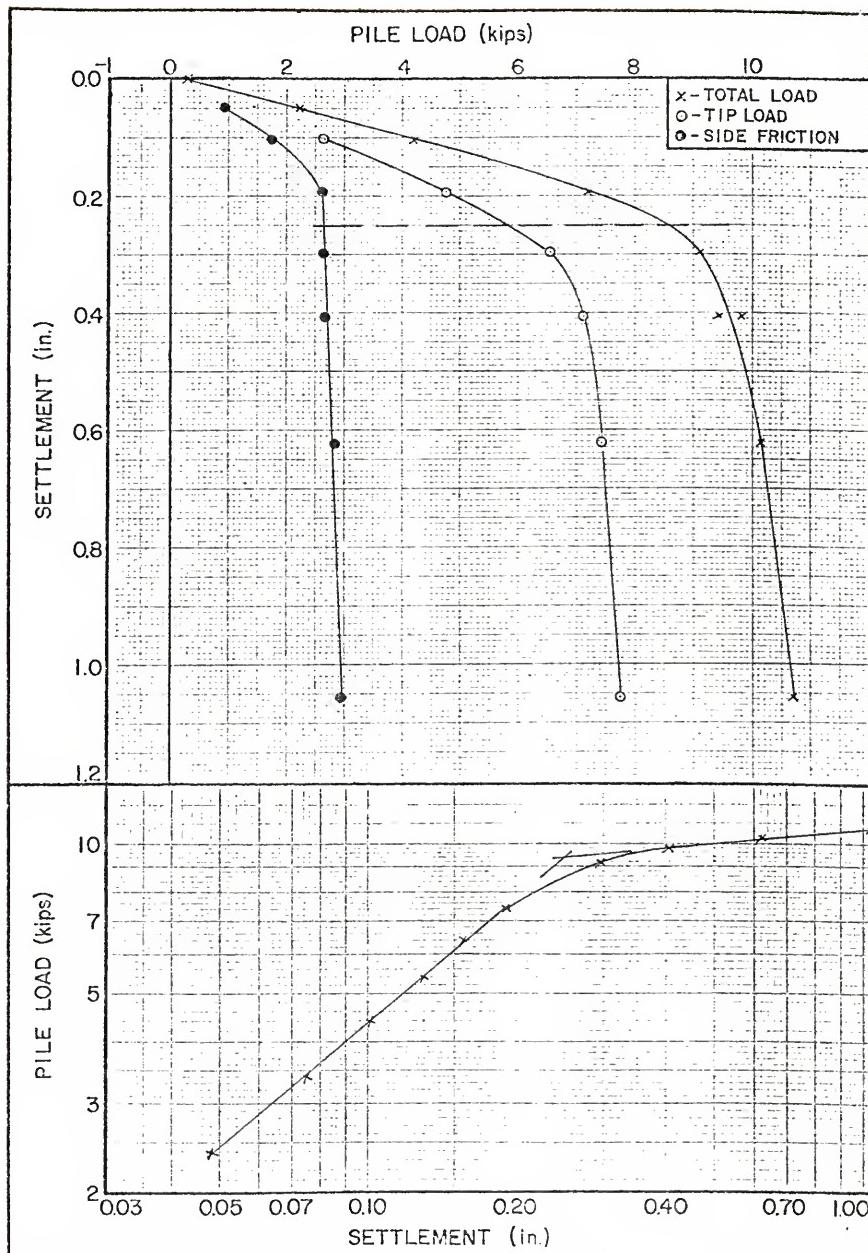


JACK-IN DATA FOR BEVILLE SITE 23 TEST

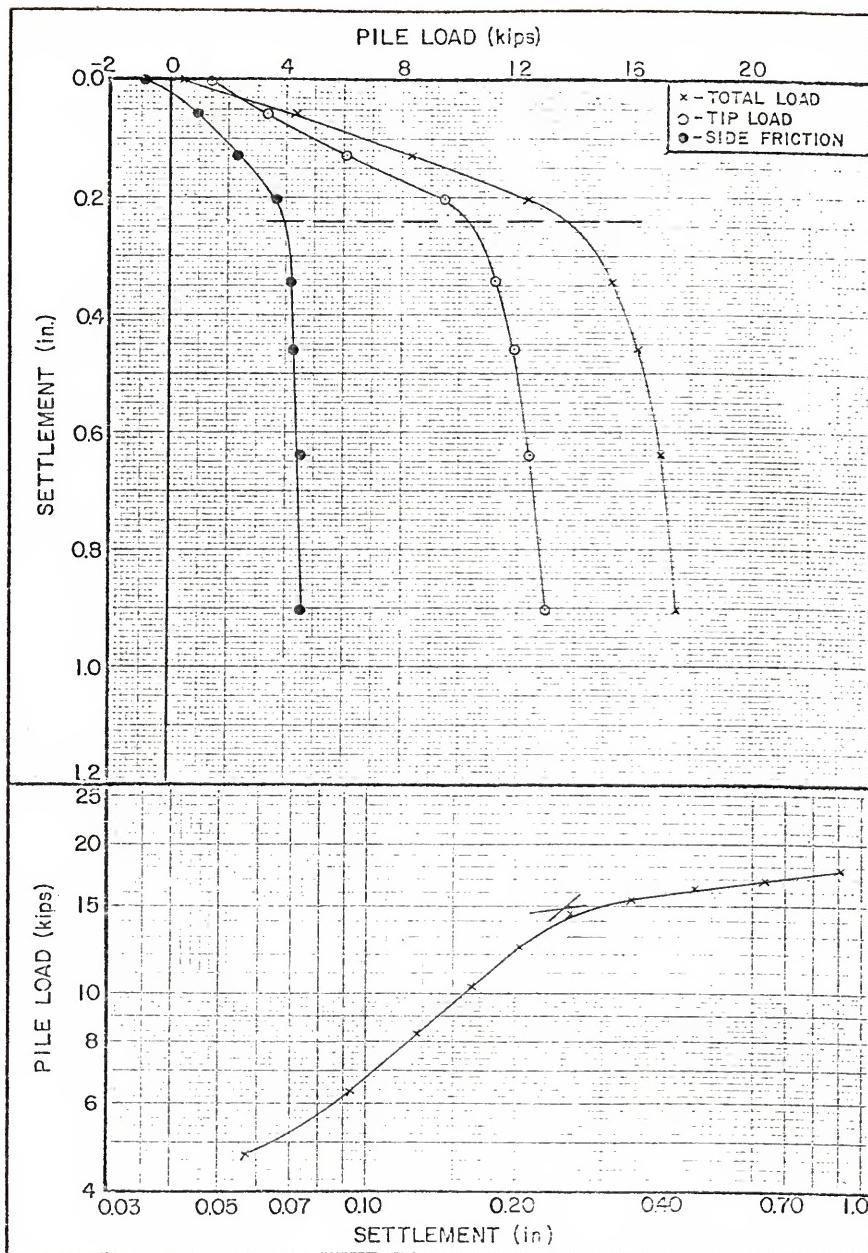
FIGURE B-80



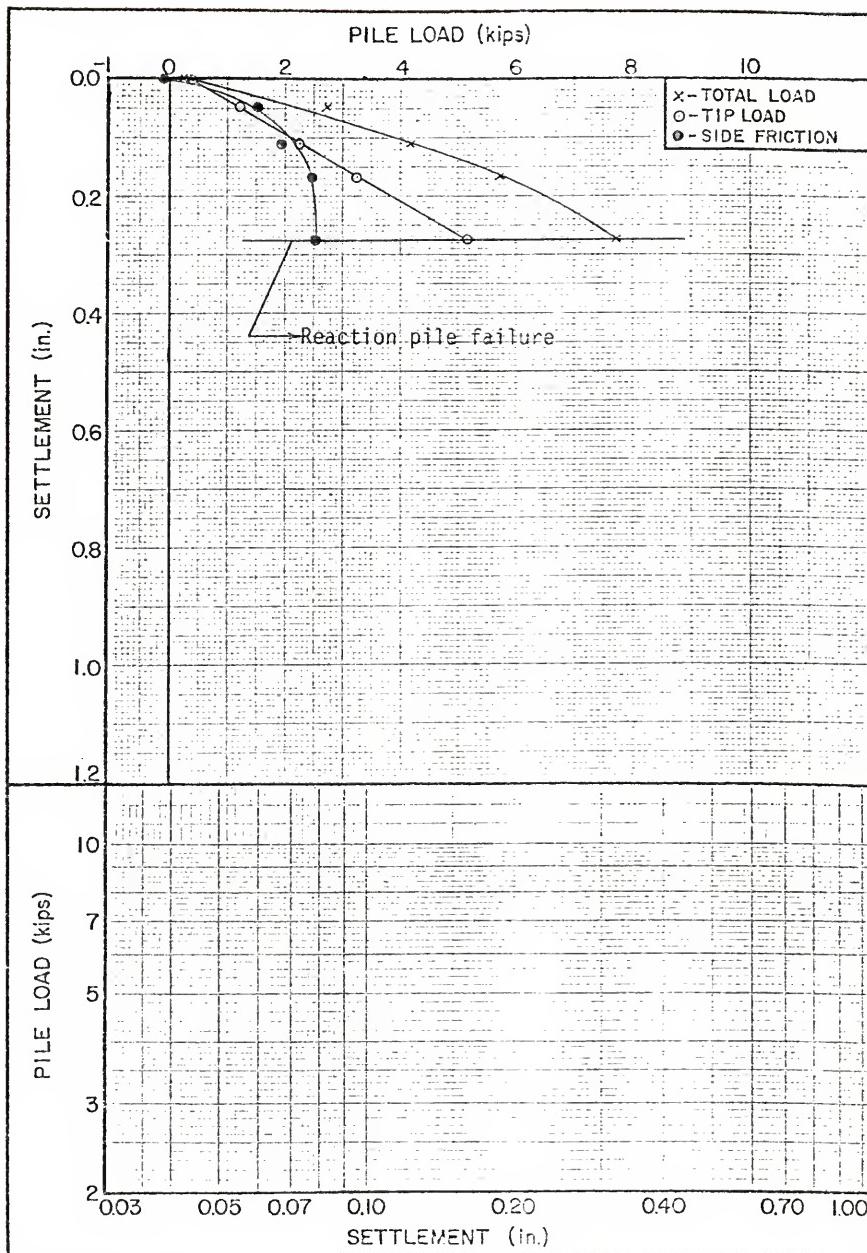
BEVILLE SITE NO 23 PILE LOAD TEST RESULTS - 3.0 FT CONCRETE PILE  
FIGURE B-81



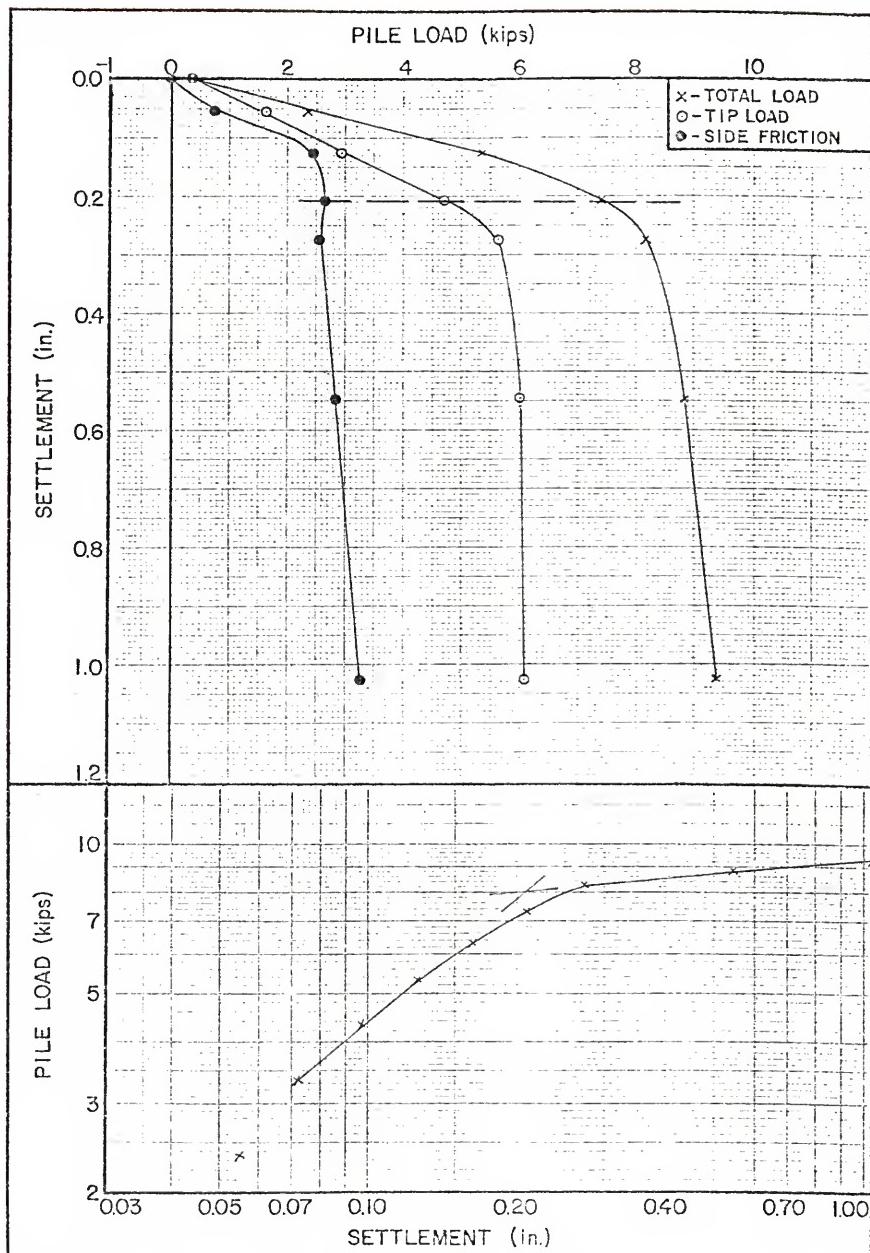
BEVILLE SITE NO 23 PILE LOAD TEST RESULTS - 6.0 FT CONCRETE PILE  
FIGURE B-82



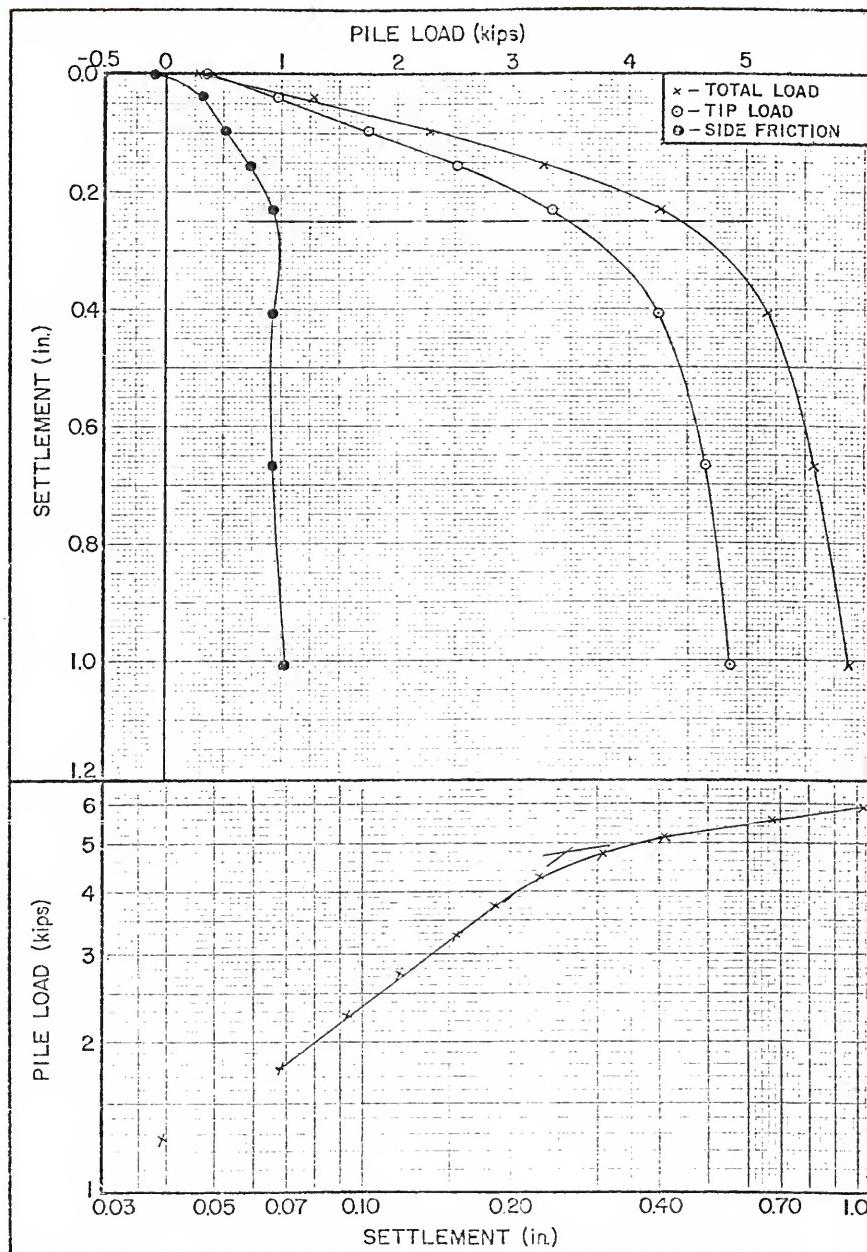
BEVILLE SITE NO 23 PILE LOAD TEST RESULTS - 8.0 FT CONCRETE PILE  
FIGURE B-83



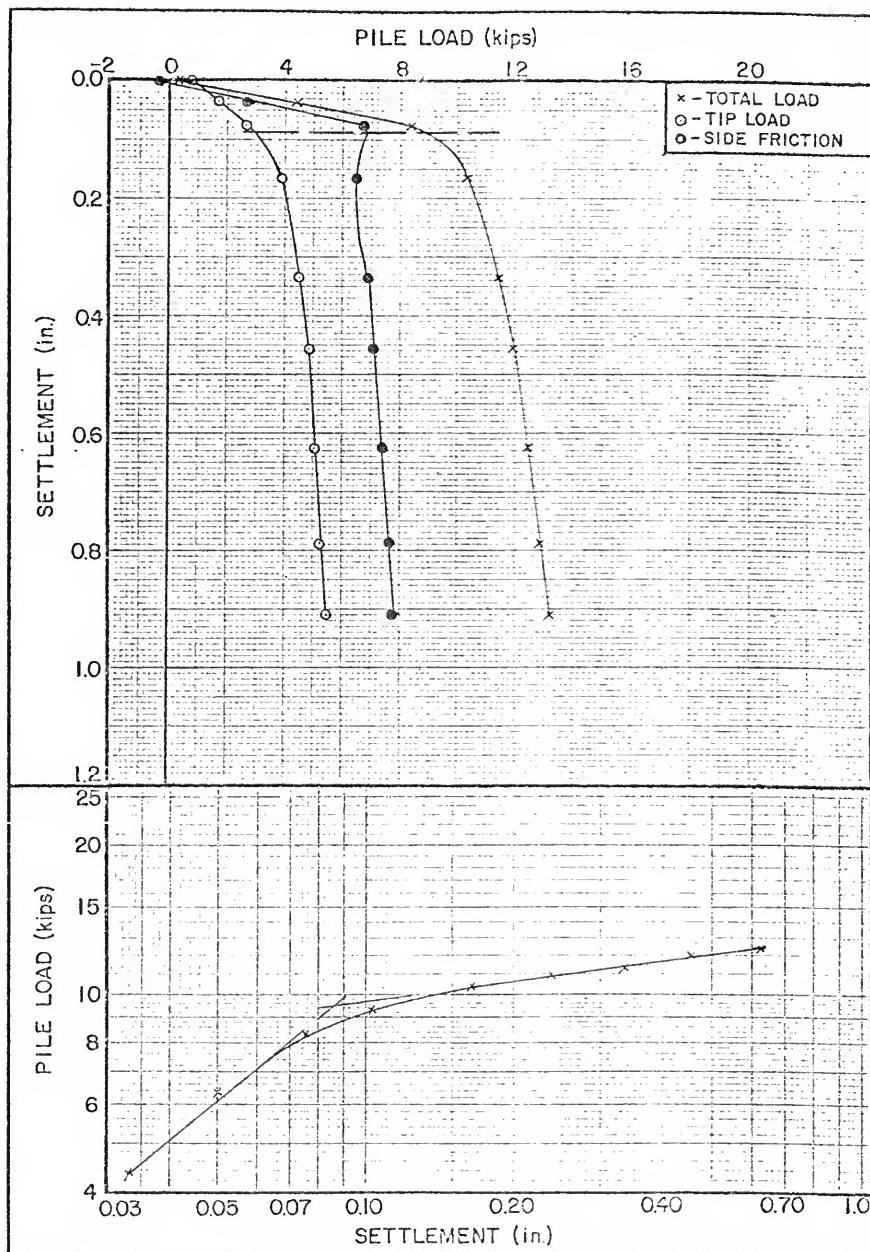
BEVILLE SITE NO 25 PILE LOAD TEST RESULTS - 3.0 FT CONCRETE PILE  
FIGURE B-84



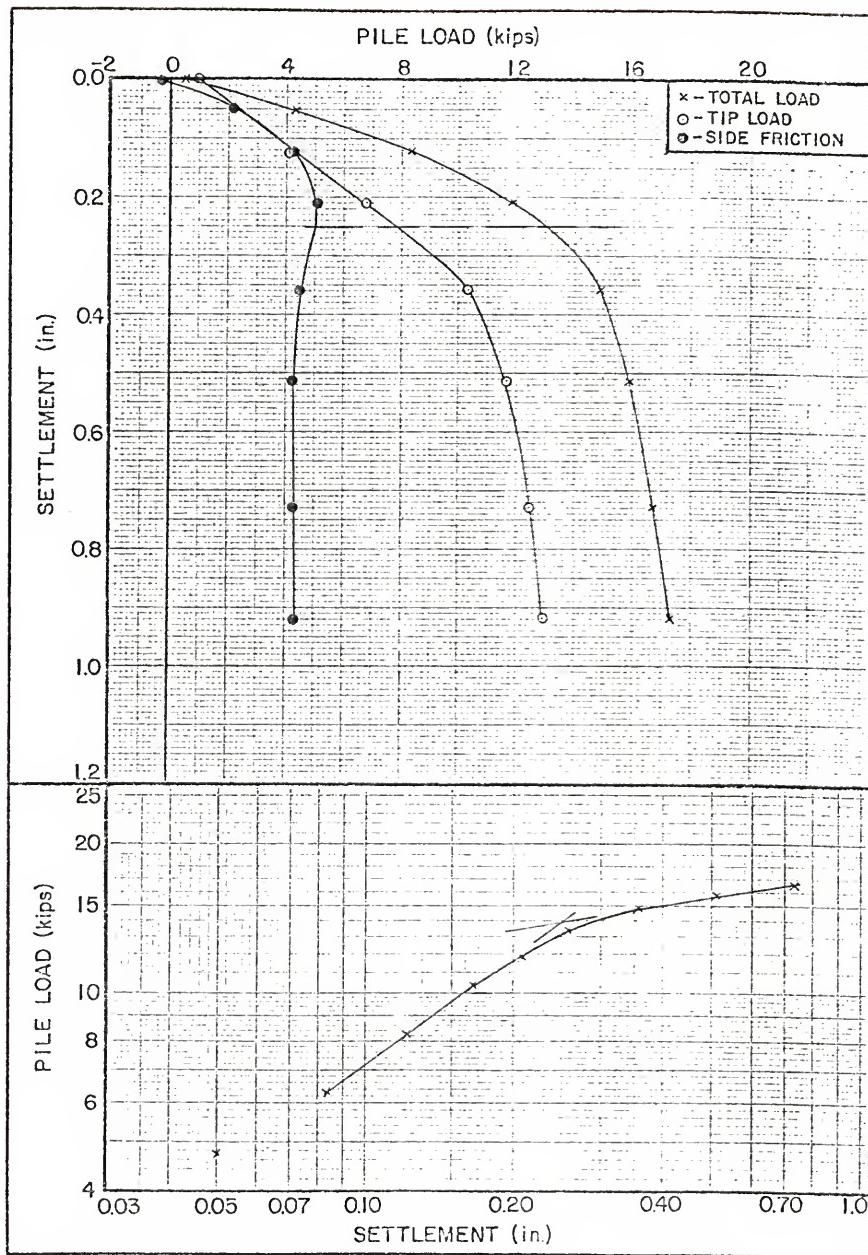
BEVILLE SITE NO 26 PILE LOAD TEST RESULTS - 6.0 FT CONCRETE PILE  
FIGURE B-85



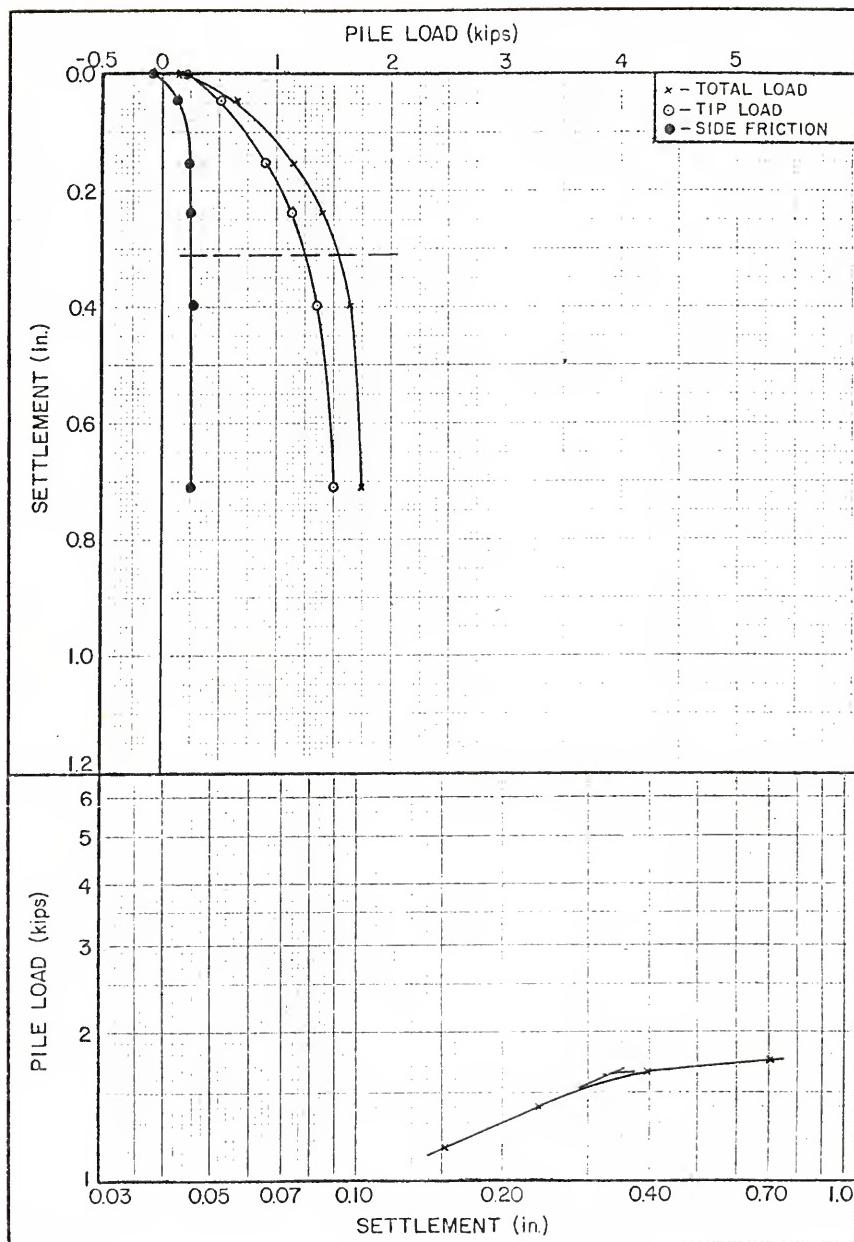
BEVILLE SITE NO 27 PILE LOAD TEST RESULTS - 3.0 FT CONCRETE PILE  
FIGURE B-86



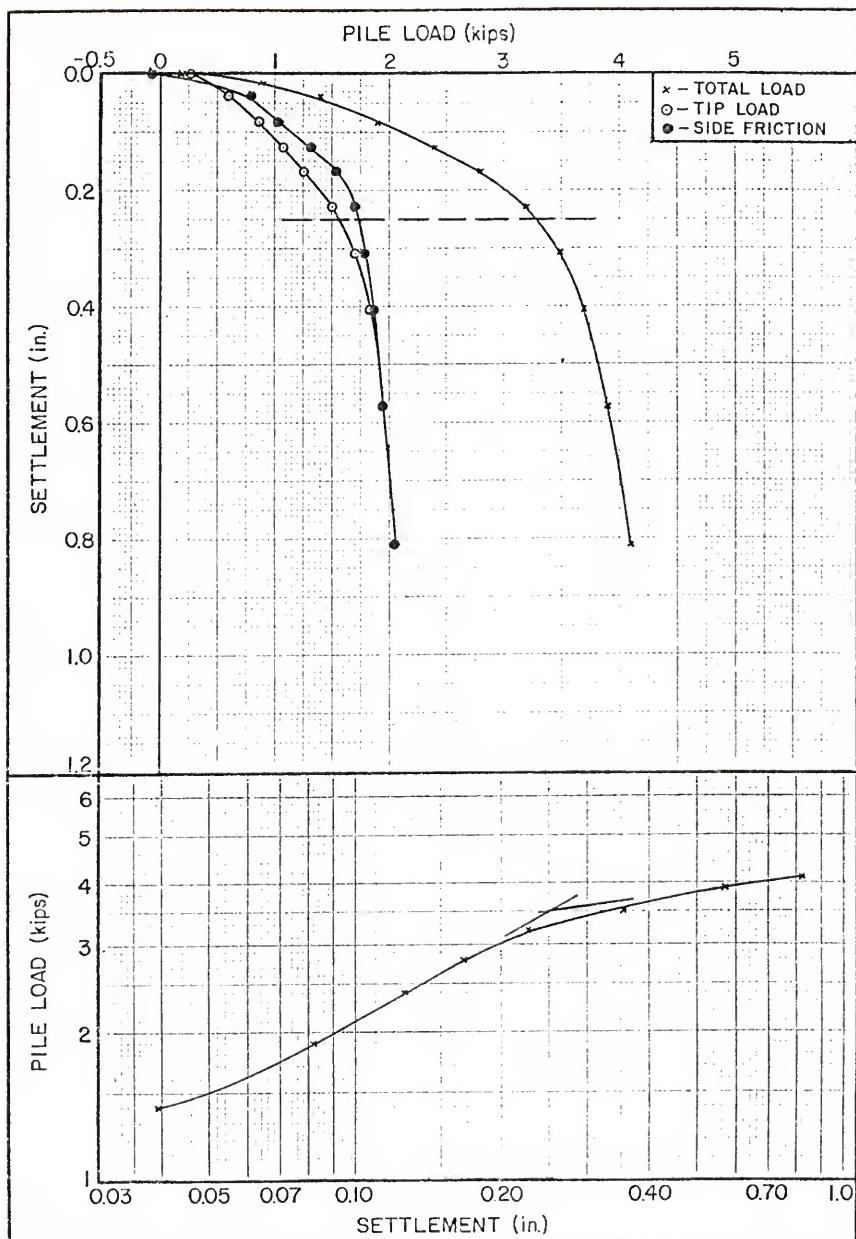
BEVILLE SITE NO 29 PILE LOAD TEST RESULTS - 8.0 FT CONCRETE PILE  
FIGURE B-87



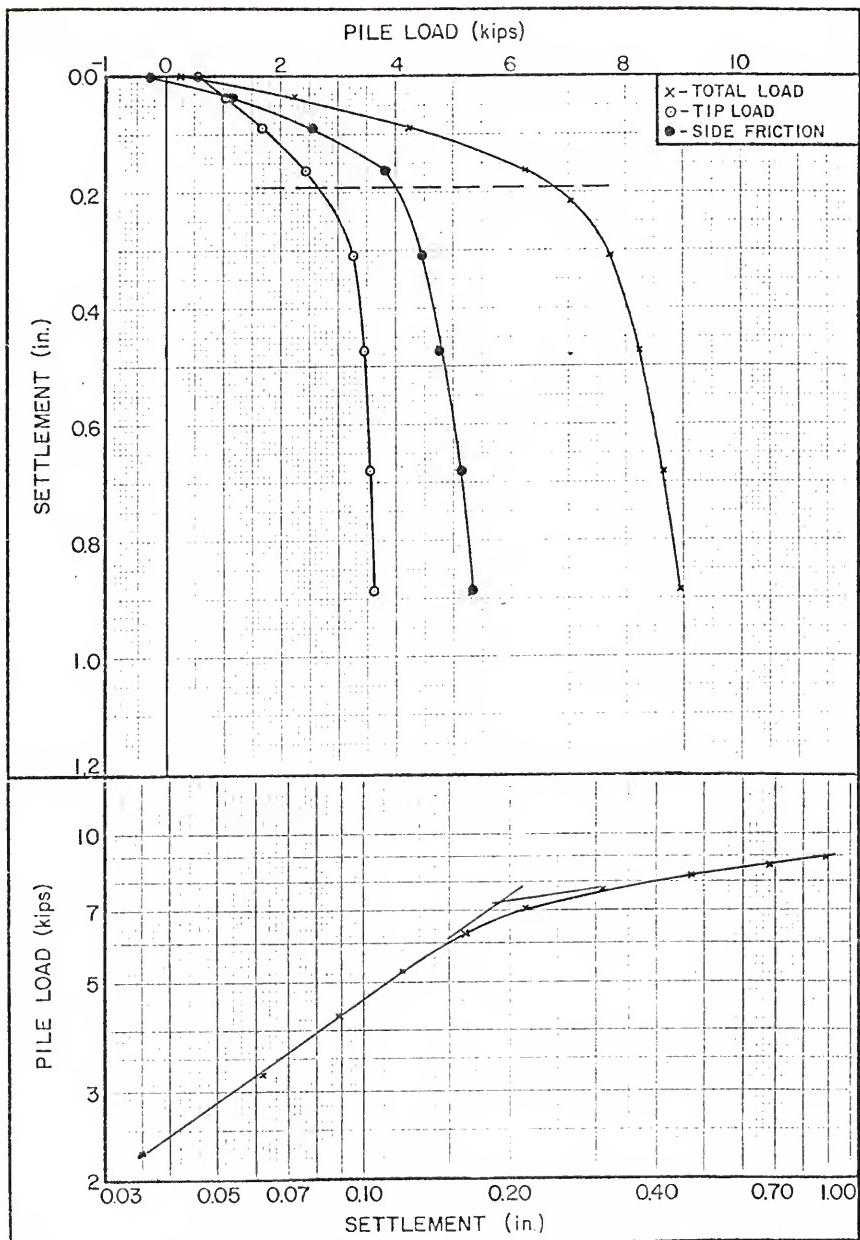
BEVILLE SITE NO 30 PILE LOAD TEST RESULTS - 8.33 FT CONCRETE PILE  
FIGURE B-88



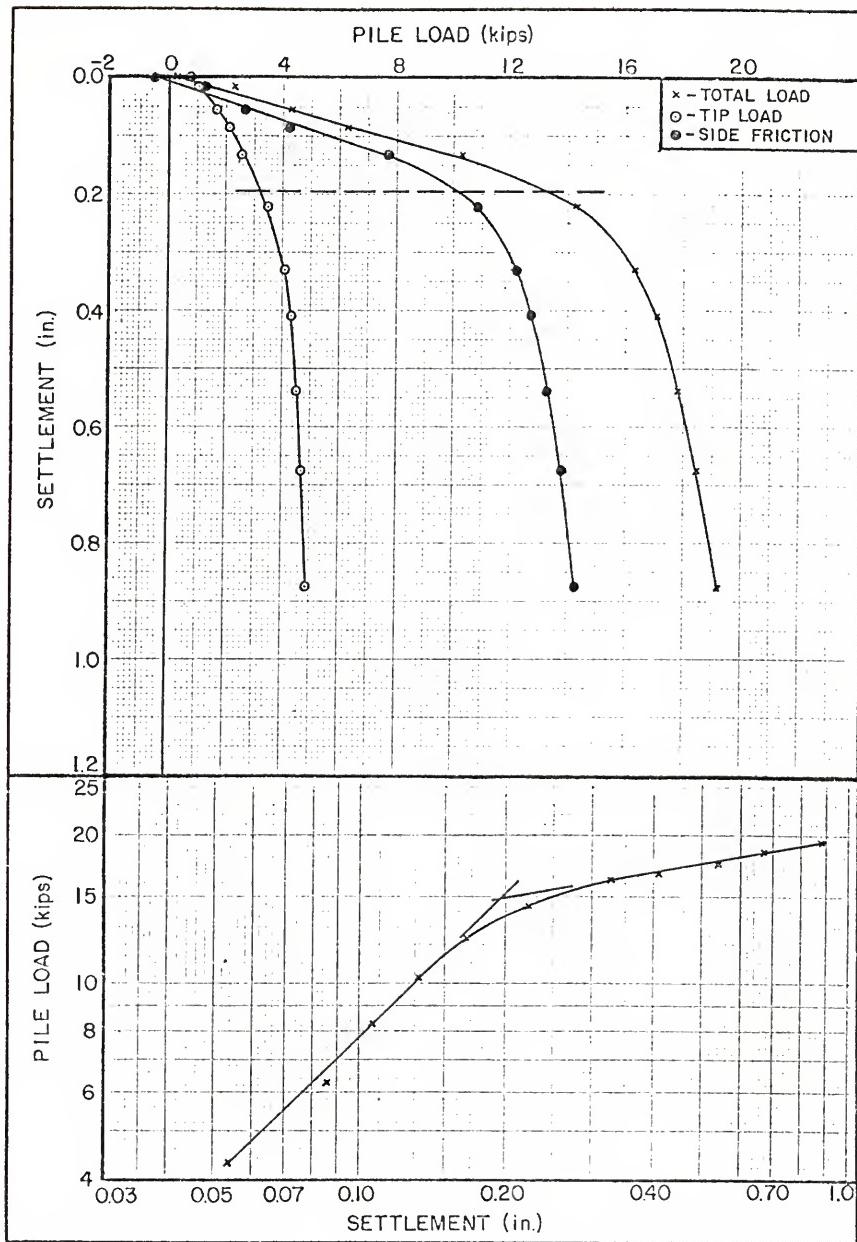
BEVILLE SITE NO 5 PILE LOAD TEST RESULTS - 2.5 FT STEP-TAPER PILE  
FIGURE B-89



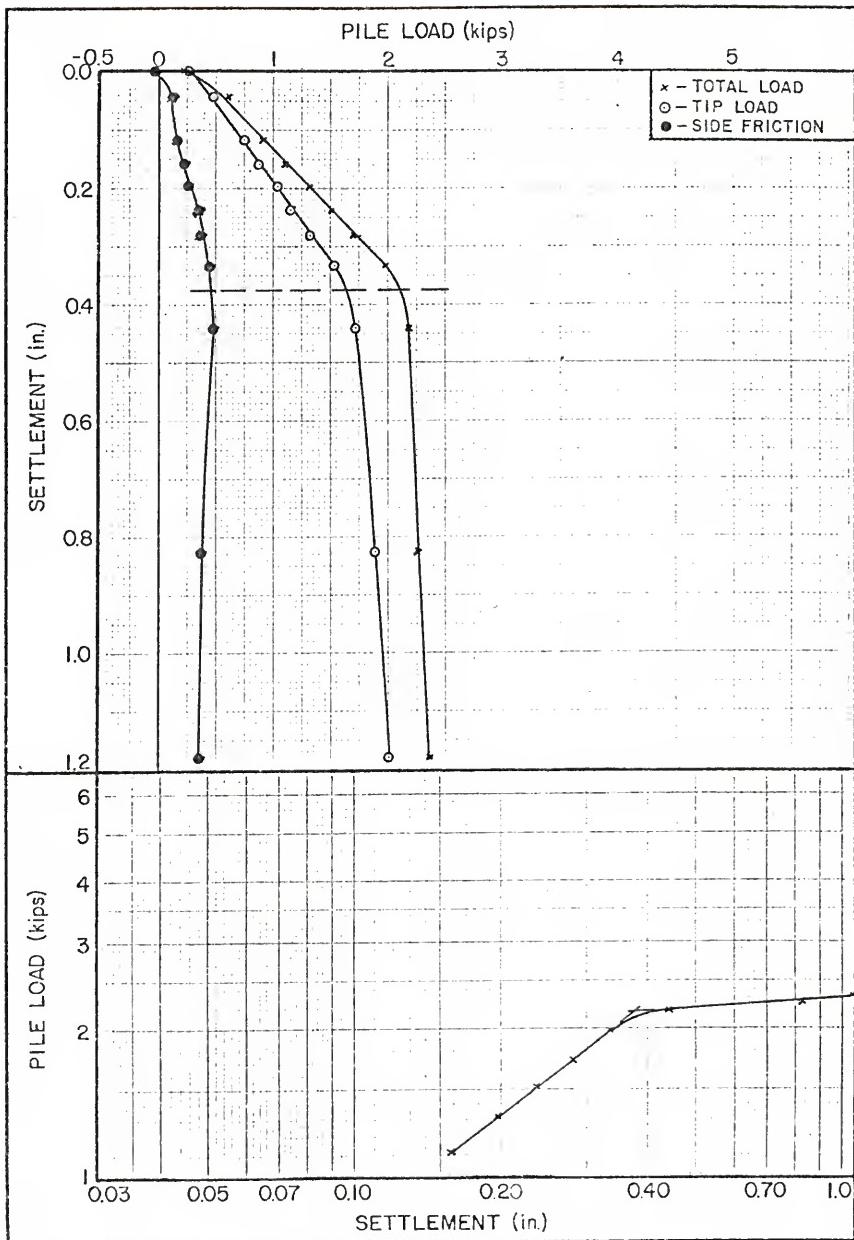
BEVILLE SITE NO 5 PILE LOAD TEST RESULTS - 4.75 FT STEP-TAPER PILE  
FIGURE B-90



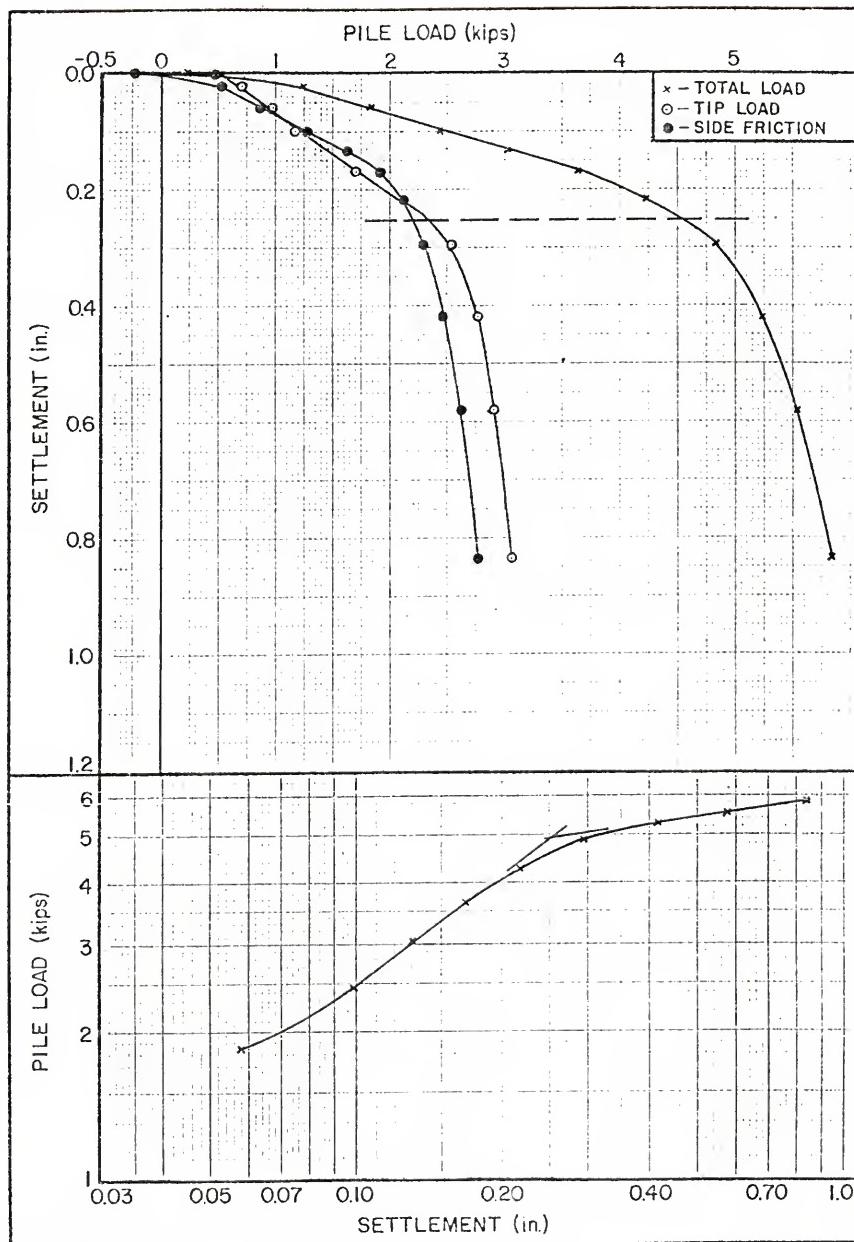
BEVILLE SITE NO 5 PILE LOAD TEST RESULTS - 7.25 FT STEP-TAPER PILE  
FIGURE B-91



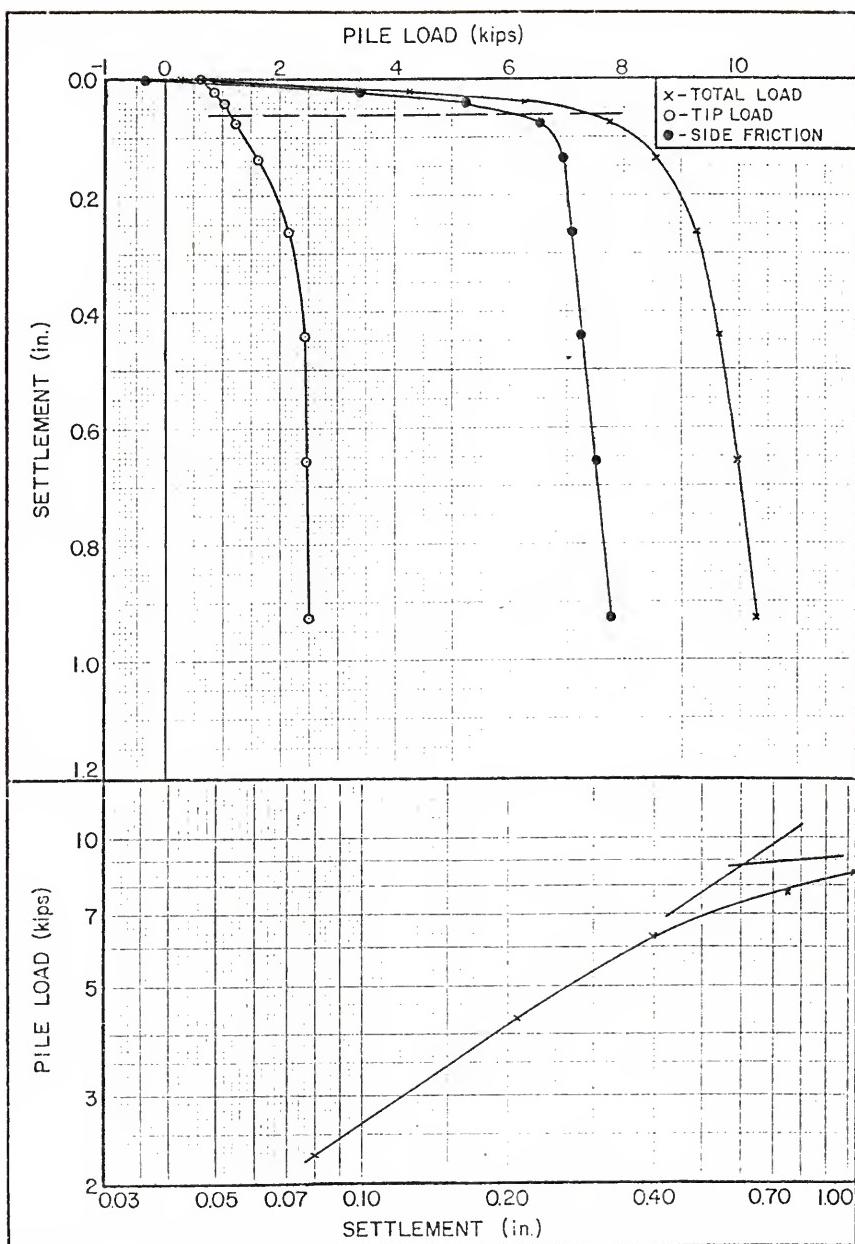
BEVILLE SITE NO 5 PILE LOAD TEST RESULTS - 9.75 FT STEP-TAPER PILE  
FIGURE B-92



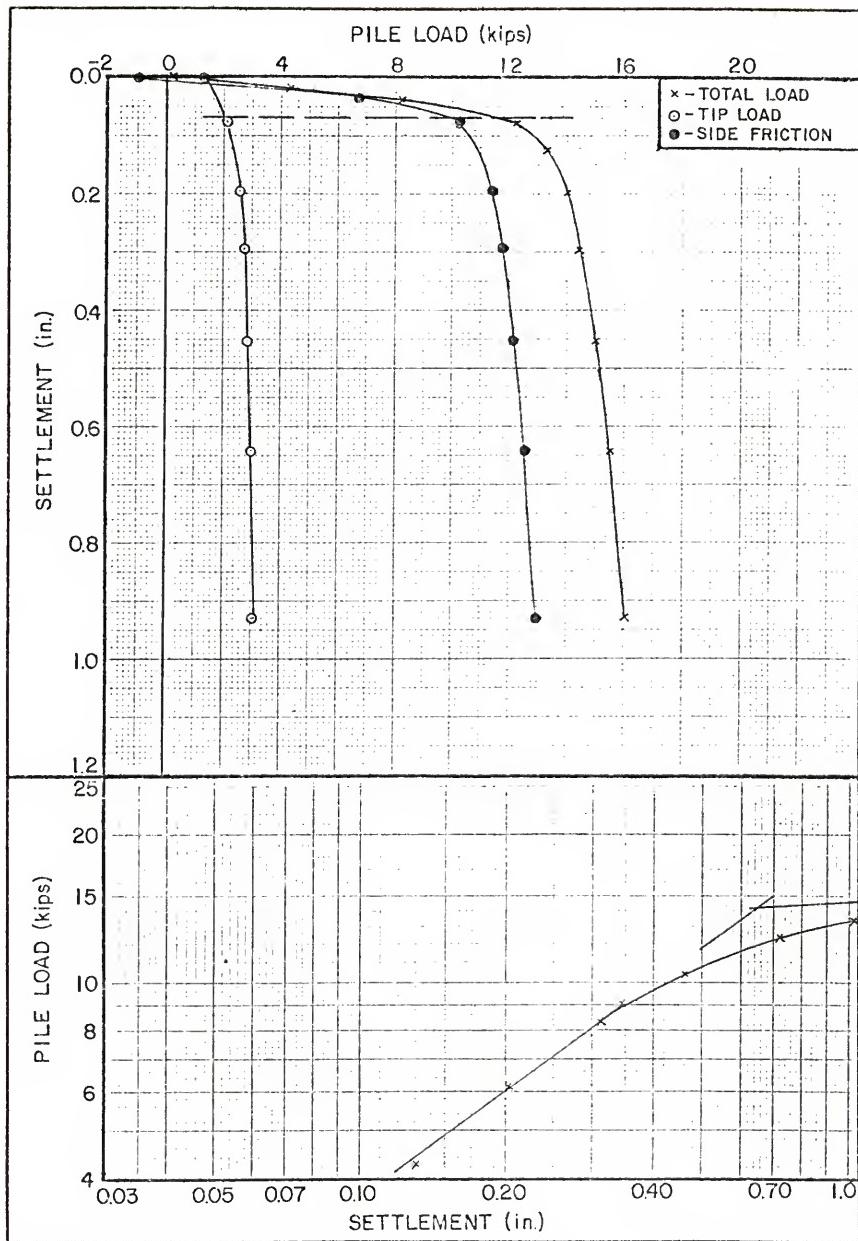
BEVILLE SITE NO 12 PILE LOAD TEST RESULTS - 2.25 FT STEP-TAPER PILE  
FIGURE B-93



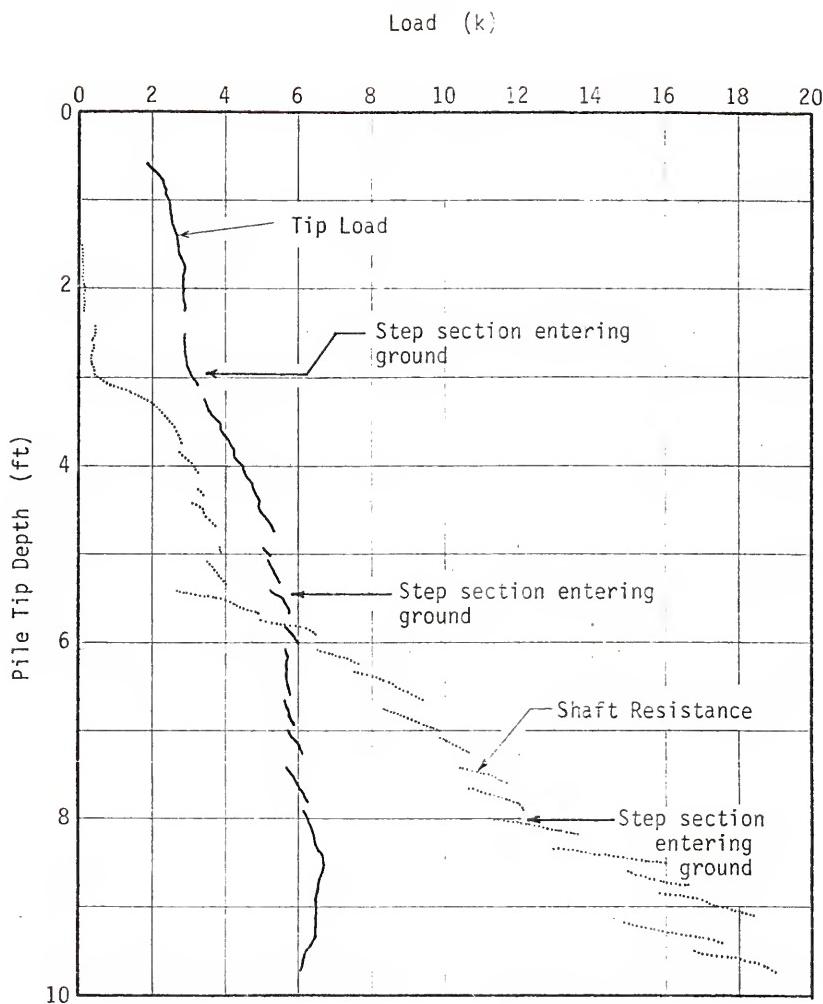
BEVILLE SITE NO 12 PILE LOAD TEST RESULTS - 4.75 FT STEP-TAPER PILE  
FIGURE B-94



BEVILLE SITE NO 12 PILE LOAD TEST RESULTS - 7.25 FT STEP-TAPER PILE  
FIGURE B-95

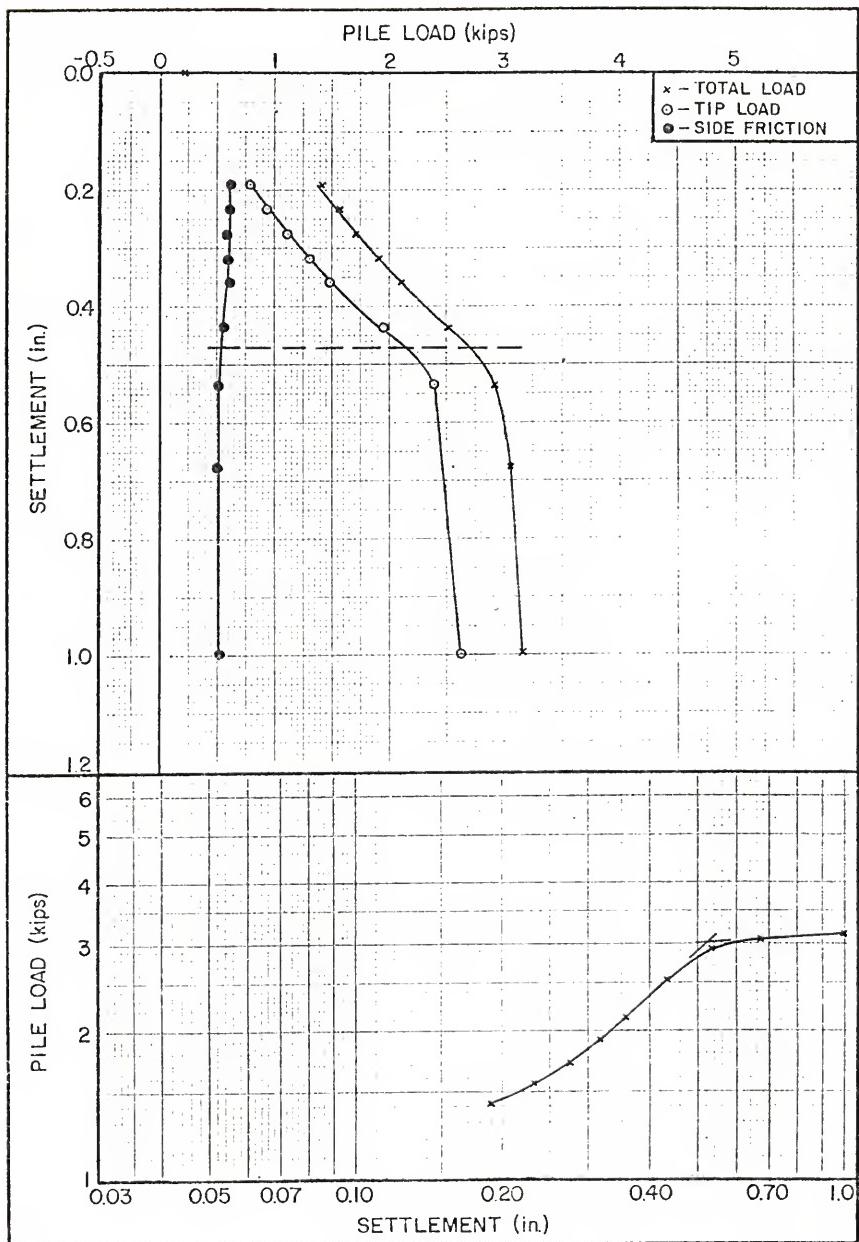


BEVILLE SITE NO 12 PILE LOAD TEST RESULTS - 9.75 FT STEP-TAPER PILE  
FIGURE B-96

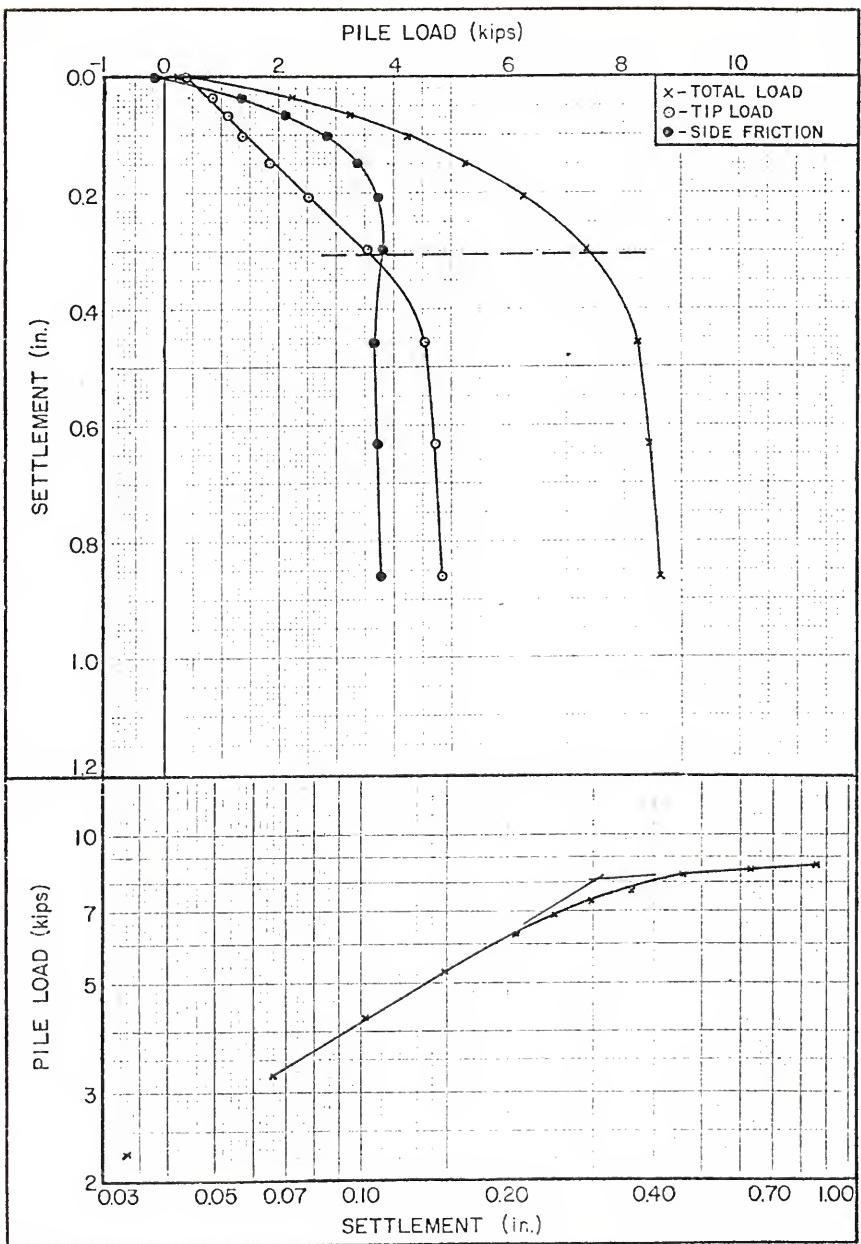


JACK-IN DATA FOR BEVILLE SITE 20 TEST

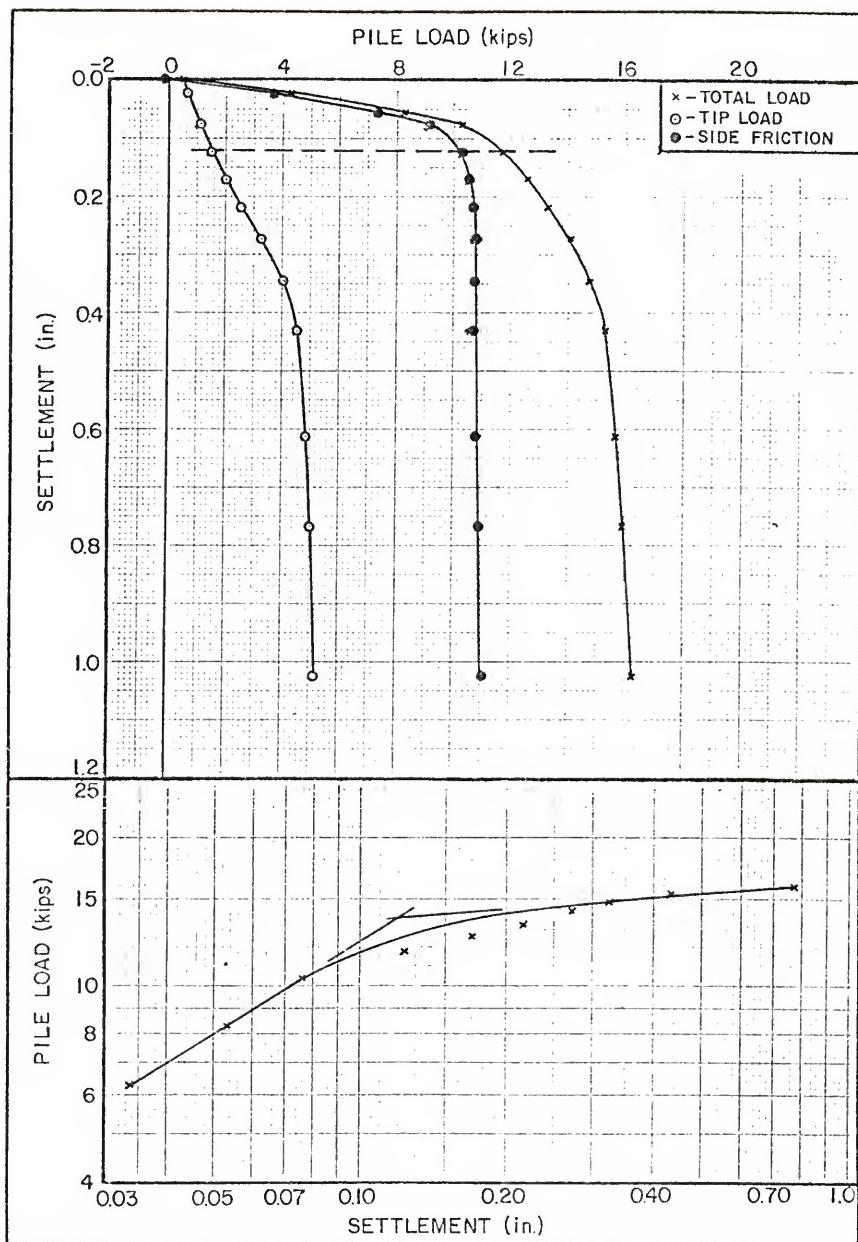
FIGURE B-97



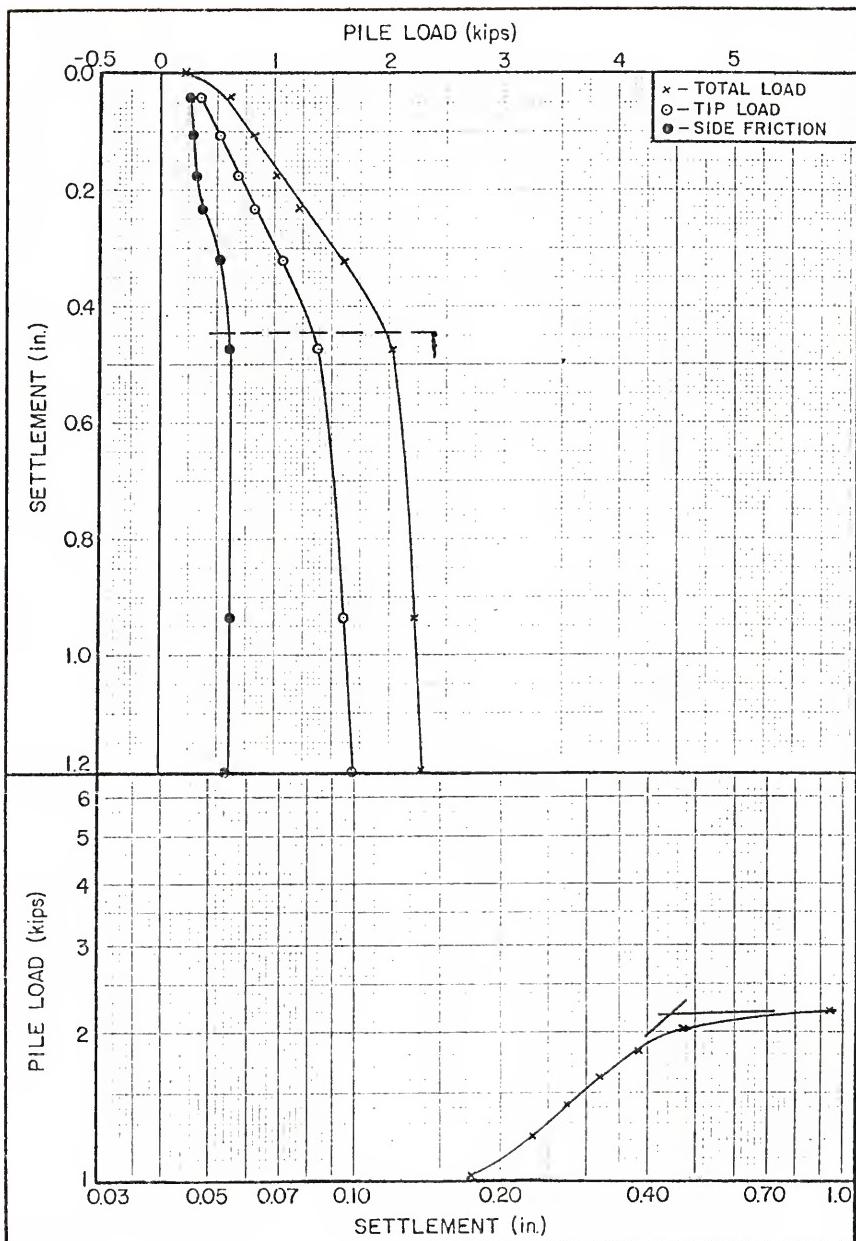
BEVILLE SITE NO 20 PILE LOAD TEST RESULTS - 2.25 FT STEP-TAPER PILE  
FIGURE B-98



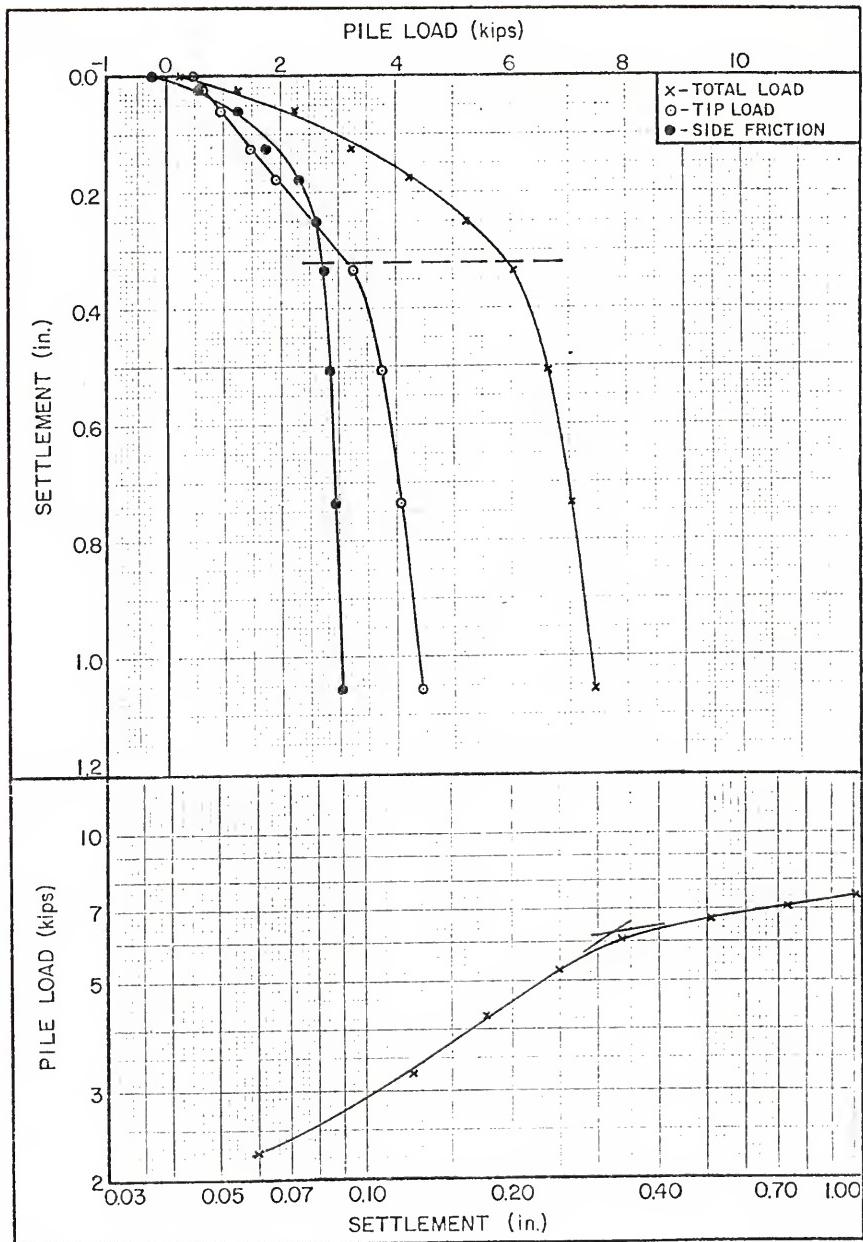
BEVILLE SITE NO 20 PILE LOAD TEST RESULTS - 4.75 FT STEP-TAPER PILE  
FIGURE B-99



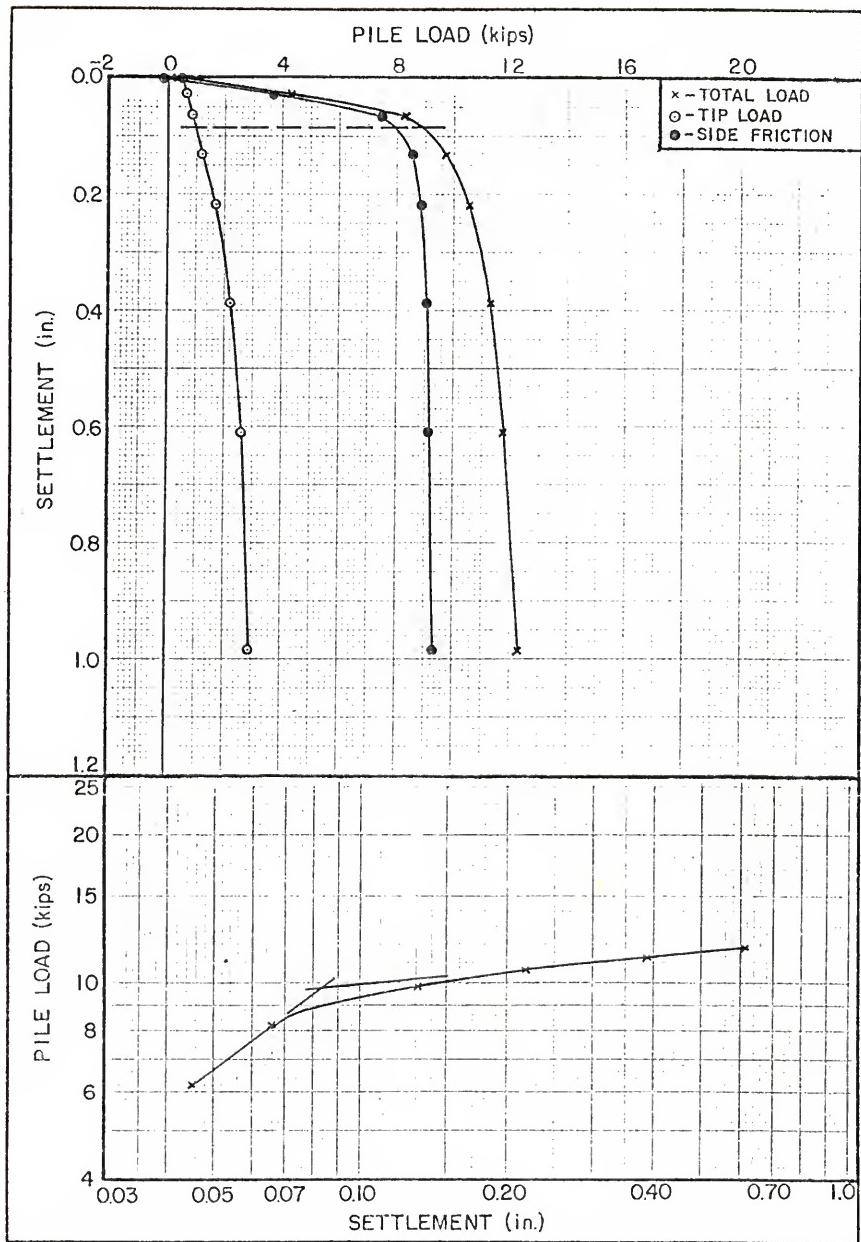
BEVILLE SITE NO 20 PILE LOAD TEST RESULTS - 7.25 FT STEP-TAPER PILE  
FIGURE B-100



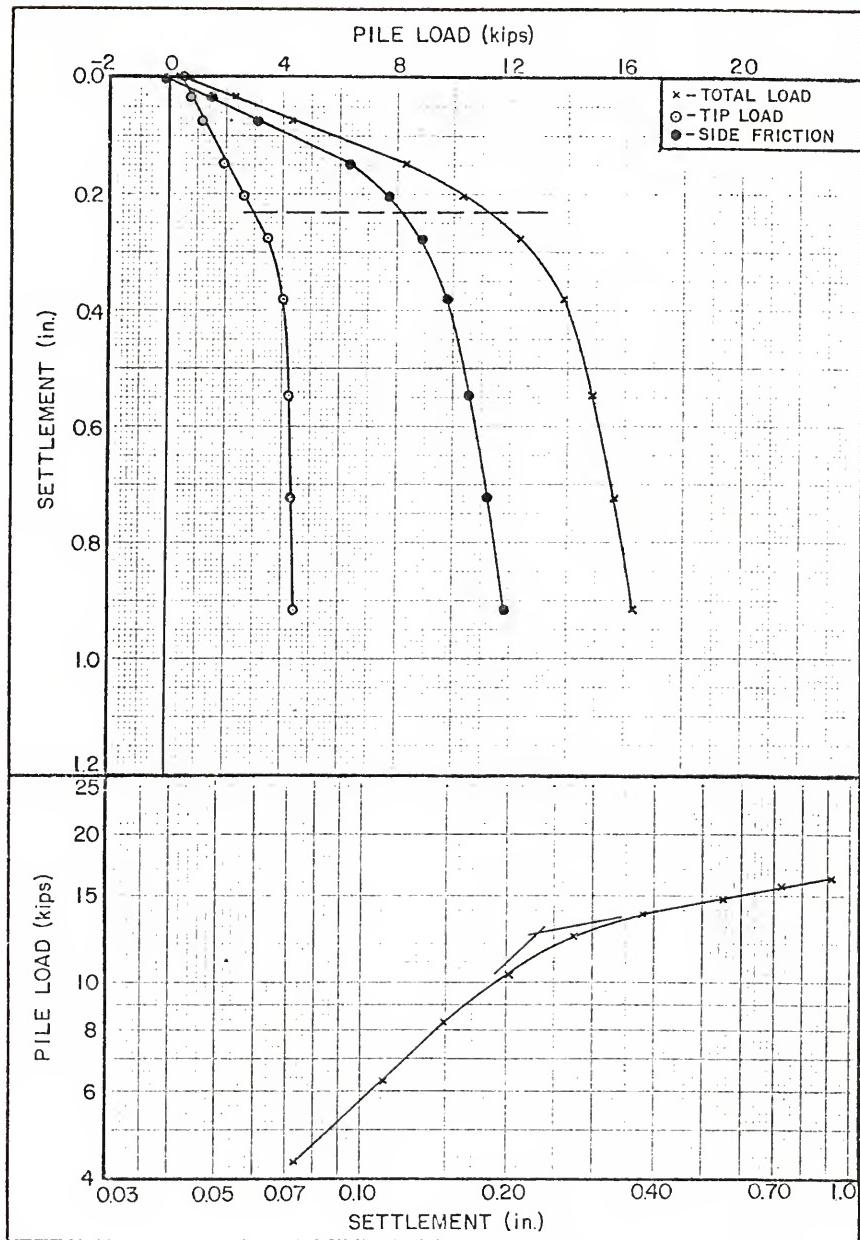
BEVILLE SITE NO 32 PILE LOAD TEST RESULTS - 2.25 FT STEP-TAPER PILE  
FIGURE B-102



BEVILLE SITE NO 32 PILE LOAD TEST RESULTS - 4.75 FT STEP-TAPER PILE  
FIGURE B-103

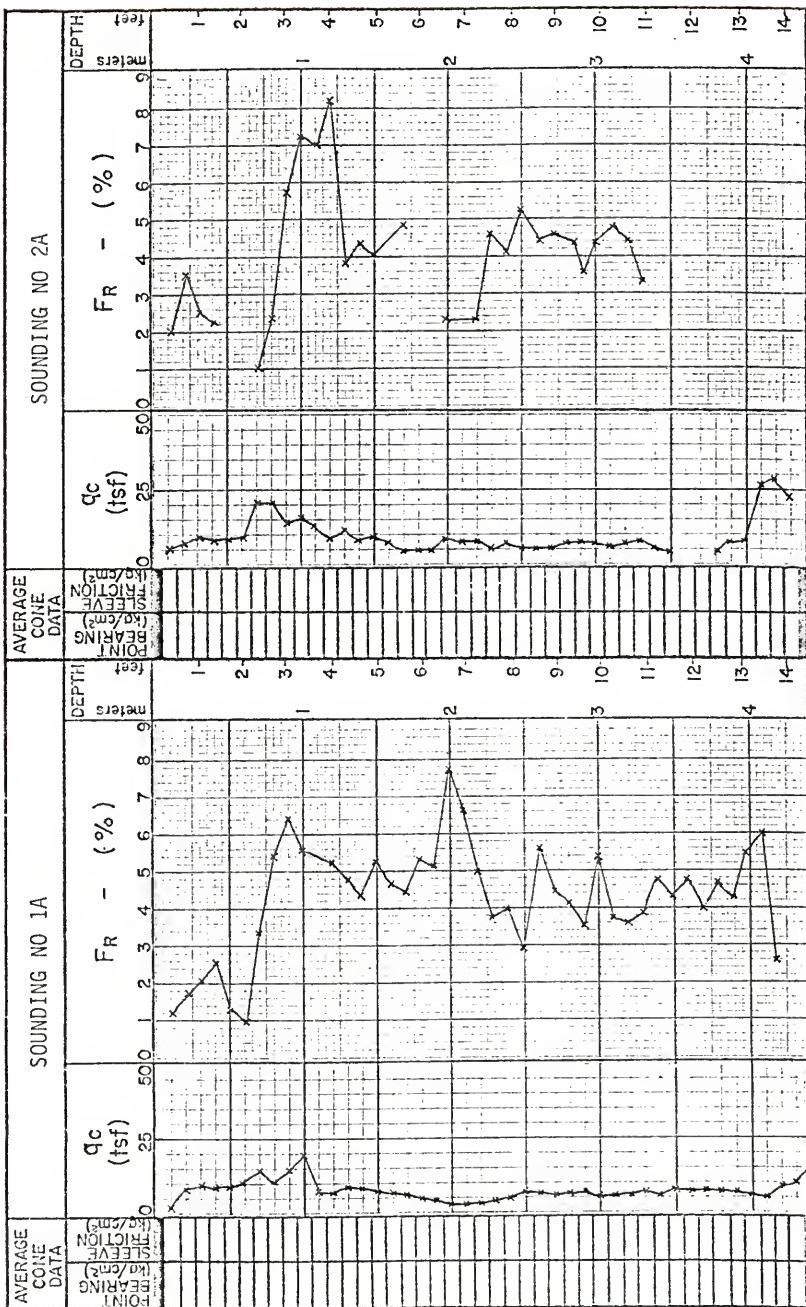


BEVILLE SITE NO 32 PILE LOAD TEST RESULTS - 7.25 FT STEP-TAPER PILE  
FIGURE B-104

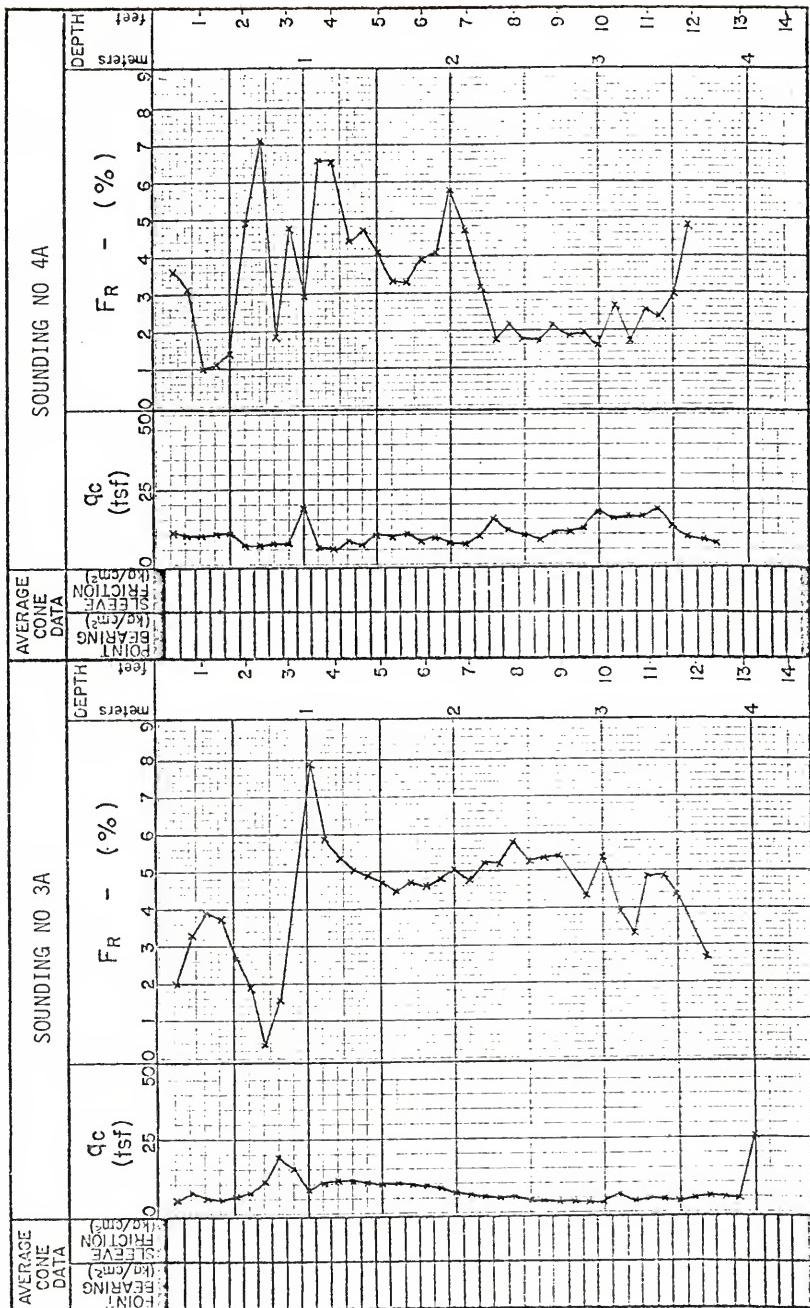


BEVILLE SITE NO 32 PILE LOAD TEST RESULTS - 9.75 FT STEP-TAPER PILE  
FIGURE B-105

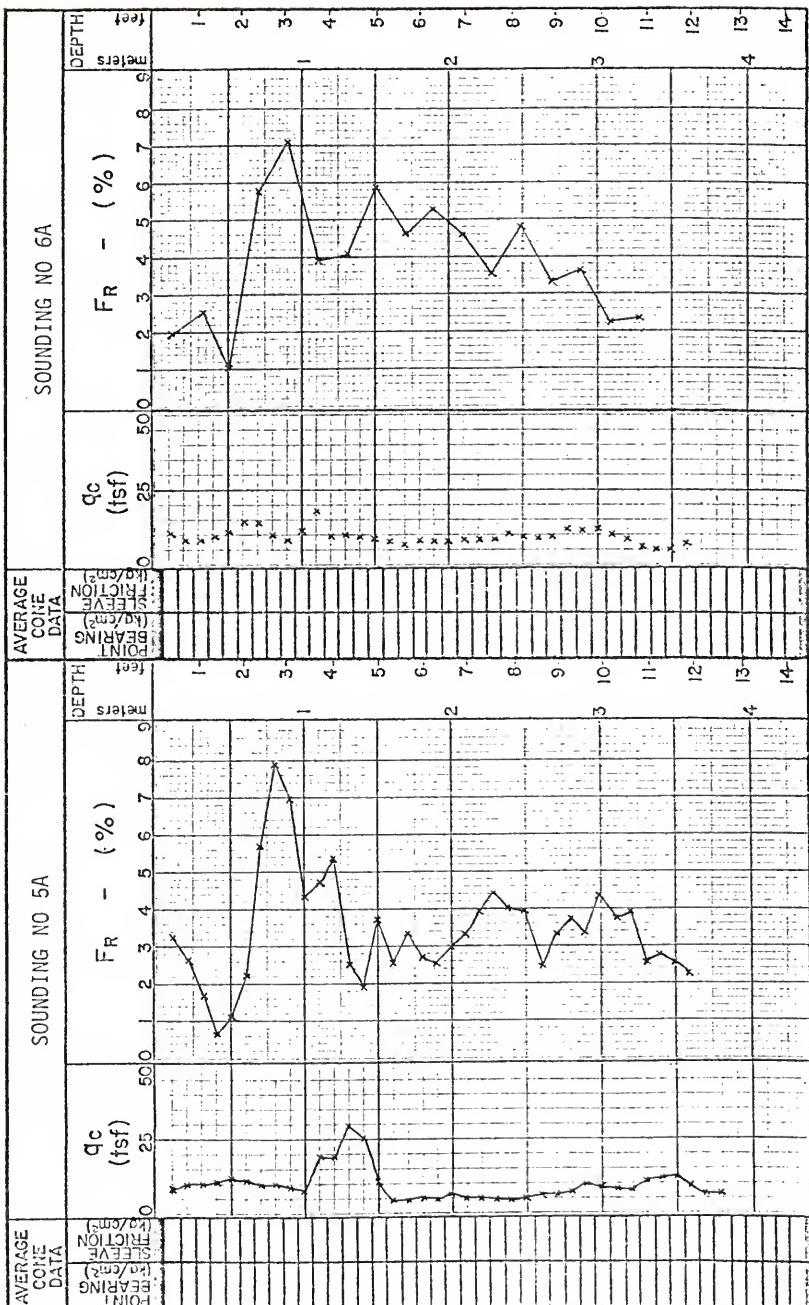
APPENDIX C  
PAINES PRAIRIE SITE TEST RESULTS



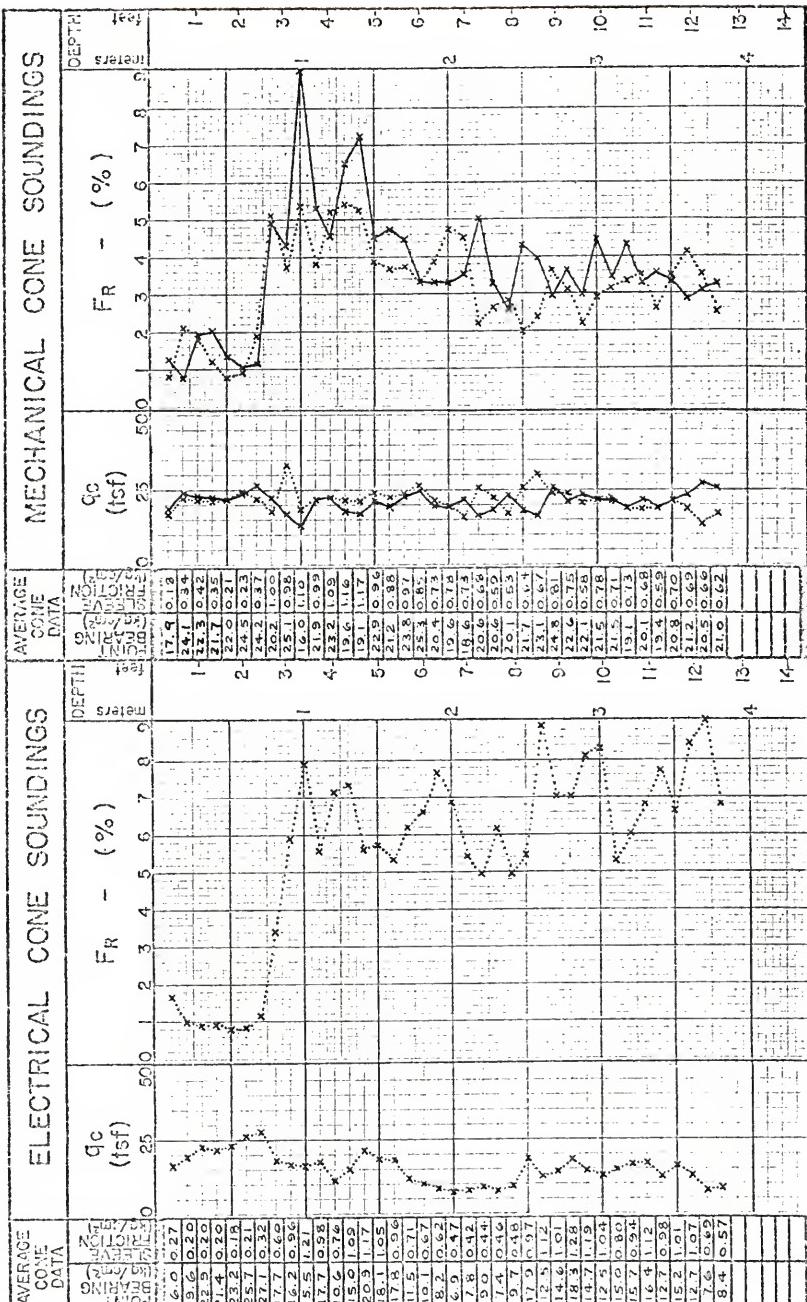
PAINES PRAIRIE PRELIMINARY CPT SOUNDING LOGS  
FIGURE C-1



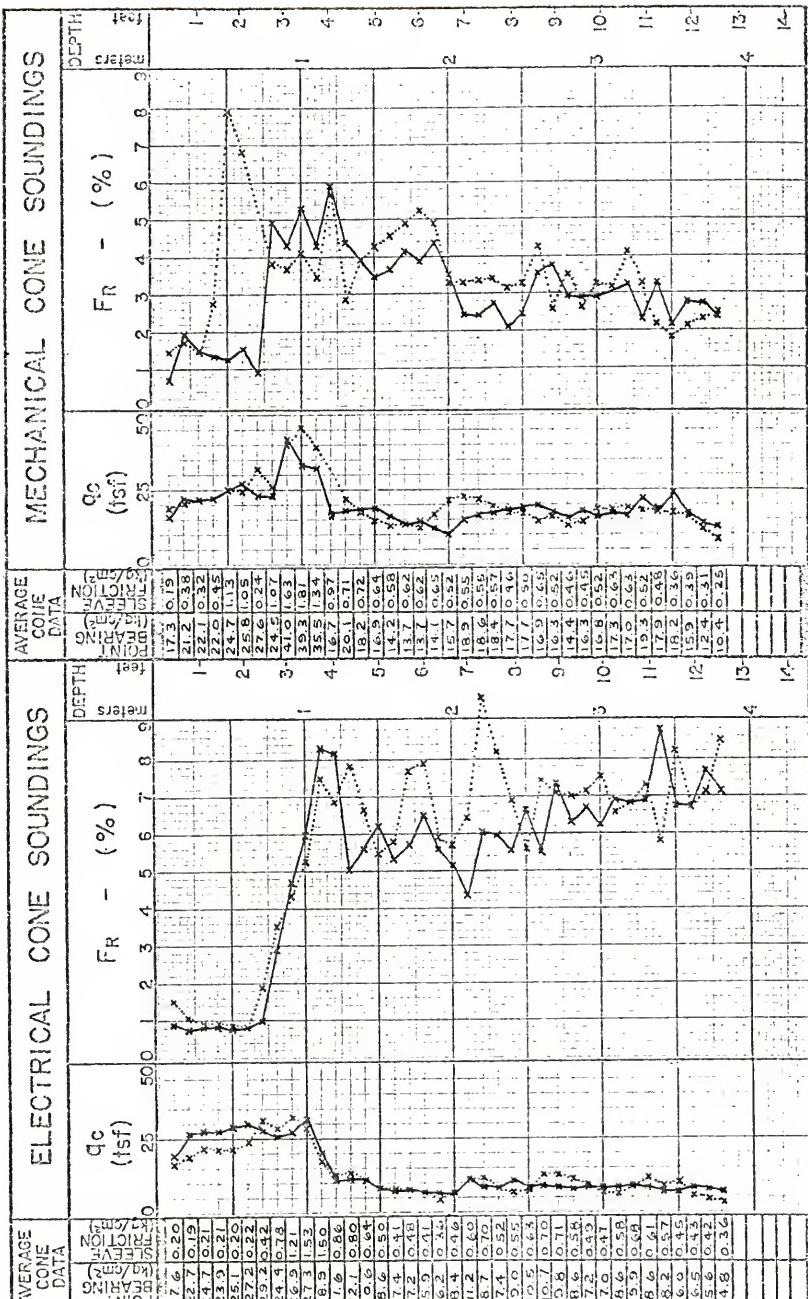
PAINES PRAIRIE PRELIMINARY CPT SOUNDING LOGS  
FIGURE C-2



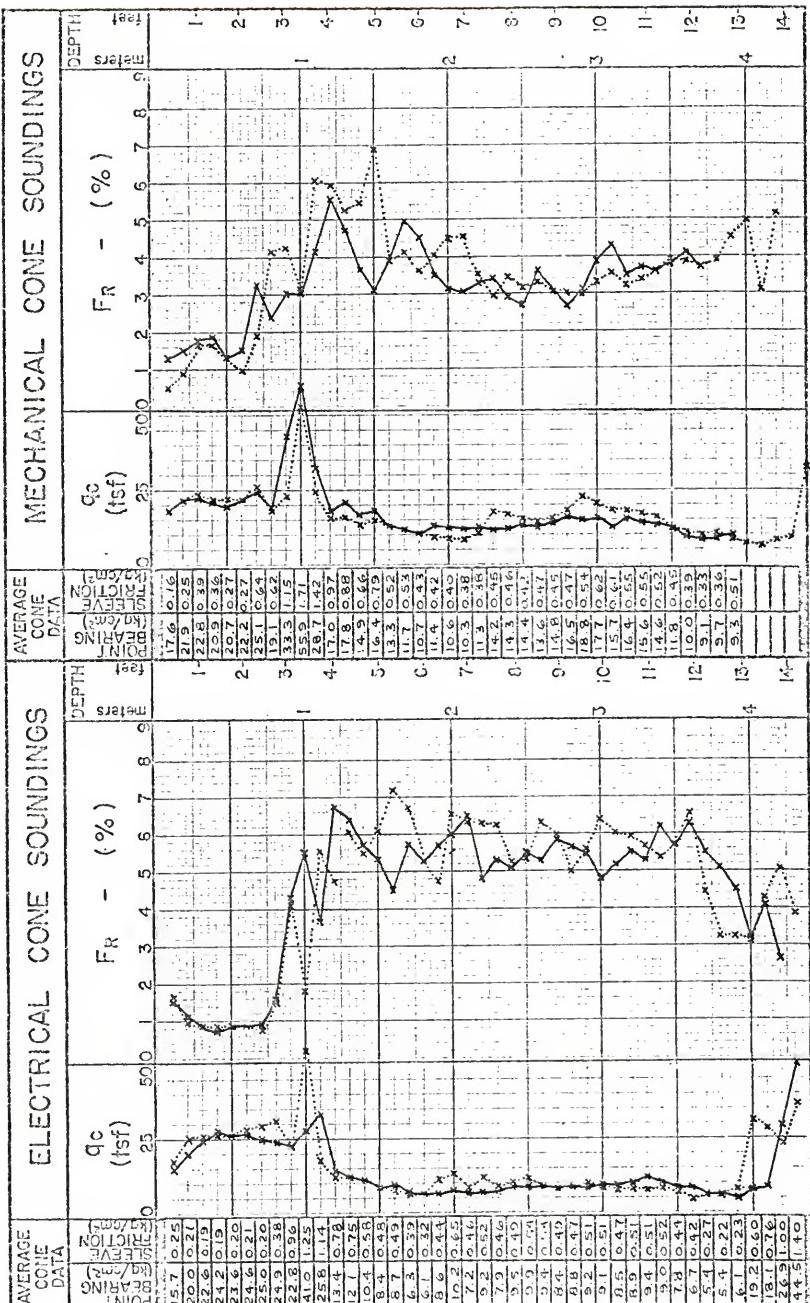
PAINES PRAIRIE PRELIMINARY CPT SOUNDING LOGS  
FIGURE C-3



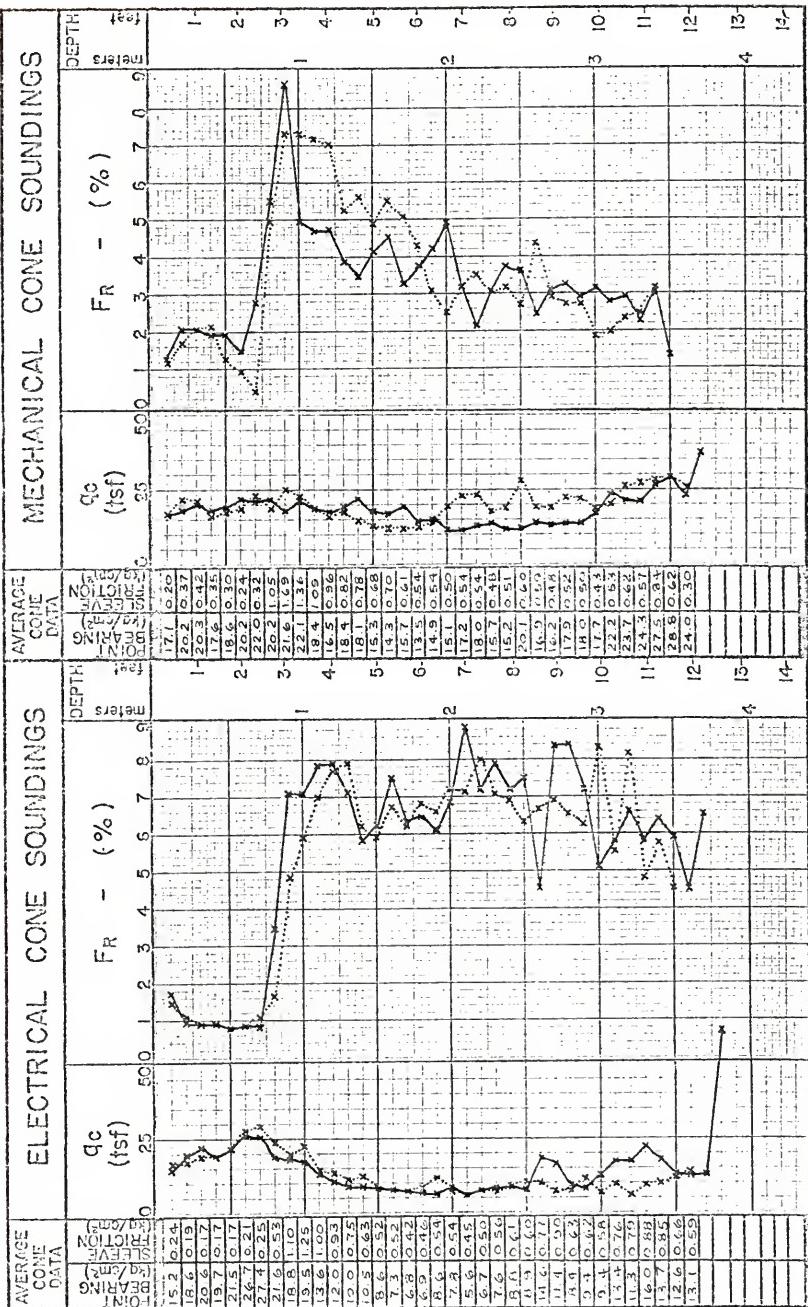
PAINES PRAIRIE SITE NO 1 CPT LOGS  
FIGURE 6-4



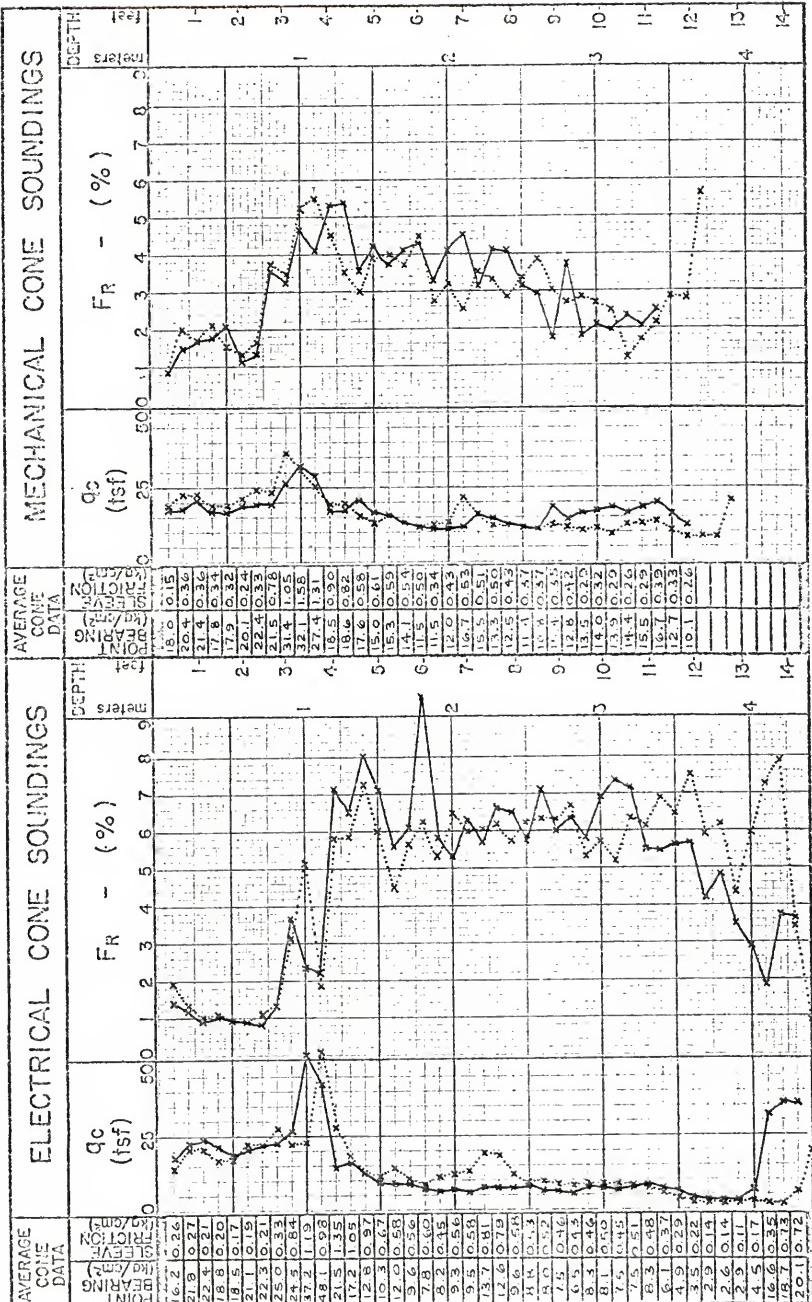
PAINES PRAIRIE SITE NO 2 CPT LOGS  
FIGURE C-5



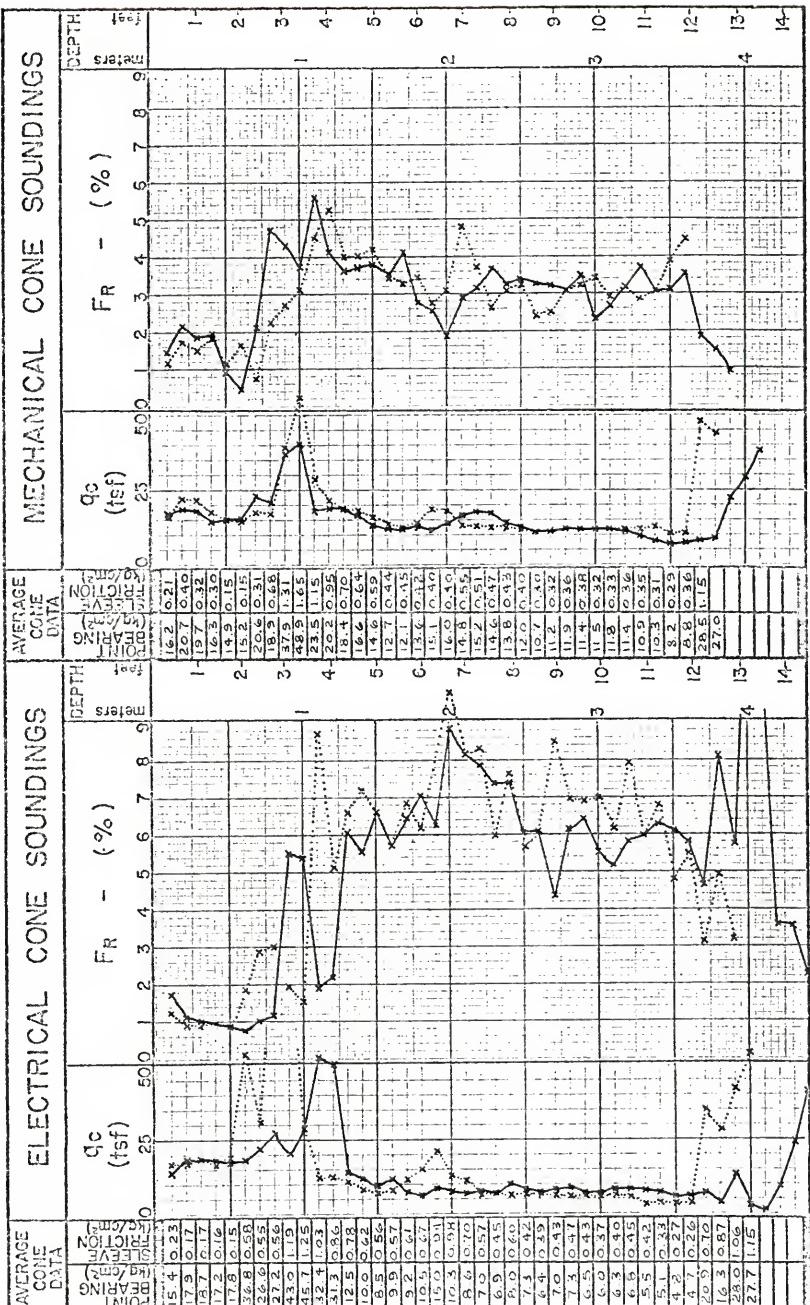
PAINES PRAIRIE SITE NO 3 CPT LOGS  
FIGURE C-6



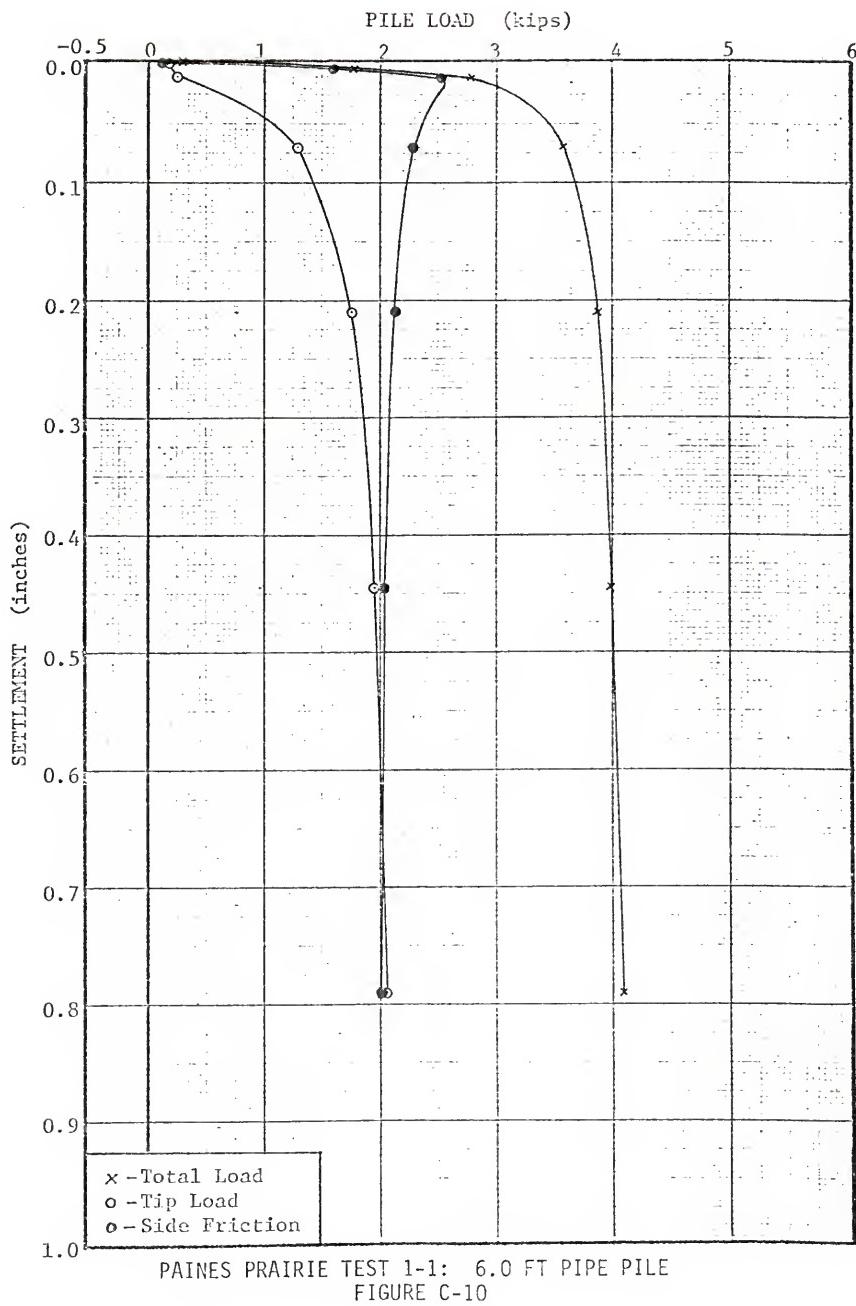
PAINES PRAIRIE SITE NO 4 CPT LOGS  
FIGURE C-7

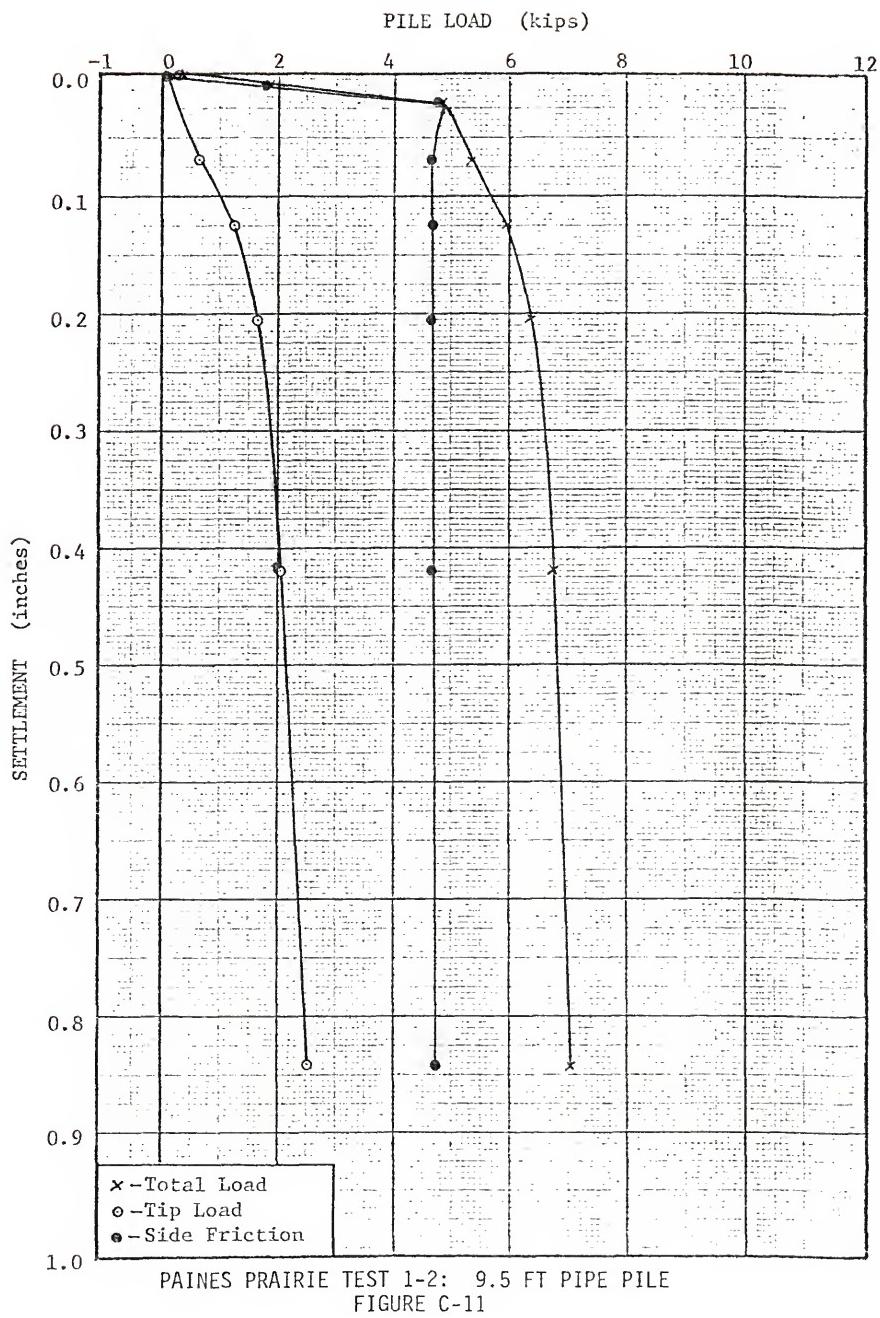


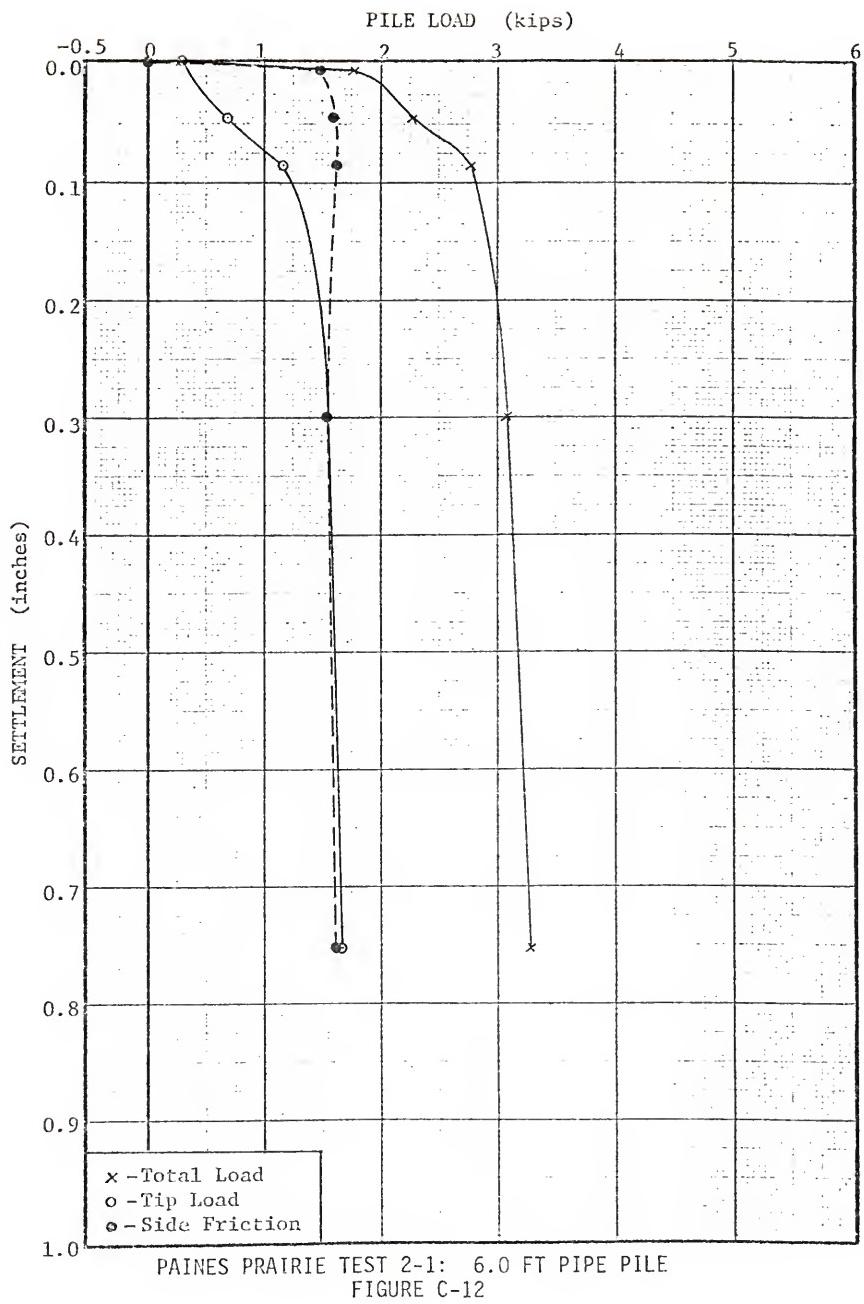
PAINES PRAIRIE SITE NO 5 CPT LOGS  
FIGURE C-8

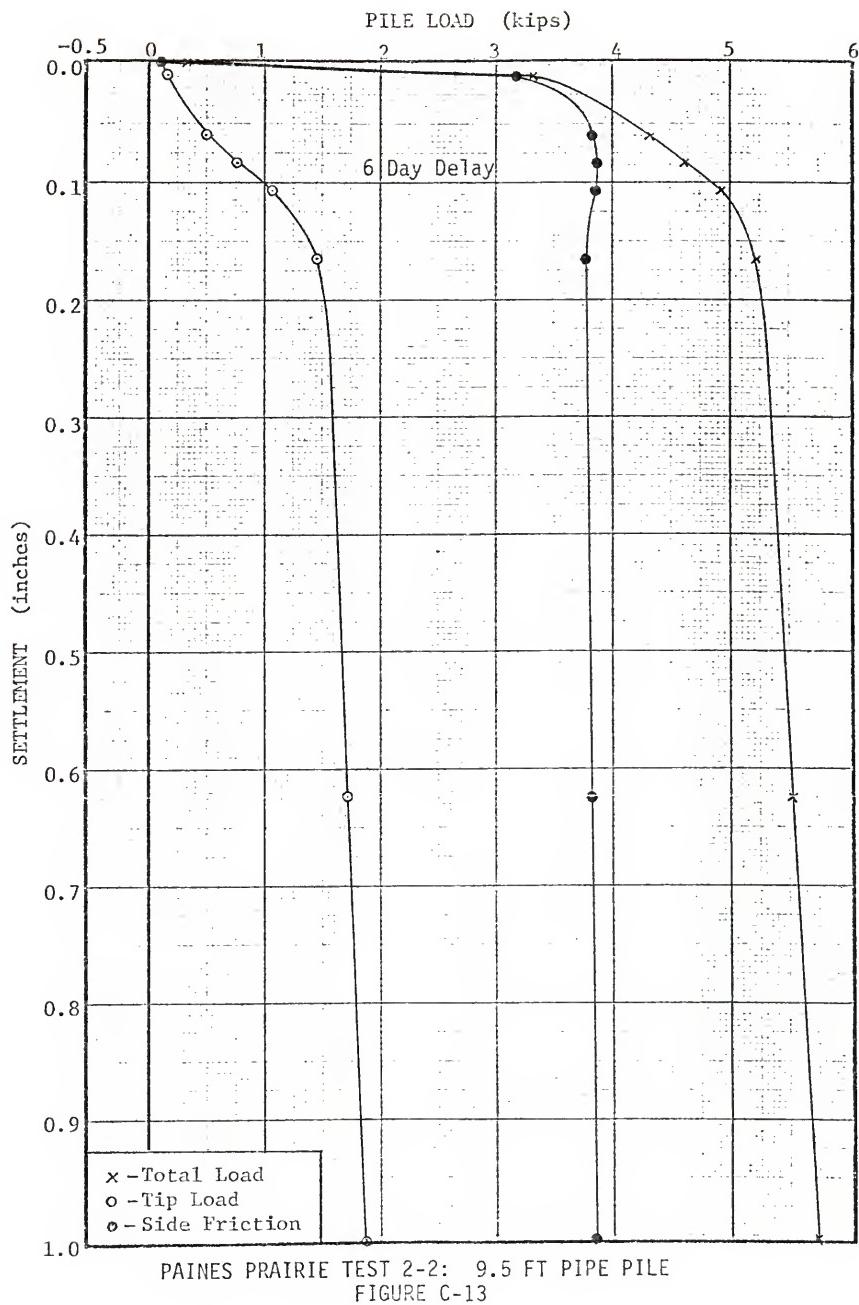


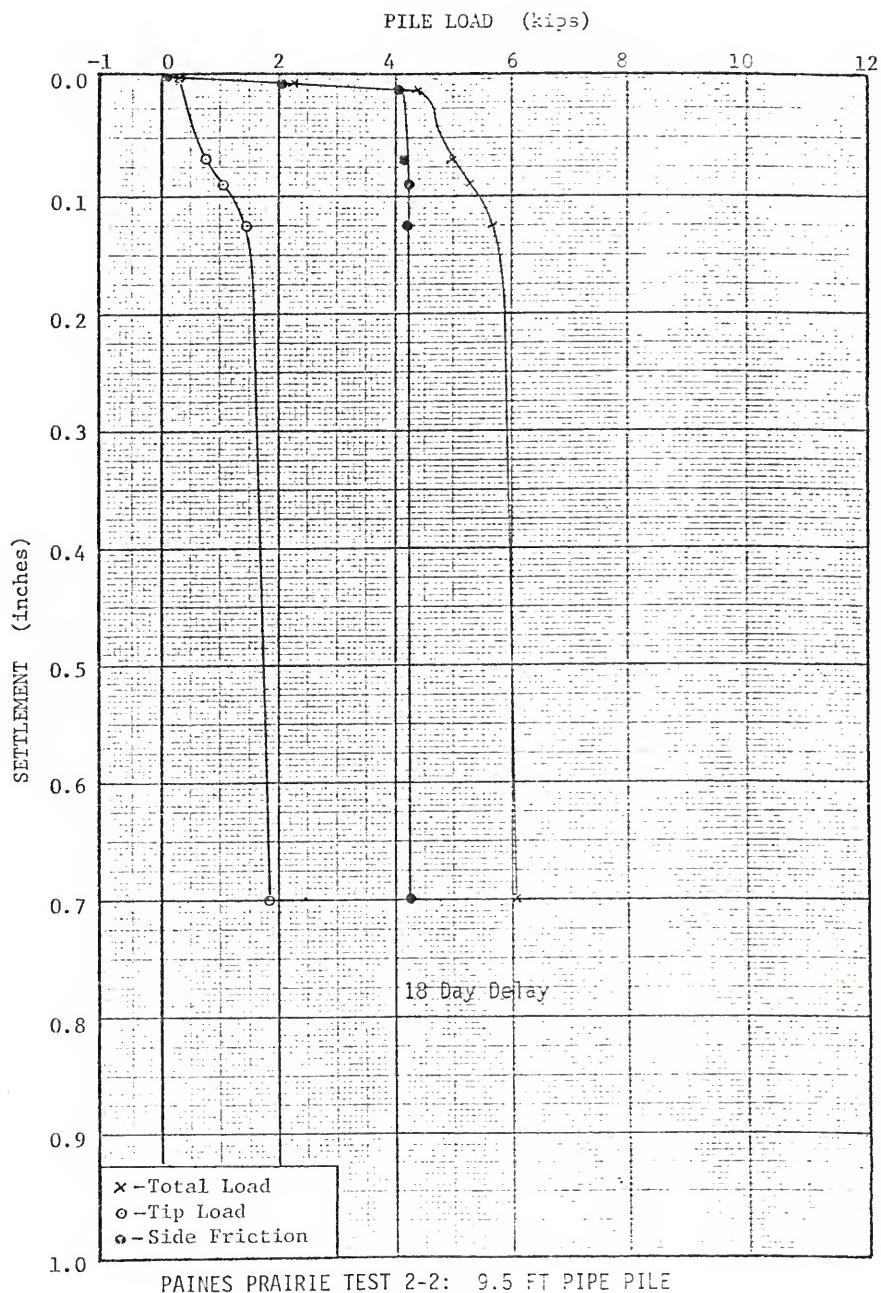
PAINES PRAIRIE SITE NO 6 CPT LOGS  
FIGURE 6.6

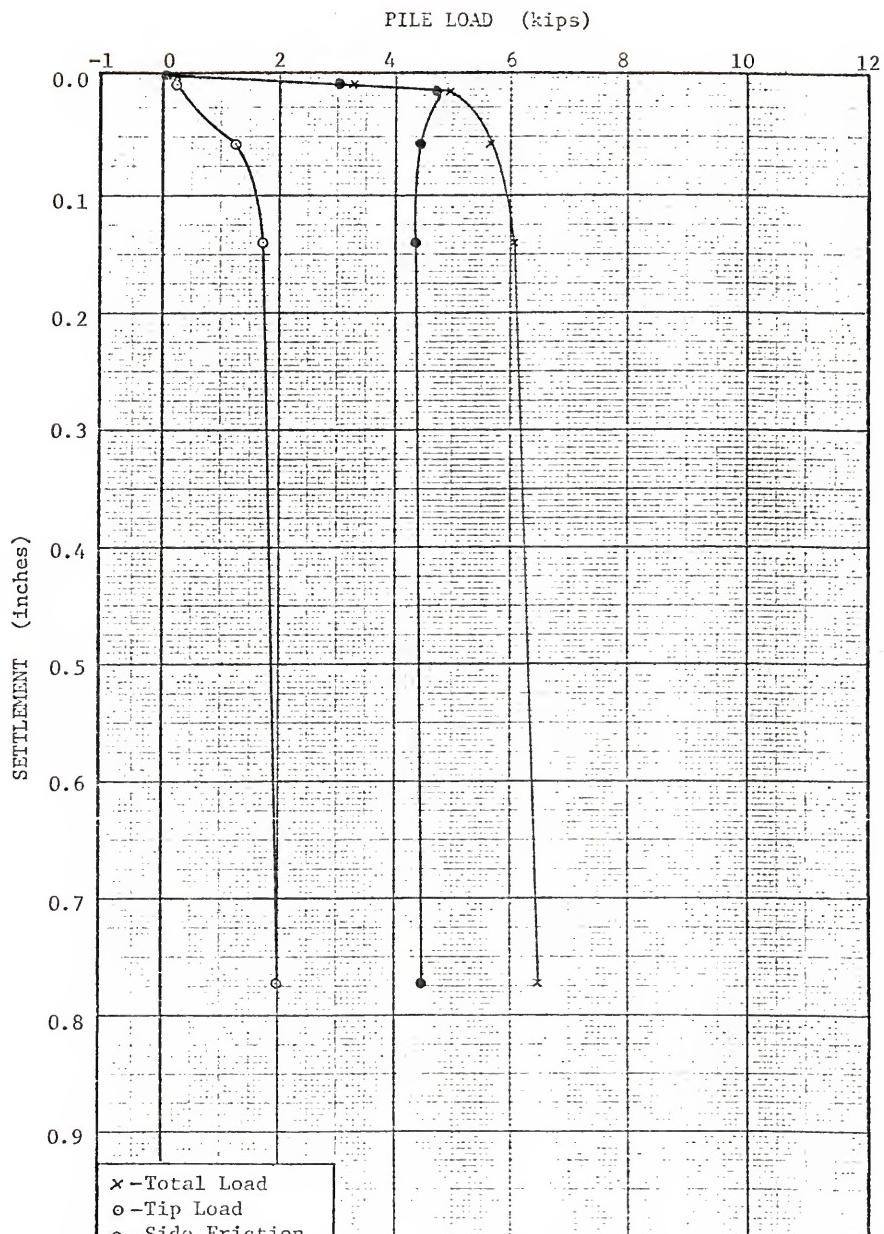




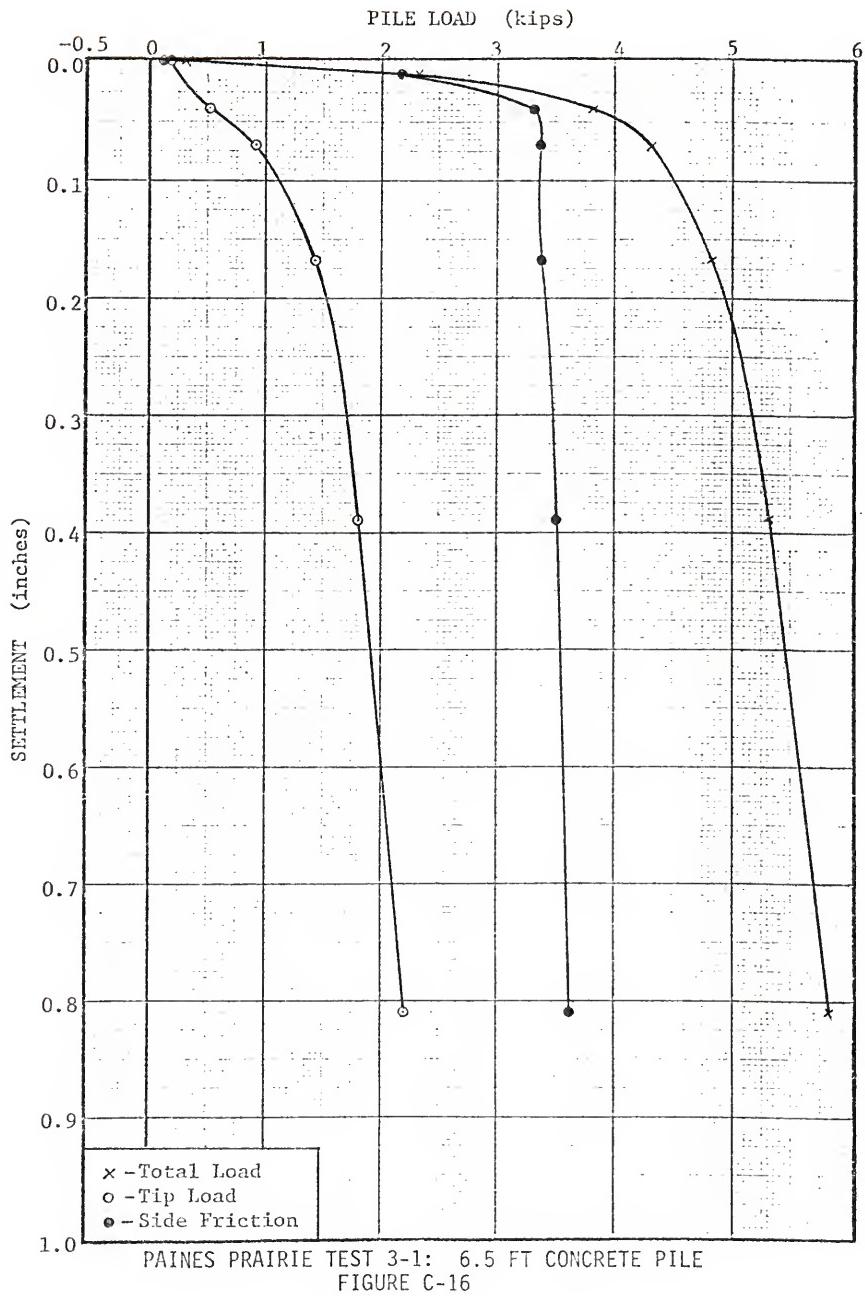


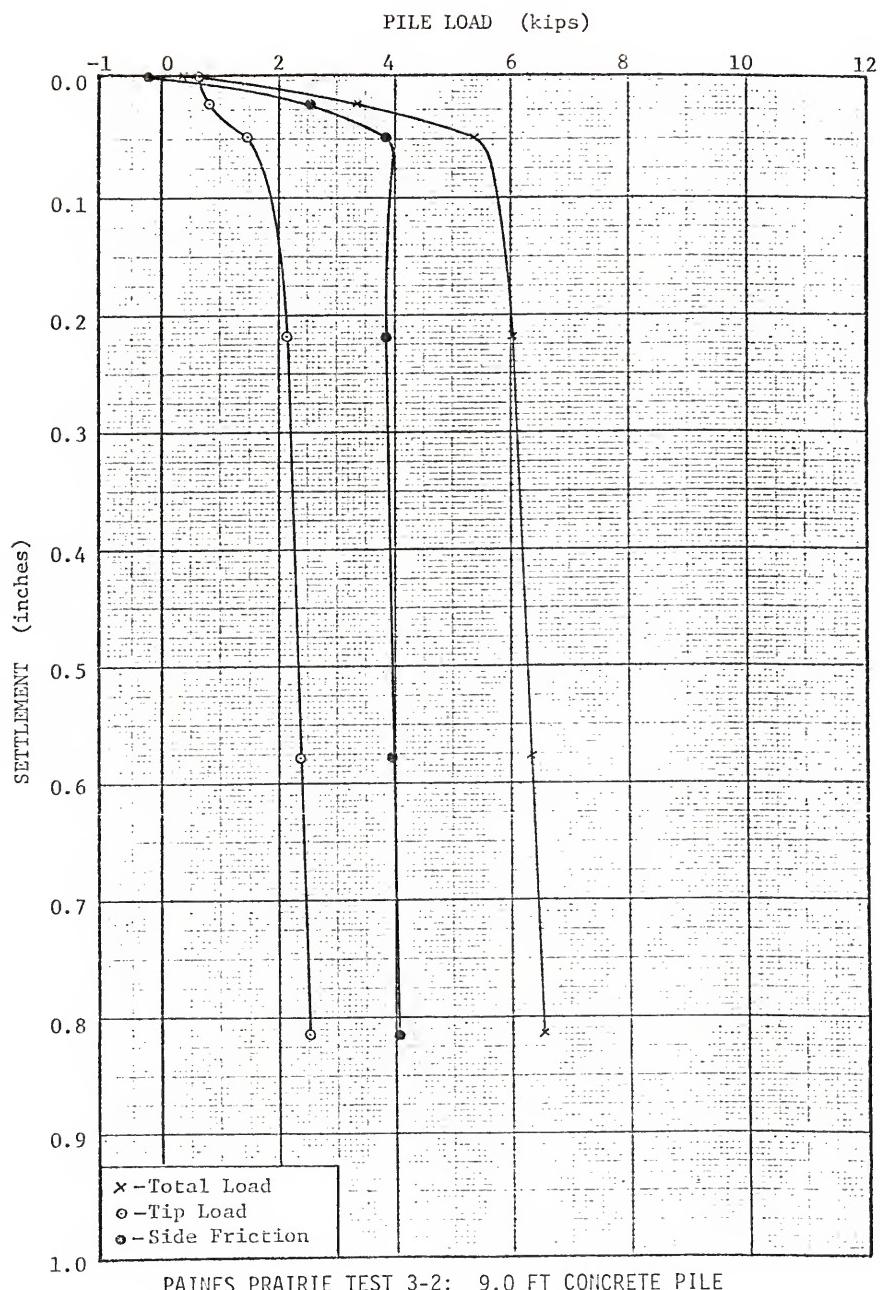




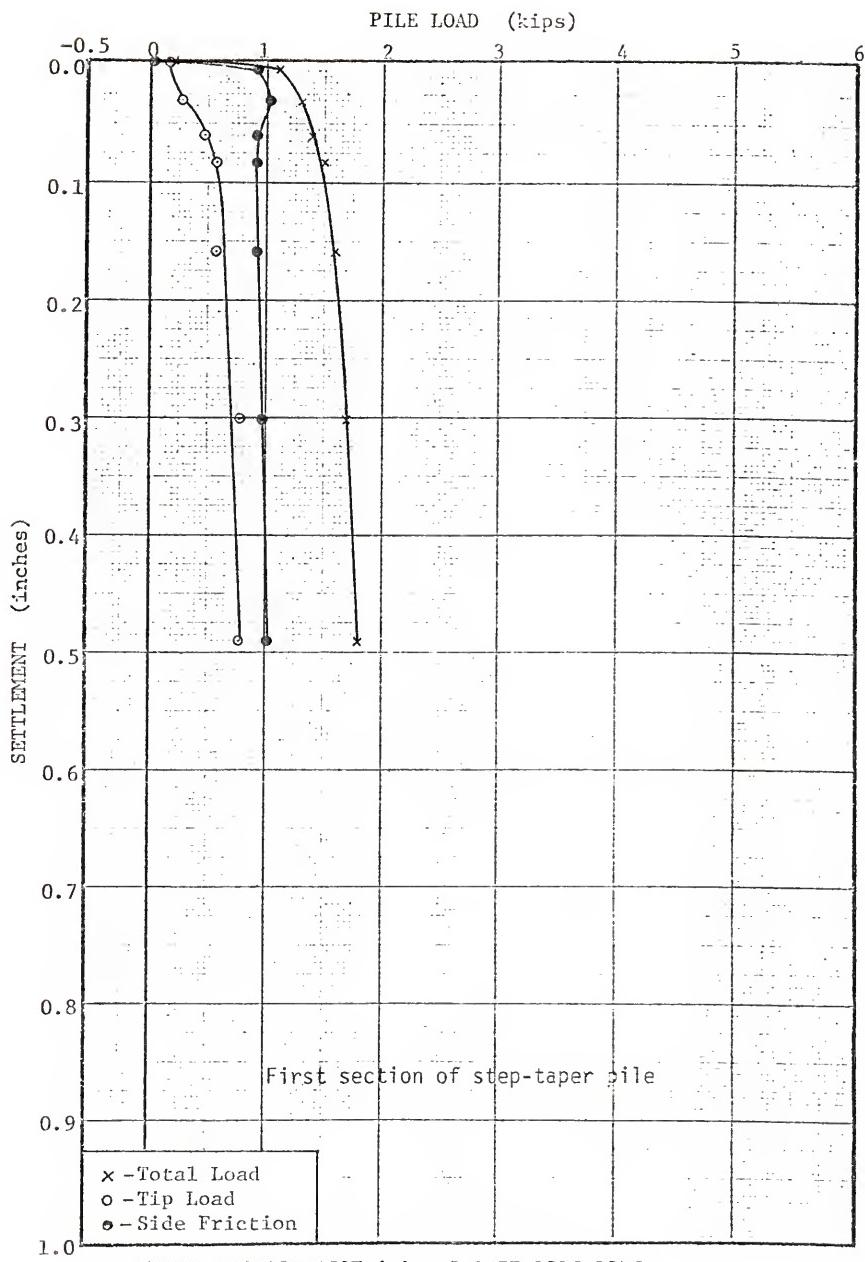


PAINES PRAIRIE TEST 2-2: 9.5 FT PIPE PILE  
FIGURE C-15

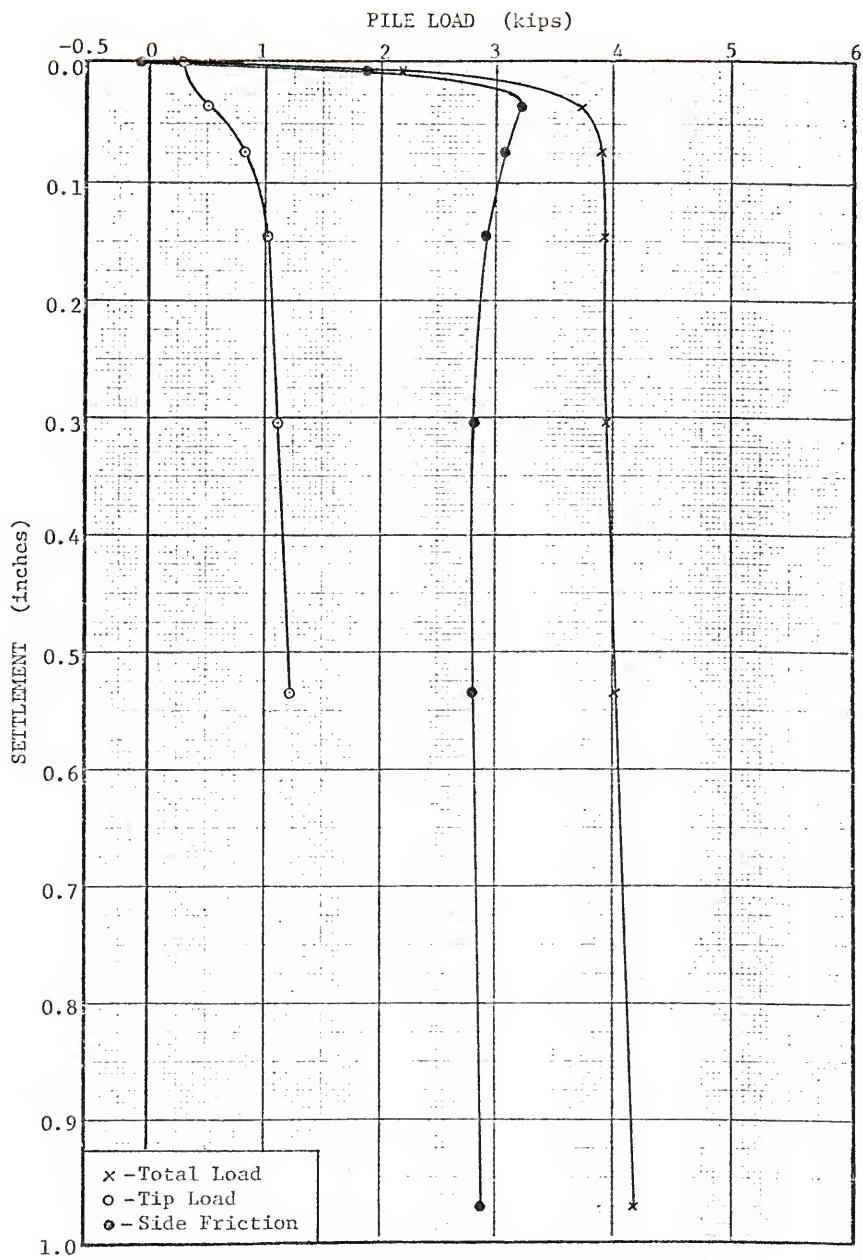




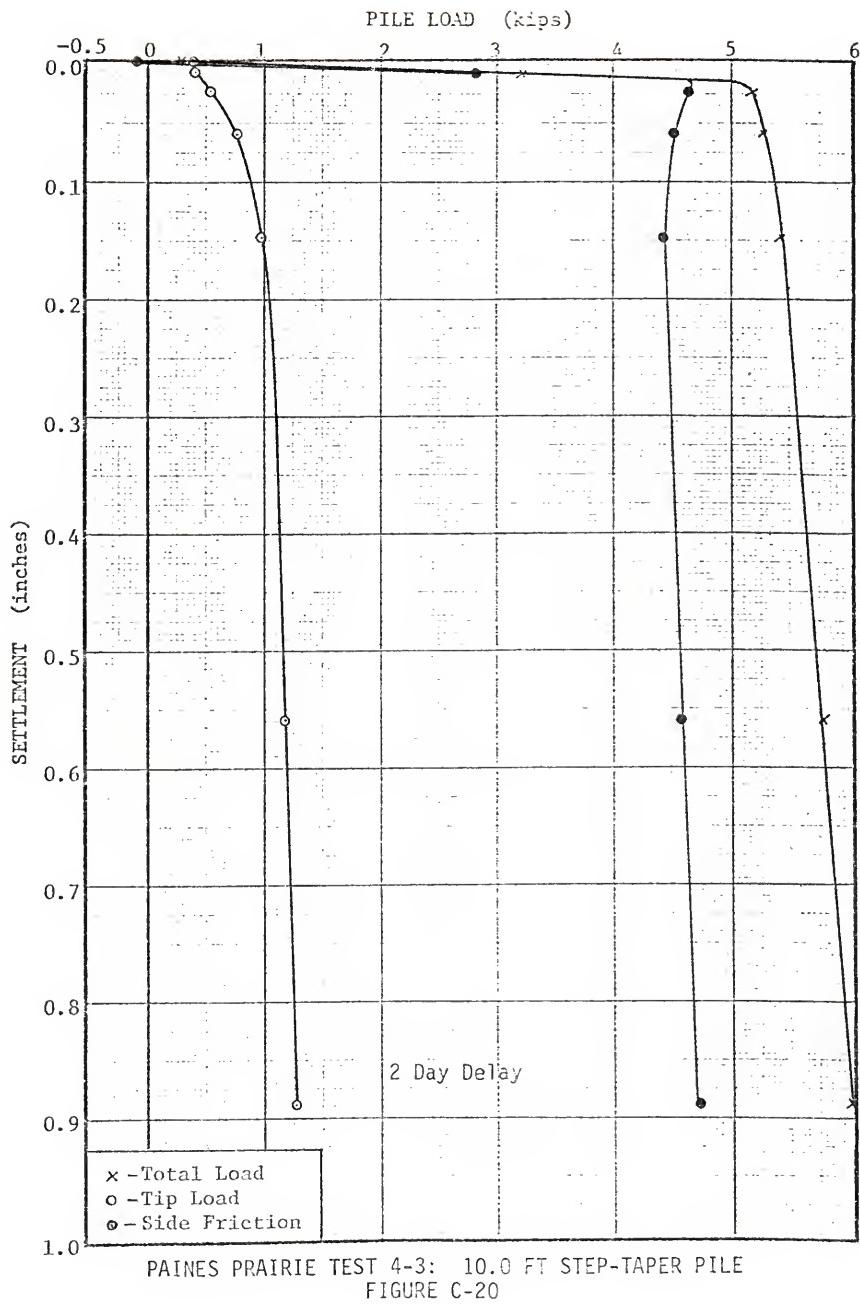
PAINES PRAIRIE TEST 3-2: 9.0 FT CONCRETE PILE  
FIGURE C-17

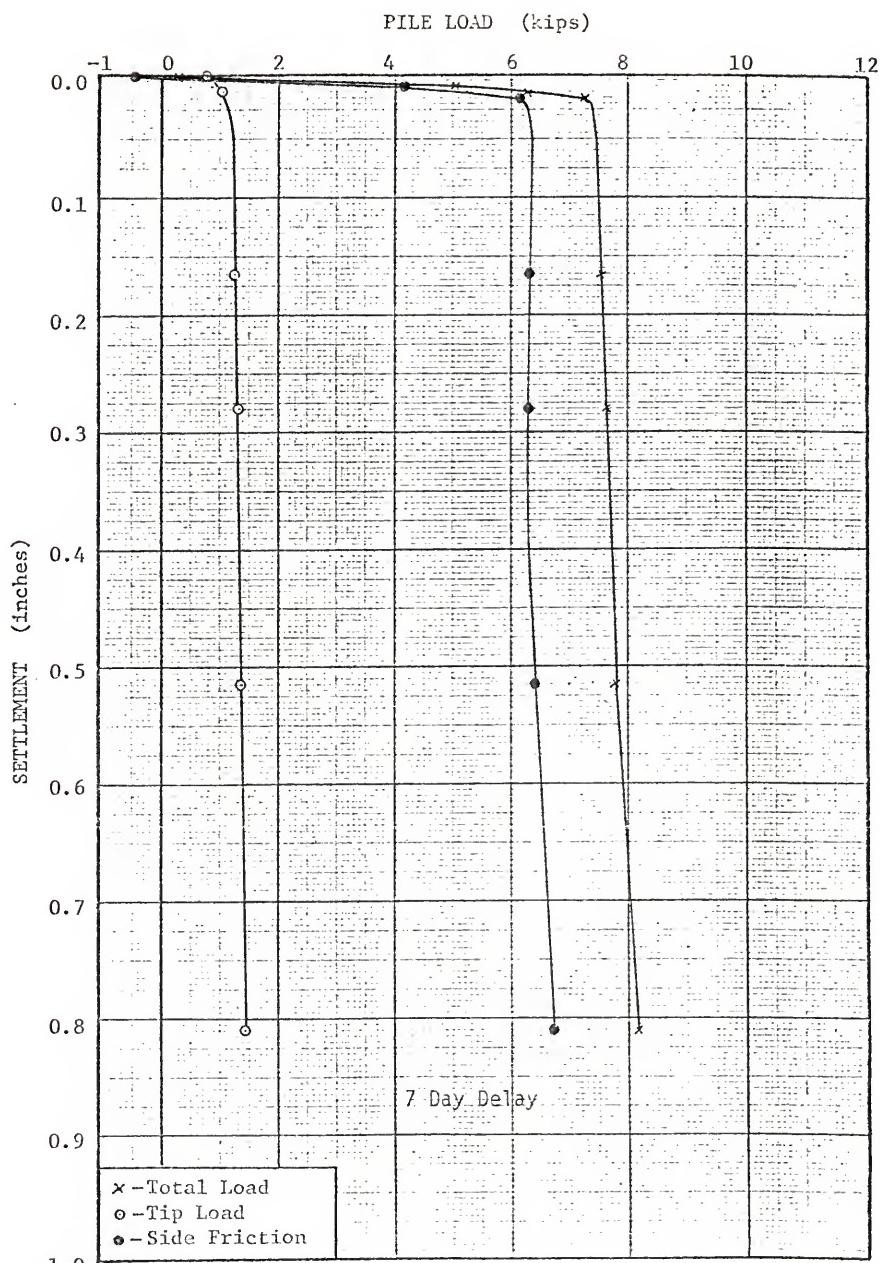


PAINES PRAIRIE TEST 4-1: 5.0 FT PIPE PILE  
FIGURE C-18

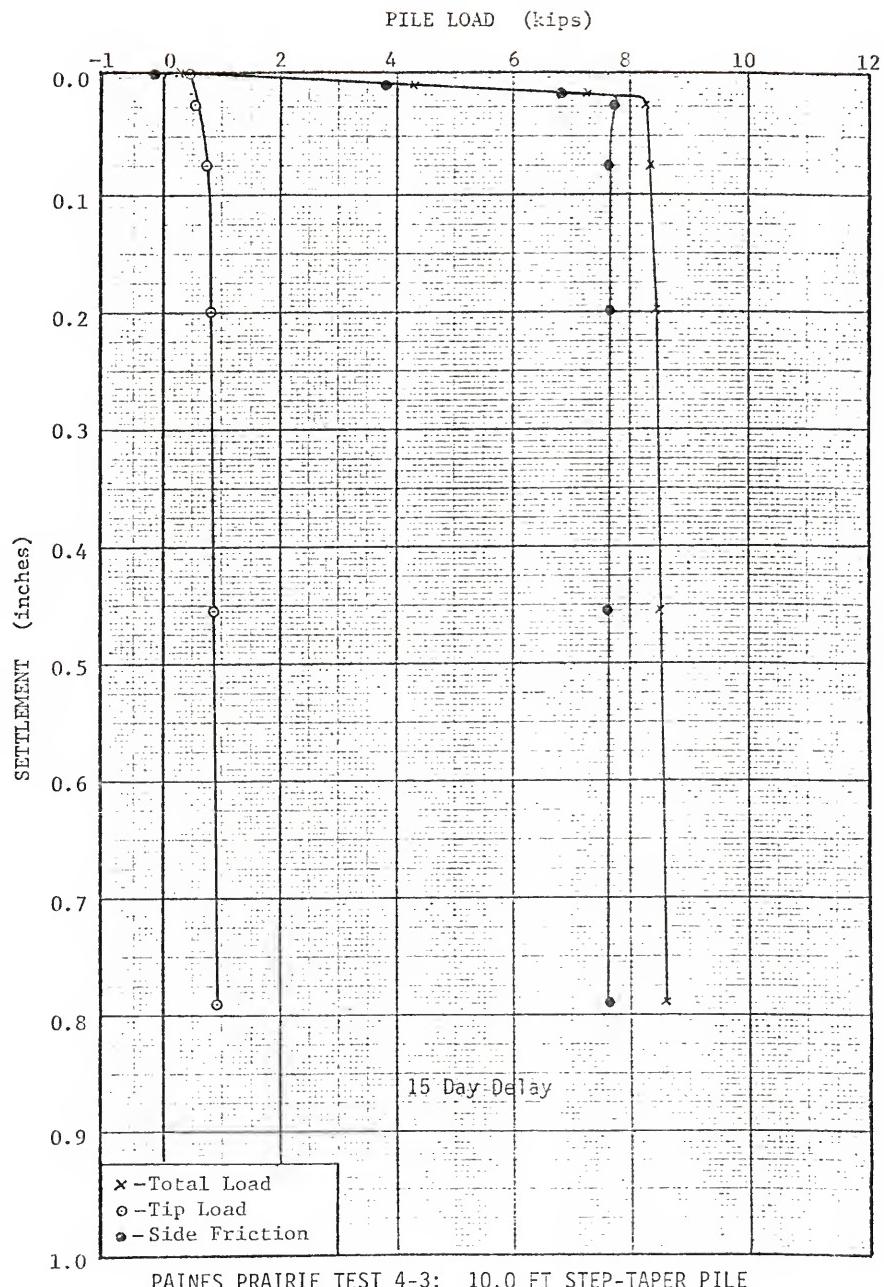


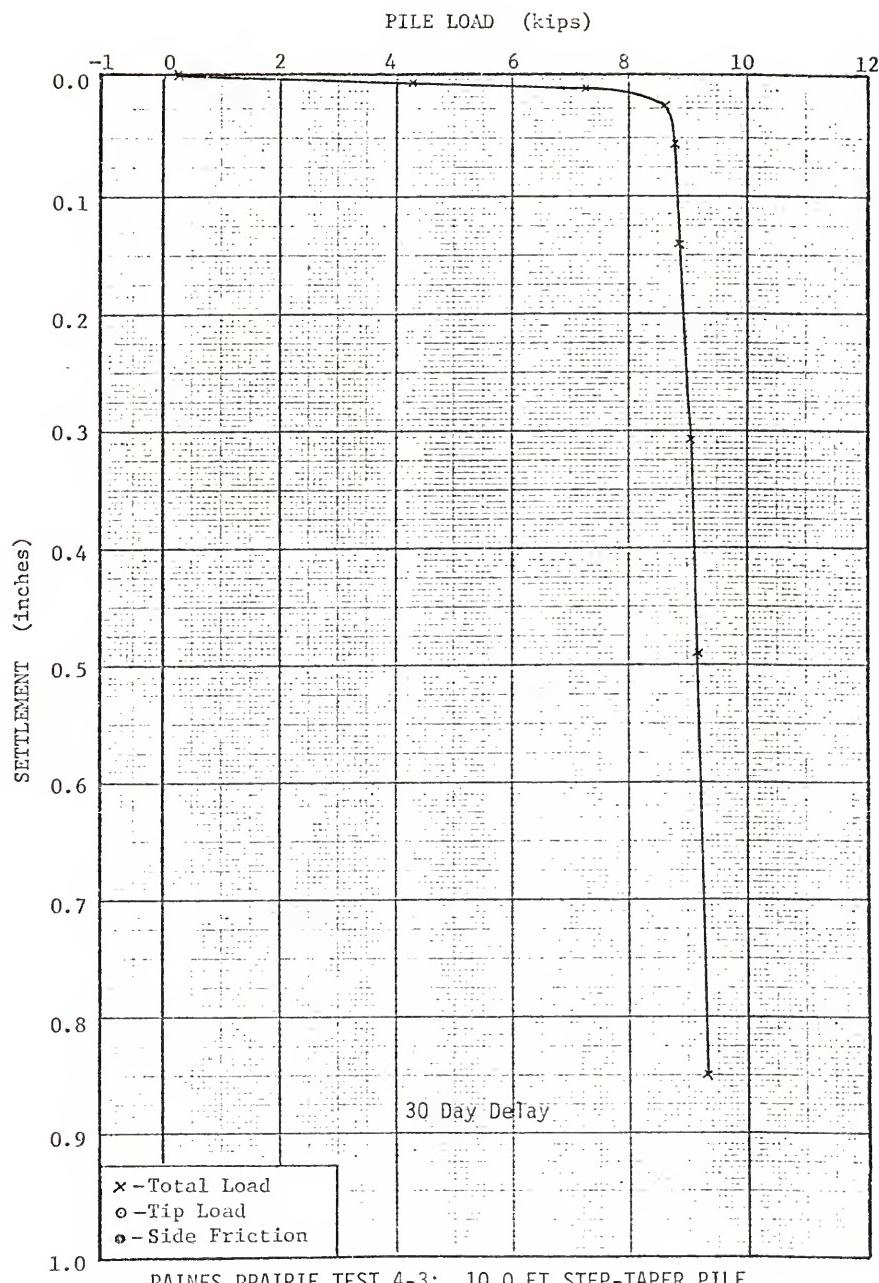
PAINES PRAIRIE TEST 4-2: 7.5 FT STEP-TAPER PILE  
FIGURE C-19

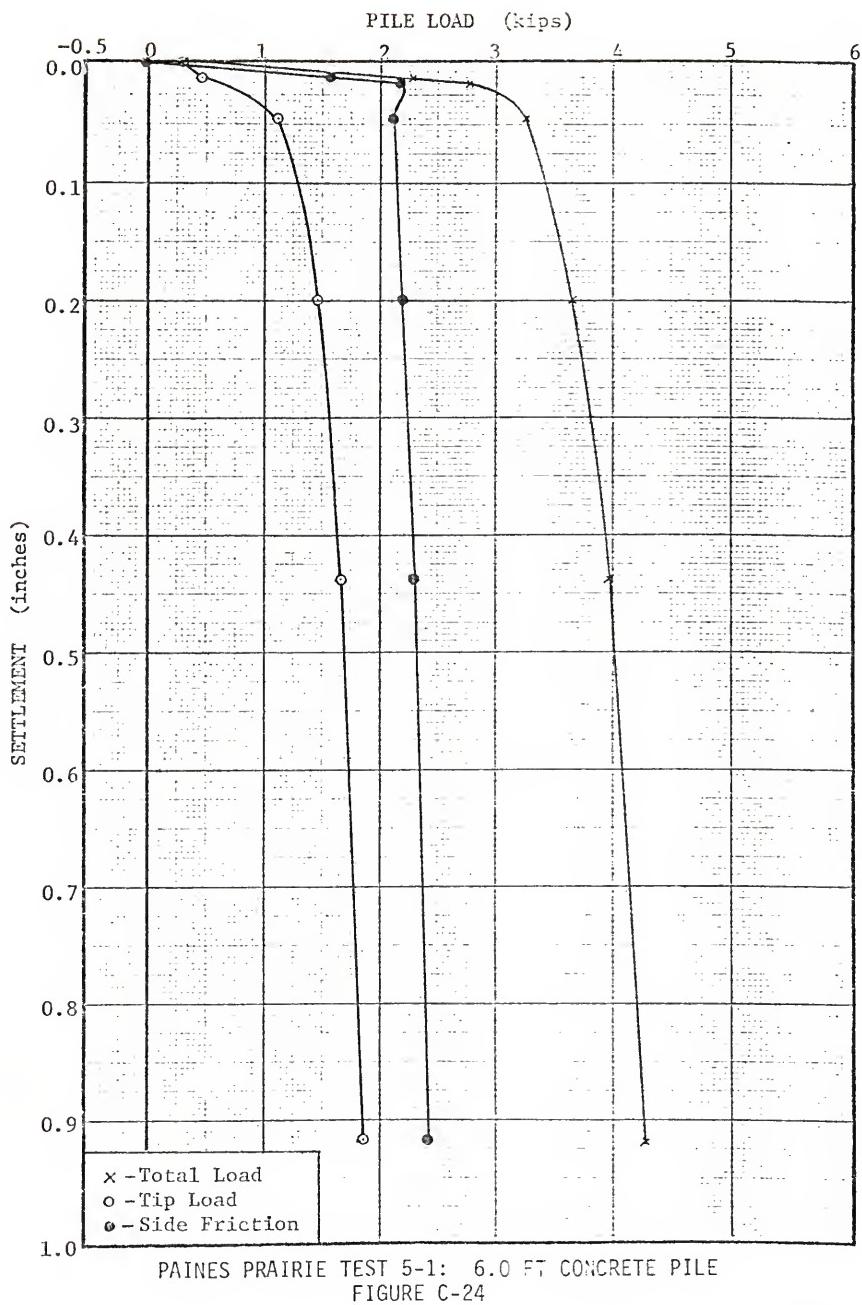


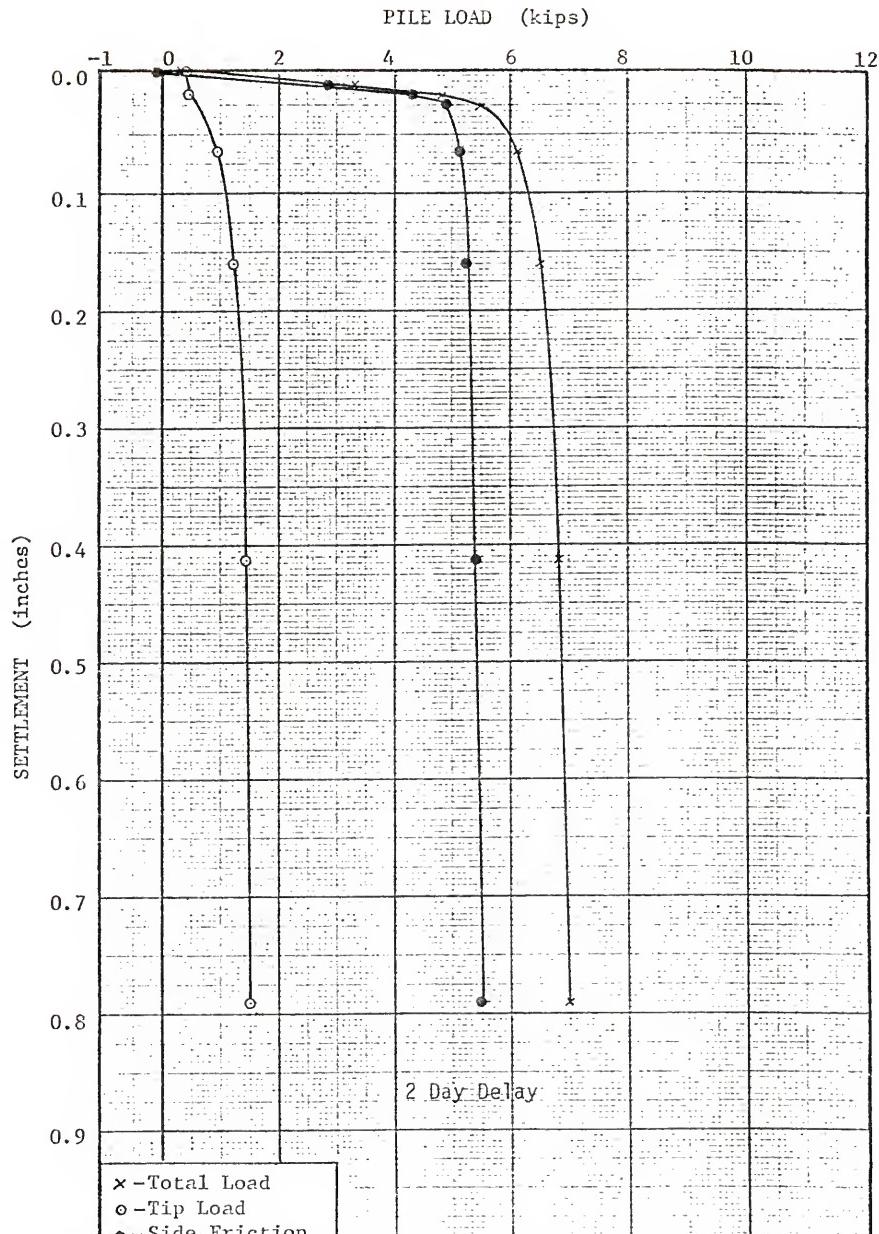


PAINES PRAIRIE TEST 4-3: 10.0 FT STEP-TAPER PILE  
FIGURE C-21

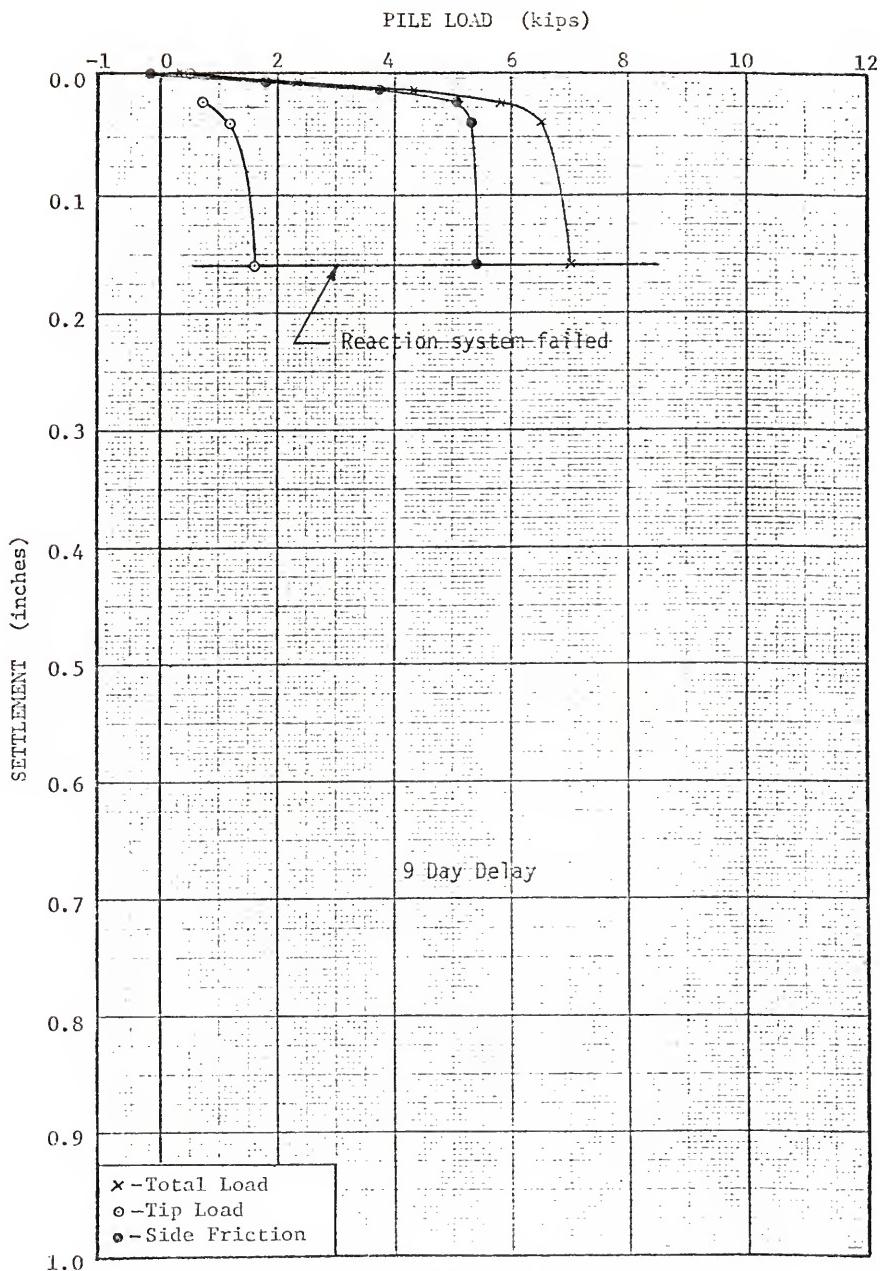








PAINES PRAIRIE TEST 5-2: 8.5 FT CONCRETE PILE  
FIGURE C-25



PAINES PRAIRIE TEST 5-2: 8.5 FT CONCRETE PILE  
FIGURE C-26

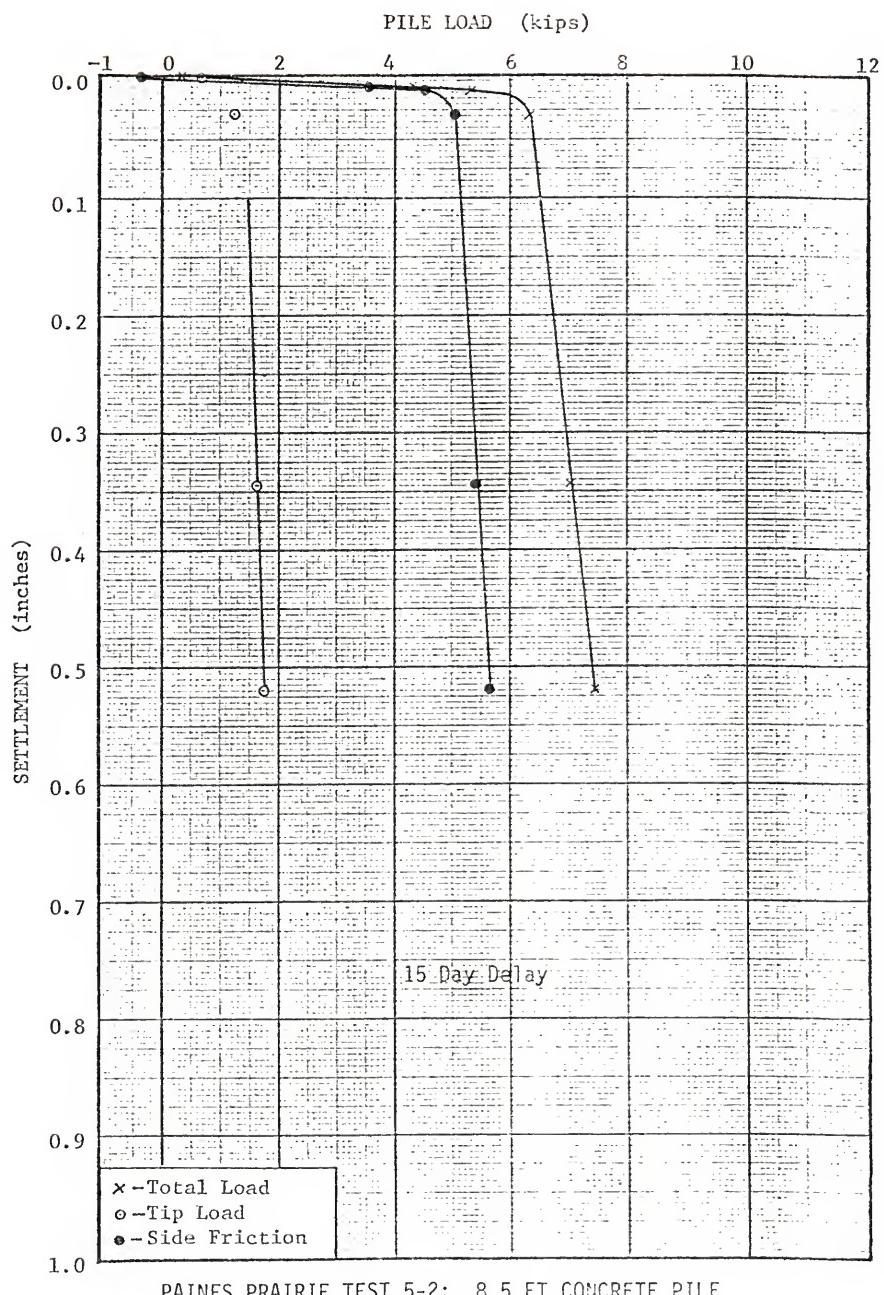
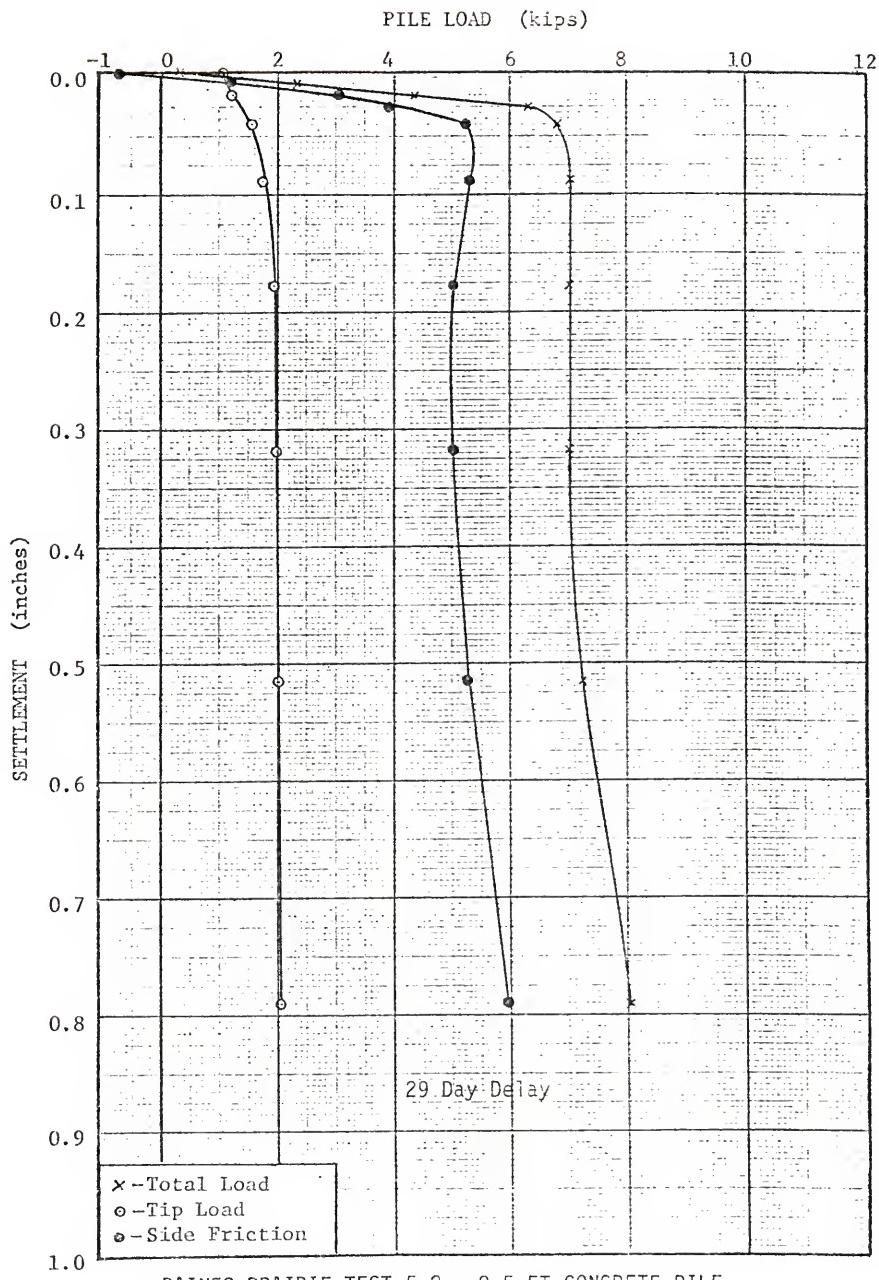
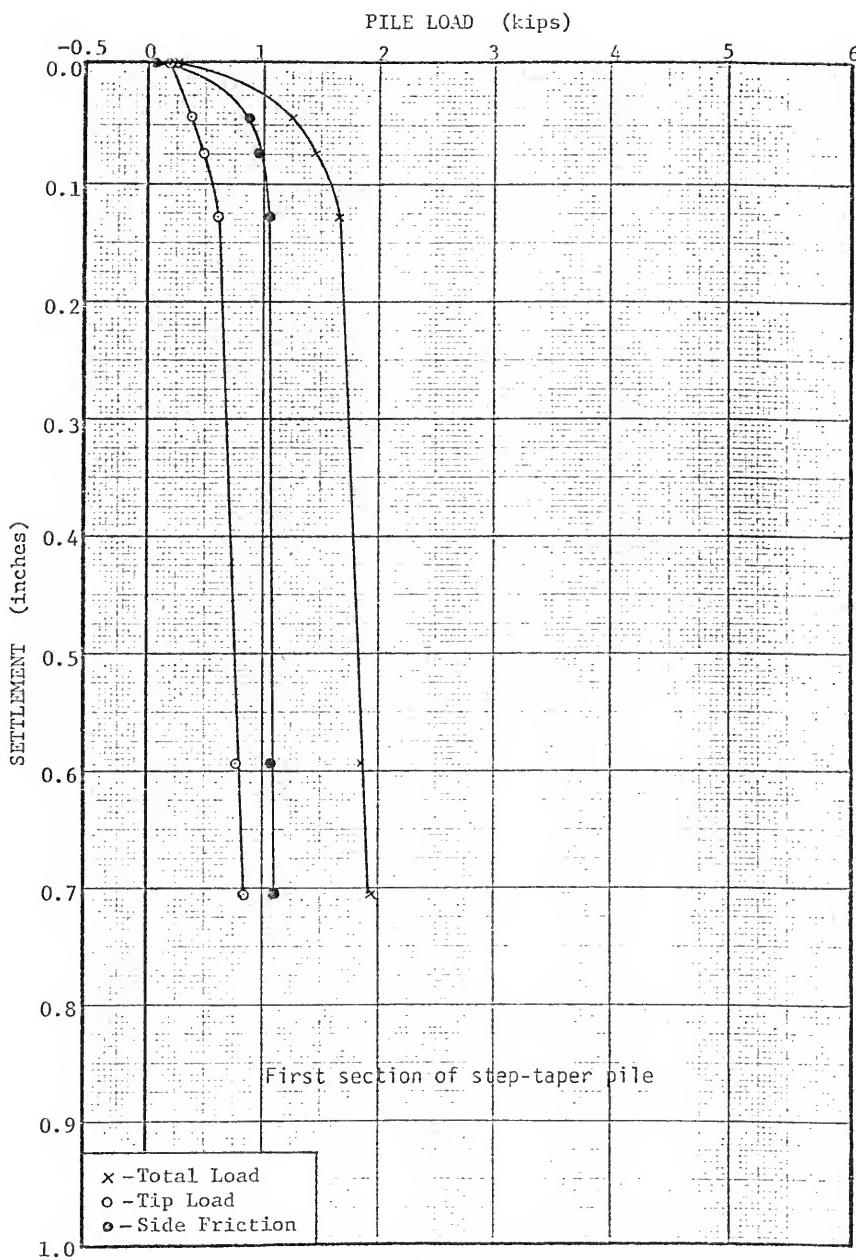


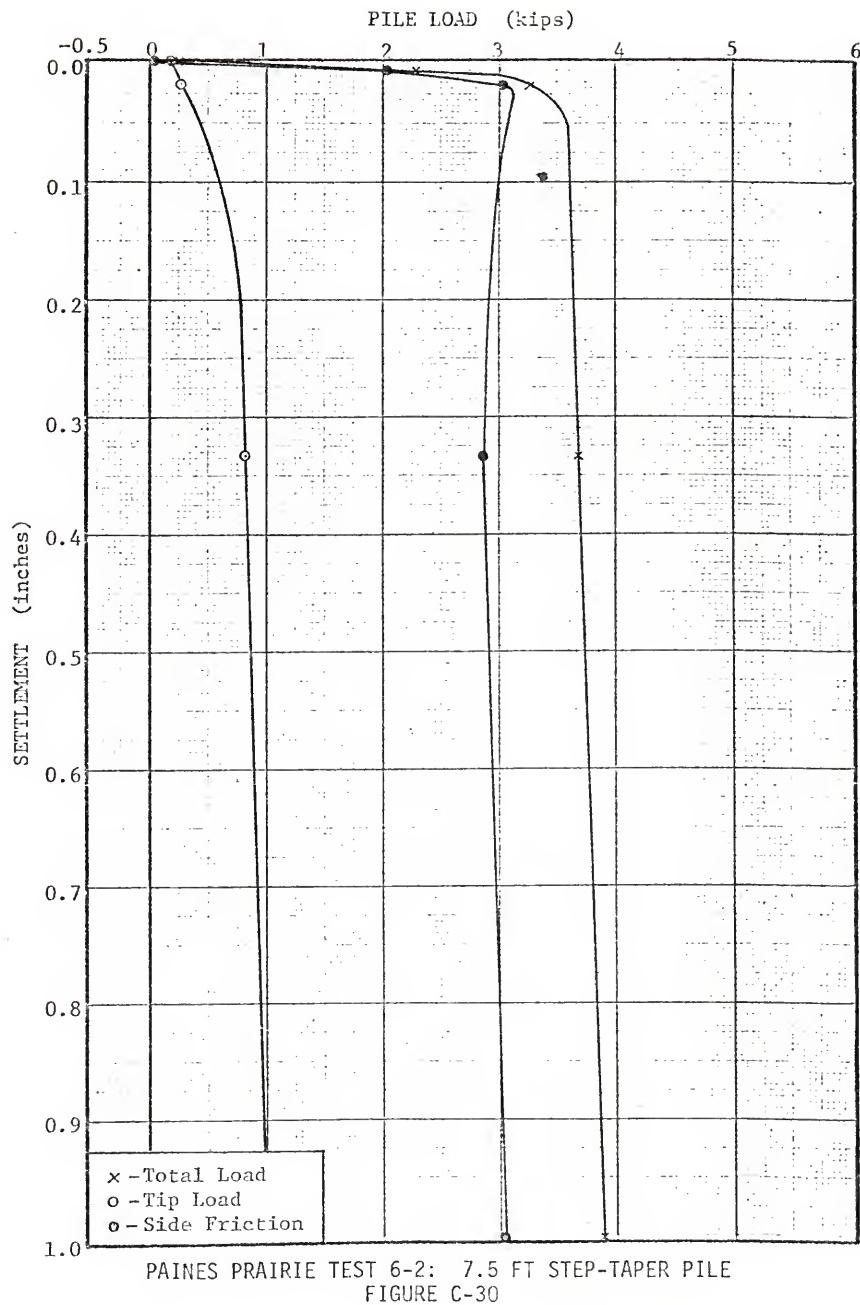
FIGURE C-27



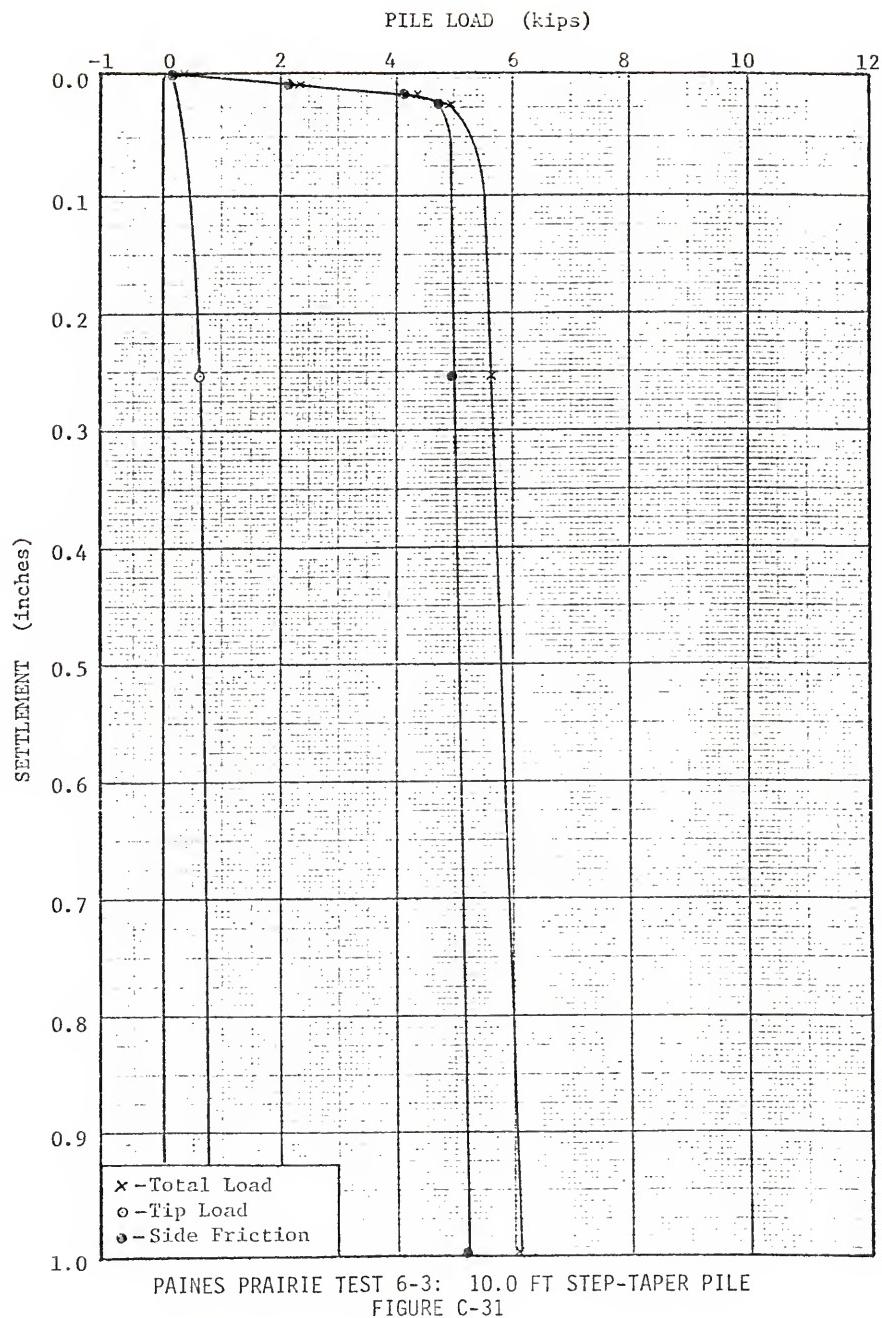
PAINES PRAIRIE TEST 5-2: 8.5 FT CONCRETE PILE  
FIGURE C-28



PAINES PRAIRIE TEST 6-1: 5.0 FT PIPE PILE  
FIGURE C-29

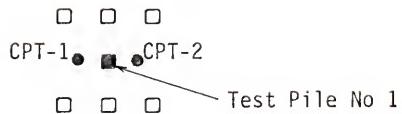


PAINES PRAIRIE TEST 6-2: 7.5 FT STEP-TAPER PILE  
FIGURE C-30

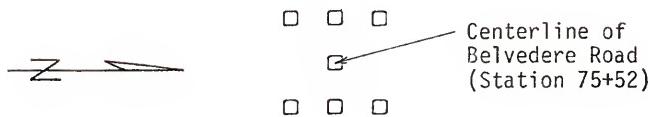


APPENDIX D  
FULL-SCALE PILE TEST RESULTS

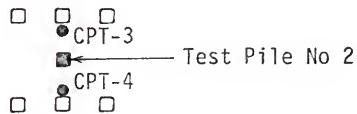
## ⊕ Boring No 1



## ⊕ Boring No 2



## ⊕ Boring No 3



## ⊕ Boring No 4

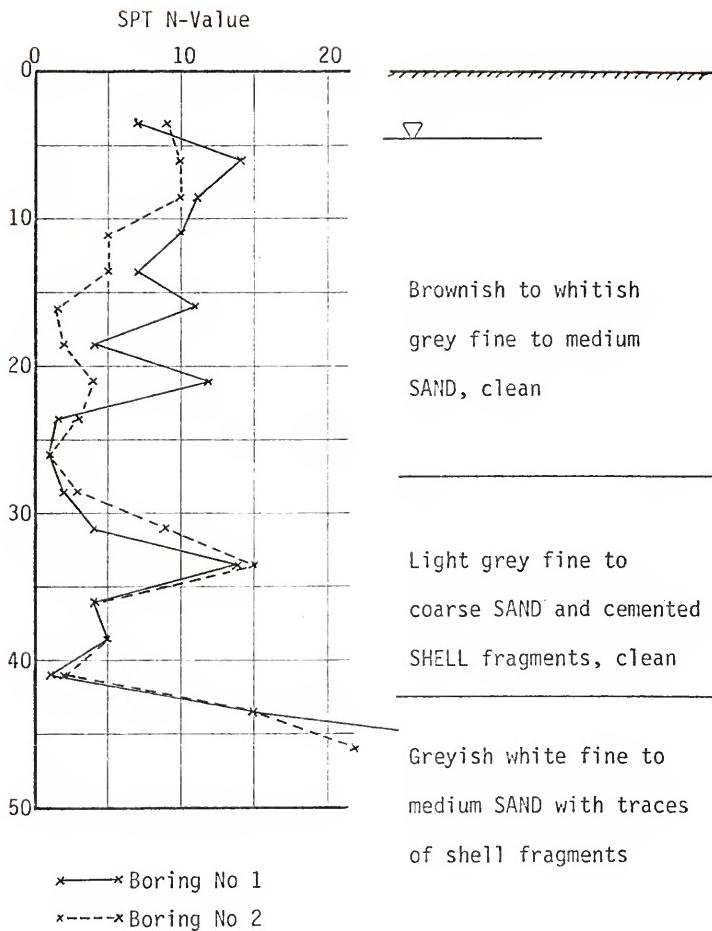
SCALE: 1" = 10'

LEGEND

- ⊕ - Test boring
- - CPT sounding

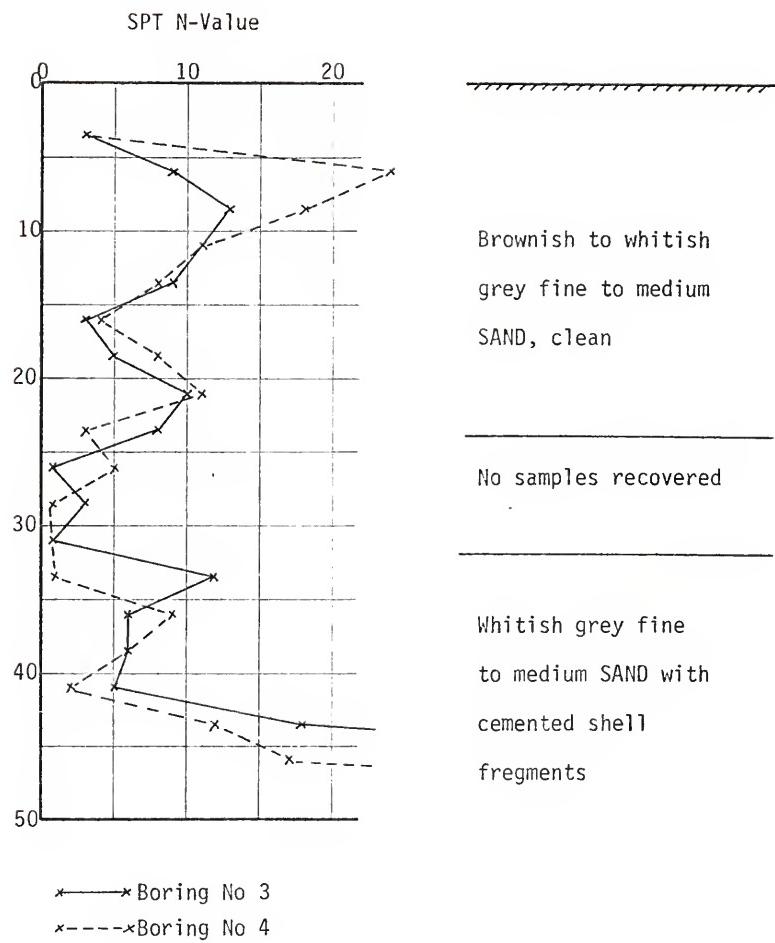
WEST PALM BEACH TEST SITE LAYOUT

FIGURE D-1



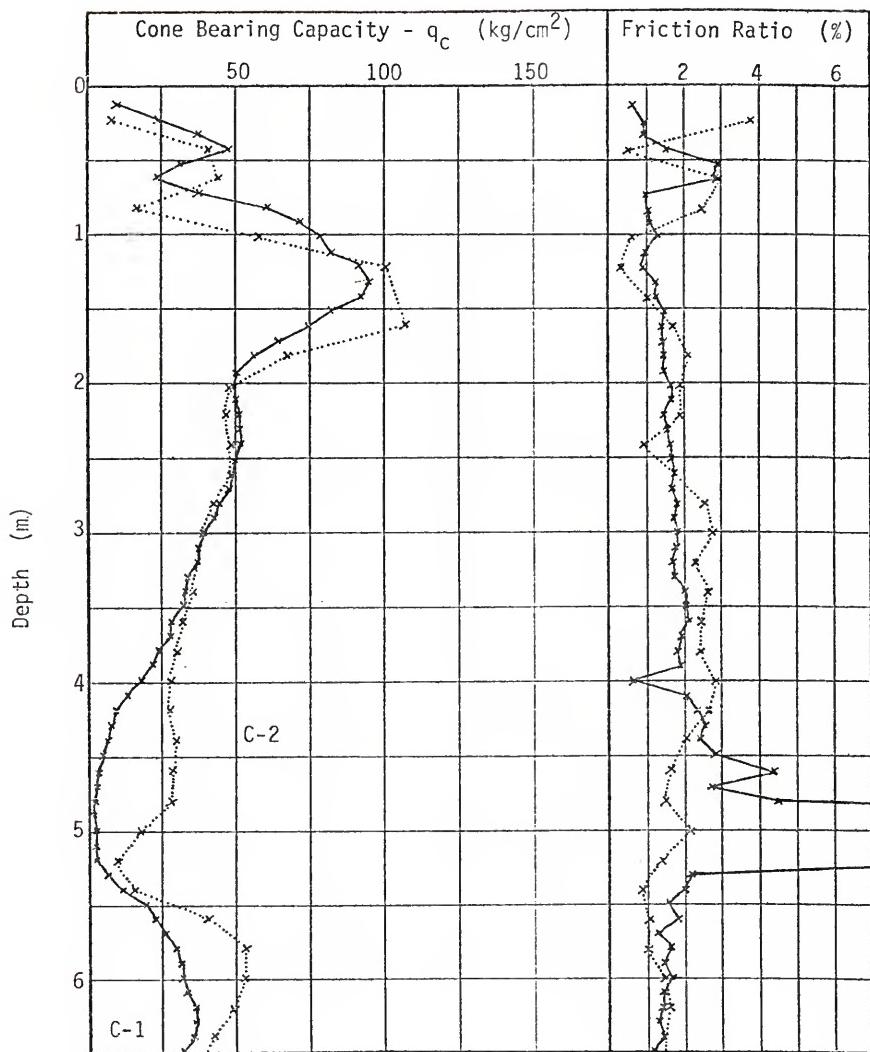
WEST PALM BEACH TEST BORING LOGS

FIGURE D-2



WEST PALM BEACH TEST BORING LOGS

FIGURE D-3



WEST PALM BEACH CPT LOGS

FIGURE D-4

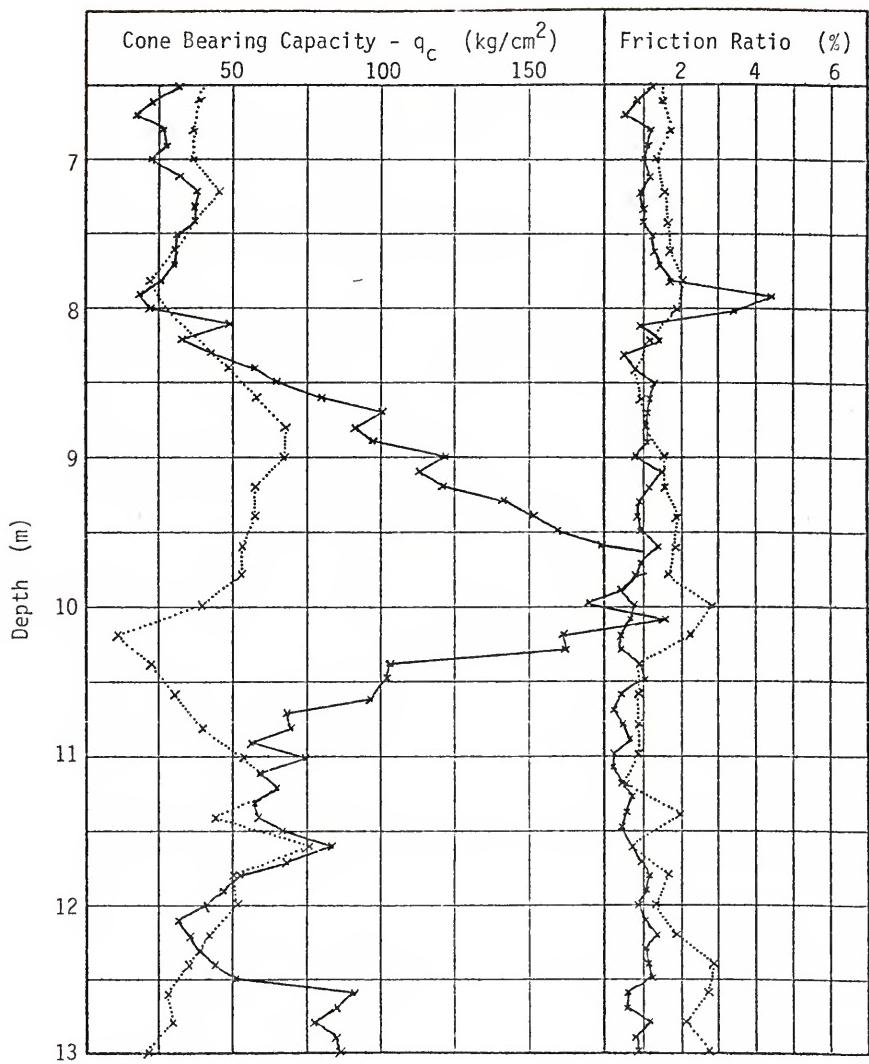


FIGURE D-4 - continued

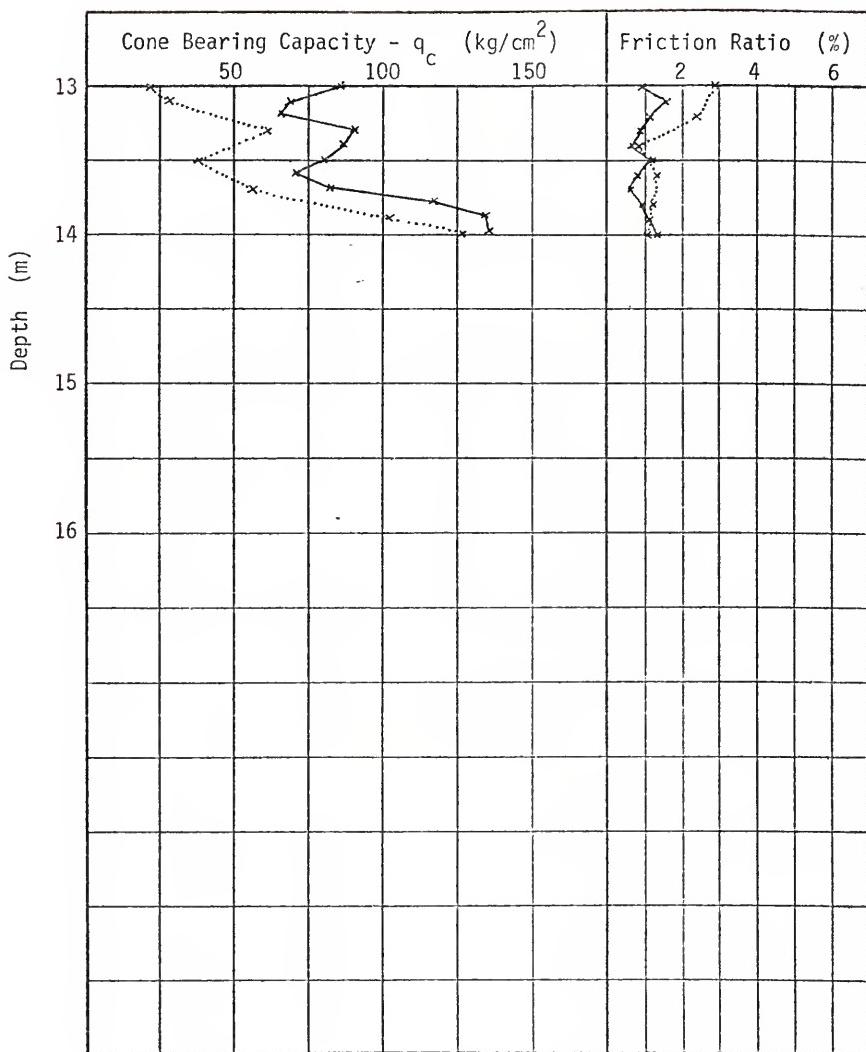
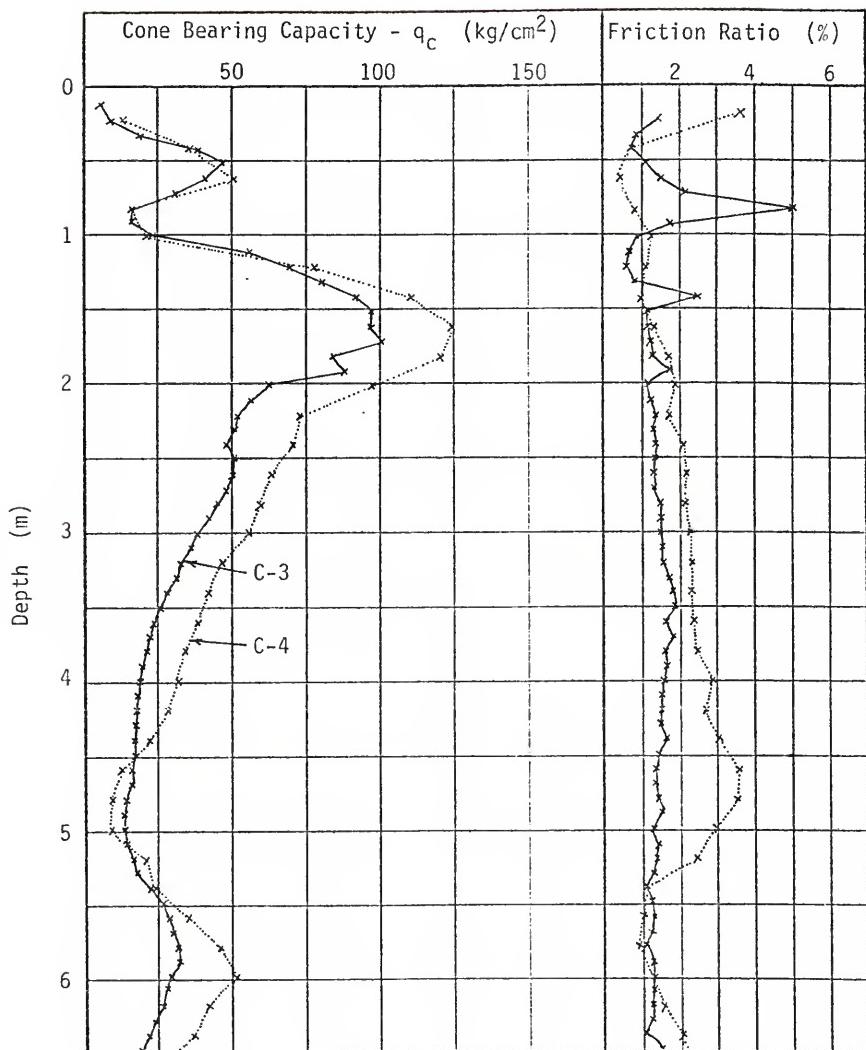


FIGURE D-4 - continued



WEST PALM BEACH CPT SOUNDING LOGS

FIGURE D-5

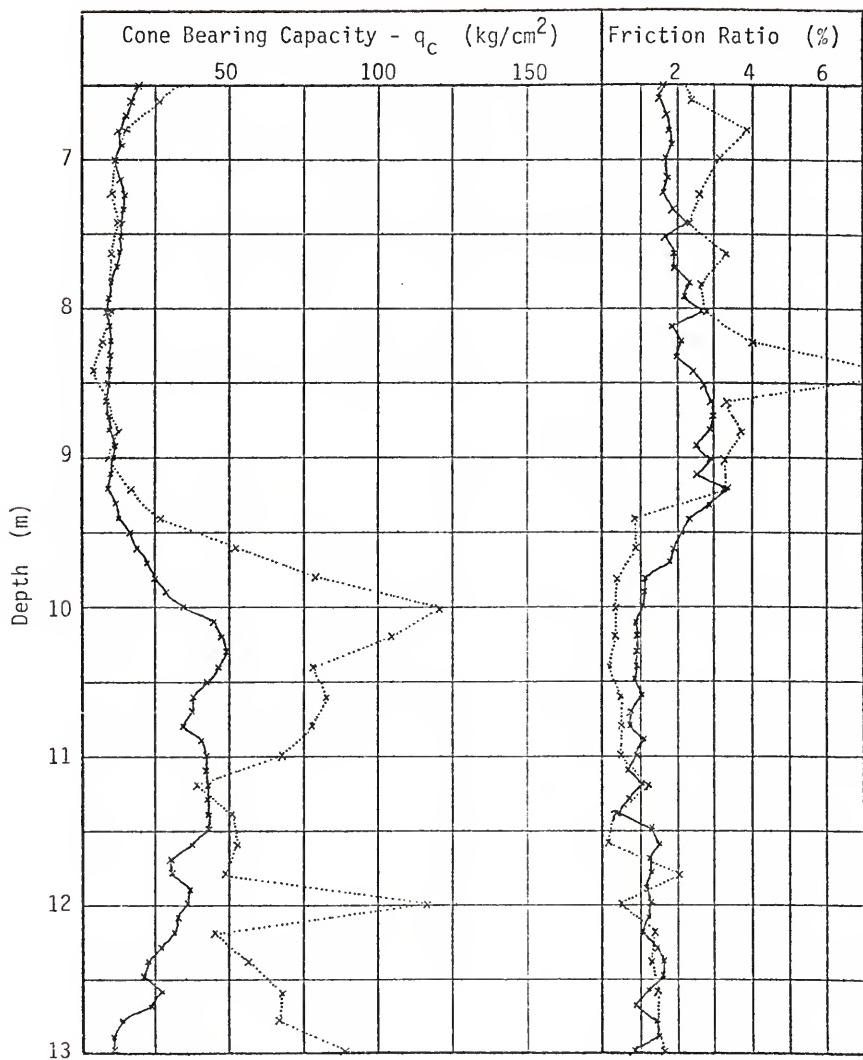
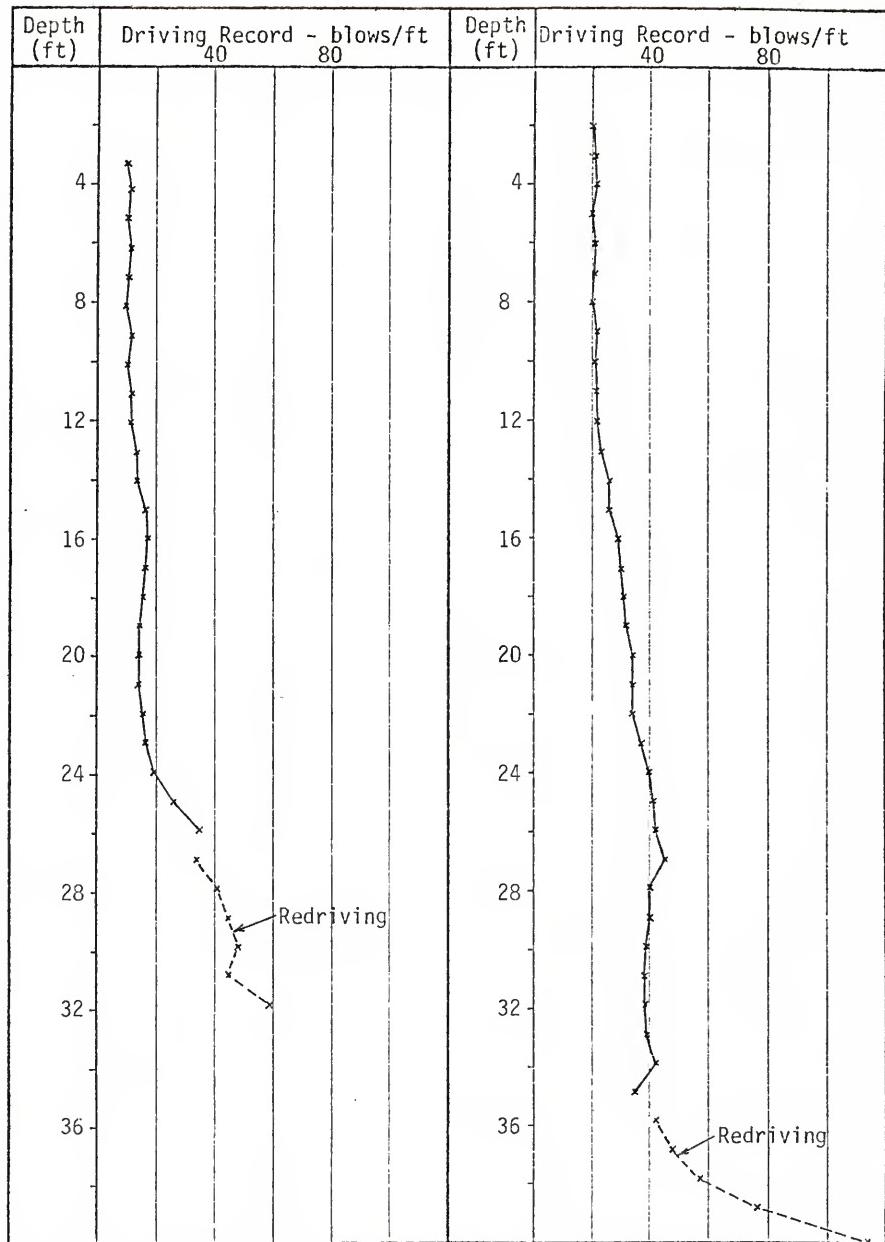
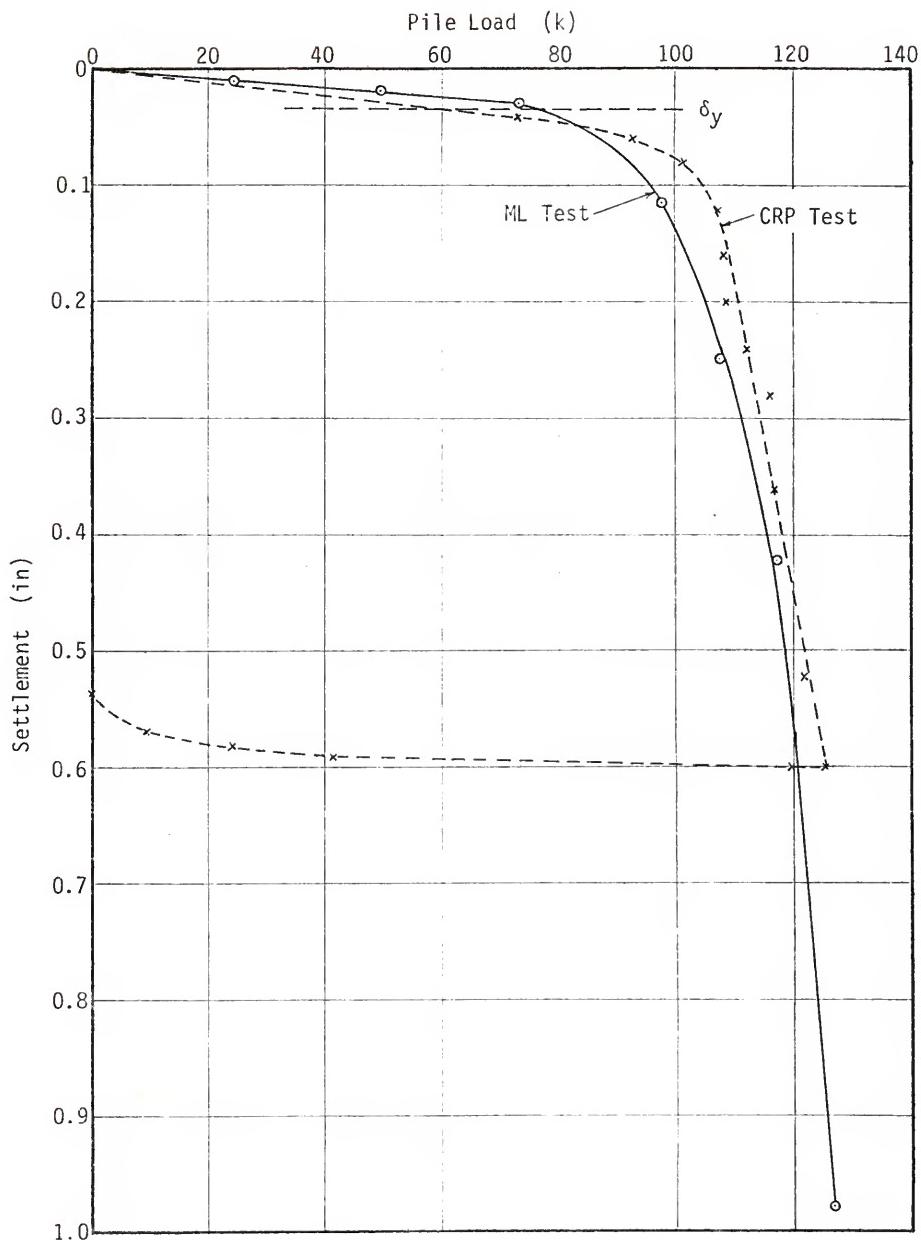


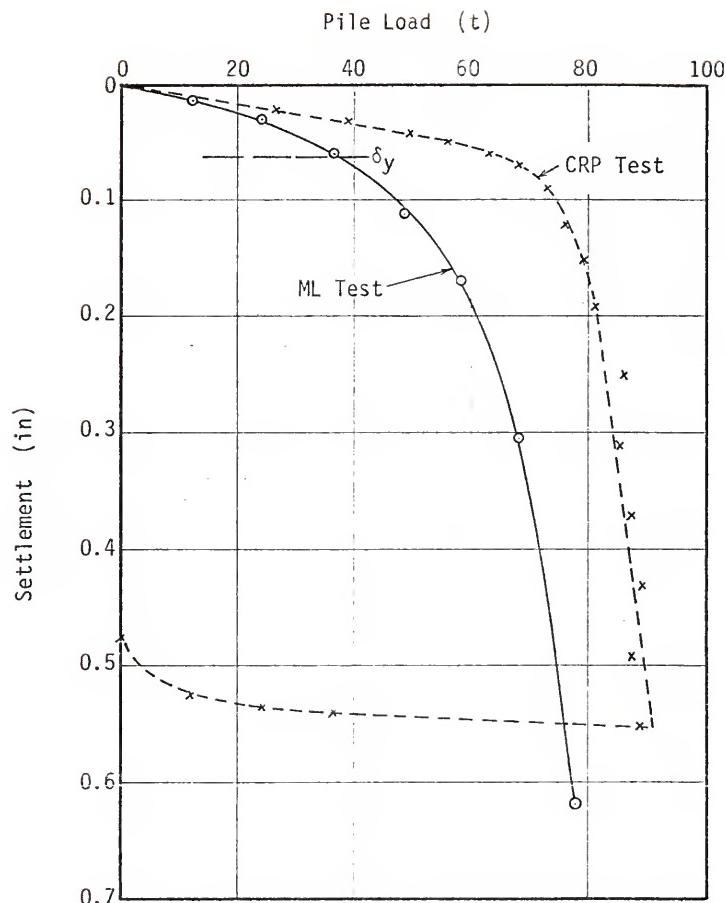
FIGURE D-5 - continued



WEST PALM BEACH PILE DRIVING RESISTANCE DATA  
FIGURE D-6

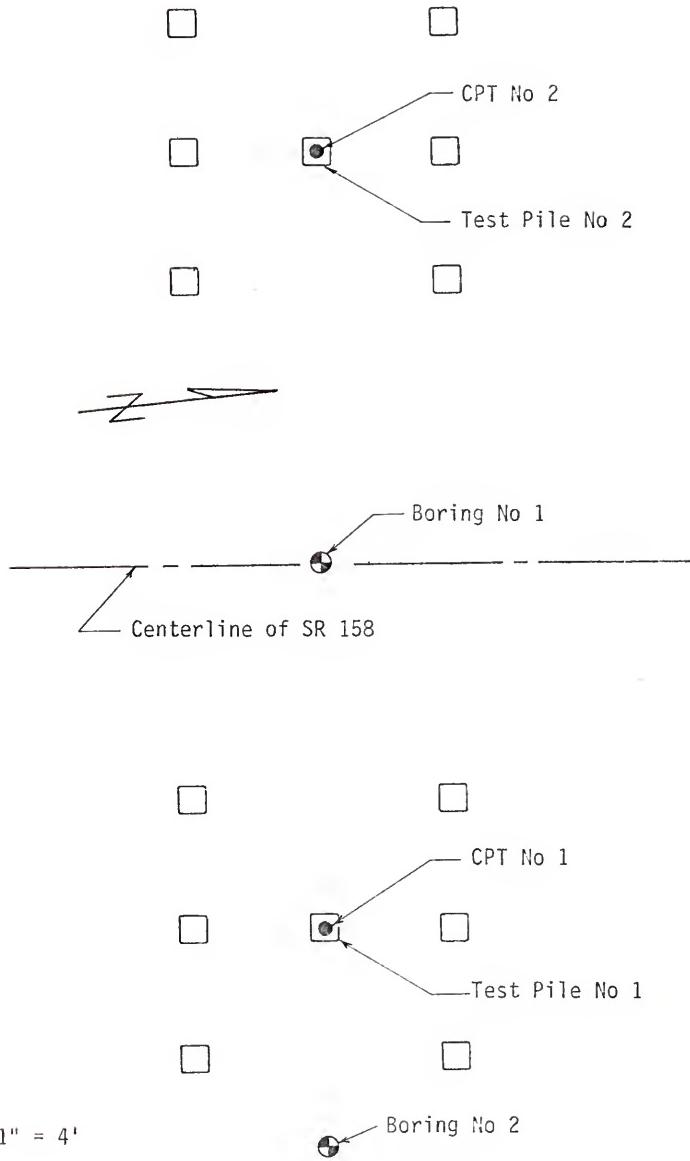


WEST PALM BEACH PILE LOAD TEST NO 1  
FIGURE D-7



WEST PALM BEACH PILE LOAD TEST NO 2

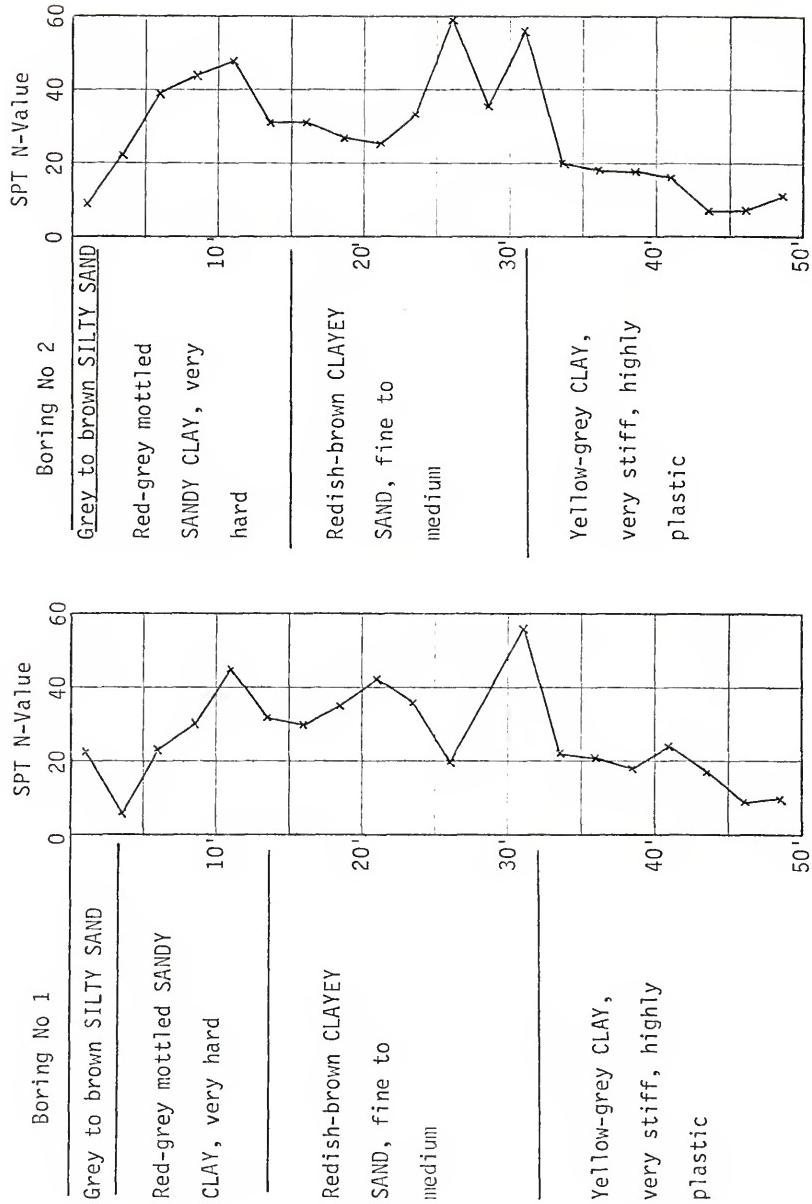
FIGURE D-8



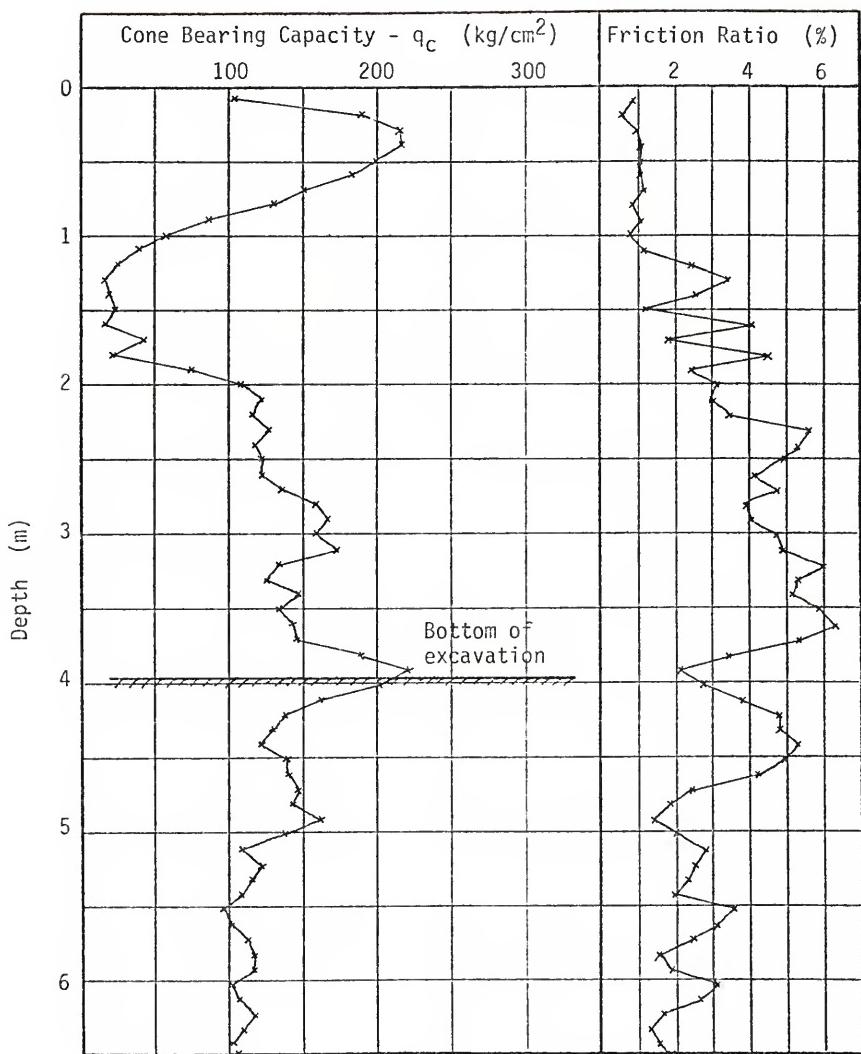
SCALE: 1" = 4'

JEFFERSON COUNTY TEST SITE LAYOUT

FIGURE D-9



JEFFERSON COUNTY TEST BORING LOGS  
FIGURE D-10



JEFFERSON COUNTY CPT SOUNDING NO 1

FIGURE D-11

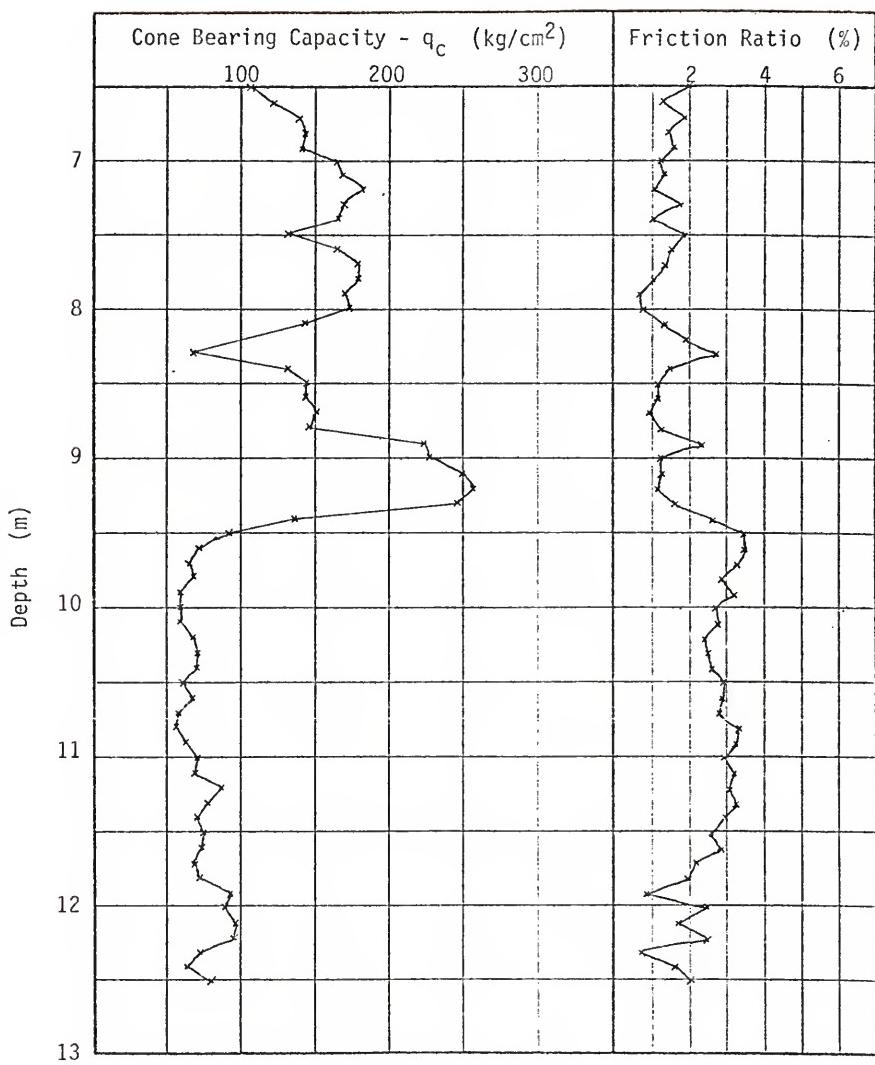
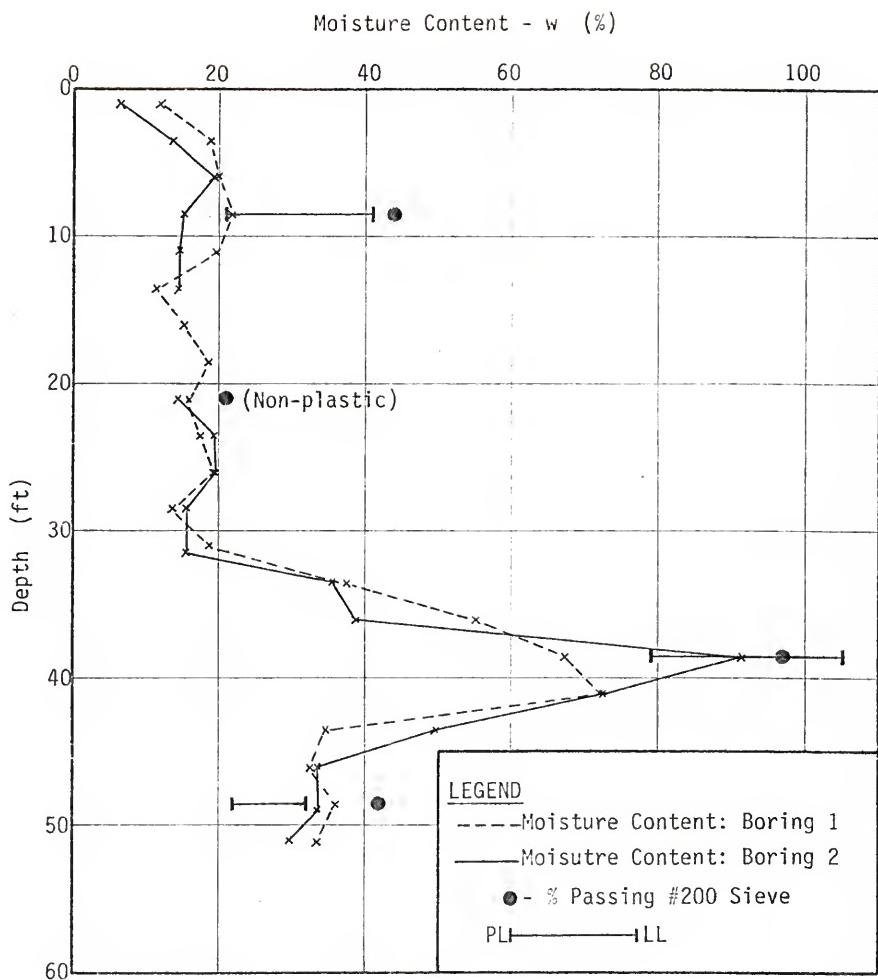
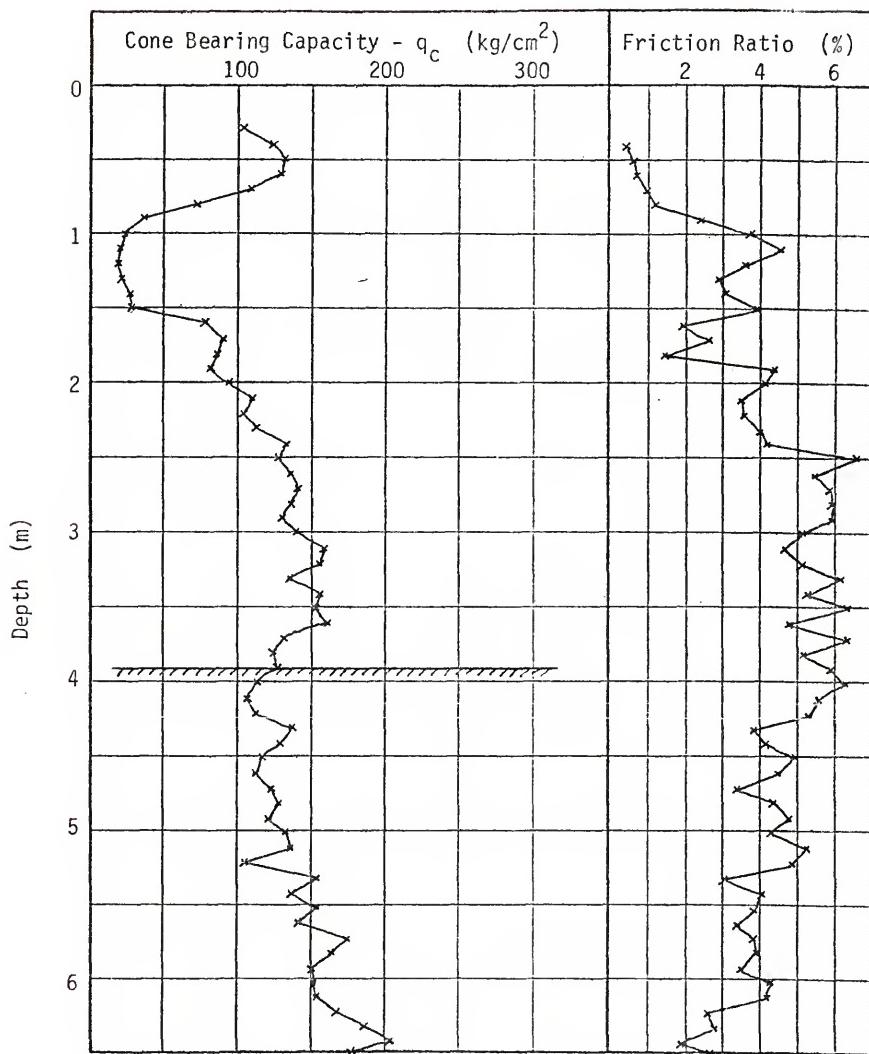


FIGURE D-11 - continued



JEFFERSON COUNTY SOIL PROPERTY DATA

FIGURE D-13



JEFFERSON COUNTY CPT SOUNDING NO 2

FIGURE D-12

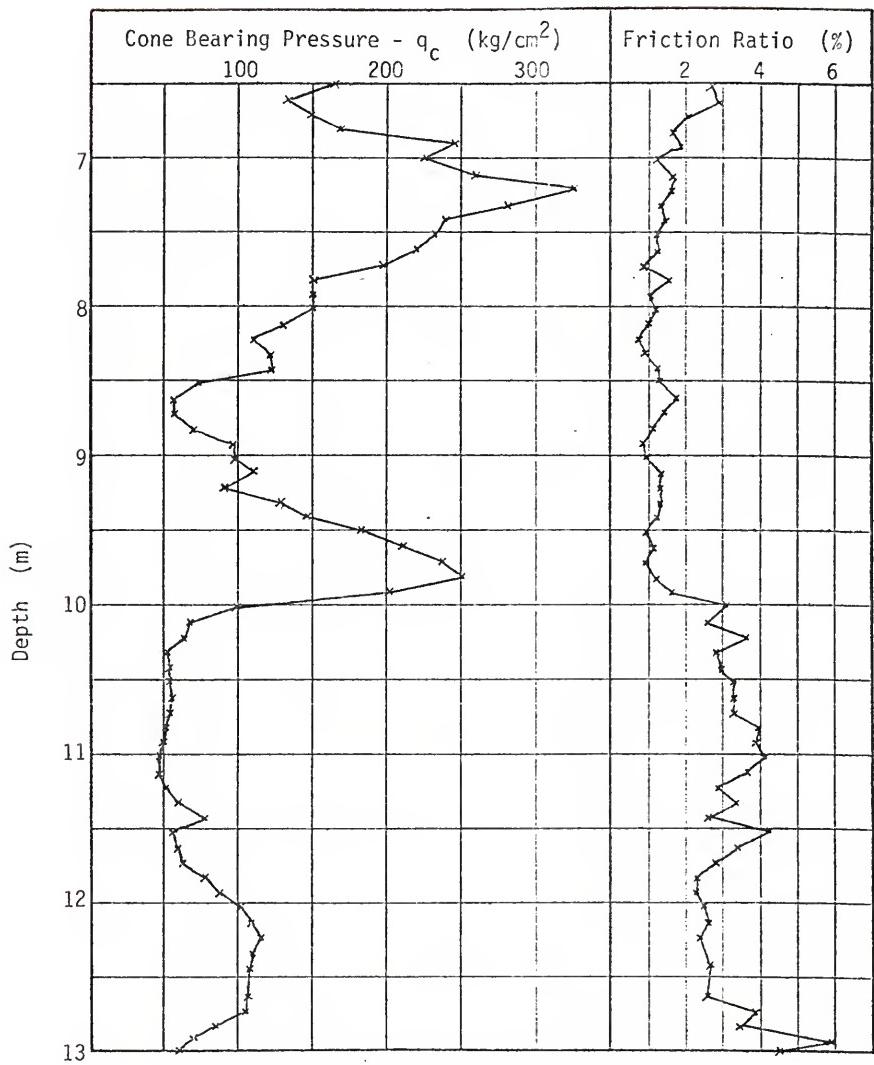


FIGURE D-12 - continued

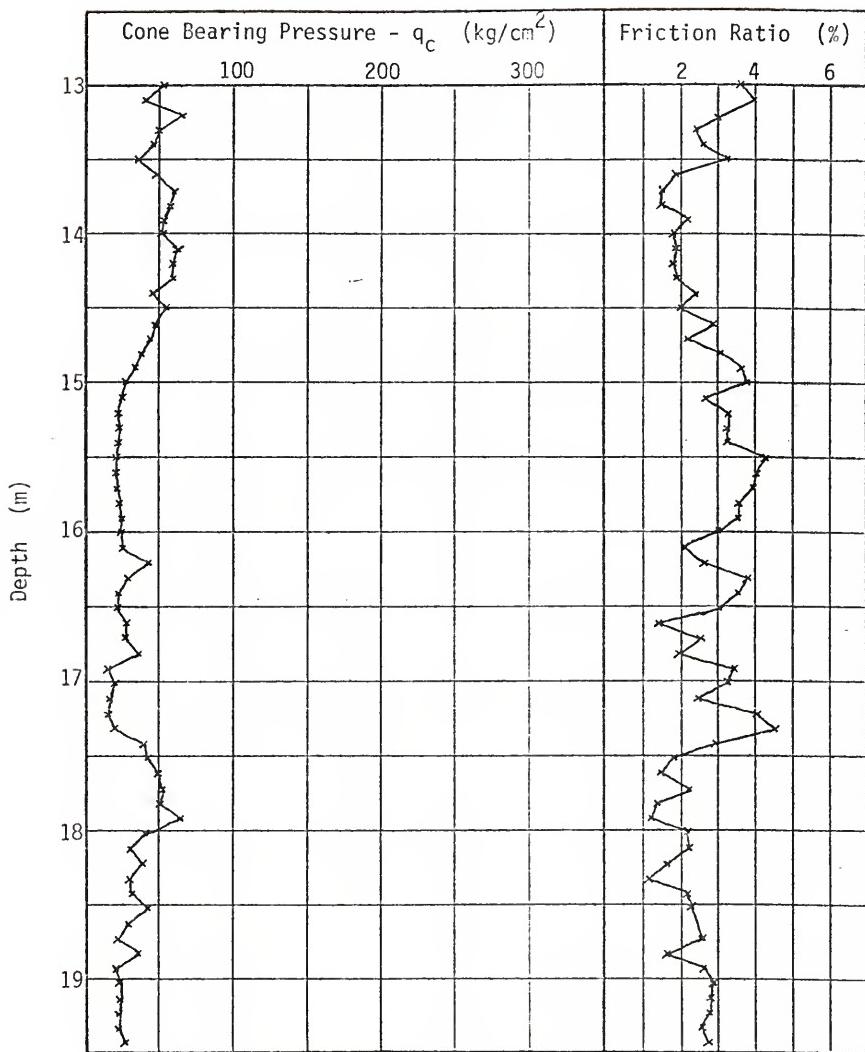
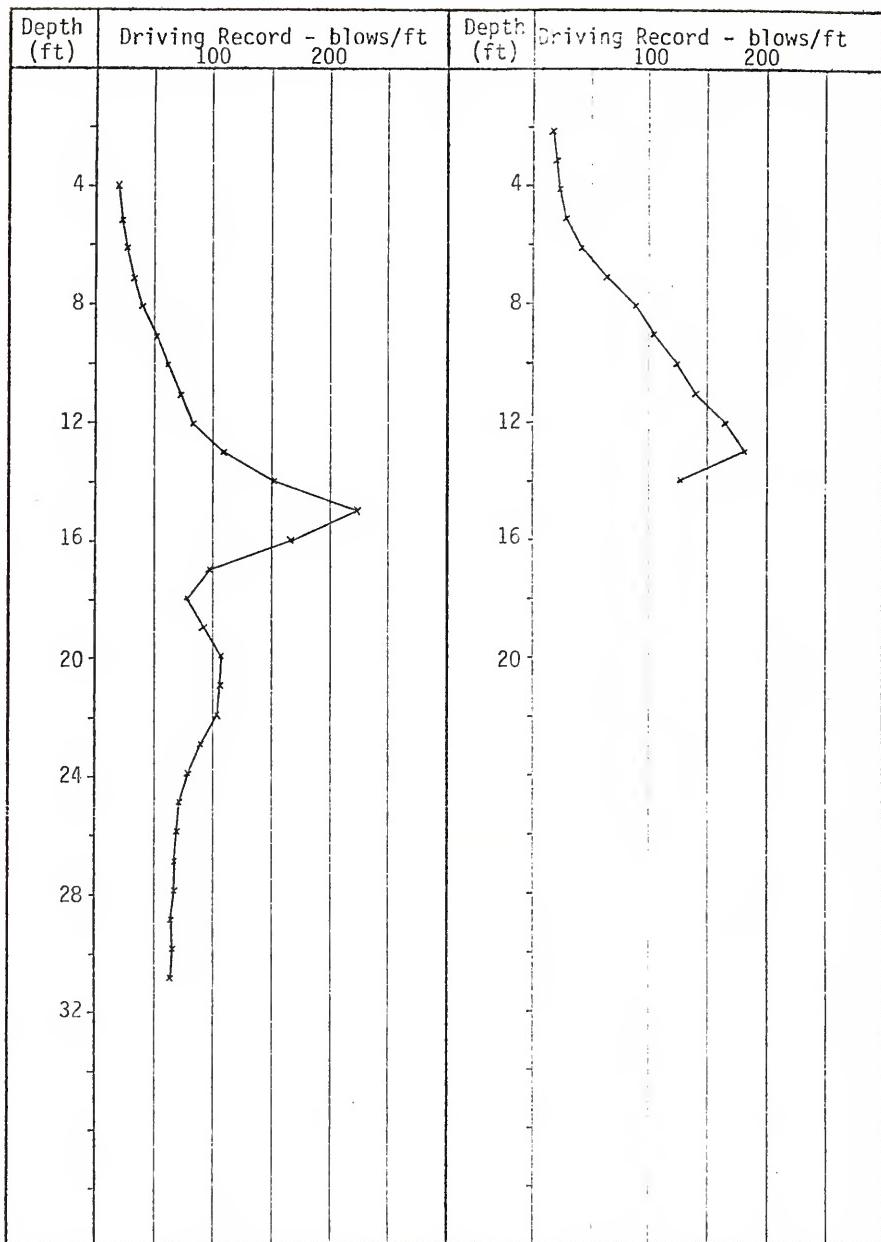
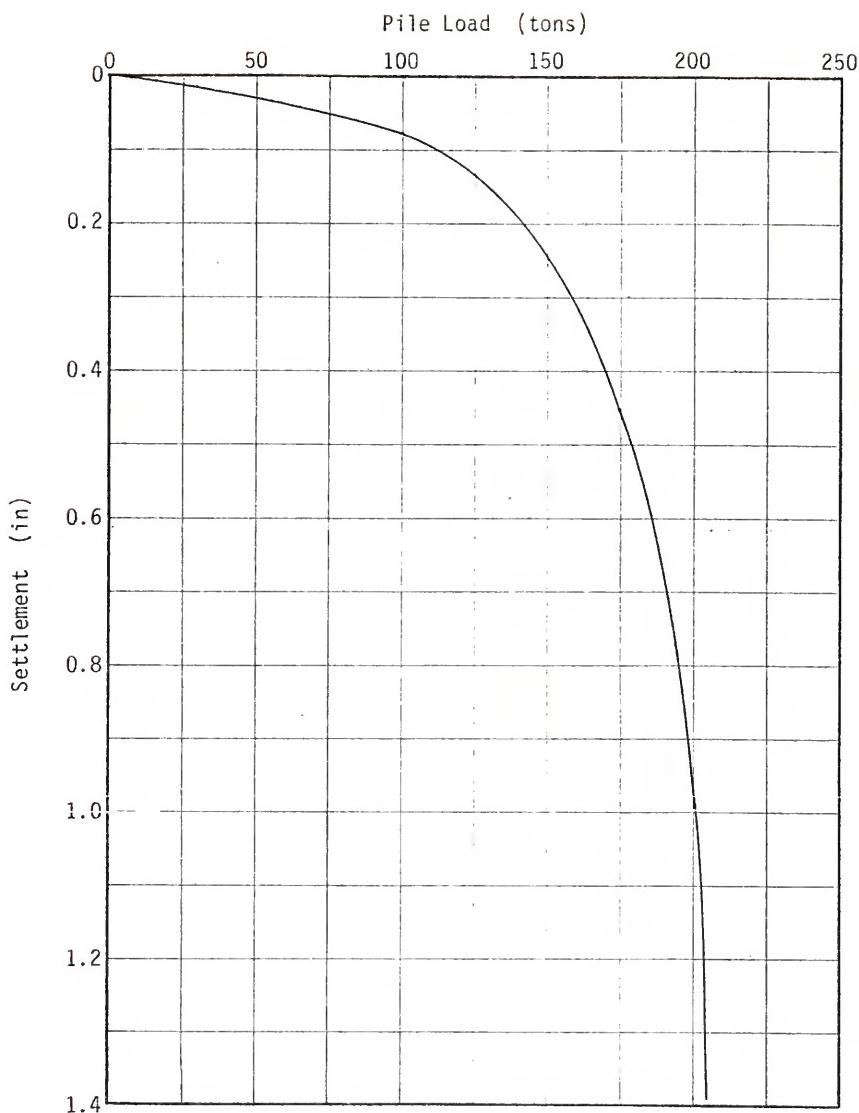


FIGURE D-12 - continued

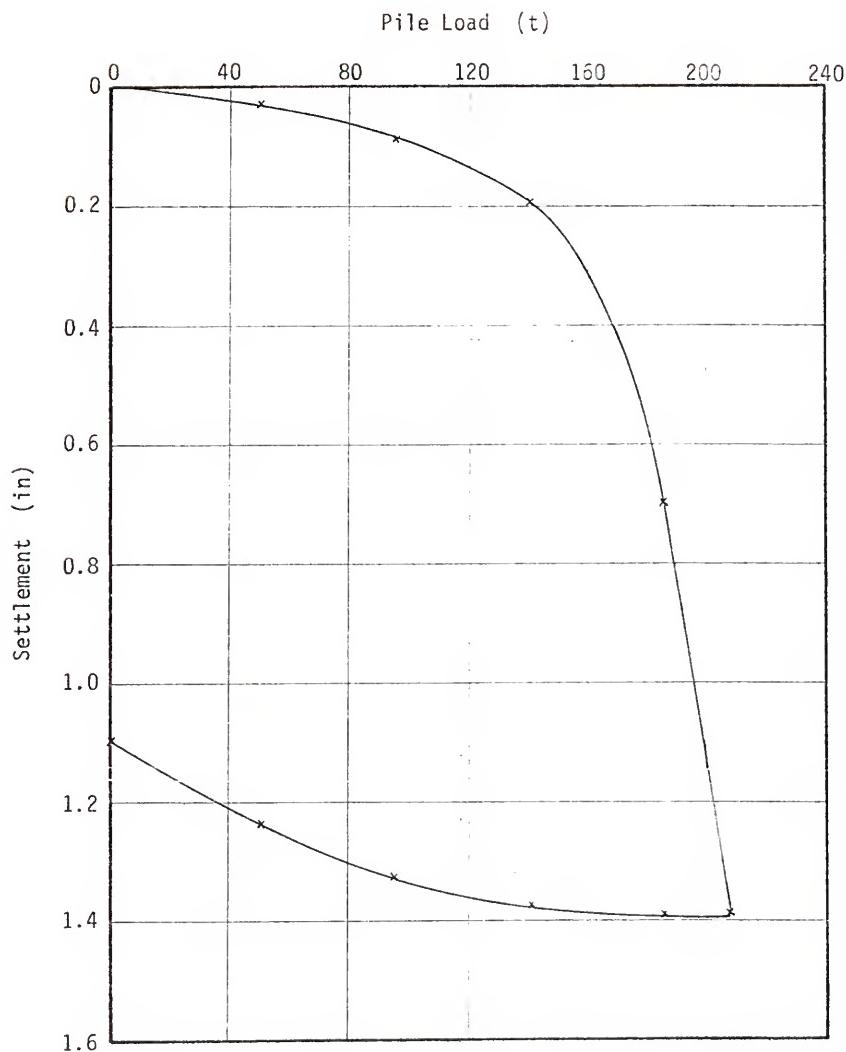


JEFFERSON COUNTY PILE DRIVING RESISTANCE DATA  
FIGURE D-14



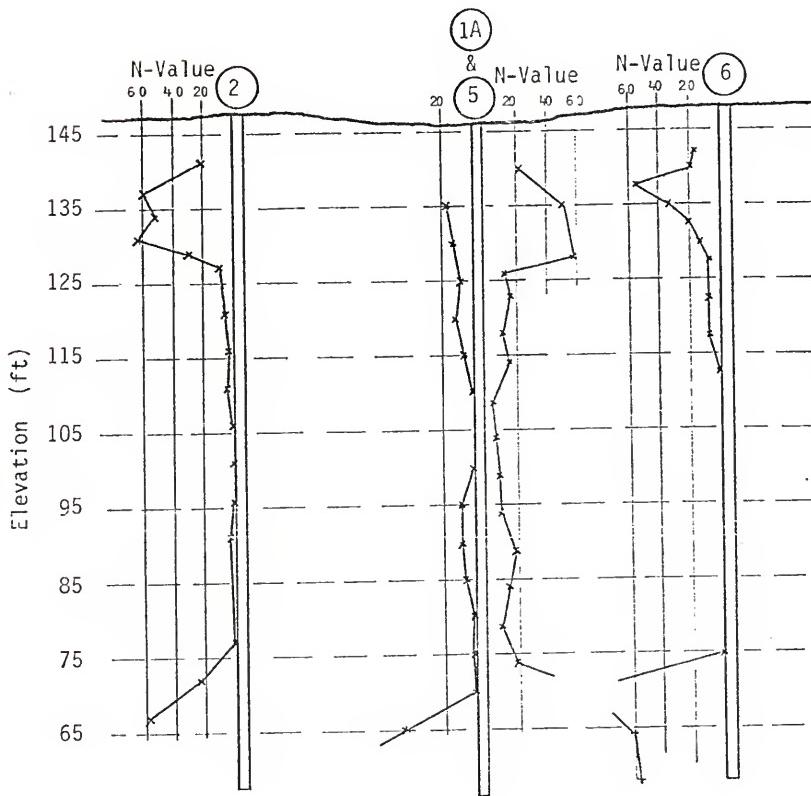
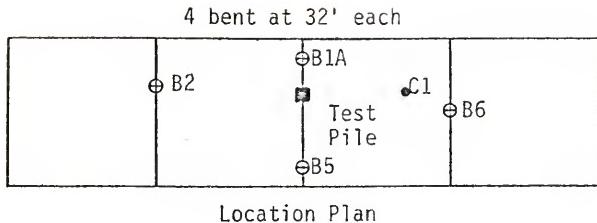
JEFFERSON COUNTY PILE LOAD TEST NO 1

FIGURE D-15



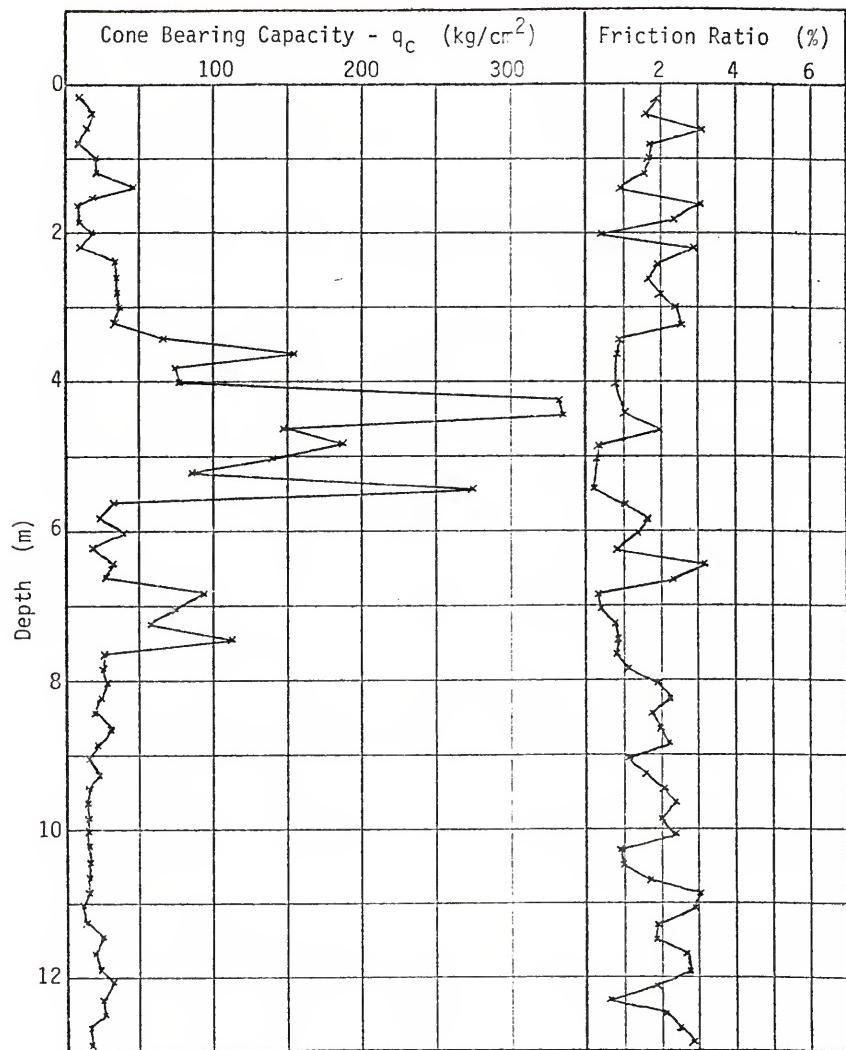
JEFFERSON COUNTY PILE LOAD TEST NO 2

FIGURE D-16



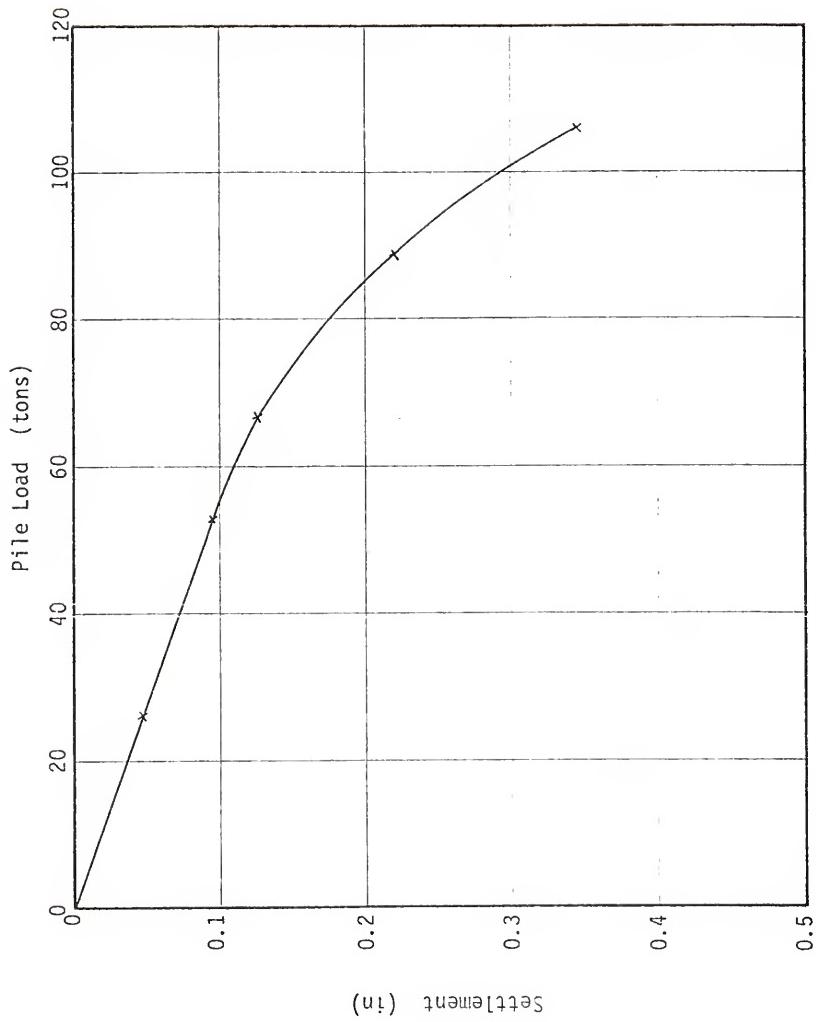
TARVER SITE LAYOUT AND BORING LOGS

FIGURE D-17



TARVER, GEORGIA CPT LOG

FIGURE D-18



TARVER SITE PILE LOAD TEST RESULTS  
FIGURE D-19

Depth (ft)	SPT N- Value	Soil Description	Depth (ft)	SPT N- Value	Soil Description
5	7	Loose tan and grey fine SAND	80	20	Firm grey fine SAND and soft slightly clayey silt layers
5	5		85	21	Boring terminated
7	11				
10	11	Firm grey fine SAND			
15	14				
20	9				
25	11	Loose to firm grey fine SAND with silt layers			
30	8				
35	38	Firm to dense fine grey SAND with silt layers			
40	11				
45	1				
50	0	Very soft dark grey clayey SILT with small shell and sand seams			
55	2				
55	2	Very loose gray SAND with soft silt layers			
60	11				
65	17	Firm grey fine SAND and soft grey slightly clayey silt layers			
70	27				
	13				
			140		
			145		

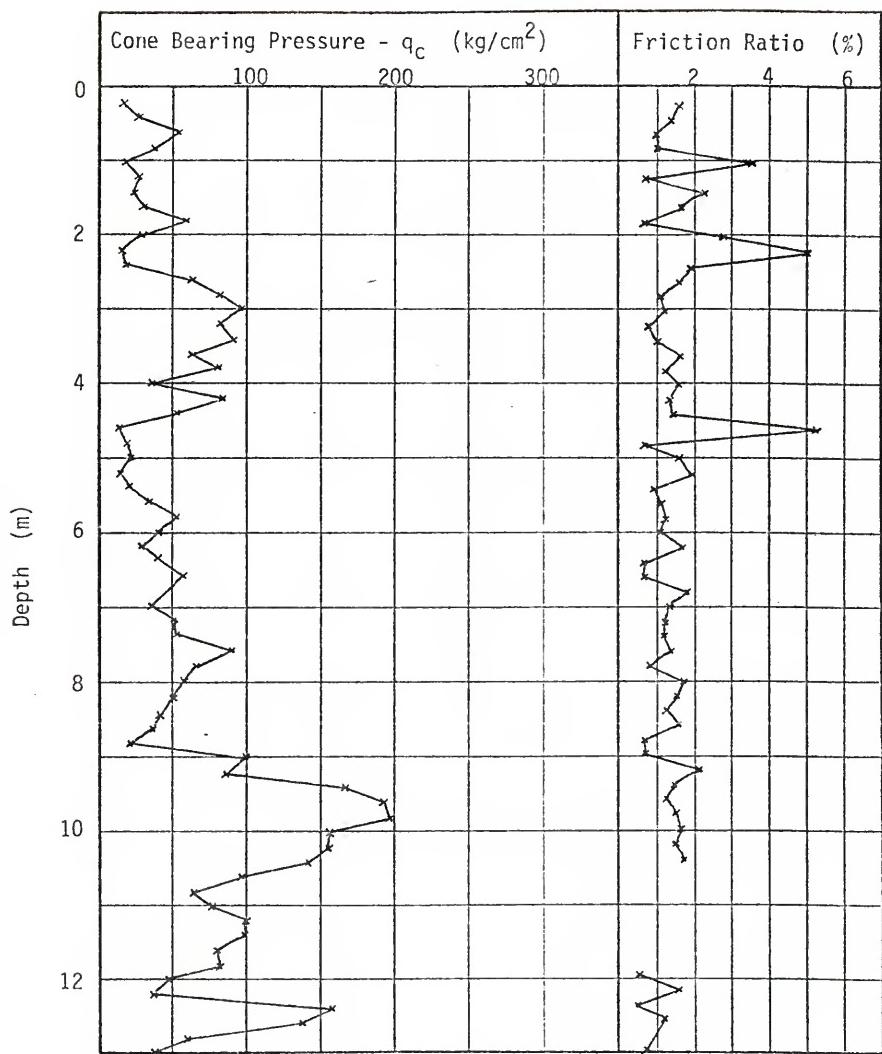
BLOUNT ISLAND SITE 215 BORING LOG

FIGURE D-20

Depth (ft)	SPT N- Value	Soil Description	Depth (ft)	SPT N- Value	Soil Description
	11	Firm grey fine SAND with shell & rock			Very hard grey clayey sandy SILT
5	35	Dense tan fine SAND with shell & rock	80	54	Very dense grey cemented SAND
	42				Very dense grey SAND
10	17		85	62	Boring terminated
	27	Firm to very firm grey and tan fine SAND with shell	90		
20	10		95		
	25	Firm grey slightly sandy SILT	100		
30	21		105		
	32	Dense to very firm grey slightly silty fine SAND	110		
40	24		115		
	6	Alternating layers of very soft grey slightly sandy SILT and loose to firm grey fine SAND	120		
50	24		125		
	8	Loose grey slightly silty fine SAND	130		
60	53	Very dense silty SAND	135		
	12	Firm grey slightly silty fine SAND	140		
70	14	Dense grey cemented silty fine SAND (LIMESTONE) with layers of firm silty sand	145		
	19				

BLOUNT ISLAND SITE 230 BORING LOG

FIGURE D-21



BLOUNT ISLAND SITE 215 CPT LOG

FIGURE D-22

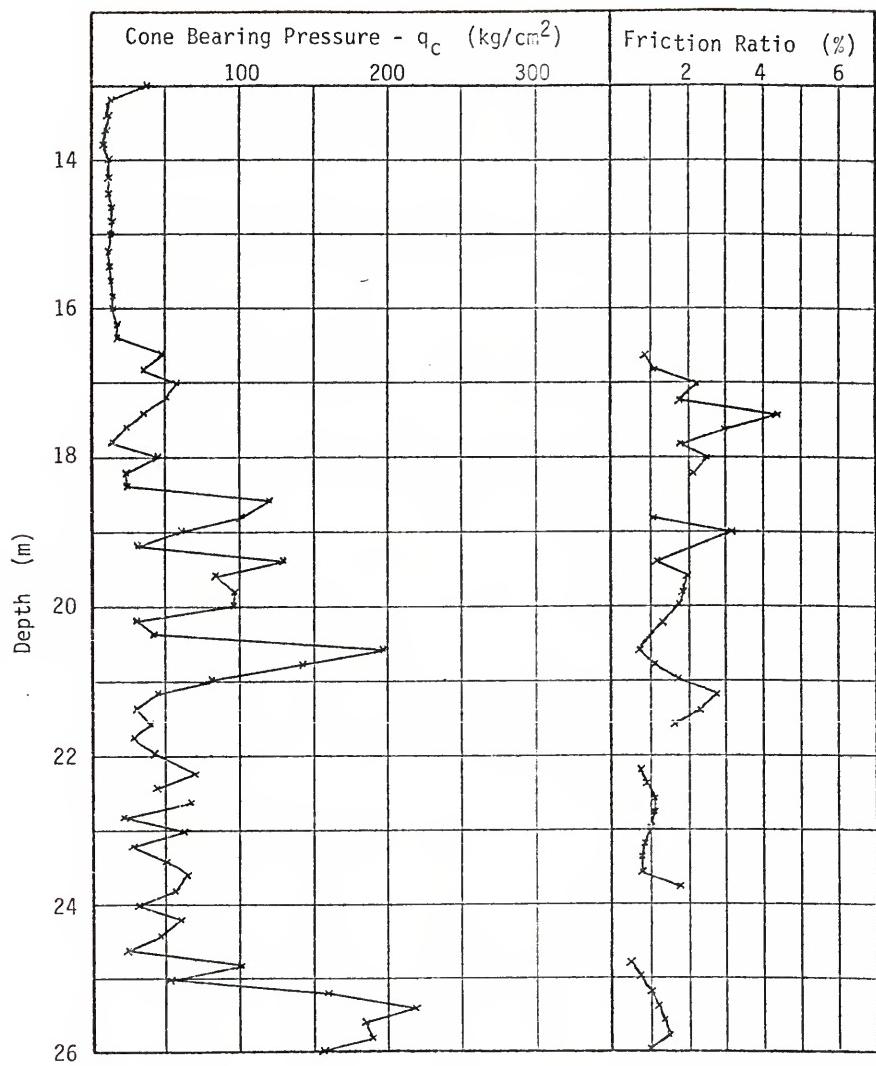


FIGURE D-22 - continued

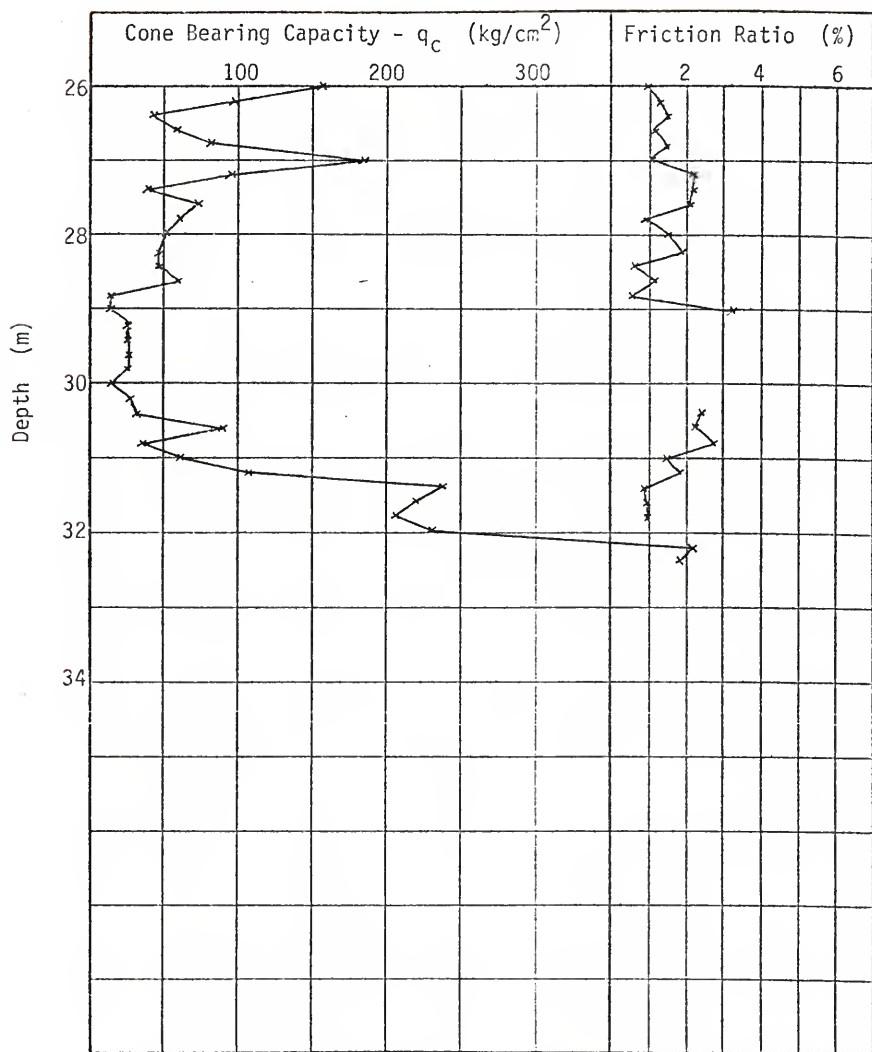
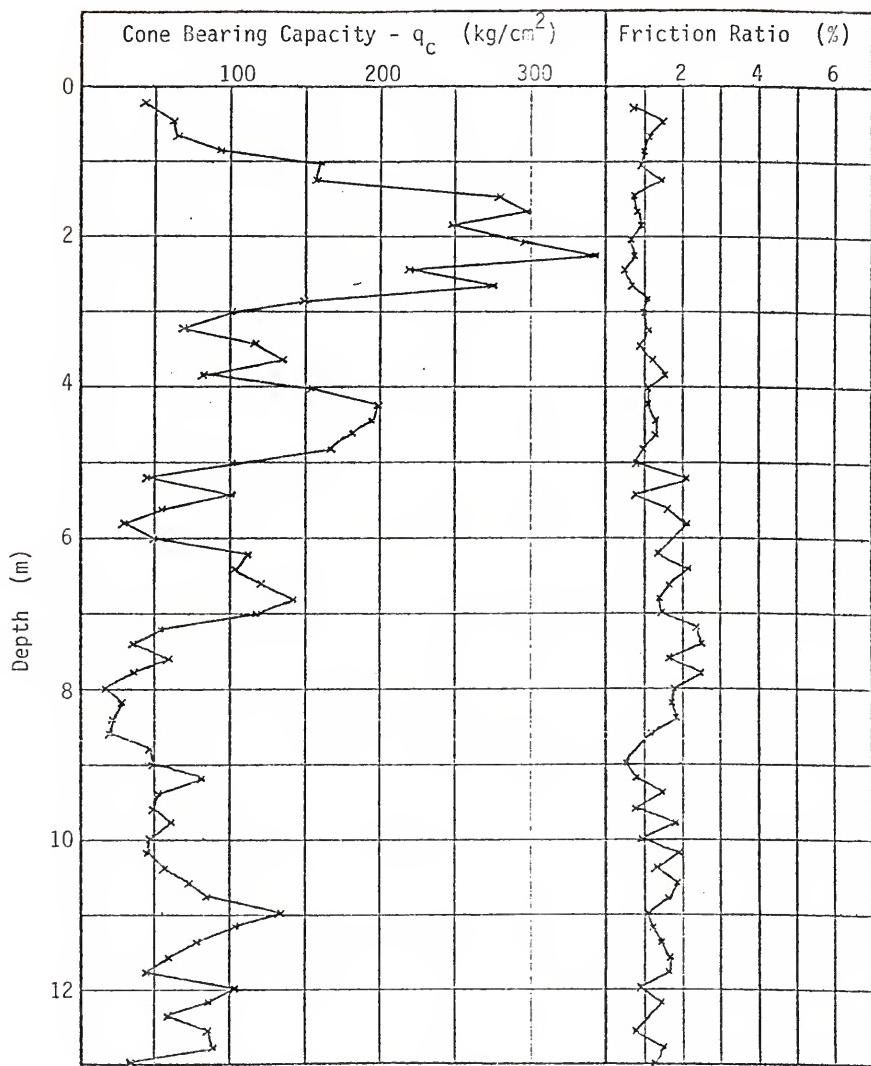


FIGURE D-22 - continued



BLOUNT ISLAND SITE 230 CPT LOG

FIGURE D-23

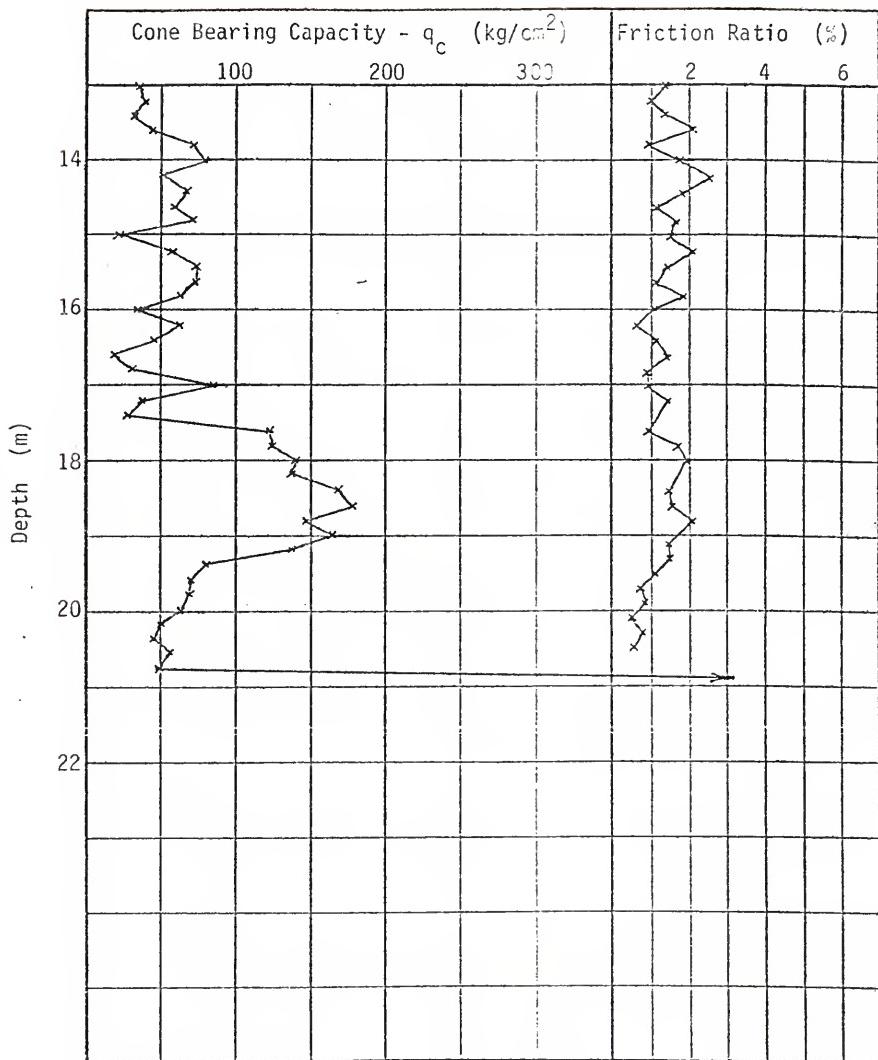


FIGURE D-23 - continued

Depth (ft)	SPT N- Value	Soil Description	Depth (ft)	SPT N- Value	Soil Description
5 -	27 13	Loose to very firm grey coarse to fine SAND with shell and rocks (Fill)	80 -	63	Very dense grey slightly clayey fine SAND
10 -	0	Very soft dark grey sandy SILT	85 -	61	
15 -	23	Very firm to very loose grey fine SAND (Fill)	90 -	100+	
20 -	4	Very soft dark grey slightly organic fine sandy SILT	95 -	100+	Very dense grey coarse to fine SAND with small gravel
25 -	1		100 -	100+	
30 -	21	Firm grey fine SAND	105 -		Boring terminated
35 -	4	Loose to very loose grey slightly silty fine SAND with shell fragments	110 -		
40 -	3		115 -		
45 -	1	Loose to very loose grey slightly silty fine SAND with layers of silt	120 -		
50 -	11	Firm grey silty coarse to fine SAND	125 -		
55 -	10	Firm grey slightly calcareous fine SAND & LIMESTONE FRAGMENTS	130 -		
60 -	20		135 -		
65 -	22	Firm brown silty fine SAND with shell fragments	140 -		
70 -	46	Dense grey-green fine SAND with silt lenses	145 -		
	9	Loose grey clayey SAND			

BLOUNT ISLAND SITE 316 BORING LOG

FIGURE D-24

Depth (ft)	SPT N- Value	Soil Description	Depth (ft)	SPT N- Value	Soil Description
5	11 10 13	Loose to firm tan and grey fine SAND with shell & rock (Fill)	80	59	Dense to very dense green-grey slightly silty fine SAND
10	19	Firm grey fine SAND (Fill)	85	85	
15	10		90	100+	Very dense grey cemented fine SAND (LIMESTONE) with layers of silt and clay
20	7	Very soft grey SILT	95	100+	
25	27	Loose grey slightly silty fine SAND	100	100+	
30	1	Very firm grey fine SAND	105		Boring terminated
35	18		110		
40	9	Loose to firm grey fine SAND with silt layers	115		
45	7		120		
50	10	Loose grey fine SAND with silt layers and wood	125		
55	10	Loose to firm grey calcareous silty fine SAND with shell	130		
60	20		135		
65	30	Dense to very dense green-grey slightly silty fine SAND	140		
70	15 48		145		

BLOUNT ISLAND SITE 322 BORING LOG

FIGURE D-25

Depth (ft)	SPT N- Value	Soil Description	Depth (ft)	SPT N- Value	Soil Description
	1	Loose grey SAND and SHELL (Fill)			
5	1	Very soft dark grey SILT	80	100+	Very dense grey cemented silty SAND (LIMESTONE)
10	0		85	100+	
10	19	Firm grey fine SAND	90	7	Loose grey calcareous silty fine SAND with cemented sand frag-ments
15	0	Very soft dark grey sandy SILT with peat	95	100+	Very dense SILTY SAND
20	9	Loose to firm grey slightly silty fine SAND with silt seams	100	100+	Very dense fine SAND
25	11				Boring terminated
30	1		105		
35	4	Very loose to loose grey silty to slightly silty fine SAND with silt seams	110		
40	9		115		
45	19	Firm grey slightly silty SAND	120		
50	15	Firm grey slightly calcareous fine SAND	125		
55	20		130		
60	18	Firm to dense brown to greenish-grey slightly clayey slightly silty fine SAND	135		
65	39		140		
70	100+	Alternating layers of cemented silty SAND (LIMESTONE) and hard grey SILT	145		
	20				

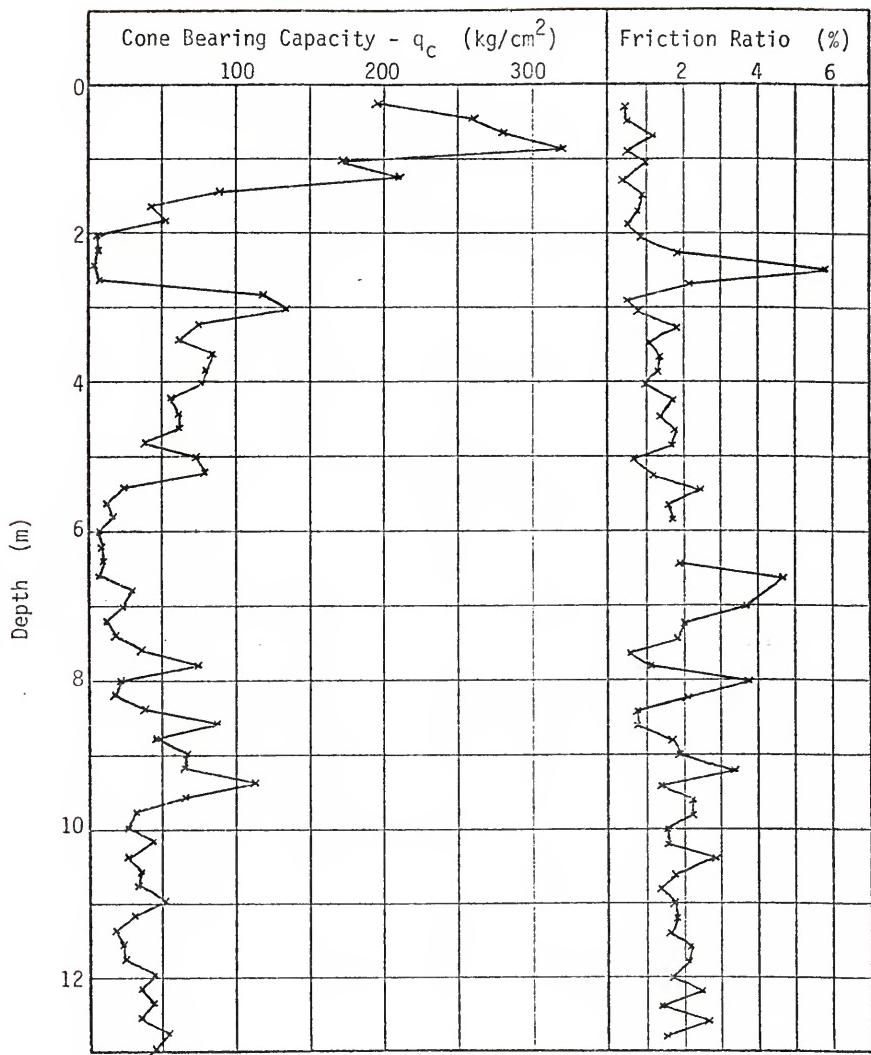
BLOUNT ISLAND SITE 343 BORING LOG

FIGURE D-26

Depth (ft)	SPT N- Value	Soil Description	Depth (ft)	SPT N- Value	Soil Description
5	6 4	Loose grey fine SAND	80	100+	
10	11 21	Firm to very firm grey fine SAND	85	69	Very dense grey- green slightly clayey slightly silty fine to medium SAND with small gravel
15	0	Very soft PEAT	90	7	Very dense grey cemented silty fine SAND (LIMESTONE) with alternating layers of firm grey clayey silt
20	17		95	100+	
25	10		100	100+	
30	7	Firm to loose grey fine SAND with silt seams	105		Boring terminated
35	7		110		
40	9		115		
45	33		120		
50	26	Dense to very firm grey fine to medium SAND	125		
55	11		130		
60	30	Firm to very dense grey-green slightly silty fine to medium SAND	135		
65	37		140		
70	23		145		
	65				

BLOUNT ISLAND SITE 348 BORING LOG

FIGURE D-27



BLOUNT ISLAND SITE 316 CPT LOG

FIGURE D-28

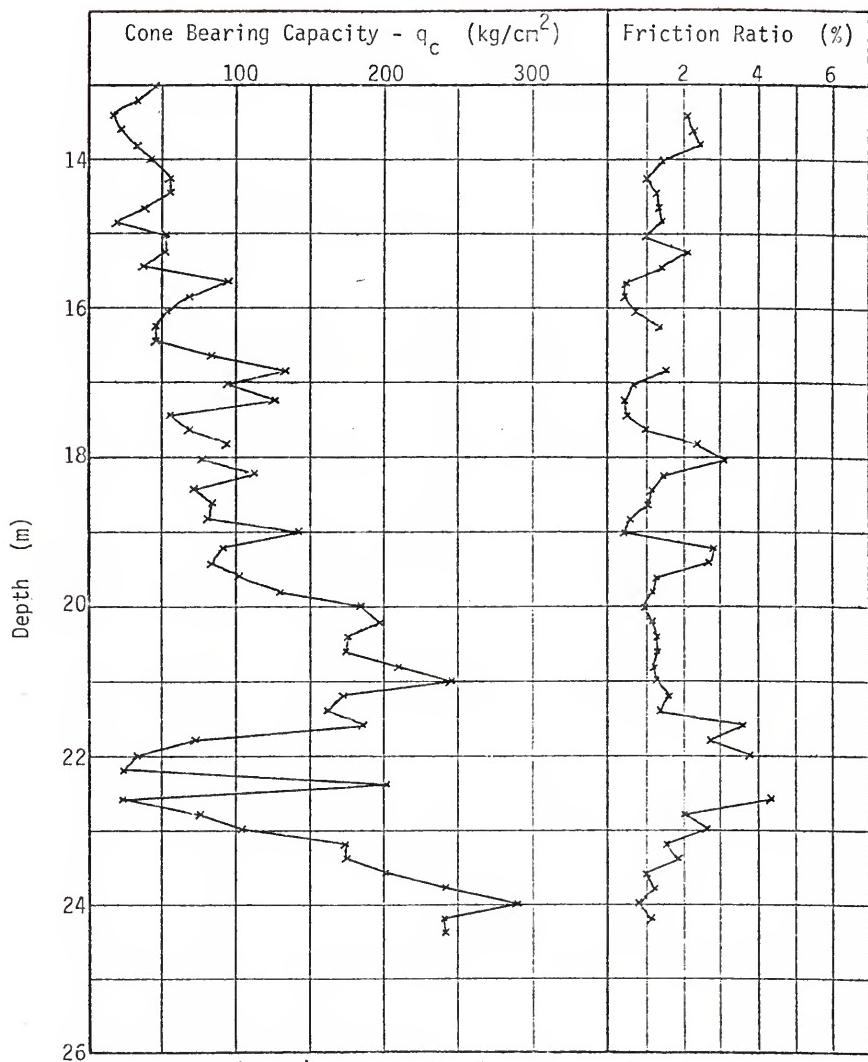
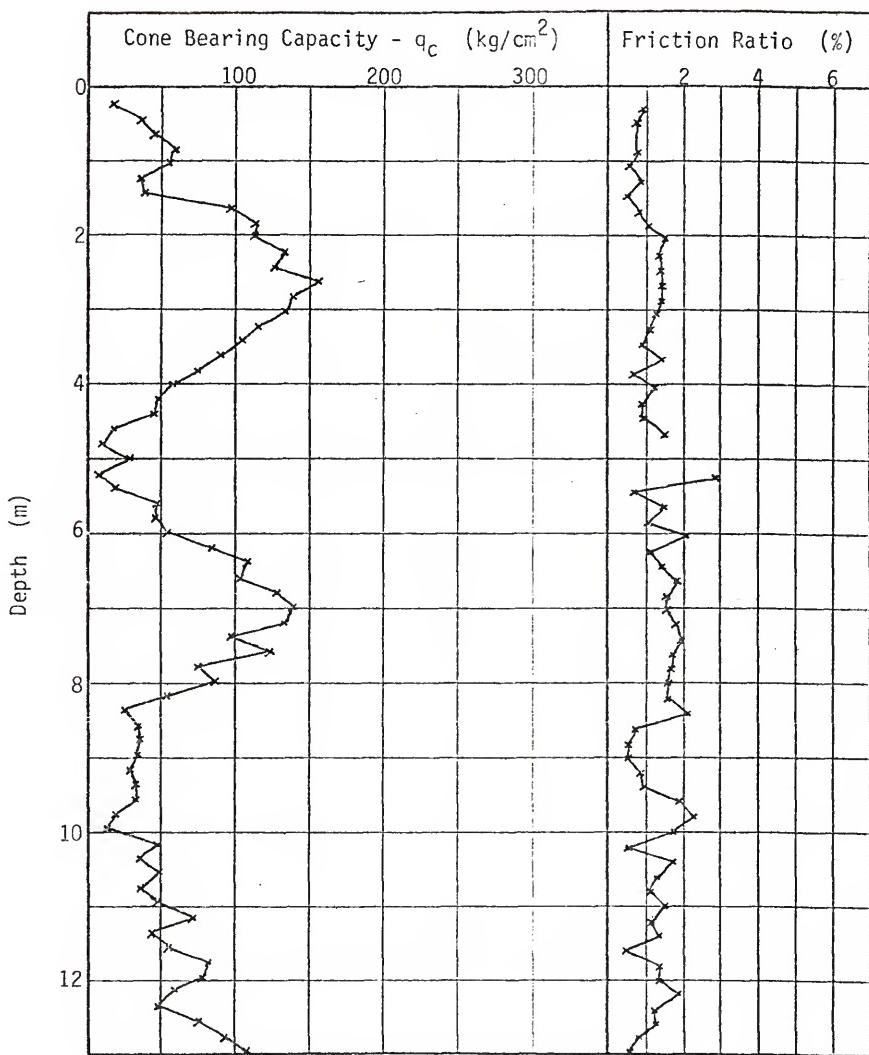


FIGURE D-28 - continued



BLOUNT ISLAND SITE 322 CPT LOG

FIGURE D-29

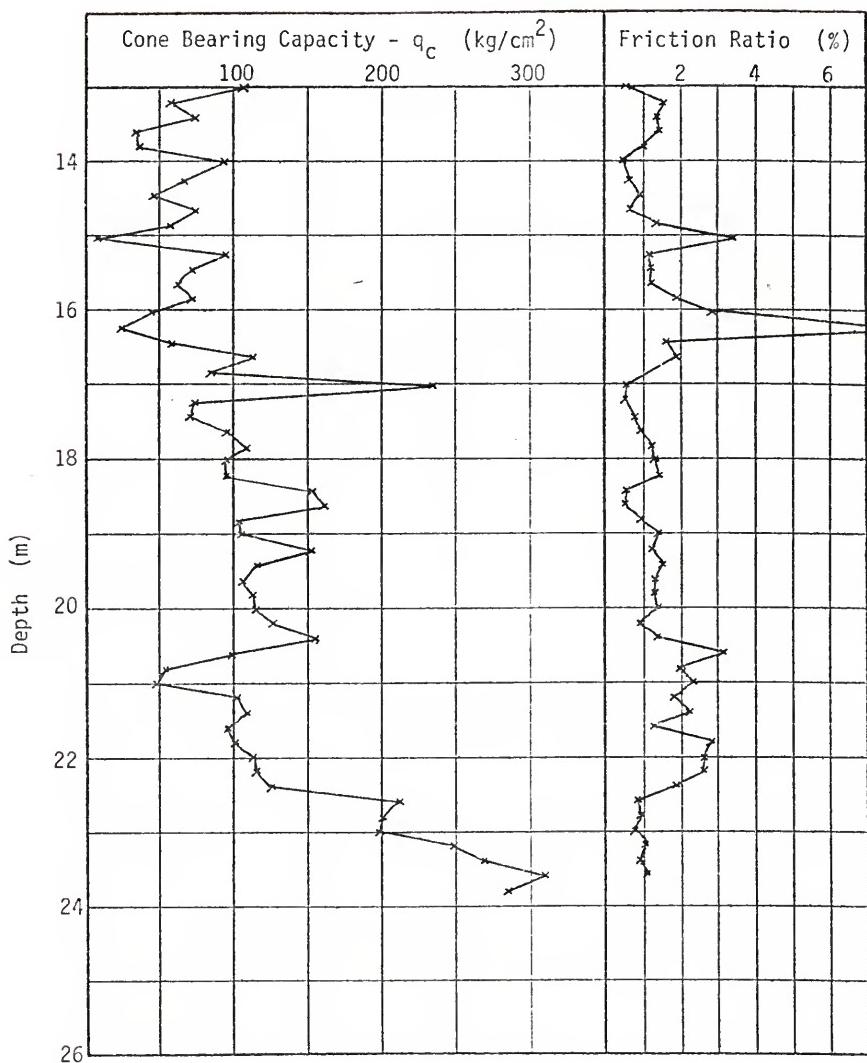
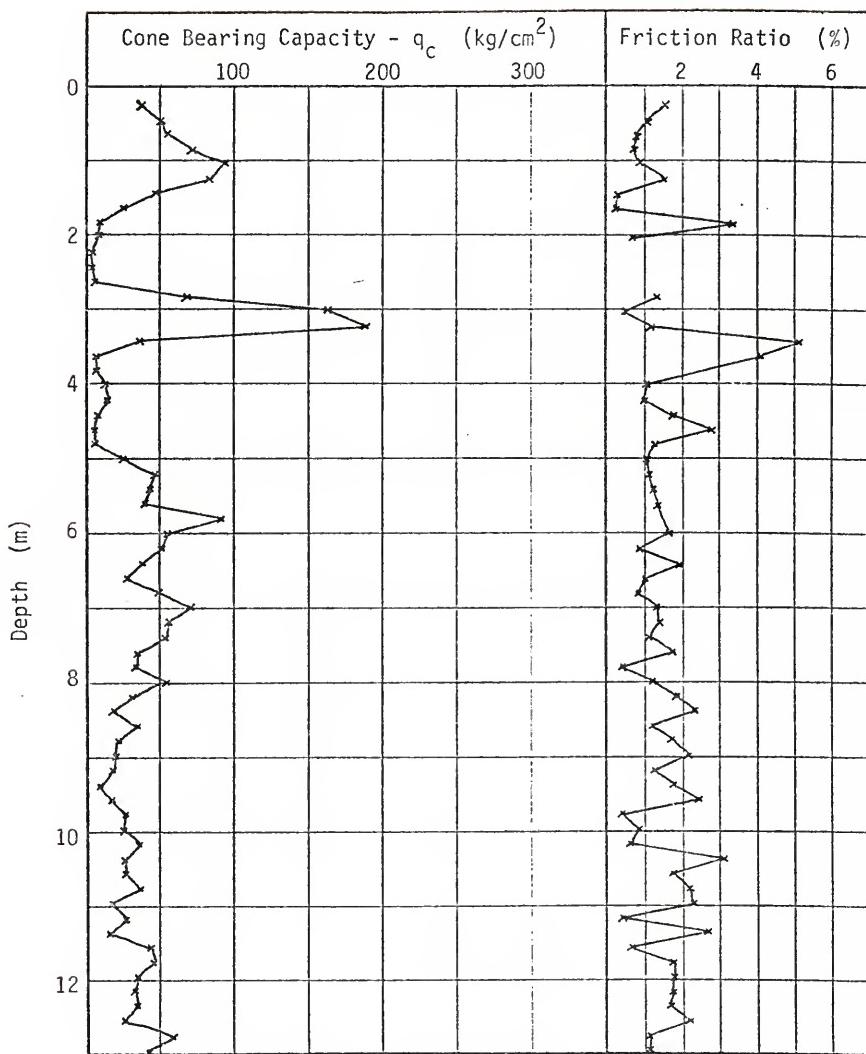


FIGURE D-29 - continued



BLOUNT ISLAND SITE 343 CPT LOG

FIGURE D-30

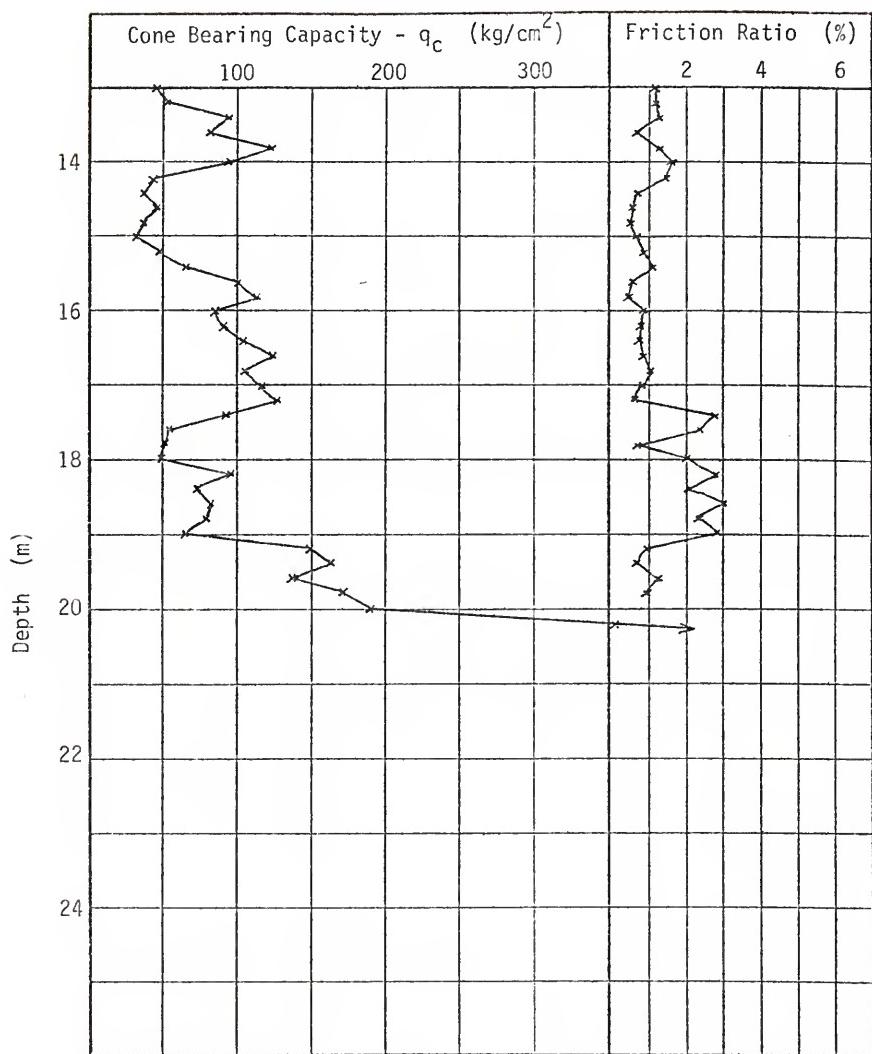
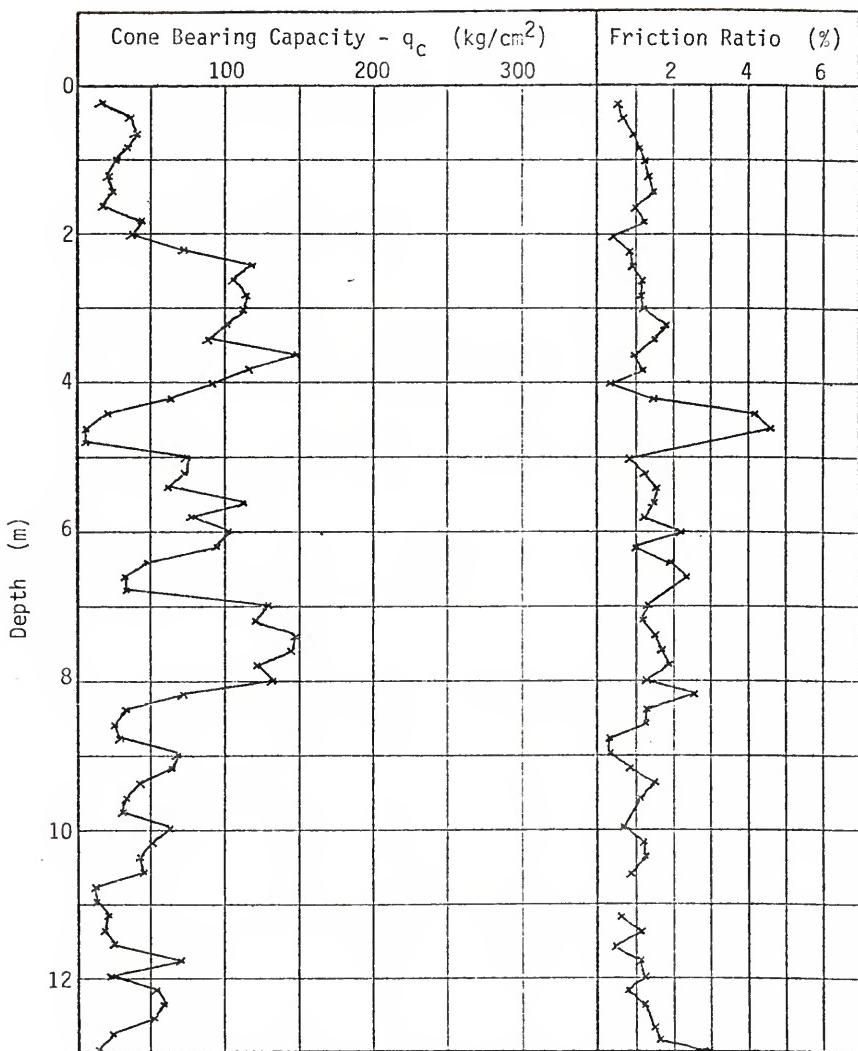


FIGURE D-30 - continued



BLOUNT ISLAND SITE 348 CPT LOG

FIGURE D-31

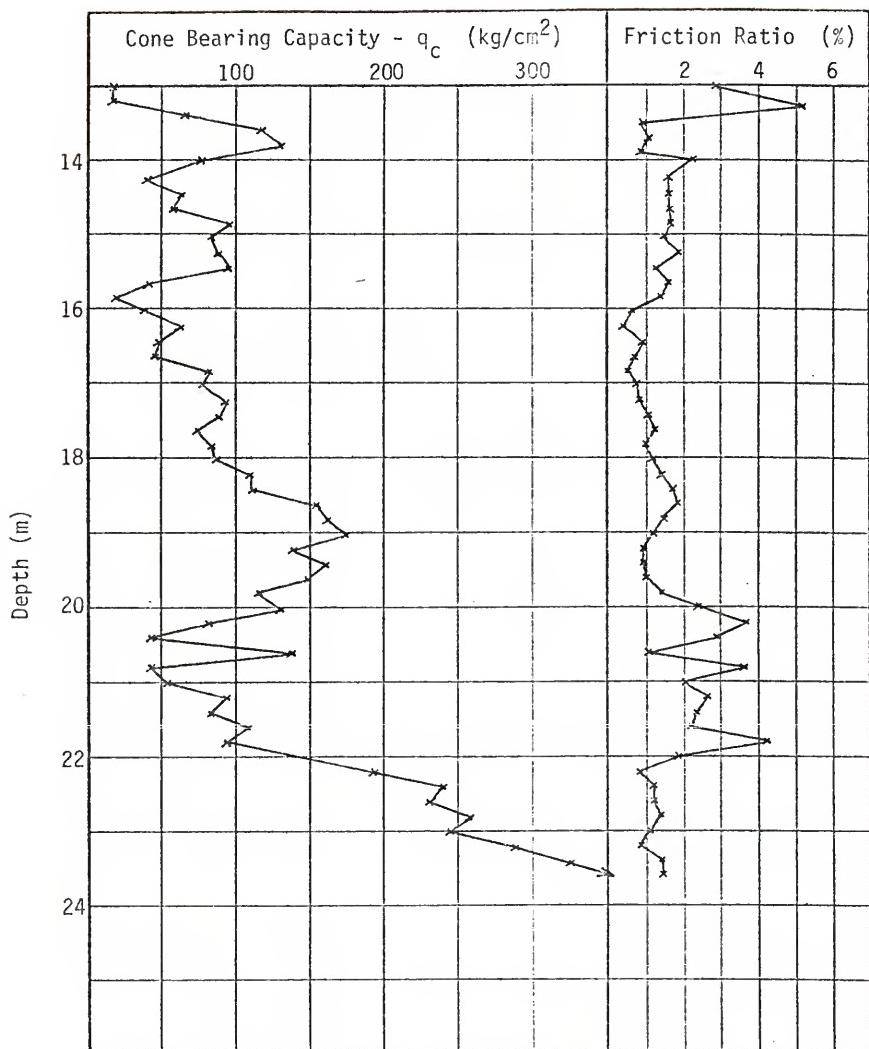
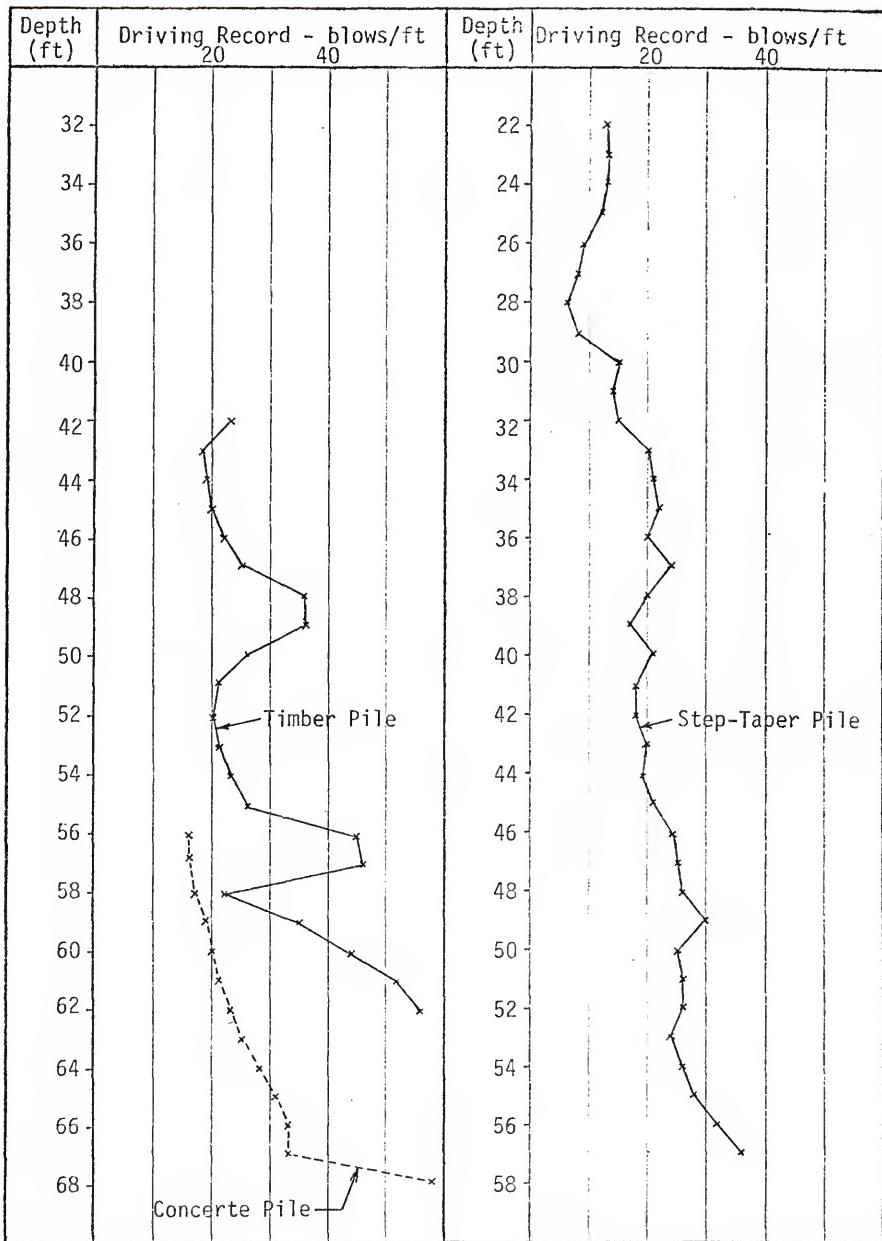
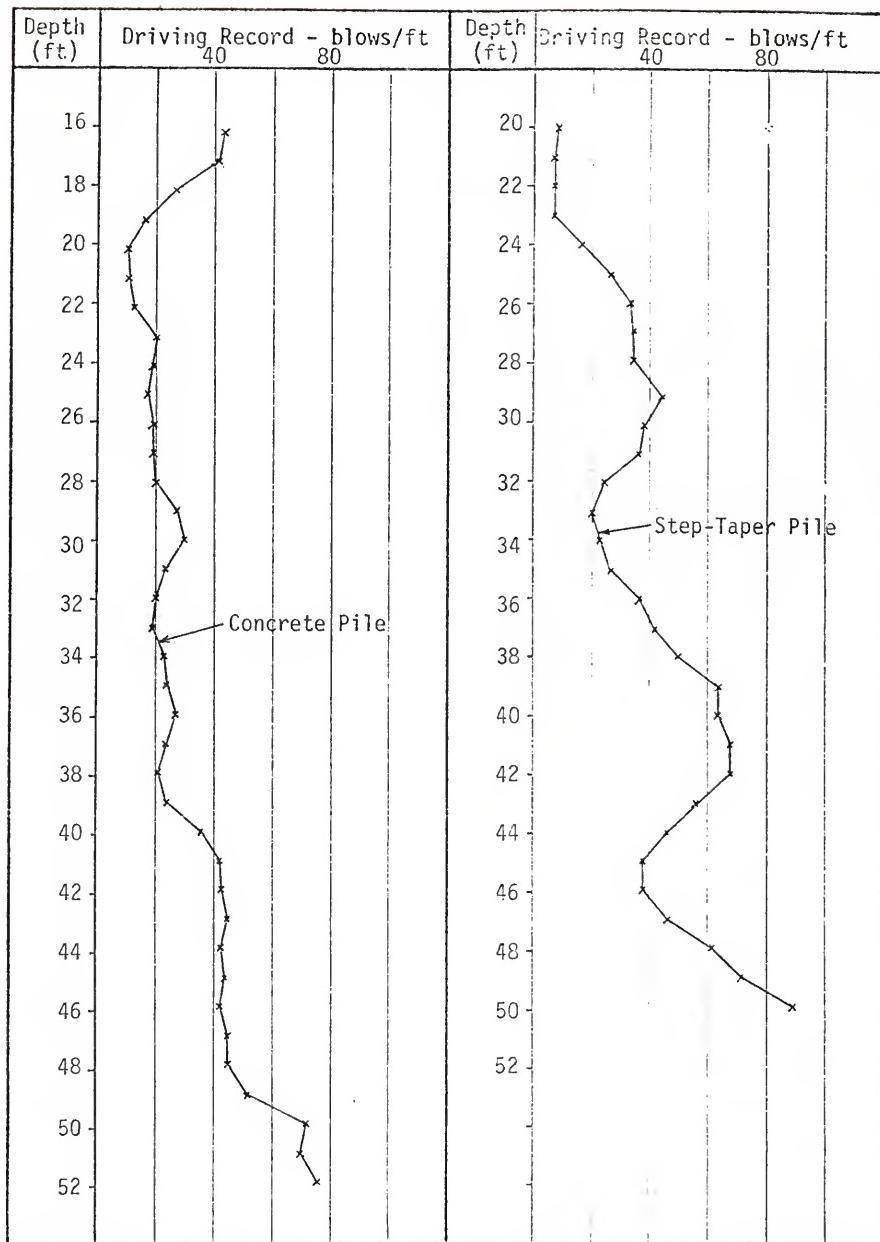


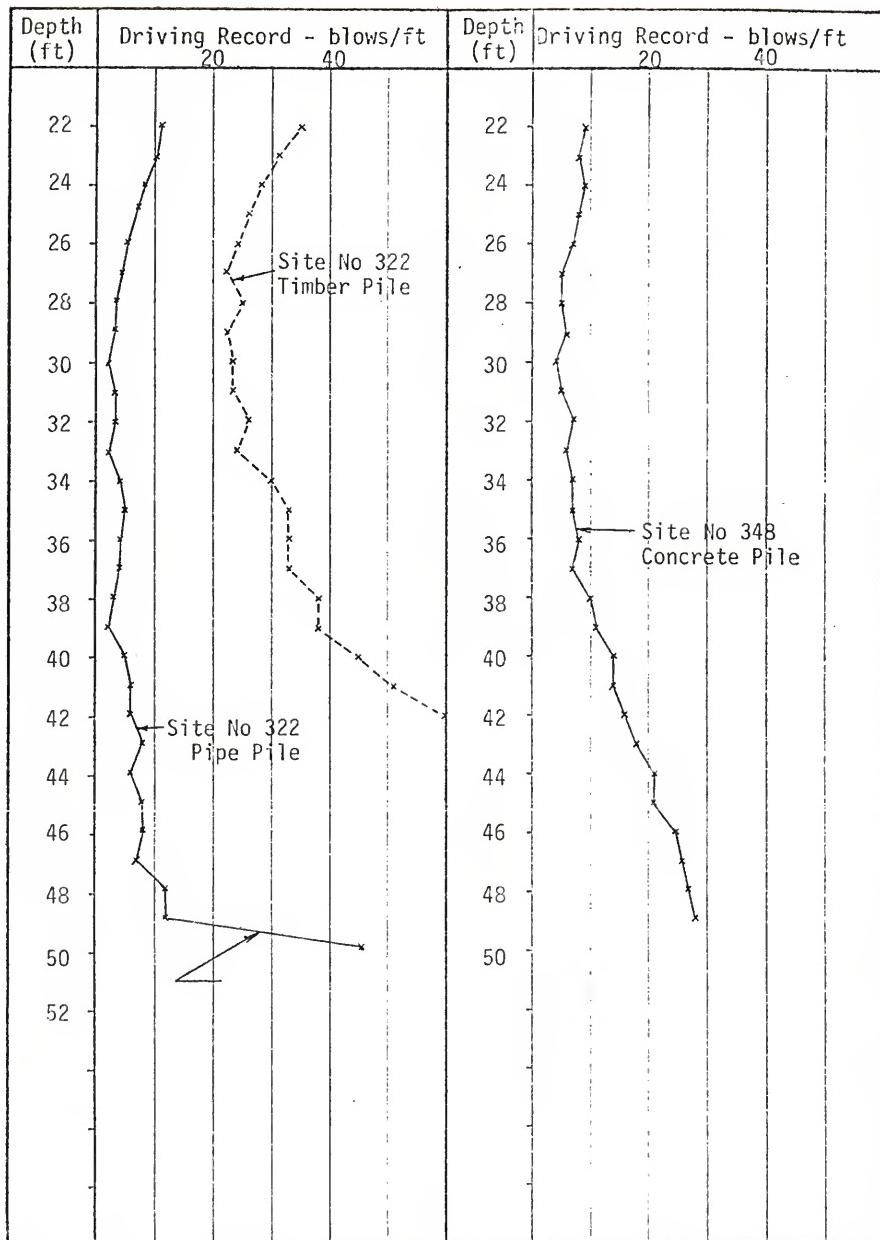
FIGURE D-31 - continued



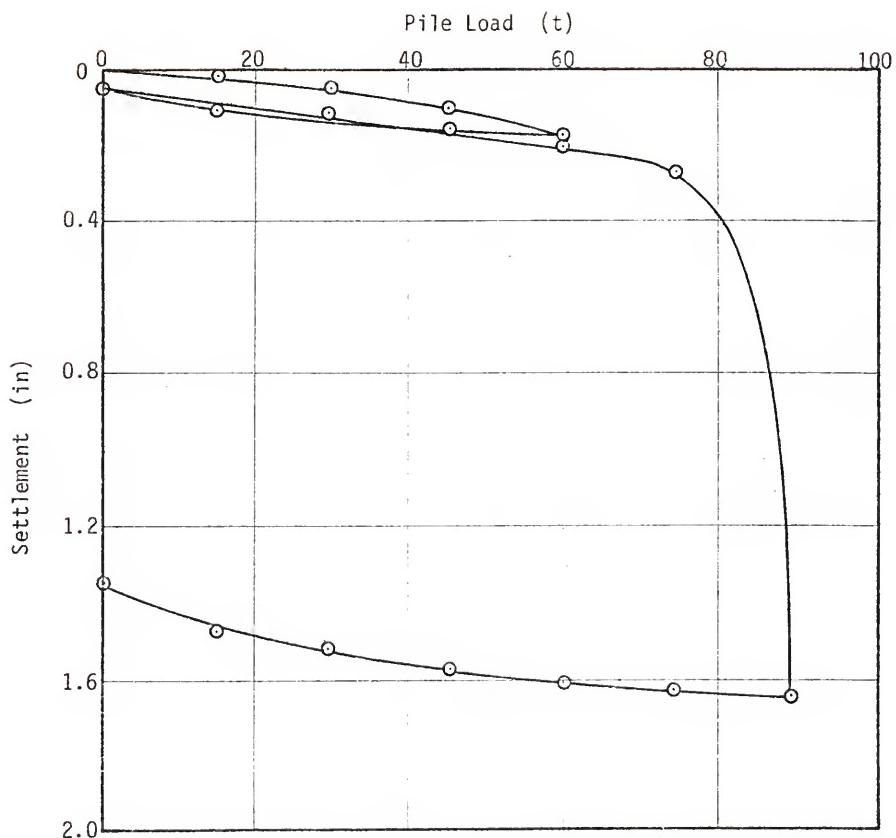
BLOUNT ISLAND SITE 215 PILE DRIVING RESISTANCE DATA  
FIGURE D-32



BLOUNT ISLAND SITE 316 PILE DRIVING RESISTANCE DATA  
FIGURE D-33



BLOUNT ISLAND PILE DRIVING RESISTANCE DATA  
FIGURE D-34

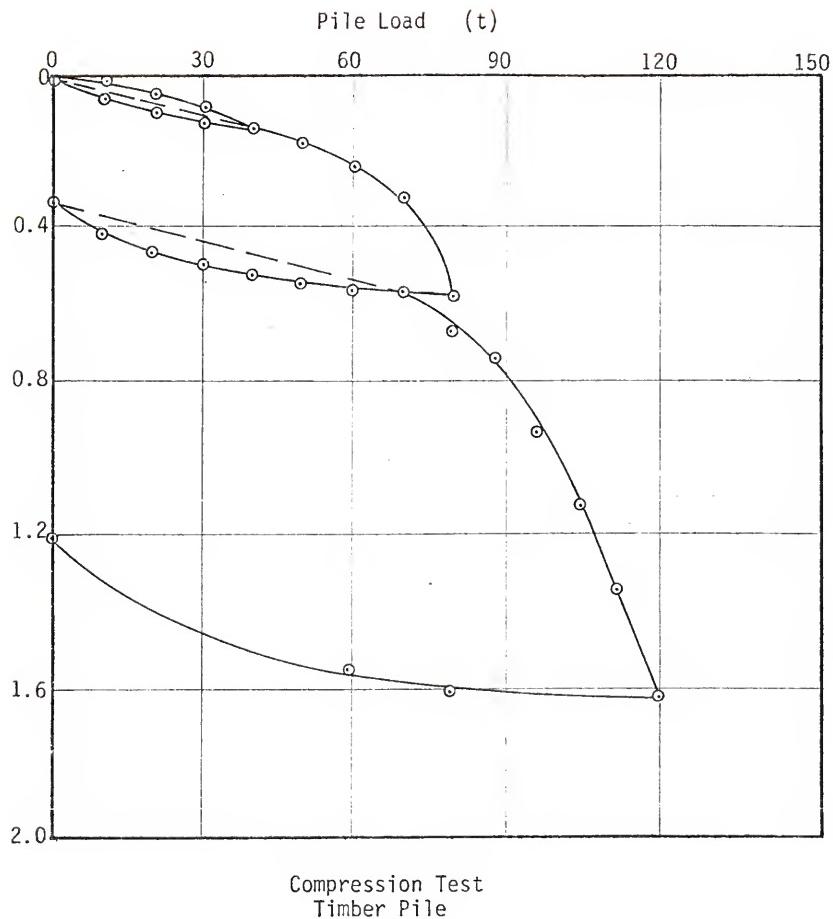


Compression Test

10 in Square Prestressed Concrete Pile

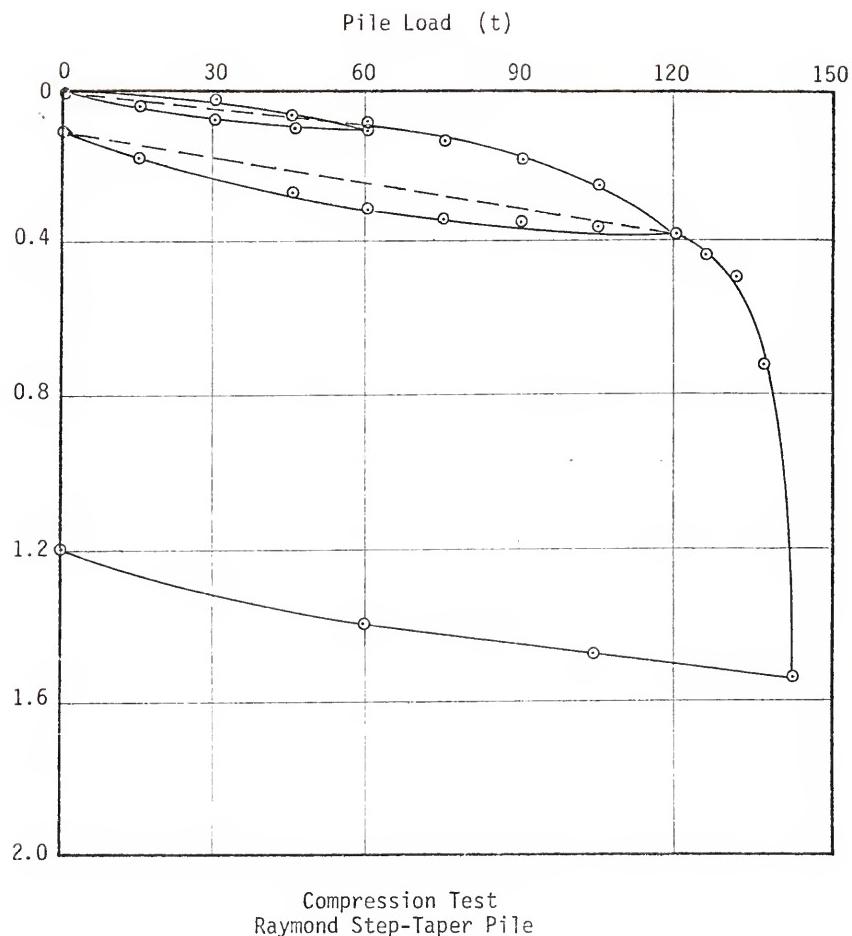
BLOUNT ISLAND PILE LOAD TEST RESULTS - SITE 215

FIGURE D-35



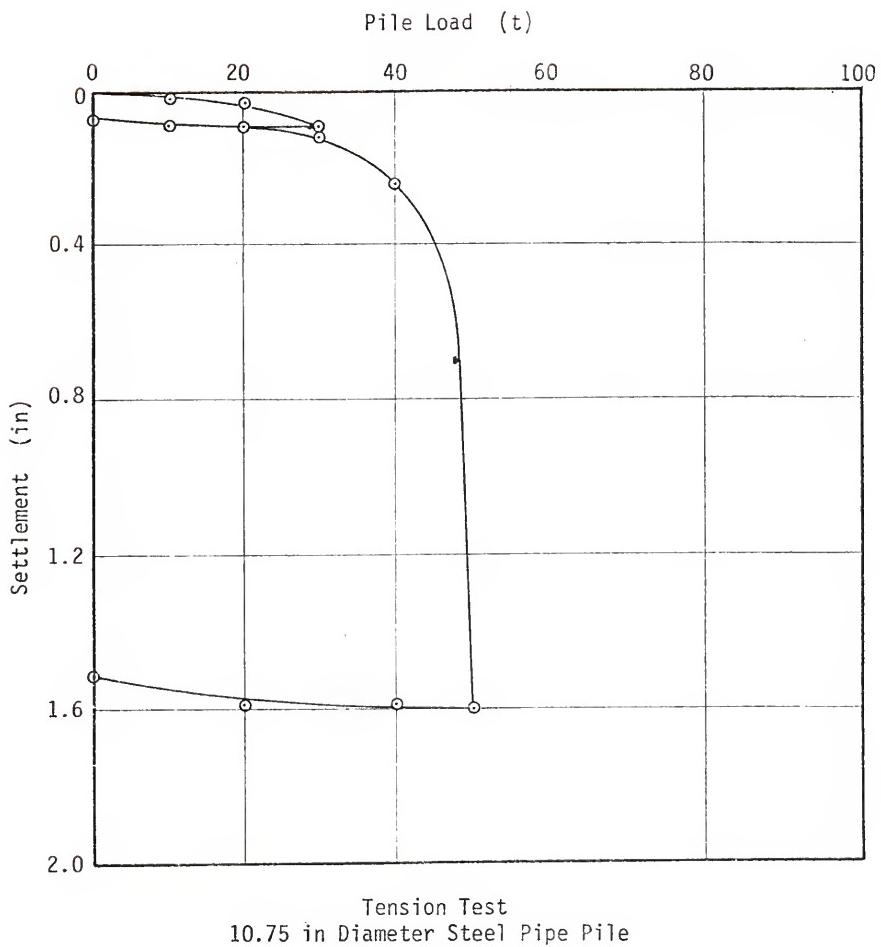
BLOUNT ISLAND PILE LOAD TEST RESULTS - SITE 215

FIGURE D-36



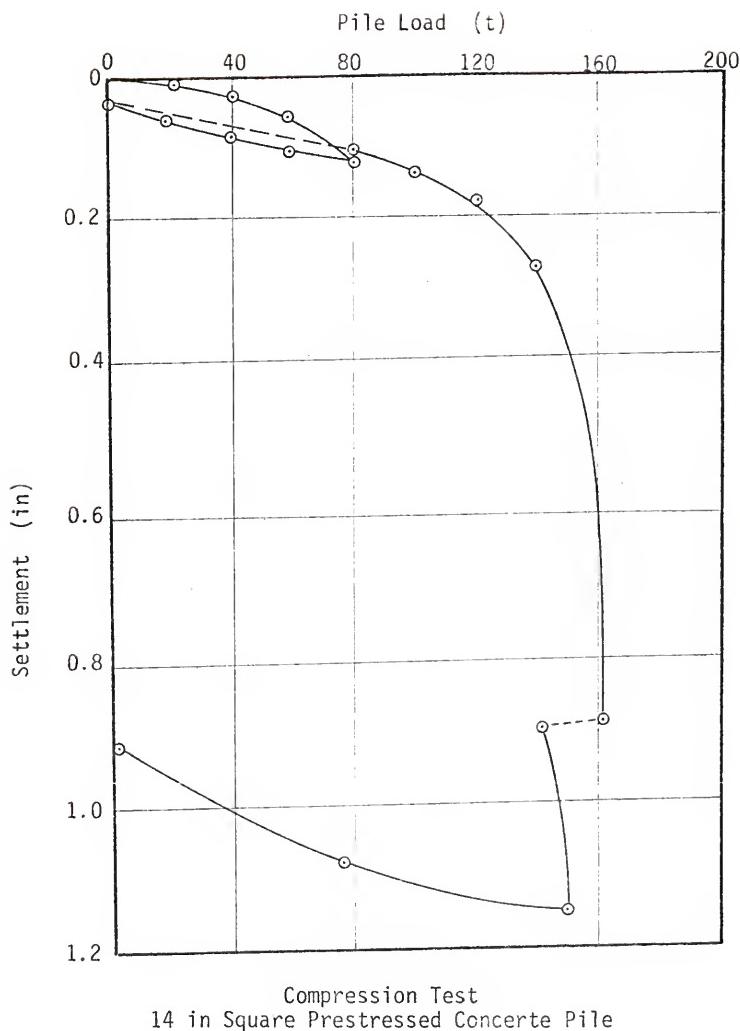
BLOUNT ISLAND PILE LOAD TEST RESULTS - SITE 215

FIGURE D-37



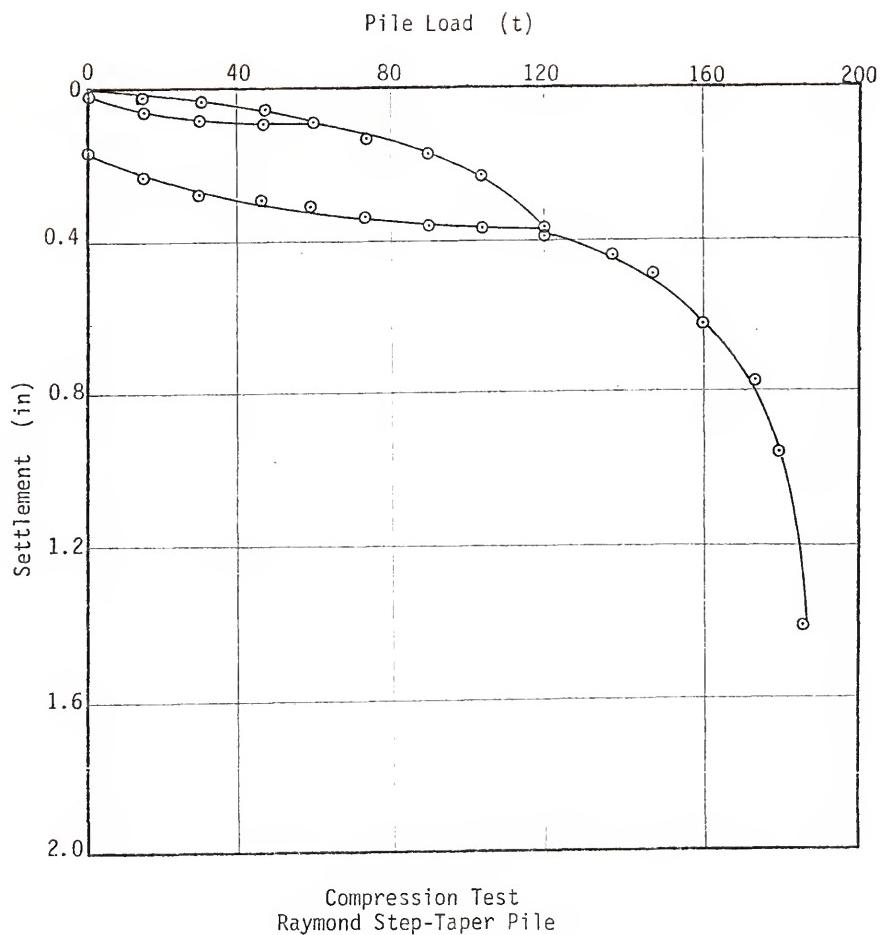
BLOUNT ISLAND PILE LOAD TEST RESULTS - SITE 227

FIGURE D-38



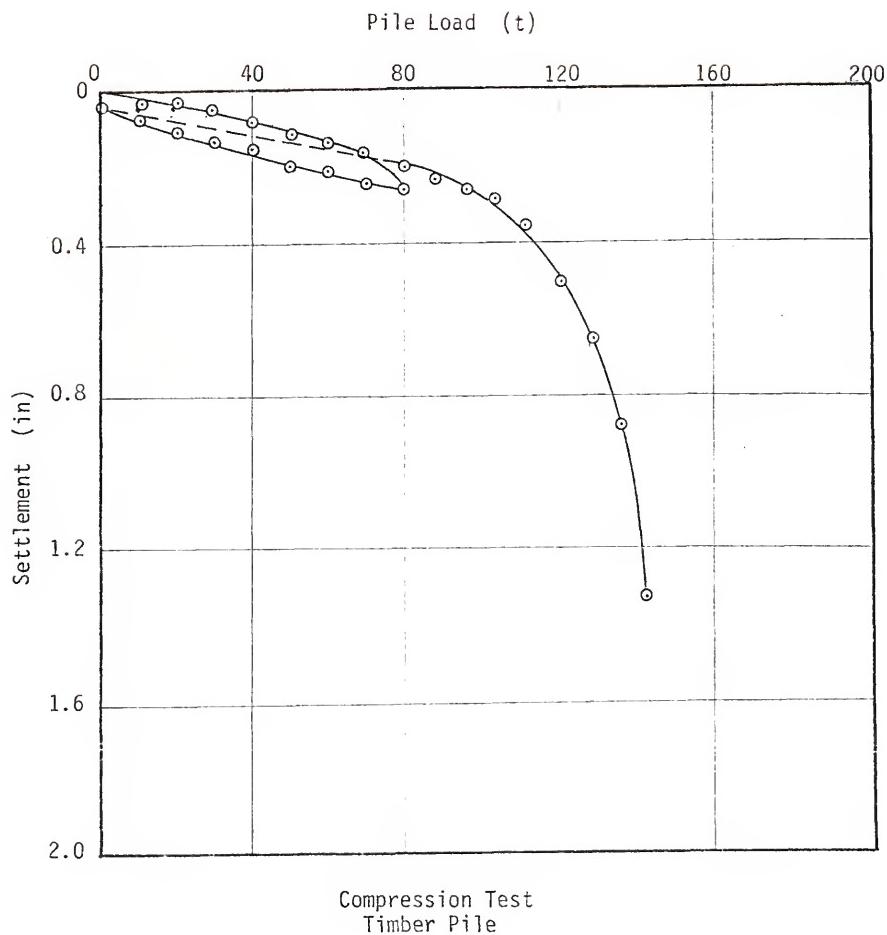
BLOUNT ISLAND PILE LOAD TEST RESULTS - SITE 316

FIGURE D-39



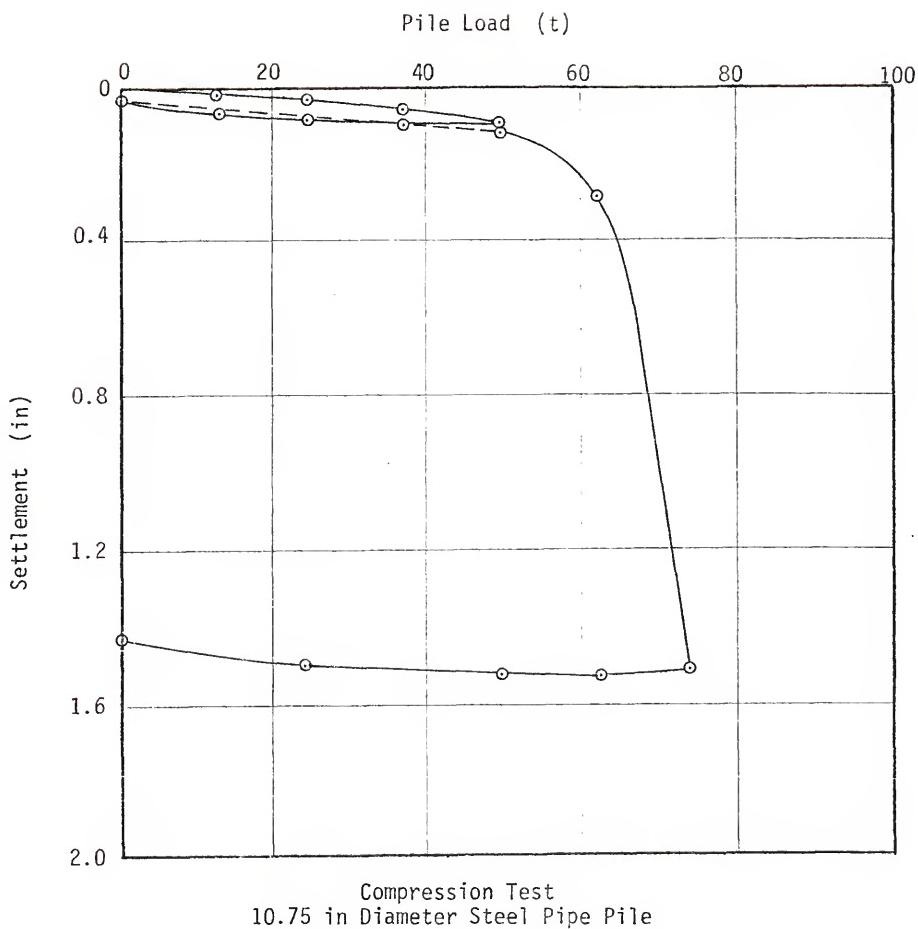
BLOUNT ISLAND PILE LOAD TEST RESULTS - SITE 316

FIGURE D-40



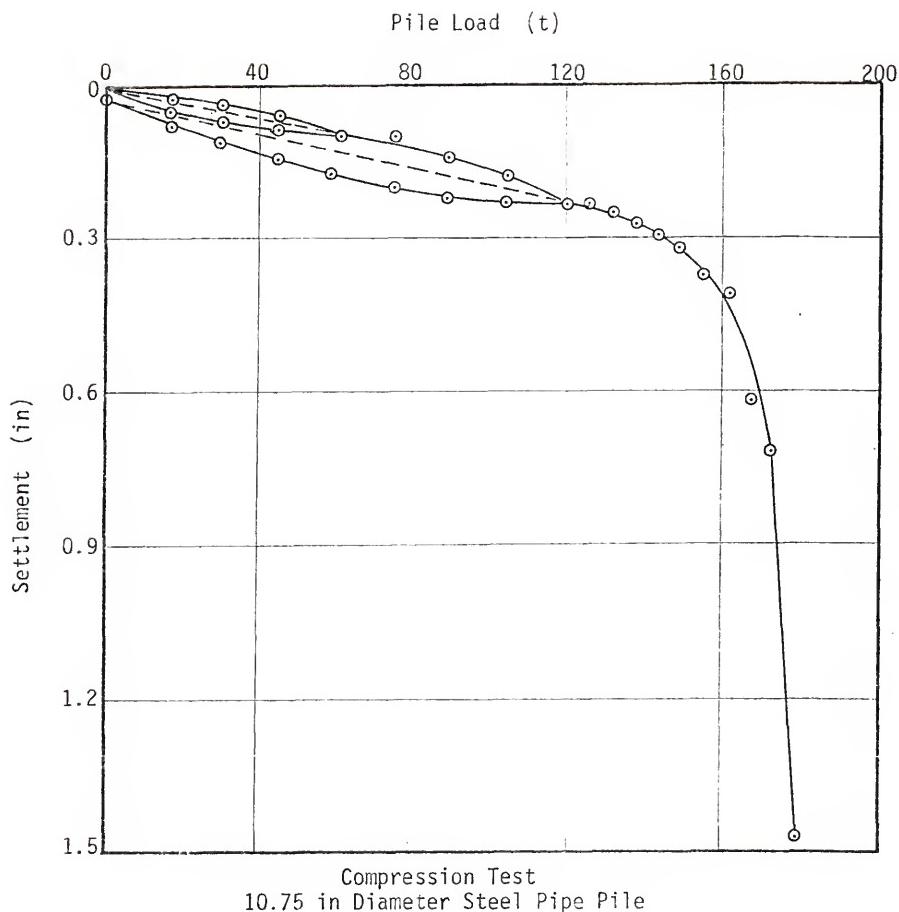
BLOUNT ISLAND PILE LOAD TEST RESULTS - SITE 322

FIGURE D-41



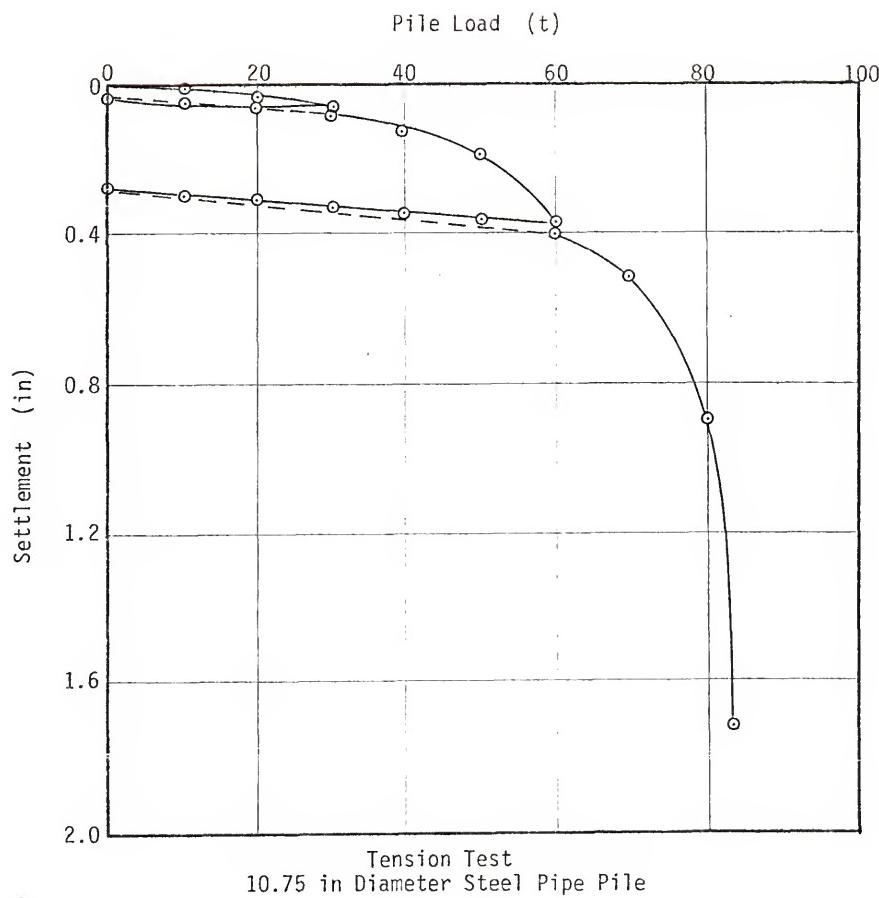
BLOUNT ISLAND PILE LOAD TEST RESULTS - SITE 322

FIGURE D-42



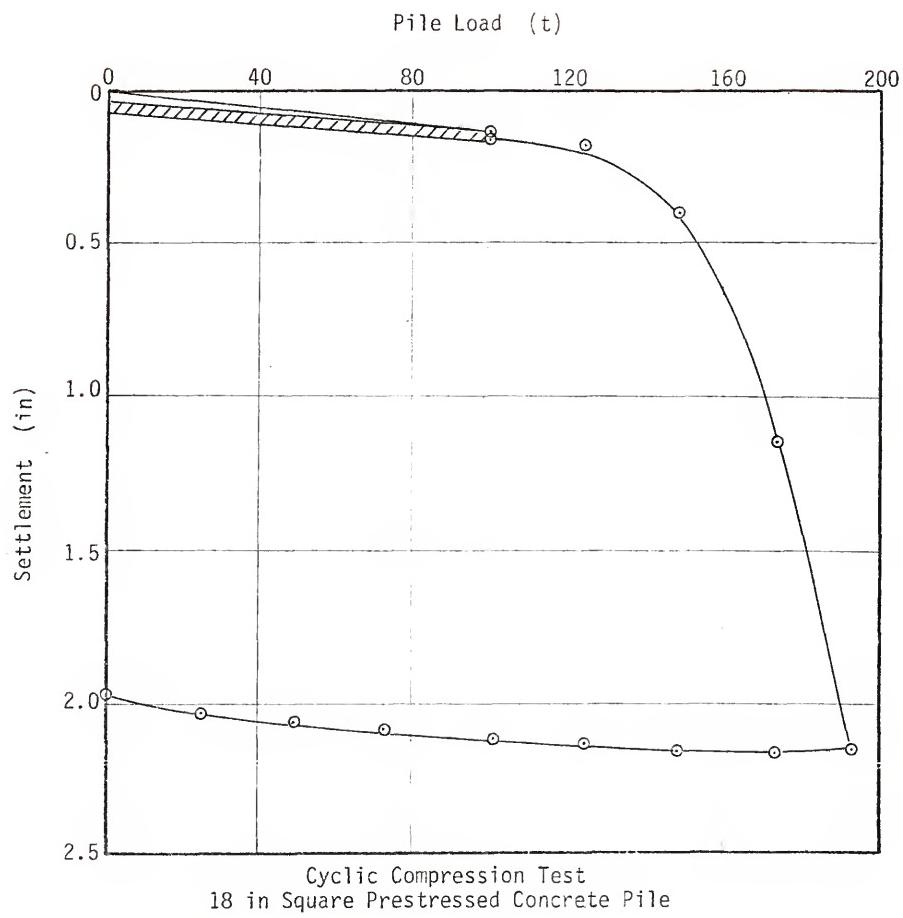
BLOUNT ISLAND PILE LOAD TEST RESULTS - SITE 322

FIGURE D-43



BLOUNT ISLAND PILE LOAD TEST RESULTS - SITE 322

FIGURE D-44



BLOUNT ISLAND PILE LOAD TEST RESULTS - SITE 348

FIGURE D-45

## BIOGRAPHY

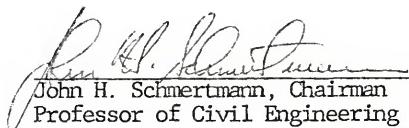
Larry C. Nottingham was born to Raymond and Darlie Nottingham on September 15, 1942, and was reared in Servia, West Virginia. He attended Servia Grade School and Gassaway High School, graduating in 1960. He entered West Virginia Institute of Technology in 1960 and graduated with a Bachelor of Science Degree in Civil Engineering in 1965. He entered graduate school at the University of Pittsburgh in 1965 and received a Master of Science Degree in 1966.

In August, 1966, he accepted employment with West Virginia Institute of Technology as Instructor of Civil Engineering. He held that position until June, 1967, when he accepted employment with A. C. Ackenheil & Associates, Inc., a geotechnical consulting firm in Charleston, West Virginia.

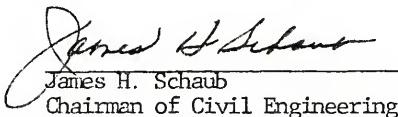
In September, 1970, Mr. Nottingham entered Graduate School at the University of Florida and began work toward a Doctor of Philosophy Degree in the field of Civil Engineering. He was employed by the Florida Department of Transportation during his stay at the University of Florida. He departed Gainesville in November, 1974, to accept employment with Fugro, Inc., a geotechnical consulting firm in Long Beach, California.

Mr. Nottingham is married to the former Carol Lambert and is the father of two children, John and Amy. He is a Registered Professional Engineer in the states of Florida and West Virginia and is an Associate Member of the American Society of Civil Engineers.

I certify that I have read this study and that in my opinion it conforms to acceptable standards of scholarly presentation and is fully adequate, in scope and quality, as a dissertation for the degree of Doctor of Philosophy.

  
John H. Schmertmann, Chairman  
Professor of Civil Engineering

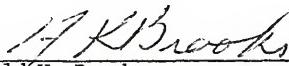
I certify that I have read this study and that in my opinion it conforms to acceptable standards of scholarly presentation and is fully adequate, in scope and quality, as a dissertation for the degree of Doctor of Philosophy.

  
James H. Schaub  
Chairman of Civil Engineering

I certify that I have read this study and that in my opinion it conforms to acceptable standards of scholarly presentation and is fully adequate, in scope and quality, as a dissertation for the degree of Doctor of Philosophy.

  
Byron E. Ruth  
Associate Professor of Civil Engineering

I certify that I have read this study and that in my opinion it conforms to acceptable standards of scholarly presentation and is fully adequate, in scope and quality, as a dissertation for the degree of Doctor of Philosophy.

  
Harold K. Brooks  
Professor of Geology

This dissertation was submitted to the Dean of the College of Engineering and to the Graduate Council, and was accepted as partial fulfillment of the requirements for the degree of Doctor of Philosophy.

June, 1975



\_\_\_\_\_  
Dean, College of Engineering

\_\_\_\_\_  
Dean, Graduate School